Linear and Hyperbranched Polyether-based Polymers as Nanocarriers for Drug Delivery

Dissertation

zur Erlangung des Grades

„Doktor der Naturwissenschaften“

im Promotionsfach Chemie

am Fachbereich Chemie, Pharmazie und Geowissenschaften der

Johannes Gutenberg-Universität Mainz

vorgelegt von

Eyleen Becker

geboren in Landau in der Pfalz

Mainz, Oktober 2021

JOHANNES GUTENBERG UNIVERSITÄT MAINZ

SFB 1066

Dekanin: Prof. Dr. Tanja Schirmeister

Prodekane: Prof. Dr. Till Opatz, Prof. Dr. Tobias Reich

1. Berichterstatter: Prof. Dr. Holger Frey

2. Berichterstatter: Prof. Dr. Pol Besenius

Tag der mündlichen Prüfung: 02.12.2021

Die als Dissertation vorgelegte Arbeit wurde im Zeitraum August 2017 bis Oktober 2021 am Department Chemie der Johannes Gutenberg-Universität Mainz in der Arbeitsgruppe von Prof. Dr. Holger Frey angefertigt.

Hiermit versichere ich gemäß § 10 Abs. 3d der Promotionsverordnung vom 24.07.2007:

a) Ich habe die jetzt als Dissertation vorgelegte Arbeit selbst angefertigt und alle benutzten Hilfsmittel (Literatur, Apparaturen, Material) in der Arbeit angegeben.

b) Ich habe oder hatte die jetzt als Dissertation vorgelegte Arbeit nicht als Prüfungsarbeit für eine andere Prüfung eingereicht

c) Ich hatte weder die jetzt als Dissertation vorgelegte Arbeit noch Teile davon bei einer anderen Fakultät bzw. einem anderen Fachbereich als Dissertation eingereicht.

Eyleen Becker

Für meine Familie

"Alice: This is impossible.

The Mad Hatter: Only if you believe it is."

Alices's Adventures in Wonderland

-Lewis Carroll

Danksagung

.

Table of Contents

Collaborations

MOTIVATION AND OBJECTIVES

The most prominent representative of the aliphatic polyethers is poly(ethylene glycol) (PEG), also known as poly(ethylene oxide) in the case of higher molecular weights.[1] It is synthesized by the anionic ring opening polymerization (AROP) of ethylene oxide (EO).[2] PEG is highly water soluble compared to the other polyethers, which makes it unique in its application.[3–5] Furthermore, it is characterized by its low toxicity,[6] immunogenicity[7] and it is chemically inert.[8] For these reasons, PEG is used in a wide range of products, from cosmetics to food additives to advanced drug delivery systems, and is considered as the "gold standard" for biomedical and pharmaceutical applications.[1,8–10] The covalent linkage of PEG can modify various surfaces, drugs, and biomolecules. This process is called "PEGylation" and is used as a strategy in biomedical and pharmaceutical applications to improve pharmacokinetic properties.[11,12] There are already several "PEGylated" pharmaceuticals on the market that have been approved by the American Drug and Food Administration (FDA). A common application is the "PEGylation" of lipids.[10,12–16] PEG lipids are mainly used for the preparation of liposomes with an increased blood circulation time.[17] By modifying the surface of the liposomes, they are not recognized as foreign by the body's immune defense system and can circulate longer in the bloodstream, which is known as the "stealth effect".[18]

However, apart from its favorable properties, PEG exhibits only two functional groups and possesses no degradability. To overcome the lack of functional groups, a novel approach represents the use of hyperbranched polyglycerol structures for the synthesis of amphiphilic lipids (*hb*PG lipids).[19,20] Hyperbranched polyglycerol lipids produce a stealth effect similar to linear PEG chains, but are characterized by a large number of functional hydroxyl groups that can be used as multiple target vectors.[21] The synthesis is also carried out by AROP, but *via* slow monomer addition (SMA) of the monomer glycidol. Another way to compensate the low number of functional groups in PEG is the copolymerization of EO with functional epoxides, resulting in multifunctional PEG (*mf*-PEG).[22]

On the other hand, a more difficult problem is the non-degradability of PEG.[23] For the safe application of PEG in the body, the molecular weight of 40 000 g/mol cannot be exceeded.

This value corresponds to the renal excretion limit. At higher molecular weights, the compounds accumulate in the tissue and organs and results in undesirable diseases.[23] On the other hand, higher molecular weights are preferred because they positively influence the pharmacokinetic properties of PEG conjugates and prolongs the blood circulation time.[24] The contradiction between desired high molecular weights and limited excretion can be overcome by the development of cleavable PEGs and is an important part of this work. A large variety of cleavable PEGs are already known, but in most cases these are based on the polyaddition or polycondensation of commercially available, end-group functionalized PEGs. However, these polymers are not suitable for medical applications. The manufacturing methods can result in poor control over the molecular weight and broad molecular weight distributions.[25] The synthesis of PEG *via* AROP allows precise and tailored molecular weights with narrow molecular weight distributions, making it the optimal choice for its use in the production of PEGs for pharmaceutical and biomedical applications.[26]

Furthermore, cleavable PEGs play a crucial role as functional components in the development of stimuli-responsive drug delivery systems.[27] Particularly sensitive cargos such as protein- and peptide-based drugs benefit significantly from delivery by polymeric drug delivery systems.[28]

In this context, the objectives of this thesis can be divided into the following main topics:

1) Strategies for the synthesis of pH-responsive polyether lipids

Chapter 2 focuses on the development and synthesis of cleavable polyether lipids based on pH-sensitive vinyl ether structures for biomedical and pharmaceutical applications. Polyether lipids are ideally suited as polymer-drug conjugates, offering a wide range of applications, for example through targeted incorporation into stealth liposomes.[29] The incorporation of a pH-sensitive cleavage site enables the PEG chains to be separated from the hydrophobic moiety. Vinyl ethers represent an ideal class of pH-sensitive groups due to their cleavage in the physiological pH of 5-4.5.[30–32] Other widely used cleavable groups are acetals or ketals.[33,34]

Polyether lipids based on cholesterol are common and extensively used.[35] By the functionalization of cholesterol with an allyl group containing moiety, a novel initiator for the AROP could be synthesized. AROP with EO allowed the preparation of amphiphilic cholesterol-based PEG lipids, which were converted to their pH sensitive vinyl ether structure by a subsequent isomerization. To enable functionalization of the end group, the polymers were provided with an alkyne group for further azide-alkine cycloaddition reactions (**Chapter 2.1**).

However, amphiphilic polyether lipids can be prepared not only by cholesterol, but also by using a hydrophobic dialkyl anchor.[36] In comparison to cholesterol, they are distinguished by their high membrane stability, especially in liposomal applications. The functionalization of the anchor by using an allyl group resulted in an initiator for the polymerization of EO *via* AROP, which formed pH-sensitive polyether lipids after the isomerization. Subsequent tests of the polyether lipids showed their good stability in liposomal formulations (**Chapter 2.2**).

The hydrophobic dialkyl anchor can not only be converted into a cleavable PEG-lipid by the incooperation of a vinyl ether group, but also by the incorporation of acetals or ketals. After the development and preparation of the amphiphilic cleavable PEG lipids, they could be used for the preparation for liposomes. Labeling by copper-catalyzed azide-alkyne click reaction with a fluorescent dye allowed the study of cleavage at different pH values (**Chapter 5.1**).

2) Development of hyperbranched polyether lipids for targeted drug delivery

Chapter 3 deals with targeted drug delivery using surface functionalized liposomes. The targeted administration of drugs is an important tool in the treatment of deadly diseases, such as cancer.[37] The focus here is on achieving the best possible effect against the disease without undesirable side effects. For targeted transport, nanocarriers such as liposomes are of great advantage due to the functionalization of the surface with PEG chains and/or ligands.[38] Hyperbranched polyether lipids have a variety of functional groups to attach different target molecules.[39] Drug targeting against prostate cancer by liposomes with hyperbranched structures on the surface was investigated. For this purpose, the synthesis

of a prostate specific membrane antigen (PSMA) as a ligand was performed. In addition, the liposomes were radioactively labeled for PET imaging studies.

3) Synthesis of stimuli-responsive functional polyethers

Chapter 4 covers the synthesis for stimuli-responsive glycidyl ethers for the copolymerization of EO. Stimuli-responsive polymers can be used for targeted release.[40] Internal stimuli in the body include pH,[41] redox processes[42] and enzymatic activity.[43] Tertiary amines in polyethers, for example, can be influenced by pH values,[44] whereas thioethers react to oxidation with a change in their properties.[45] Thiazolidines are cyclic compounds that contain both an amine function and a thioether. The development of a thiazolidine-based glycidyl ether enabled the copolymerization with EO *via* AROP to produce a new class of redox- and pH-responsive PEG polymers.

References

(1) Herzberger, J.; Niederer, K.; Pohlit, H.; Seiwert, J.; Worm, M.; Wurm, F. R.; Frey, H. Polymerization of Ethylene Oxide, Propylene Oxide, and Other Alkylene Oxides: Synthesis, Novel Polymer Architectures, and Bioconjugation. *Chem. Rev.* **2015**, acs.chemrev.5b00441. https://doi.org/10.1021/acs.chemrev.5b00441.

(2) Staudinger, H.; Schweitzer, O. Über Hochpolymere Verbindungen, 20. Mitteil.: Über Die Poly-Äthylenoxyde. *Ber. dtsch. Chem. Ges. A/B* **1929**, *62*, 2395–2405. https://doi.org/10.1002/cber.19290620879.

(3) Kadajji, V. G.; Betageri, G. V. Water Soluble Polymers for Pharmaceutical Applications. *Polymers (Basel).* **2011**, *3* (4), 1972–2009. https://doi.org/10.3390/polym3041972.

(4) Kjellander, R.; Florin, E. Water Structure and Changes in Thermal Stability of the System Poly(Ethylene Oxide)-Water. *J. Chem. Soc. Faraday Trans. 1 Phys. Chem. Condens. Phases* **1981**, *77* (9), 2053–2077. https://doi.org/10.1039/F19817702053.

(5) Klein, R.; Wurm, F. R. Aliphatic Polyethers: Classical Polymers for the 21st Century. *Macromol. Rapid Commun.* **2015**, *36* (12), 1147–1165. https://doi.org/10.1002/marc.201500013.

(6) Fruijtier-Pölloth, C. Safety Assessment on Polyethylene Glycols (PEGs) and Their Derivatives as Used in Cosmetic Products. *Toxicology* **2005**, *214* (1–2), 1–38. https://doi.org/10.1016/j.tox.2005.06.001.

(7) Garay, P. Immunogenicity of Polyethylene Glycol (PEG). *TOPROCJ* **2011**, *2*, 104–

107. https://doi.org/10.2174/2210289201102010104.

(8) Bailey, F. E. *Poly(Ethylene Oxide)*; Academic Press: New York, 1976.

(9) Thomas, A.; Müller, S. S.; Frey, H. Beyond Poly(Ethylene Glycol): Linear Polyglycerol as a Multifunctional Polyether for Biomedical and Pharmaceutical Applications. *Biomacromolecules* **2014**, *15* (6), 1935–1954. https://doi.org/10.1021/bm5002608.

(10) Dingels, C.; Schömer, M.; Frey, H. Die Vielen Gesichter Des Poly(Ethylenglykol)s: Von Der Kosmetik Zum Ionenleiter. *Chemie Unserer Zeit* **2011**, *45* (5), 338–349. https://doi.org/10.1002/ciuz.201100551.

(11) Milla, P.; Dosio, F.; Cattel, L. PEGylation of Proteins and Liposomes: A Powerful and Flexible Strategy to Improve the Drug Delivery. *Curr. Drug Metab.* **2011**, *13* (1), 105–119. https://doi.org/10.2174/138920012798356934.

(12) Veronese, F. M. *PEGylated Protein Drugs: Basic Science and Clinical Applications*; Birkenhäuser Basel: Basel, 2009.

(13) Alconcel, S. N. S.; Baas, A. S.; Maynard, H. D. FDA-Approved Poly(Ethylene Glycol)–Protein Conjugate Drugs. *Polym. Chem.* **2011**, *2* (7), 1442. https://doi.org/10.1039/c1py00034a.

(14) Bailon, P.; Won, C. Y. PEG-Modified Biopharmaceuticals. *Expert Opin. Drug Deliv.* **2009**, *6* (1), 1–16. https://doi.org/10.1517/17425240802650568.

(15) Barenholz, Y. Doxil® - The First FDA-Approved Nano-Drug: Lessons Learned. *J. Control. Release* **2012**, *160* (2), 117–134. https://doi.org/10.1016/j.jconrel.2012.03.020.

(16) Bobo, D.; Robinson, K. J.; Islam, J.; Thurecht, K. J.; Corrie, S. R. Nanoparticle-Based Medicines: A Review of FDA-Approved Materials and Clinical Trials to Date. *Pharm. Res.* **2016**, *33* (10), 2373–2387. https://doi.org/10.1007/s11095-016-1958-5.

(17) B., D. V.; Fee, C. Protein PEGylation: An Overview of Chemistry and Process Considerations. *Eur. Pharm. Rev.* **2010**, 18-26.

(18) Lasic, D. D.; Needham, D. The "Stealth" Liposome: A Prototypical Biomaterial. *Chem. Rev.* **1995**, *95* (8), 2601–2628.

(19) Fritz, T.; Hirsch, M.; Richter, F. C.; Müller, S. S.; Hofmann, A. M.; Rusitzka, K. A. K.; Markl, J.; Massing, U.; Frey, H.; Helm, M. Click Modification of Multifunctional Liposomes Bearing Hyperbranched Polyether Chains. *Biomacromolecules* **2014**, *15* (7), 2440–2448. https://doi.org/10.1021/bm5003027.

(20) Müller, S. S.; Fritz, T.; Gimnich, M.; Worm, M.; Helm, M.; Frey, H. Biodegradable Hyperbranched Polyether-Lipids with in-Chain PH-Sensitive Linkages. *Polym.*

Chem. **2016**, *7* (40), 6257–6268. https://doi.org/10.1039/C6PY01308B.

(21) Wagener, K.; Worm, M.; Pektor, S.; Schinnerer, M.; Thiermann, R.; Miederer, M.; Frey, H.; Rösch, F. Comparison of Linear and Hyperbranched Polyether Lipids for Liposome Shielding by 18 F-Radiolabeling and Positron Emission Tomography. *Biomacromolecules* **2018**, *19* (7), 2506–2516. https://doi.org/10.1021/acs.biomac.8b00115.

(22) Mangold, C.; Wurm, F.; Frey, H. Functional PEG-Based Polymers with Reactive Groups via Anionic ROP of Tailor-Made Epoxides. *Polym. Chem.* **2012**, *3* (7), 1714–1721. https://doi.org/10.1039/c2py00489e.

(23) Pasut, G.; Veronese, F. M. Polymer-Drug Conjugation, Recent Achievements and General Strategies. *Prog. Polym. Sci.* **2007**, *32* (8–9), 933–961. https://doi.org/10.1016/j.progpolymsci.2007.05.008.

(24) Yamaoka, T.; Tabata, Y.; Ikada, Y. Distribution and Tissue Uptake of Poly(Ethylene Glycol) with Different Molecular Weights after Intravenous Administration to Mice. *J. Pharm. Sci.* **1994**, *83* (4), 601–606. https://doi.org/10.1002/jps.2600830432.

(25) Dingels, C.; Frey, H. From Biocompatible to Biodegradable: Poly(Ethylene Glycol)s with Predetermined Breaking Points. In *Hierarchical Macromolecular Structures: 60 Years after the Staudinger Nobel Prize II*; Percec, V., Ed.; Springer International Publishing: Cham, 2013; pp 167–190. https://doi.org/10.1007/12_2013_235.

(26) Flory, P. J. Molecular Size Distribution in Ethylene Oxide Polymers. *J. Am. Chem. Soc.* **1940**, *62*, 1561–1565.

(27) Gil, E. S.; Hudson, S. M. Stimuli-Reponsive Polymers and Their Bioconjugates. *Prog. Polym. Sci.* **2004**, *29* (12), 1173–1222. https://doi.org/10.1016/j.progpolymsci.2004.08.003.

(28) Chamundeeswari, M.; Jeslin, J.; Verma, M. L. Nanocarriers for Drug Delivery Applications. *Environ. Chem. Lett.* **2019**, *17* (2), 849–865. https://doi.org/10.1007/s10311-018-00841-1.

(29) Howard, M. D.; Jay, M.; Dziubla, T. D.; Lu, X. PEGylation of Nanocarrier Drug Delivery Systems: State of the Art. *J. Biomed. Nanotechnol.* **2008**, *4* (2), 133–148. https://doi.org/10.1166/jbn.2008.021.

(30) Worm, M.; Leibig, D.; Dingels, C.; Frey, H. Cleavable Polyethylene Glycol: 3,4-Epoxy-1-Butene as a Comonomer to Establish Degradability at Physiologically Relevant PH. *ACS Macro Lett.* **2016**, 1357–1363. https://doi.org/10.1021/acsmacrolett.6b00735.

(31) Shin, J.; Shum, P.; Grey, J.; Fujiwara, S. I.; Malhotra, G. S.; González-Bonet, A.; Hyun, S. H.; Moase, E.; Allen, T. M.; Thompson, D. H. Acid-Labile MPEG-Vinyl Ether-1,2-Dioleylglycerol Lipids with Tunable Ph Sensitivity: Synthesis and Structural Effects on Hydrolysis Rates, DOPE Liposome Release Performance, and Pharmacokinetics. *Mol. Pharm.* **2012**, *9* (11), 3266–3276. https://doi.org/10.1021/mp300326z.

(32) Shin, J.; Shum, P.; Thompson, D. H. Acid-Triggered Release via DePEGylation of DOPE Liposomes Containing Acid-Labile Vinyl Ether PEG-Lipids. *J. Control. Release* **2003**, *91* (1–2), 187–200. https://doi.org/10.1016/S0168-3659(03)00232-3.

(33) Mustapa, M. F. M.; Grosse, S. M.; Kudsiova, L.; Elbs, M.; Raiber, E. A.; Wong, J. B.; Brain, A. P. R.; Armer, H. E. J.; Warley, A.; Keppler, M.; Ng, T.; Lawrence, M. J.; Hart, S. L.; Hailes, H. C.; Tabor, A. B. Stabilized Integrin-Targeting Ternary LPD (Lipopolyplex) Vectors for Gene Delivery Designed to Disassemble within the Target Cell. *Bioconjug. Chem.* **2009**, *20* (3), 518–532. https://doi.org/10.1021/bc800450r.

(34) Luvino, D.; Khiati, S.; Oumzil, K.; Rocchi, P.; Camplo, M.; Barthélémy, P. Efficient Delivery of Therapeutic Small Nucleic Acids to Prostate Cancer Cells Using Ketal Nucleoside Lipid Nanoparticles. *J. Control. Release* **2013**, *172* (3), 954–961. https://doi.org/10.1016/j.jconrel.2013.09.006.

(35) Hofmann, A. M.; Wurm, F.; Frey, H. Rapid Access to Polyfunctional Lipids with Complex Architecture via Oxyanionic Ring-Opening Polymerization. *Macromolecules* **2011**, *44* (12), 4648–4657. https://doi.org/10.1021/ma200367c.

(36) Hofmann, A. M.; Wurm, F.; Huhn, E.; Nawroth, T.; Langguth, P.; Frey, H. Hyperbranched Polyglycerol-Based Lipids via Oxyanionic Polymerization: Toward Multifunctional Stealth Liposomes. *Biomacromolecules* **2010**, *11* (3), 568–574. https://doi.org/10.1021/bm901123j.

(37) Manchun, S.; Dass, C. R.; Sriamornsak, P. Targeted Therapy for Cancer Using PH-Responsive Nanocarrier Systems. *Life Sci.* **2012**, *90* (11–12), 381–387. https://doi.org/10.1016/j.lfs.2012.01.008.

(38) Torchilin, V. P. *Passive and Active Drug Targeting: Drug Delivery to Tumors as an Example*; 2010; Vol. 197. https://doi.org/10.1007/978-3-642-00477-3_1.

(39) Reibel, A. T.; Müller, S. S.; Pektor, S.; Bausbacher, N.; Miederer, M.; Frey, H.; Rösch, F. Fate of Linear and Branched Polyether-Lipids in Vivo in Comparison to Their Liposomal Formulations by 18F-Radiolabeling and Positron Emission Tomography. *Biomacromolecules* **2015**, *16* (3), 842–851. https://doi.org/10.1021/bm5017332.

(40) Avramović, N.; Mandić, B.; Savić-Radojević, A.; Simić, T. Polymeric Nanocarriers of Drug Delivery Systems in Cancer Therapy. *Pharmaceutics* **2020**, *12* (4), 1–17.

https://doi.org/10.3390/pharmaceutics12040298.

(41) Rodrigues, P. C. A.; Beyer, U.; Schumacher, P.; Roth, T.; Fiebig, H. H.; Unger, C.; Messori, L.; Orioli, P.; Paper, D. H.; Mülhaupt, R.; Kratz, F. Acid-Sensitive Polyethylene Glycol Conjugates of Doxorubicin: Preparation, in Vitro Efficacy and Intracellular Distribution. *Bioorganic Med. Chem.* **1999**, *7* (11), 2517–2524. https://doi.org/10.1016/S0968-0896(99)00209-6.

(42) Zhang, P.; Wu, J.; Xiao, F.; Zhao, D.; Luan, Y. Disulfide Bond Based Polymeric Drug Carriers for Cancer Chemotherapy and Relevant Redox Environments in Mammals. *Med. Res. Rev.* **2018**, *38* (5), 1485–1510. https://doi.org/10.1002/med.21485.

(43) Roy, D.; Cambre, J. N.; Sumerlin, B. S. Future Perspectives and Recent Advances in Stimuli-Responsive Materials. *Prog. Polym. Sci.* **2010**, *35* (1–2), 278–301. https://doi.org/10.1016/j.progpolymsci.2009.10.008.

(44) Lee, A.; Lundberg, P.; Klinger, D.; Lee, B. F.; Hawker, C. J.; Lynd, N. a. Physiologically Relevant, PH-Responsive PEG-Based Block and Statistical Copolymers with N,N-Diisopropylamine Units. *Polym. Chem.* **2013**, *4* (24), 5735. https://doi.org/10.1039/c3py00747b.

(45) Herzberger, J.; Fischer, K.; Leibig, D.; Bros, M.; Thiermann, R.; Frey, H. Oxidation-Responsive and "Clickable" Poly(Ethylene Glycol) via Copolymerization of 2-(Methylthio)Ethyl Glycidyl Ether. *J. Am. Chem. Soc.* **2016**, jacs.6b04548. https://doi.org/10.1021/jacs.6b04548.

ABSTRACT

The aim of this work is the synthesis of linear and hyperbranched polyether lipids and multifunctional polyether (co)polymers based on poly(ethylene glycol) (PEG) as nanocarriers for targeted drug delivery. The linear polymer structures are equipped with stimuli-responsive groups to expand the scope of degradable polymer materials for biomedical applications. One of the most important polymers for use in pharmaceutical or biomedical applications is PEG, which is often used for conjugation to therapeutically active molecules ("PEGylation") or in liposomes to modify their pharmacokinetic properties („Stealth Liposomes"). PEG is characterized by its high water solubility, low toxicity and low immunogenicity. In contrast to its favorable properties, however, there is a distinct disadvantage: PEG is not biodegradable. To counteract this drawback, various stimuli-responsive PEGs have been developed in this work. Hyperbranched polymer lipids were synthesized to produce multifunctional liposomes. Therefore, the present dissertation is motivated both by the fundamental issues of synthesis and by the potential applicability of the polymer compounds in biological applications.

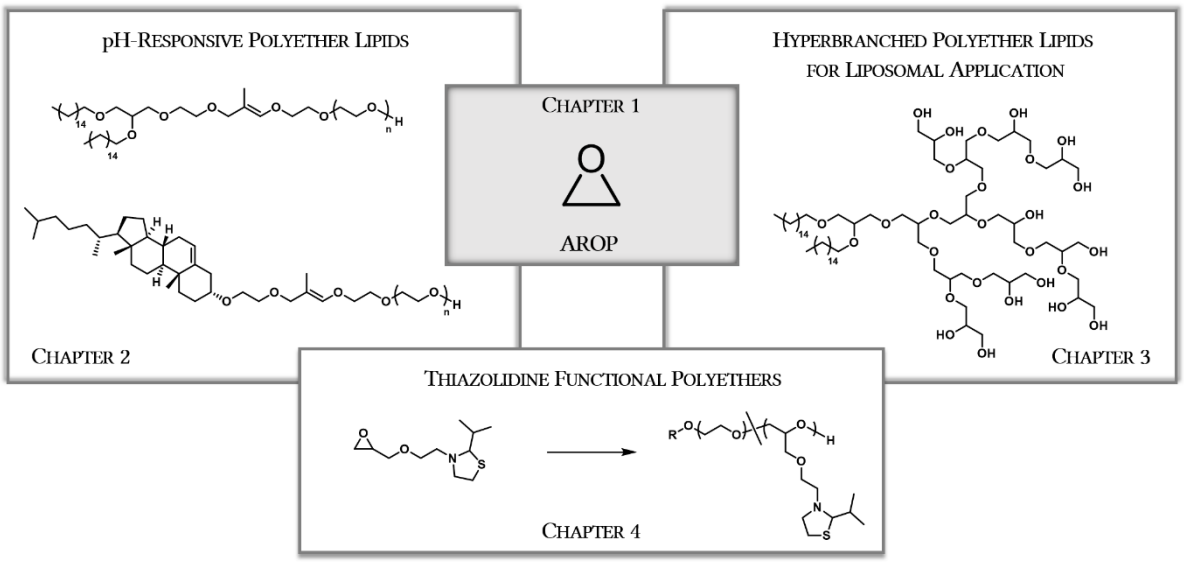

Scheme 1: Synopsis of the main topics of this thesis.

Chapter 1 provides an introduction to this thesis. **Chapter 1.1** gives an overview of the class of aliphatic polyethers. The most important representative for this work, poly(ethylene glycol) (PEG), is highlighted with an emphasis on its preparation, properties and applications. **Chapter 1.2** discusses anionic ring-opening polymerization (AROP) as a preparation method for the synthesis of PEG. The degradability of polyethers is discussed in **Chapter 1.3**, as well as the functional groups that can be incorporated into the polymer to enable cleavage. In **Chapter 1.4**, nanocarriers for targeted drug delivery are presented, as well as the transport mechanisms through active and passive targeting. Furthermore, the release strategies *via* external and internal stimuli are explained.

Chapter 2 deals with the preparation of pH-responsive polyether lipids. The introduction of the pH-sensitive cleavage site is in the form of a vinyl ether unit between the hydrophilic and the hydrophobic part of the lipid. In **Chapter 2.1**, the synthesis of a pH-cleavable polyether lipid based on cholesterol is shown. For the preparation, the synthesis of a pH-stable initiator developed first, which then reacts with ethylene oxide (EO) in an AROP to give the amphiphilic PEG lipid. The subsequent conversion of the pH-stable allyl group of the PEG lipid into the pH-sensitive vinyl ether group was achieved by isomerization to give the cleavable PEG lipid. A subsequent post-modification of the pH-responsive polyether lipid with an alkyne end group enables further conjugations of active ingredients, dyes and other compounds by azide-alkyne cycloaddition.

Based on the same synthesis strategy, dialkyl PEG lipids for the use in pH-sensitive liposomes were prepared in **Chapter 2.2**. Based on a long-chain dialkyl anchor, an initiator for AROP was developed. Polymerization of EO was followed by reaction of the pH-stable polymer lipids to pH-labile lipids by isomerization. After modification of the PEG lipids with an alkyne group, they were incorporated into liposomes by dual centrifugation. The size of the liposomes was determined, as well as their stability. Toxicity was excluded by MTT assay.

In **Chapter 3**, hyperbranched polyether lipids were prepared for liposome applications. Alkyne-functionalized hyperbranched polyglycerols (*hb*PG) were synthesized with a dialkyl anchor and functionalized by Cu(I)-catalyzed alkyne-azide cycloaddition (CuAAC) with a prostate-specific membrane antigen (PSMA) inhibitor and radiolabeling with ^{18}Fluorine.

The functionalized hyperbranched lipids were then used to prepare liposomes as a promising system for future targeted drug delivery for the treatment of prostate cancer.

Chapter 4 describes the development of a new glycidyl ether based on thiazolidine. The development of the monomer as well as the copolymerization with ethylene oxide and the homopolymerization are explained. The microstructure of the polymers was investigated by *in-situ* ^{1}H NMR kinetics studies. Furthermore, the responsive behavior of the copolymers was tested and investigated by oxidation with hydrogen peroxide. For a possible application in medical systems, the polymers were analyzed in toxicity studies by cell testing.

The appendix in **Chapter 5** contains contributions from the author of this thesis with other collaborators. In **Chapter 5.1**, a novel strategy for asymmetric ketals in polymers was developed to access pH-responsive PEG lipids. The hydrolysis rates of the ketal lipids were investigated at acidic pH using ^{1}H NMR kinetics studies. Furthermore, an investigation of the lipids in liposomal formulations was carried out using time-resolved fluorescence spectroscopy and gel electrophoresis assays. The cleavage of PEG chains from the liposome surface occurred at slightly acidic pH values (pH = 6.5-5.5), demonstrating the great potential of ketal PEG lipids for drug delivery strategies. In **Chapter 5.2**, the influence of the long-chain dialkyl-PEG lipids on the stability of the liposomal membrane was investigated. For this purpose, different formulations with different PEG lipids were used to prepare liposomes and labeled with a fluorescent dye. Subsequently, lipid exchange was analyzed by flow cytometry.

ZUSAMMENFASSUNG

Ziel dieser Arbeit ist die Synthese linearer und hyperverzweigter Polyether-Lipide und multifunktioneller Polyether-(Co)polymere auf Basis von Poly(ethylenglykol) (PEG), die zur Herstellung von Nanocarrier zum zielgerichteten Wirkstofftransport genutzt werden sollen. Die linearen Polymerstrukturen sind mit stimuli-responsiven Gruppen ausgestattet, um den Einsatzbereich von abbaubaren Polymermaterialien für biomedizinische Anwendungen zu erweitern. Eines der wichtigsten Polymere für den Einsatz im pharmazeutischen oder biomedizinischen Bereich stellt dabei PEG dar, das häufig zur Konjugation an therapeutisch aktive Moleküle angebunden wird („PEGylierung“) oder in Liposomen zur Änderung der pharmakokinetischen Eigenschaften eingesetzt wird („Stealth Liposomen“). PEG zeichnet sich dabei durch seine gute Wasserlöslichkeit, geringen Toxizität und geringer Immunogenität aus. Neben den guten Eigenschaften gibt es aber einen deutlichen Nachteil: PEG ist nicht bioabbaubar. Um diesem Nachteil entgegenzuwirken wurden in dieser Arbeit verschiedene stimuli-responsive PEGs entwickelt. Zur Herstellung von multifunktionellen Liposomen wurden hyperverzweigte Polymer-Lipide synthetisiert. Die vorliegende Dissertation ist daher sowohl von den grundsätzlichen Fragestellungen zur Synthese als auch durch die mögliche Anwendbarkeit der Polymerverbindungen in biologischen Anwendungen motiviert, wie in **Schema 1** gezeigt.

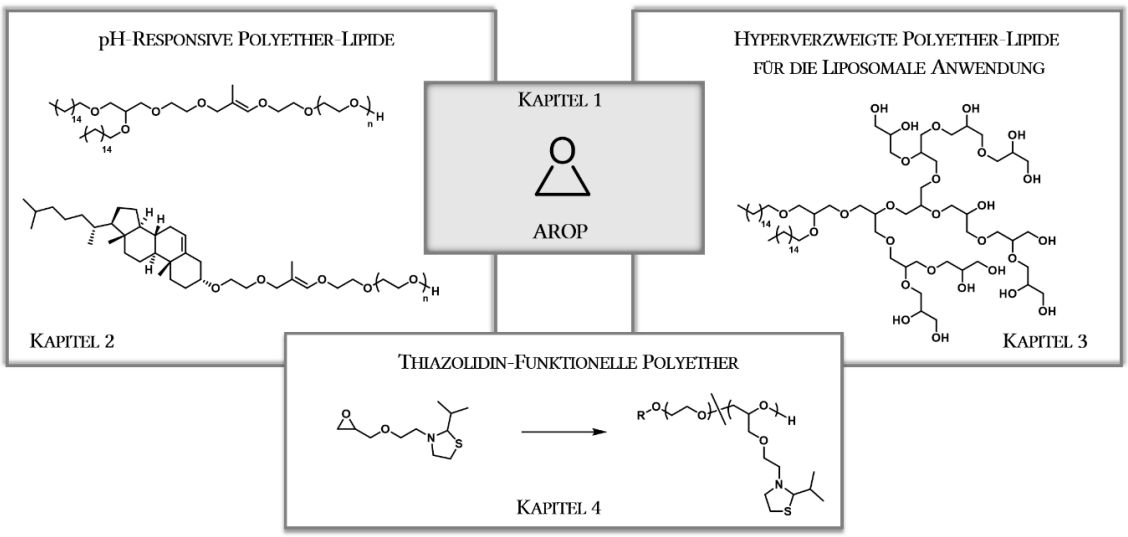

Schema 1: Zusammenfassung der Hauptthemen dieser Arbeit.

Kapitel 1.1 gibt einen Überblick über die Klasse der aliphatischen Polyether. Der für diese Arbeit wichtigste Vertreter Poly(ethylenglykol) (PEG) wird diskutiert, mit Schwerpunkten auf der Herstellung, den Eigenschaften und den Anwendungen. **Kapitel 1.2** behandelt die anionische ringöffnende Polymerisation (AROP) als eine Herstellungsmethode für die Synthese von PEG. Die Abbaubarkeit der Polyether wird im **Kapitel 1.3** behandelt, sowie die funktionellen Gruppen, die für eine Spaltung in das Polymer eingebaut werden können. In **Kapitel 1.4** werden Nanocarrier für den zielgerichteten Wirkstofftransport vorgestellt sowie die Transportmechanismen durch aktiven und passiven Transport. Weiterhin werden die Freisetzungsstrategien über externe und interne Stimuli erläutert.

Kapitel 2 behandelt die Herstellung von pH-responsiven Polyether-Lipide. Die Einführung der pH-sensitiven Spaltstelle erfolgt in Form einer Vinylether-Einheit zwischen dem hydrophilen und dem hydrophoben Teil des Lipids. In **Kapitel 2.1** wird die Synthese eines pH-spaltbaren Polyether-Lipids auf Basis von Cholesterin gezeigt. Für die Herstellung erfolgt zuerst die Synthese eines pH-stabilen Initiators, der anschließend in einer AROP mit Ethylenoxid (EO) zum amphiphilen PEG-Lipid reagiert. Die anschließende Überführung der pH-stabilen Allyl-Gruppe des PEG-Lipids in die pH-sensitive Vinylether-Gruppe erfolgt mittels Isomerisierung. Eine anschließende Post-Modifizierung des pH-responsiven Polyether-Lipids mit einer Alkin-Endgruppe ermöglicht weitere Konjugationen von Wirkstoffen, Farbstoffen und anderen Verbindungen durch Azid-Alkin-Cycloaddition.

Basierend auf der gleichen Synthesestrategie wurden im **Kapitel 2.2** Dialkyl-PEG-Lipide für den Einsatz in pH-sensitiven Liposomen hergestellt. Auf Basis eines langkettigen Dialkyl-Ankers wurde ein Initiator für die AROP entwickelt. Nach der Polymerisation mit EO erfolgte wieder die Umwandlung der pH-stabilen Polymer-Lipide in pH-labile Lipide durch Isomerisierung. Nach der Modifikation der PEG-Lipide mit einer Alkingruppe wurden diese mittels Dualer Zentrifugation in Liposomen eingebaut. Die Größe der Liposomen wurde bestimmt, sowie ihre Stabilität. Mittels MTT Assay wurde eine Toxizität ausgeschlossen.

In **Kapitel 3** wurden hyperverzweigte Polyether-Lipide für die Anwendung in Liposomen hergestellt. Alkin-funktionalisierte, hyperverzweigte Polyglycerine (*hb*PG) wurden mit einem langkettigen Dialkyl-Anker synthetisiert und mittels Cu(I)-katalysierter Alkin-Azid-Cycloaddition (CuAAC) mit einem Prostata-spezifischen Membran Antigen (PSMA)

Inhibitor und einer Radiomarkierung mit ^{18}Fluor funktionalisiert. Die funktionalisierten, hyperverzweigten Lipide wurden dann zur Herstellung von Liposomen genutzt als vielversprechendes System für die künftige gezielte Verabreichung von Medikamenten zur Behandlung von Prostatakrebs.

Kapitel 4 beschreibt die Entwicklung eines neuen Glycidylether Monomers, basierend auf Thiazolidin. Die Entwicklung des Monomers sowie die Copolymerisation mit Ethylenoxid und die Homopolymerisation werden erläutert. Die Mikrostruktur der Polymere wurde mittels *in situ* ^{1}H NMR Kinetik Studien untersucht. Weiterhin wurde das responsive Verhalten der Copolymere durch Oxidation mit Wasserstoffperoxid getestet und untersucht. Für eine mögliche Anwendung in medizinischen Systemen wurden die Polymere in Toxizitätsstudien durch Zelltests analysiert.

Der Anhang in **Kapitel 5** enthält weitere Beiträge des Autors dieser Arbeit zusammen mit anderen Kooperationspartnern. In **Kapitel 5.1** wurde eine neuartige Strategie für asymmetrische Ketale in Polymeren entwickelt, die den Zugang zu pH-responsiven PEG-Lipiden ermöglicht. Die Hydrolysegeschwindigkeit der Ketal-Lipide bei saurem pH-Wert wurde mittels ^{1}H NMR Kinetik Studien untersucht. Weiterhin erfolgte eine Untersuchung der Lipide in liposomalen Formulierungen mittels zeitaufgelöster Fluoreszenzspektroskopie und Gelelektrophorese-Assays. Die Abspaltung der PEG-Ketten von der Liposomenoberfläche erfolgte bei leicht sauren pH-Werten (pH = 6.5-5.5) und zeigt das große Potential der Ketal-PEG-Lipide für „Drug Delivery“ Strategien. In **Kapitel 5.2** wurde der Einfluss der langkettigen Dialkyl-PEG-Lipide auf die Stabilität der liposomalen Membran untersucht. Dafür wurden verschiedene Formulierungen mit unterschiedlichen PEG-Lipiden für die Herstellung von Liposomen verwendet und mit einem Fluoreszenzfarbstoff markiert. Anschließend wurde der Lipid-Austausch durch Durchflusszytometrie analysiert.

GRAPHICAL ABSTRACT

CHAPTER 1: INTRODUCTION

Chapter 1.3 Nanocarriers for Drug Delivery

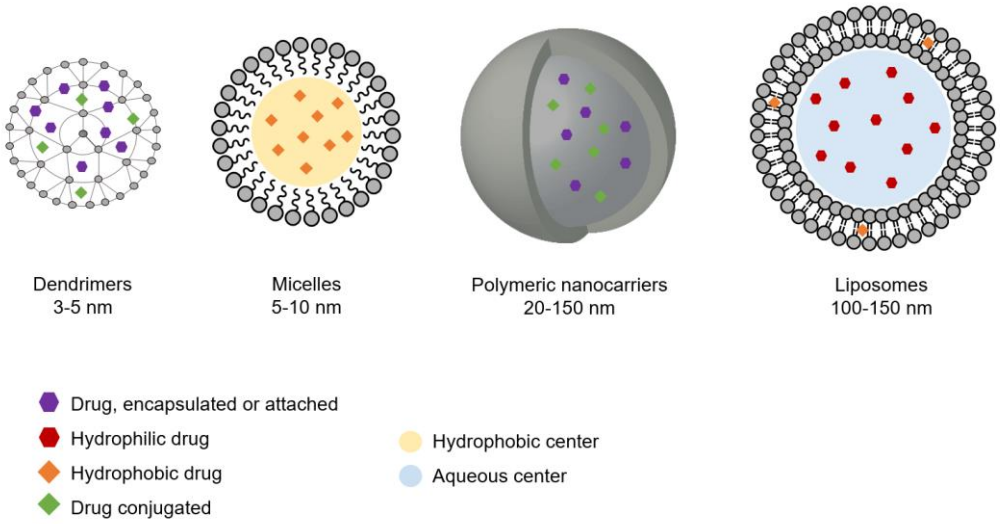

CHAPTER 2: PH-RESPONSIVE POLYETHER LIPIDS

Chapter 2.1: Design of pH-Degradable Cholesterol-based Polyether Lipids for the Conjugation of Small Molecules

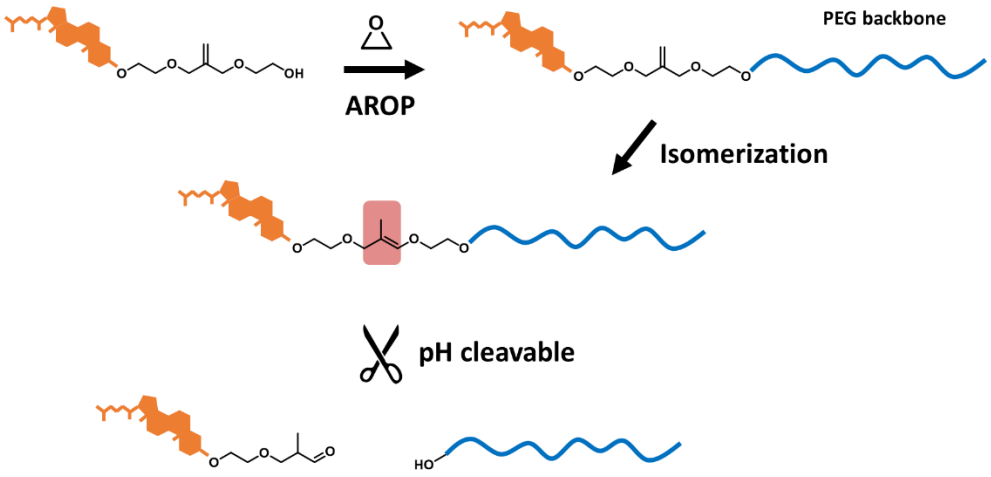

Chapter 2.2: Vinylether-functional Dialkyl-PEG Lipids for pH-Responsive Liposomes

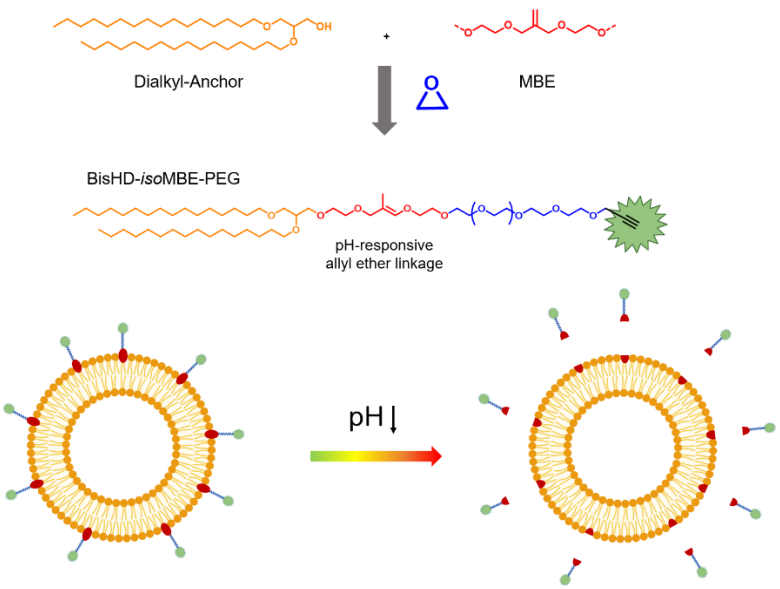

CHAPTER 3: HYPERBRANCHED POLYETHER LIPIDS FOR LIPOSOMAL APPLICATION

Chapter 3.1: ^{18}F-labeled, PSMA-specific liposomes: promising and PET-traceable tool for future targeted drug delivery in the treatment of prostate cancer

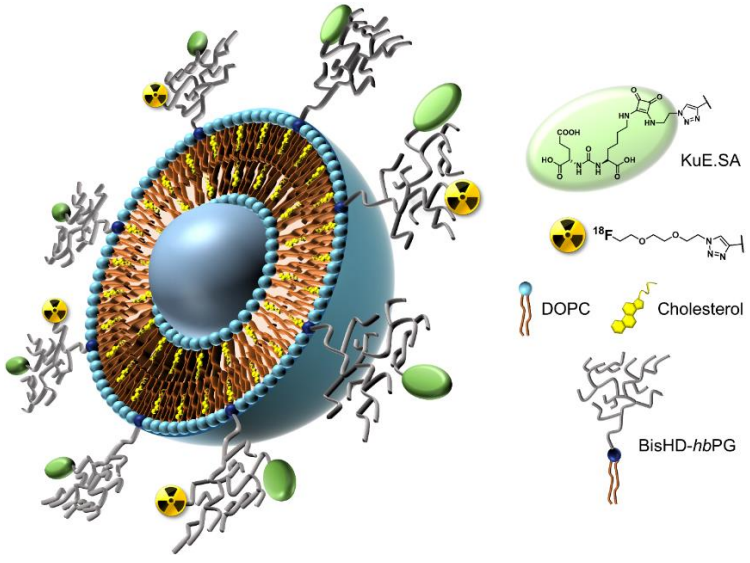

CHAPTER 4: THIAZOLIDINE FUNCTIONAL POLYETHERS

Chapter 4.1: Thiazolidine-based Glycidyl Ethers for the Anionic Ring-Opening Polymerization

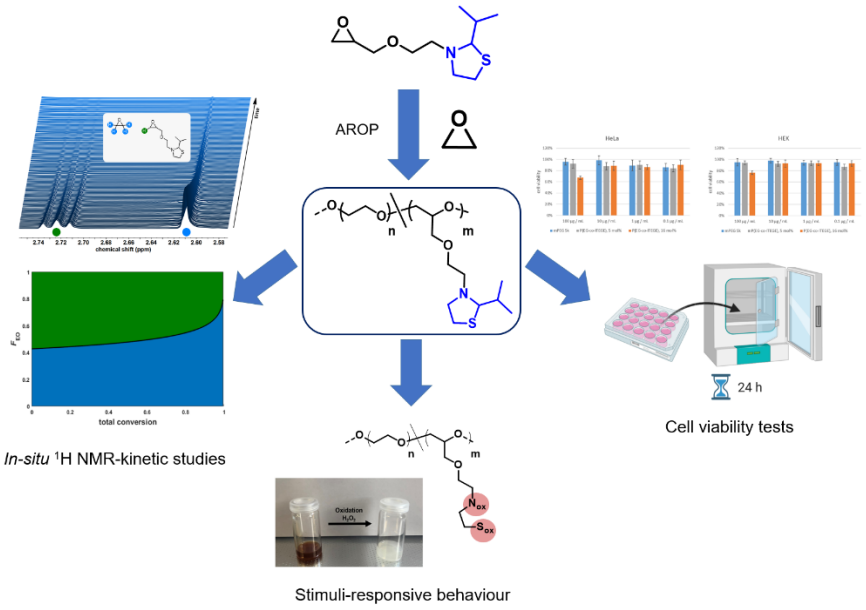

CHAPTER 5: APPENDIX

Chapter 5.1: Ketal- and Acetal-Functional Dialkyl-PEG Lipids for pH-Sheddable Stealth Liposomes

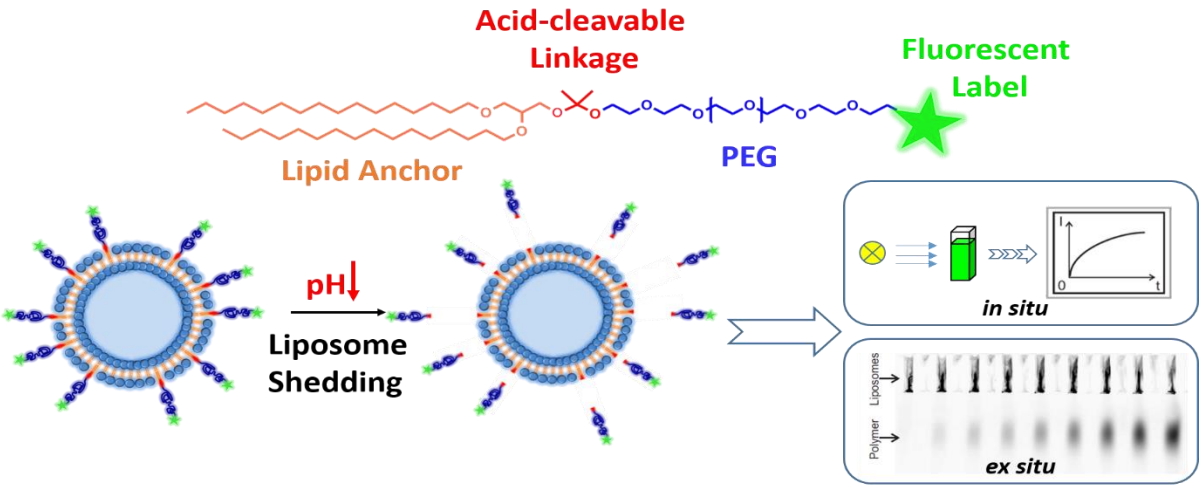

1 Introduction

This chapter will give a brief overview of polyethers, with a focus on the most prominent representatives in biomedical applications: poly(ethylene glycol) (PEG). The first section will highlight the structure and properties of aliphatic polyethers with a focus on PEG. Subsequently, polymerization techniques will be presented. In the second chapter, nanocarriers for drug delivery will be discussed. First, the different types of nanocarriers will be described and advantages and disadvantages of the systems will be highlighted. Subsequently, drug targeting will be considered in more detail. The last section deals with stimuli-sensitive nanocarriers for targeted drug delivery.

1.1 Aliphatic Polyethers

Polyethers represent an important class of polymers and exhibit unique properties. They play a crucial role in both academia and industry and they are used in various products.[1] Especially aliphatic polyethers are of interest, due to their high chain flexibility and low glass transition temperature.[2] Aliphatic polyethers exhibit in each repeating unit an ether unit with the general formula $(R\text{-}O\text{-}R')_n$, where R and R' represents an alkyl group and n the degree of polymerization. The C-O bond length is 143 pm and the ether bond possesses an angle of 112°.[3] The most prominent and commercially relevant representatives of polyethers are shown in Scheme 1.

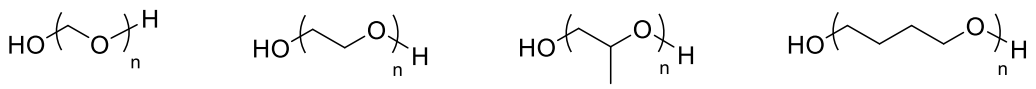

Scheme 1: Overview of the most relevant aliphatic polyether structures: poly(oxymethylene) (POM), poly(ethylene glycol) (PEG), poly(propylene oxide) (PPO) and poly(tetrahydrofuran) (PTHF).

Aliphatic polyethers can be classified by the number of carbon atoms of their repeating unit. Poly(oxymethylene) (POM) has the simplest structure with only one CH_2 group next to the oxygen atom in the polymer backbone. By increasing the number of CH_2 groups, poly(ethylene glycol) (PEG) and the structurally related poly(propylene oxide) are obtained. Compared to PEG, PPO has an additional methyl group attached to the backbone as a side

chain. Continuing the series, poly(tetrahydrofuran) (PTHF) follows as a further representative.

POM would at first glance be classified as a polyether, but it is strictly speaking a poly(acetal). Auerbach and Barschall first described the synthesis of POM,[4] and later POM was studied by Staudinger and others.[5–7] POM is highly crystalline and has a melting temperature of T_m = 180 °C. In the 1960s it was commercialized by DuPont under the product name Delrin®. Nowadays, it is used as a durable engineering plastic in gear wheels or Playmobil® toys, for example.[8,9]

PPO was first described by Levene and Walti, who synthesized it from the monomer propylene oxide (PO) in the presence of KOH.[10] Later, it was investigated by Pierre and Price.[11] Despite the similar structure as PEG, PPO is not water-soluble at room temperature and non-crystalline, due to the additional methyl group in the backbone and its atactic arrangement.[12,13] PPO-based structures are of immense interest in many different fields, such as lubricants,[14] anti-foaming agents[13] or non-ionic surfactants.[15,16] The synthesis of PPO is usually carried out *via* classical anionic ring-opening polymerization (AROP).[17] However, high molecular weight PPO (exceeding 10 000 g/mol) cannot be prepared by this technique due to proton abstraction at the α-carbon, which leads to chain termination or transfer reactions.[18] Carlotti and Deffieux *et al.* synthesized high molecular weight PPO (up to 170 000 g/mol) using the monomer-activated anionic ring-opening polymerization (MAROP).[19,20]

PTHF was developed in the 1930s by Meerwein *et al.*[21] and is mainly used as a polyether component in the production of foams and fibers.[22,23]

In the context of this thesis, PEG is the most important polyether-based polymer. For this reason, the properties, applications and synthesis will be discussed in detail in the next sections.

1.1.1 Poly(ethylene glycol) (PEG)

In the class of aliphatic polyethers poly(ethylene glycol) (PEG) is by far the most important representative.[18] The synthesis is usually carried out *via* anionic polymerization of ethylene oxide (EO) and was first described by Staudinger and Schweitzer in 1929.[24] PEG with a

molecular weight below 20 000 g/mol is called polyethylene glycol (PEG), while polymers with a higher molecular weight are usually referred to as polyethylene oxide (PEO).[25] In medicine, the abbreviation PEG is most common and exclusively used.[26]

The state of aggregation or melting point of PEG is strongly dependent on the degree of polymerization and therefore on the molecular weight. Polymers in the range of 200-600 g/mol appear as colorless oil, from 1000-6000 g/mol as a waxy solid, and at higher molecular weights as semi-crystalline solids. The melting point for high molecular weight PEG is in the range of 66 °C, and the glass transition temperature (T_g) is approximately -53 °C.[1,18]

Compared to all other aliphatic polyethers, PEG is characterized by its outstanding water solubility.[1,18] The high hydrophilicity can be explained by the structure of the polymer backbone. The distances of the oxygen atoms in the backbone are similar to the distances between the hydrogen atoms of water molecules in the liquid state. This allows the building of a network of hydrogen bonds between water and the PEG backbone, leading to its exceptional hydration and water-solubility.[27,28] Unlike most other substances, the aqueous solubility of PEG and its copolymers cannot be increased by heating. Polymers with this property belong to the group of thermoresponsive polymers.[29] The hydrate shell around the hydrophilic surface of the polymer can only form below the cloud point temperature, because of the relatively stretched polymer chains. Above the cloud point, the hydration shell disintegrates and the entropy of the system is increased due to free water molecules. As a result, the polymer becomes insoluble in water and precipitates.[30] Thermoresponsive polymers with this behavior have a lower critical solution temperature (LCST). The LCST of PEG in water is approx. 98 °C.[31] The LCST behavior can be lowered by copolymerization with other, less polar epoxides, and the cloud point can be adjusted to a physiologically interesting range.[32,33]

PEG is of great importance in many biomedical and pharmaceutical applications due to its low toxicity,[34] antigenicity[35] and immunogenicity.[36] It is chemically inert[37] and therefore considered as the "gold standard" in this field.[18] The pharmacokinetic properties of biomolecules such as drugs, proteins and peptides can be optimized by the covalent attachment of PEG chains, which is known as "PEGylation".[38–41] The "PEGylation" process

increases the aqueous solubility of drugs, and shielding by the PEG chains can be achieved (stealth effect). The recognition of the drug by cells of the immune system is thereby reduced or prevented, resulting in a significant prolongation of the blood circulation time in the body.[42,43] A prerequisite for the medical application of PEG is a narrow molecular weight distribution of the polymers and molecular weights below 40 000 g/mol. Polymers with higher molecular weights can no longer be excreted by renal filtration through the kidney, which can lead to accumulation in organs such as the liver.[43] Numerous "PEGylated" pharmaceuticals and formulations are approved by the American Food and Drug Administration (FDA).[44–48]

In addition to its wide range of applications in medicine and pharmaceuticals, PEG is used in a wide variety of areas, such as the food industry, in cosmetics, as formulations in creams or lotions, in engineering, as lubricant and mold release agent, and for the preparation and restoration of excavation finds or old wooden objects.[1,18,37] In industry, PEG is used in non-ionic surfactants. For this purpose, the PEG chains are end-functionalized as a hydrophilic block with hydrophobic moieties, such as fatty acid esters or alkyl chains.[49] An important class of non-ionic surfactants are ABA triblock-copolymers based on PEG and PPO, which are used among other things as suspension and emulsion stabilizers. The properties of the compounds can be specifically influenced and adjusted by varying the different block lengths. Compounds of this type are known as "poloxamers" and are marketed under the trade name Pluronics®.[15,16]

In addition to the many useful properties, for some applications PEG has a distinct disadvantage: it exhibits only a low number of functional groups. This problem can be overcome by copolymerization of EO with functional epoxides, resulting in multifunctional PEG (*mf*-PEG).[50] The synthesis of *mf*-PEG is typically achieved *via* classical anionic ring-opening polymerization (AROP).[51] An alternative synthesis procedure is the copolymerization *via* monomer-activated anionic ring-opening polymerization (MAROP), especially for comonomers with functional groups that are not stable under AROP conditions.[52–54]

1.2 Anionic Ring-Opening Polymerization (AROP)

PEG and PPO can be prepared by various methods. One of the most common polymerization technique is the ring-opening polymerization of epoxides, for instance the classical anionic ring-opening polymerization (AROP) and the monomer-activated anionic ring-opening polymerization (MAROP). In the next section, AROP will be described in more detail, because it is the main polymerization method empoyed in this work.

The AROP for the synthesis of PEG was first reported in the 19th century by Lourenço and Wurtz.[55–58] The preparation of high molecular weight PEGs by polymerization in the presence of hydroxides was later carried out by Staudinger and Schweitzer.[24,59] AROP is a polymerization technique with a "living character". Characteristics of a living anionic polymerization are the lack of termination and chain transfer reactions, resulting in narrow distributions with low dispersity. Furthermore, AROP is characterized by an outstanding control of the molecular weight *via* the monomer-to-initiator ratio. The concept of living anionic polymerization of EO was introduced by Flory in 1940ies.[60] These properties result in a Poisson distribution of the degree of polymerization (P_n) of an individual polymer chain.[61]

$$Đ = \frac{M_w}{M_n} \approx 1 + \frac{1}{P_n} \qquad (1)$$

Hence, the dispersity ($Đ$) only depends on the weight (M_w) and number (M_n) average molecular weight and is directly connected to the degree of polymerization (P_n). In the following **Scheme 2** the mechanism of the AROP for a functional epoxide monomer in the presence of an alkoxide is shown.

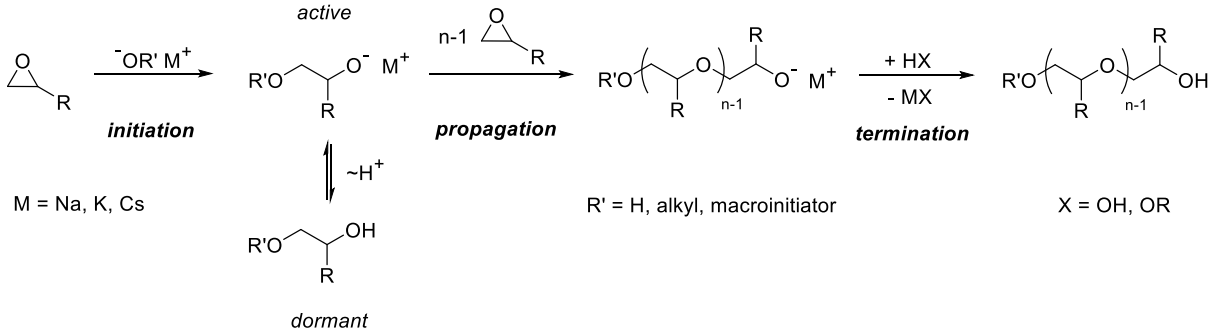

Scheme 2: Reaction mechanism of the AROP of a functional epoxide monomer.

Strongly basic compounds, such as metal hydrides, alkoxides, metal alkyls or aryls, can induce the initiation.[61] The base reacts in a nucleophilic reaction with the carbon atom of the epoxide ring. This results in ringopening and the formation of a new alkoxide species, which can react with another monomer. The reaction thus proceeds as a bimolecular, nucleophilic substitution. This reaction is driven by the ring strain of the epoxide ring, which is 115.4 kJ/mol for ethylene oxide.[62] The chain propagation can be terminated by addition of protic solvents such as methanol. Alternatively, targeted end functionalization can be achieved by adding a suitable electrophile, or the sequential addition of further epoxide monomers can enable the synthesis of block copolymers. **Scheme 3** shows some prominent examples for the termination of the alkoxide end groups with suitable electrophiles to provide access to functional PEGs. Examples of functional groups that have been attached to PEG by conversion of the reactive end group are mesylates,[63] vinyl benzyl ethers,[64] hemisuccinates,[65] methacrylates,[66,67] and propargyl ethers.[68]

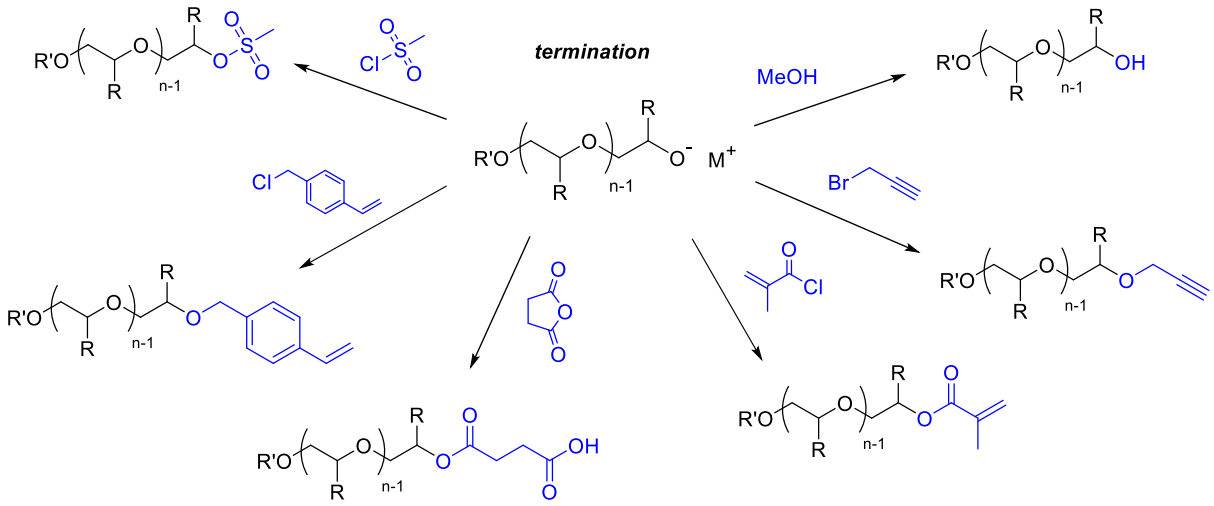

Scheme 3: Termination of the alkoxide end groups with suitable electrophiles provides access to functional PEGs.

The compilation shown above shows only a few examples of the preparation of functional PEGs by termination. A wide range of chemical modifications can be derived from the terminal groups. Mesylates can be conveniently converted to halides, azides and thiols *via* nucleophilic substitution reactions.[63,68] Alkynes and succinates are often used to conjugate other functional molecules, such as polymeric substrates,[69,70] peptides, and proteins.[71,72] Methacrylates and vinyl benzyl ethers, on the other hand, can be polymerized into PEG-

based hydrogels or nanogels by radical or UV-initiated polymerization. The broad spectrum of end-functionalized PEGs has been reviewed by Riffle and co-workers.[73]

The reaction conditions like the choice of solvent and counterion are crucial for the propagation rate of the AROP, due to their significant impact on the reactivity of the active chain end. The solvation of the counterion, such as alkali metal ions, rises with increasing polarity of the solvent.[52] As a result, the reactive chain end becomes less coordinated, leading to an increase in the propagation rate.[74] A further increase in the reactivity of the chain end can be achieved by the addition of suitable crown ethers or cryptands, which show complex formation with the counterions. A common example is the addition of 18-crown-6 to complex the potassium counterion.[52,75,76] In the following **Scheme 4**, the influence of the solvent on the active chain end is shown schematically.

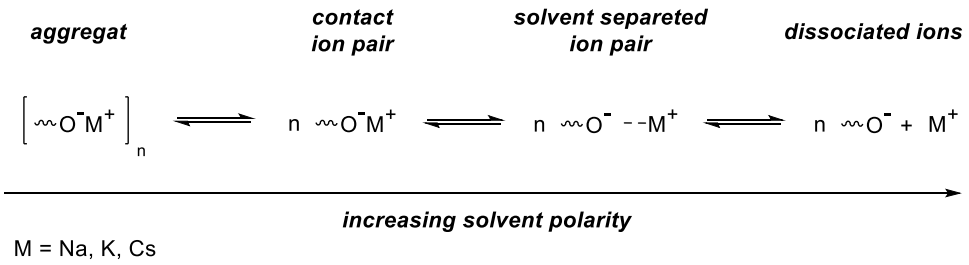

Scheme 4: Possible structures of metal alkoxide chain ends in solution.

The influence of the metal alkoxide on the reactivity of the chain end can be explained by the HSAB (hard and soft acids and bases) concept according to Pearson.[77] The reactive species in the polymerization of EO is an oxygen anion, which represents a hard base according to the HSAB concept. The charge-to-radius ratio of the alkali metal ion plays a crucial role. The larger the ratio, the more unreactive is the active chain end. For this reason, hard alkali metal counterions, such as lithium, form unreactive chain ends (lithium alkoxides) due to the rather covalent bond characteristics.[18] Therefore, they are unsuitable as initiators for AROP. The propagation rate of alkali metal alkoxide initiated polymerizations of epoxides corresponds according to this principle with the size of the counter ion as follows: $Na^+ < K^+ < Cs^+$.[78]

The combination of alkali metal alkoxide and the appropriate alcohol is often chosen as initiator system for the AROP. Partial deprotonation of the alcohol increases the solubility

of the initiator, and aggregation can thus be prevented. During the reaction, in addition to the active chain end (alkoxide), a dormant alcohol species is present, which undergoes a chain transfer reaction by a rapid exchange of protons. For this reason, AROP cannot be considered a living polymerization by definition in this case.[79] The reversible proton exchange, however, takes place considerably faster than the monomer addition. Therefore, similar to the living anionic polymerization, excellent control of the molecular weight and molecular weight distribution ($Đ$) can be achieved.[80] In this context, the terms "degenerative proton transfer" as well as active and dormant species are used.[52] Because of these characteristics, AROP is often referred to as "living-like". Furthermore, it bears mechanistic similarity to controlled radical polymerization techniques, which are also based on dormant species and degenerative transfer.[79]

However, AROP also has some limitations. Many functional polymers cannot be prepared under the harsh and strongly basic conditions of the AROP. Functional groups such as carbonyl groups, cyanides and halides cannot be introduced due the protic character of the side chains and possible interactions with the base or active chain end.[52,81,82] Even epoxide monomers, such as PO or glycidyl ethers, with a slightly acidic proton, lead to side reactions like chain termination and transfer reactions due to proton abstraction.[83–85] Hence, for these monomers high molecular weight polyethers are not accessible *via* AROP. These disadvantages can be overcome by polymerization *via* monomer-activated anionic ring-opening polymerization (MAROP). In this polymerization technique, the ring-opening polymerization is supported by an initiator/catalyst system, which consists of a weak base and a Lewis acid.[86]

1.3 Cleavable Polyethers

Many polymers were originally designed with the aim of achieving good mechanical and thermal properties and the highest possible resistance to environmental influences.[87] These properties also apply to polyethers, which are stable under harsh conditions and are chemically inert.[37] However, in long-term *in vivo* experiments, degradation under the influence of oxidative stress by reactive oxygen species (ROS) was observed.[88] Aromatic polyethers exhibit a higher stability against oxidation compared to aliphatic polyethers.[89]

This can be explained by the low water solubility of aromatic polyether systems. Furthermore, the degradation by electrochemical degradation,[90] UV light,[91] ultrasonication[92] and temperature[91] is described in literature. The degradation rate is strongly dependent on whether the experiment was performed in bulk or in aqueous solutions. A major influencing factor is the pH value in aqueous solutions.[93]

Cleavable polyethers play a significant role for specific biomedical applications, such as reversible PEGylation.[18,94] As described above, PEG is considered as the "gold standard" for use in pharmaceutical and medical applications, for instance in the form of polymer-drug conjugates to prolong blood circulation time.[18,38–41] Nevertheless, PEG is not biodegradable and can only be used in the body up to a molecular weight of 40 000 g/mol. The molecular weight is limited by the renal excretion of the kidney. At larger molecular weights, accumulation of PEG takes place in human tissues, predominantly in the liver, eventually leading to inflammation and liver damage or cancer.[95] However, the increase in blood circulation time is directly related to the increase in molecular weight. In order to utilize the favorable properties of PEG as effective as possible without obtaining undesirable side reactions, the design of cleavable PEG derivatives is of great interest.[96] A variety of different stimuli can be used to trigger cleavage of the PEG backbone or detachment of PEG from the drug conjugate. Examples of these stimuli are the pH value, redox reactions, enzymatic reactions or light. Dingels *et al.* published a comprehensive review article on the strategies for incorporating cleavable components into PEG chains and PEG conjugates, which was used as a guide for the following **Scheme 5**.[97]

Cleavable polyether-based lipids have gained increasing attraction. They are ideally suited for the development of surface-modified liposomes (stealth liposomes) for targeted drug delivery.[98] The stimuli-cleavable linker in the lipid structure enables shedding of the liposomes in cellular compartments, such as the lysosome, or tissues. This process increases the efficiency of liposomal formulations.

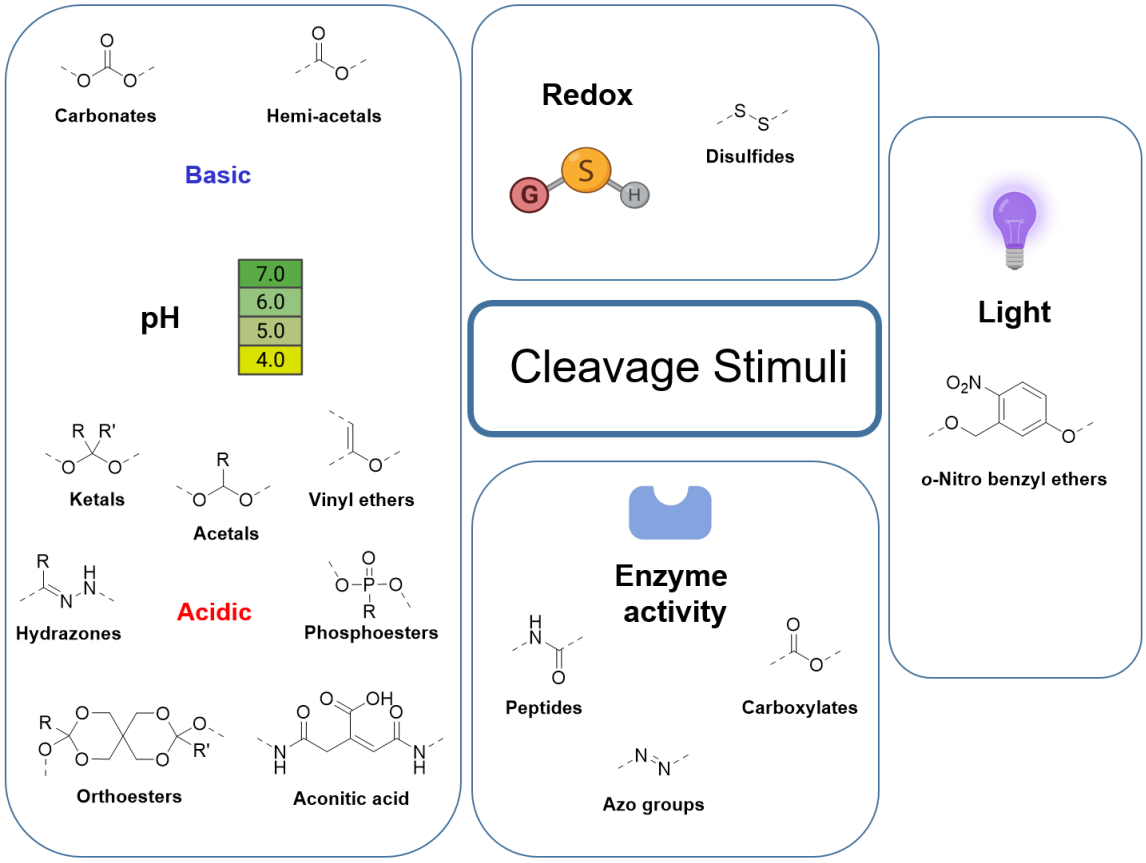

Scheme 5: Cleavable components with the respective stimuli for the application in cleavable polyethers.

Numerous reports on acid-labile PEG-lipids based on cholesterol with cleavable compounds, such as aconitic acid, hydrazones, ketals, acetals or vinyl ethers have already been established.[99–102] Chapter 2.1 and 2.2 discuss the syntheses of a novel class of pH-responsive polyether-lipids based on vinyl ethers as cleavage site. For this reason, the next section will describe vinyl ethers in PEG in general.

1.3.1 pH-Responsive Vinyl Ethers in PEG

In the 1960s, vinyl ethers and their precursors, the allyl ethers, were used specifically in carbohydrate chemistry as protecting groups for hydroxyl groups.[103] The simple formation and cleavage under mild conditions are tolerated by many other protective groups. These properties made allyl ether a common choice for orthogonal synthesis strategies.[104] The transformation of allyl ether into vinyl ether and the cleavage under acidic conditions is shown in **Scheme 6**.

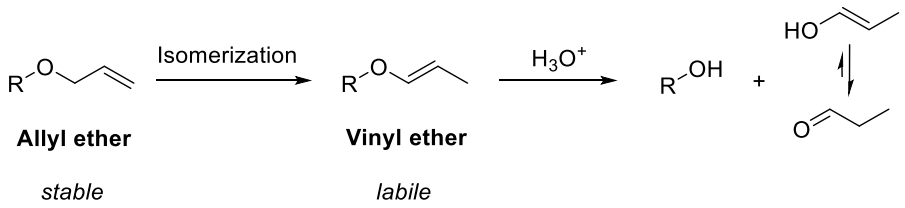

Scheme 6: Transformation of the allyl ether group to a vinyl ether and ensuing cleavage.

The stable allyl ether group can be converted to the labile vinyl ether by isomerization. The cleavage can be performed in different ways, in which the most common methods are acidic hydrolysis or oxidation.[103] A central step in this process is the isomerization, which can be carried out by a broad variety of different methods. The isomerization is often base-catalyzed with potassium *tert*-butoxide (KO^{t}Bu) in DMSO under heat or using Wilkinson's catalyst ($RhCl(PPh_3)_3$). In addition to the two systems described, other catalytic systems have been investigated and applied as well.[105–108] In addition to the protection of hydroxyl groups, thiols and amines can also be protected by the use of allyl ethers. This is applied, among other fields, in polymer research with the protected amine monomer *N*,*N*-diallylglycidylamine (DAGA), which enables access to amine-functionalized PEGs.[108–110]

Thompson *et al.* described the use of vinyl ethers as acid-cleavable linkers for lipids in various reports already in 1998.[111–113] Also cleavable PEG-lipids were synthesized and used, for example, for the preparation of liposomes as drug delivery systems. **Scheme 7** shows the acid-catalyzed vinyl ether hydrolysis reaction of a polyether lipid as an example, synthesized by Thompson and co-workers.[114]

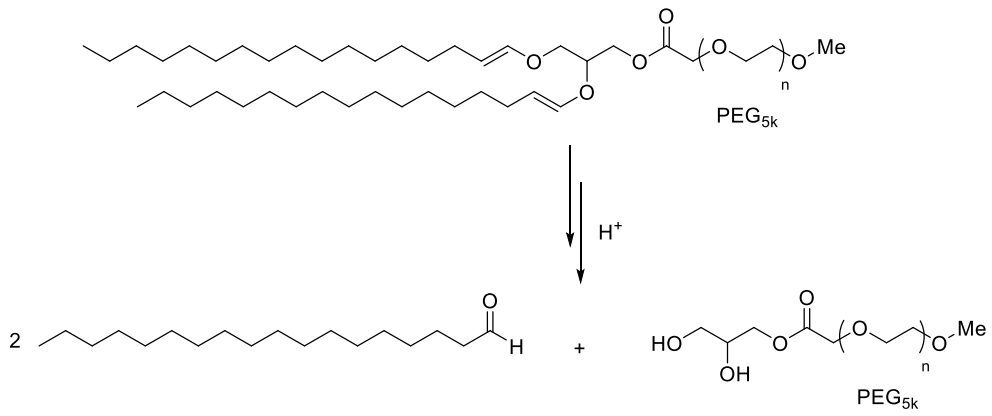

Scheme 7: Acid-catalyzed vinyl ether hydrolysis reactions of a polyether lipid.

Worm *et al.* developed a synthetic strategy for the preparation of cleavable PEGs by incorporating several pH-sensitive vinyl ether moieties into the polyether backbone.[115] Copolymerization of EO and the epoxide monomer 3,4-epoxy-1-butene (EPB) *via* AROP provides access to a PEG backbone with allyl units that can be isomerized to pH-cleavable propenyl units (*iso*EPB). The synthesis procedure is shown in **Scheme 8**.

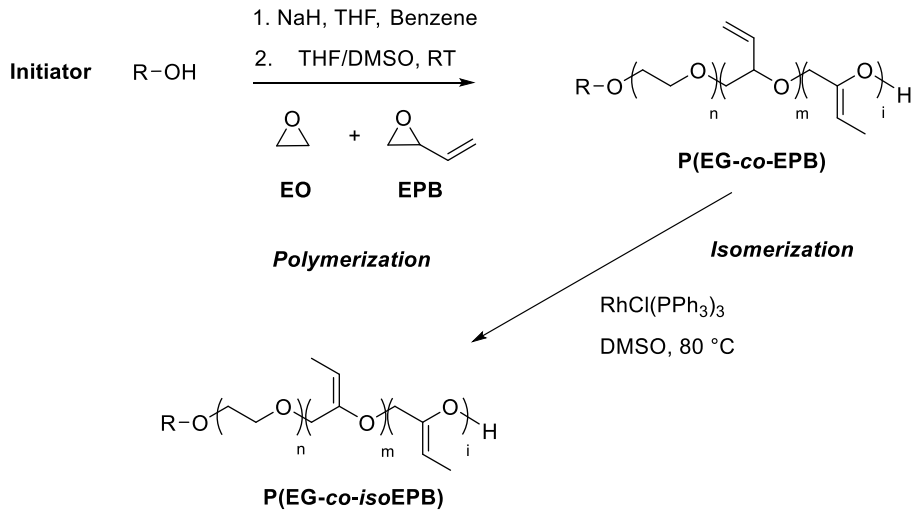

Scheme 8: Synthesis procedure for P(EG-*co*-*iso*MBE) copolymers.

Well-defined, degradable PEGs could be prepared with this technique with molecular weights up to M_n = 10 000 g/mol. In addition, the degradation kinetics were determined *via* online ^{1}H NMR spectroscopy. For the measurements, at pD 5 half-life values in the range of $t_{1/2}$ = 20-34 h were obtained, and at pD 4.4 from $t_{1/2}$ = 9-20 h. These values are in the range of the degradation kinetics of ketals and acetals and correspond to the slightly acidic pH in inflammatory or tumor tissue.[116–118] Compared to pH-sensitive ketal structures, vinyl ethers are excellent stable for the storage at neutral pH. In a report of Shin *et al.*, the pH sensitivity is further fine-tuned by different substitution patterns at the vinyl ether.[119]

References

(1) Dingels, C.; Schömer, M.; Frey, H. Die Vielen Gesichter Des Poly(Ethylenglykol)s: Von Der Kosmetik Zum Ionenleiter. *Chemie Unserer Zeit* **2011**, *45* (5), 338–349. https://doi.org/10.1002/ciuz.201100551.

(2) Price, C. C. Polyethers. *Acc. Chem. Res.* **1974**, 294–301.

(3) Klein, R.; Wurm, F. R. Aliphatic Polyethers: Classical Polymers for the 21st Century. *Macromol. Rapid Commun.* **2015**, *36* (12), 1147–1165.

https://doi.org/10.1002/marc.201500013.

(4) Auerbach, F.; Barschall, H. Über Die Festen Polymeren Des Formaldehyds. *Fresenius, Zeitrschrift für Anal. Chemie* **1908**, *47*, 515–518. https://doi.org/10.1007/BF01362685.

(5) Staudinger, H.; Lüthy, M. Hochpolymere Verbindungen. 3. Mitteilung. Über Die Konstitution Der Poly-oxymethylene. *Helv. Chim. Acta* **1925**, *8* (1), 41–64. https://doi.org/10.1002/hlca.19250080111.

(6) Staudinger, H. Hochpolymere Verbindungen. 5. Mitteilung. Über Die Konstitution Der Poly-Oxymethylene Und Anderen Hochpolymeren Verbindungen. *Helv. Chim. Acta* **1925**, *8*, 67–70. https://doi.org/10.1002/hlca.19250080113.

(7) Mie, G.; Hengstenberg, J.; Staudinger, H.; Johner, H.; Lüthy, M.; Signer, R. Der Polymere Formaldehyd, Ein Modell Der Cellulose. *Zeitschrift für Phys. Chemie* **1927**, 425–448. https://doi.org/10.1515/zpch-1927-12628.

(8) Koltzenburg, S.; Maskos, M.; Nuyken, O.; Mülhaupt, R. *Polymere: Synthese, Eigenschaften Und Anwendungen*; Springer Spektrum: Berlin, 2014.

(9) Carraher, C. E. *Introduction to Polymer Chemistry*, 4th ed.; Taylor & Francis: Boca Raton: London, New York, 2017.

(10) Levene, P. A.; Walti, A. On Condensation Products of Propylene Oxide and of Glycidol. *J. Biol. Chem.* **1927**, *75* (1), 325–336. https://doi.org/10.1016/s0021-9258(18)84205-3.

(11) Pierre, L. E.; Price, C. C. The Room Temperature Polymerization of Propylene Oxide. *J. Am. Chem. Soc.* **1956**, *78* (14), 3432–3436. https://doi.org/10.1021/ja01595a047.

(12) Dai, S.; Tam, K. C. Isothermal Titration Calorimetric Studies on the Temperature Dependence of Binding Interactions between Poly(Propylene Glycol)s and Sodium Dodecyl Sulfate. *Langmuir* **2004**, *20* (6), 2177–2183. https://doi.org/10.1021/la0357559.

(13) Chattopadhyay, D. K.; Raju, K. V. S. N. Structural Engineering of Polyurethane Coatings for High Performance Applications. *Prog. Polym. Sci.* **2007**, *32* (3), 352–418. https://doi.org/10.1016/j.progpolymsci.2006.05.003.

(14) Paredes, X.; Pensado, A. S.; Comuñas, M. J. P.; Fernández, J. How Pressure Affects the Dynamic Viscosities of Two Poly(Propylene Glycol) Dimethyl Ether Lubricants. *J. Chem. Eng. Data* **2010**, *55* (9), 4088–4094. https://doi.org/10.1021/je100285a.

(15) Almeida, M.; Magalhães, M.; Veiga, F.; Figueiras, A. Poloxamers, Poloxamines and Polymeric Micelles: Definition, Structure and Therapeutic Applications in Cancer. *J. Polym. Res.* **2018**, *25* (1). https://doi.org/10.1007/s10965-017-1426-x.

(16) Pitto-Barry, A.; Barry, N. P. E. Pluronic® Block-Copolymers in Medicine: From Chemical and Biological Versatility to Rationalisation and Clinical Advances. *Polym. Chem.* **2014**, *5* (10), 3291–3297. https://doi.org/10.1039/c4py00039k.

(17) Gagnon, S. D. Propylene Oxide and Higher 1,2-Epoxide Polymers. *Encycl. Polym. Sci. Technol.* **2008**. https://doi.org/10.1002/0471440264.pst530.

(18) Herzberger, J.; Niederer, K.; Pohlit, H.; Seiwert, J.; Worm, M.; Wurm, F. R.; Frey, H. Polymerization of Ethylene Oxide, Propylene Oxide, and Other Alkylene Oxides: Synthesis, Novel Polymer Architectures, and Bioconjugation. *Chem. Rev.* **2015**, acs.chemrev.5b00441. https://doi.org/10.1021/acs.chemrev.5b00441.

(19) Billouard, C.; Carlotti, S.; Desbois, P.; Deffieux, A. "Controlled" High-Speed Anionic Polymerization of Propylene Oxide Initiated by Alkali Metal Alkoxide/Trialkylaluminum Systems. *Macromolecules* **2004**, *37* (11), 4038–4043. https://doi.org/10.1021/ma035768t.

(20) Walther, P.; Krauß, A.; Naumann, S. Lewis Pair Polymerization of Epoxides via Zwitterionic Species as a Route to High-Molar-Mass Polyethers. *Angew. Chemie - Int. Ed.* **2019**, *58* (31), 10737–10741. https://doi.org/10.1002/anie.201904806.

(21) Meerwein, H.; Delfs, D.; Morschel, H. Die Polymerisation Des Tetrahydrofurans. *Angew. Chemie* **1960**, *72*, 926–934. https://doi.org/10.1002/ange.19600722402.

(22) Engels, H. W.; Pirkl, H. G.; Albers, R.; Albach, R. W.; Krause, J.; Hoffmann, A.; Casselmann, H.; Dormish, J. Polyurethanes: Versatile Materials and Sustainable Problem Solvers for Today's Challenges. *Angew. Chemie - Int. Ed.* **2013**, *52* (36), 9422–9441. https://doi.org/10.1002/anie.201302766.

(23) Saunders, K. J. *Organic Polymer Chemistry: An Introduction to the Organic Chemistry of Adhesives, Fibres, Paints, Plastics and Rubbers*, 2nd ed.; Springer Netherlands: Dordrecht, 1988.

(24) Staudinger, H.; Schweitzer, O. Über Hochpolymere Verbindungen, 20. Mitteil.: Über Die Poly-Äthylenoxyde. *Ber. dtsch. Chem. Ges. A/B* **1929**, *62*, 2395–2405. https://doi.org/10.1002/cber.19290620879.

(25) Sedlák, M. Recent Advances in Chemistry and Applications of Substituted Poly(Ethylene Glycol)S. *Collect. Czech. Chem. Commun.* **2005**, *70*, 269–291. https://doi.org/10.1135/cccc20050269.

(26) Thomas, A.; Müller, S. S.; Frey, H. Beyond Poly(Ethylene Glycol): Linear Polyglycerol as a Multifunctional Polyether for Biomedical and Pharmaceutical Applications. *Biomacromolecules* **2014**, *15* (6), 1935–1954. https://doi.org/10.1021/bm5002608.

(27) Shikata, T.; Okuzono, M.; Sugimoto, N. Temperature-Dependent Hydration/Dehydration Behavior of Poly(Ethylene Oxide)s in Aqueous Solution. *Macromolecules* **2013**, *46* (5), 1956–1961. https://doi.org/10.1021/ma3026282.

(28) Kjellander, R.; Florin, E. Water Structure and Changes in Thermal Stability of the System Poly(Ethylene Oxide)-Water. *J. Chem. Soc. Faraday Trans. 1 Phys. Chem. Condens. Phases* **1981**, *77* (9), 2053–2077. https://doi.org/10.1039/F19817702053.

(29) Ward, M. A.; Georgiou, T. K. Thermoresponsive Polymers for Biomedical Applications. *Polymers (Basel).* **2011**, *3* (3), 1215–1242. https://doi.org/10.3390/polym3031215.

(30) Somcynsky, T. The Lower Critical Solution Temperature (LCST) of Non-polar Polymer Solutions: An Introduction. *Polym. Eng. Sci.* **1982**, *22* (2), 58–63. https://doi.org/10.1002/pen.760220203.

(31) Wang, X.; Qiu, X.; Wu, C. Comparison of the Coil-to-Globule and the Globule-to-Coil Transitions of a Single Poly(N-Isopropylacrylamide) Homopolymer Chain in Water. *Macromolecules* **1998**, *31* (9), 2972–2976. https://doi.org/10.1021/ma971873p.

(32) Mangold, C.; Obermeier, B.; Wurm, F.; Frey, H. From an Epoxide Monomer Toolkit to Functional PEG Copolymers with Adjustable LCST Behavior. *Macromol. Rapid Commun.* **2011**, *32* (23), 1930–1934. https://doi.org/10.1002/marc.201100489.

(33) Reuss, V. S.; Werre, M.; Frey, H. Thermoresponsive Copolymers of Ethylene Oxide and N,N-Diethyl Glycidyl Amine: Polyether Polyelectrolytes and PEGylated Gold Nanoparticle Formation. *Macromol. Rapid Commun.* **2012**, *33* (18), 1556–1561. https://doi.org/10.1002/marc.201200307.

(34) Fruijtier-Pölloth, C. Safety Assessment on Polyethylene Glycols (PEGs) and Their Derivatives as Used in Cosmetic Products. *Toxicology* **2005**, *214* (1–2), 1–38. https://doi.org/10.1016/j.tox.2005.06.001.

(35) Veronese, F. M.; Pasut, G. PEGylation, Successful Approach to Drug Delivery. *Drug Discov. Today* **2005**, *10* (21), 1451–1458.

(36) Garay, P. Immunogenicity of Polyethylene Glycol (PEG). *TOPROCJ* **2011**, *2*, 104–107. https://doi.org/10.2174/2210289201102010104.

(37) Bailey, F. E. *Poly(Ethylene Oxide)*; Academic Press: New York, 1976.

(38) Milla, P.; Dosio, F.; Cattel, L. PEGylation of Proteins and Liposomes: A Powerful and Flexible Strategy to Improve the Drug Delivery. *Curr. Drug Metab.* **2011**, *13* (1), 105–119. https://doi.org/10.2174/138920012798356934.

(39) Hamley, I. W. PEG – Peptide Conjugates. *Biomacromolecules* **2014**, *15* (5), 1543–

1559.

(40) Khandare, J.; Minko, T. Polymer-Drug Conjugates: Progress in Polymeric Prodrugs. *Prog. Polym. Sci.* **2006**, *31* (4), 359–397. https://doi.org/10.1016/j.progpolymsci.2005.09.004.

(41) Milton Harris, J.; Chess, R. B. Effect of Pegylation on Pharmaceuticals. *Nat. Rev. Drug Discov.* **2003**, *2* (3), 214–221. https://doi.org/10.1038/nrd1033.

(42) Zalipsky, S. Chemistry of Polyethylene Glycol Conjugates with Biologically Active Molecules. *Adv. Drug Deliv. Rev.* **1995**, *16* (2–3), 157–182. https://doi.org/10.1016/0169-409X(95)00023-Z.

(43) Veronese, F. M. Peptide and Protein PEGylation: A Review of Problems and Solutions. *Biomaterials* **2001**, *22* (5), 405–417. https://doi.org/10.1016/S0142-9612(00)00193-9.

(44) Alconcel, S. N. S.; Baas, A. S.; Maynard, H. D. FDA-Approved Poly(Ethylene Glycol)–Protein Conjugate Drugs. *Polym. Chem.* **2011**, *2* (7), 1442. https://doi.org/10.1039/c1py00034a.

(45) Bailon, P.; Won, C. Y. PEG-Modified Biopharmaceuticals. *Expert Opin. Drug Deliv.* **2009**, *6* (1), 1–16. https://doi.org/10.1517/17425240802650568.

(46) Barenholz, Y. Doxil® - The First FDA-Approved Nano-Drug: Lessons Learned. *J. Control. Release* **2012**, *160* (2), 117–134. https://doi.org/10.1016/j.jconrel.2012.03.020.

(47) Bobo, D.; Robinson, K. J.; Islam, J.; Thurecht, K. J.; Corrie, S. R. Nanoparticle-Based Medicines: A Review of FDA-Approved Materials and Clinical Trials to Date. *Pharm. Res.* **2016**, *33* (10), 2373–2387. https://doi.org/10.1007/s11095-016-1958-5.

(48) Veronese, F. M. *PEGylated Protein Drugs: Basic Science and Clinical Applications*; Birkenhäuser Basel: Basel, 2009.

(49) Schmolka, I. R.; Corp, B. W. A Review of Block Polymer Surfactants. *J. Am. Oil Chem. Soc.* **1976**, *54*, 110–116.

(50) Obermeier, B.; Wurm, F.; Mangold, C.; Frey, H. Multifunctional Poly(Ethylene Glycol)S. *Angew. Chemie - Int. Ed.* **2011**, *50* (35), 7988–7997. https://doi.org/10.1002/anie.201100027.

(51) Mangold, C.; Wurm, F.; Frey, H. Functional PEG-Based Polymers with Reactive Groups via Anionic ROP of Tailor-Made Epoxides. *Polym. Chem.* **2012**, *3* (7), 1714–1721. https://doi.org/10.1039/c2py00489e.

(52) Brocas, A. L.; Mantzaridis, C.; Tunc, D.; Carlotti, S. Polyether Synthesis: From

Activated or Metal-Free Anionic Ring-Opening Polymerization of Epoxides to Functionalization. *Prog. Polym. Sci.* **2013**, *38* (6), 845–873. https://doi.org/10.1016/j.progpolymsci.2012.09.007.

(53) Gervais, M.; Brocas, A. L.; Cendejas, G.; Deffieux, A.; Carlotti, S. Synthesis of Linear High Molar Mass Glycidol-Based Polymers by Monomer-Activated Anionic Polymerization. *Macromolecules* **2010**, *43* (4), 1778–1784. https://doi.org/10.1021/ma902286a.

(54) Kubisa, P.; Bednarek, M.; Biedron, T.; Biela, T.; Penczek, S. Progress in Activated Monomer Polymerization. Kinetics of AM Polymerization. *Macromol. Symp.* **2000**, *153*, 217–226.

(55) Lourenço, A. V. Intermediäre Aether Des Glykols. *J. Prakt. Chem.* **1860**, *79*, 212–213.

(56) Lourenço, A. V. Ueber Die Polyäthylenalkohole. *J. Prakt. Chem.* **1862**, *85*, 389–392.

(57) Wurtz, A. Neue Untersuchungen Über Das Aethylenoxy. *Ann. Chem. Pharm.* **1860**, *116*, 249–252.

(58) Wurtz, A. Synthese Des Glycols Aus Aethylenoxyd Und Wasser. *Ann. Chem. Pharm.* **1860**, *113*, 255–256.

(59) Staudinger, H.; Lohmann, H. Über Hochpolymere Verbindungen, 81. Mitteilung Über Eukolloides Polyäthylenoxyd. *Ann. Chem. Pharm.* **1933**, *505*, 41–51.

(60) Flory, P. J. Molecular Size Distribution in Ethylene Oxide Polymers. *J. Am. Chem. Soc.* **1940**, *62*, 1561–1565.

(61) Penczek, S.; Cypryk, M.; Duda, A.; Kubisa, P.; Słomkowski, S. Living Ring-Opening Polymerizations of Heterocyclic Monomers. *Prog. Polym. Sci.* **2007**, *32* (2), 247–282. https://doi.org/10.1016/j.progpolymsci.2007.01.002.

(62) Aresta, M. *Reaction Mechanisms in Carbon Dioxide Conversion*; Springer, 2015.

(63) Akiyama, Y.; Otsuka, H.; Nagasaki, Y.; Kato, M.; Kataoka, K. Selective Synthesis of Heterobifunctional Poly (Ethylene Glycol). **2000**, 947–950.

(64) Hayashi, H.; Iijima, M.; Kataoka, K.; Nagasaki, Y. PH-Sensitive Nanogel Possessing Reactive PEG Tethered Chains on the Surface. *Macromolecules* **2004**, *37* (14), 5389–5396. https://doi.org/10.1021/ma049199g.

(65) Ishii, T.; Yamada, M.; Hirase, T.; Nagasaki, Y. New Synthesis of Heterobifunctional Poly(Ethylene Glycol) Possessing a Pyridyl Disulfide at One End and a Carboxylic Acid at the Other End. *Polym. J.* **2005**, *37* (3), 221–228. https://doi.org/10.1295/polymj.37.221.

(66) Yagci, Y.; Ito, K. Macromolecular Architecture Based on Anionically Prepared Poly(Ethylene Oxide) Macromonomers. *Macromol. Symp.* **2005**, *226*, 87–96. https://doi.org/10.1002/masy.200550809.

(67) Ishizu, K.; Furukawa, T. Synthesis of Functionalized Poly (Ethylene Oxide) Macromonomers. **2001**, *42*, 7233–7236.

(68) Hiki, S.; Kataoka, K. Versatile and Selective Synthesis of "Click Chemistry" Compatible Heterobifunctional Poly(Ethylene Glycol)s Possessing Azide and Alkyne Functionalities. *Bioconjug. Chem.* **2010**, *21* (2), 248–254. https://doi.org/10.1021/bc900253p.

(69) Jing, R.; Wang, G.; Zhang, Y.; Huang, J. One-Pot Synthesis of PS-b-PEO-b-PtBA Triblock Copolymers via Combination of SET-LRP and "Click" Chemistry Using Copper(0)/PMDETA as Catalyst System. *Macromolecules* **2011**, *44* (4), 805–810. https://doi.org/10.1021/ma102621k.

(70) Opsteen, J. A.; Van Hest, J. C. M. Modular Synthesis of Block Copolymers via Cycloaddition of Terminal Azide and Alkyne Functionalized Polymers. *Chem. Commun.* **2005**, No. 1, 57–59. https://doi.org/10.1039/b412930j.

(71) Deiters, A.; Cropp, T. A.; Summerer, D.; Mukherji, M.; Schultz, P. G. Site-Specific PEGylation of Proteins Containing Unnatural Amino Acids. *Bioorganic Med. Chem. Lett.* **2004**, *14* (23), 5743–5745. https://doi.org/10.1016/j.bmcl.2004.09.059.

(72) Atassi, M. Z.; Manshouri, T. Synthesis of Tolerogenic Monomethoxypolyethylene Glycol and Polyvinyl Alcohol Conjugates of Peptides. *J. Protein Chem.* **1991**, *10* (6), 623–627. https://doi.org/10.1007/BF01025714.

(73) Thompson, M. S.; Vadala, T. P.; Vadala, M. L.; Lin, Y.; Riffle, J. S. Synthesis and Applications of Heterobifunctional Poly(Ethylene Oxide) Oligomers. *Polymer (Guildf).* **2008**, *49* (2), 345–373. https://doi.org/10.1016/j.polymer.2007.10.029.

(74) Brocas, A.; Mantzaridis, C.; Tunc, D.; Carlotti, S. Progress in Polymer Science Polyether Synthesis : From Activated or Metal-Free Anionic Ring-Opening Polymerization of Epoxides to Functionalization. *Prog. Polym. Sci.* **2013**, *38* (6), 845–873. https://doi.org/10.1016/j.progpolymsci.2012.09.007.

(75) Deffieux, A.; Graf, E.; Boileau, S. Anionic Polymerization of Ethylene Oxide with Cryptates as Counterions. *Polymer (Guildf).* **1981**, *22*, 549–552.

(76) Ding, J.; Price, C.; Booth, C. Use of Crown Ether in the Anionic Polymerization of Propylene Oxide. *Eur. Polym. J.* **1991**, *27*, 891–894.

(77) Pearson, R. G. Hard and Soft Acids and Bases. *J. Am. Chem. Soc.* **1963**, *85*, 3533–

3539.

(78) Esswein, B.; Moiler, M. Polymerization of Ethylene Oxide with Alkyllithium Compounds and the Phosphazene Base "TBu-P4." *Angew. Chem. Int. Ed. Engl.* **1996**, *35*, 623–625. https://doi.org/10.1002/anie.199606231.

(79) Szwarc, M. "Living" Polymers. *Nature* **1956**, *178* (4), 1168–1169. https://doi.org/10.1016/0927-0256(95)00032-2.

(80) Wojtech, V. B. Zur Darstellung Hochmolekularer Polyäthylenoxyde. *Die Makromol. Chemie* **1963**, *66* (1), 180–195. https://doi.org/10.1002/macp.1963.020660118.

(81) Herzberger, J.; Leibig, D.; Langhanki, J.; Moers, C.; Opatz, T.; Frey, H. "Clickable PEG" via Anionic Copolymerization of Ethylene Oxide and Glycidyl Propargyl Ether. *Polym. Chem.* **2017**, *8*, 1882–1887. https://doi.org/10.1039/C7PY00173H.

(82) Rejsek, V.; Sauvanier, D.; Billouard, C.; Desbois, P.; Deffieux, A. Controlled Anionic Homo- and Copolymerization of Ethylene Oxide and Propylene Oxide by Monomer Activation. **2007**, 6510–6514.

(83) Simons, D. M.; Verbanc, J. J. The Polymerization of Propylene Oxide. *J. Polym. Sci.* **1960**, *44*, 303–311. https://doi.org/doi.org/10.1002/pol.1960.1204414403.

(84) Steiner, E. C.; Pelletier, R. R.; Trucks, R. O. A Study of the Polymerization of Propylene Oxide Catalyzed by Anhydrous Potassium Hydroxide. *J. Am. Chem. Soc.* **1964**, *86* (21), 4678–4686. https://doi.org/10.1021/ja01075a031.

(85) Blanchard, L. P.; Hornof, V.; Moinard, J. Anionic Polymerization of Propylene Oxide. **1972**, *10* (2), 3089–3102.

(86) Carlotti, S.; Desbois, P.; Billouard, C.; Deffieux, A. Reactivity Control in Anionic Polymerization of Ethylenic and Heterocyclic Monomers through Formation of 'Ate' Complexes. *Polym. Int.* **2006**, *55*, 1126–1131. https://doi.org/10.1002/pi.

(87) Welzel, K.; Müller, R.-J.; Deckwer, W.-D. Enzymatischer Abbau von Polyester-Nanopartikeln. *Chemie Ing. Tech.* **2002**, *74* (10), 1496–1500. https://doi.org/10.1002/1522-2640(20021015)74:10<1496::aid-cite1496>3.0.co;2-p.

(88) Ulbricht, J.; Jordan, R.; Luxenhofer, R. On the Biodegradability of Polyethylene Glycol, Polypeptoids and Poly(2-Oxazoline)S. *Biomaterials* **2014**, *35* (17), 4848–4861. https://doi.org/10.1016/j.biomaterials.2014.02.029.

(89) Jayakannan, M.; Ramakrishnan, S. Recent Developments in Polyether Synthesis. *Macromol. Rapid Commun.* **2001**, *22* (18), 1463–1473. https://doi.org/10.1002/1521-3927(20011201)22:18<1463::AID-MARC1463>3.0.CO;2-F.

(90) Harding, J. R.; Amanchukwu, C. V.; Hammond, P. T.; Shao Horn, Y. Instability of Poly(Ethylene Oxide) upon Oxidation in Lithium Air Batteries. *J. Phys. Chem. C* **2015**, *119* (13), 6947–6955. https://doi.org/10.1021/jp511794g.

(91) De Sainte Claire, P. Degradation of PEO in the Solid State: A Theoretical Kinetic Model. *Macromolecules* **2009**, *42* (10), 3469–3482. https://doi.org/10.1021/ma802469u.

(92) Kawasaki, H.; Takeda, Y.; Arakawa, R. Mass Spectrometric Analysis for High Molecular Weight Synthetic Polymers Using Ultrasonic Degradation and the Mechanism of Degradation. *Anal. Chem.* **2007**, *79* (11), 4182–4187. https://doi.org/10.1021/ac062304v.

(93) Hassouna, F.; Morlat-Thérias, S.; Mailhot, G.; Gardette, J. L. Influence of Water on the Photodegradation of Poly(Ethylene Oxide). *Polym. Degrad. Stab.* **2007**, *92* (11), 2042–2050. https://doi.org/10.1016/j.polymdegradstab.2007.07.016.

(94) Peleg-Shulman, T.; Tsubery, H.; Mironchik, M.; Fridkin, M.; Schreiber, G.; Shechter, Y. Reversible PEGylation: A Novel Technology to Release Native Interferon A2 over a Prolonged Time Period. *J. Med. Chem.* **2004**, *47* (20), 4897–4904. https://doi.org/10.1021/jm0497693.

(95) Pasut, G.; Veronese, F. . . Polymer-Drug Conjugation, Recent Achievements and General Strategies. *Prog. Polym. Sci.* **2007**, *32*, 933–961. https://doi.org/10.1016/j.progpolymsci.2007.05.008.

(96) Yamaoka, T.; Tabata, Y.; Ikada, Y. Distribution and Tissue Uptake of Poly(Ethylene Glycol) with Different Molecular Weights after Intravenous Administration to Mice. *J. Pharm. Sci.* **1994**, *83* (4), 601–606. https://doi.org/10.1002/jps.2600830432.

(97) Dingels, C.; Frey, H. From Biocompatible to Biodegradable: Poly(Ethylene Glycol)s with Predetermined Breaking Points. In *Hierarchical Macromolecular Structures: 60 Years after the Staudinger Nobel Prize II*; Percec, V., Ed.; Springer International Publishing: Cham, 2013; pp 167–190. https://doi.org/10.1007/12_2013_235.

(98) Pattni, B. S.; Chupin, V. V.; Torchilin, V. P. New Developments in Liposomal Drug Delivery. *Chem. Rev.* **2015**, *115* (19), 10938–10966. https://doi.org/10.1021/acs.chemrev.5b00046.

(99) De Graaf, A. J.; Kooijman, M.; Hennink, W. E.; Mastrobattista, E. Nonnatural Amino Acids for Site-Specific Protein Conjugation. *Bioconjug. Chem.* **2009**, *20* (7), 1281–1295. https://doi.org/10.1021/bc800294a.

(100) De Vrieze, J.; Van Herck, S.; Nuhn, L.; De Geest, B. G. Design of PH-Degradable

Polymer-Lipid Amphiphiles Using a Ketal-Functionalized RAFT Chain Transfer Agent. *Macromol. Rapid Commun.* **2020**, *41* (18), 1–6. https://doi.org/10.1002/marc.202000034.

(101) De Vrieze, J.; Louage, B.; Deswarte, K.; Zhong, Z.; De Coen, R.; Van Herck, S.; Nuhn, L.; Kaas Frich, C.; Zelikin, A. N.; Lienenklaus, S.; Sanders, N. N.; Lambrecht, B. N.; David, S. A.; De Geest, B. G. Amphiphile Polymer-Lipidkonjugate Zur Potenten Lymphatischen Anreicherung von TLR7/8-Agonisten Ermöglichen Eine Örtlich Begrenzte Aktivierung Des Angeborenen Immunsystems. *Angew. Chemie* **2019**, *131* (43), 15535–15541. https://doi.org/10.1002/ange.201905687.

(102) Jangra, S.; De Vrieze, J.; Choi, A.; Rathnasinghe, R.; Laghlali, G.; Uvyn, A.; Van Herck, S.; Nuhn, L.; Deswarte, K.; Zhong, Z.; Sanders, N. N.; Lienenklaus, S.; David, S. A.; Strohmeier, S.; Amanat, F.; Krammer, F.; Hammad, H.; Lambrecht, B. N.; Coughlan, L.; García-Sastre, A.; De Geest, B. G.; Schotsaert, M. Sterilizing Immunity against SARS-CoV-2 Infection in Mice by a Single-Shot and Lipid Amphiphile Imidazoquinoline TLR7/8 Agonist-Adjuvanted Recombinant Spike Protein Vaccine**. *Angew. Chemie* **2021**, 9467–9473. https://doi.org/10.1002/ange.202015362.

(103) Wuts, P. G. M.; T.W., G. *Greene's Protective Groups in Organic Synthesis*, 5th ed.; Wiley: Hoboken, New Jersey, 2014.

(104) Guibé, F. Allylic Protecting Groups and Their Use in a Complex Environment Part I : Allylic Protection of Alcohols. *Tetrahedron* **1997**, *53* (40), 1350–13556.

(105) Cunningham, J.; Gigg, R.; Warren, C. D. The Allyl Ether as a Protecting Group in Carbohydrate Chemistry. *Tetrahedron Lett.* **1964**, *19*, 1191–1196. https://doi.org/10.1016/S0040-4039(00)90699-3.

(106) Cadot, C.; Dalko, P. I.; Cossy, J. Olefin Isomerization by a Ruthenium Carbenoid Complex. Cleavage of Allyl and Homoallyl Groups. *Tetrahedron Lett.* **2002**, *43* (10), 1839–1841. https://doi.org/10.1016/S0040-4039(02)00991-7.

(107) Gent, P. A.; Gigg, R. The Allyl Ether as a Protecting Group in Carbohydrate Chemistry. Isomerisations with Tristriphenylphosphinerhodium(I) Chloride. *J. Chem. Soc. Chem. Commun.* **1974**, No. 7, 277–278. https://doi.org/10.1039/C39740000277.

(108) Price, C. C.; Snyder, W. H. Solvent Effects in the Base-Catalyzed Isomerization of Allyl to Propenyl Ethers. *J. Am. Chem. Soc.* **1961**, *83* (7), 1773. https://doi.org/10.1021/ja01468a062.

(109) Reuss, V. S.; Obermeier, B.; Dingels, C.; Frey, H. N,N -Diallylglycidylamine: A Key

Monomer for Amino-Functional Poly(Ethylene Glycol) Architectures. *Macromolecules* **2012**, *45* (11), 4581–4589. https://doi.org/10.1021/ma300292m.

(110) E., L. W.; T., L. The Isomerization by Base of Alkyl Allyl Sulfides to Alkyl Propenyl Sulfides. The Mechanism of the Reaction. *J. Am. Chem. Soc.* **1956**, *78* (10), 2259–2264.

(111) Rui, Y.; Wang, S.; Low, P. S.; Thompson, D. H. Diplasmenylcholine-Folate Liposomes: An Efficient Vehicle for Intracellular Drug Delivery. *J. Am. Chem. Soc.* **1998**, *120* (44), 11213–11218. https://doi.org/10.1021/ja9742949.

(112) Qualls, M. M.; Thompson, D. H. Chloroaluminum Phthalocyanine Tetrasulfonate Delivered via Acid-Labile Diplasmenylcholine-Folate Liposomes: Intracellular Localization and Synergistic Phototoxicity. *Int. J. Cancer* **2001**, *93* (3), 384–392. https://doi.org/10.1002/ijc.1339.

(113) Thompson, D. H.; Shin, J.; Boomer, J.; Kim, J. M. Preparation of Plasmenylcholine Lipids and Plasmenyl-Type Liposome Dispersions. *Methods Enzymol.* **2004**, *387*, 153–168. https://doi.org/10.1016/s0076-6879(04)87010-1.

(114) Gerasimov, O. V.; Boomer, J. A.; Qualls, M. M.; Thompson, D. H. Cytosolic Drug Delivery Using PH- and Light-Sensitive Liposomes. *Adv. Drug Deliv. Rev.* **1999**, *38* (3), 317–338. https://doi.org/10.1016/S0169-409X(99)00035-6.

(115) Worm, M.; Leibig, D.; Dingels, C.; Frey, H. Cleavable Polyethylene Glycol: 3,4-Epoxy-1-Butene as a Comonomer to Establish Degradability at Physiologically Relevant PH. *ACS Macro Lett.* **2016**, *5* (12), 1357–1363. https://doi.org/10.1021/acsmacrolett.6b00735.

(116) Schmaljohann, D. Thermo- and PH-Responsive Polymers in Drug Delivery. *Adv. Drug Deliv. Rev.* **2006**, *58* (15), 1655–1670. https://doi.org/10.1016/j.addr.2006.09.020.

(117) Vaupel, P.; Kallinowski, F.; Okunieff, P. Blood Flow, Oxygen and Nutrient Supply, and Metabolic Microenvironment of Human Tumors: A Review. *Cancer Res.* **1989**, *49*, 6449–6465.

(118) Rofstad, E. K.; Mathiesen, B.; Kindem, K.; Galappathi, K. Acidic Extracellular PH Promotes Experimental Metastasis of Human Melanoma Cells in Athymic Nude Mice. *Cancer Res.* **2006**, *66* (13), 6699–6707. https://doi.org/10.1158/0008-5472.CAN-06-0983.

(119) Shin, J.; Shum, P.; Grey, J.; Fujiwara, S. I.; Malhotra, G. S.; González-Bonet, A.; Hyun, S. H.; Moase, E.; Allen, T. M.; Thompson, D. H. Acid-Labile MPEG-Vinyl Ether-1,2-Dioleylglycerol Lipids with Tunable Ph Sensitivity: Synthesis and Structural Effects

on Hydrolysis Rates, DOPE Liposome Release Performance, and Pharmacokinetics. *Mol. Pharm.* **2012**, *9* (11), 3266–3276. https://doi.org/10.1021/mp300326z.

1.4 Nanocarriers for Drug Delivery

In recent years, nanotechnology has gained increasing interest and is applied in various fields such as medicine, cosmetics, environmental and neutraceutical research areas.[1] There are various forms of nanostructures such as nanocomposites, nanotubes, nanofibers and nanoparticles, which effectively serve for the diagnosis and treatment of various diseases. If these nanostructures are used as carrier molecules, they are called nanocarriers.[2–4] For example, they can be used as transport agents for vaccines, drugs, genes, proteins and enzymes.[5–8] In general, nanocarriers are defined as objects having at least one dimension in the 1–100 nanometer scale, although some sources include dimensions less than 500 nm as nano-sized.[9]

The process of transporting therapeutic agents into the body with appropriate pharmacokinetics is called drug delivery.[10] The administration of drugs into the body is generally mediated through the gastrointestinal tract or other routes. The conventional mode for drug administration is mediated by the enteral or parenteral pathway. For the drug delivery, the enteral route of the drug occurs through oral, rectal or sublingual administration, involving gastrointestinal tract, while the parenteral route of the drug is through intravenous, intramuscular or subcutaneous administration. This involves routes other than the gastrointestinal tract.[11,12] The strongly preferred route is *via* the enteral route of distribution due to its noninvasive nature. A distinct disadvantage, however, is that the bioavailability of the drug decreases. This is due to incomplete drug absorption and the fact that the drug undergoes first-pass metabolism.[13,14]

There are many treatment approaches to deal with deadly diseases such as cancer. Common treatment methods include removal of the tumor via surgery, radiation or chemotherapy. However, the last two methods in particular are associated with severe side effects, because diseased cells cannot be differentiated from healthy cells, resulting in damage to both. For this reason, it is of great importance that the drug is transported to the target tissue in an organized structure to suppress undesirable side effects.[15] Nanocarriers are used selectively to achieve a sustained release of the drug. They change the pharmacokinetics of transport and distribution. For example, a longer circulation time in the blood can be achieved or a

targeted distribution.[16,17] In addition, nanocarriers can prevent the degradation of active drugs. This allows higher and more efficient concentrations in target tissues, while potentially reducing undesirable toxic side effects.[18,19] Furthermore, nanocarriers can be linked to specific ligands that mediate transport to selected tissues.[20] However, cancer cells have special defense mechanisms that make them difficult to control. They can overexpress, have self-repairing capacities or can downregulate the metabolism of the drug.[21,22] Nevertheless, the best possible therapy is achieved by the use of specialized nanocarriers to overcome the defense mechanisms.

In the following sections, the different forms of nanocarriers are described, with a focus on polymeric and lipid-based carriers. In addition, the different transport mechanisms will be highlighted.

1.4.1 Types of Nanocarriers

In general, nanocarriers can be divided into three predominant types: the organic nanocarriers, the inorganic nanocarriers, and the hybrid nanocarriers.

Organic nanocarriers include solid lipid nanocarriers, micelles, polymeric or lipid-based carriers such as liposomes, dendrimers and viral nanocarriers. [23,24] Organic nanocarriers can be highly customized and versatile, and inherently have lower toxicity. Furthermore, a variety of drugs as well as ligands can be conjugated for drug delivery. Studies showed that especially drugs transported by micelles or liposomes have the properties to accumulate in tissues.[25] The reason for this is the enhanced permeability and retention effect (EPR effect).[26]

Inorganic nanocarriers include gold, magnetic nanocarriers, quantum dots, nanotubes and mesoporous silica.[27] One advantage of inorganic nanocarriers is their tractable properties. Their preferred application is in biosensing, cell labeling, targeting, imaging and diagnostics.[28] However, the use of heavy metals as inorganic nanocarriers can lead to health problems in the longer term.[29]

Hybrid nanocarriers, as the name implies, combine two or more organic and inorganic nanomaterials together or individually in one carrier. They can combine organic-inorganic, inorganic-inorganic or multi components in one carrier. Two examples of hybrid

nanocarriers are lipid-polymer hybrids and ceramic polymer hybrids. They use the advantages of both systems.

1.4.1.1 Polymeric and lipid-based Nanocarriers

In this section, the polymeric and lipid-based nanocarriers will be described in further detail. The schematic structures of common representatives is shown in **Figure 1** below. The exact structure will be explained in detail in the following sections.

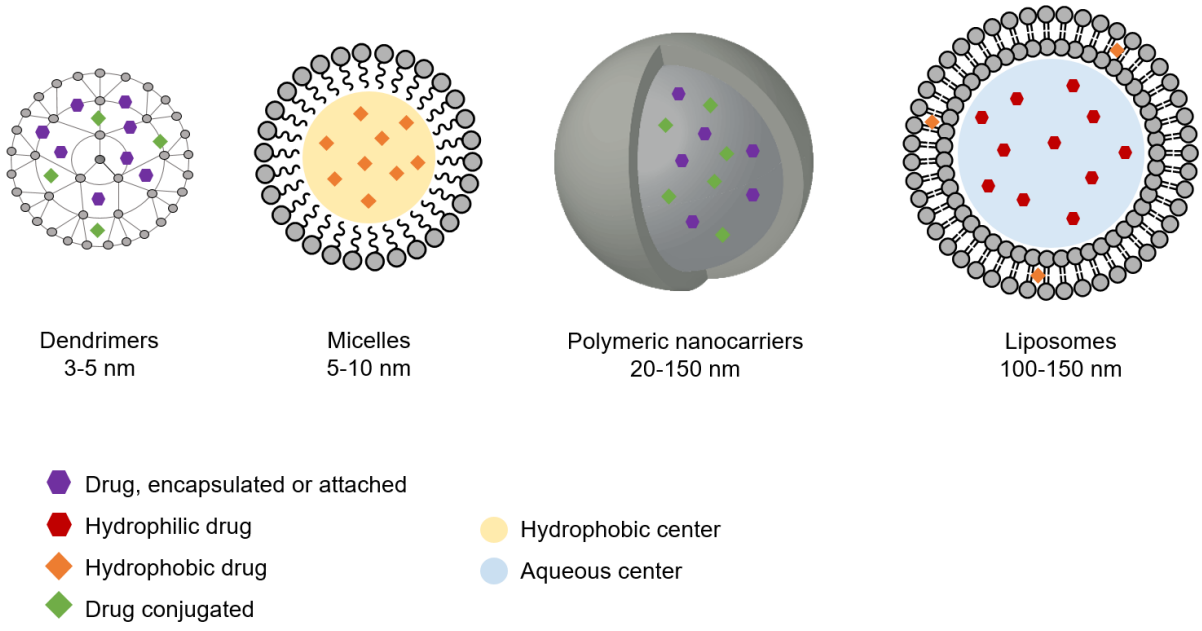

Figure 1: Schematic structures of polymeric and lipid-based nanocarriers.

Dendrimers

Dendrimers are nano-sized compounds consisting of a central core (initiator core) from which tree-like arms or branches form. Their structure is highly symmetric, well-defined and monodisperse.[30,31] Dendrimers can be formed from nucleotides, sugar molecules or amino acids, for example.[32–34] Their synthesis takes place in a step-by-step process and thus enables an irregular, well-arranged formation of the branching patterns of the dendrimer.[35] Their diverse peripheral groups and distinct molecular weight make them a unique source for drug delivery. The transport of drugs *via* dendrimers can take place in different ways.[36] One possibility is to encapsulate the drugs in the core. This can be done by hydrophobic or chemical interactions or hydrogen bonds. Furthermore, direct covalent attachment of the drugs to the terminal active groups of the branches can also occur.[37] However, a

disadvantage of transporting drugs by dendrimers is that dissociation of the attached molecules can happen.[38] Nevertheless, the use of dendrimers is diverse: they can not only used as drug delivery systems,[39] but can also be used for magnetic resonance imaging contrast agents,[40] gene delivery,[41,42] photodynamic therapy,[43–46] transdermal drug delivery[47] and dendritic sensor.[48]

Micelles

Micelles are nanoscopic structures formed by the spontaneous aggregation of amphiphilic molecules or surfactants in a dispersion medium (usually water). The non-polar tails (hydrophobic) are arranged in the center, the polar heads (hydrophilic) point outward into the external solvent.[49] A particular class of micelles form the polymeric micelles. They consist of amphiphilic block copolymers. The core is formed by the insoluble copolymer, whereas the shell is formed by the soluble copolymer.[50] When non-polar solvents are used, equally inverse micelles can be prepared. Then the head points to the center and the tail is directed outward. Polymeric micelles are excellent suitable for drug delivery applications, because of their modifiable properties.[51] There are countless ways to produce polymeric micelles, but the most common systems are based on polyethylene glycol (PEG) as a hydrophilic copolymer. Poly(β-benzyl-L-aspartate) (PBLA), poly(L-lactid acid) (PLA) and various lipids are some examples for the hydrophobic block. The hydrophobic blocks PBLA and PLA are biodegradable into non-toxic byproducts in vivo.[51] The drug is transported in the micelles by encapsulation. Therefore, water-insoluble drugs are particularly suitable for the transport in micelles.[52,53] However, this also results in a clear disadvantage of the system: either hydrophobic or hydrophilic drugs can be encapsulated. But the positive aspects and the great variety and possibilities of these drug delivery systems outweigh this.[54,55]

Polymeric Nanocarriers

Polymeric nanoparticles are colloidal solid nanoparticles that can be formed from any biodegradable natural or synthetic polymers.[56] Natural polymers for polymeric nanocarriers can be chitosan, gelatin, albumin, collagen and alginate. As synthetic polymers, for example, poly(lactid-*co*-glycolic acid) (PLGA), polyethylene glycol (PEG), poly(glutamic acid) (PGA)

and poly(caprolactone) (PCL) can be used.[57] Two basic types can be distinguished: nanocapsules and nanospheres. Nanocapsules have a reservoir in which the drug is dissolved or dispersed in the core of the polymer.[58] Nanospheres form a polymer matrix in which the drug can be trapped.[59] Furthermore, in both types, chemical conjugation or adsorption of the drug can take place on the surface.[60] Biodegradation of such nanocarriers in the body produces monomers that are easily degraded by metabolic pathways.[61] The high variability of their properties makes them attractive drug delivery systems.[62] Furthermore, polymeric nanocarriers possess some advantages with respect to other nanocarriers. They are characterized by their higher stability, they have a high drug concentration, a longer circulation time in the bloodstream and a sustained release of the drug.[63] However, a clear disadvantage of the system is that substances from the body, such as proteins, can also accumulate on the surface. This makes it difficult to study the models under physiological conditions.[64,65]

Liposomes

Liposomes are bilayered structures consisting of natural phospholipids.[66] Two types are distinguished: unilamellar liposomes, which are formed from one bilayer, or multilamellar liposomes, which are formed from more than one bilayer. They arrange themselves in a spherical structure, with an aqueous core surrounded by the lipophilic bilayer.[67] Both can transport hydrophilic and hydrophobic drugs. Furthermore, they possess good biocompatibility, biodegradability and low toxicity. These positive properties make them ideal for the transport of biologically active agents.[55] However, liposomes have a significant disadvantage compared to other nanocarrier systems. They have a shorter blood circulation time.[68] The reason for this is their comparatively much larger size. This means that they are more quickly detected as foreign by the body's defense mechanisms.[69] In the meantime, however, there are various strategies and approaches to significantly extend the circulation time in the blood. One approach, for example, is to modify the surface of the liposomes with polymeric compounds. A common method for surface modification is the coating with polyethylene glycol (PEG).[70] For this process, PEGylated lipids are incorporated into the bilayer of the liposomes. The PEG chains point into the aqueous medium and enclose the surface, forming sterically stabilized liposomes (SSL), which are also called "stealth

liposomes".[71] Compared to conventional liposomes, stealth liposomes have a prolonged serum half-life and an improved safety profile.[72–74]

Nonvesicular Lipid Nanocarriers

In addition to vesicular nanocarriers, such as liposomes, there are also some nonvesicular forms of lipid nanoparticles (LNP). These include solid lipid nanoparticles (SLN) and the new generation nanocarriers such as nanostructured lipid carriers (NLC) and lipid drug conjugates (LDC). Unlike vesicular lipid nanocarriers, emulsifiers or surfactants must be used to stabilize the structures. The nanocarriers can be used for drug delivery *via* topical applications, parenteral and oral administration.[75]

Solid lipid nanoparticles (SLN) are colloidal carriers with a size of 50-1000 nm. They are prepared by dispersion of molten lipids in water, stabilized by addition of surfactants.[76] Lipids that are biocompatible, biodegradable and solid at room temperature are used for their preparation. These include free fatty alcohols or fatty acids, steroids or waxes and mono-, di- and triglycerides.[77] They are suitable for transporting lipophilic drugs. The drug can be incorporated into the matrix, the shell or the core. This depends on the production conditions and the composition. Compared to other carrier systems, they are characterized by a better stability.[78] They have unique properties, such as a large surface area. However, disadvantages of the systems are a low drug loading capacity and a spontaneous burst release of the drug.[79]

Nanostructured lipid carriers (NLC) combine solid and liquid lipids.[75] This combination gives them a less organized internal structure.[80] Compared to solid lipid nanoparticles, they have a higher drug-loading capacity and less drug expulsion property.[81,82] The liquid lipids, which were used, are mainly medium chain triglycerides and oleic acid, as well as natural edible oils.[83]

Lipid drug conjugates (LDC) are water insoluble carrier molecules consisting of a drug covalently modified with a lipid.[84] They have several advantages, such as reduced drug toxicity compared to direct administration of the drug, high entrapment efficiency of hydrophilic drugs, improved oral bioavailability and targeting of tumor tissue.[75] Based on the chemical structures of drugs and lipids, various conjugation strategies and chemical

linkers can be used for the synthesis of LDCs. Common systems consist of conjugates of drugs with fatty acids, steroids, glycerides or phospholipids.[85] Here, the drugs are covalently linked direct to the lipid anchor. A combination is often made between a lipid nanocarriers and a lipid drug conjugate: for this purpose, the drug is first conjugated to a lipid and then additionally used for the synthesis of another nanocarrier.[86–88] This is done to take advantage of the good properties of both systems.

1.4.2 Drug Targeting

The major challenges in clinical research are, on the one hand, the targeted diagnosis of a disease and finding a suitable drug for treatment. On the other hand, it is of immense importance to find the best strategy for the targeted delivery of the drug to the specific site. This insight was already recognized by Paul Ehrlich in 1910. He postulated the use of a "magic bullet" for targeted drug delivery and its importance in fighting diseases.[89] The targeted delivery increases the therapeutic effect by reducing the non-specific distribution of the drug and its side effect.

Two fundamental transport mechanisms are distinguished for the targeted transport of nanocarriers: passive targeting and active targeting. In the following sections, both mechanisms will be considered in more detail for the targeted drug delivery in cancer cells. Cancer cells have some differences from normal tissues. These differences include vascular abnormalities, oxygenation, perfusion, pH and metabolic stages.[90] These differences can be used for the design of nanocarriers as targeted tumor-drug delivery systems.

Passive targeting

Passive targeting is the transport of nanocarriers by convection or passive diffusion.[91] The accumulation of nanocarriers in diseased tissue, such as tumor tissue, occurs through the enhanced permeability and retention effect (EPR effect).[92] Matsamura and Maeda first explained the EPR effect in 1986.[93] Diseases, such as cancer, lead to a leaky vasculature where the endothelial cells are many times larger than in healthy blood vessels.[94] This allows nanocarriers to extravasate through the leaky vasculature into the inflamed areas, tumor tissue or ichemic tissue. The EPR effect therefore forms the basis for passive targeting and is now becoming the gold standard in cancer-targeting drug designing.[95] The EPR effect

can be used in all rapidly growing solid tumors, and therefore it forms a guiding system for all nanocarriers.[96] However, exceptions where the EPR effect cannot be used are hypovascular tumors, such as prostate cancer or pancreatic cancer.[97,98] The transport of nanocarriers *via* passive targeting is shown schematically in **Figure 2** below.

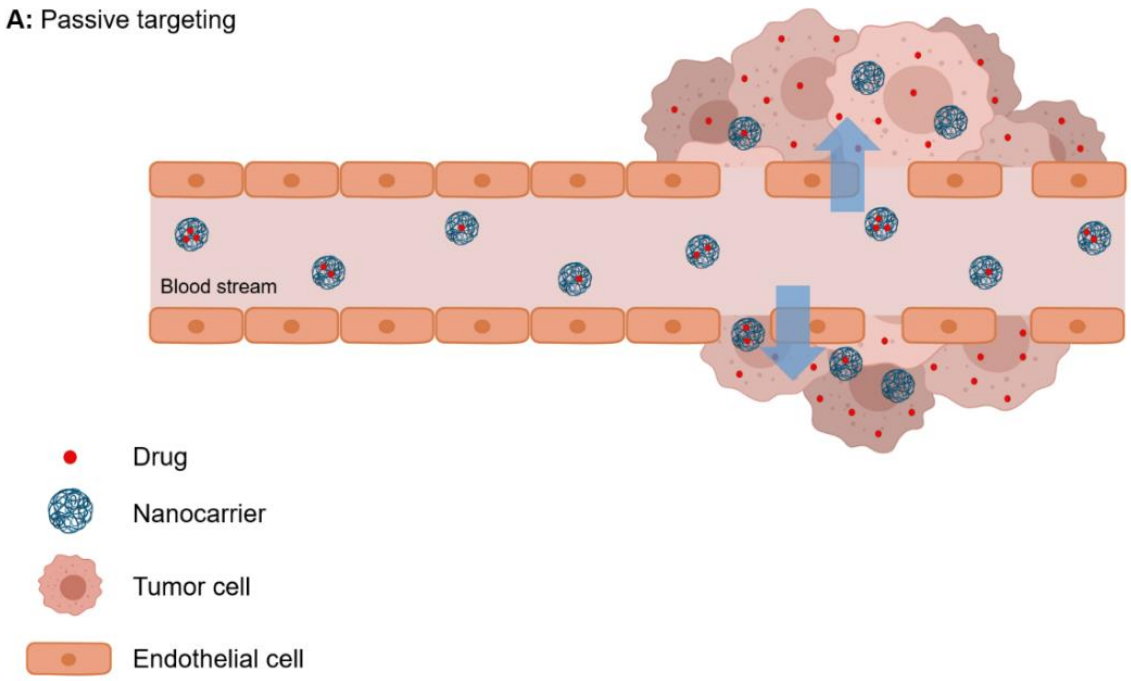

Figure 2: Passive targeting of nanocarriers.

For the optimal accumulation of the nanocarriers *via* EPR effect, immune surveillance must be evaded to maintain blood circulation time for a long period. The local concentration of drug-loaded nanocarriers can be 10-50-fold higher in tumor tissue than in normal tissue within 1-2 days.[99] To this end, nanocarriers must fulfill three main properties. First, the size of the nanocarriers plays an important role. They should be between 10-100 nm in size. Nanocarriers larger than 100 nm can accumulate in the liver, carriers smaller than 10 nm are excreted by the filtration of the kidney.[100] Furthermore, the particles should be neutral or anionically charged to efficiently avoid renal elimination. Last, the nanocarriers must be able to hide from the reticulo-endothelial system. This is responsible for the destruction of any foreign material through opsonization followed by phagocytosis.[55,101]

There are also some limitations for the passive transport. Passive transport depends on the degree of vascularization and angiogenesis of the tumor.[102] This may result in leakage of

the nanocarriers from the tumor tissue into the surrounding tissue. The tumor types and the anatomical sites of the tumor influence this. In solid tumors, there is high pressure caused by the interstitial fluid.[103] It prevents the successful uptake and homogeneous distribution of drugs, which are not entrapped in a carrier. Small molecules can diffuse more easily into the tumor, but also back into the blood. This leads to a rapid decrease in their effective concentration in the tumor drug-loaded nanocarriers cannot diffuse back because of their size. They accumulate in the tumor tissue.[104] This process also explains the size relationship of the nanocarriers with the EPR effect.[105]

Active targeting

In the process of active targeting, the surface of the nanocarrier is functionalized with small ligand molecules that can actively bind to specific receptors on diseased cells. Cancer or tumor cells in particular overexpress specific proteins on their surface. This allows the nanocarriers to bind selectively and with high affinity to the target cell. Thus, active targeting enables increased uptake of the drug by the diseased cells.[106] The first knowledge of active targeting was obtained by Leserman *et al.* in 1980 using antibodies crafted onto the surface of liposomes.[107] Other examples of targeting ligands are small molecules, lectins, lipoproteins, peptides (arginyl glycylaspartic acid), hormones, glycoproteins (transferrin), polysaccharides, low molecular weight vitamins (folic acid), nucleic acids and growth factors.[90,108,109] The nanocarriers can also be equipped with several different ligands on the surface due to their large surface-to-volume ratio.[110] The active targeting process for the targeting of cancer cells is shown schematically in **Figure 3**.

Cell surface receptors overexpressed in cancer cells are critical for successful drug targeting.[111] The basis for the efficacy of nanocarriers is their ability to be internalized after binding to the target cell.[112] In this strategy, ligand-targeted nanocarriers lead directly to the death of the cell and have a cytotoxic effect on cells located in the tumor periphery that are independent of angiogenesis.[113] There are four types of receptors that are well studied and allow the internalization. These receptors include the transferrin receptor, the folate receptor, glycoproteins expressed on the cell surface, and the epidermal growth factor receptor.[15,90]

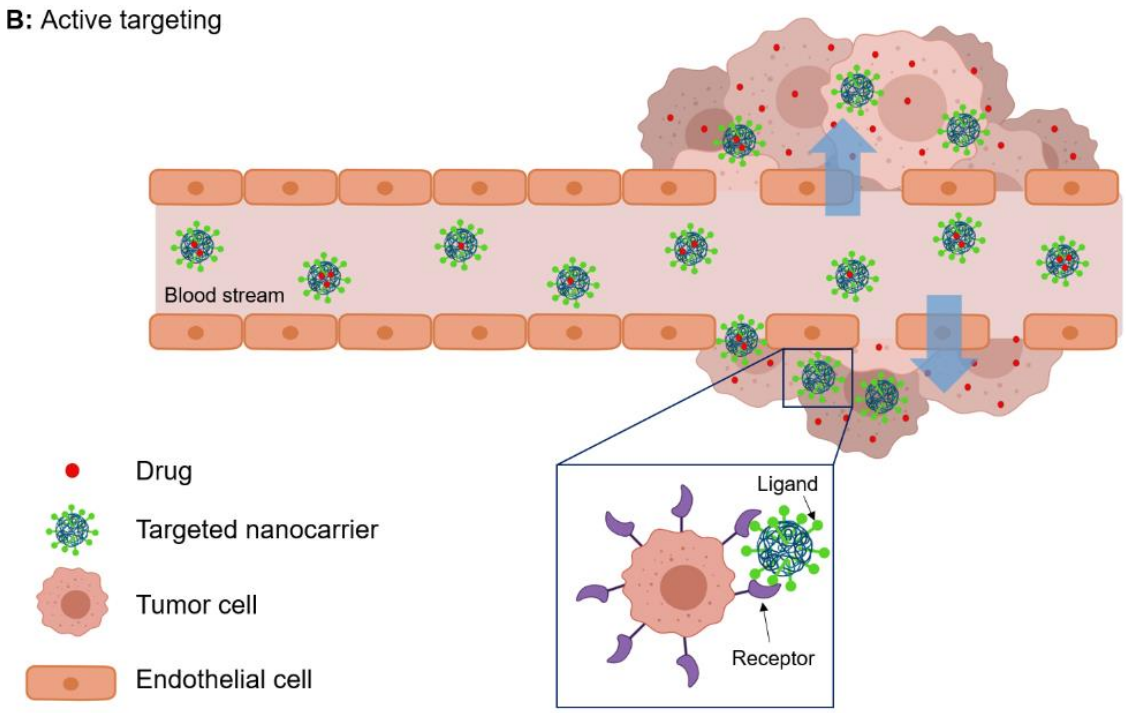

Figure 3: Active targeting of nanocarriers.

Transferrin is a glycoprotein in the serum that is responsible for the transport of iron through the blood into the cells. For uptake into cells, it binds to the transferrin receptor and is internalized by receptor-mediated endocytosis.[114] The transferrin receptor is a protein responsible for homeostasis and the regulation of cell growth.[115] In cancer cells, the expression of transferrin receptors is 100-fold higher than in normal cells. This receptor is an attractive target for cancer therapy, because of its extracellular accessibility, its ability to internalize and its central role in the cellular pathology of human cancer.[116]

The folate receptor is a well-known tumor marker. It binds to the vitamin folic acid, but also to folate-drug conjugates or folate-functionalized nanocarriers. It has a high affinity and transports the molecules into the cell by receptor-mediated endocytosis.[117] Folic acid is essential for the synthesis of nucleotide bases, because it is required for metabolic reactions with one carbon, which contributes significantly to the synthesis.[118] The alpha-isoform of the folate receptor in particular is overexpressed on 40% of human cancers.[119]

Lectins are proteins of non-immunological origin and play a role associated with glycoproteins at the cell surface. They recognize carbohydrate parts attached to

glycoproteins and can bind to them.[120] Different glycoproteins are often expressed by cancer cells compared to normal cells. The interaction of lectins with certain carbohydrates is very specific. Targeting can take place in two different ways. In direct lectin targeting, the lectins are incorporated into the nanocarrier and directed to the cell-surface carbohydrates. In reverse lectin targeting, carbohydrate moieties are coupled to nanoparticles to target lectins.[121] Lectins and neoglycoconjugates are mainly used for drug targeting in the colon.[122]

The epidermal growth factor receptor (EGFR) belongs to the tyrosine kinase receptor family.[123] Activation of the receptor stimulates important processes involved in tumor growth and progression. These processes include proliferation, angiogenesis, invasion and metastasis.[124] Overexpression is found in many cancers, but predominantly in breast cancer, but a significant role in progression can also be found in other human malignancies.[125,126] Expression or overexpression has also been detected in several solid tumors, such as colorectal cancer, non-small cell lung cancer and squamous cell carcinoma of the head and neck, as well as ovarian, kidney, pancreatic and prostate cancer.[127]

In general, active targeting is preferred to passive targeting, because it prevents off-target drug delivery and reduces multi-drug resistance.[128] Furthermore, targeting can take place anywhere in the body, regardless of the EPR effect. Thereby cancer cells can also be combated without a defined location, as in the case of metastases, for example. This is particularly important to prevent the proliferation of cancer cells to other organs.[129]

A clear disadvantage, however, is that the development and production of functionalized nanocarriers is much more complex and usually associated with high costs.[130] A reduction in the manufacturing costs for the development of economically valuable therapeutics for the treatment of diseases is therefore essential.

1.4.3 Stimuli-sensitive nanocarriers

In recent years, research interest in "smart" or “responsive” nanocarriers has been growing.[131,132] These are systems, which consists of materials that can change their properties in response to stimuli.[133] Two groups of stimuli can be divided: stimuli that are induced from the outside are called external stimuli, stimuli that are induced from the inside are called internal stimuli.

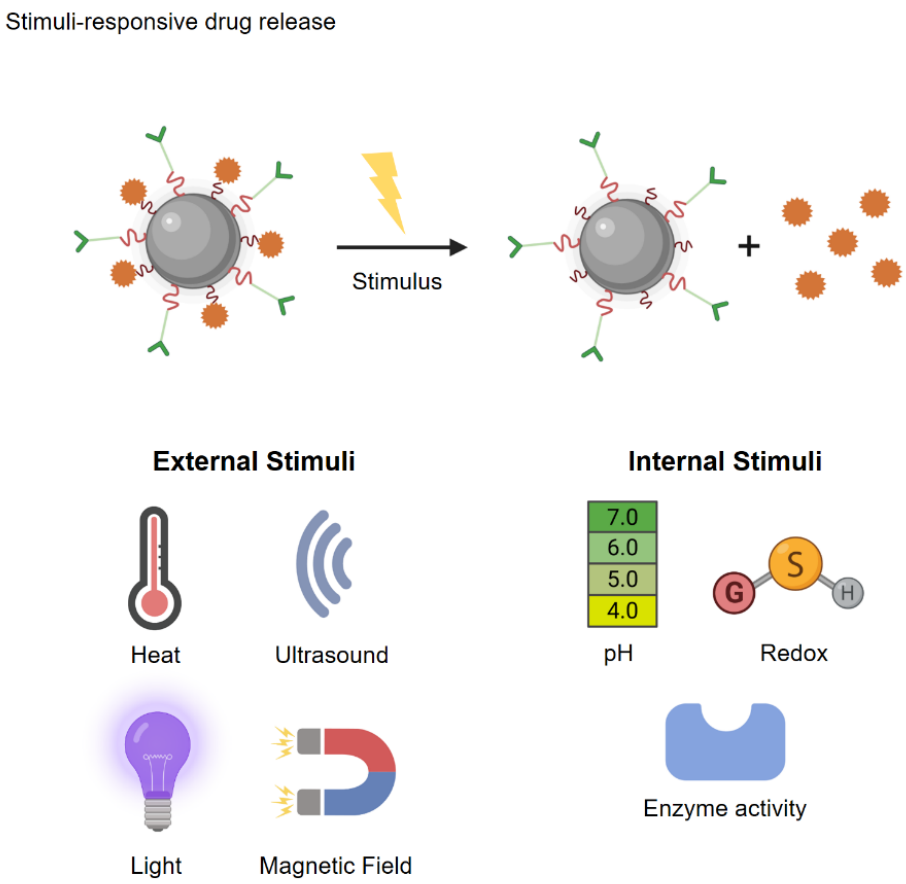

Figure 4: Stimuli-responsive drug release *via* external or internal stimuli.

External stimuli include heat, ultrasound, light and the magnetic field, whereas pH, redox processes and enzyme activity belong to the internal stimuli. These stimuli can be used to induce targeted drug release.[134] In particular, in cancer cells, the stimuli can be perfectly used for targeted drug release or interaction with a specific target due to the unique extracellular tumor environment. Furthermore, drug retention can be controlled by nanocarriers. For example, by applying external stimuli, a controlled and selective targeting of cells can be triggered.[135] In the next sections, the different stimuli will be discussed in a more detailed way.

External stimuli

Many pathological areas show distinct hyperthermia.[136] In the development of temperature-sensitive nanocarriers, various polymers with a low critical solution temperature (LCST) are of great interest. These materials undergo a phase separation from solution upon a temperature change. The release of a drug in a temperature-sensitive nanocarrier occurs by

precipitation of the polymer when the temperature is above the LCST (in the tumor).[137] The structure of the nanocarrier is thus destroyed, resulting in the release of the drug. The most widely used polymer for thermos-responsive nanocarriers is poly(*N*-isopropylacrylamide) (PNIPAM), because of its outstanding properties.[138] Various physical processes can achieve local heating of the tumor.

Ultrasound is a preferred method to induce local heating *via* high-intensity focused ultrasound (HIFU). This method is least invasive, easy and cheap.[139] However, ultrasound can not only trigger thermal effects through local heating, but is also suitable for mechanical effects, for example through transient cavitation.[140]

Another external stimulus can be triggered *via* the magnetic field. Magnetic nanoparticles, such as superparamagnetic iron oxide nanoparticles (SPION) are used for this purpose.[141] These were originally developed for magnetic resonance imaging by passive targeting, but are also used as drug targeting systems.[142,143] For this purpose, the SPION systems are coated with targeting ligands and transported *via* active targeting. By using an external magnetic field, it is possible to guide the nanoparticles to the target site.[144] Furthermore, the magnetic process leads to a local increase in temperature when the SPION nanoparticles are used with an alternating magnetic field.[145] This allows the elimination of the tumor. The procedure is called "magnetic thermal ablation".[146]

When light is used as an external stimulus, photo-responsive polymers are applied. These molecules can change their properties under the influence of light of a certain wavelength. The influence of light induces a structural change in a specific function of these polymers in general.[147] An example of a photo-responsive system is the use of pyrene-containing hydrophobic methacrylate units in micelles. Irradiation with UV causes cleavage of the pyrenyl-methyl ester units, leading to transformation of the previously hydrophobic methacrylate units to hydrophilic units and results in the dissociation of the micelles.[148] However, the systems controlled with light from the UV or visible wavelength ranges have some limitations, because they can be absorbed by the skin and cause undesirable side reactions. For this reason, researchers are interested in photo-responsive polymer systems that can be modified with infra-red or near infra-red light.[149,150]

Internal stimuli

Within the body, pH values can vary significantly. This ranges from the strongly acidic pH in the stomach to a basic pH of the intestine, but also intracellular components such as the cytoplasm, endosomes, lysosomes, mitochondria and nuclei have their own characteristic pH values.[151–154] This property can be used not only for drug targeting in general, but especially as an internal stimulus in targeted drug release in cancer. The pH in both primary and metastasized tumors is lower than the pH in healthy tissue.[155] Because of this, acidic pH serves as an ideal internal stimulus in drug delivery *via* pH-responsive nanocarriers.[156] The transport of the pH-responsive nanocarriers to the target site is carried out by active or passive targeting and the drug release occurs by the deformation of the nanocarriers.[157] The most common components for pH-responsive nanocarriers are polymers, which undergo a change in their physical properties under the influence of small pH changes. These changes in physical properties include size, shape or hydrophobicity and leads to a destabilization of the nanocarrier which triggered the release of the drug.[156] Further details about pH-responsive polymers can be found in Chapter 1.3. pH-responsive nanocarriers can overcome the lack of selectivity of conventional anticancer methods and, together with EPR, enhance the efficacy of therapeutic agents including siRNA, drugs or radioisotopes.[158]

Enzymatic activity can also be used as an internal stimulus. For this purpose, nanocarriers can be activated by overexpressed enzymes in the tumor. A special therapeutic approach is based on tumor site-specific enzymatic activation of a prodrug. In this approach, either an accumulation by the enzyme in the tumor takes place or an ineffective prodrug is converted by the enzyme into its cytotoxic form in the tumor area.[159] When enzymes are used for drug delivery from nanocarriers, enzymatically induced cleavage of a linker on the nanocarrier usually occurs, which controls the release of the drug.[160]

Another class of responsive polymers reacts to redox processes. One of the most important example are the redox/thiol sensitive polymers.[161] The conversion of disulfides and thiols in biological processes is a key step. Disulfide bonds can be reversibly converted to thiols by various reducing agents and undergo disulfide exchange in the presence of other thiols.[162] For this reason, polymers containing disulfide bonds can be considered both redox and thiol responsive.[163] Oxidative processes take place in the extracellular fluid, in inflamed

tissue and tumor tissue, whereas reductive processes take place in the cells.[164] This property allows redox-responsive polymers to be used for the controlled release of drugs in inflamed and tumor tissues.[165] There, reactive oxygen species (ROS) are released by activated macrophages, which can trigger the transformation of redox-responsive nanocarriers.[166,167] This leads to a change in the physical properties of the polymers and consequently to the release of the drug. However, redox-responsive systems can not only be used for the drug delivery, but also for imaging.[168]

References

(1) Nie, S.; Xing, Y.; Kim, G. J.; Simons, J. W. Nanotechnology Applications in Cancer. *Annu. Rev. Biomed. Eng.* **2007**, *9*, 257–288. https://doi.org/10.1146/annurev.bioeng.9.060906.152025.

(2) Hamoudeh, M.; Kamleh, M. A.; Diab, R.; Fessi, H. Radionuclides Delivery Systems for Nuclear Imaging and Radiotherapy of Cancer. *Adv. Drug Deliv. Rev.* **2008**, *60* (12), 1329–1346. https://doi.org/10.1016/j.addr.2008.04.013.

(3) Cho, K.; Wang, X.; Nie, S.; Chen, Z. G.; Shin, D. M. Therapeutic Nanoparticles for Drug Delivery in Cancer. *Clin. Cancer Res.* **2008**, *14*, 1310–1316.

(4) Torchilin, V. P. Multifunctional Nanocarriers. *Adv. Drug Deliv. Rev.* **2006**, *58* (14), 1532–1555. https://doi.org/10.1016/j.addr.2006.09.009.

(5) Petkar, K. C.; Patil, S. M.; Chavhan, S. S.; Kaneko, K.; Sawant, K. K.; Kunda, N. K.; Saleem, I. Y. An Overview of Nanocarrier-Based Adjuvants for Vaccine Delivery. *Pharmaceutics* **2021**, *13* (4), 1–29. https://doi.org/10.3390/pharmaceutics13040455.

(6) Mody, N.; Sharma, R.; Agrawal, U.; Dubey, S.; Vyas, S. P. Chapter 5 - Nanobiomaterials: Emerging Platform in Cancer Theranostics. In *Nanobiomaterials in Cancer Therapy*; Grumezescu, A. M., Ed.; William Andrew Publishing, 2016; pp 117–146. https://doi.org/https://doi.org/10.1016/B978-0-323-42863-7.00005-0.

(7) Bhaw-Luximon, A.; Goonoo, N.; Jhurry, D. Chapter 6 - Nanotherapeutics Promises for Colorectal Cancer and Pancreatic Ductal Adenocarcinoma. In *Nanobiomaterials in Cancer Therapy*; Grumezescu, A. M., Ed.; William Andrew Publishing, 2016; pp 147–201. https://doi.org/https://doi.org/10.1016/B978-0-323-42863-7.00006-2.

(8) Patel, N. R.; Pattni, B. S.; Abouzeid, A. H.; Torchilin, V. P. Nanopreparations to Overcome Multidrug Resistance in Cancer. *Adv. Drug Deliv. Rev.* **2013**, *65* (13–14), 1748–1762. https://doi.org/10.1016/j.addr.2013.08.004.

(9) Chacko, A. M.; Hood, E. D.; Zern, B. J.; Muzykantov, V. R. Targeted Nanocarriers for

Imaging and Therapy of Vascular Inflammation. *Curr. Opin. Colloid Interface Sci.* **2011**, *16* (3), 215–227. https://doi.org/10.1016/j.cocis.2011.01.008.

(10) Allen, T. M.; Cullis, P. R. Drug Delivery Systems: Entering the Mainstream. *Science (80-.).* **2004**, *303* (5665), 1818–1822. https://doi.org/10.1126/science.1095833.

(11) Bardal, S. K.; Waechter, J. E.; Martin, D. S. Chapter 2 - Pharmacokinetics. In *Applied Pharmacology*; Bardal, S. K., Waechter, J. E., Martin, D. S., Eds.; W.B. Saunders: Philadelphia, 2011; pp 17–34. https://doi.org/https://doi.org/10.1016/B978-1-4377-0310-8.00002-6.

(12) Viswanathan, P.; Muralidaran, Y.; Ragavan, G. Chapter 7 - Challenges in Oral Drug Delivery: A Nano-Based Strategy to Overcome. In *Nanostructures for Oral Medicine*; Andronescu, E., Grumezescu, A. M., Eds.; Micro and Nano Technologies; Elsevier, 2017; pp 173–201. https://doi.org/https://doi.org/10.1016/B978-0-323-47720-8.00008-0.

(13) Sala, M.; Diab, R.; Elaissari, A.; Fessi, H. Lipid Nanocarriers as Skin Drug Delivery Systems: Properties, Mechanisms of Skin Interactions and Medical Applications. *Int. J. Pharm.* **2018**, *535* (1), 1–17. https://doi.org/https://doi.org/10.1016/j.ijpharm.2017.10.046.

(14) Chowdary, K. P. R.; Rao, Y. S. Mucoadhesive Microspheres for Controlled Drug Delivery. *Biol. Pharm. Bull.* **2004**, *27* (11), 1717–1724. https://doi.org/10.1248/bpb.27.1717.

(15) Chamundeeswari, M.; Jeslin, J.; Verma, M. L. Nanocarriers for Drug Delivery Applications. *Environ. Chem. Lett.* **2019**, *17* (2), 849–865. https://doi.org/10.1007/s10311-018-00841-1.

(16) Wicki, A.; Witzigmann, D.; Balasubramanian, V.; Huwyler, J. Nanomedicine in Cancer Therapy: Challenges, Opportunities, and Clinical Applications. *J. Control. Release* **2015**, *200*, 138–157. https://doi.org/10.1016/j.jconrel.2014.12.030.

(17) Shi, J.; Kantoff, P. W.; Wooster, R.; Farokhzad, O. C. Cancer Nanomedicine: Progress, Challenges and Opportunities. *Nat. Rev. Cancer* **2017**, *17* (1), 20–37. https://doi.org/10.1038/nrc.2016.108.

(18) Allard, E.; Passirani, C.; Benoit, J. P. Convection-Enhanced Delivery of Nanocarriers for the Treatment of Brain Tumors. *Biomaterials* **2009**, *30* (12), 2302–2318. https://doi.org/10.1016/j.biomaterials.2009.01.003.

(19) Zhang, Z.; Tsai, P. C.; Ramezanli, T.; Michniak-Kohn, B. B. Polymeric Nanoparticles-Based Topical Delivery Systems for the Treatment of Dermatological Diseases.

Wiley Interdiscip. Rev. Nanomedicine Nanobiotechnology **2013**, *5* (3), 205–218. https://doi.org/10.1002/wnan.1211.

(20) Peer, D.; Karp, J. M.; Hong, S.; Farokhzad, O. C.; Margalit, R.; Langer, R. *Nanocarriers as an Emerging Platform for Cancer Therapy*; 2007; Vol. 2. https://doi.org/10.1038/nnano.2007.387.

(21) Gottesman, M. M. Mechanism of Cancer Drug Resistance. *Annu. Rev. med.* **2002**, *53*, 615–627.

(22) Bradshaw, D. M.; Arceci, R. J. Clinical Relevance of Transmembrane Drug Efflux as a Mechanism of Multidrug Resistance. *J. Clin. Oncol.* **1998**, *16* (11), 3674–3690. https://doi.org/10.1200/JCO.1998.16.11.3674.

(23) Esfahani, D. R.; Tangen, K. M.; Sadeh, M.; Seksenyan, A.; Neisewander, B. L.; Mehta, A. I.; Linninger, A. A. *Systems Engineers' Role in Biomedical Research. Convection-Enhanced Drug Delivery*, 1st ed.; Elsevier B.V., 2018; Vol. 42. https://doi.org/10.1016/B978-0-444-63964-6.00009-X.

(24) Manju, S.; Sreenivasan, K. Functionalised Nanoparticles for Targeted Drug Delivery. *Biointegration Med. Implant Mater. Sci. Des.* **2010**, 267–297. https://doi.org/10.1533/9781845699802.2.267.

(25) López-Dávila, V.; Seifalian, A. M.; Loizidou, M. Organic Nanocarriers for Cancer Drug Delivery. *Curr. Opin. Pharmacol.* **2012**, *12* (4), 414–419. https://doi.org/https://doi.org/10.1016/j.coph.2012.02.011.

(26) Torchilin, V. Tumor Delivery of Macromolecular Drugs Based on the EPR Effect. *Adv. Drug Deliv. Rev.* **2011**, *63* (3), 131–135. https://doi.org/10.1016/j.addr.2010.03.011.

(27) Liang, R.; Wei, M.; Evans, D. G.; Duan, X. Inorganic Nanomaterials for Bioimaging, Targeted Drug Delivery and Therapeutics. *Chem. Commun.* **2014**, *50* (91), 14071–14081. https://doi.org/10.1039/c4cc03118k.

(28) Santos, H. A.; Bimbo, L. M.; Peltonen, L.; Hirvonen, J. Inorganic Nanoparticles in Targeted Drug Delivery and Imaging. In *Targeted Drug Delivery : Concepts and Design*; Devarajan, P. V, Jain, S., Eds.; Springer International Publishing: Cham, 2015; pp 571–613. https://doi.org/10.1007/978-3-319-11355-5_18.

(29) Ma, P.; Xiao, H.; Li, C.; Dai, Y.; Cheng, Z.; Hou, Z.; Lin, J. Inorganic Nanocarriers for Platinum Drug Delivery. *Mater. Today* **2015**, *18* (10), 554–564. https://doi.org/https://doi.org/10.1016/j.mattod.2015.05.017.

(30) Kresge C, Leonowicz M, R. W. Dendrimers and Dendrons: Concepts, Syntheses,

Applications,; VCH: Weinheim, 2001; pp 7291–7309.

(31) Sampathkumar, S.; Yarema, K. J. Dendrimers in Cancer Treatment and Diagnosis; Wiley: New York, 2007; Vol. 7.

(32) Gorzkiewicz, M.; Klajnert-Maculewicz, B. Dendrimers as Nanocarriers for Nucleoside Analogues. *Eur. J. Pharm. Biopharm.* **2017**, *114*, 43–56. https://doi.org/10.1016/j.ejpb.2016.12.030.

(33) Szulc, A.; Appelhans, D.; Voit, B.; Bryszewska, M.; Klajnert, B. Characteristics of Complexes between Poly(Propylene Imine) Dendrimers and Nucleotides. *New J. Chem.* **2012**, *36* (8), 1610–1615. https://doi.org/10.1039/c2nj40165g.

(34) Kim, Y.; Zeng, F.; Zimmerman, S. C. Peptide Dendrimers from Natural Amino Acids. *Chem. - A Eur. J.* **1999**, *5* (7), 2133–2138. https://doi.org/10.1002/(sici)1521-3765(19990702)5:7<2133::aid-chem2133>3.3.co;2-a.

(35) Fréchet, J. M. J.; Tomalia, D. A. *Dendrimers and Other Dendritic Polymers*; Wiley series in polymer science, 2001.

(36) Markowicz, M.; Szymański, P.; Ciszewski, M.; Kłys, A.; Mikiciuk-Olasik, E. Evaluation of Poly(Amidoamine) Dendrimers as Potential Carriers of Iminodiacetic Derivatives Using Solubility Studies and 2D-NOESY NMR Spectroscopy. *J. Biol. Phys.* **2012**, *38* (4), 637–656. https://doi.org/10.1007/s10867-012-9277-5.

(37) Mintzer, M. A.; Grinstaff, M. W. Biomedical Applications of Dendrimers: A Tutorial. *Chem. Soc. Rev.* **2011**, *40* (1), 173–190. https://doi.org/10.1039/b901839p.

(38) De Groot, F. M. H.; Albrecht, C.; Koekkoek, R.; Beusker, P. H.; Scheeren, H. W. "Cascade-Release Dendrimers" Liberate All End Groups upon a Single Triggering Event in the Dendritic Core. *Angew. Chemie - Int. Ed.* **2003**, *42* (37), 4490–4494. https://doi.org/10.1002/anie.200351942.

(39) Stiriba, S. E.; Frey, H.; Haag, R. Dendritic Polymers in Biomedical Applications: From Potential to Clinical Use in Diagnostics and Therapy. *Angew. Chemie - Int. Ed.* **2002**, *41* (8), 1329–1334. https://doi.org/10.1002/1521-3773(20020415)41:8<1329::AID-ANIE1329>3.0.CO;2-P.

(40) Patel, H. N.; Patel, P. M. Dendrimer Applications - A Review. *Int. J. Pharma Bio Sci.* **2013**, *4* (2), 454–463.

(41) Fu, H. L.; Cheng, S. X.; Zhang, X. Z.; Zhuo, R. X. Dendrimer/DNA Complexes Encapsulated in a Water Soluble Polymer and Supported on Fast Degrading Star Poly(Dl-Lactide) for Localized Gene Delivery. *J. Control. Release* **2007**, *124* (3), 181–188. https://doi.org/10.1016/j.jconrel.2007.08.031.

(42) Dutta, T.; Garg, M.; Jain, N. K. Poly(Propyleneimine) Dendrimer and Dendrosome Mediated Genetic Immunization against Hepatitis B. *Vaccine* **2008**, *26* (27–28), 3389–3394. https://doi.org/10.1016/j.vaccine.2008.04.058.

(43) Battah, S. H.; Chee, C. E.; Nakanishi, H.; Gerscher, S.; MacRobert, A. J.; Edwards, C. Synthesis and Biological Studies of 5-Aminolevulinic Acid-Containing Dendrimers for Photodynamic Therapy. *Bioconjug. Chem.* **2001**, *12* (6), 980–988. https://doi.org/10.1021/bc010027n.

(44) Nishiyama, N.; Stapert, H. R.; Zhang, G. D.; Takasu, D.; Jiang, D. L.; Nagano, T.; Aida, T.; Kataoka, K. Light-Harvesting Ionic Dendrimer Porphyrins as New Photosensitizers for Photodynamic Therapy. *Bioconjug. Chem.* **2003**, *14* (1), 58–66. https://doi.org/10.1021/bc025597h.

(45) Calin, M. A.; Parasca, S. V. Photodynamic Therapy in Oncology. *J. Optoelectron. Adv. Mater.* **2006**, *8* (3), 1173–1179. https://doi.org/10.1634/theoncologist.11-9-1034.

(46) Zhang, G. D.; Harada, A.; Nishiyama, N.; Jiang, D. L.; Koyama, H.; Aida, T.; Kataoka, K. Polyion Complex Micelles Entrapping Cationic Dendrimer Porphyrin: Effective Photosensitizer for Photodynamic Therapy of Cancer. *J. Control. Release* **2003**, *93* (2), 141–150. https://doi.org/10.1016/j.jconrel.2003.05.002.

(47) Yiyun, C.; Na, M.; Tongwen, X.; Rongqiang, F.; Xueyuan, W.; Xiaomin, W.; Longping, W. Transdermal Delivery of Nonsteroidal Anti-Inflammatory Drugs Mediated by Polyamidoamine (PAMAM) Dendrimers**Cheng Yiyun and Wen Longping Designed the Experiments and Wrote This Manuscript, Man Na and Other Coauthors Did the Experiments and Analyzed the Da. *J. Pharm. Sci.* **2007**, *96* (3), 595–602. https://doi.org/https://doi.org/10.1002/jps.20745.

(48) Beer, P. D.; Gale, P. A.; Smith, D. K. *Supramolecular Chemistry*; Oxford University Press: Oxford, 1999.

(49) Wennerström, H.; Lindman, B. Micelles. Physical Chemistry of Surfactant Association. *Phys. Rep.* **1979**, *52* (1), 1–86. https://doi.org/10.1016/0370-1573(79)90087-5.

(50) Riess, G. Micellization of Block Copolymers. *Prog. Polym. Sci.* **2003**, *28* (7), 1107–1170. https://doi.org/10.1016/S0079-6700(03)00015-7.

(51) Kwon, G. S.; Okano, T. Polymeric Micelles as New Drug Carriers. *Adv. Drug Deliv. Rev.* **1996**, *21* (2), 107–116. https://doi.org/10.1016/S0169-409X(96)00401-2.

(52) Aliabadi, H. M.; Lavasanifar, A. Polymeric Micelles for Drug Delivery. *Expert Opin. Drug Deliv.* **2006**, *3* (1), 139–162. https://doi.org/10.1517/17425247.3.1.139.

(53) Ahmad, Z.; Shah, A.; Siddiq, M.; Kraatz, H. B. Polymeric Micelles as Drug Delivery Vehicles. *RSC Adv.* **2014**, *4* (33), 17028–17038. https://doi.org/10.1039/c3ra47370h.

(54) Bhatia, S. Nanoparticles Types, Classification, Characterization, Fabrication Methods and Drug Delivery Applications. In *Natural Polymer Drug Delivery Systems: Nanoparticles, Plants, and Algae*; Springer International Publishing: Cham, 2016; pp 33–93. https://doi.org/10.1007/978-3-319-41129-3_2.

(55) Malam, Y.; Loizidou, M.; Seifalian, A. M. Liposomes and Nanoparticles: Nanosized Vehicles for Drug Delivery in Cancer. *Trends Pharmacol. Sci.* **2009**, *30* (11), 592–599. https://doi.org/10.1016/j.tips.2009.08.004.

(56) Avramović, N.; Mandić, B.; Savić-Radojević, A.; Simić, T. Polymeric Nanocarriers of Drug Delivery Systems in Cancer Therapy. *Pharmaceutics* **2020**, *12* (4), 1–17. https://doi.org/10.3390/pharmaceutics12040298.

(57) Wang, X.; Wang, Y.; Chen, Z. G.; Shin, D. M. Advances of Cancer Therapy by Nanotechnology. *Cancer Res. Treat.* **2009**, *41* (1), 1. https://doi.org/10.4143/crt.2009.41.1.1.

(58) Meier, W. Polymer Nanocapsules. *Chem. Soc. Rev.* **2000**, *29* (5), 295–303. https://doi.org/10.1039/a809106d.

(59) Gref, R.; Minamitake, Y.; Peracchia, M. T.; Trubetskoy, V.; Torchilin, V.; Langer, R. Biodegradable Long-Circulating Polymeric Nanospheres. *Science (80-.).* **1994**, *263* (March), 1600.

(60) Prabhu, R. H.; Patravale, V. B.; Joshi, M. D. Polymeric Nanoparticles for Targeted Treatment in Oncology: Current Insights. *Int. J. Nanomedicine* **2015**, *10*, 1001–1018. https://doi.org/10.2147/IJN.S56932.

(61) Mishra, B.; Patel, B. B.; Tiwari, S. Colloidal Nanocarriers: A Review on Formulation Technology, Types and Applications toward Targeted Drug Delivery. *Nanomedicine Nanotechnology, Biol. Med.* **2010**, *6* (1), 9–24. https://doi.org/10.1016/j.nano.2009.04.008.

(62) Abasian, P.; Ghanavati, S.; Rahebi, S.; Nouri Khorasani, S.; Khalili, S. Polymeric Nanocarriers in Targeted Drug Delivery Systems: A Review. *Polym. Adv. Technol.* **2020**, *31* (12), 2939–2954. https://doi.org/10.1002/pat.5031.

(63) Iyisan, B.; Landfester, K. *Polymeric Nanocarriers*; Springer International Publishing, 2019. https://doi.org/10.1007/978-3-030-12461-8_3.

(64) Ritz, S.; Schöttler, S.; Kotman, N.; Baier, G.; Musyanovych, A.; Kuharev, J.; Landfester, K.; Schild, H.; Jahn, O.; Tenzer, S.; Mailänder, V. Protein Corona of

Nanoparticles: Distinct Proteins Regulate the Cellular Uptake. *Biomacromolecules* **2015**, *16* (4), 1311–1321. https://doi.org/10.1021/acs.biomac.5b00108.

(65) Schöttler, S.; Becker, G.; Winzen, S.; Steinbach, T.; Mohr, K.; Landfester, K.; Mailänder, V.; Wurm, F. R. Protein Adsorption Is Required for Stealth Effect of Poly(Ethylene Glycol)- and Poly(Phosphoester)-Coated Nanocarriers. *Nat. Nanotechnol.* **2016**, *11* (4), 372–377. https://doi.org/10.1038/nnano.2015.330.

(66) Bangham, A. D.; Glover, J. C.; Hollingshead, S.; Pethica, B. A. The Surface Properties of Some Neoplastic Cells. *Biochem. J.* **1962**, *84* (3), 513–517. https://doi.org/10.1042/bj0840513.

(67) Mansoori Agrawal, M. A.; Jawade, S.; Khan, S.; I., M. A Review on Liposome. *Int. J. Adv. Res. Pharm. Bio Sci.* **2012**, *2*, 453+.

(68) Ahl, P. L.; Bhatia, S. K.; Meers, P.; Roberts, P.; Stevens, R.; Dause, R.; Perkins, W. R.; Janoff, A. S. Enhancement of the in Vivo Circulation Lifetime of L-α-Distearoylphosphatidylcholine Liposomes, Importance of Liposomal Aggregation versus Complement Opsonization. *Biochim. Biophys. Acta - Biomembr.* **1997**, *1329* (2), 370–382. https://doi.org/10.1016/S0005-2736(97)00129-6.

(69) Bradley, A. J.; Devine, D. V.; Ansell, S. M.; Janzen, J.; Brooks, D. E. Inhibition of Liposome-Induced Complement Activation by Incorporated Poly(Ethylene Glycol)-Lipids. *Arch. Biochem. Biophys.* **1998**, *357* (2), 185–194. https://doi.org/10.1006/abbi.1998.0798.

(70) Woodle, M. C. Surface-Modified Liposomes: Assessment and Characterization for Increased Stability and Prolonged Blood Circulation. *Chem. Phys. Lipids* **1993**, *64* (1–3), 249–262. https://doi.org/10.1016/0009-3084(93)90069-F.

(71) Lasic, D. .; Needham, D. The "Stealth" Liposome: A Prototypical Biomaterial. *Chem. Rev.* **1995**, *95* (8), 2601–2628.

(72) Veronese, F. M.; Pasut, G. PEGylation, Successful Approach to Drug Delivery. *Drug Discov. Today* **2005**, *10* (21), 1451–1458.

(73) Pasut, G.; Veronese, F. . . Polymer-Drug Conjugation, Recent Achievements and General Strategies. *Prog. Polym. Sci.* **2007**, *32*, 933–961. https://doi.org/10.1016/j.progpolymsci.2007.05.008.

(74) Pasut, G.; Paolino, D.; Celia, C.; Mero, A.; Joseph, A. S.; Wolfram, J.; Cosco, D.; Schiavon, O.; Shen, H.; Fresta, M. Polyethylene Glycol (PEG)-Dendron Phospholipids as Innovative Constructs for the Preparation of Super Stealth Liposomes for Anticancer Therapy. *J. Control. Release* **2015**, *199*, 106–113.

https://doi.org/10.1016/j.jconrel.2014.12.008.

(75) Shukla, T.; Upmanyu, N.; Prakash Pandey, S.; Gosh, D. *Lipid Nanocarriers*; Elsevier Inc., 2018. https://doi.org/10.1016/B978-0-12-813687-4.00001-3.

(76) Kesharwani, R.; Sachan, A.; Singh, S.; Patel, D. Formulation and Evaluation of Solid Lipid Nanoparticle (SLN) Based Topical Gel of Etoricoxib. *J. Appl. Pharm. Sci.* **2016**, *6* (10), 124–131. https://doi.org/10.7324/JAPS.2016.601017.

(77) Üner, M.; Yener, G. Importance of Solid Lipid Nanoparticles (SLN) in Various Administration Routes and Future Perspective. *Int. J. Nanomedicine* **2007**, *2* (3), 289–300.

(78) Mu, H.; Holm, R. Solid Lipid Nanocarriers in Drug Delivery: Characterization and Design. *Expert Opin. Drug Deliv.* **2018**, *15* (8), 771–785. https://doi.org/10.1080/17425247.2018.1504018.

(79) Morel, S.; Terreno, E.; Ugazio, E.; Aime, S.; Gasco, M. R. NMR Relaxometric Investigations of Solid Lipid Nanoparticles (SLN) Containing Gadolinium(III) Complexes. *Eur. J. Pharm. Biopharm.* **1998**, *45* (2), 157–163. https://doi.org/10.1016/S0939-6411(97)00107-0.

(80) H. Muller, R.; Shegokar, R.; M. Keck, C. 20 Years of Lipid Nanoparticles (SLN & NLC): Present State of Development & Industrial Applications. *Curr. Drug Discov. Technol.* **2011**, *8* (3), 207–227. https://doi.org/10.2174/157016311796799062.

(81) Soni, K.; Kukereja, B. K.; Kapur, M.; Kohli, K. Lipid Nanoparticles: Future of Oral Drug Delivery and Their Current Trends and Regulatory Issues. *Int. J. Curr. Pharm. Rev. Res.* **2016**, *7* (1), 1–18.

(82) Selvamuthukumar, S.; Velmurugan, R. Nanostructured Lipid Carriers: A Potential Drug Carrier for Cancer Chemotherapy. *Lipids Health Dis.* **2012**, *11* (1), 1–8. https://doi.org/10.1186/1476-511X-11-159.

(83) Fang, C.-L.; A. Al-Suwayeh, S.; Fang, J.-Y. Nanostructured Lipid Carriers (NLCs) for Drug Delivery and Targeting. *Recent Pat. Nanotechnol.* **2013**, *7* (1), 41–55. https://doi.org/10.2174/1872210511307010041.

(84) Banerjee, S.; Kundu, A. Lipid-Drug Conjugates: A Potential Nanocarrier System for Oral Drug Delivery Applications. *DARU, J. Pharm. Sci.* **2018**, *26* (1), 65–75. https://doi.org/10.1007/s40199-018-0209-1.

(85) Irby, D.; Du, C.; Li, F. Lipid-Drug Conjugate for Enhancing Drug Delivery. *Mol. Pharm.* **2017**, *14* (5), 1325–1338. https://doi.org/10.1021/acs.molpharmaceut.6b01027.

(86) Li, F.; Snow-Davis, C.; Du, C.; Bondarev, M. L.; Saulsbury, M. D.; Heyliger, S. O.

Preparation and Characterization of Lipophilic Doxorubicin Pro-Drug Micelles. *J. Vis. Exp.* **2016**, *2016* (114), 1–8. https://doi.org/10.3791/54338.

(87) Shao, W.; Paul, A.; Zhao, B.; Lee, C.; Rodes, L.; Prakash, S. Carbon Nanotube Lipid Drug Approach for Targeted Delivery of a Chemotherapy Drug in a Human Breast Cancer Xenograft Animal Model. *Biomaterials* **2013**, *34* (38), 10109–10119. https://doi.org/10.1016/j.biomaterials.2013.09.007.

(88) Sun, B.; Luo, C.; Li, L.; Wang, M.; Du, Y.; Di, D.; Zhang, D.; Ren, G.; Pan, X.; Fu, Q.; Sun, J.; He, Z. Core-Matched Encapsulation of an Oleate Prodrug into Nanostructured Lipid Carriers with High Drug Loading Capability to Facilitate the Oral Delivery of Docetaxel. *Colloids Surfaces B Biointerfaces* **2016**, *143*, 47–55. https://doi.org/10.1016/j.colsurfb.2016.02.065.

(89) Winau, F.; Westphal, O.; Winau, R. Paul Ehrlich - In Search of the Magic Bullet. *Microbes Infect.* **2004**, *6* (8), 786–789. https://doi.org/10.1016/j.micinf.2004.04.003.

(90) Danhier, F.; Feron, O.; Préat, V. To Exploit the Tumor Microenvironment: Passive and Active Tumor Targeting of Nanocarriers for Anti-Cancer Drug Delivery. *J. Control. Release* **2010**, *148* (2), 135–146. https://doi.org/10.1016/j.jconrel.2010.08.027.

(91) Haley, B.; Frenkel, E. Nanoparticles for Drug Delivery in Cancer Treatment. *Urol. Oncol. Semin. Orig. Investig.* **2008**, *26* (1), 57–64. https://doi.org/10.1016/j.urolonc.2007.03.015.

(92) Maeda, H.; Wu, J.; Sawa, T.; Matsumura, Y.; Hori, K. Tumor Vascular Permeability and the EPR Effect in Macromolecular Therapeutics: A Review. *J. Control. Release* **2000**, *65* (1–2), 271–284. https://doi.org/10.1016/S0168-3659(99)00248-5.

(93) Matsumura, Y.; Maeda, H. A New Concept for Macromolecular Therapeutics in Cancer Chemotherapy: Mechanism of Tumoritropic Accumulation of Proteins and the Antitumor Agent Smancs. *Cancer Res.* **1986**, *46* (12 Part 1), 6387–6392.

(94) Chrastina, A.; Massey, K. A.; Schnitzer, J. E. Overcoming in Vivo Barriers to Targeted Nanodelivery. *Wiley Interdiscip. Rev. Nanomedicine Nanobiotechnology* **2011**, *3* (4), 421–437. https://doi.org/10.1002/wnan.143.

(95) Kobayashi, H.; Watanabe, R.; Choyke, P. L. Improving Conventional Enhanced Permeability and Retention (EPR) Effects; What Is the Appropriate Target? *Theranostics* **2014**, *4* (1), 81–89. https://doi.org/10.7150/thno.7193.

(96) Maeda, H.; Bharate, G. Y.; Daruwalla, J. Polymeric Drugs for Efficient Tumor-Targeted Drug Delivery Based on EPR-Effect. *Eur. J. Pharm. Biopharm.* **2009**, *71* (3), 409–419. https://doi.org/10.1016/j.ejpb.2008.11.010.

(97) Maeda, H.; Sawa, T.; Konno, T. Mechanism of Tumor-Targeted Delivery of Macromolecular Drugs, Including the EPR Effect in Solid Tumor and Clinical Overview of the Prototype Polymeric Drug SMANCS. *J. Control. Release* **2001**, *74* (1–3), 47–61. https://doi.org/10.1016/S0168-3659(01)00309-1.

(98) Unezaki, S.; Maruyama, K.; Hosoda, J. I.; Nagae, I.; Koyanagi, Y.; Nakata, M.; Ishida, O.; Iwatsuru, M.; Tsuchiya, S. Direct Measurement of the Extravasation of Polyethyleneglycol-Coated Liposomes into Solid Tumor Tissue by in Vivo Fluorescence Microscopy. *Int. J. Pharm.* **1996**, *144* (1), 11–17. https://doi.org/10.1016/S0378-5173(96)04674-1.

(99) Iyer, A. K.; Khaled, G.; Fang, J.; Maeda, H. Exploiting the Enhanced Permeability and Retention Effect for Tumor Targeting. *Drug Discov. Today* **2006**, *11* (17–18), 812–818. https://doi.org/10.1016/j.drudis.2006.07.005.

(100) Fang, J.; Nakamura, H.; Maeda, H. The EPR Effect: Unique Features of Tumor Blood Vessels for Drug Delivery, Factors Involved, and Limitations and Augmentation of the Effect. *Adv. Drug Deliv. Rev.* **2011**, *63* (3), 136–151. https://doi.org/10.1016/j.addr.2010.04.009.

(101) Gullotti, E.; Yeo, Y. Extracellularly Activated Nanocarriers: A New Paradigm of Tumor Targeted Drug Delivery. *Mol. Pharm.* **2009**, *6* (4), 1041–1051. https://doi.org/10.1021/mp900090z.

(102) Bae, Y. H. Drug Targeting and Tumor Heterogeneity. *J. Control. Release* **2009**, *133* (1), 2–3. https://doi.org/10.1016/j.jconrel.2008.09.074.

(103) Heldin, C. H.; Rubin, K.; Pietras, K.; Östman, A. High Interstitial Fluid Pressure - An Obstacle in Cancer Therapy. *Nat. Rev. Cancer* **2004**, *4* (10), 806–813. https://doi.org/10.1038/nrc1456.

(104) Pirollo, K. F.; Chang, E. H. Does a Targeting Ligand Influence Nanoparticle Tumor Localization or Uptake? *Trends Biotechnol.* **2008**, *26* (10), 552–558. https://doi.org/10.1016/j.tibtech.2008.06.007.

(105) Lee, H.; Fonge, H.; Hoang, B.; Reilly, R. M.; Allen, C. The Effects of Particle Size and Molecular Targeting on the Intratumoral and Subcellular Distribution of Polymeric Nanoparticles. *Mol. Pharm.* **2010**, *7* (4), 1195–1208. https://doi.org/10.1021/mp100038h.

(106) Torchilin, V. P. *Passive and Active Drug Targeting: Drug Delivery to Tumors as an Example*; 2010; Vol. 197. https://doi.org/10.1007/978-3-642-00477-3_1.

(107) Leserman, L. D.; Barbet, J.; Kourilsky, F.; Weinstein, J. N. Targeting to Cells of

Fluorescent Liposomes Covalently Coupled with Monoclonal Antibody or Protein A. *Nature* **1980**, *288* (5791), 602–604. https://doi.org/10.1038/288602a0.

(108) Pérez-Herrero, E.; Fernández-Medarde, A. Advanced Targeted Therapies in Cancer: Drug Nanocarriers, the Future of Chemotherapy. *Eur. J. Pharm. Biopharm.* **2015**, *93*, 52–79. https://doi.org/10.1016/j.ejpb.2015.03.018.

(109) Allen, T. M. Ligand-Targeted Therapeutics in Anticancer Therapy. *Nat. Rev. Cancer* **2002**, *2* (10), 750–763. https://doi.org/10.1038/nrc903.

(110) Sun, T.; Zhang, Y. S.; Pang, B.; Hyun, D. C.; Yang, M.; Xia, Y. Engineered Nanoparticles for Drug Delivery in Cancer Therapy. *Angew. Chemie - Int. Ed.* **2014**, *53* (46), 12320–12364. https://doi.org/10.1002/anie.201403036.

(111) Sikorski, A. F.; Toporkiewicz, M.; Meissner, J.; Matusewicz, L.; Czogalla, A. Toward a Magic or Imaginary Bullet? Ligands for Drug Targeting to Cancer Cells: Principles, Hopes, and Challenges. *Int. J. Nanomedicine* **2015**, 1316–1399.

(112) Kirpotin, D. B.; Drummond, D. C.; Shao, Y.; Shalaby, M. R.; Hong, K.; Nielsen, U. B.; Marks, J. D.; Benz, C. C.; Park, J. W. Antibody Targeting of Long-Circulating Lipidic Nanoparticles Does Not Increase Tumor Localization but Does Increase Internalization in Animal Models. *Cancer Res.* **2006**, *66* (13), 6732–6740. https://doi.org/10.1158/0008-5472.CAN-05-4199.

(113) Pastorino, F.; Brignole, C.; Di Paolo, D.; Nico, B.; Pezzolo, A.; Marimpietri, D.; Pagnan, G.; Piccardi, F.; Cilli, M.; Longhi, R.; Ribatti, D.; Corti, A.; Allen, T. M.; Ponzoni, M. Targeting Liposomal Chemotherapy via Both Tumor Cell-Specific and Tumor Vasculature-Specific Ligands Potentiates Therapeutic Efficacy. *Cancer Res.* **2006**, *66* (20), 10073–10082. https://doi.org/10.1158/0008-5472.CAN-06-2117.

(114) de Jong, G.; van Dijk, J. P.; van Eijk, H. G. The Biology of Transferrin. *Clin. Chim. Acta* **1990**, *190* (1–2), 1–46. https://doi.org/10.1016/0009-8981(90)90278-Z.

(115) Ponka, P.; Lok, C. N. The Transferrin Receptor: Role in Health and Disease. *Int. J. Biochem. Cell Biol.* **1999**, *31* (10), 1111–1137. https://doi.org/10.1016/S1357-2725(99)00070-9.

(116) Daniels, T. R.; Delgado, T.; Helguera, G.; Penichet, M. L. The Transferrin Receptor Part II: Targeted Delivery of Therapeutic Agents into Cancer Cells. *Clin. Immunol.* **2006**, *121* (2), 159–176. https://doi.org/10.1016/j.clim.2006.06.006.

(117) Sudimack, J.; Lee, R. J. Targeted Drug Delivery via the Folate Receptor. *Adv. Drug Deliv. Rev.* **2000**, *41* (2), 147–162. https://doi.org/10.1016/S0169-409X(99)00062-9.

(118) Reynolds, E. Vitamin B12, Folic Acid, and the Nervous System. *Lancet Neurol.* **2006**,

5 (11), 949–960. https://doi.org/10.1016/S1474-4422(06)70598-1.

(119) Low, P. S.; Kularatne, S. A. Folate-Targeted Therapeutic and Imaging Agents for Cancer. *Curr. Opin. Chem. Biol.* **2009**, *13* (3), 256–262. https://doi.org/10.1016/j.cbpa.2009.03.022.

(120) Ghazarian, H.; Idoni, B.; Oppenheimer, S. B. A Glycobiology Review: Carbohydrates, Lectins and Implications in Cancer Therapeutics. *Acta Histochem.* **2011**, *113* (3), 236–247. https://doi.org/10.1016/j.acthis.2010.02.004.

(121) Bies, C.; Lehr, C. M.; Woodley, J. F. Lectin-Mediated Drug Targeting: History and Applications. *Adv. Drug Deliv. Rev.* **2004**, *56* (4), 425–435. https://doi.org/10.1016/j.addr.2003.10.030.

(122) Minko, T. Drug Targeting to the Colon with Lectins and Neoglycoconjugates. *Adv. Drug Deliv. Rev.* **2004**, *56* (4), 491–509. https://doi.org/10.1016/j.addr.2003.10.017.

(123) Jorissen, R. N.; Walker, F.; Pouliot, N.; Garrett, T. P. J.; Ward, C. W.; Burgess, A. W. Epidermal Growth Factor Receptor: Mechanisms of Activation and Signalling. In *The EGF Receptor Family*; Carpenter, G., Ed.; Academic Press: Burlington, 2003; pp 33–55. https://doi.org/https://doi.org/10.1016/B978-012160281-9/50004-9.

(124) Normanno, N.; De Luca, A.; Bianco, C.; Strizzi, L.; Mancino, M.; Maiello, M. R.; Carotenuto, A.; De Feo, G.; Caponigro, F.; Salomon, D. S. Epidermal Growth Factor Receptor (EGFR) Signaling in Cancer. *Gene* **2006**, *366* (1), 2–16. https://doi.org/10.1016/j.gene.2005.10.018.

(125) Acharya, S.; Dilnawaz, F.; Sahoo, S. K. Targeted Epidermal Growth Factor Receptor Nanoparticle Bioconjugates for Breast Cancer Therapy. *Biomaterials* **2009**, *30* (29), 5737–5750. https://doi.org/10.1016/j.biomaterials.2009.07.008.

(126) Scaltriti, M.; Baselga, J. The Epidermal Growth Factor Receptor Pathway: A Model for Targeted Therapy. *Clin. Cancer Res.* **2006**, *12* (18), 5268–5272. https://doi.org/10.1158/1078-0432.CCR-05-1554.

(127) Lurje, G.; Lenz, H. J. EGFR Signaling and Drug Discovery. *Oncology* **2010**, *77* (6), 400–410. https://doi.org/10.1159/000279388.

(128) Van Vlerken, L. E.; Duan, Z.; Seiden, M. V.; Amiji, M. M. Modulation of Intracellular Ceramide Using Polymeric Nanoparticles to Overcome Multidrug Resistance in Cancer. *Cancer Res.* **2007**, *67* (10), 4843–4850. https://doi.org/10.1158/0008-5472.CAN-06-1648.

(129) Bertrand, N.; Wu, J.; Xu, X.; Kamaly, N.; Farokhzad, O. C. Cancer Nanotechnology: The Impact of Passive and Active Targeting in the Era of Modern Cancer Biology.

Adv. Drug Deliv. Rev. **2014**, *66*, 2–25. https://doi.org/10.1016/j.addr.2013.11.009.

(130) Cheng, Z.; Al Zaki, A.; Hui, J. Z.; Muzykantov, V. R.; Tsourkas, A. Multifunctional Nanoparticles: Cost versus Benefit of Adding Targeting and Imaging Capabilities. *Science (80-.).* **2012**, *338* (6109), 903–910. https://doi.org/10.1126/science.1226338.

(131) Mura, S.; Nicolas, J.; Couvreur, P. Stimuli-Responsive Nanocarriers for Drug Delivery. *Nat. Mater.* **2013**, *12*, 991–1103.

(132) Ganta, S.; Devalapally, H.; Shahiwala, A.; Amiji, M. A Review of Stimuli-Responsive Nanocarriers for Drug and Gene Delivery. *J. Control. Release* **2008**, *126* (3), 187–204. https://doi.org/10.1016/j.jconrel.2007.12.017.

(133) Theato, P.; Sumerlin, B. S.; O'reilly, R. K.; Epp, T. H. Stimuli Responsive Materials. *Chem. Soc. Rev.* **2013**, *42* (17), 7055–7056. https://doi.org/10.1039/c3cs90057f.

(134) Hu, X.; Zhang, Y.; Xie, Z.; Jing, X.; Bellotti, A.; Gu, Z. Stimuli-Responsive Polymersomes for Biomedical Applications. *Biomacromolecules* **2017**, acs.biomac.6b01704. https://doi.org/10.1021/acs.biomac.6b01704.

(135) Torchilin, V. Multifunctional and Stimuli-Sensitive Pharmaceutical Nanocarriers. *Eur. J. Pharm. Biopharm.* **2009**, *71* (3), 431–444. https://doi.org/10.1016/j.ejpb.2008.09.026.

(136) Field, S. B.; Bleehen, N. M. Hyperthermia in the Treatment of Cancer. *Cancer Treat. Rev.* **1979**, *6*, 63–94. https://doi.org/10.5694/j.1326-5377.1990.tb120944.x.

(137) Bordat, A.; Boissenot, T.; Nicolas, J.; Tsapis, N. Thermoresponsive Polymer Nanocarriers for Biomedical Applications. *Adv. Drug Deliv. Rev.* **2019**, *138*, 167–192. https://doi.org/https://doi.org/10.1016/j.addr.2018.10.005.

(138) Kono, K.; Yoshino, K.; Takagishi, T. Effect of Poly(Ethylene Glycol) Grafts on Temperature-Sensitivity of Thermosensitive Polymer-Modified Liposomes. *J. Control. Release* **2002**, *80* (1–3), 321–332. https://doi.org/10.1016/S0168-3659(02)00018-4.

(139) Wu, F.; Wang, Z. B.; Cao, Y. De; Xu, Z. L.; Zhou, Q.; Zhu, H.; Chen, W. Z. Heat Fixation of Cancer Cells Ablated with High-Intensity-Focused Ultrasound in Patients with Breast Cancer. *Am. J. Surg.* **2006**, *192* (2), 179–184. https://doi.org/10.1016/j.amjsurg.2006.03.014.

(140) Schroeder, A.; Kost, J.; Barenholz, Y. Ultrasound, Liposomes, and Drug Delivery: Principles for Using Ultrasound to Control the Release of Drugs from Liposomes. *Chem. Phys. Lipids* **2009**, *162* (1–2), 1–16. https://doi.org/10.1016/j.chemphyslip.2009.08.003.

(141) Neuberger, T.; Schöpf, B.; Hofmann, H.; Hofmann, M.; Von Rechenberg, B. Superparamagnetic Nanoparticles for Biomedical Applications: Possibilities and Limitations of a New Drug Delivery System. *J. Magn. Magn. Mater.* **2005**, *293* (1), 483–496. https://doi.org/10.1016/j.jmmm.2005.01.064.

(142) Veiseh, O.; Gunn, J. W.; Zhang, M. Design and Fabrication of Magnetic Nanoparticles for Targeted Drug Delivery and Imaging. *Adv. Drug Deliv. Rev.* **2010**, *62* (3), 284–304. https://doi.org/10.1016/j.addr.2009.11.002.

(143) Mahmoudi, M.; Sant, S.; Wang, B.; Laurent, S.; Sen, T. Superparamagnetic Iron Oxide Nanoparticles (SPIONs): Development, Surface Modification and Applications in Chemotherapy. *Adv. Drug Deliv. Rev.* **2011**, *63* (1–2), 24–46. https://doi.org/10.1016/j.addr.2010.05.006.

(144) McBain, S. C.; Yiu, H. H. P.; Dobson, J. Magnetic Nanoparticles for Gene and Drug Delivery. *Int. J. Nanomedicine* **2008**, *3* (2), 169–180. https://doi.org/10.2147/ijn.s1608.

(145) Wilson, M. W.; Kerlan, R. K.; Fidelman, N. A.; Venook, A. P.; LaBerge, J. M.; Koda, J.; Gordon, R. L. Hepatocellular Carcinoma: Regional Therapy with a Magnetic Targeted Carrier Bound to Doxorubicin in a Dual MR Imaging/ Conventional Angiography Suite-Initial Experience with Four Patients. *Radiology* **2004**, *230* (1), 287–293. https://doi.org/10.1148/radiol.2301021493.

(146) Hilger, I.; Hiergeist, R.; Hergt, R.; Winnefeld, K.; Schubert, H.; Kaiser, W. A. Thermal Ablation of Tumors Using Magnetic Nanoparticles: An in Vivo Feasibility Study. *Invest. Radiol.* **2002**, *37* (10), 580–586. https://doi.org/10.1097/00004424-200210000-00008.

(147) Bertrand, O.; Gohy, J. F. Photo-Responsive Polymers: Synthesis and Applications. *Polym. Chem.* **2017**, *8* (1), 52–73. https://doi.org/10.1039/c6py01082b.

(148) Ghosh, S.; Yesilyurt, E.; Savariar, K.; Irvin, S.; Thayumanavan, S. Redox, Ionic Strength, and PH Sensitive Supramolecular Polymer Assemblies. *J. Polym. Sci. Part A Polym. Chem.* **2009**, *47*, 1052–1060. https://doi.org/10.1002/pola.

(149) Goodwin, A. P.; Mynar, J. L.; Yingzhong, M.; Fleming, G. R.; Fréchet, J. M. J. Synthetic Micelle Sensitive to IR Light via a Two-Photon Process. *J. Am. Chem. Soc.* **2005**, *127*, 9952–9953.

(150) Jiang, J.; Tong, X.; Morris, D.; Zhao, Y. Toward Photocontrolled Release Using Light-Dissociable Block Copolymer Micelles. *Macromolecules* **2006**, *39* (13), 4633–4640. https://doi.org/10.1021/ma060142z.

(151) Schmaljohann, D. Thermo- and PH-Responsive Polymers in Drug Delivery. *Adv.*

Drug Deliv. Rev. **2006**, *58* (15), 1655–1670. https://doi.org/10.1016/j.addr.2006.09.020.

(152) Vaupel, P.; Kallinowski, F.; Okunieff, P. Blood Flow, Oxygen and Nutrient Supply, and Metabolic Microenvironment of Human Tumors: A Review. *Cancer Res.* **1989**, *49*, 6449–6465.

(153) Rofstad, E. K.; Mathiesen, B.; Kindem, K.; Galappathi, K. Acidic Extracellular PH Promotes Experimental Metastasis of Human Melanoma Cells in Athymic Nude Mice. *Cancer Res.* **2006**, *66* (13), 6699–6707. https://doi.org/10.1158/0008-5472.CAN-06-0983.

(154) Grabe, M.; Oster, G. Regulation of Organelle Acidity. *J. Gen. Physiol.* **2001**, *117* (4), 329–344. https://doi.org/10.1085/jgp.117.4.329.

(155) Gerweck, L. E.; Seetharaman, K. Cellular PH Gradient in Tumor versus Normal Tissue: Potential Exploitation for the Treatment of Cancer. *Cancer Res.* **1996**, *56* (6), 1194–1198.

(156) Manchun, S.; Dass, C. R.; Sriamornsak, P. Targeted Therapy for Cancer Using PH-Responsive Nanocarrier Systems. *Life Sci.* **2012**, *90* (11–12), 381–387. https://doi.org/10.1016/j.lfs.2012.01.008.

(157) Rodrigues, P. C. A.; Beyer, U.; Schumacher, P.; Roth, T.; Fiebig, H. H.; Unger, C.; Messori, L.; Orioli, P.; Paper, D. H.; Mülhaupt, R.; Kratz, F. Acid-Sensitive Polyethylene Glycol Conjugates of Doxorubicin: Preparation, in Vitro Efficacy and Intracellular Distribution. *Bioorganic Med. Chem.* **1999**, *7* (11), 2517–2524. https://doi.org/10.1016/S0968-0896(99)00209-6.

(158) Kanamala, M.; Wilson, W. R.; Yang, M.; Palmer, B. D.; Wu, Z. Mechanisms and Biomaterials in PH-Responsive Tumour Targeted Drug Delivery: A Review. *Biomaterials* **2016**, *85*, 152–167. https://doi.org/10.1016/j.biomaterials.2016.01.061.

(159) Schellmann, N.; Deckert, P. M.; Bachran, D.; Fuchs, H.; Bachran, C. Targeted Enzyme Prodrug Therapies. *Mini-Reviews Med. Chem.* **2010**, *10* (10), 887–904. https://doi.org/10.2174/138955710792007196.

(160) Roy, D.; Cambre, J. N.; Sumerlin, B. S. Future Perspectives and Recent Advances in Stimuli-Responsive Materials. *Prog. Polym. Sci.* **2010**, *35* (1–2), 278–301. https://doi.org/10.1016/j.progpolymsci.2009.10.008.

(161) Zhang, P.; Wu, J.; Xiao, F.; Zhao, D.; Luan, Y. Disulfide Bond Based Polymeric Drug Carriers for Cancer Chemotherapy and Relevant Redox Environments in Mammals. *Med. Res. Rev.* **2018**, *38* (5), 1485–1510. https://doi.org/10.1002/med.21485.

(162) Huo, M.; Yuan, J.; Tao, L.; Wei, Y. Redox-Responsive Polymers for Drug Delivery:

From Molecular Design to Applications. *Polym. Chem.* **2014**, *5* (5), 1519–1528. https://doi.org/10.1039/c3py01192e.

(163) Liu, G.; Zhou, L.; Guan, Y.; Su, Y.; Dong, C. M. Multi-Responsive Polypeptidosome: Characterization, Morphology Transformation, and Triggered Drug Delivery. *Macromol. Rapid Commun.* **2014**, *35* (19), 1673–1678. https://doi.org/10.1002/marc.201400343.

(164) Meng, F. H.; Zhong, Z. Y.; Feijen, J. Stimuli-Responsive Polymersomes for Programmed Drug Delivery. *Biomacromolecules* **2009**, *10* (2), 197–209. https://doi.org/10.1021/bm801127d.

(165) McCarley, R. L. Redox-Responsive Delivery Systems. *Annu. Rev. Anal. Chem.* **2012**, *5*, 391–411. https://doi.org/10.1146/annurev-anchem-062011-143157.

(166) Liang, J.; Liu, B. ROS-Responsive Drug Delivery Systems. *Bioeng. Transl. Med.* **2016**, *1* (3), 239–251. https://doi.org/10.1002/btm2.10014.

(167) Lee, S. H.; Gupta, M. K.; Bang, J. B.; Bae, H.; Sung, H. J. Current Progress in Reactive Oxygen Species (ROS)-Responsive Materials for Biomedical Applications. *Adv. Healthc. Mater.* **2013**, *2* (6), 908–915. https://doi.org/10.1002/adhm.201200423.

(168) Sowers, M. A.; Mccombs, J. R.; Wang, Y.; Paletta, J. T.; Morton, S. W.; Dreaden, E. C.; Boska, M. D.; Francesca Ottaviani, M.; Hammond, P. T.; Rajca, A.; Johnson, J. A. Redox-Responsive Branched-Bottlebrush Polymers for in Vivo MRI and Fluorescence Imaging. *Nat. Commun.* **2014**, *5* (May), 1–9. https://doi.org/10.1038/ncomms6460.

2 pH-responsive Polyether Lipids

2.1 Design of pH-Degradable Cholesterol-based Polyether Lipids for the Conjugation of Small Molecules

Eyleen Becker,[†] [redacted],[†] [redacted]*,[†]

[†]Department of Chemistry, Johannes Gutenberg University Mainz, Duesbergweg 10-14, 55128 Mainz, Germany

*E-Mail: [redacted]

to be submitted

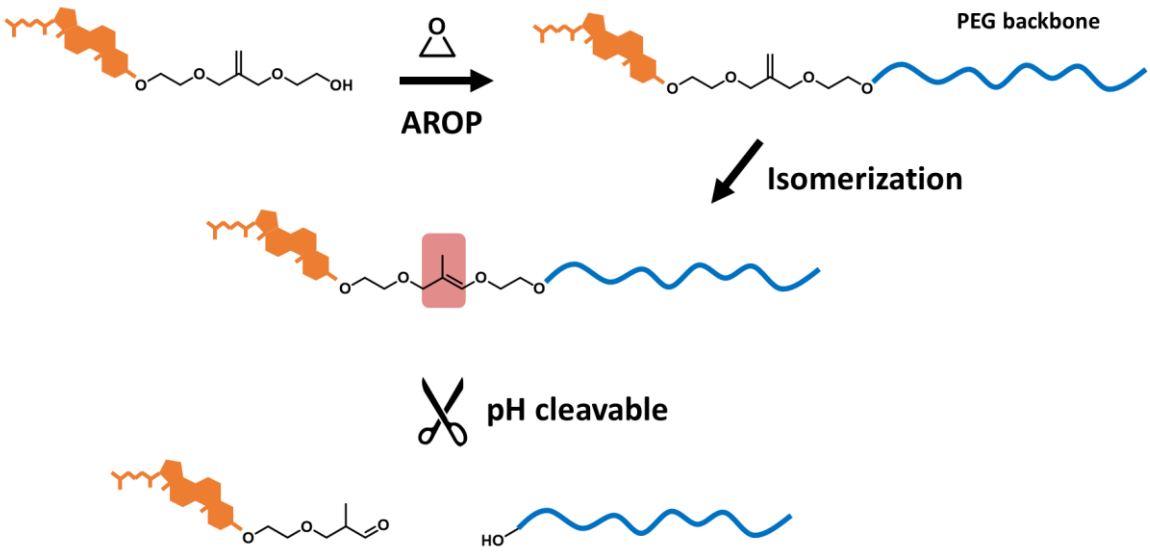

Abstract

Polyether-based lipids can be used in many ways as drug delivery systems, for example in liposomal formulations but also for the direct conjugation of small molecules. Due to the stealth effect of the polyether moiety and the mediated binding to albumin or other serum molecules, polyether lipids offer a promising opportunity to modify the pharmacokinetic profile of these small molecules. To prevent unwanted binding of the conjugates with hydrophobic pockets of serum proteins or phospholipid membranes, a pH-responsive cleavage site between the hydrophobic lipid anchor and the polymer chain may be of interest. In this work, we present the synthesis of a cholesterol-based initiator for the preparation of pH-responsive polyether lipids *via* anionic ring-opening polymerization (AROP) of ethylene oxide.

2.1.1 Introduction

Amphiphilic polymer lipids are widely used in different biomedical and therapeutic applications. Poly(ethylene glycol) (PEG) is the most prominent example in polymer materials for biomedical applications and is used as the hydrophilic part of the polymeric lipid due to its special properties like water solubility, biocompatibility and low toxicity.[1–3] Polyether-based polymer lipids are attractive drug carriers for small molecules, because they strongly alter the pharmacokinetic properties or improve the solubility.[4] Small molecules exhibit a fast deposition and renal clearance, whereas binding to a polymer lipid can prolong the blood circulation by a multiple time. The hydrophobic part induces the binding to serum proteins with hydrophobic pockets, such as albumin, whereas the hydrophilic part induces the stealth effect of PEGylated systems.[4–7] Due to albumin binding and an increased accumulation of albumin in the cancer milieu, the intravenous administration of the polymeric lipid-drug can result in a higher tumor accumulation *via* enhanced permeability and retention (EPR) effect.[8] Enrichment enables a drug depot in the tumor tissue for sustained release of the drug. With an optimal adjustment of the amphiphilic structure and a balanced water solubility, the lymphatic albumin flow can be interrupted and the active substance can accumulate in the lymphoid tissue.[9,10] The accumulation in lymphoid tissue is of great interest with regard to vaccination and immunotherapy. Various approaches developed from this realization. For example, the Irvin group dealt with the effect of semi macromolecular drugs based on oligonucleotides and peptides.[11] In contrast, the group of De Geest *et al.* investigated the immune-modulatory of small molecule agonists of Toll like receptor 7.[12] Recent publications by the group of De Geest and Schotsaert *et al.* dealt with the effect of a lipid amphiphile consisting of an imidazoquinoline conjugated to the chain end of a cholesterol-poly(ethylene glycol) macromolecule against the coronavirus 2 (SARS-CoV-2).[13] In most cases, the drug is directly attached to the amphiphilic polymer lipid. By incorporating a degradable site between the hydrophobic lipid and the hydrophilic polymer chain, entirely new properties and the resulting application possibilities can be generated. For example, the accessibility of the drug may be limited by the anchoring of the lipid motif to the endosomal phospholipid membrane. This may lead to reduced receptor interaction or activation of metabolic enzymes.[14]

In this work, the synthesis of a novel cholesterol-based, pH-responsive polyether lipid is presented. Among the many possibilities to introduce a cleavage site in the PEG backbone, vinyl ethers are the most promising functional group to achieve this goal. Vinyl ether-containing PEG polymers are characterized by rapid hydrolysis kinetics at a pH around 5, but have excellent stability at pH 7.4 as well as under dry storage conditions.[15,16] Adequate stability is not only a requirement for good storage but also for the handling and application-specific chemical modification of the materials. Furthermore, premature cleavage of the polymer backbone, for example on the way to the targeted tissue or cell compartment, should be prevented. Therefore, the time frame, controlled by the specific stimulus, is crucial for the successful use of pH-responsive polymers. The unique combination of moderate stability and fast hydrolysis kinetics at physiologically relevant pH values make vinyl ether-containing PEGs to promising candidates for various biomedical applications. Cholesterol was chosen for the hydrophobic part in the amphiphilic polymer. Conjugates of cholesterol are known for their spontaneous anchoring in the cell membrane and their albumin-binding properties.[17,18]

2.1.2 Experimental part

Terminology

The allyl ether based diol is named 2,2'-((2-methylenepropane-1,3-diyl)bis(oxy))bis(ethan-1-ol) (MBE) and after protection of one hydroxyl group with 3,4-dihydropyran (DHP) it is named 2-((2-((2-((tetrahydro-2H-pyran-2-yl)oxy)ethoxy)methyl)allyl)oxy)ethan-1-ol (THP-MBE). The protected MBE was transformed in the tosylated product with the synonym 2-((2-((2-((tetrahydro-2H-pyran-2-yl)oxy)ethoxy)methyl)allyl)oxy)ethyl 4-methylbenzenesulfonate (THP-MBE-Ts). The reaction of cholesterol and THP-MBE-Ts leads to cholesteryl-MBE-THP (Chol-MBE-THP) and after cleavage of the protecting group under acidic conditions to the initiator cholesteryl-MBE-OH (Chol-MBE-OH). The amphiphilic polymer lipid based on the initiator is called cholesteryl-MBE-Poly(ethylene glycol) (Chol-MBE-PEG) and after the isomerization cholesteryl-*iso*MBE-Poly(ethylene glycol) (Chol-*iso*MBE-PEG). The comparison structures without cleavage site are called cholesteryl-Poly(ethylene glycol) (Chol-PEG).

Instrumentation

^{1}H NMR (300 MHz), ^{13}C NMR (75 MHz) and 2D spectra were recorded on a Bruker Avance III HD 300 (5 mm BBFO-Probe with z-Gradient and ATM). ^{1}H NMR (400 MHz), ^{13}C NMR (100 MHz) and 2D spectra were measured on a Bruker Avance II 400 MHz (5 mm BBFO-Probe Z-gradient and ATM, SampleXPress 60 auto sampler). The chemical shifts were internally referred to residual proton signals of the deuterated solvent.

Size exclusion chromatography (SEC) was performed at 50 °C in *N,N*-dimethylformamide (with 1 g/L lithium bromide added) as eluent on an Agilent 1,100 Series equipped with Polymer Standards Service (PSS) HEMA columns with 300/100/40 Å porosity and a RI detector. The determination of the molecular weights was determined by a calibration with poly(ethylene glycol) standards by PSS.

Differential scanning calorimetry (DSC) measurements were carried out under a nitrogen atmosphere using a Perkin Elmer DSC 8,500 in the temperature range of -95 °C to 100 °C, with heating rates of 20 °C/min for the first and 10 °C/min for the second heating run.

MALDI-ToF MS measurements were performed on a Shimadzu Axima CFR MALDI-ToF or a Bruker Rapiflex. Samples were prepared trans-2-[3-(4-tert-Butylphenyl)-2-methyl-2-propenylidene]malononitrile (DCTB) as a matrix and potassium trifluoroacetate as a cationization agent.

Materials

All solvents and reagents were purchased generally from the suppliers Acros Organics, Tokyo Chemical Industry (TCI), Sigma-Aldrich, Fluka, Fisher Scientific, Alfa Aesar and were used as received unless otherwise stated. Deuterated solvents were purchased from Deutero GmbH. Dialysis membranes (regenerated cellulose, MWCO = 1000 g/mol) were purchased from Orange Scientific.

Synthesis procedure

Synthesis of 2,2'-((2-methylenepropane-1,3-diyl)bis(oxy))bis(ethan-1-ol) (MBE)

The synthesis of MBE was carried out in a slightly modified form according to literature.[19]

Ethylene glycol (200 mL) was slowly added under argon atmosphere to a suspension of sodium hydride (10.08 g, 0.42 mol, 2.1 eq.) in dry THF (200 mL). The resulting mixture was stirred at room temperature for 30 minutes. Subsequently, 3-chloro-2-(chloromethyl)prop-1-ene (25.00 g, 0.20 mol, 1 eq.) was added slowly, and the mixture was refluxed for 24 hours. THF and excess of ethylene glycol were removed under reduced pressure, and the residue was treated with ethanol (150 mL). After filtration of the solid and evaporation of the ethanol, the product was obtained by distillation (b.p.=130 °C, 0.001 mbar) as a colorless oil (yield: 11.06 g, 0.06 mol, 30 %).

^{1}H NMR (300 MHz, chloroform-*d*) δ [ppm] = 5.20 (s, 2H, H_2C=C), 4.08 (s, 4H, CH_2OH), 3.76 – 3.70 (m, 4H, H_2C=(C-$CH_2O)_2$), 3.59 – 3.51 (m, 4H, CH_2O).

^{13}C NMR (75 MHz, chloroform-*d*) δ [ppm] = 142.41 (1C, H_2C=*C*), 115.94 (1C, H_2C=C), 72.31 (2C, H_2C=(C-$CH_2O)_2$), 71.63 (2C, CH_2-O-CH_2), 61.83 (2C, CH_2OH).

Synthesis of 2-((2-((2-((tetrahydro-2H-pyran-2-yl)oxy)ethoxy)methyl)allyl)oxy)ethan-1-ol (THP-MBE)

MBE (6.90 g, 39.18 mmol, 5.90 mL, 1 eq.) was dissolved in dichloromethane (80 mL), the solution was cooled to 0 °C and pyridinium *p*-toluenesulfonate (PPTS) (1.97 g, 7.84 mmol, 0.2 eq.) was added to the cooled solution. Subsequently, 3,4-dihydropyran (DHP) (3.30 g, 39.18 mmol, 3.58 mL, 1 eq.) was slowly added *via* syringe. After 1.5 hours the cooling mixture was removed and the reaction mixture was stirred for 3 hours at room temperature. To the solution saturated $NaHCO_3$ was added and the product was extracted from the aqueous solution with dichloromethane (3 x 20 mL). The organic layer was dried and evaporated under reduced pressure. The monofunctional product and bifunctional product were separated *via* column chromatography (ethyl acetate/cyclohexane 3:1, R_f (mono) = 0.43, R_f (bi) = 0.81). The monofunctional product THP-MBE was obtained as a colorless oil (yield: 3.28 g, 12.60 mmol, 32 %).

^{1}H NMR (300 MHz, DMSO-d_6) δ [ppm] = 5.18 – 5.07 (m, *J* = 1.1 Hz, 2H, H_2C=C), 4.64 – 4.53 (m, 2H, O-C*H*-O, -O*H*), 3.99 – 3.87 (m, 4H, H_2C=(C-$CH_2O)_2$), 3.80 – 3.64 (m, 2H, O-CH-O-CH_2), 3.57 – 3.29 (m, 8H, O-CH_2-CH_2-O), 1.80 – 1.33 (m, 6H, CH_2-CH_2-CH_2).

^{13}C NMR (75 MHz, DMSO-d_6) δ [ppm] = 143.29 (1C, H_2C=*C*), 112.53 (1C, H_2*C*=C), 97.94 (1C, O-*C*H-O), 71.60 (1C, O-CH-O-*C*H_2), 70.73 (2C, H_2C=(C-*C*$H_2O)_2$), 68.94 (1C, O-*C*H_2-CH_2-OH), 65.95 (1C, O-CH_2-*C*H_2-O), 61.12 (1C, O-CH_2-*C*H_2-OH), 60.19 (1C, O-CH-O-*C*H_2), 30.21 (1C, O-CH_2-CH_2-CH_2-*C*H_2), 25.03 (1C, O-CH_2-*C*H_2-CH_2-CH_2), 19.05 (1C, O-CH_2-CH_2-*C*H_2-CH_2).

Synthesis of 2-((2-((2-((tetrahydro-2H-pyran-2-yl)oxy)ethoxy)methyl)allyl)oxy)ethyl 4-methylbenzenesulfonate (THP-MBE-Ts)

The synthesis of THP-MBE-Ts was carried out in a modified form according to literature.[20]

Under argon atmosphere THP-MBE (5.16 g, 19.82 mmol, 1 eq.) and triethylamine (5 mL) were dissolved in dichloromethane (15 mL), the solution was cooled to 0 °C and *p*-toluenesulfonic acid chloride (3.78 g, 19.82 mmol, 1 eq.) was added. The mixture was stirred on ice for 20 hours. The solvent was removed under reduced pressure, the residue floated in diethyl ether and filtered off. The diethyl ether was removed, and the crude product was obtained as an orange liquid. The crude product was purified using column chromatography (cyclohexane/ethyl acetate 4:1) and the product was obtained as a viscous, colorless liquid (yield: 5.34 g, 12.88 mmol, 65 %).

^{1}H NMR (300 MHz, DMSO-d_6) δ [ppm] = 7.79 (d, *J* = 8.3 Hz, 2H, *H*$_{aromat}$), 7.48 (d, 2H, *J* = 8.0 Hz, *H*$_{aromat}$), 5.08 (d, 2H, *J* = 16.9 Hz, *H*$_2$C=C), 4.58 (s, 1H, O-C*H*-O), 4.21 – 4.08 (m, 2H, C*H*$_2$-Ts), 3.88 (d, *J* = 4.4 Hz, 4H, H_2C=(C-C*H*$_2O)_2$), 3.72 (q, *J* = 12.5, 11.9 Hz, 2H, O-CH-O-C*H*$_2$), 3.58 – 3.36 (m, 6H, O-C*H*$_2$-C*H*$_2$-O, O-C*H*$_2$-CH_2-Ts), 2.43 (s, 3H, C*H*$_3$), 1.81 – 1.42 (m, 6H, C*H*$_2$-C*H*$_2$-C*H*$_2$).

^{13}C NMR (75 MHz, DMSO-d_6) δ [ppm] = 145.38 (1C, SO_3-*C*), 143.15 (1C, H_2C=*C*), 132.89 (1C, *C*$_{aromat}$), 130.61 (1C, *C*$_{aromat}$), 128.07 (1C, *C*$_{aromat}$), 113.41 (1C, H_2*C*=C), 98.42 (1C, O-*C*H-O), 71.03 (1C, O-CH-O-*C*H_2), 70.42 (2C, H_2C=(C-*C*$H_2O)_2$), 69.40 (1C, O-*C*H_2-CH_2-Ts), 67.53 (1C, O-CH_2-*C*H_2-O), 66.40 (1C, O-CH_2-*C*H_2-Ts), 61.60 (1C, O-CH-O-*C*H_2), 30.67 (1C, O-CH_2-CH_2-CH_2-*C*H_2), 25.48 (1C, O-CH_2-*C*H_2-CH_2-CH_2), 21.55 (1C, *C*H_3), 19.51 (1C, O-CH_2-CH_2-*C*H_2-CH_2).

Synthesis of cholesteryl-MBE-THP (Chol-MBE-THP)

Dry dioxane (25 mL) was placed in a Schlenk flask and sodium hydride (0.23 g, 9.65 mmol, 1 eq.) was added under argon atmosphere. Cholesterol (4.10 g, 10.61 mmol, 1.1 eq.) was dissolved in dry dioxane (5 mL) and slowly added to the suspension *via* syringe. The solution was stirred for 1 h until no gas evolution could be detected. The reaction mixture was cooled to 0 °C, and the THP-MBE-Ts (4.00 g, 9.65 mmol, 1 eq.) was added *via* syringe. The solution was then heated to 110 °C for 48 hours under reflux. After the reaction time, dioxane was removed in vacuo. The residue was dissolved in ethyl acetate, the organic phase was extracted with $NaHCO_3$-solution, dried over $NaSO_4$ and the organic solvent was evaporated. The crude product was purified by column chromatography (cyclohexane/ethyl acetate 10:1), and the product was obtained as a viscous, colorless liquid (yield: 2.50 g, 3.97 mmol, 41 %).

^{1}H NMR (300 MHz, chloroform-*d*) δ [ppm] = 5.28 (d, *J* = 5.1 Hz, 1H, C*H*=C_{chol}), 5.14 (s, 2H, *H*$_2$C=C), 4.59 (t, *J* = 3.4 Hz, 1H, O-C*H*-O), 4.00 (s, 4H, H_2C=(C-C*H*$_2$O)$_2$), 3.87 – 3.74 (m, 2H, O-CH-O-C*H*$_2$), 3.63 – 3.39 (m, 8H, O-C*H*$_2$-C*H*$_2$-O), 3.20 – 3.06 (m, 1H, O-C*H*$_{chol}$), 2.34 (d, *J* = 4.4 Hz, 1H, O-CH-C*H*$_{2\ chol}$), 2.23 – 2.10 (m, 1H, O-CH-C*H*$_{2\ chol}$), 2.01 – 0.75 (m, 48H, cholesteryl, -C*H*$_2$-C*H*$_2$-C*H*$_2$-), 0.63 (s, 3H, C*H*$_{3\ chol}$).

^{13}C NMR (75 MHz, chloroform-*d*) δ [ppm] = 142.65 (1C, H_2C=*C*), 140.88 (1C, CH=*C*$_{chol}$), 121.49 (1C, *C*H=C_{chol}), 113.77 (1C, H_2*C*=C), 98.76 (1C, O-*C*H-O), 79.45 (1C, O-*C*H$_{chol}$), 71.79, 71.72 (2C, H_2C=(C-*C*$H_2O)_2$), 69.77, 69.37 (2C, O-CH_2-*C*H_2-O), 67.25 (1C, Chol-O-*C*H_2-CH_2-O), 66.53 (1C, O-CH_2-*C*H_2-O-THP), 62.00 (1C, O-CH-O-*C*H_2), 56.75, 56.14, 50.16, 42.29, 39.78, 39.50, 39.06, 37.23, 36.83, 36.18, 35.78, 31.93, 31.86 (13C, cholesteryl), 30.53 (1C, O-CH_2-CH_2-CH_2-*C*H_2), 28.36, 27.98 (2C, cholesteryl), 25.45 (1C, O-CH_2-*C*H_2-CH_2-CH_2), 24.28, 23.83, 22.82, 22.56, 21.05 (5C, cholesteryl) 19.39, 19.35, 18.71 (3C, cholesteryl, O-CH_2-CH_2-*C*H_2-CH_2), 11.84 (1C, *C*H$_{3\ chol}$).

Deprotection of cholesteryl-MBE-THP for the synthesis of the initiator cholesteryl-MBE-OH (Chol-MBE-OH)

Cholesteryl-MBE-THP (2.07 g, 3.29 mmol, 1 eq.) was dissolved in methanol (50 mL), and 4 g of an acidic ion exchange resin (Dowex 50WX8) was added to the solution to cleave the

cyclic acetal protecting group. The solution was stirred and heated to 50 °C overnight. Afterwards, the resin was removed by filtration and the solvent was removed partly in vacuo. The product was obtained as a light orange wax (yield: 1.47 g, 2.70 mmol, 82 %).

^{1}H NMR (400 MHz, chloroform-*d*) δ [ppm] = 5.36 (d, *J* = 5.3 Hz, 1H, C*H*=C$_{chol}$), 5.21 (s, 2H, *H*$_2$C=C), 4.08 (s, 4H, H$_2$C=(C-C*H*$_2$O)$_2$), 3.76 (d, *J* = 4.7 Hz, 2H, CH$_2$-C*H*$_2$-OH), 3.68 – 3.64 (m, 2H, Chol-O-C*H*$_2$), 3.61 – 3.56 (m, 4H, Chol-O-CH$_2$-C*H*$_2$-O, O-C*H*$_2$-CH$_2$-OH), 3.27 – 3.15 (m, 1H, O-C*H*$_{chol}$), 2.45 – 2.34 (m, 1H, O-CH-C*H*$_{2\,chol}$), 2.24 – 2.10 (m, 1H, O-CH-C*H*$_{2\,chol}$), 2.10 – 0.80 (m, 42H, cholesteryl), 0.69 (s, 3H, C*H*$_{3\,chol}$).

^{13}C NMR (101 MHz, chloroform-*d*) δ [ppm] = 142.60 (1C, H$_2$C=*C*), 140.96 (1C, CH=*C*$_{chol}$), 121.58 (1C, *C*H=C$_{chol}$), 114.65 (1C, H$_2$*C*=C), 79.55 (1C, O-*C*H$_{chol}$), 72.01 (1C, Chol-O-CH$_2$-*C*H$_2$-O), 71.77, 71.38 (2C, H$_2$C=(C-*C*H$_2$O)$_2$), 69.80 (1C, Chol-O-*C*H$_2$-CH$_2$-O), 67.27 (1C, O-*C*H$_2$-CH$_2$-OH), 61.82 (1C, O-CH$_2$-*C*H$_2$-OH), 56.79, 56.16, 50.19, 42.33, 39.79, 39.53, 39.05, 37.24, 36.89, 36.20, 35.79, 31.96, 31.90, 28.35, 28.24, 28.02, 24.30, 23.83, 22.83, 22.57, 21.08, 19.39, 18.72 (23C, cholesteryl), 11.87 (1C, *C*H$_{3\,chol}$).

Synthesis of cholesterol-initiated PEG polymers

The polymerization of ethylene oxide (EO) using cholesterol as initiator was performed on the basis of literature procedures for other glycidyl ethers with adjusted reaction procedure.[2,21]

The synthesis is described for Chol-PEG$_{82}$ as a representative example. All other samples were synthesized in the same fashion with varied monomer equivalents.

In a dry Schlenk flask the initiator cholesterol (519.00 mg, 1.34 mmol, 1 eq.) and potassium *tert*-butoxide (136.00 mg, 1.21 mmol, 0.9 eq.) were dissolved in benzene (5 mL) and dry THF (5 mL), stirred under slightly reduced pressure at 60 °C for 30 minutes and subsequently dried in high vacuum for 16 hours. The resulting initiator salt was dissolved in dry THF (15 mL), and the flask was cooled to -70 °C with an ethanol/nitrogen cooling bath. Ethylene oxide (4.85 g, 109.88 mmol, 5.00 mL, 82 eq.) was condensed *via* a graduated ampule into the flask. The reaction mixture was heated in vacuo to 60 °C for 48 hours. Subsequently, methanol (1 mL) was added, and the flask was flushed with argon. The resulting polymer

Chol-PEG$_{82}$ was precipitated three times in diethyl ether and separated *via* centrifuge. The polymer was dried under reduced pressure at room temperature for 24 hours (yield: 90 %).

^{1}H NMR (300 MHz, chloroform-*d*) δ [ppm] = 5.32 (d, *J* = 5.2 Hz, 1H, C*H*=C$_{chol}$), 3.88 - 3.38 (m, 327H, C*H*O polyether backbone), 3.22 - 3.13 (m, 1H, O-C*H*$_{chol}$), 2.38 – 2.32 (m, 1H, O-CH-C*H*$_{2\,chol}$), 2.23 - 2.15 (m, 1H, O-CH-C*H*$_{2\,chol}$), 2.05 – 0.79 (m, 42H, cholesteryl), 0.66 (s, 3H, C*H*$_{3\,chol}$).

^{13}C NMR (75 MHz, chloroform-*d*) δ [ppm] = 140.96 (1C, CH=*C*$_{chol}$), 121.52 (1C, *C*H=C$_{chol}$), 79.45 (1C, O-*C*H$_{chol}$), 72.53 (1C, Chol-O-CH$_2$-*C*H$_2$-O), 70.87 - 70.31(164C, *C*HO polyether backbone), 67.28 (1C, Chol-O-*C*H$_2$-CH$_2$-O), 65.84 (1C, O-*C*H$_2$-CH$_2$-OH), 61.67 (1C, O-CH$_2$-*C*H$_2$-OH), 56.75, 56.12, 50.15, 42.30, 39.76, 39.49, 39.05, 37.22, 36.85, 36.16, 35.76, 31.93, 31.87, 28.34, 28.22, 27.99, 24.27, 23.79, 22.82, 22.56, 21.04, 19.38, 18.71 (23C, cholesteryl), 15.27, 11.85 (1C, *C*H$_{3\,chol}$).

Synthesis of cholesteryl-MBE-OH initiated PEG polymers

The polymerization of ethylene oxide (EO) using Chol-MBE-OH as initiator was performed on the basis of literature procedures for other glycidyl ethers with adjusted reaction procedure.[2,21]

The synthesis is described for Chol-MBE-PEG$_{105}$ as a representative example. All other samples were synthesized in the same fashion with varied monomer equivalents.

In a dry Schlenk flask the initiator cholesteryl-MBE-OH (765.00 mg, 1.40 mmol, 1 eq.) and potassium *tert*-butoxide (142.00 mg, 1.26 mmol, 0.9 eq.) were dissolved in benzene (5 mL) and dry THF (5 mL), stirred under slightly reduced pressure at 60 °C for 30 minutes and subsequently dried in high vacuum for 16 hours. The resulting initiator salt was dissolved in dry THF (15 mL) and the flask was cooled to -70 °C with an ethanol/nitrogen cooling bath. Ethylene oxide (4.85 g, 109.88 mmol, 5.00 mL, 78 eq.) was condensed *via* a graduated ampule into the flask. The reaction mixture was heated in vacuo to 50 °C for 48 hours. Subsequently, methanol (1 mL) was added, and the flask was flushed with argon. The resulting polymer Chol-MBE-PEG$_{105}$ was precipitated three times in diethyl ether and separated *via* centrifuge. The polymer was dried under reduced pressure at room temperature for 24 hours (yield: 85–90 %). During the polymerization, an in situ

isomerization of the polymer of about 60 % took place. The signals of the isomerized polymer are labeled *iso* in the NMR spectrum.

^{1}H NMR (400 MHz, chloroform-*d*) δ [ppm] = 6.10 (s, 0.62H, C=C*H*$_{iso}$), 5.34 (d, *J* = 5.3 Hz, 1H, C*H*=C$_{chol}$), 5.18 (s, 0.53H, *H*$_2$C=C), 4.02 (s, 1H, H$_2$C=(C-C*H*$_2$O)$_2$), 3.87 – 3.45 (m, 437H, C*H*O polyether backbone), 3.21 – 3.14 (m, 1H, O-C*H*$_{chol}$), 2.39 – 2.34 (m, 1H, O-CH-C*H*$_{2\,chol}$), 2.24 – 2.16 (m, 1H, O-CH-C*H*$_{2\,chol}$), 2.03 – 1.79 (m, 6H, cholesteryl), 1.63 (d, *J* = 1.2 Hz, 1.84H, C*H*$_3$-C=CH$_{iso}$), 1.59 – 0.85 (m, 39H, cholesteryl), 0.67 (s, 3H, C*H*$_{3\,chol}$).

^{13}C NMR (75 MHz, methylene chloride-*d*$_2$) δ [ppm] = 144.58 (1C, C=*C*H$_{iso}$), 140.94 (1C, CH=*C*$_{chol}$), 121.45 (1C, *C*H=C$_{chol}$), 113.21 (1C, H$_2$*C*=C), 110.53 (1C, *C*=CH$_{iso}$), 79.50 (1C, O-*C*H$_{chol}$), 73.12, 72.51 (2C, H$_2$C=(C-*C*H$_2$O)$_2$), 70.75 – 70.27 (210C, *C*HO polyether backbone), 68.20 (1C, Chol-O-CH$_2$-*C*H$_2$-O), 66.96 (1C, O-*C*H$_2$-CH$_2$-OH), 61.54 (1C, O-CH$_2$-*C*H$_2$-OH), 56.80, 56.16, 50.23, 42.27, 39.81, 39.47, 39.06, 37.21, 36.82, 36.17, 35.79, 31.94, 31.88, 28.36, 28.18, 28.00, 24.23, 23.77, 22.55, 22.30, 21.05, 19.17, 18.49 (23C, cholesteryl), 11.61 (1C, *C*H$_{3\,chol}$), 11.11 (1C, *C*H$_3$-C=CH$_{iso}$).

Isomerization of Chol-MBE-PEG to Chol-isoMBE-PEG

The synthesis is described for the isomerization of Chol-MBE-PEG$_{105}$ to Chol-*iso*MBE-PEG$_{105}$ as a representative example. All other samples were isomerized in the same fashion with varied equivalents of potassium *tert*-butoxide.

Chol-MBE-PEG$_{105}$ (150.00 mg, 37.13 mmol, 1 eq.) and potassium *tert*-butoxide (8.33 mg, 74.26 mmol, 2 eq.) were dissolved in dry DMSO (2 mL) in a Schlenk tube under argon condition. The solution was stirred and heated to 60 °C under reduced pressure overnight. The resulting isomerized polymer Chol-*iso*MBE-PEG$_{105}$ was precipitated three times in a mixture of diethyl ether/acetone (70:30 vol%) and separated *via* centrifuge. The polymer was dried under reduced pressure at room temperature for 24 hours (yield: 60 %).

^{1}H NMR (300 MHz, benzene-*d*$_6$) δ [ppm] = 6.09 – 6.00 (m, 1H, CH$_3$-C=C*H*), 5.38 (d, *J* = 3.4 Hz, 1H), 3.84 (d, *J* = 10.8 Hz, 2H, C*H*$_2$-CH=CH), 3.73 - 3.37 (m, 472H, C*H*O polyether backbone), 3.21 – 3.11 (m, 1H, O-C*H*$_{chol}$), 2.56 – 2.22 (m, 4H, cholesteryl), 1.90 (s, 3H, C*H*$_3$-C=CH), 1.78 – 0.83 (m, 37H, cholesteryl), 0.66 (s, 3H, C*H*$_{3\,chol}$).

^{13}C NMR (75 MHz, benzene-d_6) δ [ppm] = 144.76 (1C, C=*C*H), 140.77 (1C, CH=*C*$_{chol}$), 121.45 (1C, *C*H=C$_{chol}$), 110.56 (1C, *C*=CH), 79.41 (1C, O-*C*H$_{chol}$), 73.24, 72.78 (2C, *C*H$_2$-CH=CH), 71.64 - 70.23 (236C, *C*HO polyether backbone), 68.92 (1C, Chol-O-*C*H$_2$-CH$_2$-O), 67.56 (1C, O-*C*H$_2$-CH$_2$), 67.08 (1C, O-CH$_2$-*C*H$_2$), 61.51 (1C, O-CH$_2$-*C*H$_2$-OH), 56.68, 56.21, 50.26, 42.25, 39.85, 39.58, 39.36, 37.22, 36.32, 35.87, 32.02, 31.88, 28.57, 28.29, 28.06, 24.26, 24.00, 22.69, 22.43, 21.10, 19.17, 18.69 (23C, cholesteryl), 11.74 (1C, *C*H$_{3\ chol}$), 11.52 (1C, *C*H$_3$-C=CH).

Post-polymerization modification

The functionalization of Chol-PEG with propargyl bromide is described for Chol-PEG$_{78}$ as a representative example.

Chol-PEG$_{78}$ (0.40 g, 0.10 mmol, 1 eq.) was placed in a Schlenk flask and dissolved in THF (10 mL). The solution was cooled to 0 °C, and sodium hydride (7.00 mg, 0.31 mmol, 3 eq.) was added. The solution was stirred for 1 hour at 0 °C to ensure complete deprotonation. Subsequently, propargyl bromide (0.35 mL, 0.31 mmol, 3 eq.) (80 wt% in toluene) was added and the mixture was allowed to slowly reach room temperature. The solution was stirred at room temperature overnight. Afterwards, water (2 mL) was added, and the solvent was removed under reduced pressure. The crude product was precipitated three times in diethyl ether and separated *via* centrifuge. The polymer was dried under reduced pressure at room temperature for 24 hours (yield: 75 %).

^{1}H NMR (300 MHz, chloroform-*d*) δ [ppm] = 5.33 (d, *J* = 5.0 Hz, 1H, C*H*=C$_{chol}$), 4.20 (d, *J* = 2.4 Hz, 2H, OC*H*$_2$-CCH), 3.89 – 3.38 (m, 339H, C*H*O polyether backbone), 3.25 – 3.08 (m, 1H, O-C*H*$_{chol}$), 2.45 (t, *J* = 2.4 Hz, 1H, OCH$_2$-CC*H*), 2.41 – 2.31 (m, 1H, O-CH-C*H*$_{2\ chol}$), 2.29 – 0.75 (m, 42H, cholesteryl), 0.67 (s, 3H, C*H*$_{3\ chol}$).

^{13}C NMR (75 MHz, chloroform-*d*) δ [ppm] = 140.95 (1C, CH=*C*$_{chol}$), 121.52 (1C, *C*H=C$_{chol}$), 79.64 (1C, OCH$_2$-*C*CH), 79.45 (1C, O-*C*H$_{chol}$), 74.60 (1C, OCH$_2$-C*C*H), 72.56 (1C, Chol-O-CH$_2$-*C*H$_2$-O), 70.86 - 70.24 (170C, *C*HO polyether backbone), 69.08 (1C, OCH$_2$-C*C*H), 67.27 (1C, Chol-O-*C*H$_2$-CH$_2$-O), 61.64 (1C, Chol-O-CH$_2$-*C*H$_2$-O), 58.38 (1C, O*C*H$_2$-CCH), 56.75, 56.11, 50.15, 42.29, 39.76, 39.49, 39.04, 37.21, 36.84, 36.16, 35.76, 31.92, 31.87, 28.33, 28.21, 27.99, 24.27, 23.79, 22.82, 22.56, 21.04, 19.37, 18.70 (23C, cholesteryl), 11.85(1C, *C*H$_{3\ chol}$).

The functionalization of Chol-*iso*MBE-PEG with propargyl bromide is described for Chol-*iso*MBE-PEG$_{105}$ as a representative example.

Chol-*iso*MBE-PEG$_{105}$ (34.00 mg, 0.01 mmol, 1 eq.) was placed in a Schlenk flask and dissolved in THF (10 mL). The solution was cooled to 0 °C, and sodium hydride (1.00 mg, 0.03 mmol, 3 eq.) was added. The solution was stirred for 1 hour at 0 °C to ensure complete deprotonation. Subsequently, propargyl bromide (5.00 µL, 0.03 mmol, 3 eq.) (80 wt% in toluene) was added and the mixture was allowed to slowly reach room temperature. The solution was stirred at room temperature overnight. Afterwards, water (0.5 mL) was added, and the solvent was removed under reduced pressure. The crude product was precipitated three times in diethyl ether and separated *via* centrifuge. The polymer was dried under reduced pressure at room temperature for 24 hours (yield: 85 %).

^{1}H NMR (400 MHz, benzene-d_6) δ [ppm] = 6.08 – 6.04 (m, 1H, CH_3-C=C*H*), 5.41 (d, *J* = 4.9 Hz, 1H), 3.94 (d, *J* = 2.4 Hz, 2H, OC*H*$_2$-CCH), 3.86 (d, *J* = 15.0 Hz, 2H, C*H*$_2$-CH=CH), 3.74 - 3.25 (m, 410H, C*H*O polyether backbone), 3.25 – 3.13 (m, 1H, O-C*H*$_{chol}$), 2.64 – 2.33 (m, 3H, cholesteryl), 2.12 (t, *J* = 2.3 Hz, 1H, OCH_2-CC*H*), 2.07 – 1.96 (m, 2H, cholesteryl), 1.93 (s, 3H, C*H*$_3$-C=CH), 1.89 – 0.86 (m, 46H, cholesteryl), 0.68 (s, 3H, C*H*$_{3\,chol}$).

2.1.3 Results and discussion

A wide variety of approaches already exists for introducing vinyl ether structures into PEG-based polymers. One possibility is to perform an AROP of ethylene oxide (EO) with the commercially available epoxide monomer 3,4-epoxy-1-butene (EPB). Subsequent isomerization of the allyl ether moieties by Wilkinson's catalyst leads to the acid cleavable vinyl ether structures. In addition to polymerization and isomerization, Worm *et al.* performed pH-dependent degradation studies using ^{1}H NMR spectroscopy, which confirmed cleavage of the polymers at different pH values.[15] However, the introduction of vinyl ether groups using EPB also has some weaknesses. During polymerization, β–elimination occurs as a side reaction due to the acidic proton at the allyl ether position. This side reaction can be reduced by adjusting the reaction conditions, such as the base used, the solvent and the reaction temperature, but it can never be completely prevented. Another problem arises after cleavage of the polymers at acidic pH. Due to the

copolymerization, the EPB units are randomly distributed in the polymer backbone. During cleavage, polymer fragments of different sizes are formed, which lead to a strong broadening of the molecular weight distribution. In the synthesis of cholesterol-initiated copolymers of EO and EPB, well-defined structures could be synthesized, but complete isomerization could not be obtained for any polymer. The reason for this is that the amphiphilic structures assemble into micellar structures under the synthesis conditions of isomerization and the required transition state of the catalyst for isomerization is prevented. For this reason, the introduction of pH-sensitive vinyl ether groups *via* copolymerization of EO and EPB is not suitable for the formation of amphiphilic structures.

For the preparation of cleavable polymer lipids as drug delivery systems a single pH-responsive group between the hydrophobic and the hydrophilic moiety should be realized. In our group a new class of allyl ether initiators based on 2-(methylene)-1,3-propanediol (MPD) was introduced as lead structure (**Scheme 1**).[22] In this work, a novel cholesterol-based initiator for AROP was developed on this basis in a multi-step synthesis procedure. In the following sections, the individual synthesis steps will be discussed in more detail.

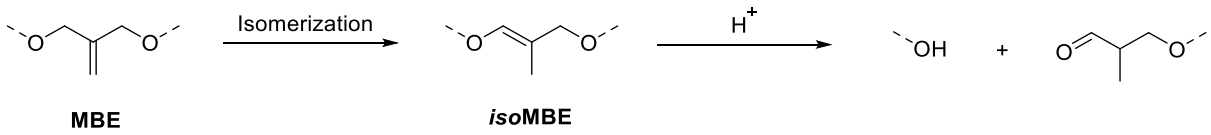

Scheme 1: Isomerization and hydrolysis of MPD-derived substructures.

2.1.3.1 Initiator synthesis

Synthesis of bifunctional MBE

For the introduction of the allyl ether moieties 2,2'-((2-methylenepropane-1,3-diyl)bis(oxy))bis(ethan-1-ol) (MBE) was synthesized in a convenient one-step reaction of 3-chloro-2-(chloromethyl)prop-1-ene with ethylene glycol in a nucleophilic substitution reaction (**Scheme 2**). This leads of the addition of two ethylene glycol spacers at the terminal hydroxyl groups of the lead structure 2-(methylene)-1,3-propanediol (MPD) and enables improved handling. Furthermore, the compound can be synthesized on a multi gram-scale. The purification can be done by fractional distillation with good yields, high purity and low

costs. The detailed NMR analysis of this compound can be found in the Supporting Information (**SI-Figure 1**, **SI-Figure 2**)

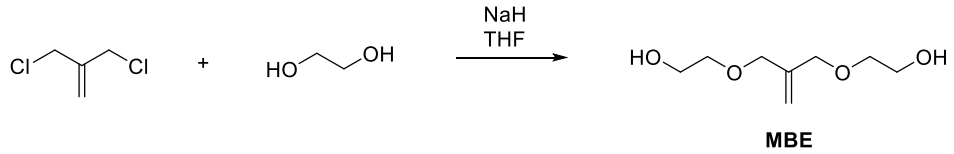

Scheme 2: Synthesis of bifunctional MBE.

Synthesis of monofunctional MBE

For controlled binding of MBE to cholesterol, one hydroxyl group had to be selectively protected to prevent double binding of cholesterol. Furthermore, it was important that the protective group could be easily cleaved again after the reaction in order to be able to use the initiator for the AROP. For this reason, 3,4-dihydropyran (DHP) was used as the protecting group to synthesize THP-MBE (**Scheme 3**). After purification by column chromatography, the mono-protected product was obtained with a yield of 30-40 %. The double-protected product can be recovered by acid cleavage back to the starting compound MBE.

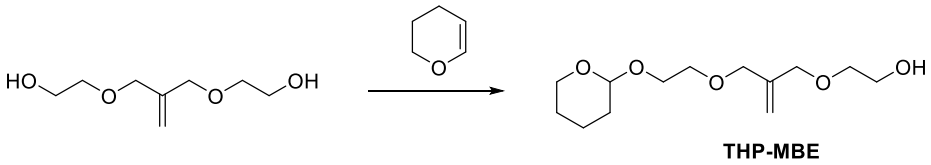

Scheme 3: Synthesis of monofunctional MBE.

Synthesis of cholesteryl-MBE-THP and cholesteryl-MBE-OH initiator

To attach cholesterol to MBE, the hydroxyl group was tosylated according to a synthesis route known in the literature.[23] Tosylation of hydroxyl-functionalized substrates is an important transformation to activate hydroxyl groups, thus yielding substrates for further nucleophilic substitution. Subsequently, the nucleophilic substitution reaction of cholesteryl tosylate with MBE was carried out (**Scheme 4**). After purification of the resulting product and analysis by NMR spectroscopy, it became clear that the product did not correspond to the cholesteryl-MBE-THP, but that elimination at the cholesterol had occurred (**Figure 1**). A comparison with the literature confirmed this common side reaction.[24]

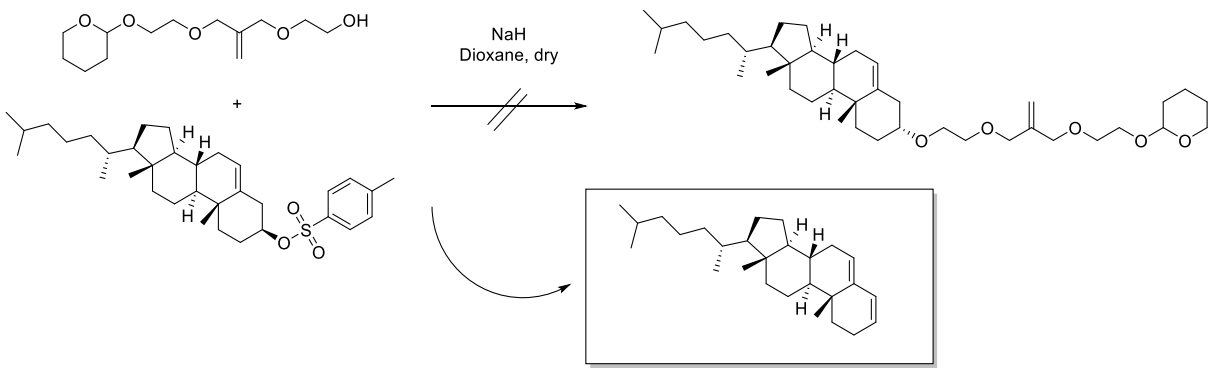

Scheme 4: Elimination reaction of the cholesteryl tosylate.

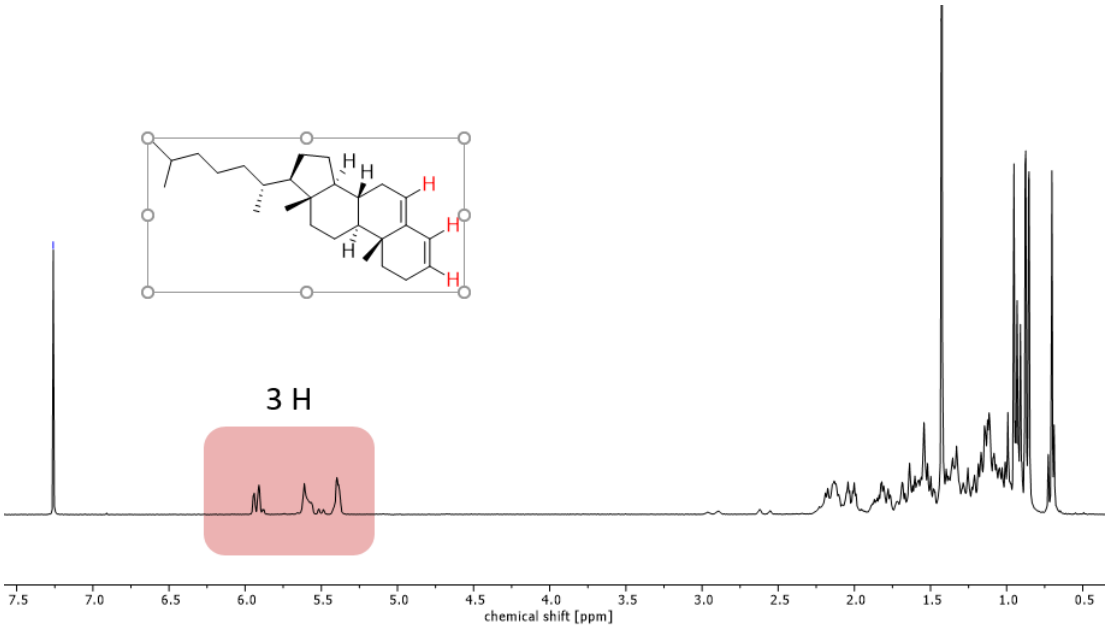

Figure 1: ^{1}H NMR spectrum (300 MHz, chloroform-*d*) of the elimination reaction of cholesteryl tosylate.

To prevent elimination at the cholesterol, the THP-MBE was transferred to the tosylate in place of the cholesterol. Afterwards, the substitution reaction of cholesterol and THP-MBE-Ts was repeated with adjusted conditions (**Scheme 5**). For better separation of the product from cholesterol, which was used in slight excess, the THP protecting group was removed by acid cleavage. Subsequently, the product cholesteryl-MBE-OH initiator was purified by column chromatography in good yields.

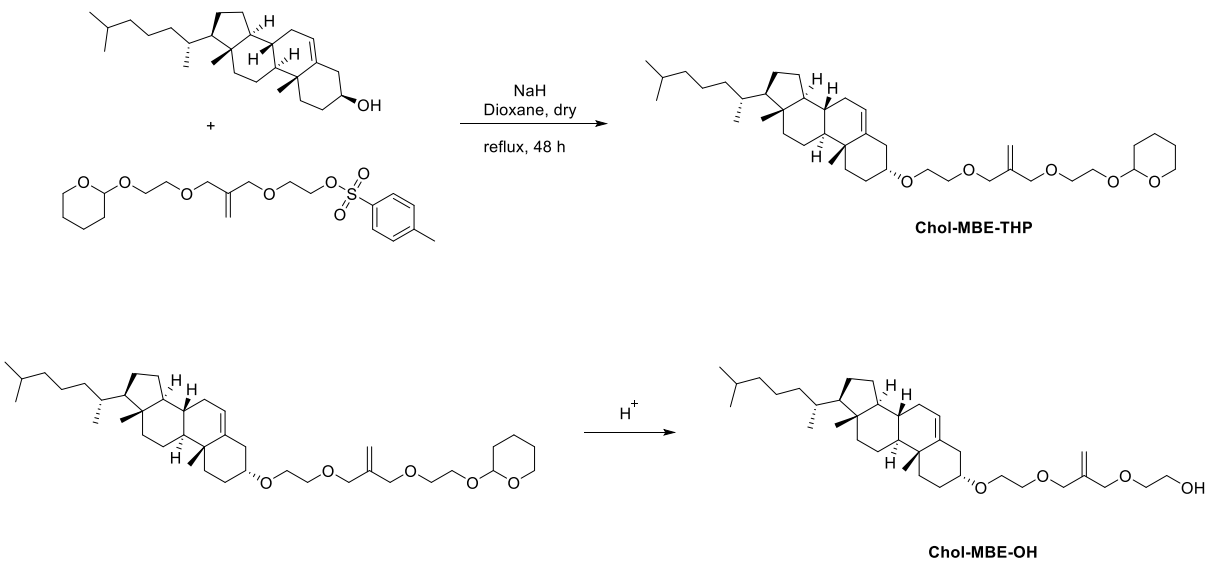

Scheme 5: Synthesis route of Chol-MBE-THP with subsequent deprotection to Chol-MBE-OH initiator.

The cholesteryl-MBE-OH initiator was analyzed by NMR spectroscopy (**Figure 2**). All signals could be unambiguously assigned, and the number of protons determined by integration of the signals agree with those of the molecule.

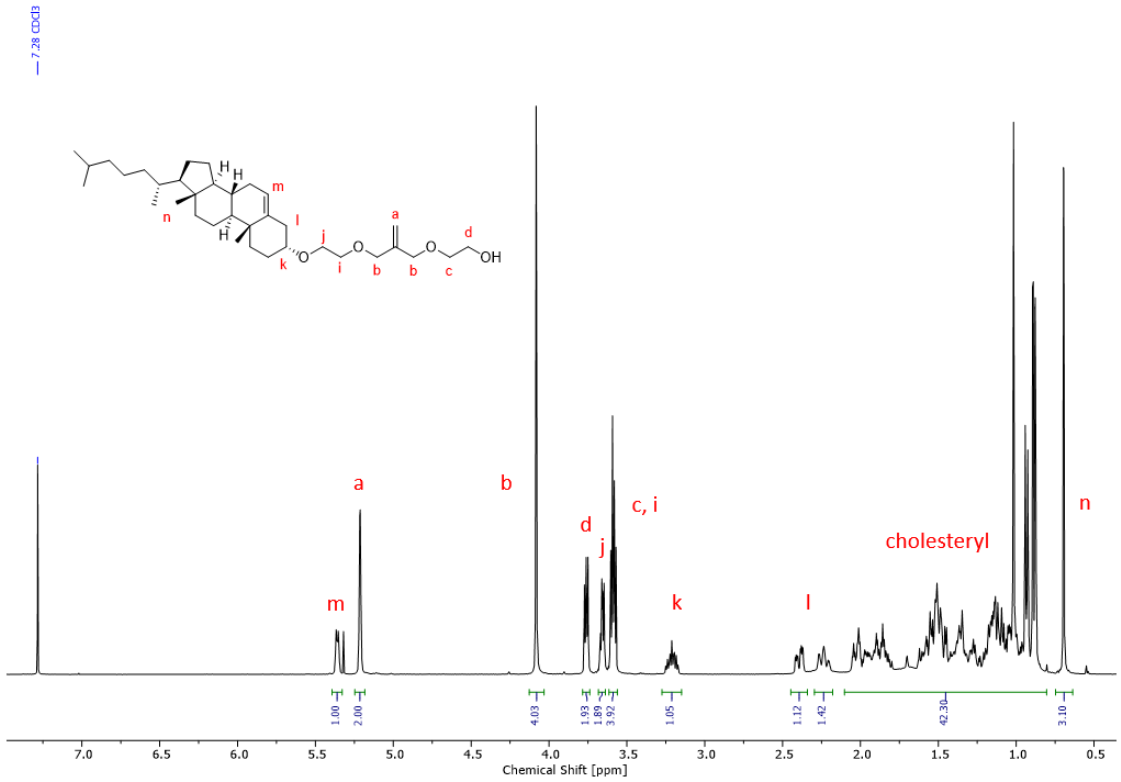

Figure 2: ^{1}H NMR spectrum (400 MHz, chloroform-*d*) of the initiator Chol-MBE-OH.

2.1.3.2 Polymer synthesis and characterization

In this work all presented polymers were synthesized *via* anionic ring-opening polymerization (AROP) of ethylene oxide (EO). This method is commonly used to generate FDA-approved PEGs.[1] Two polymers with different molecular weights were synthesized with the initiator Chol-MBE-OH to demonstrate the excellent control over the molecular weights. Furthermore, polymers without a cleavage site with cholesterol as initiator were prepared as comparative structures with similar molecular weights.

Cholesterol-initiated PEG

For the synthesis of cholesterol-initiated PEG polymers as comparative structures, the cholesterol was deprotonated with potassium *tert*-butoxide with a degree of deprotonation of 90 %. The polymerization with EO was performed in THF at 60 °C for 48 hours. Full monomer conversion was determined *via* ^{1}H NMR spectroscopy. The synthesis route of the polymerization of Chol-PEG polymers is shown in **Scheme 6**.

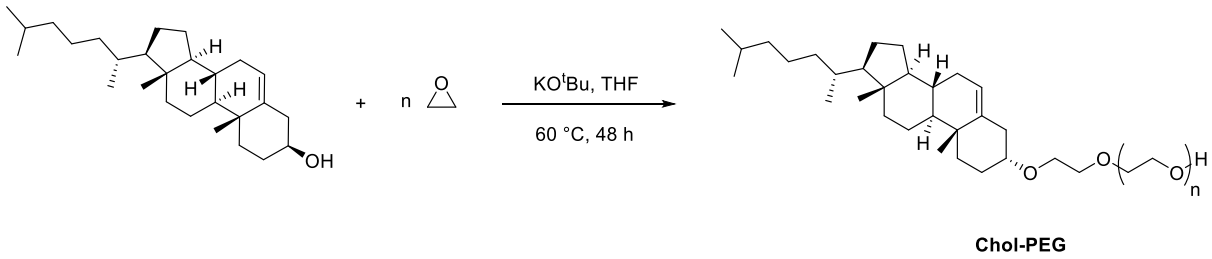

Scheme 6: Synthesis route of the Chol-PEG polymers.

The key characterization data of the Chol-PEG polymers are summarized in **Table 1**. The targeted degree of polymerization is in good agreement with the determined values for obtained PEGs. The molecular weight (M_n) was obtained from SEC in DMF using PEG standards with narrow size distributions ($Đ$ < 1.10). The corresponding SEC traces are shown in **Figure 3**.

Table 1: Characterization data of the Chol-PEG polymers.

Composition [a]	M_n theo g·mol^{-1}	M_n NMR [a] g·mol^{-1}	M_n SEC [b] g·mol^{-1}	$Đ$ [b]
Chol-PEG$_{78}$	4000	3820	2790	1.06
Chol-PEG$_{134}$	6000	6280	3830	1.10

[a] Obtained from ^{1}H NMR spectroscopy. [b] Determined *via* SEC (RI, DMF, PEG standards).

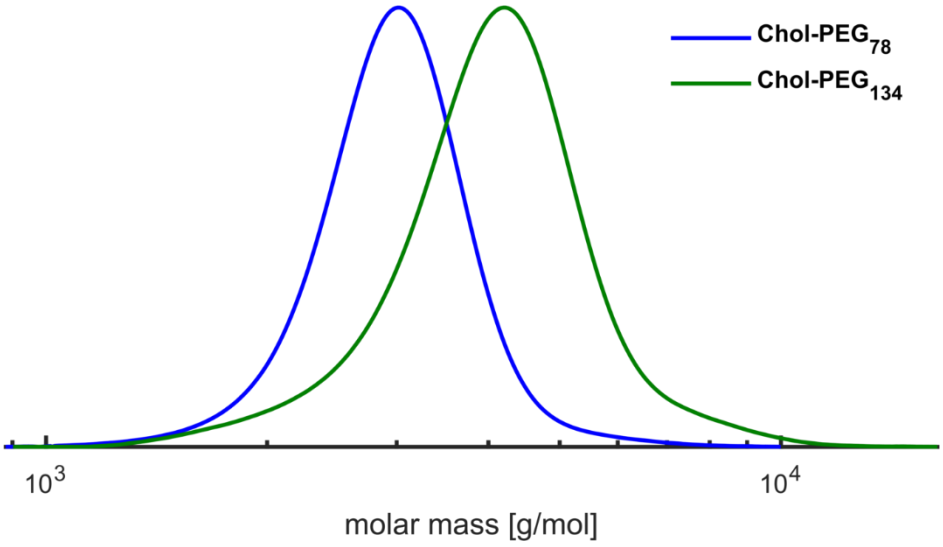

Figure 3: SEC traces (RI detector, DMF, PEG standards) of the Chol-PEG polymers.

The molecular weights from ^{1}H NMR spectroscopy were determined *via* integration of the methyl signals of the cholesterol (signal **n**) and are in good agreement with the molecular weights measured from SEC. For more details, NMR spectra are shown in **SI-Figure 11**.

To determine the end-groups of the cholesterol-initiated PEGs, MALDI-ToF mass spectrometry was performed. The full spectra and a zoom-in of the polymer Chol-PEG$_{78}$ are depicted in **Figure 4**. The spectrum of Chol-PEG$_{134}$ is shown in the Supporting Information (**SI-Figure 30**). The obtained mass spectra show PEG chains exclusively initiated by cholesterol and underlined the formation of well-defined polymers. The mass spectra demonstrate the formation of polymers with the absence of side reactions.

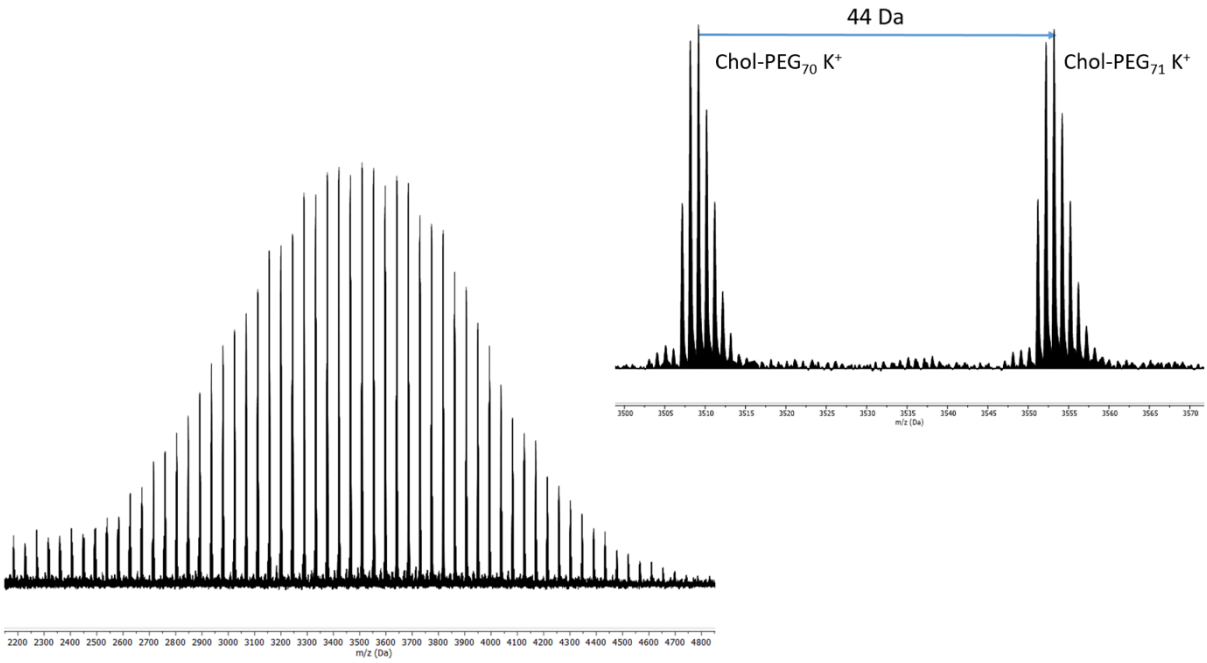

Figure 4: MALDI-ToF MS spectrum of Chol-PEG$_{78}$ (left) and the zoom-in spectrum (right).

Chol-MBE-OH initiated PEG

The synthesis route of PEG with the initiator Chol-MBE-OH is shown in **Scheme 7**. As previously described for the polymerization of Chol-PEG, a deprotonation of the Chol-MBE-OH initiator of 90 % was achieved with potassium *tert*-butoxide. The polymerization of EO was carried out in THF at 50 °C for 48 hours.

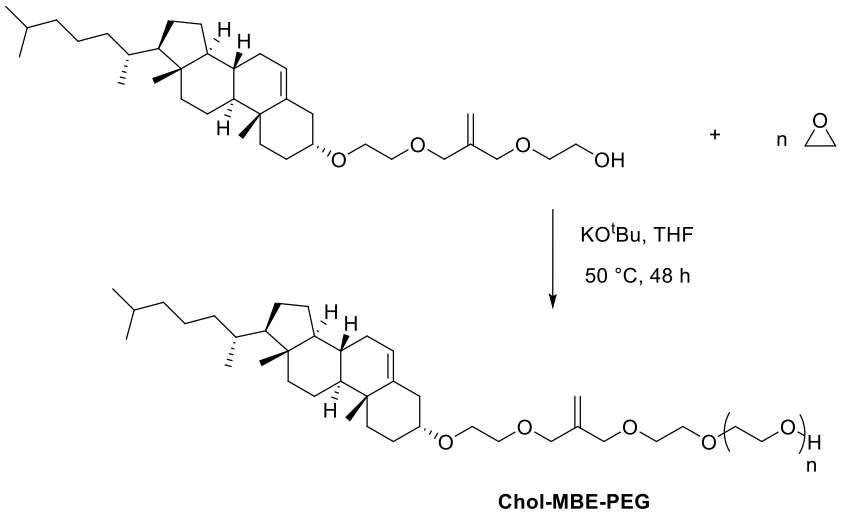

Scheme 7: Synthesis route of Chol-MBE-PEG.

The key characterization data of the Chol-MBE-PEG polymers is shown in **Table 2**. The targeted degree of polymerization deviates from the values obtained. In both cases, the molecular weights are higher than the targeted ones. The reason for this could be, for example, the change in temperature at which the EO was condensed into the ampule. The density of EO is strongly temperature dependent. Furthermore, only smaller amounts of EO were used for the approaches. This means that an error in the amount of EO can have a greater effect on the molecular weight. Both polymers were prepared at the same time with the same set-up. It is therefore likely that one or more of the above-mentioned sources of error occurred. The molecular weight (M_n) was obtained from SEC in DMF using PEG standards with narrow size distributions ($Đ < 1.11$). The polymer with the higher molecular weight exhibits slight tailing at higher molecular weights. However, this proportion is small and changes the size distribution only minimally. The corresponding SEC traces are shown in **Figure 5**.

Table 2: Characterization data of the Chol-MBE-PEG polymers.

Composition [a]	M_n theo g·mol^{-1}	M_n NMR [a] g·mol^{-1}	M_n SEC [b] g·mol^{-1}	$Đ$ [b]
Chol-MBE-PEG$_{105}$	4000	5160	4010	1.07
Chol-MBE-PEG$_{167}$	6000	7880	6490	1.11

[a] Obtained from ^{1}H NMR spectroscopy. [b] Determined *via* SEC (RI, DMF, PEG standards).

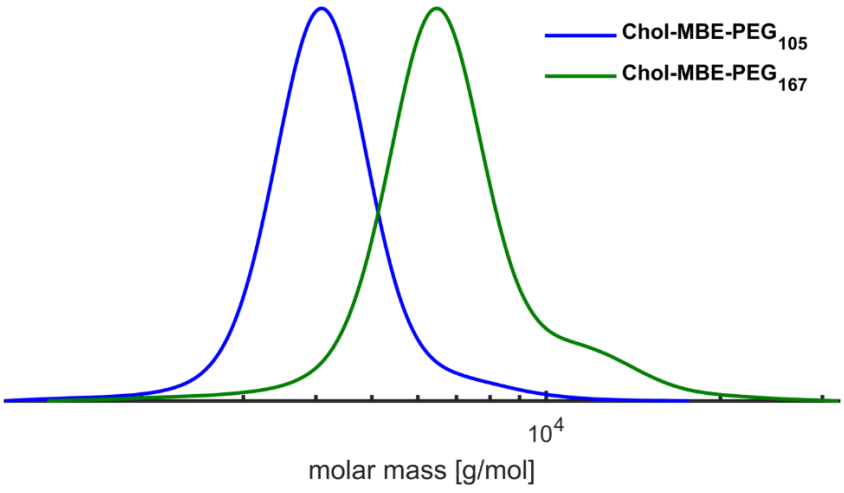

Figure 5: SEC traces (RI detector, DMF, PEG standards) of the Chol-MBE-PEG polymers.

As described previously for the Chol-PEG polymers, the molecular weights from ^{1}H NMR spectroscopy were determined *via* integration of the methyl signals of the cholesterol (signal **n**) and are also in good agreement with the molecular weights measured from SEC. The ^{1}H NMR spectrum is shown in **Figure 6**. During the analysis of the spectrum, it was found that the polymer was already partially isomerized (about 60–80 %) under the conditions of the AROP. The signals of the vinyl ether group after isomerization are shown in blue (signal **a** and **b**).

The isomerization of the allyl ether group to the vinyl ether group has been studied in various publications.[22,25,26] One possibility of isomerization is the use of the base potassium *tert*-butoxide in polar solvents at 60-80 °C. The influence of the solvent on isomerization is important. Complete isomerization is only possible in DMSO due to the formation of a complex of the potassium *tert*-butoxide and the proton of the allyl ether group. In other solvents, the catalyst is less soluble or the hydrogen bond to the alcohol decreases.[26] For this reason, complete isomerization cannot take place in THF.

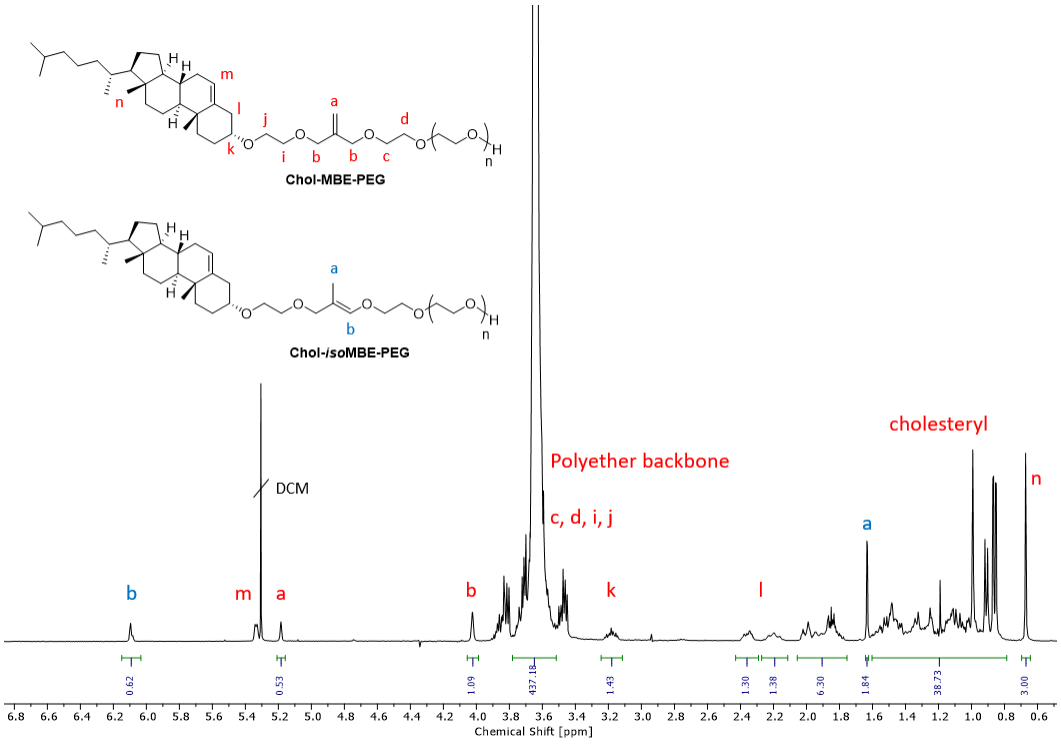

Figure 6: ^{1}H NMR spectrum (400 MHz, chloroform-*d*) of the Chol-MBE-PEG and Chol-*iso*MBE-PEG polymers. Characteristic signals of Chol-MBE-PEG are assigned in red, signals of Chol-*iso*MBE-PEG are assigned in blue.

In **Figure 7** the MALDI-ToF mass spectrometry of Chol-MBE-PEG$_{105}$ and a zoom-in is shown to determine the end-groups. The spectrum of Chol-MBE-PEG$_{167}$ is shown in the Supporting Information (**SI-Figure 32**). The main distribution corresponds to polymer initiated by Chol-MBE-OH. However, upon closer inspection, a second species can be detected. This corresponds to cholesterol-initiated PEG. When purifying the initiator, no traces of cholesterol could be detected in the NMR spectra and by thin-layer chromatography. However, the detection limit by NMR spectroscopy is higher and can falsify the result at small concentrations of impurities. However, the amount of cholesterol-initiated polymer is less than 5 %. The same initiator was used to prepare both polymers with different molecular weights, which is why cholesterol-initiated PEGs can be detected in both MALDI-ToF MS spectra.

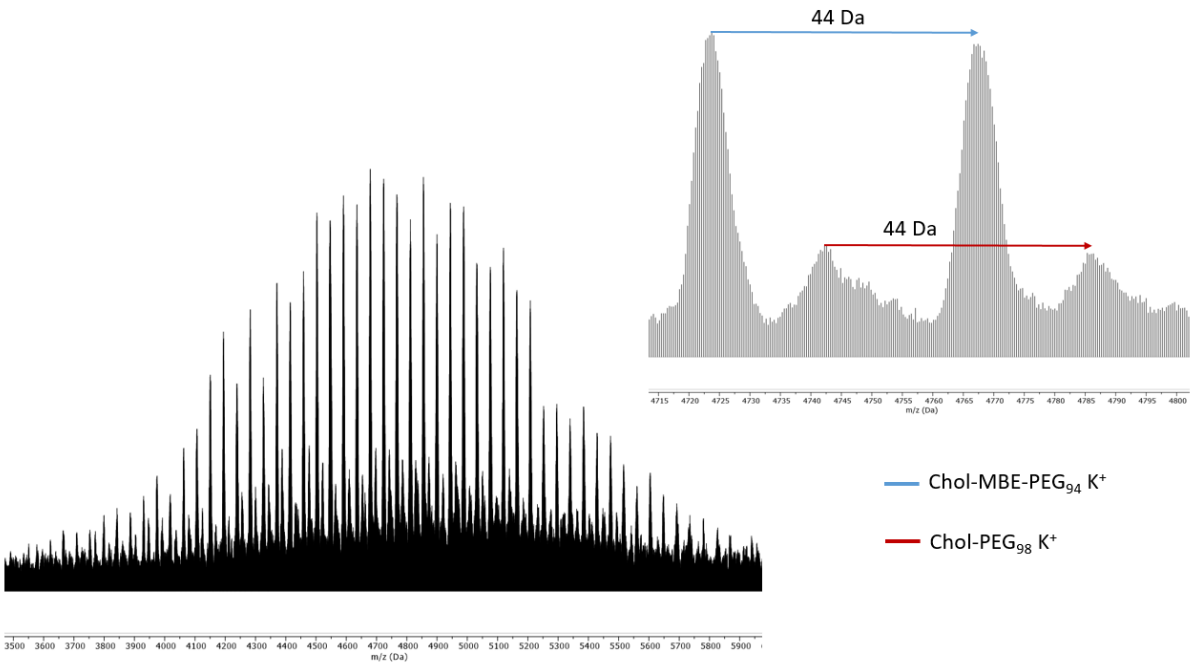

Figure 7: MALDI-ToF MS spectrum of Chol-MBE-PEG$_{105}$ (left) and the zoom-in spectrum (right).

Isomerization of Chol-MBE-PEG to Chol-isoMBE-PEG

In order to obtain complete isomerization of the polymers, the polymers were dissolved in DMSO and heated with potassium *tert*-butoxide for 12 hours. The synthesis route of the isomerization is shown in **Scheme 8**.

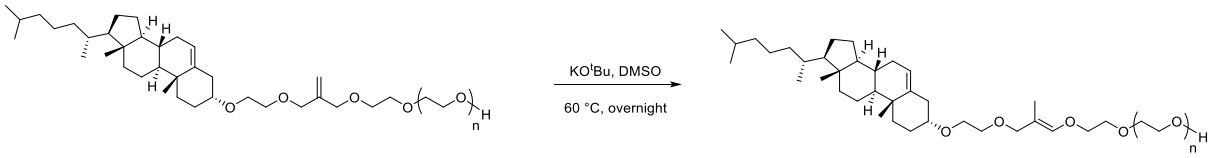

Scheme 8: Synthesis route of the isomerization of Chol-MBE-PEG to Chol-*iso*MBE-PEG.

The amount of base and the temperature were varied to study the influence of both. The temperature (60 °C or 80 °C) had no significant effect on the isomerization. For the amount of base, 1.5, 2 and 4 equivalents were tested. With 1.5 eq. no complete isomerization could be obtained, whereas with the amount of 4 eq. a side reaction occurred. More details about the side reaction are in the Supporting Information (**SI-Figure 28**). Complete isomerization with 2 eq. base without side products could be obtained *via* ^{1}H NMR spectroscopy. The ^{1}H NMR spectrum of Chol-*iso*MBE-PEG$_{167}$ is shown in **Figure 8** as a representative example. For the proton at position **b**, two signals are obtained in the ^{1}H NMR spectrum due to E/Z-isomerization. Due to the transition state during isomerization, the Z-isomer is formed preferentially.

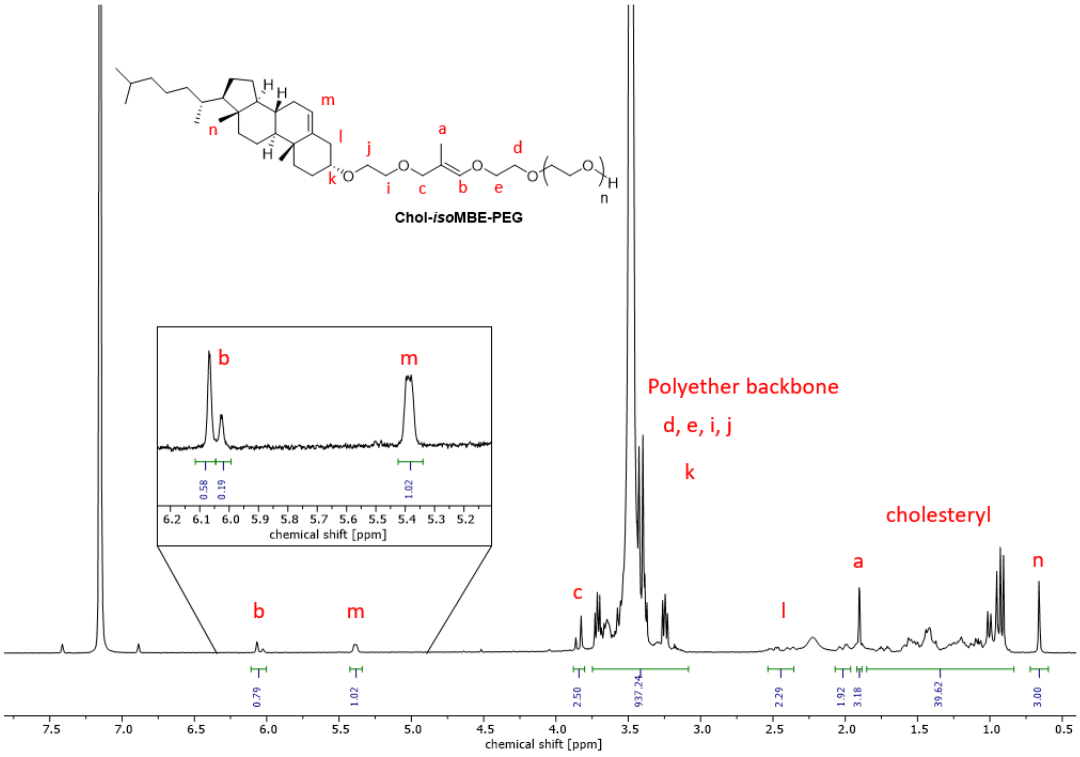

Figure 8: ^{1}H NMR spectrum (400 MHz, benzene-d_6) of the Chol-*iso*MBE-PEG polymer.

In order to exclude a cleavage or change of the polymer due to the isomerization, SEC measurements were performed in addition to the NMR spectra (**Figure 9**). The dashed curves correspond to the polymers before isomerization, the continuous curves after isomerization. The curves are congruent. Degradation or cleavage of the product could not be detected, neither by NMR spectroscopy nor SEC measurements.

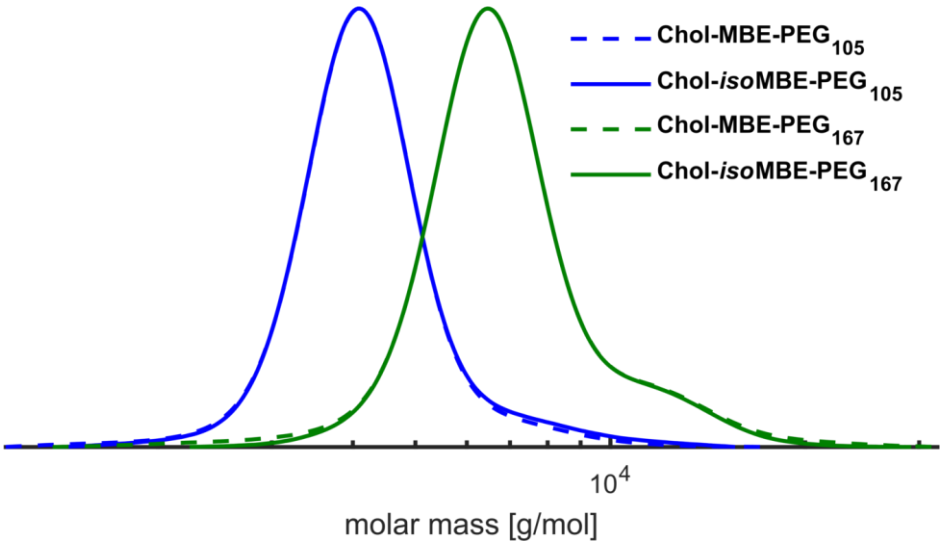

Figure 9: SEC traces (RI detector, DMF, PEG standards) of the Chol-MBE-PEG polymers (dashed) and Chol-*iso*MBE-PEG polymers (continuous).

Post-polymerization modification

There are several ways to transport a drug in the body. One possibility is the use of nanomaterials, such as micelles, liposomes, polymersomes or amphiphilic polymer lipids. In this particular case, the drug can be covalently bound to the polymers or entrapped due to other interactions. There are different approaches for covalent binding. For this purpose, the polymers are post-modified after polymerization. The active ingredients are usually also given specific groups for targeted binding to the polymers. Established systems for binding are click reactions, such as the thiol-ene click or the azide-alkyne click but also the use of Diels-Alder reactions or the formation of reactive esters.[16,27–30]

In this work, the polymers were modified with an alkyne group according to an established synthesis procedure that has been used many times in our group.[2,31,32] To attach alkyne

moieties, the amphiphilic polymer lipids were deprotonated using sodium hydride (NaH) and functionalized with propargyl bromide. Both polymers, the Chol-PEG polymer and the Chol-*iso*MBE-PEG polymer were modified. The successful functionalization was proven *via* NMR spectroscopy. The synthesis route for the post-polymerization modification for the Chol-PEG polymer and the Chol-*iso*MBE-PEG polymer is shown in **Scheme 9**.

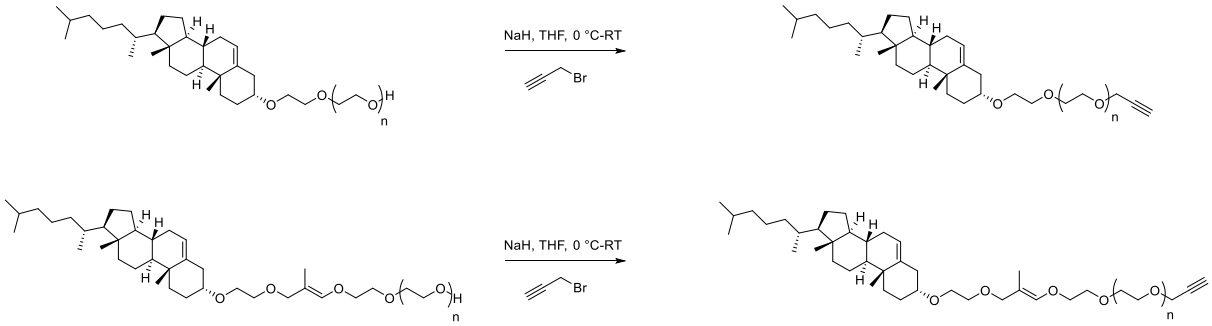

Scheme 9: Synthesis route of the post-polymerization modification of Chol-PEG (top) and Chol-*iso*MBE-PEG (bottom) with propargyl bromide.

Details about the NMR spectra, the SEC data and the MALDI-ToF MS spectra of the reference structure Chol-PEG-alkyne can be found in the Supporting Information (**SI-Figure 26**, **SI-Figure 29**, **SI-Figure 31**).

In **Figure 10** the ^{1}H NMR spectra of Chol-*iso*MBE-PEG before and after functionalization is shown. The characteristic signals for the protons of the alkyne moieties are highlighted in blue.

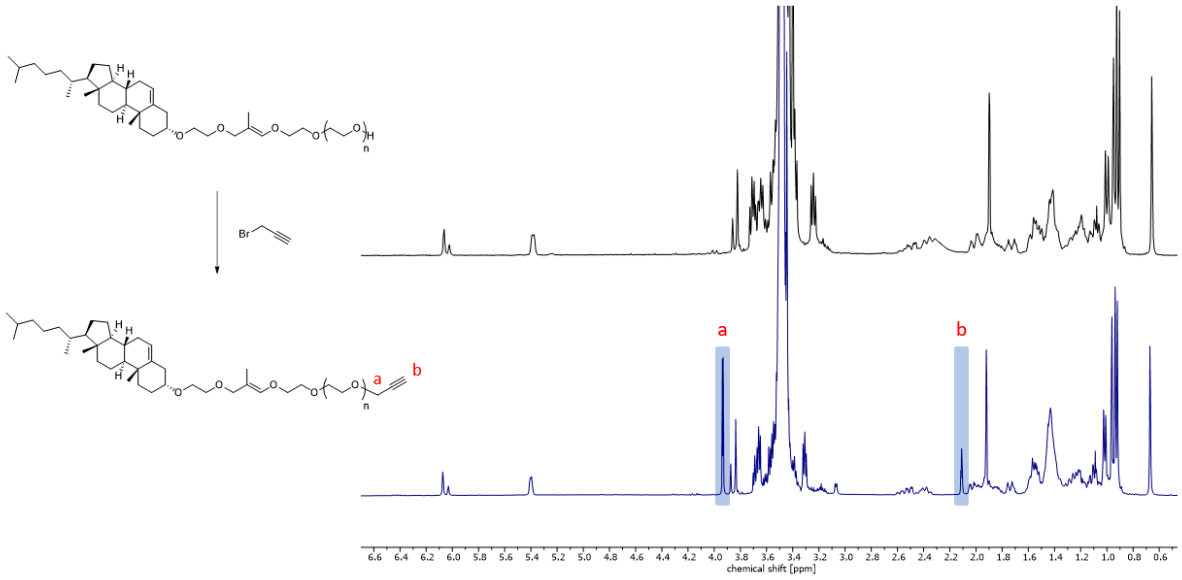

Figure 10: ^{1}H NMR spectra (400 MHz, benzene-d_6) of the Chol-*iso*MBE-PEG polymer before (top) and after (bottom) the post-polymerization modification with propargyl bromide.

SEC measurements showed no changes in the polymers before and after functionalization. The SEC data of Chol-*iso*MBE-PEG and Chol-*iso*MBE-PEG-alkyne can be taken from the following **Figure 11**.

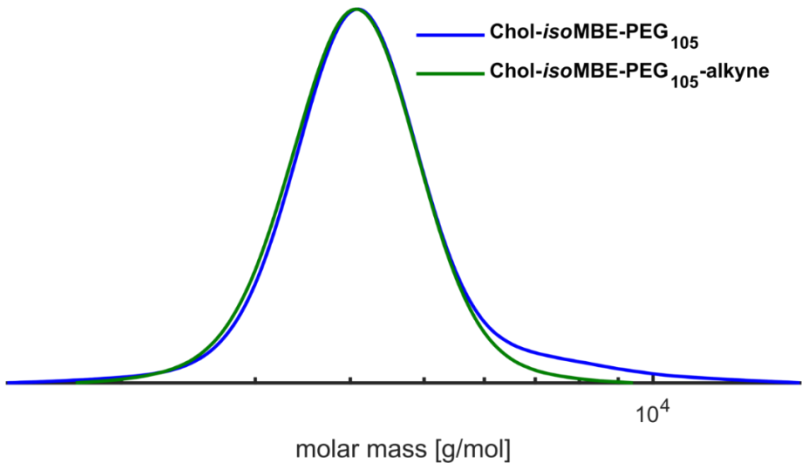

Figure 11: SEC traces (RI detector, DMF, PEG standards) of the Chol-*iso*MBE-PEG polymer before (blue) and after (green) post-modification with propargyl bromide.

Using MALDI-ToF MS spectra, complete functionalization using propargyl bromide was additionally confirmed. The spectrum of Chol-*iso*MBE-PEG$_{105}$-alkyne as well as the zoom-in spectrum are shown in **Figure 12**.

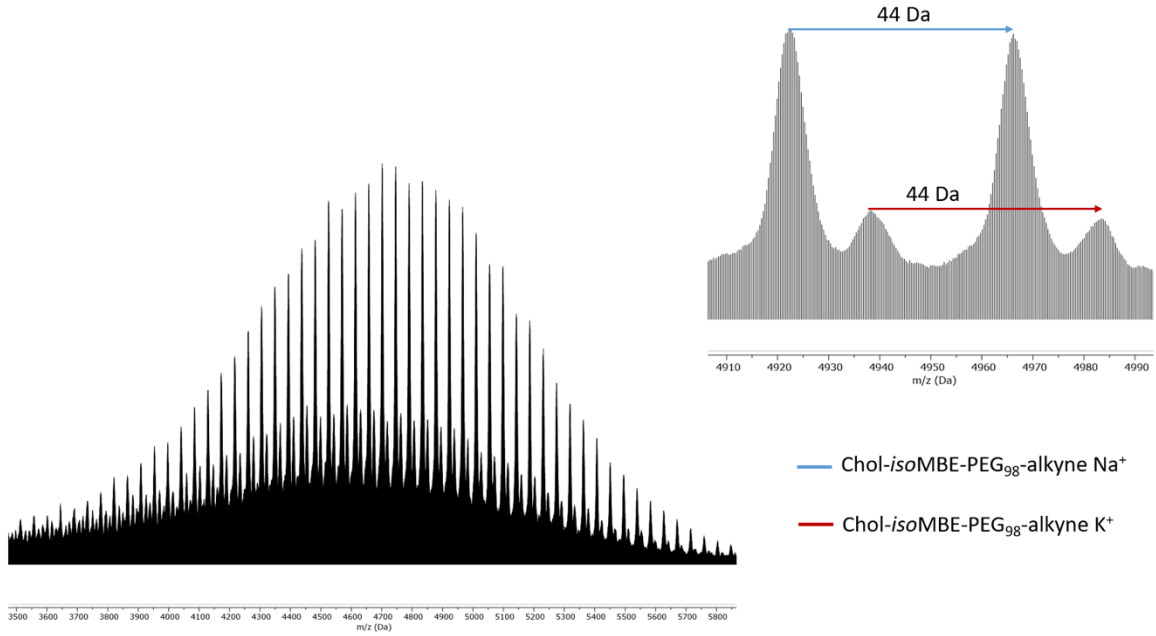

Figure 12: MALDI-ToF MS spectrum of Chol-*iso*MBE-PEG$_{105}$-alkyne (left) and the zoom-in spectrum (right).

Degradation Studies of the Chol-isoMBE-PEG polymers

To obtain more detailed information about the degradation products of the amphiphilic polymer lipids, they were incubated at acidic pH value. For this purpose, the Chol-*iso*MBE-PEG polymer (5 mg) was dissolved in a dilute hydrochloric acid solution (1 mL) and treated for 24 hours with continuous shaking. The pH value was chosen low enough to ensure complete cleavage of all polymers. After 24 hours, the aqueous polymer solution was filtered over basic aluminum oxide to neutralize it and dried in high vacuum. Finally, the hydrolysis fragments were analyzed by SEC. **Figure 13** shows the SEC traces of the polymer before and after hydrolysis. The hydrolysis products of acidic cleavage are shown in **Scheme 10**.

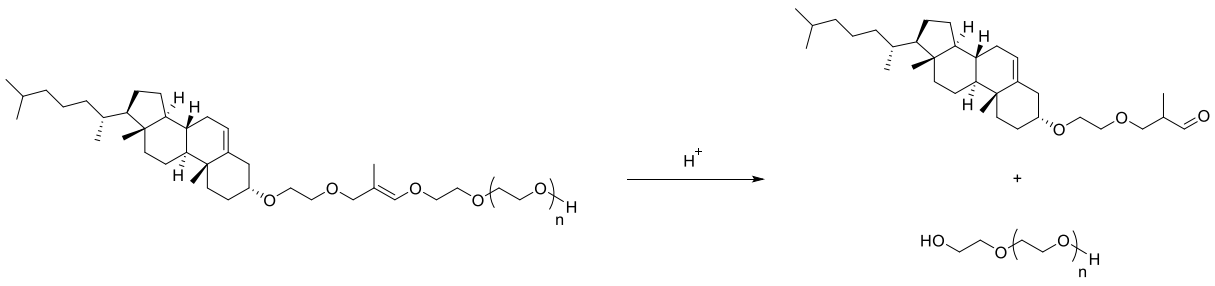

Scheme 10: Products of the acidic hydrolysis.

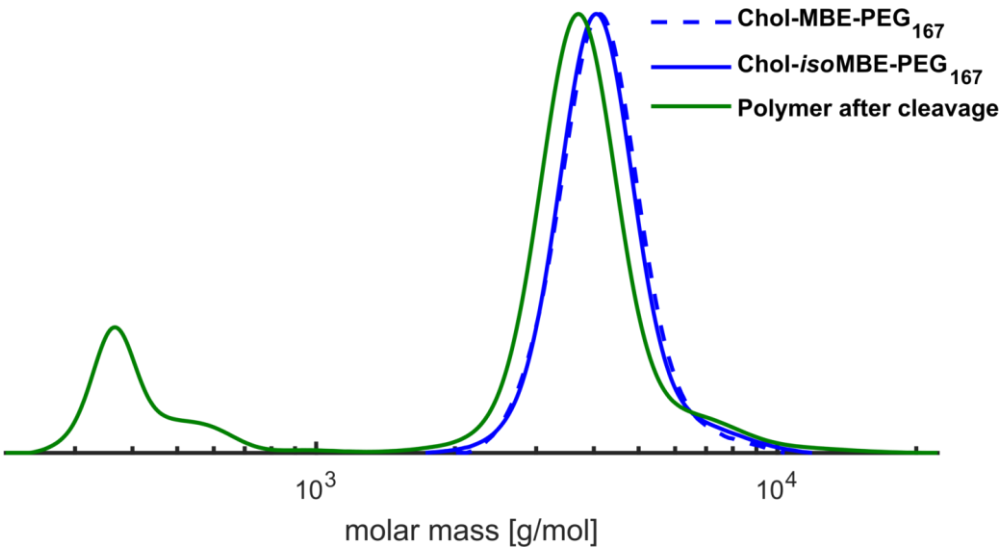

Figure 13: SEC traces (RI detector, DMF, PEG standards) of the Chol-MBE-PEG polymer (dashed), the Chol-*iso*MBE-PEG polymer (continuous) and the fragments after acidic hydrolysis (green).

For the analysis of the fragments by SEC measurement, the polymer solution was neutralized and the solvent removed. The hydrolysis products were then added to the SEC column as a mixture without purification. As expected, two compounds could be detected. One compound with a molecular weight of about 3200 g/mol, the other with a molecular weight of about 500 g/mol. These molecular weights correspond quite closely to the hydrolysis products. A shift to lower molecular weights in the higher molecular range additionally confirms the cleavage of the hydrophobic initiator from the PEG backbone.

2.1.4 Conclusion

In this work, the synthesis of a new class of acid-cleavable cholesterol-based polyether lipids was presented. Here, a cholesterol-based initiator was first prepared *via* a multistep synthesis procedure, which was then used in an anionic ring-opening polymerization (AROP) with ethylene oxide (EO) to produce amphiphilic polyether lipids. To allow cleavage at pH values in the acidic range, the allyl position between the hydrophobic cholesterol anchor and the hydrophilic polyether moiety was isomerized to obtain a vinyl ether structure. Comparative structures without a cleavage site were also prepared. All polymers were analyzed and characterized by NMR spectroscopy, Size Exclusion chromatography (SEC) and Matrix Assisted Laser Desorption Ionization-Time of Flight Mass spectrometry

(MALDI-ToF MS). Polymers with narrow molecular weight distributions were obtained ($Đ$ < 1.11). Furthermore, SEC cleavage studies were performed to obtain information about the fragments after cleavage. To enable further functionalization, for example with an active ingredient, an antibody or even a dye, the polymers were post-modified using propargyl bromide. This allows further reaction using Cu(I)-catalyzed alkyne-azide cycloaddition (CuAAC).

2.1.5 Acknowledgment

E.B. thanks [redacted] for the SEC measurements, [redacted] for the MALDI-ToF measurements and the DFG in the context of the SFB 1066 for financial support.

References

(1) Herzberger, J.; Niederer, K.; Pohlit, H.; Seiwert, J.; Worm, M.; Wurm, F. R.; Frey, H. Polymerization of Ethylene Oxide, Propylene Oxide, and Other Alkylene Oxides: Synthesis, Novel Polymer Architectures, and Bioconjugation. *Chem. Rev.* **2015**, acs.chemrev.5b00441. https://doi.org/10.1021/acs.chemrev.5b00441.

(2) Hofmann, A. M.; Wurm, F.; Frey, H. Rapid Access to Polyfunctional Lipids with Complex Architecture via Oxyanionic Ring-Opening Polymerization. *Macromolecules* **2011**, *44* (12), 4648–4657. https://doi.org/10.1021/ma200367c.

(3) Dingels, C.; Schömer, M.; Frey, H. Die Vielen Gesichter Des Poly (Ethylenglykol) S. *Chemie unserer Zeit* **2011**, *45* (5), 338–349. https://doi.org/10.1002/ciuz.201100551.

(4) Pasut, G.; Veronese, F. M. Polymer-Drug Conjugation, Recent Achievements and General Strategies. *Prog. Polym. Sci.* **2007**, *32* (8–9), 933–961. https://doi.org/10.1016/j.progpolymsci.2007.05.008.

(5) Veronese, F. M.; Pasut, G. PEGylation, Successful Approach to Drug Delivery. *Drug Discov. Today* **2005**, *10* (21), 1451–1458.

(6) Nuhn, L.; Vanparijs, N.; De Beuckelaer, A.; Lybaert, L.; Verstraete, G.; Deswarte, K.; Lienenklaus, S.; Shukla, N. M.; Salyer, A. C. D.; Lambrecht, B. N.; Grooten, J.; David, S. A.; De Koker, S.; De Geest, B. G. PH-Degradable Imidazoquinoline-Ligated Nanogels for Lymph Node-Focused Immune Activation. *Proc. Natl. Acad. Sci.* **2016**, *113* (29), 8098–8103. https://doi.org/10.1073/pnas.1600816113.

(7) Lynn, G. M.; Laga, R.; Darrah, P. A.; Ishizuka, A. S.; Balaci, A. J.; Dulcey, A. E.; Pechar, M.; Pola, R.; Gerner, M. Y.; Yamamoto, A.; Buechler, C. R.; Quinn, K. M.;

Smelkinson, M. G.; Vanek, O.; Cawood, R.; Hills, T.; Vasalatiy, O.; Kastenmüller, K.; Francica, J. R.; Stutts, L.; Tom, J. K.; Ryu, K. A.; Esser-Kahn, A. P.; Etrych, T.; Fisher, K. D.; Seymour, L. W.; Seder, R. A. In Vivo Characterization of the Physicochemical Properties of Polymer-Linked TLR Agonists That Enhance Vaccine Immunogenicity. *Nat. Biotechnol.* **2015**, *33* (11), 1201–1210. https://doi.org/10.1038/nbt.3371.

(8) Torchilin, V. Tumor Delivery of Macromolecular Drugs Based on the EPR Effect. *Adv. Drug Deliv. Rev.* **2011**, *63* (3), 131–135. https://doi.org/10.1016/j.addr.2010.03.011.

(9) Hu, L.; Quach, T.; Han, S.; Lim, S. F.; Yadav, P.; Senyschyn, D.; Trevaskis, N. L.; Simpson, J. S.; Porter, C. J. H. Glyceride-Mimetic Prodrugs Incorporating Self-Immolative Spacers Promote Lymphatic Transport, Avoid First-Pass Metabolism, and Enhance Oral Bioavailability. *Angew. Chemie* **2016**, *128* (44), 13904–13909. https://doi.org/10.1002/ange.201604207.

(10) De Vrieze, J.; Louage, B.; Deswarte, K.; Zhong, Z.; De Coen, R.; Van Herck, S.; Nuhn, L.; Kaas Frich, C.; Zelikin, A. N.; Lienenklaus, S.; Sanders, N. N.; Lambrecht, B. N.; David, S. A.; De Geest, B. G. Amphiphile Polymer-Lipidkonjugate Zur Potenten Lymphatischen Anreicherung von TLR7/8-Agonisten Ermöglichen Eine Örtlich Begrenzte Aktivierung Des Angeborenen Immunsystems. *Angew. Chemie* **2019**, *131* (43), 15535–15541. https://doi.org/10.1002/ange.201905687.

(11) Liu, H.; Moynihan, K. D.; Zheng, Y.; Szeto, G. L.; Li, A. V.; Huang, B.; Van Egeren, D. S.; Park, C.; Irvine, D. J. Structure-Based Programming of Lymph-Node Targeting in Molecular Vaccines. *Nature* **2014**, *507* (7493), 519–522. https://doi.org/10.1038/nature12978.

(12) De Vrieze, J.; Van Herck, S.; Nuhn, L.; De Geest, B. G. Design of PH-Degradable Polymer-Lipid Amphiphiles Using a Ketal-Functionalized RAFT Chain Transfer Agent. *Macromol. Rapid Commun.* **2020**, *41* (18). https://doi.org/10.1002/marc.202000034.

(13) Jangra, S.; De Vrieze, J.; Choi, A.; Rathnasinghe, R.; Laghlali, G.; Uvyn, A.; Van Herck, S.; Nuhn, L.; Deswarte, K.; Zhong, Z.; Sanders, N. N.; Lienenklaus, S.; David, S. A.; Strohmeier, S.; Amanat, F.; Krammer, F.; Hammad, H.; Lambrecht, B. N.; Coughlan, L.; García-Sastre, A.; De Geest, B. G.; Schotsaert, M. Sterilizing Immunity against SARS-CoV-2 Infection in Mice by a Single-Shot and Lipid Amphiphile Imidazoquinoline TLR7/8 Agonist-Adjuvanted Recombinant Spike Protein Vaccine**. *Angew. Chemie* **2021**, 9467–9473. https://doi.org/10.1002/ange.202015362.

(14) Wu, T. Y.-H.; Singh, M.; Miller, A. T.; De Gregorio, E.; Doro, F.; D\textquoterightOro,

U.; Skibinski, D. A. G.; Mbow, M. L.; Bufali, S.; Herman, A. E.; Cortez, A.; Li, Y.; Nayak, B. P.; Tritto, E.; Filippi, C. M.; Otten, G. R.; Brito, L. A.; Monaci, E.; Li, C.; Aprea, S.; Valentini, S.; Calabró, S.; Laera, D.; Brunelli, B.; Caproni, E.; Malyala, P.; Panchal, R. G.; Warren, T. K.; Bavari, S.; O\textquoterightHagan, D. T.; Cooke, M. P.; Valiante, N. M. Rational Design of Small Molecules as Vaccine Adjuvants. *Sci. Transl. Med.* **2014**, *6* (263), 263ra160--263ra160. https://doi.org/10.1126/scitranslmed.3009980.

(15) Worm, M.; Leibig, D.; Dingels, C.; Frey, H. Cleavable Polyethylene Glycol: 3,4-Epoxy-1-Butene as a Comonomer to Establish Degradability at Physiologically Relevant PH. *ACS Macro Lett.* **2016**, *5* (12), 1357–1363. https://doi.org/10.1021/acsmacrolett.6b00735.

(16) Steiert, E.; Ewald, J.; Wagner, A.; Hellmich, U. A.; Frey, H.; Wich, P. R. PH-Responsive Protein Nanoparticles: Via Conjugation of Degradable PEG to the Surface of Cytochrome C. *Polym. Chem.* **2020**, *11* (2), 551–559. https://doi.org/10.1039/c9py01162e.

(17) Gleue, L.; Schupp, J.; Zimmer, N.; Becker, E.; Frey, H.; Tuettenberg, A.; Helm, M. Stability of Alkyl Chain-Mediated Lipid Anchoring in Liposomal Membranes. *Cells* **2020**, *9* (10), 1–13. https://doi.org/10.3390/cells9102213.

(18) Woods, E. C.; Yee, N. A.; Shen, J.; Bertozzi, C. R. Glycocalyx Engineering with a Recycling Glycopolymer That Increases Cell Survival in Vivo. *Angew. Chemie - Int. Ed.* **2015**, *54* (52), 15782–15788. https://doi.org/10.1002/anie.201508783.

(19) An, H.; Bradshaw, J. S.; Krakowiak, K. E.; Zhu, C.; Dailey, N. K.; Izatt, R. M. Synthesis and Complexation Properties of Suitcase-Shaped Macrotricyclic and Butterfly-Shaped Macrobicyclic Polyether Ligands. *J.Org.Chem.* **1992**, No. 13, 4998–5005.

(20) de Vries, E. F. J.; Steenwinkel, P.; Brussee, J.; Kruse, C. G.; van der Gen, A. Synthesis of Chiral Diaza-18-Crown-6 Derivatives from Optically Active Diethanolamines. *J. Org. Chem.* **1993**, *58* (16), 4315–4325. https://doi.org/10.1021/jo00068a029.

(21) Reibel, A. T.; Müller, S. S.; Pektor, S.; Bausbacher, N.; Miederer, M.; Frey, H.; Rösch, F. Fate of Linear and Branched Polyether-Lipids in Vivo in Comparison to Their Liposomal Formulations by 18F-Radiolabeling and Positron Emission Tomography. *Biomacromolecules* **2015**, *16* (3), 842–851. https://doi.org/10.1021/bm5017332.

(22) Ewald, J. Vinyl Ether Moieties as a Key Component for Cleavable Poly (Ethylene Glycol) Copolymers. **2020**.

(23) Bajaj, A.; Mishra, S. K.; Kondaiah, P.; Bhattacharya, S. Effect of the Headgroup Variation on the Gene Transfer Properties of Cholesterol Based Cationic Lipids

Possessing Ether Linkage. *Biochim. Biophys. Acta - Biomembr.* **2008**, *1778* (5), 1222–1236. https://doi.org/10.1016/j.bbamem.2007.12.010.

(24) Lichtfouse, E.; Albrecht, P. Synthesis of Triaromatic Steroid Hydrocarbons Methylated at Position 2, 3 or 6: Molecular Fossils of yet Unknown Biological Origin. *Tetrahedron* **1994**, *50* (6), 1731–1744. https://doi.org/10.1016/S0040-4020(01)80848-6.

(25) Prosser, T. J. The Rearrangement of Allyl Ethers to Propenyl Ethers. *J. Am. Chem. Soc.* **1961**, *83* (7), 1701–1704. https://doi.org/10.1021/ja01468a035.

(26) Price, C. C.; Snyder, W. H. Solvent Effects in the Base-Catalyzed Isomerization of Allyl to Propenyl Ethers. *J. Am. Chem. Soc.* **1961**, *83* (7), 1773. https://doi.org/10.1021/ja01468a062.

(27) Van Dijk, M.; Rijkers, D. T. S.; Liskamp, R. M. J.; Van Nostrum, C. F.; Hennink, W. E. Synthesis and Applications of Biomedical and Pharmaceutical Polymers via Click Chemistry Methodologies. *Bioconjug. Chem.* **2009**, *20* (11), 2001–2016. https://doi.org/10.1021/bc900087a.

(28) Wagener, K.; Bros, M.; Krumb, M.; Langhanki, J.; Pektor, S.; Worm, M.; Schinnerer, M.; Montermann, E.; Miederer, M.; Frey, H.; Opatz, T.; Rösch, F. Targeting of Immune Cells with Trimannosylated Liposomes. *Adv. Ther.* **2020**, *3* (6), 1900185. https://doi.org/10.1002/adtp.201900185.

(29) Miron, T.; Wilchek, M. A Simplified Method for the Preparation of Succinimidyl Carbonate Polyethylene Glycol for Coupling to Proteins. *Bioconjug. Chem.* **1993**, *4* (6), 568–569. https://doi.org/10.1021/bc00024a022.

(30) Gandini, A. The Furan/Maleimide Diels-Alder Reaction: A Versatile Click-Unclick Tool in Macromolecular Synthesis. *Prog. Polym. Sci.* **2013**, *38* (1), 1–29. https://doi.org/10.1016/j.progpolymsci.2012.04.002.

(31) Wagener, K.; Worm, M.; Pektor, S.; Schinnerer, M.; Thiermann, R.; Miederer, M.; Frey, H.; Rösch, F. Comparison of Linear and Hyperbranched Polyether Lipids for Liposome Shielding by 18 F-Radiolabeling and Positron Emission Tomography. *Biomacromolecules* **2018**, *19* (7), 2506–2516. https://doi.org/10.1021/acs.biomac.8b00115.

(32) Herzberger, J.; Fischer, K.; Leibig, D.; Bros, M.; Thiermann, R.; Frey, H. Oxidation-Responsive and "Clickable" Poly(Ethylene Glycol) via Copolymerization of 2-(Methylthio)Ethyl Glycidyl Ether. *J. Am. Chem. Soc.* **2016**, jacs.6b04548. https://doi.org/10.1021/jacs.6b04548.

2.1.6 Supporting Information

2.1.6.1 Initiator synthesis

Synthesis of bifunctional MBE

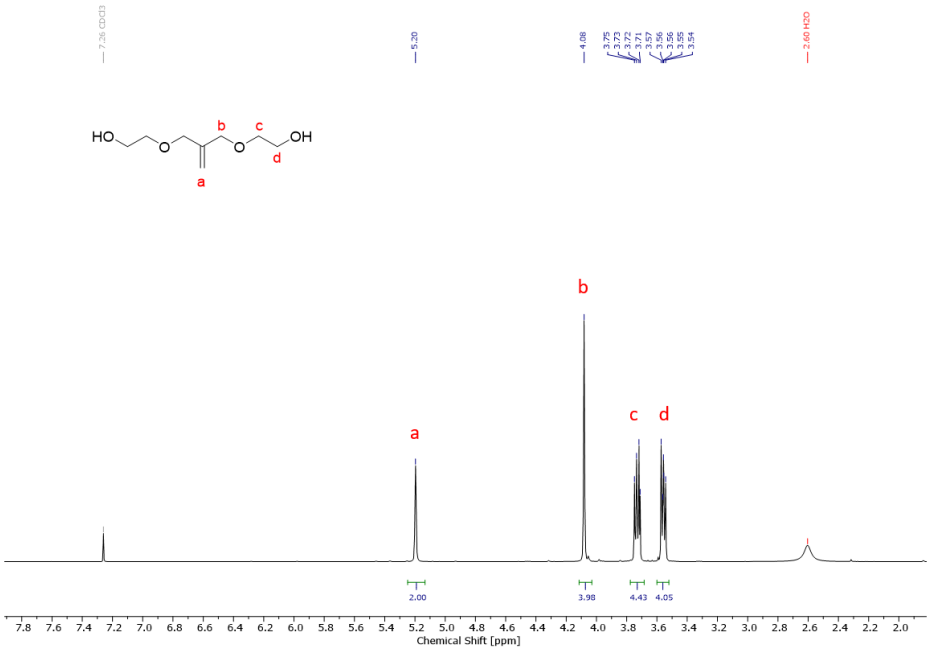

SI-Figure 1: ^{1}H NMR spectrum (300 MHz, chloroform-*d*) of MBE.

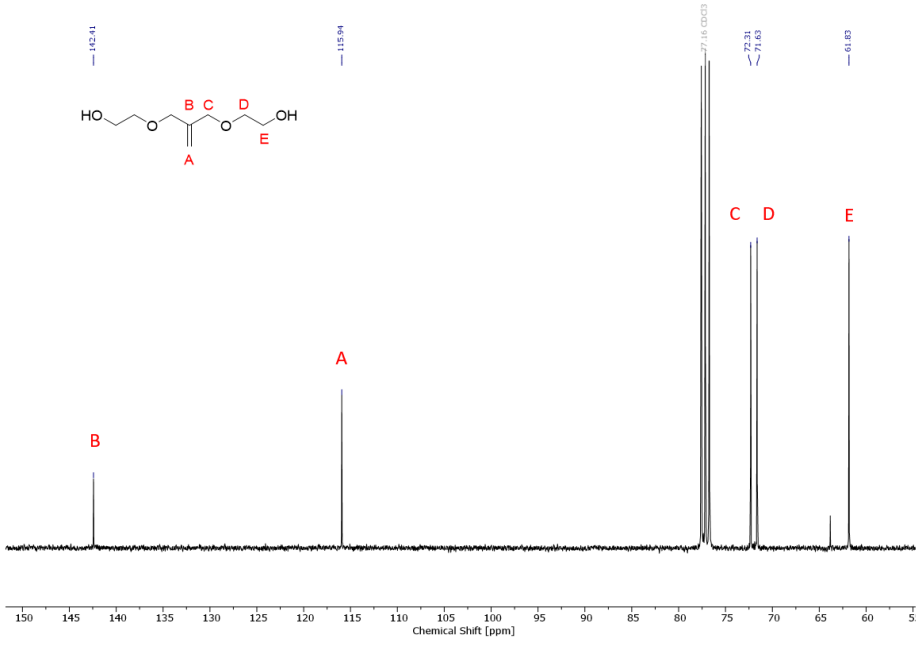

SI-Figure 2: ^{13}C NMR spectrum (75 MHz, chloroform-*d*) of MBE.

Synthesis of monofunctional THP-MBE-OH

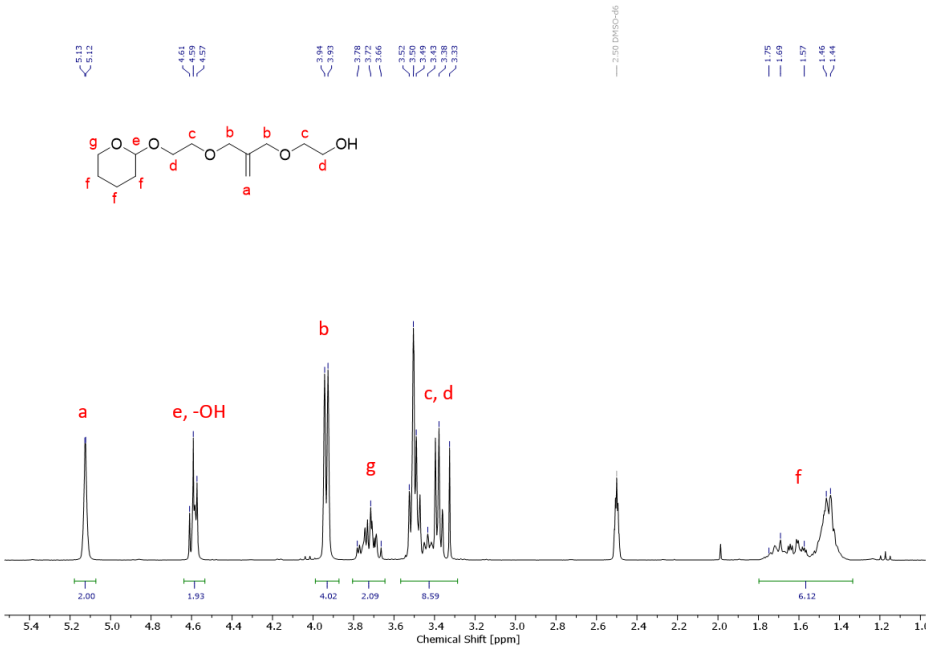

SI-Figure 3: ^{1}H NMR spectrum (300 MHz, DMSO-d_6) of THP-MBE-OH.

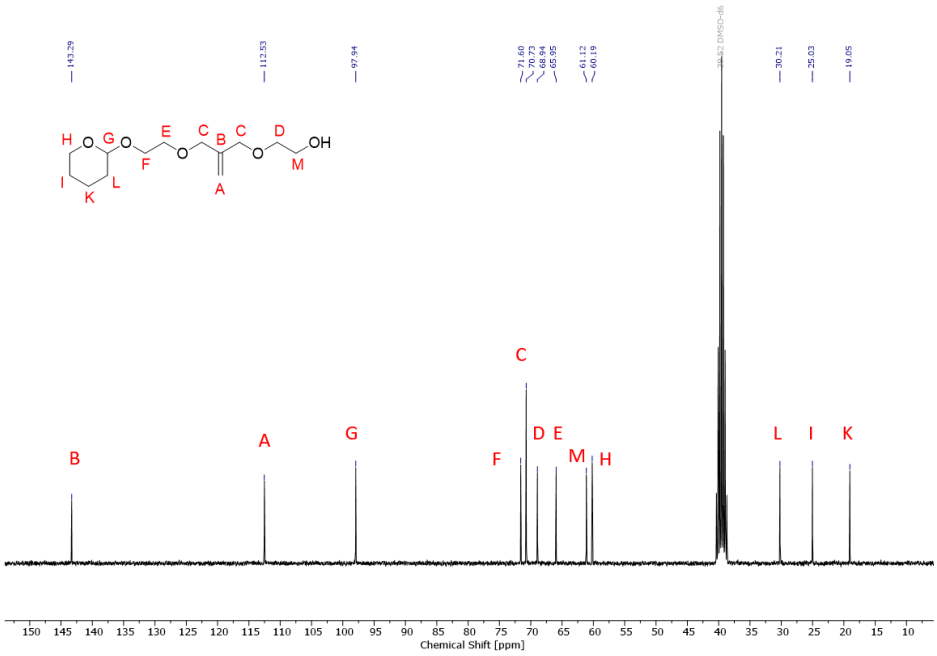

SI-Figure 4: ^{13}C NMR spectrum (75 MHz, DMSO-d_6) of THP-MBE-OH.

Synthesis of THP-MBE-Ts

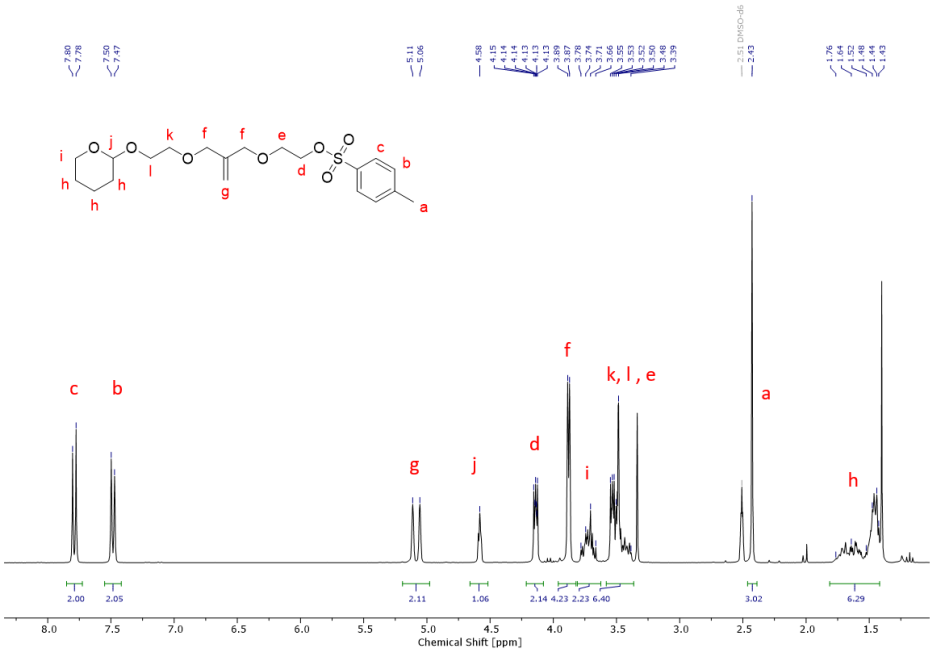

SI-Figure 5: ^{1}H NMR spectrum (300 MHz, DMSO-d_6) of THP-MBE-Ts.

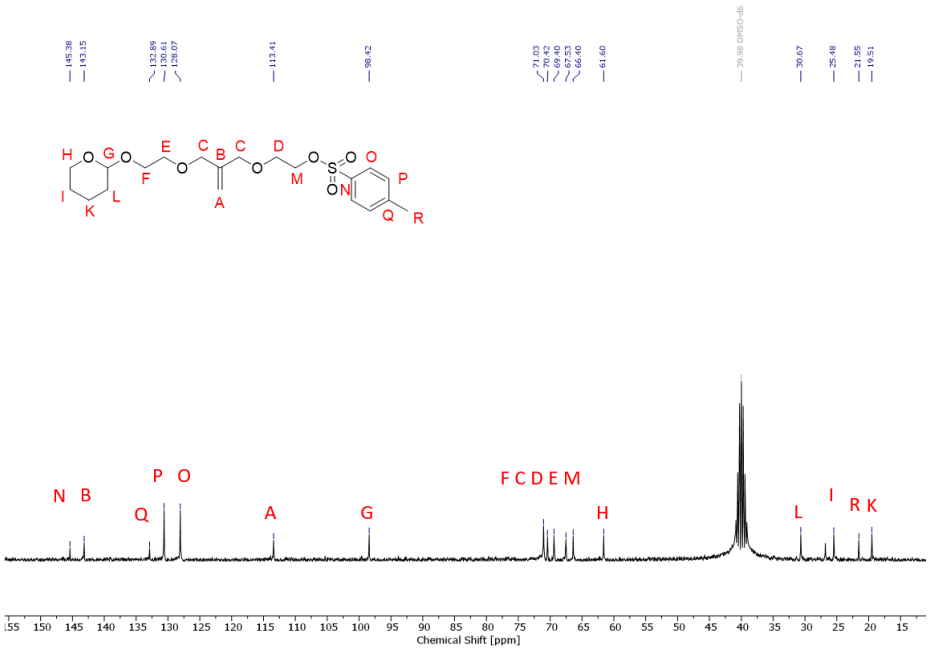

SI-Figure 6: ^{13}C NMR spectrum (75 MHz, DMSO-d_6) of THP-MBE-Ts.

Synthesis of cholesteryl-MBE-THP

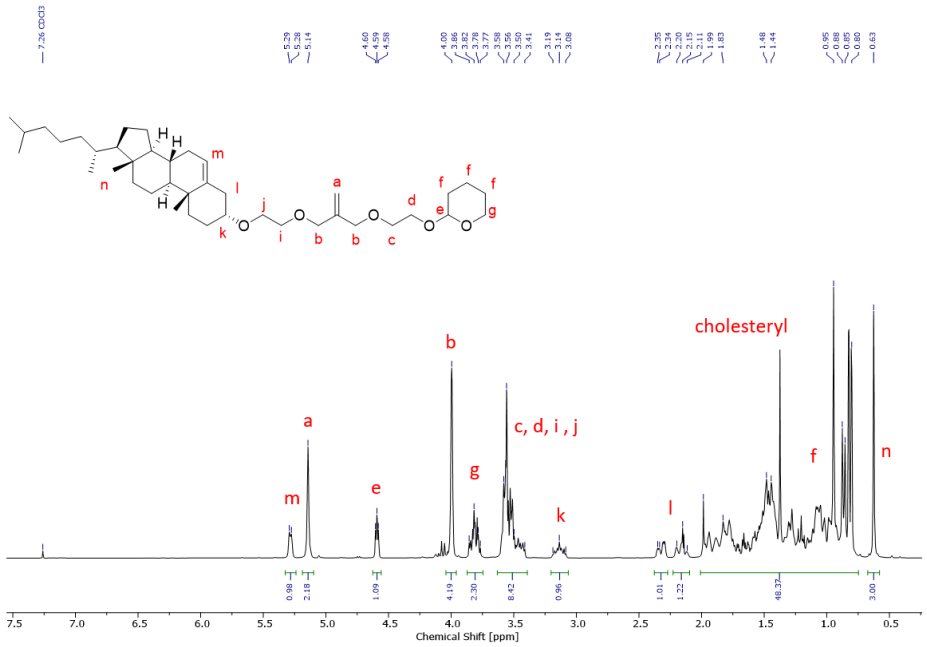

SI-Figure 7: ^{1}H NMR spectrum (300 MHz, chloroform-*d*) of cholesteryl-MBE-THP.

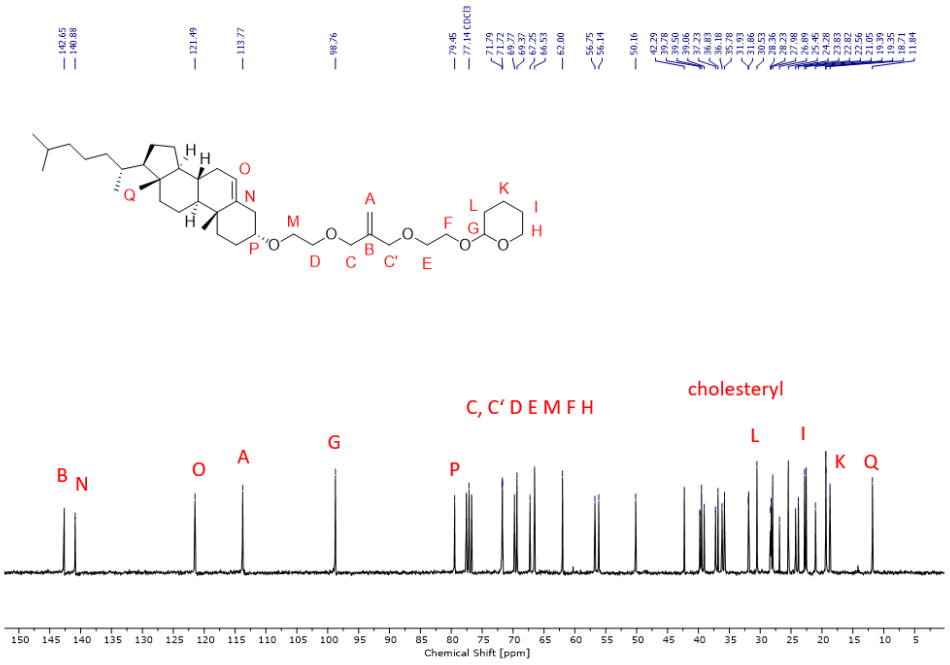

SI-Figure 8: ^{13}C NMR spectrum (75 MHz, chloroform-*d*) of cholesteryl-MBE-THP.

Synthesis of the initiator Chol-MBE-OH

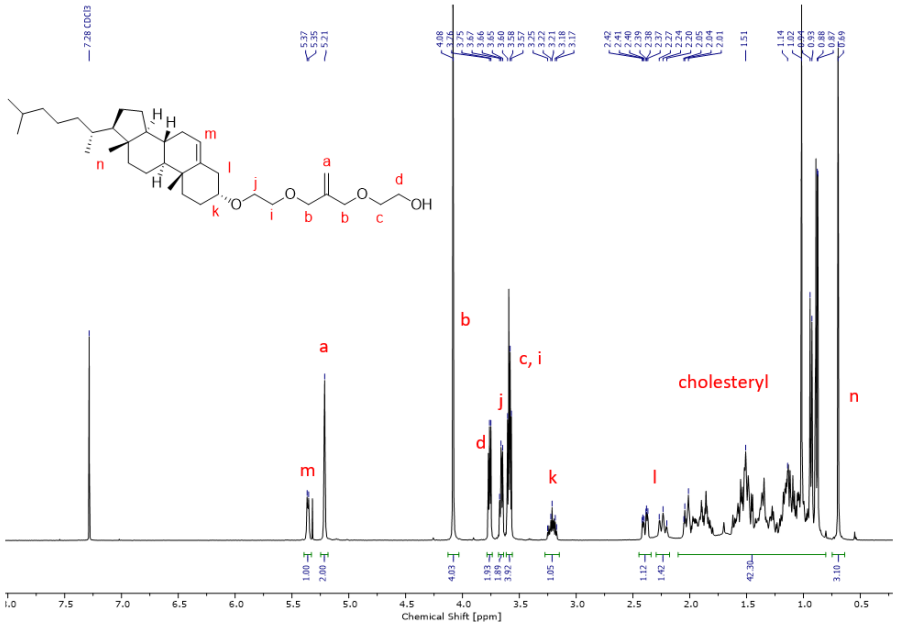

SI-Figure 9: ^{1}H NMR spectrum (300 MHz, chloroform-*d*) of Chol-MBE-OH.

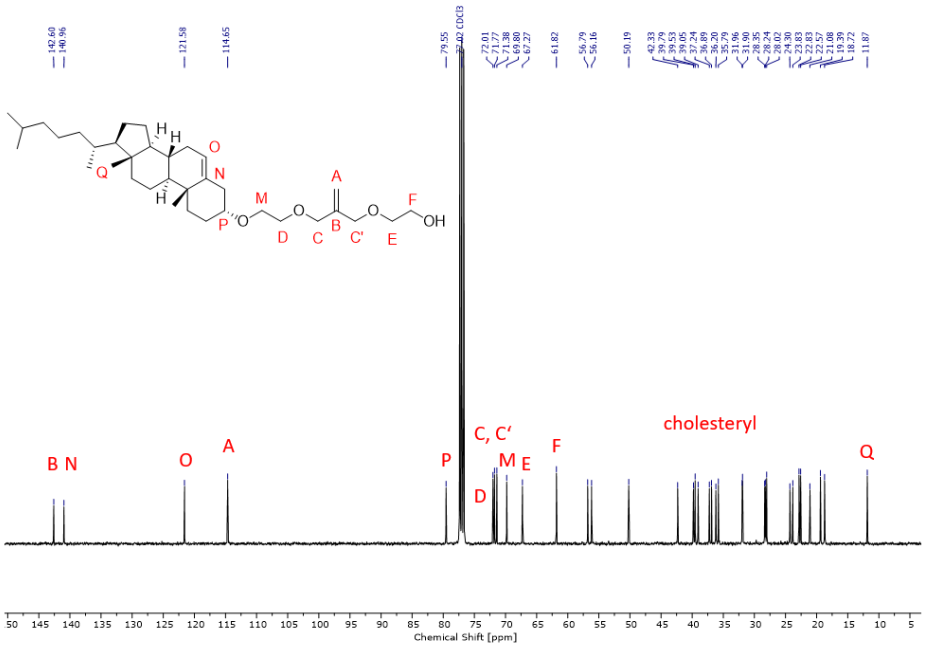

SI-Figure 10: ^{13}C NMR spectrum (75 MHz, chloroform-*d*) of Chol-MBE-OH.

2.1.6.2 Polymer synthesis

Synthesis of Chol-PEG

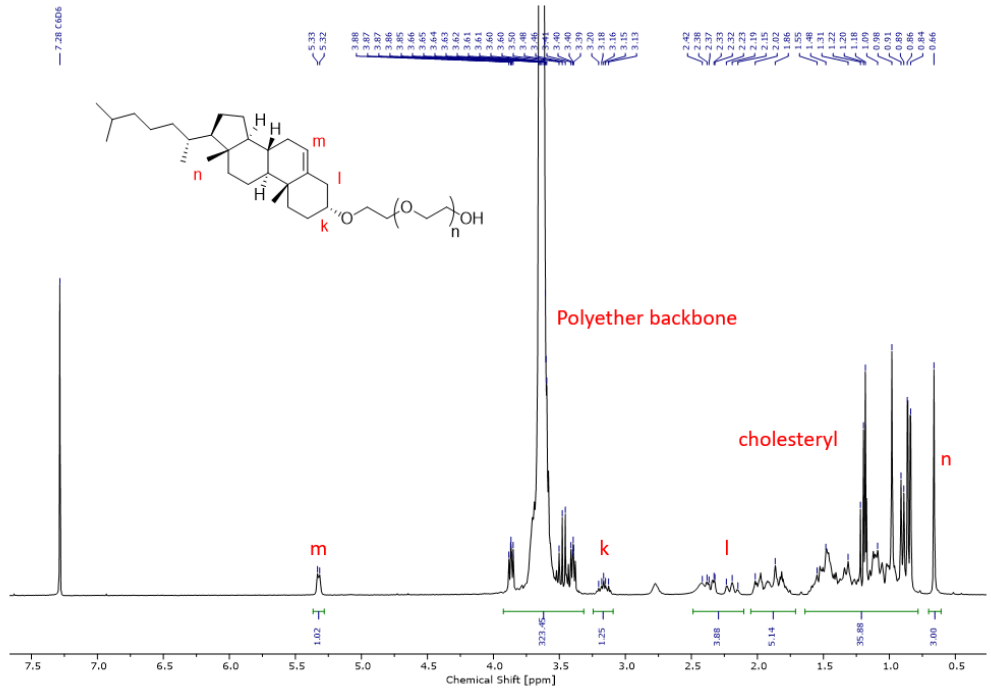

SI-Figure 11: ^{1}H NMR spectrum (300 MHz, benzene-d_6) of Chol-PEG.

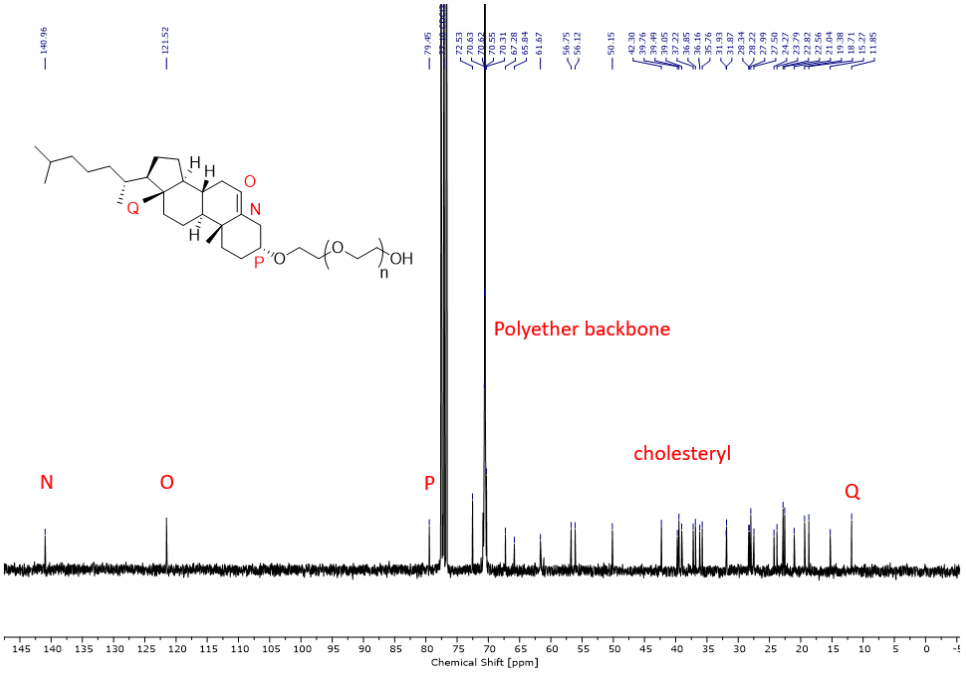

SI-Figure 12: ^{13}C NMR spectrum (75 MHz, chloroform-d) of Chol-PEG.

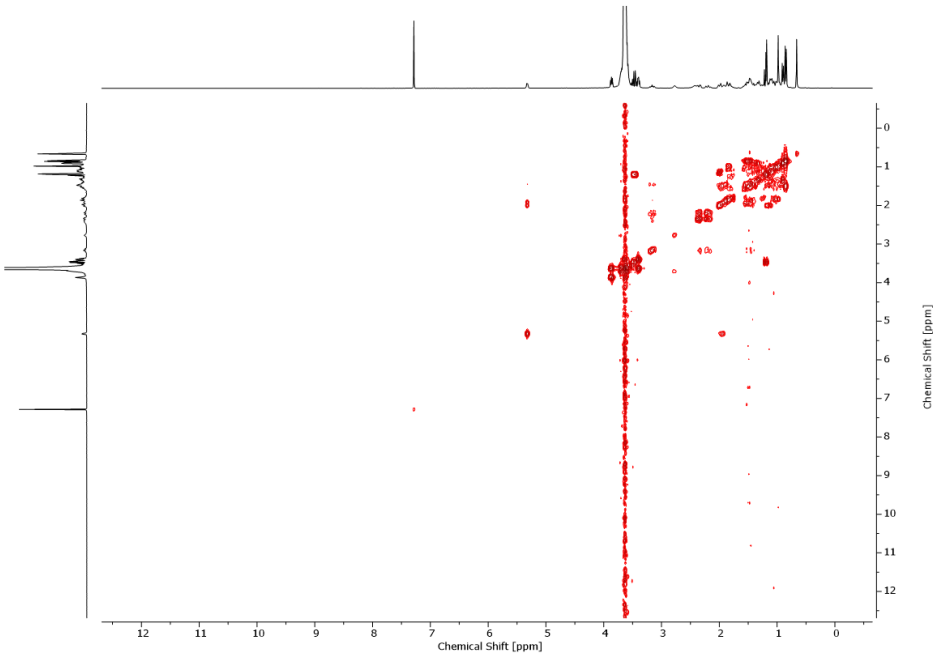

SI-Figure 13: ^{1}H, ^{1}H COSY NMR spectrum (300 MHz, chloroform-*d*) of Chol-PEG.

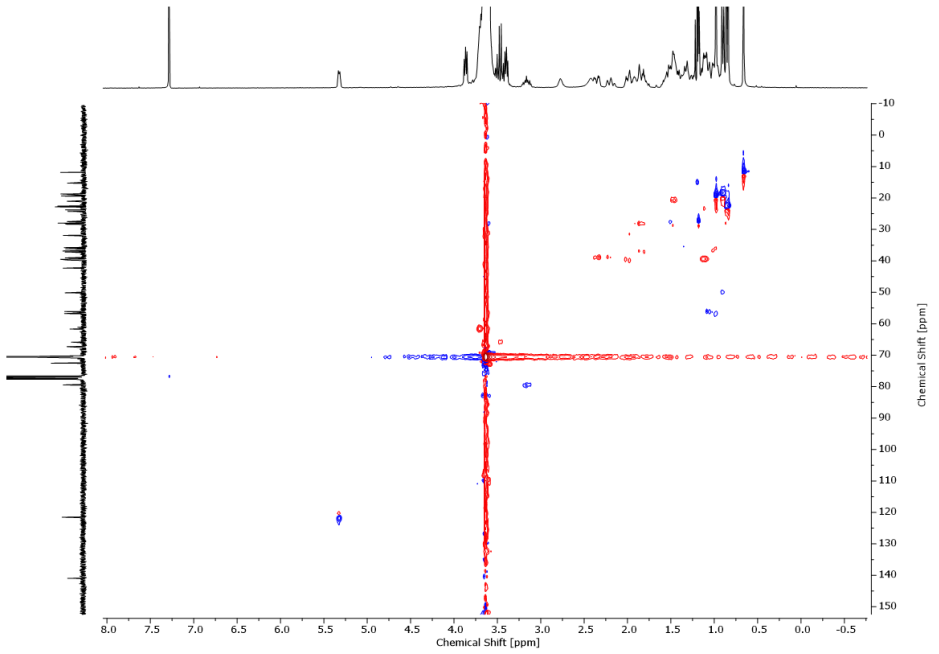

SI-Figure 14: ^{1}H, ^{13}C HSQC NMR spectrum (300 MHz, chloroform-*d*) of Chol-PEG.

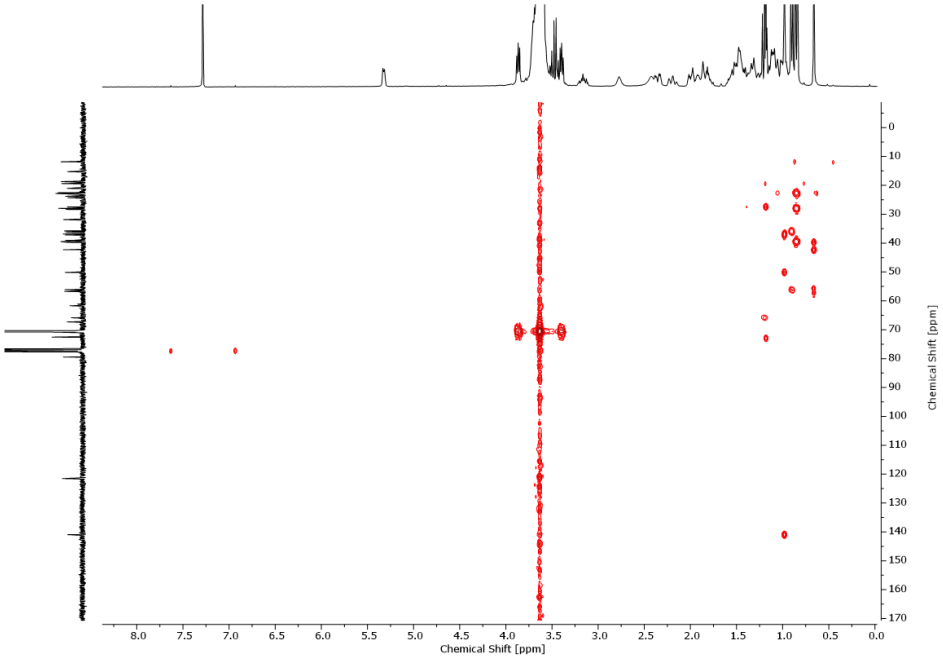

SI-Figure 15: ^{1}H, ^{13}C HMBC NMR spectrum (300 MHz, chloroform-*d*) of Chol-PEG.

Synthesis of Chol-MBE-PEG

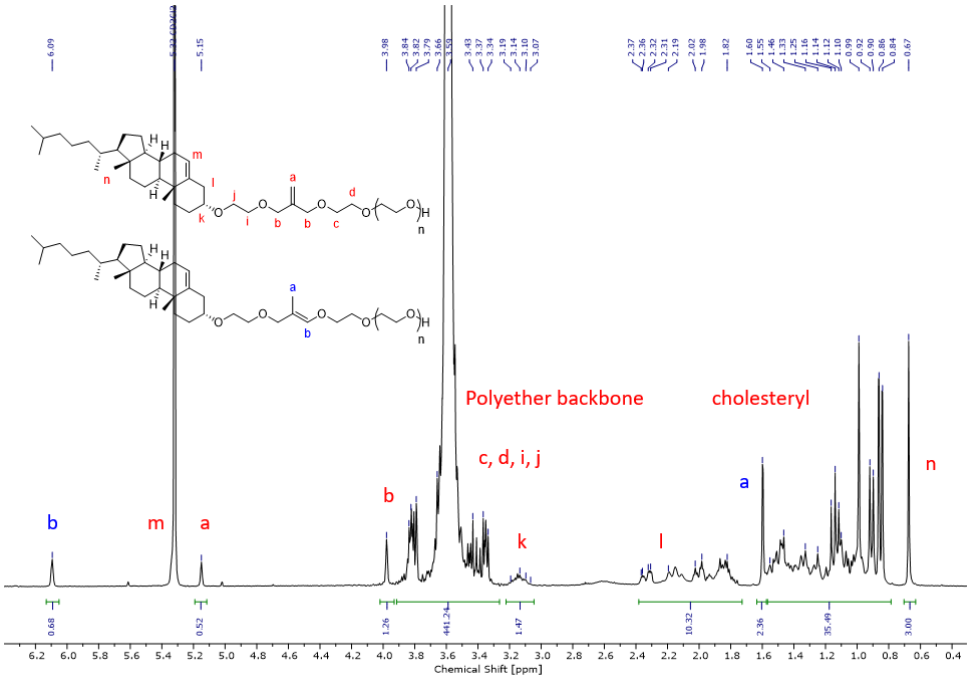

SI-Figure 16: ^{1}H NMR spectrum (300 MHz, methylene chloride-d_2) of Chol-MBE-PEG.

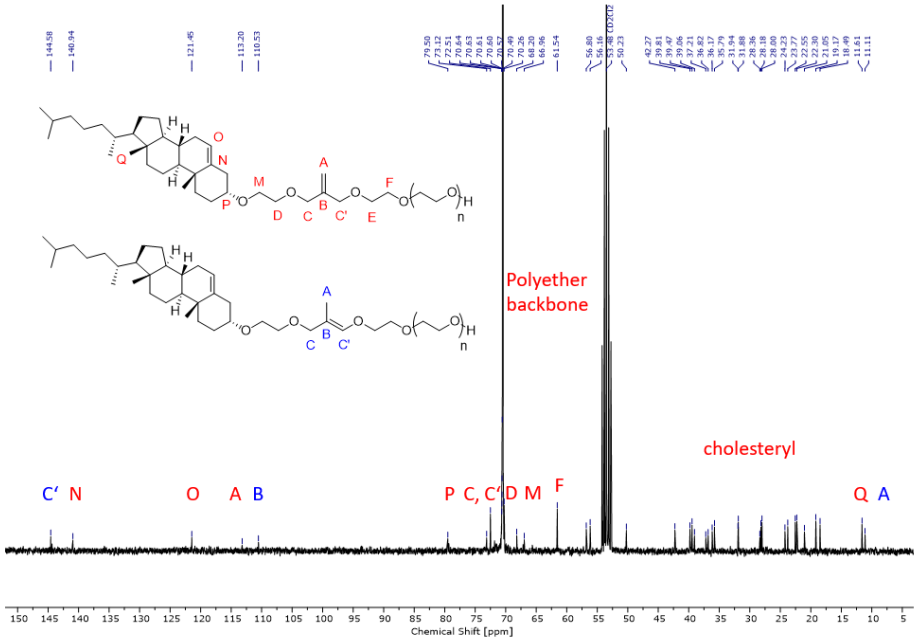

SI-Figure 17: ^{13}C NMR spectrum (75 MHz, methylene chloride-d_2) of Chol-MBE-PEG.

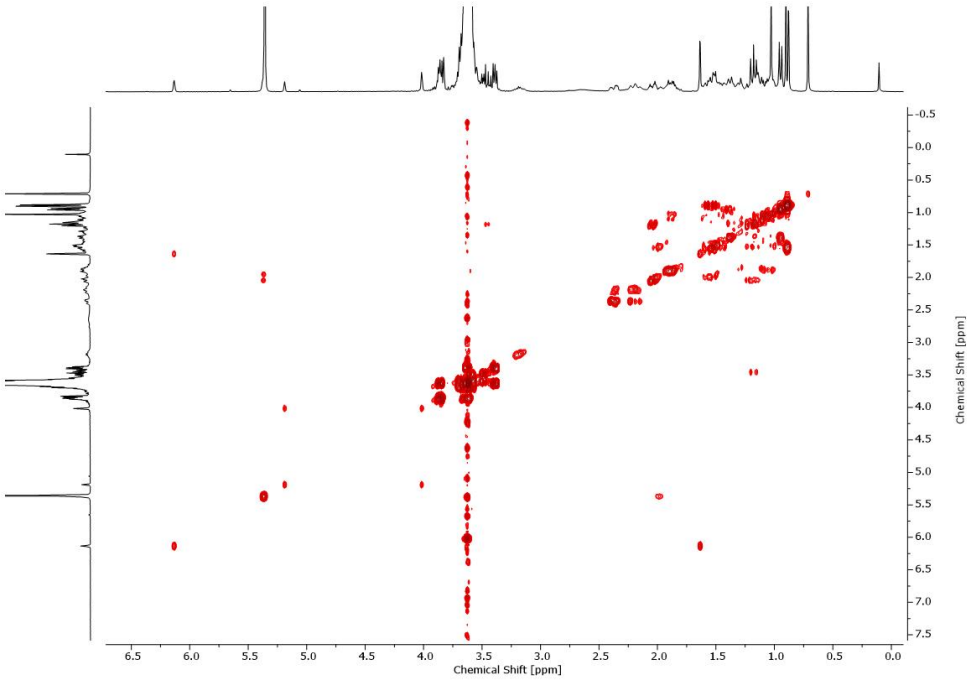

SI-Figure 18: ^{1}H, ^{1}H COSY NMR spectrum (300 MHz, methylene chloride-d_2) of Chol-MBE-PEG.

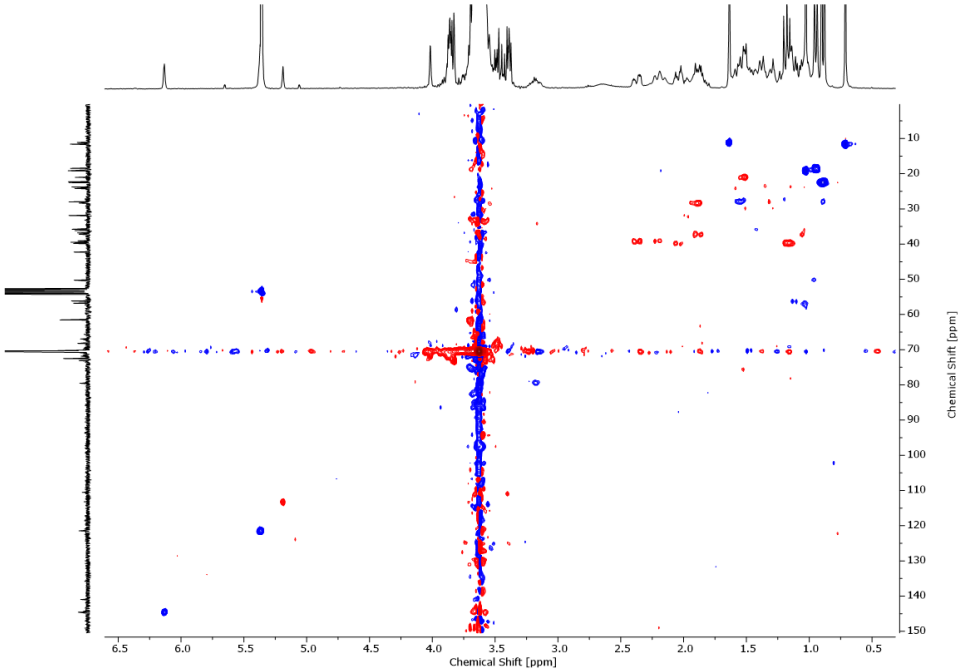

SI-Figure 19: ^{1}H, ^{13}C HSQC NMR spectrum (300 MHz, methylene chloride-d_2) of Chol-MBE-PEG.

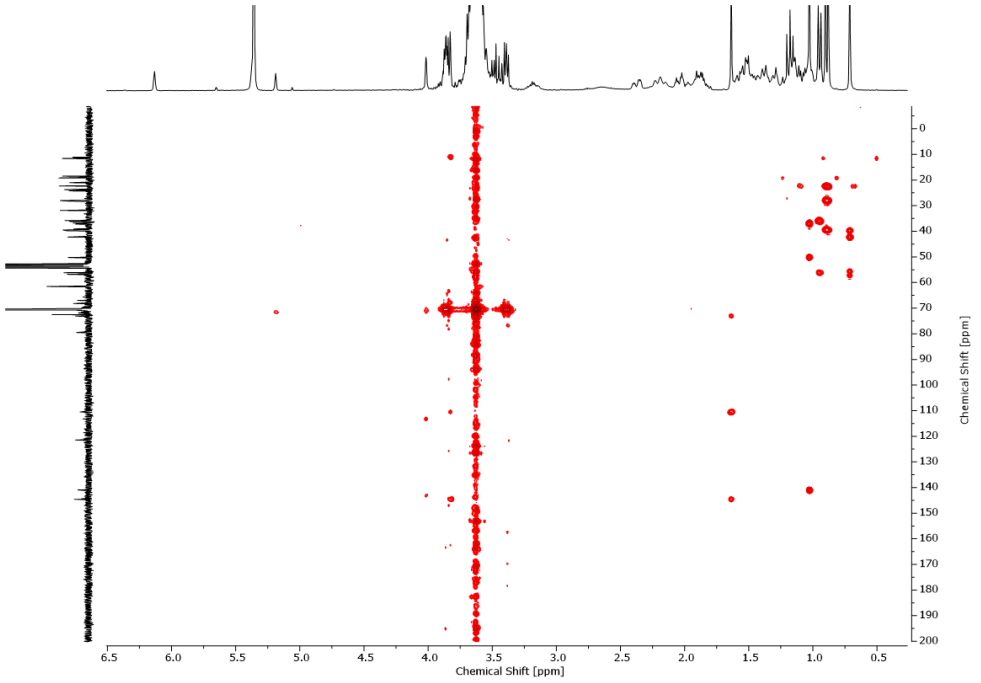

SI-Figure 20: ^{1}H, ^{13}C HMBC NMR spectrum (300 MHz, methylene chloride-d_2) of Chol-MBE-PEG.

Isomerization of Chol-MBE-PEG to Chol-isoMBE-PEG

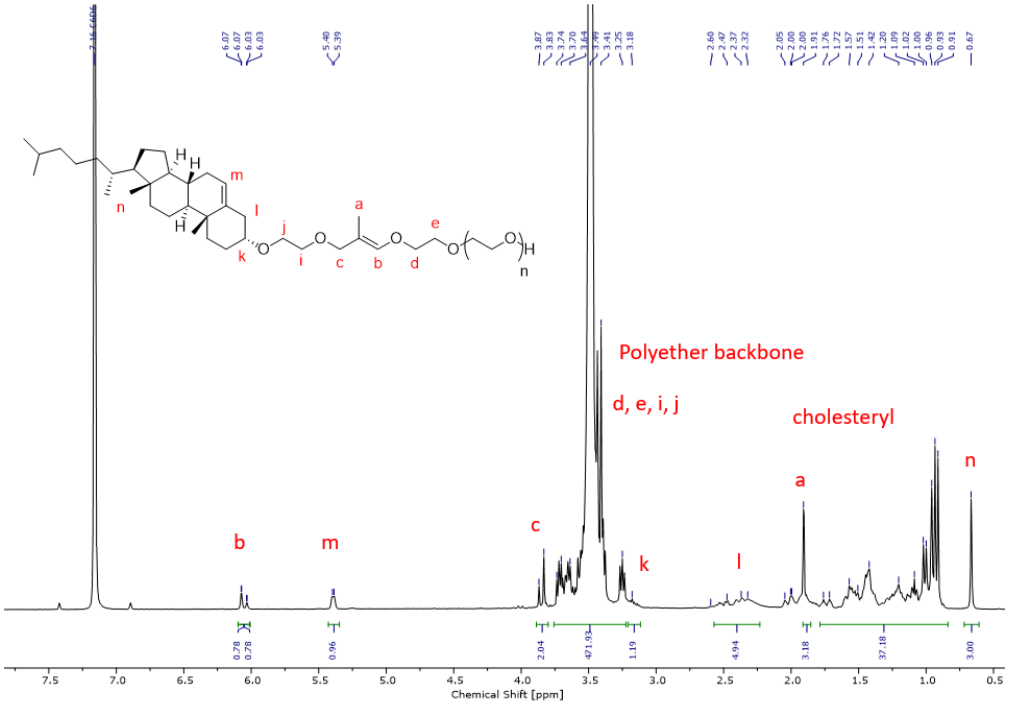

SI-Figure 21: ^{1}H NMR spectrum (300 MHz, benzene-d_6) of Chol-*iso*MBE-PEG.

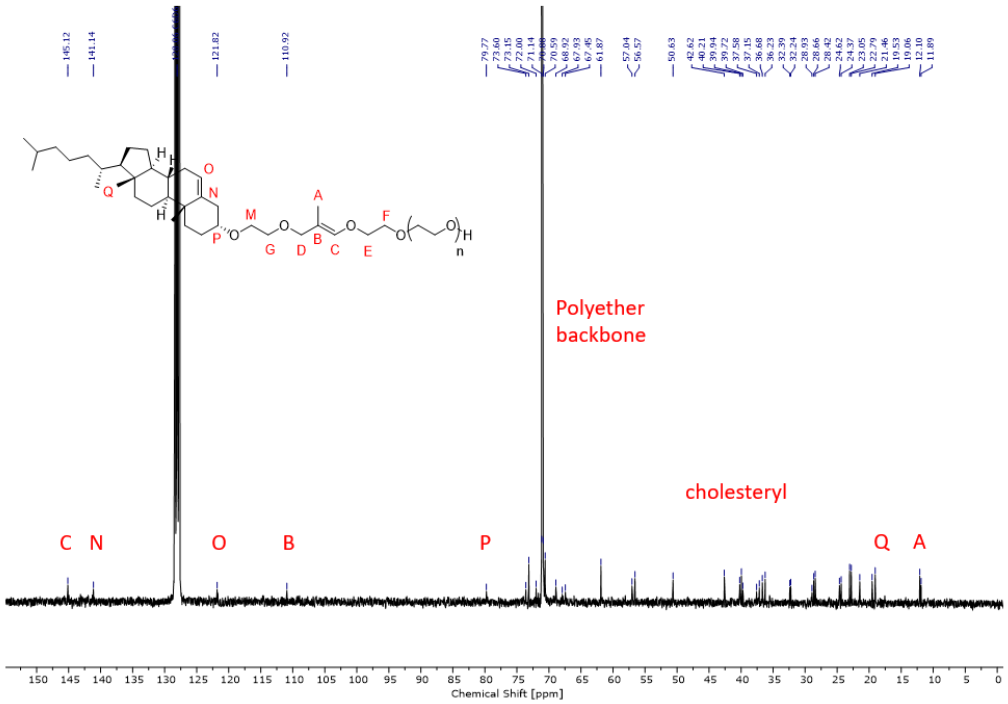

SI-Figure 22: ^{13}C NMR spectrum (75 MHz, benzene-d_6) of Chol-*iso*MBE-PEG.

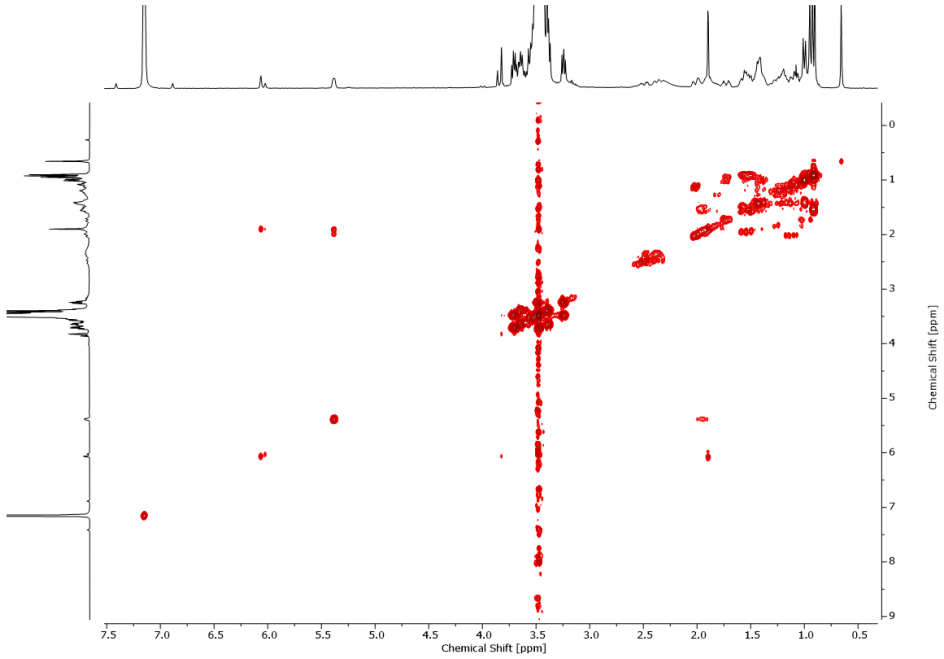

SI-Figure 23: ^{1}H, ^{1}H COSY NMR spectrum (300 MHz, benzene-d_6) of Chol-*iso*MBE-PEG.

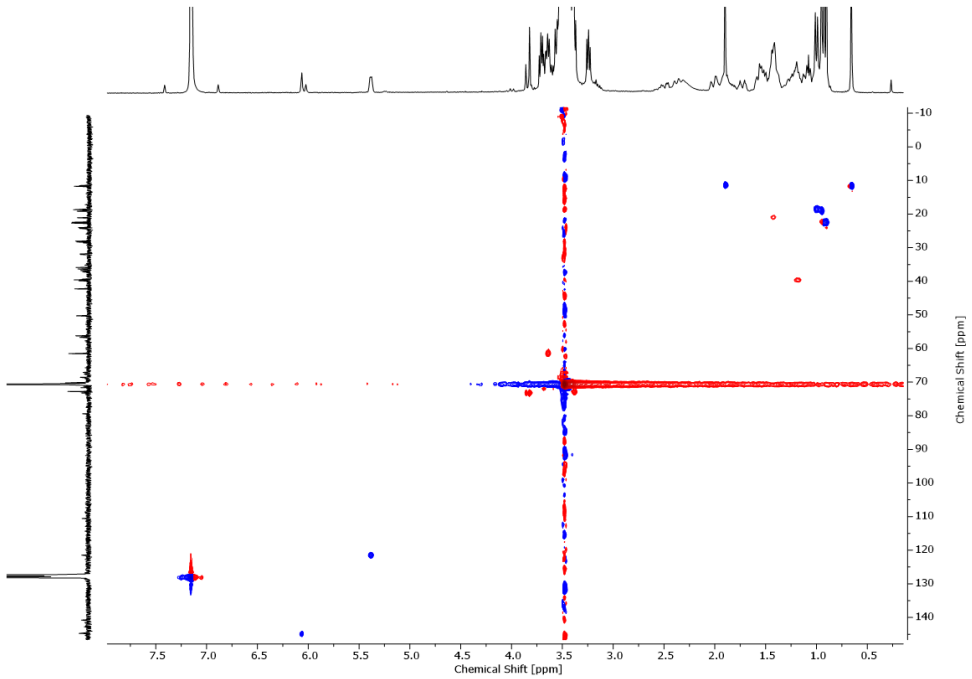

SI-Figure 24: ^{1}H, ^{13}C HSQC NMR spectrum (300 MHz, benzene-d_6) of Chol-*iso*MBE-PEG.

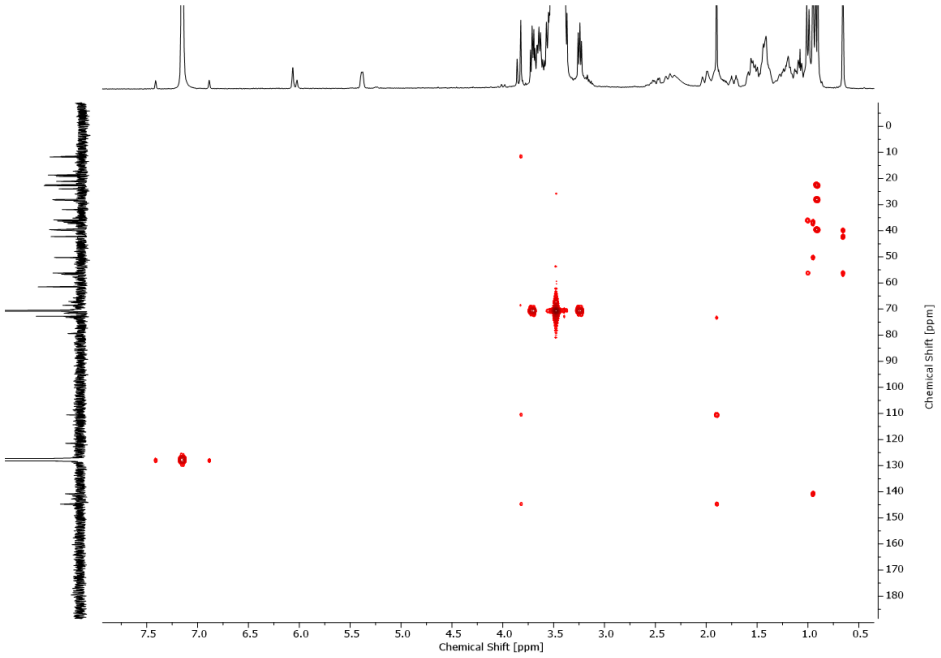

SI-Figure 25: ^{1}H, ^{13}C HMBC NMR spectrum (300 MHz, benzene-d_6) of Chol-*iso*MBE-PEG.

Post-polymerization modification

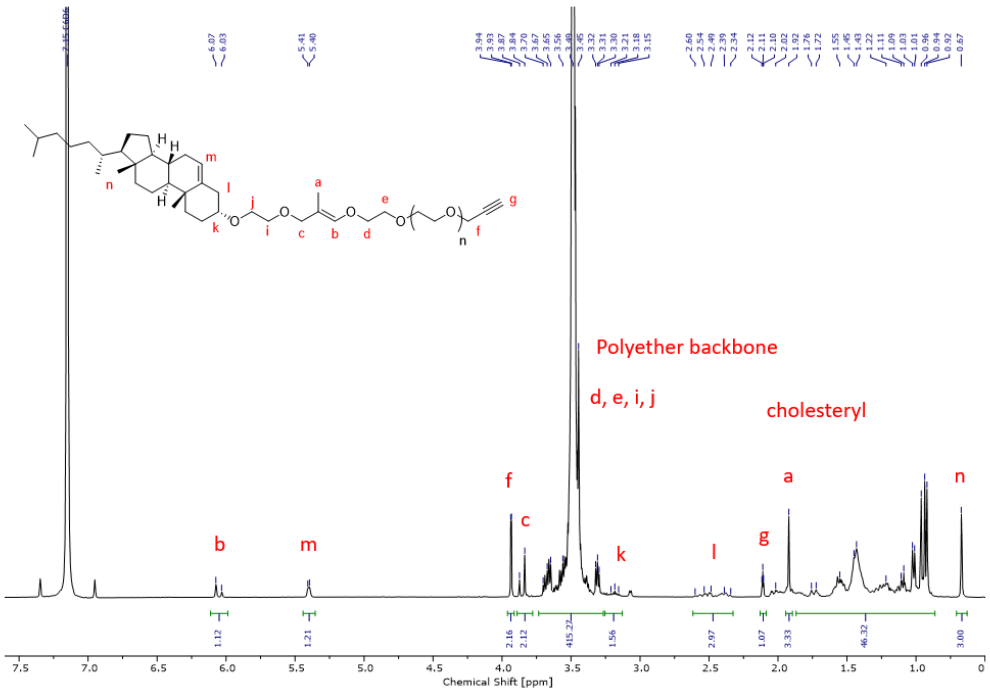

SI-Figure 26: ^{1}H NMR spectrum (400 MHz, benzene-d_6) of Chol-PEG-alkyne.

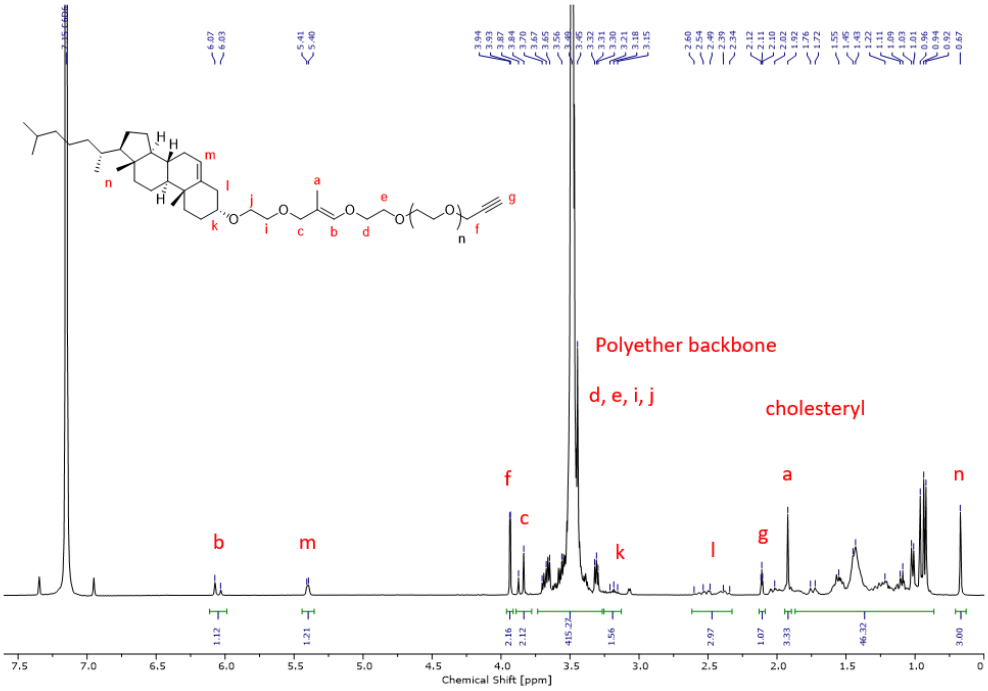

SI-Figure 27: ^{1}H NMR spectrum (400 MHz, benzene-d_6) of Chol-*iso*MBE-PEG-alkyne.

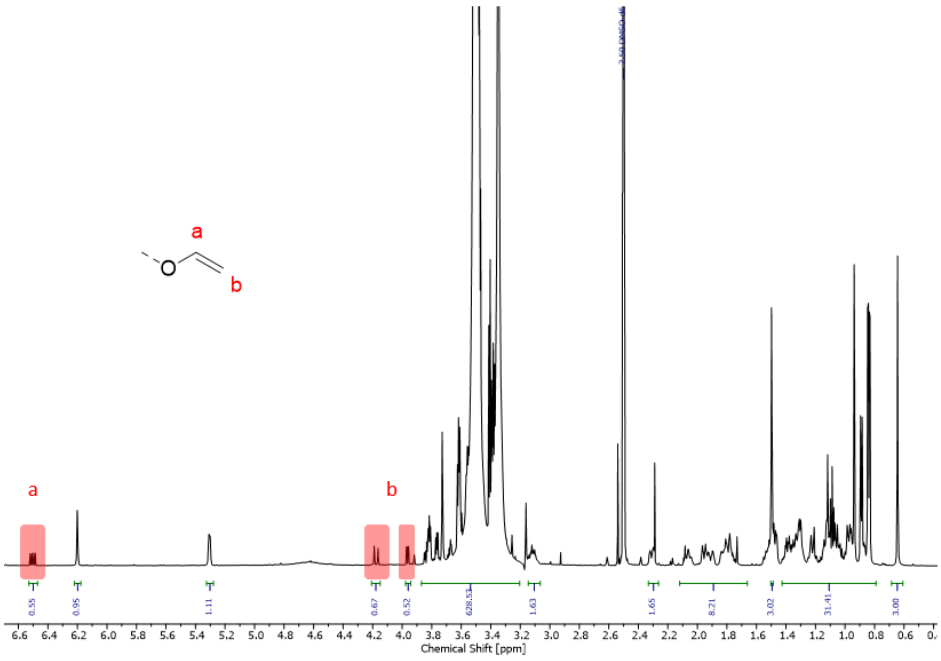

SI-Figure 28: ^{1}H NMR spectrum (300 MHz, DMSO-d_6) of the side reaction during the isomerization with 4 eq. KO^{t}Bu.

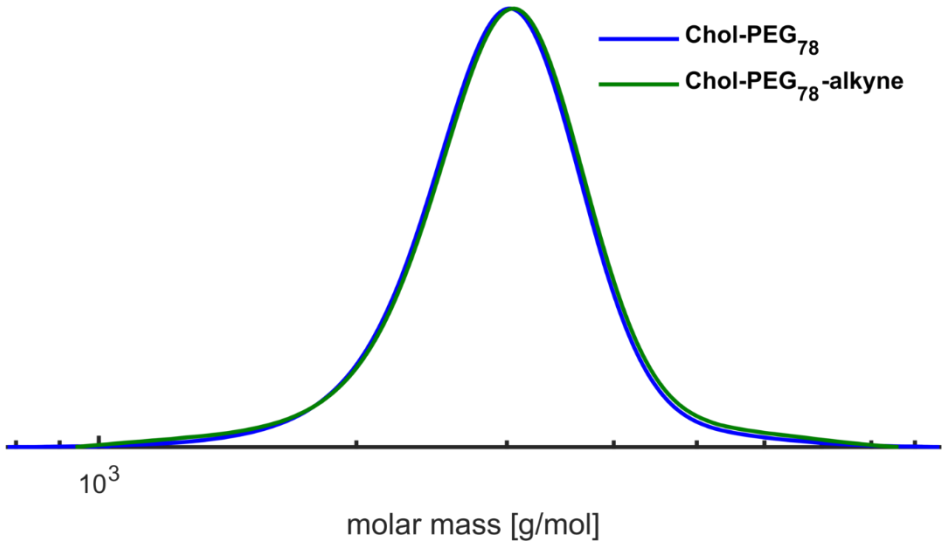

SI-Figure 29: SEC traces (RI detector, DMF, PEG standards) of the Chol-PEG polymer before (blue) and after (green) post-modification with propargyl bromide.

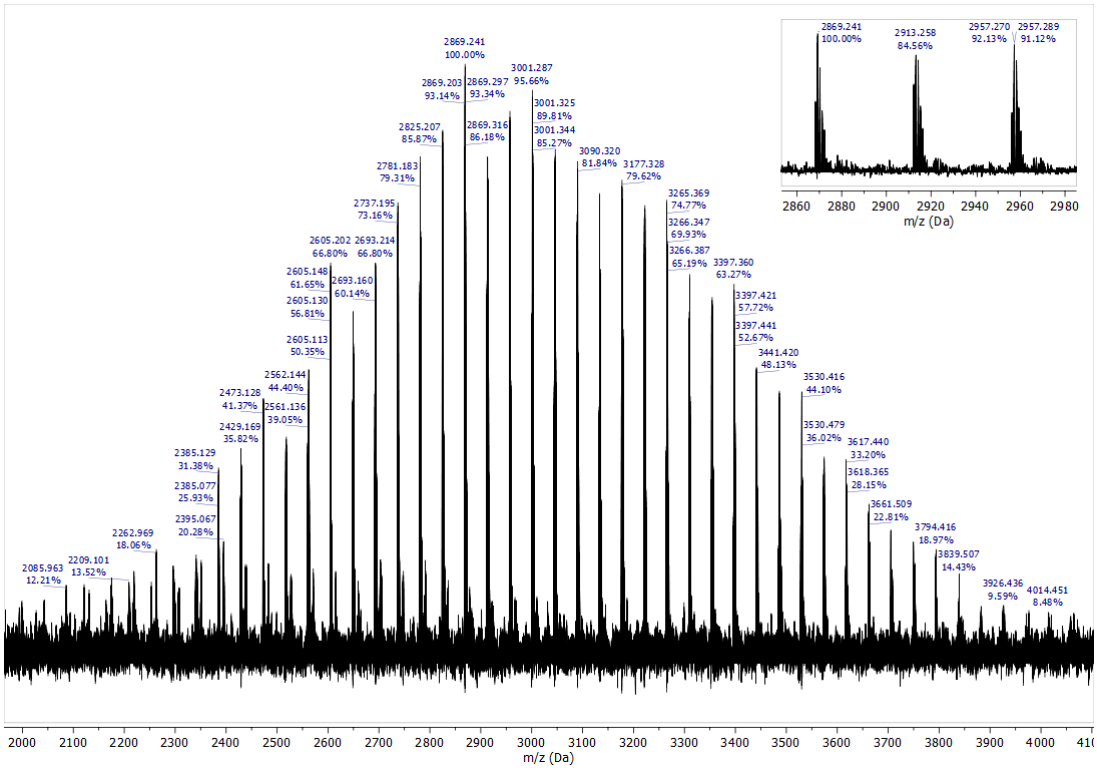

SI-Figure 30: MALDI-ToF MS spectrum of Chol-PEG$_{134}$ (left) and the zoom-in spectrum (right).

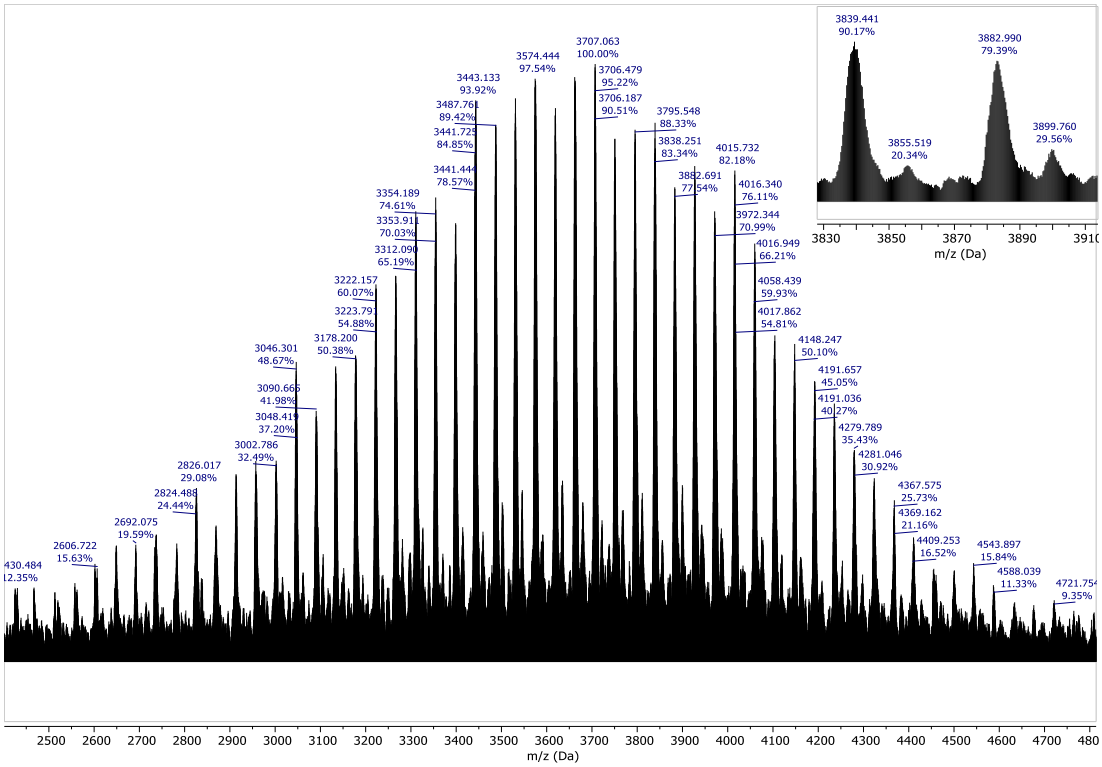

SI-Figure 31: MALDI-ToF MS spectrum of Chol-PEG$_{134}$-alkyne (left) and the zoom-in spectrum (right).

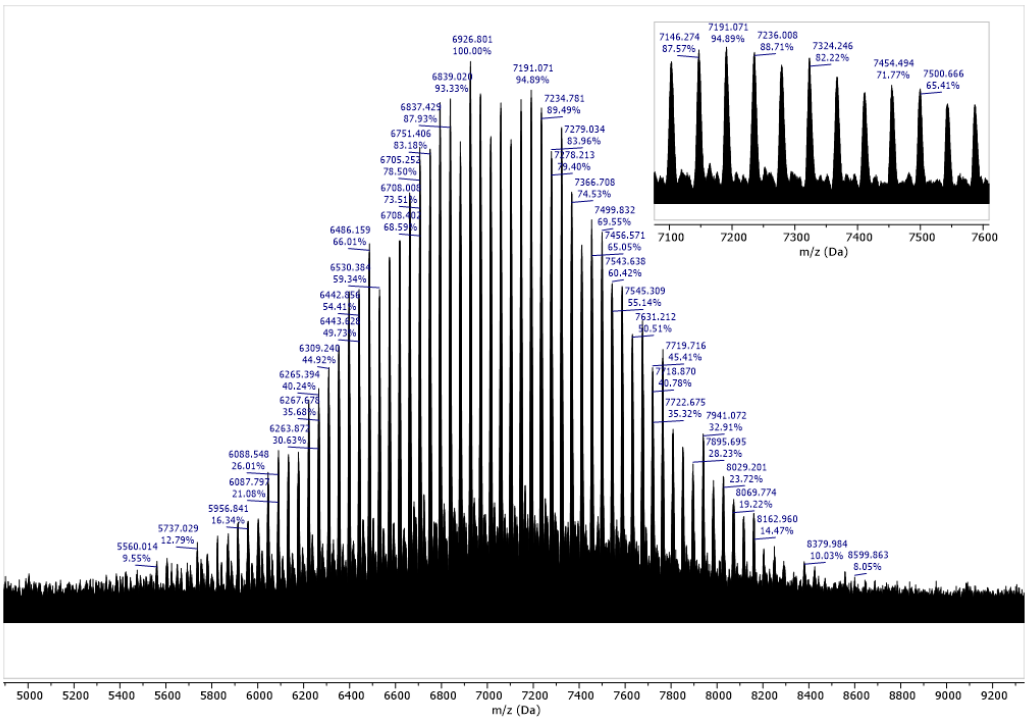

SI-Figure 32: MALDI-ToF MS spectrum of Chol-MBE-PEG$_{167}$ (left) and the zoom-in spectrum (right).

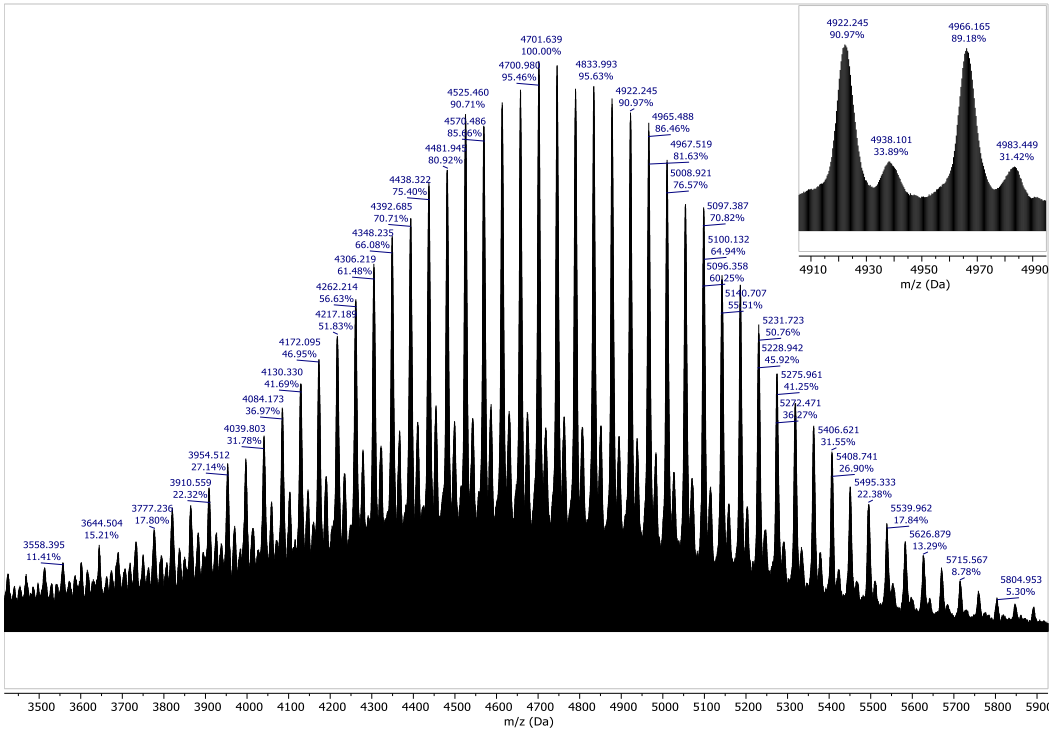

SI-Figure 33: MALDI-ToF MS spectrum of Chol-*iso*MBE-PEG$_{167}$-alkyne (left) and the zoom-in spectrum (right).

2.2 Vinylether-functional Dialkyl-PEG Lipids for pH-Responsive Liposomes

Eyleen Becker,[†] [redacted],[§] [redacted]*,[†], [redacted]*,[§]

[†]Department of Chemistry, Johannes Gutenberg University Mainz, Duesbergweg 10-14, 55128 Mainz, Germany

[§]Institute of Pharmacy and Biochemistry, Johannes Gutenberg University Mainz, Staudingerweg 5, 55128 Mainz, Germany

*E-Mail: [redacted], [redacted]

to be submitted

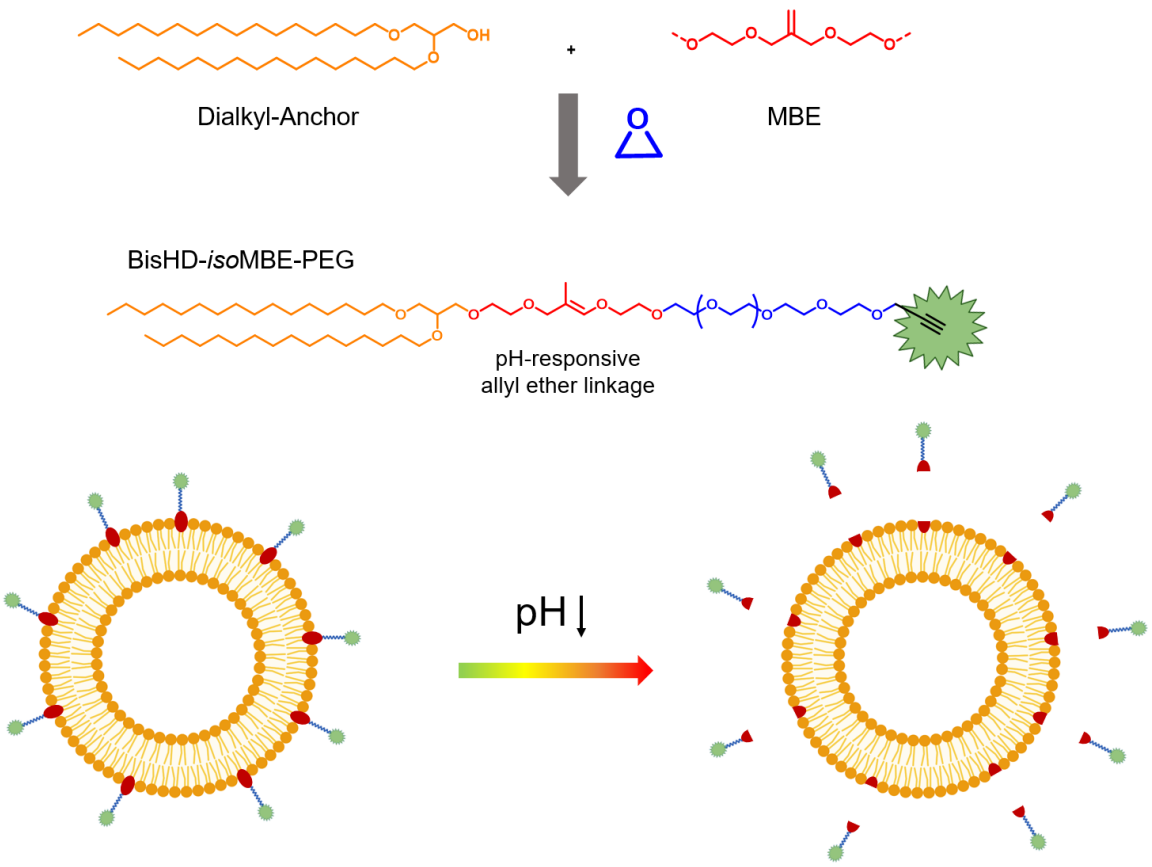

Abstract

Targeted drug delivery is playing an increasingly important role in the treatment of many diseases. The key objective in this context is to maximize efficacy and minimize unwanted side effects. A promising approach is the use of "stealth" liposomes with PEG-lipids in their membrane as a potent drug delivery system for cancer therapy. Besides the stealth effect, polyether-based lipids offer a promising opportunity to change the pharmacokinetic profile. In this work, we present the synthesis of a pH-responsive polyether lipid comprising a pH-sensitive vinyl ether cleavage site. To prepare the cleavable PEG-lipids, a modified bishexadecyl glycerol is used as an initiator for the anionic ring-opening polymerization (AROP) with ethylene oxide (EO) to obtain well-defined amphiphilic polymer structures. The subsequent transformation of the allyl group into a pH-responsive vinyl ether group was achieved by isomerization. To allow post-modification *via* Cu(I)-catalyzed alkyne-azide cycloaddition (CuAAC) with a dye label, a small molecule, a drug or a radioisotope, the polymer was equipped with alkyne moieties. Subsequently, the PEG-lipids were used to prepare liposomes. Toxicity could be excluded by MTT assays. The findings demonstrate the potential of these functionalizable, pH-responsive PEG-lipids for the use in liposomes.

2.2.1 Introduction

Targeted drug delivery has become increasingly important in recent years.[1] It has long been recognized that there is a tremendous need to deliver especially highly toxic drugs to a specific site without affecting healthy organs, tissues and cells.[2] For this reason, various strategies have been developed to optimize the targeted drug delivery. One attractive option, for example, is the use of nanocarriers, such as liposomes.

Liposomes are artificial vesicles with a spherical shape composed of cholesterol and natural phospholipids.[3] Due to the amphiphilic character of lipids, they can transport both water-soluble and water-insoluble drugs. Furthermore, they are characterized by their good biocompatibility, biodegradability and low toxicity, which makes them ideal drug delivery systems.[4] Compared to other nanocarrier, liposome have one significant disadvantage: their short blood circulation time.[5] Due to their size, they are quickly recognized by the body's defense systems.[6] This leads to rapid uptake by the cells of the reticuloendothelial system (RES), which are mainly located in the liver and spleen, and significantly shortens the blood circulation time.[7] However, blood circulation time can be increased multiple times by using so called "stealth liposomes".[8] In these liposomes, the surface is modified by attaching poly(ethylene glycol) (PEG) chains. PEGylated lipids are used for the modification, which are integrated into the lipid bilayer.[9] The modified surface properties prevent rapid uptake and thus significantly increase the circulation time in the blood compared to conventional liposomes.[10–12]

PEG not only plays a significant role in stealth liposomes, it is in general the gold standard in polymers for biomedical and therapeutic applications. This is due to its exceptional properties, such as good water solubility, biocompatibility and low toxicity.[11,13] Polyether-based polymer lipids can not only be used in stealth liposomes, but are also suitable as drug delivery systems for small molecules. A central objective is the incorporation of pH-cleavable building blocks into PEG and its conjugates to facilitate the release of the drug in a target manner.[14] These approaches are based on the lower pH values for endosomal and lysosomal cell compartments, but also for the microenvironment of various tumor cell lines and inflammatory tissue.[15] In liposomal research, pH-responsive PEG lipids generate increasing attention. By separating the PEG chains of the stealth liposomes in the target

tissue, the efficacy of the respective drug carriers can be improved.[16,17] While the PEG stealth layer can increase circulation time in the blood, it can also, conversely, hinder cellular uptake of liposomes and drug release.[18–20] The use of pH-cleavable PEG chains can circumvent the drawbacks of PEG in liposomes. There are various approaches to incorporate acid-cleavable moieties into pH-responsive liposomes. These include hydrazones,[17,21–23] orthoesters,[23–25] acetals,[26] vinyl ethers[27,28] and cyclic ketals.[29] The existing strategies are mostly based on the chemical modification of commercially available methoxy PEG (mPEG). However, the disadvantage of this system is its low functionality, which excludes attaching further functional structures, such as dye labels or radioactive tracers.

In this work, we present the synthesis of a pH-responsive polyether lipid, which is subsequently used for the preparation of liposomes. Among the many possibilities to integrate a cleavage site into the PEG backbone, vinyl ethers represent the most promising group. They are characterized by rapid hydrolysis at pH values around 5, but have excellent stability at pH 7.4, as well as under dry storage conditions.[30–32] Many polymer lipids comprise cholesterol as a component. In this work, a dialkyl anchor is used as the hydrophobic moiety. In contrast to cholesterol, dialkyl glyceryl lipids with a chain of 18-20 methylene units show increased stability in liposomes, matching the typical chain length in biological membranes.[33] In the first synthesis steps, the hydrophobic dialkyl anchor was combined with a protected allyl ether alcohol. After deprotection, it was used as an initiator for the anionic ring-opening polymerization (AROP) of ethylene oxide (EO) to form the hydrophilic PEG moiety. To obtain the pH-labile vinyl ether structure, the allyl group of the polymer was converted to the vinyl function by isomerization. To allow further functionalization with, for example, a dye, a radioactive label or a ligand *via* Cu(I)-catalyzed alkyne-azide cycloaddition (CuAAC) the polymer was provided with an alkyne function. The pH-responsive PEG-lipid was then used for liposome preparation by dual centrifugation (DC). Dual centrifugation is a special centrifugation technique in which efficient mixing results from the high shear forces applied to the sample. Compared to other preparation methods, DC is characterized by a narrow size distribution of the liposomal vesicles.[34] MTT

assays were used to exclude toxicity of the liposomes. **Scheme 1** shows an overview of the synthesis steps.

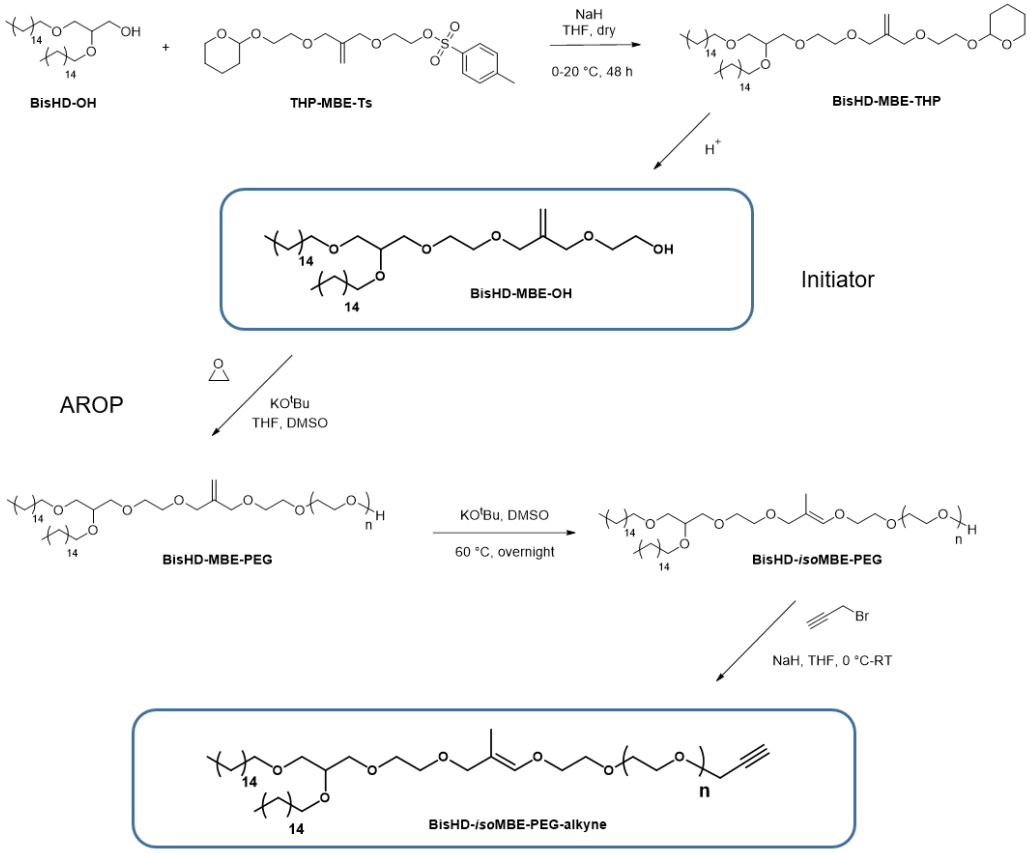

Scheme 1: Overview of the synthesis steps for the pH-responsive polyether lipid.

2.2.2 Experimental part

Terminology

The allyl ether based diol is designated 2,2'-((2-methylenepropane-1,3-diyl)bis(oxy))bis(ethan-1-ol) (MBE) and after protection of one hydroxyl group with 3,4-dihydropyran (DHP) it is named 2-((2-((2-((tetrahydro-2H-pyran-2-yl)oxy)ethoxy)methyl)allyl)oxy)ethan-1-ol (THP-MBE). The protected MBE was transformed in the tosylated product with the synonym 2-((2-((2-((tetrahydro-2H-pyran-2-yl)oxy)ethoxy)methyl)allyl)oxy)ethyl 4-methylbenzenesulfonate (THP-MBE-Ts). The hydrophobic anchor 1,2-bis-*n*-hexadecyl glyceryl ether (BisHD-OH) was synthesized according to literature.[35] The reaction of BisHD-OH with THP-MBE-Ts leads to BisHD-

MBE-THP and after cleavage of the protecting group under acidic conditions to the initiator BisHD-MBE-OH. The amphiphilic polymer lipid based on the initiator is called BisHD-MBE-Poly(ethylene glycol) (BisHD-MBE-PEG) and after the isomerization BisHD-*iso*MBE-Poly(ethylene glycol) (BisHD-*iso*MBE-PEG). The comparison structures without cleavage site are called BisHD-Poly(ethylene glycol) (BisHD-PEG).

Instrumentation

^{1}H NMR (300 MHz), ^{13}C NMR (75 MHz) and 2D spectra were recorded on a Bruker Avance III HD 300 (5 mm BBFO-Probe with z-Gradient and ATM). ^{1}H NMR (400 MHz), ^{13}C NMR (101 MHz) and 2D spectra were measured on a Bruker Avance II 400 MHz (5 mm BBFO-Probe Z-gradient and ATM, SampleXPress 60 auto sampler). The chemical shifts were internally referred to residual proton signals of the deuterated solvent.

Size exclusion chromatography (SEC) was performed at 50 °C in *N,N*-dimethylformamide (with 1 g/L lithium bromide added) as eluent on an Agilent 1,100 Series equipped with Polymer Standards Service (PSS) HEMA columns with 300/100/40 Å porosity and a RI detector. The determination of the molecular weights was determined by a calibration with poly(ethylene glycol) standards by PSS.

MALDI-ToF measurements were performed on a Shimadzu Axima CFR MALDI-ToF or a Bruker Rapiflex. Samples were prepared with trans-2-[3-(4-tert-Butylphenyl)-2-methyl-2-propenylidene]malononitrile (DCTB) as a matrix and potassium trifluoroacetate as a cationization agent.

Cell viability studies (MTT assays) were measured using a Spark 10M plate reader from the Tecan group.

Materials

All solvents and reagents were purchased generally from the suppliers Acros Organics, Tokyo Chemical Industry (TCI), Sigma-Aldrich, Fluka, Fisher Scientific, Alfa Aesar and were used as received unless otherwise stated. Deuterated solvents were purchased from Deutero GmbH. Dialysis membranes (regenerated cellulose, MWCO = 1000 g/mol) were purchased from Orange Scientific. HeLa and HEK293 cell lines were purchased from DSMZ.

Synthesis procedure

Synthesis of 2,2'-((2-methylenepropane-1,3-diyl)bis(oxy))bis(ethan-1-ol) (MBE)

The synthesis of MBE was carried out in a slightly modified form according to literature.[36]

Ethylene glycol (200 mL) was slowly added under argon atmosphere to a suspension of sodium hydride (10.08 g, 0.42 mol, 2.1 eq.) in dry THF (200 mL). The resulting mixture was stirred at room temperature for 30 minutes. Subsequently, 3-chloro-2-(chloromethyl)prop-1-ene (25.00 g, 0.20 mol, 1 eq.) was added slowly, and the mixture was refluxed for 24 hours. THF and excess of ethylene glycol were removed under reduced pressure, and the residue was treated with ethanol (150 mL). After filtration of the solid and evaporation of the ethanol, the product was obtained by distillation (b.p.=130 °C, 0.001 mbar) as a colorless oil (yield: 11.06 g, 0.06 mol, 30 %).

^{1}H NMR (300 MHz, chloroform-*d*) δ [ppm] = 5.20 (s, 2H, H_2C=C), 4.08 (s, 4H, CH_2OH), 3.76 – 3.70 (m, 4H, H_2C=(C-$CH_2O)_2$), 3.59 – 3.51 (m, 4H, CH_2O).

^{13}C NMR (75 MHz, chloroform-*d*) δ [ppm] = 142.41 (1C, H_2C=*C*), 115.94 (1C, H_2C=C), 72.31 (2C, H_2C=(C-$CH_2O)_2$), 71.63 (2C, CH_2-O-CH_2), 61.83 (2C, CH_2OH).

Synthesis of 2-((2-((2-((tetrahydro-2H-pyran-2-yl)oxy)ethoxy)methyl)allyl)oxy)ethan-1-ol (THP-MBE)

MBE (6.90 g, 39.18 mmol, 5.90 mL, 1 eq.) was dissolved in dichloromethane (80 mL), the solution was cooled to 0 °C and pyridinium *p*-toluenesulfonate (PPTS) (1.97 g, 7.84 mmol, 0.2 eq.) was added to the cooled solution. Subsequently, 3,4-dihydropyran (DHP) (3.30 g, 39.18 mmol, 3.58 mL, 1 eq.) was slowly added *via* syringe. After 1.5 hours the cooling mixture was removed and the reaction mixture was stirred for 3 hours at room temperature. To the solution saturated $NaHCO_3$ was added, and the product was extracted from the aqueous solution with dichloromethane (3 x 20 mL). The organic layer was dried and evaporated under reduced pressure. The monofunctional product and bifunctional product were separated *via* column chromatography (ethyl acetate/cyclohexane 3:1, R_f (mono) = 0.43, R_f (bi) = 0.81). The monofunctional product THP-MBE was obtained as a colorless oil (yield: 3.28 g, 12.60 mmol, 32 %).

^{1}H NMR (300 MHz, DMSO-d_6) δ [ppm] = 5.18 – 5.07 (m, J = 1.1 Hz, 2H, H_2C=C), 4.64 – 4.53 (m, 2H, O-C*H*-O, -O*H*), 3.99 – 3.87 (m, 4H, H_2C=(C-CH_2O)$_2$), 3.80 – 3.64 (m, 2H, O-CH-O-CH_2), 3.57 – 3.29 (m, 8H, O-CH_2-CH_2-O), 1.80 – 1.33 (m, 6H, CH_2-CH_2-CH_2).

^{13}C NMR (75 MHz, DMSO-d_6) δ [ppm] = 143.29 (1C, H_2C=*C*), 112.53 (1C, H_2*C*=C), 97.94 (1C, O-*C*H-O), 71.60 (1C, O-CH-O-*C*H_2), 70.73 (2C, H_2C=(C-*C*H_2O)$_2$), 68.94 (1C, O-*C*H_2-CH$_2$-OH), 65.95 (1C, O-CH$_2$-*C*H_2-O), 61.12 (1C, O-CH$_2$-*C*H_2-OH), 60.19 (1C, O-CH-O-*C*H_2), 30.21 (1C, O-CH$_2$-CH$_2$-CH$_2$-*C*H_2), 25.03 (1C, O-CH$_2$-*C*H_2-CH$_2$-CH$_2$), 19.05 (1C, O-CH$_2$-CH$_2$-*C*H_2-CH$_2$).

Synthesis of 2-((2-((2-((tetrahydro-2H-pyran-2-yl)oxy)ethoxy)methyl)allyl)oxy)ethyl 4-methylbenzenesulfonate (THP-MBE-Ts)

The synthesis of THP-MBE-Ts was carried out in a modified form according to literature.[37]

Under argon atmosphere THP-MBE (5.16 g, 19.82 mmol, 1 eq.) and triethylamine (5 mL) were dissolved in dichloromethane (15 mL), the solution was cooled to 0 °C and *p*-toluenesulfonic acid chloride (3.78 g, 19.82 mmol, 1 eq.) was added. The mixture was stirred on ice for 20 hours. The solvent was removed under reduced pressure, the residue floated in diethyl ether and filtered off. The diethyl ether was removed, and the crude product was obtained as an orange liquid. The crude product was purified using column chromatography (cyclohexane/ethyl acetate 4:1) and the product was obtained as a viscous, colorless liquid (yield: 5.34 g, 12.88 mmol, 65 %).

^{1}H NMR (300 MHz, DMSO-d_6) δ [ppm] = 7.79 (d, J = 8.3 Hz, 2H, H_{aromat}), 7.48 (d, 2H, J = 8.0 Hz, H_{aromat}), 5.08 (d, 2H, J = 16.9 Hz, H_2C=C), 4.58 (s, 1H, O-C*H*-O), 4.21 – 4.08 (m, 2H, CH_2-Ts), 3.88 (d, J = 4.4 Hz, 4H, H_2C=(C-CH_2O)$_2$), 3.72 (q, J = 12.5, 11.9 Hz, 2H, O-CH-O-CH_2), 3.58 – 3.36 (m, 6H, O-CH_2-CH_2-O, O-CH_2-CH$_2$-Ts), 2.43 (s, 3H, CH_3), 1.81 – 1.42 (m, 6H, CH_2-CH_2-CH_2).

^{13}C NMR (75 MHz, DMSO-d_6) δ [ppm] = 145.38 (1C, SO$_3$-*C*), 143.15 (1C, H_2C=*C*), 132.89 (1C, C_{aromat}), 130.61 (1C, C_{aromat}), 128.07 (1C, C_{aromat}), 113.41 (1C, H_2*C*=C), 98.42 (1C, O-*C*H-O), 71.03 (1C, O-CH-O-*C*H_2), 70.42 (2C, H_2C=(C-*C*H_2O)$_2$), 69.40 (1C, O-*C*H_2-CH$_2$-Ts), 67.53 (1C, O-CH$_2$-*C*H_2-O), 66.40 (1C, O-CH$_2$-*C*H_2-Ts), 61.60 (1C, O-CH-O-*C*H_2), 30.67 (1C, O-

CH_2-CH_2-CH_2-*C*H_2), 25.48 (1C, O-CH_2-*C*H_2-CH_2-CH_2), 21.55 (1C, *C*H_3), 19.51 (1C, O-CH_2-CH_2-*C*H_2-CH_2).

Synthesis of BisHD-MBE-OH

Dry THF (30 mL) was placed in a Schlenk flask, sodium hydride (0.04 g, 1.85 mmol, 1.1 eq.) and BisHD-OH (1.00 g, 1.85 mmol, 1.1 eq.) were added under argon atmosphere The solution was stirred for 1 h until no gas evolution could be detected. The reaction mixture was cooled to 0 °C, and the THP-MBE-Ts (0.70 g, 1.68 mmol, 1 eq.) was added *via* syringe. The solution was then heated to 60 °C for 48 hours under reflux. After the reaction time, THF was removed in vacuo, the residue was dissolved in cyclohexane and the organic phase was extracted with a saturated $NaHCO_3$-solution, dried over $NaSO_4$ and the organic solvent was evaporated. The crude product was dissolved in methanol (30 mL) and 2 g of an acidic ion exchange resin (Dowex 50WX8) was added to the solution to cleave the cyclic acetal protecting group. The solution was stirred and heated to 50 °C overnight. Afterwards, the resin was removed by filtration and the solvent was removed partly in vacuo. The product was purified by column chromatography (cyclohexane/ethyl acetate 2:1), and the product was obtained as a light orange wax (yield: 0.35 g, 0.50 mmol, 30 %).

^{1}H NMR (300 MHz, chloroform-*d*) δ [ppm] = 5.24 – 5.14 (m, 2H, *H*$_2$C=C), 4.05 (s, 4H, H_2C=(C-C*H*$_2$O)$_2$), 3.77 – 3.69 (m, 2H, C*H*$_2$-OH), 3.67 – 3.36 (m, 15H, (C*H*$_2$-O)$_2$-C*H*$_2$-C*H*-C*H*$_2$-O-C*H*$_2$-C*H*$_2$, C*H*$_2$-CH_2-OH), 1.62 – 1.48 (m, 4H, C*H*$_2$-CH_2-O), 1.25 (s, 52H, C*H*$_2$), 0.88 (t, 6H, , *J* = 6.8 Hz, C*H*$_3$-CH_2).

^{13}C NMR (75 MHz, chloroform-*d*) δ [ppm] = 142.56 (1C, H_2C=*C*), 114.63 (1C, H_2*C*=C), 77.90 (1C, O-CH_2-*C*H-O-CH_2), 71.95 – 70.65 (9C, (*C*H_2-O)$_2$-*C*H_2-CH-*C*H_2-O-*C*H_2-*C*H_2, *C*H_2-CH_2-OH, H_2C=(C-*C*H_2O)$_2$), 69.50 (1C, *C*H_2-CH_2-OH), 61.81 (1C, CH_2-*C*H_2-OH), 31.94 (1C, *C*H_2-CH_2-CH_3), 30.11 – 29.38 (22C, *C*H_2), 26.14, 26.10 (2C, *C*H_2-CH_2-CH_2O), 22.71 (2C, *C*H_2-CH_3), 14.14 (2C, CH_2-*C*H_3).

Synthesis of BisHD-OH initiated PEG polymers

The polymerization of ethylene oxide (EO) using BisHD-OH as initiator was performed on the basis of literature procedures for other glycidyl ethers with adjusted reaction procedure.[38,39]

The synthesis is described for BisHD-PEG$_{72}$ as a representative example.

In a dry Schlenk flask the initiator BisHD-OH (455.00 mg, 0.84 mmol, 1 eq.) and potassium *tert*-butoxide (85.00 mg, 0.75 mmol, 0.9 eq.) were dissolved in benzene (5 mL) and dry THF (5 mL), stirred under slightly reduced pressure at 60 °C for 30 minutes and subsequently dried in high vacuum for 16 hours. The resulting initiator salt was dissolved in dry THF (15 mL), and the flask was cooled to -70 °C with an ethanol/nitrogen cooling bath. Ethylene oxide (2.91 g, 66.10 mmol, 3.00 mL, 79 eq.) was condensed *via* a graduated ampule into the flask. The reaction mixture was heated in vacuo to 60 °C for 48 hours. Subsequently, methanol (1 mL) was added, and the flask was flushed with argon. The resulting polymer BisHD-PEG$_{72}$ was precipitated three times in diethyl ether and separated *via* centrifuge. The polymer was dried under reduced pressure at room temperature for 24 hours (yield: 90 %).

^{1}H NMR (300 MHz, methylene chloride-d_2) δ [ppm] = 3.86 – 3.33 (m, 299H, (C*H*$_2$-O)$_2$-C*H*$_2$-C*H*-C*H*$_2$-O, polyether backbone), 1.59 – 1.45 (m, 4H, C*H*$_2$-CH$_2$-O), 1.25 (s, 52H, C*H*$_2$), 0.87 (t, 6H, , J = 6.8 Hz, C*H*$_3$-CH$_2$).

^{13}C NMR (75 MHz, methylene chloride-d_2) δ [ppm] = 78.42 (1C, O-CH$_2$-*C*H-O-CH$_2$), 73.06, 72.00, 71.76 – 70.77 (148C, (*C*H$_2$-O)$_2$-*C*H$_2$-CH-*C*H$_2$-O, polyether backbone), 62.05 (1C, CH$_2$-*C*H$_2$-OH), 32.45 (1C, *C*H$_2$-CH$_2$-CH$_3$), 30.27 – 29.88 (22C, *C*H$_2$), 26.69, 26.65 (2C, *C*H$_2$-CH$_2$-CH$_2$O), 23.21 (2C, *C*H$_2$-CH$_3$), 14.42 (2C, CH$_2$-*C*H$_3$).

Synthesis of BisHD-MBE-OH initiated PEG polymers

The polymerization of ethylene oxide (EO) using BisHD-MBE-OH as initiator was performed on the basis of literature procedures for other glycidyl ethers with adjusted reaction procedure.[38,39]

The synthesis is described for BisHD-MBE-PEG$_{84}$ as a representative example.

In a dry Schlenk flask the initiator BisHD-MBE-OH (158.00 mg, 0.23 mmol, 1 eq.) and potassium *tert*-butoxide (23.00 mg, 0.20 mmol, 0.9 eq.) were dissolved in benzene (5 mL) and dry THF (5 mL), stirred under slightly reduced pressure at 60 °C for 30 minutes and subsequently dried in high vacuum for 16 hours. The resulting initiator salt was dissolved

in dry THF (5 mL) and the flask was cooled to -70 °C with an ethanol/nitrogen cooling bath. Ethylene oxide (0.97 g, 22.00 mmol, 1.00 mL, 98 eq.) was condensed *via* a graduated ampule into the flask. The reaction mixture was heated in vacuo to 50 °C for 48 hours. Subsequently, methanol (1 mL) was added, and the flask was flushed with argon. The resulting polymer BisHD-MBE-PEG$_{84}$ was precipitated three times in diethyl ether and separated *via* centrifuge. The polymer was dried under reduced pressure at room temperature for 24 hours (yield: 85–90 %).

^{1}H NMR (300 MHz, benzene-d_6) δ [ppm] = 5.24 (s, 2H, H_2C=C), 3.97 (s, 4H, H$_2$C=(C-CH_2O)$_2$), 3.74 – 3.22 (m, 344H, (CH_2-O)$_2$-CH_2-CH-CH_2-O-CH_2-CH_2, CH_2-CH$_2$-OH, polyether backbone), 1.69 – 1.56 (m, 4H, CH_2-CH$_2$-O), 1.32 (s, 52H, CH_2), 0.91 (t, 6H, J = 6.8 Hz, CH_3-CH$_2$).

^{13}C NMR (75 MHz, benzene-d_6) δ [ppm] = 112.98 (1C, H$_2$*C*=C), 78.76 (1C, O-CH$_2$-*C*H-O-CH$_2$), 73.17, 72.20 (2C, H$_2$C=(C-*C*H$_2$O)$_2$), 72.11 – 70.09 (177C, (*C*H$_2$-O)$_2$-*C*H$_2$-CH-*C*H$_2$-O, polyether backbone), 61.89 (1C, CH$_2$-*C*H$_2$-OH), 32.36 (1C, *C*H$_2$-CH$_2$-CH$_3$), 30.38 – 29.85 (22C, *C*H$_2$), 26.75 (2C, *C*H$_2$-CH$_2$-CH$_2$O), 23.13 (2C, *C*H$_2$-CH$_3$), 14.40 (2C, CH$_2$-*C*H$_3$).

Isomerization of BisHD-MBE-PEG to BisHD-isoMBE-PEG

The synthesis is described for the isomerization of BisHD-MBE-PEG$_{84}$ to BisHD-*iso*MBE-PEG$_{84}$ as a representative example.

BisHD-MBE-PEG$_{84}$ (100.00 mg, 0.02 mmol, 1 eq.) and potassium *tert*-butoxide (8.00 mg, 0.07 mmol, 3 eq.) were dissolved in dry DMSO (1 mL) in a Schlenk tube under argon condition. The solution was stirred and heated to 60 °C under reduced pressure overnight. The resulting isomerized polymer BisHD-*iso*MBE-PEG$_{84}$ was precipitated three times in a mixture of diethyl ether/acetone (70:30 vol%) and separated *via* centrifuge. The polymer was dried under reduced pressure at room temperature for 24 hours (yield: 70 %).

^{1}H NMR (400 MHz, benzene-d_6) δ [ppm] = 6.01 (s, 1H, CH$_3$-C=CH), 3.83 (s, 2H, CH_2-CH=CH), 3.67 – 3.30 (m, 416H, (CH_2-O)$_2$-CH_2-CH-CH_2-O-CH_2-CH_2, CH_2-CH$_2$-OH, polyether backbone), 1.90 (s, 3H, CH_3-C=CH), 1.71 – 1.51 (m, 4H, CH_2-CH$_2$-O), 1.32 (s, 52H, CH_2), 0.91 (t, 6H, J = 6.8 Hz, CH_3-CH$_2$).

^{13}C NMR (101 MHz, benzene-d_6) δ [ppm] = 144.63 (1C, C=*C*H), 78.52 (1C, O-CH$_2$-*C*H-O-CH$_2$), 73.25 (1C, O-*C*H$_2$-CH$_3$C=CH), 71.48 – 70.68 (177C, (*C*H$_2$-O)$_2$-*C*H$_2$-CH-*C*H$_2$-O, polyether backbone), 61.61 (1C, CH$_2$-*C*H$_2$-OH), 32.01 (1C, *C*H$_2$-CH$_2$-CH$_3$), 30.19 – 29.85 (22C, *C*H$_2$), 26.54 (2C, *C*H$_2$-CH$_2$-CH$_2$O), 22.84 (2C, *C*H$_2$-CH$_3$), 14.01 (2C, CH$_2$-*C*H$_3$), 11.44 (1C, *C*H$_3$-C=CH).

Post-polymerization modification

The functionalization of BisHD-PEG with propargyl bromide is described for BisHD-PEG$_{72}$ as a representative example.

BisHD-PEG$_{72}$ (0.39 g, 0.10 mmol, 1 eq.) was placed in a Schlenk flask and dissolved in THF (10 mL). The solution was cooled to 0 °C, and sodium hydride 10.30 mg, 0.43 mmol, 3 eq.) was added. The solution was stirred for 1 hour at 0 °C to ensure complete deprotonation. Subsequently, propargyl bromide (0.35 mL, 0.31 mmol, 3 eq.) (80 wt% in toluene) was added and the mixture was allowed to slowly reach room temperature. The solution was stirred at room temperature overnight. Afterwards, water (2 mL) was added, and the solvent was removed under reduced pressure. The crude product was precipitated three times in diethyl ether and separated *via* centrifuge. The polymer was dried under reduced pressure at room temperature for 24 hours (yield: 80 %).

^{1}H NMR (300 MHz, chloroform-*d*) δ [ppm] = 4.17 (d, *J* = 2.4 Hz, 2H, OC*H*$_2$-CCH), 3.89 – 3.32 (m, 301H, (C*H*$_2$-O)$_2$-C*H*$_2$-C*H*-C*H*$_2$-O, polyether backbone), 2.42 (t, *J* = 2.4 Hz, 1H, OCH$_2$-CC*H*), 1.60 – 1.44 (m, 4H, C*H*$_2$-CH$_2$-O), 1.22 (s, 52H, C*H*$_2$), 0.85 (t, 6H, *J* = 6.8 Hz, C*H*$_3$-CH$_2$).

The functionalization of BisHD-*iso*MBE-PEG with propargyl bromide is described for BisHD-*iso*MBE-PEG$_{84}$ as a representative example.

BisHD-*iso*MBE-PEG$_{84}$ (50.00 mg, 0.01 mmol, 1 eq.) was placed in a Schlenk flask and dissolved in THF (10 mL). The solution was cooled to 0 °C, and sodium hydride (1.00 mg, 0.03 mmol, 3 eq.) was added. The solution was stirred for 1 hour at 0 °C to ensure complete deprotonation. Subsequently, propargyl bromide (10.00 µL, 0.03 mmol, 3 eq.) (80 wt% in toluene) was added and the mixture was allowed to slowly reach room temperature. The solution was stirred at room temperature overnight. Afterwards, water (0.5 mL) was added,

and the solvent was removed under reduced pressure. The crude product was precipitated three times in diethyl ether and separated *via* centrifuge. The polymer was dried under reduced pressure at room temperature for 24 hours (yield: 75 %).

^{1}H NMR (400 MHz, benzene-d_6) δ [ppm] = 6.01 (s, 1H, CH_3-C=C*H*), 3.94 (d, *J* = 2.4 Hz, 2H, OC*H*$_2$-CCH), 3.83 (s, 2H, C*H*$_2$-CH=CH), 3.68 −3.30 (m, 363H, (C*H*$_2$-O)$_2$-C*H*$_2$-C*H*-C*H*$_2$-O-C*H*$_2$-C*H*$_2$, C*H*$_2$-CH_2-OH, polyether backbone), 2.11 (t, *J* = 2.4 Hz, 1H, OCH_2-CC*H*), 1.90 (t, *J* = 1.6 Hz, 3H, C*H*$_3$-C=CH), 1.71 − 1.55 (m, 4H, C*H*$_2$-CH_2-O), 1.33 (s, 52H, C*H*$_2$), 0.92 (t, 6H, *J* = 6.8 Hz, C*H*$_3$-CH_2).

Cell viability studies

Prior to the cytotoxicity tests the corresponding polymers were purified by dialysis (regenerated cellulose, MWCO = 1000 g/mol) in PBS buffer solution and dried *via* freeze-pump technique.

A 3-(4,5-dimethylthiazol-2-yl)-2,5-diphenyltetrazolium bromide-based (MTT) (#M5655-500MG, Sigma Aldrich, St. Louis, MO, USA) cell viability assay was performed to investigate the cell toxicity of polymer-modified liposomes on HEK293 (#ACC 305, DSMZ, Braunschweig, Germany) and HeLa (#ACC 57, DSMZ, Braunschweig, Germany) cell lines.

The cells were cultivated at 37 °C and 5 vol-% CO_2 in a growth medium without phenol red (#31966-047, Thermo Fisher Scientific, Waltham, MA, USA) containing 0.1 vol-% Glutamax™ supplement (#35050061, Thermo Fisher Scientific, Waltham, MA, USA), 0.1 vol-% sodium pyruvate solution (#11360039, Thermo Fisher Scientific, Waltham, MA, USA), 0.1 vol-% Penicilin and Streptomycin (#15140122, Thermo Fisher Scientific, Waltham, MA, USA), 0.2 vol-% glucose solution (#A2494001, Thermo Fisher Scientific, Waltham, MA, USA) and 10 vol-% Fetal Bovine Serum (#10500064, Thermo Fisher Scientific, Waltham, MA, USA). 24 h before the assay started, 7.5 k HEK293 or HeLa cells in 200 µL medium per well were seeded in 96-weell plates (#M0812-100EA, Sigma Aldrich, St. Louis, MO, USA).

For incubation, the cell culture medium was replaced with fresh medium containing 100, 10, 1 or 0.1 mg/mL liposomes (total lipid). After 24 h incubation, 30 µL of a 5 mg/mL MTT solution in DPBS (#14190169, Thermo Fisher Scientific, Waltham, MA, USA) were added

per well and incubated for 1 h. The Medium was removed and 200 µL of a mixture containing (1:8, v/v) glycine buffer pH 10 (#120072500, Thermo Fisher Scientific, Waltham, MA, USA) and DMSO mixture (#D8418-100ML, Sigma Aldrich, St. Louis, MO, USA) were added per well. The 96-well plate was shaken for 15 min and final for analysis of cell viability, the absorbances at 595 nm and the background 670 nm were measured by using a plate reader (Spark 10M, Tecan Group, Männedorf, Switzerland).

Liposome preparation

To prepare liposomes, lipids dissolved in dichlormethane (#320269-1L, Sigma Aldrich, St. Louis, MO, USA) were first combined in 2.2 mL tubes (#3225, Hettich Lab Technology, Tuttlingen, Germany) in proportion to their mol% ratio, shown in **Table 2**. Afterwards, the solvents were removed under low pressure by using a vacuum concentrator (#5305, Thermo Fisher Scientific, Waltham, MA, USA) for 2 h at 45 °C.

Then, 9.3 µL DPBS and 325 mg beads (#96035-362, Sigmund Lindner GmbH, Warmensteinach, Germany) were added to 5 µMol dry lipids and were incubated for 10 min at room temperature. For the release studies, 9.3 µL DPBS containing 50 mM Sulforhodamine B (341738-1G, Sigma Aldrich, St. Louis, MO, USA) was used. The mixture was homogenized by dual centrifugation (#3200, Hettich Lab Technology, Tuttlingen, Germany) for 20 min at 2500 rpm and 4 °C, followed by the addition of 77.2 µL DPBS and mixing twice times for 2 min at 2500 rpm and 4 °C using the dual centrifuge.

The liposomal suspension was purified by size exclusion chromatography. For this the suspension was injected in a system consisting of an high-performance liquid chromatography (HPLC) system (#G1311A + #G1313A + #G1316A + #G1322A + #G1365A + #G1364C, Agilent Technologies, Santa Clara, CA, USA) and a Bio-RAD UNO Q1 column (#7200001, Bio-Rad, filled with 2 mL Sephacryl S500-HR (#GE17-0613-01, Sigma Aldrich, St. Louis, MO, USA). The purified liposomes were automatically collected in 2.0 mL vials (#XC84.1, Carl Roth, Karlsruhe, Germany) by a fraction collector.

(50 mol-% phosphatidyl choline 3 (#527600, lipoid, Ludwigsharfen, Germany), 45 mol-% cholesterol (#22749.233, VWR, Radnor, USA) and 5 mol-% polymer.

Dynamic light scattering

To determine the physicochemical properties by dynamic light scattering (DLS) of liposomes, 10 µL of liposome suspension in 1 mL DPBS were measured in a folded zeta-capillary cells (#DTS1070, Malvern Panalytical, Worcestershire, UK) with a Zetasizer (#Zetasizer Nano ZS, Malvern Panalytical, Worcestershire, UK). The temperature was set to 25 °C with a refractive index of 1.33 and a water viscosity of 0.8872. The scattering angle was set to 173°.

Release studies

The release and stability studies were performed always at 37 °C with purified liposomes with encapsulated sulforhodamine b dye. 100 µL liposomal suspension were incubated for investigation of pH-sensitivity in the equal volume of citrate buffer pH 5.4 (0.1 M disodium phosphate (#P030.1, Carl Roth, Karlsruhe, Germany), 0.11 M citric acid (#7624.1, Carl Roth, Karlsruhe, Germany) or in the same volume of DPBS for incubation studies under physiological pH values. Afterwards, the retention of dye was analyzed by absorbance measurement at 550 nm after separation via size exclusion chromatography and HPLC.

2.2.3 Results and discussion

There are different approaches to introduce vinyl ether structures into PEG-based polymers. One possibility was presented by Worm et al., who used ethylene oxide (EO) combined with the epoxide monomer 3,4-epoxy-1-butene (EPB) in an anionic ring-opening copolymerization (AROP). To convert the allyl ether groups at the chains formed into the pH sensitive vinyl ethers, an isomerization with Wilkinson's catalyst was performed.[40]Despite the valuable character of this method, further investigations also revealed weaknesses. For example, β–elimination can occur as a side reaction during the polymerization and, especially when working with amphiphilic structures, problems were observed in the complete implementation of the isomerization due to aggregate formation of the polymer chains.

In order to nevertheless produce cleavable polymer lipids with vinyl ether moieties, a new synthesis strategy was used to prepare them. In our group a new class of allyl ether based initiators based on 2-(methylene)-1,3-propanediol (MPD) as lead structure was introduced.[41]

In this work, these new structures were linked to a hydrophobic dialkyl anchor to enable the synthesis of novel pH sensitive polymer lipids. In the following sections, the steps of initiator synthesis, as well as polymer syntheses and post-modification are described. Furthermore, the respective polymers were used in further steps to prepare liposomes, and the stability of the systems at different pH values was investigated.

2.2.3.1 Initiator synthesis

Synthesis of bifunctional MBE

For the introduction of the allyl ether moieties 2,2'-((2-methylenepropane-1,3-diyl)bis(oxy))bis(ethan-1-ol) (MBE) was synthesized in a convenient one-step reaction of 3-chloro-2-(chloromethyl)prop-1-ene with ethylene glycol in a nucleophilic substitution reaction (**Scheme 2**). This leads of the addition of two ethylene glycol spacers at the terminal hydroxyl groups of the lead structure 2-(methylene)-1,3-propanediol (MPD) and enables improved handling. Furthermore, the compound can be synthesized on a multi gram-scale. Purification is achieved by fractional distillation with good yields, high purity and low costs. Detailed NMR characterization of this compound can be found in the Supporting Information (**SI-Figure 1**, **SI-Figure 2**)

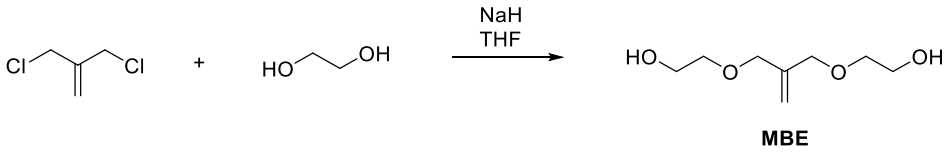

Scheme 2: Synthesis of bifunctional MBE.

Synthesis of monofunctional MBE

For controlled binding of MBE to cholesterol, one hydroxyl group had to be selectively protected to prevent double attachment of cholesterol. Furthermore, it was important that the protective group could be easily cleaved again after the reaction in order to be able to use the initiator for the ensuing AROP. For this reason, 3,4-dihydropyran (DHP) was used as a protecting group to synthesize THP-MBE (**Scheme 3**). After purification by column chromatography, the mono-protected product was obtained with a yield of 30-40 %. The double-protected product can be recovered by acid cleavage back to the starting compound MBE.

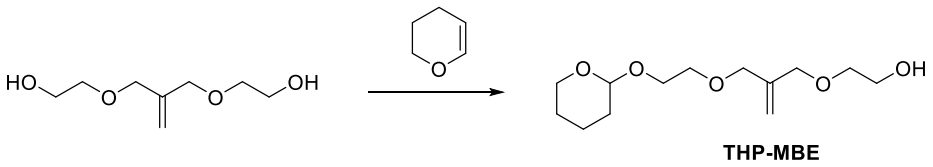

Scheme 3: Synthesis of monofunctional MBE.

Synthesis of the hydrophobic anchor (BisHD-OH)

BisHD-OH was synthesized as described in literature.[35] More details are given in the Supporting Information (**SI-Scheme 1**, **SI-Figure 7**)

Synthesis of THP-MBE-Ts and BisHD-MBE-OH initiator

For the attachement of BisHD-OH to MBE, the hydroxyl group of the THP-MBE was tosylated according to a synthesis route known in the literature (**Scheme 4**).[42] The tosylation of hydroxyl-functionalized substrates is an important transformation to activate hydroxyl groups, thus yielding substrates for further nucleophilic substitution.

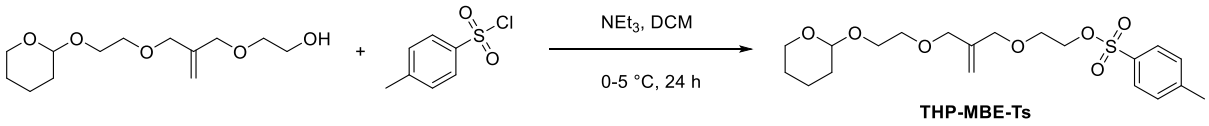

Scheme 4: Synthesis route of THP-MBE-Ts.

Subsequently, the nucleophilic substitution reaction of BisHD-OH with THP-MBE-Ts was carried out. For better separation of the product from BisHD-OH, which was used in slight excess, the THP protecting group was removed by acidic cleavage. The synthesis route of both steps are shown in **Scheme 5**. The BisHD-MBE-OH initiator was purified by column chromatography.

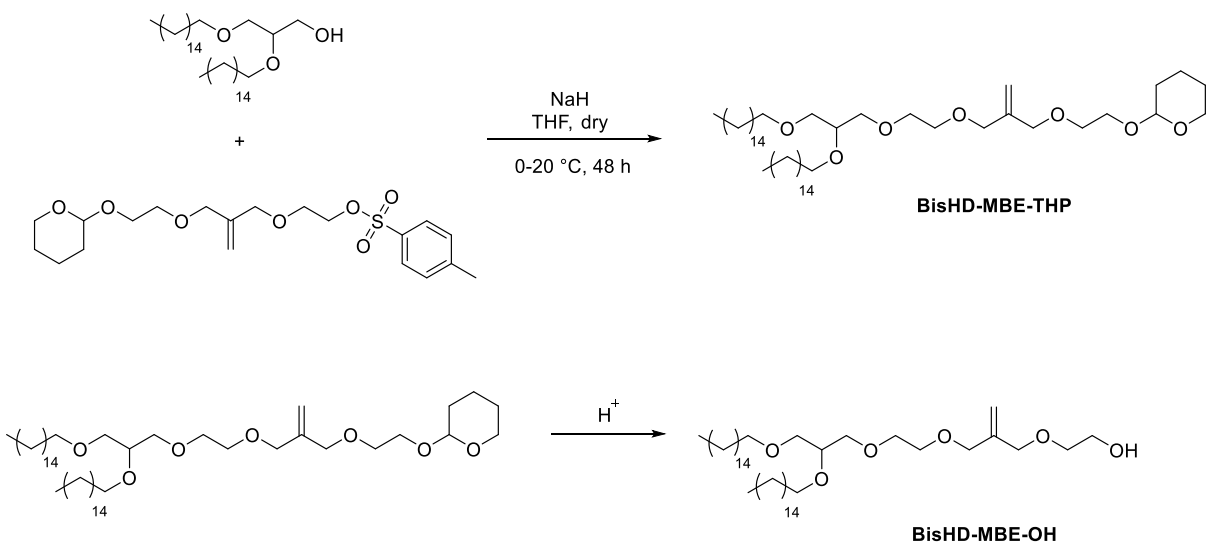

Scheme 5: Synthesis route of BisHD-MBE-THP with subsequent deprotection to BisHD-MBE-OH initiator.

The BisHD-MBE-OH initiator was characterized by NMR spectroscopy (**Figure 1**). All signals could be assigned, and the number of protons determined by integration of the signals agree with those of the molecule.

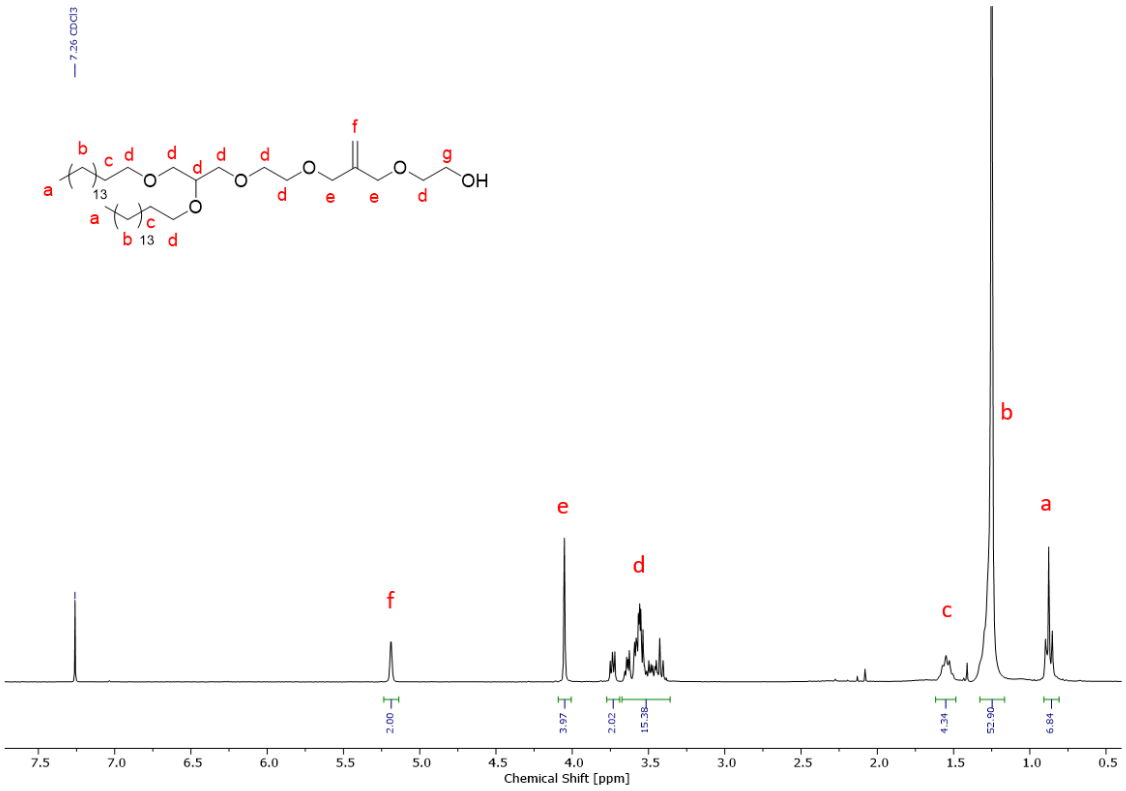

Figure 1: ^{1}H NMR spectrum (400 MHz, chloroform-*d*) of the initiator BisHD-MBE-OH.

2.2.3.2 Polymer synthesis and characterization.

All polymers prepared in this work were synthesized *via* anionic ring-opening polymerization (AROP) of ethylene oxide (EO) as a commonly used method to generate FDA-approved PEGs.[13] Polymers with and without a cleavage site were prepared. For the pH responsive polymers the initiator BisHD-MBE-OH was used and for the polymers without a cleavage site the initiator BisHD-OH.

BisHD-OH initiated PEG and BisHD-isoMBE-OH initiated PEG

Both polymer structures, with or without a cleavage site, were prepared by analogous experimental procedures. The procedure was based on methods for the preparation of amphiphilic polyether lipids known from the literature.[38] For the polymerizations, the initiators BisHD-OH and BisHD-MBE-OH were deprotonated with potassium *tert*-butoxide with a degree of deprotonation of 90 %. The polymerization with EO was performed in THF at 50 °C in case of the BisHD-MBE-OH initiator and 60 °C for the BisHD-OH initiator for 48 hours. Full monomer conversion was determined *via* ^{1}H NMR spectroscopy. The synthesis routes employed for the polymerizations are shown in **Scheme 6**.

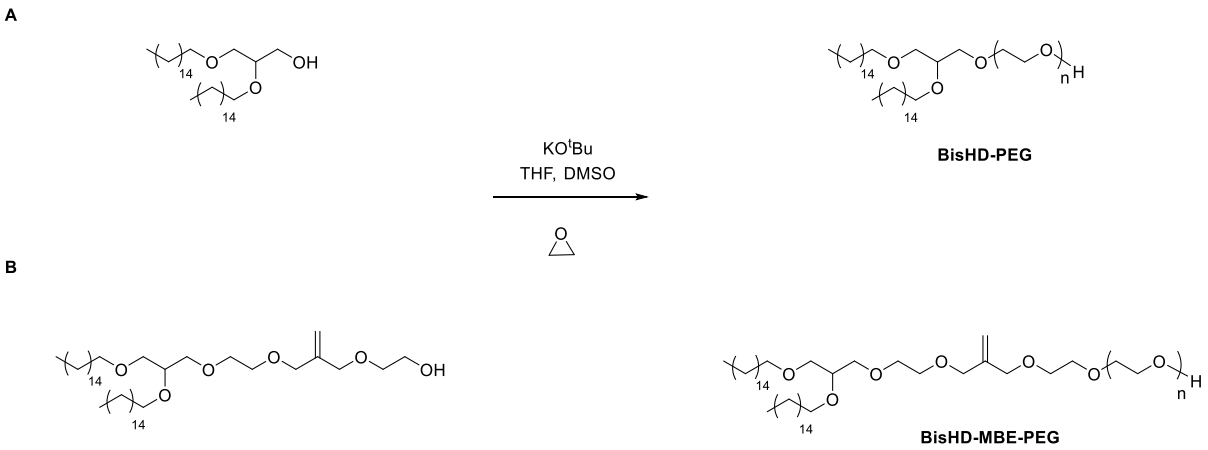

Scheme 6: Synthesis route of the BisHD-PEG polymer (**A**) and the BisHD-MBE-PEG polymer (**B**).

The key characterization data of the BisHD-PEG and the BisHD-MBE-PEG polymers are summarized in **Table 1**. The targeted degree of polymerization is in good agreement with the determined values for the obtained PEGs in case of the BisHD-PEG polymer. For the BisHD-MBE-PEG polymer, molecular weights are higher than targeted. The reason for this

could be, e.g., at change in temperature at which the EO was condensed into the ampule. The density of EO is strongly temperature dependent. Furthermore, only a smaller amount of EO was used for the approach compared to the synthesis of BisHD-PEG. This means that an error in the amount of EO can have a significant effect on the molecular weight. Both polymers were prepared at the same time with the same set-up. It is therefore likely that one or more of the above-mentioned sources of error occurred. The molecular weight (M_n) was obtained from SEC in DMF using PEG standards with narrow size distributions ($Đ$ < 1.07). The corresponding SEC traces are shown in **Figure 2**.

Table 1: Characterization data of the BisHD-PEG and BisHD-MBE-PEG polymers.

Composition [a]	M_n theo g·mol^{-1}	M_n NMR [a] g·mol^{-1}	M_n SEC [b] g·mol^{-1}	$Đ$ [b]
BisHD-PEG$_{72}$	4000	3710	2620	1.07
BisHD-MBE-PEG$_{84}$	4000	4400	3620	1.04

[a] Obtained from ^{1}H NMR spectroscopy. [b] Determined *via* SEC (RI, DMF, PEG standards).

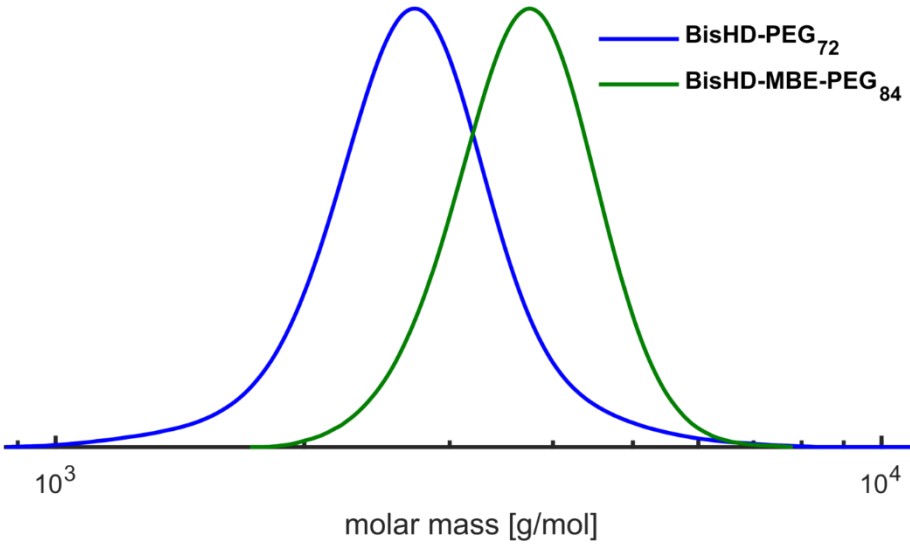

Figure 2: SEC traces (RI detector, DMF, PEG standards) of the BisHD-PEG and BisHD-MBE-PEG polymers.

The molecular weights based on ^{1}H NMR spectroscopy were determined *via* integration of the methyl signals of the BisHD-OH initiator (signal **a**) and are in good agreement with the molecular weights measured *via* SEC. For more details, NMR spectra of the BisHD-PEG

polymer are shown in **SI-Figure 10** and **SI-Figure 11**. The ^{1}H NMR spectrum of the BisHD-MBE-PEG polymer is shown in **Figure 3**.

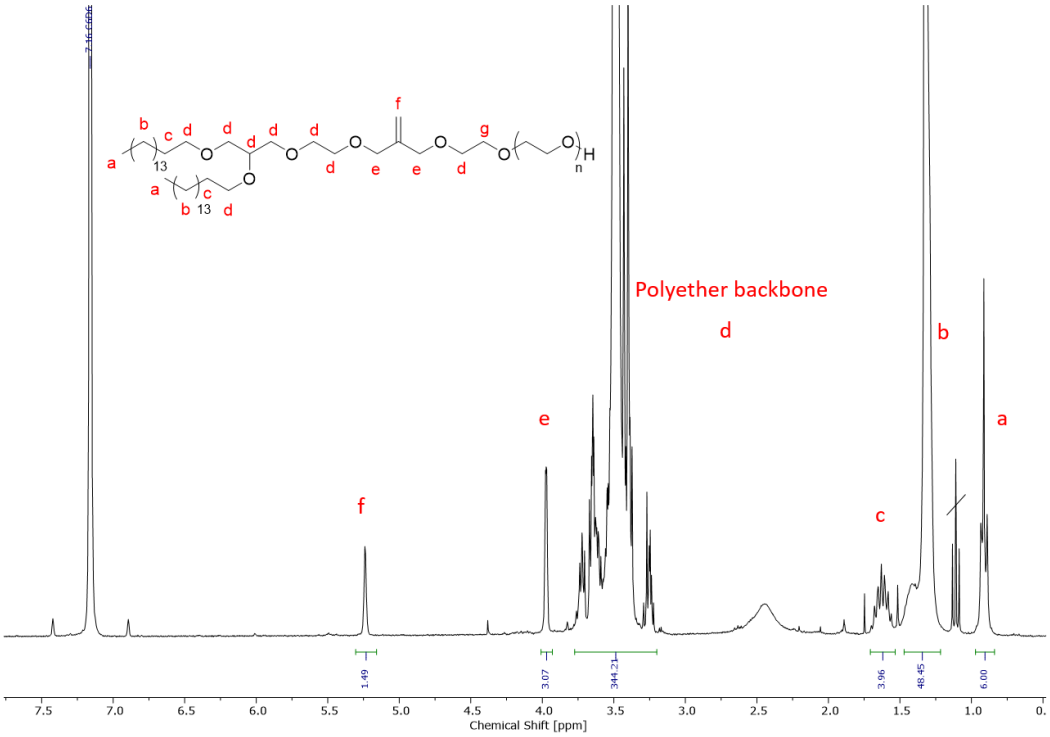

Figure 3: ^{1}H NMR spectrum (300 MHz, benzene-d_6) of the BisHD-MBE-PEG.

To determine the end-groups of the BisHD-OH and BisHD-MBE-OH initiated PEGs, MALDI-ToF mass spectrometry was performed. The spectrum of BisHD-PEG is shown in the Supporting Information (**SI-Figure 21**). For the polymerization of BisHD-OH with EO, the MALDI-ToF spectra show PEG chains exclusively initiated by the inititator BisHD-OH and underline the formation of well-defined polymers. The mass spectra demonstrate the formation of polymers with the absence of side reactions. In **Figure 4** the MALDI-ToF mass spectrometry of BisHD-MBE-PEG and a zoom-in is shown to determine the end-groups. The main distribution corresponds to polymer initiated by BisHD-MBE-OH. However, upon closer inspection, a second species can be detected. This corresponds to BisHD-initiated PEG. When purifying the initiator, no traces of BisHD-OH could be detected in the NMR spectra and by thin-layer chromatography. However, the detection limit by NMR spectroscopy is higher and can falsify the result at small concentrations of impurities. However, the amount of BisHD-initiated polymer is less than 5 % based on MALDI-ToF.

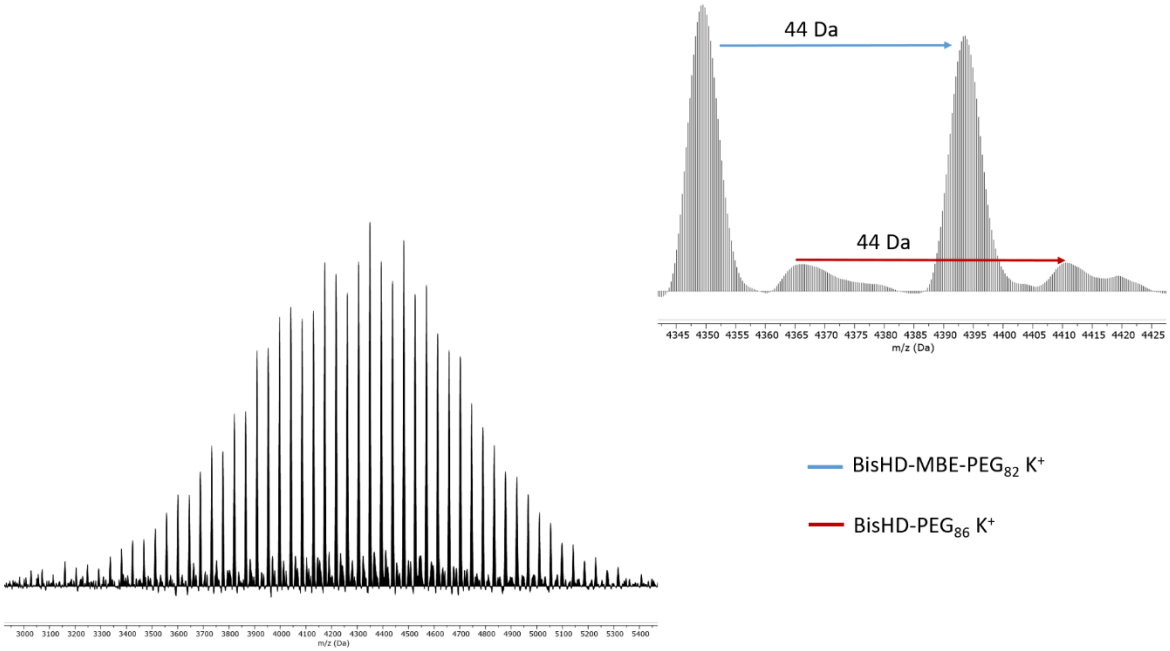

Figure 4: MALDI-ToF MS spectrum of BisHD-MBE-PEG (left) and the zoom-in spectrum (right).

Isomerization of BisHD-MBE-PEG to BisHD-isoMBE-PEG

In order to obtain complete isomerization of the polymers, the polymers were dissolved in DMSO and heated with potassium *tert*-butoxide for 12 hours (**Scheme 7**).

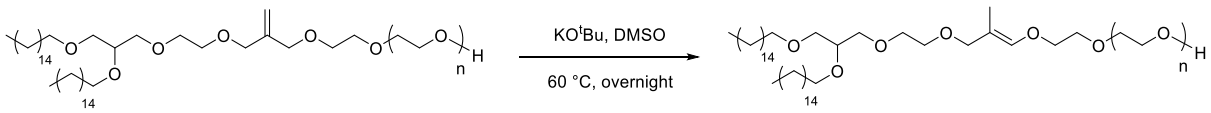

Scheme 7: Synthesis route of the isomerization of BisHD-MBE-PEG to BisHD-*iso*MBE-PEG.

For complete isomerization, the equivalents of base were varied. Using 2 eq base, only about 65 % of the polymer could be isomerized. The equivalents of base were then increased to 3, 4, and 5 eq. Higher amounts of base resulted in complete isomerization, but a side reaction was also observed to increase with the amount of base. The best results were obtained with 3 eq. base were obtained, because here the side reaction took place below 5 %. The next **Figure 5** shows the ^{1}H NMR spectra of the reactions with different amounts of base. The signals of the molecule of the side reaction are marked in blue.

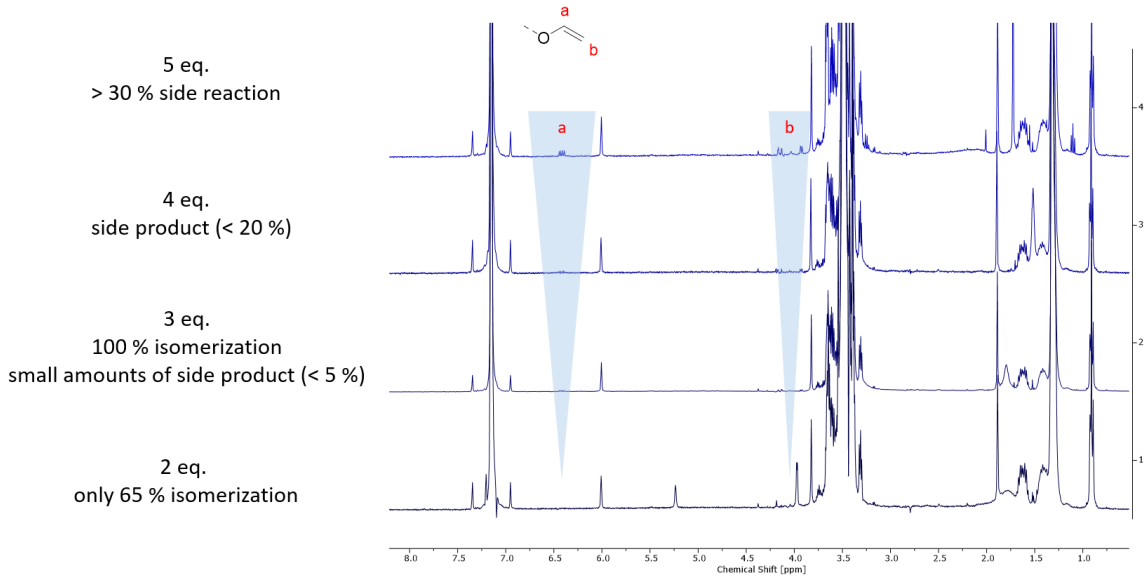

Figure 5: ^{1}H NMR spectra (400 MHz, benzene-d_6) of the BisHD-*iso*MBE-PEG polymer with the influence of different amounts of base.

The ^{1}H NMR of the reaction with 3 eq. base is shown below in **Figure 6** with the assignment of the signals.

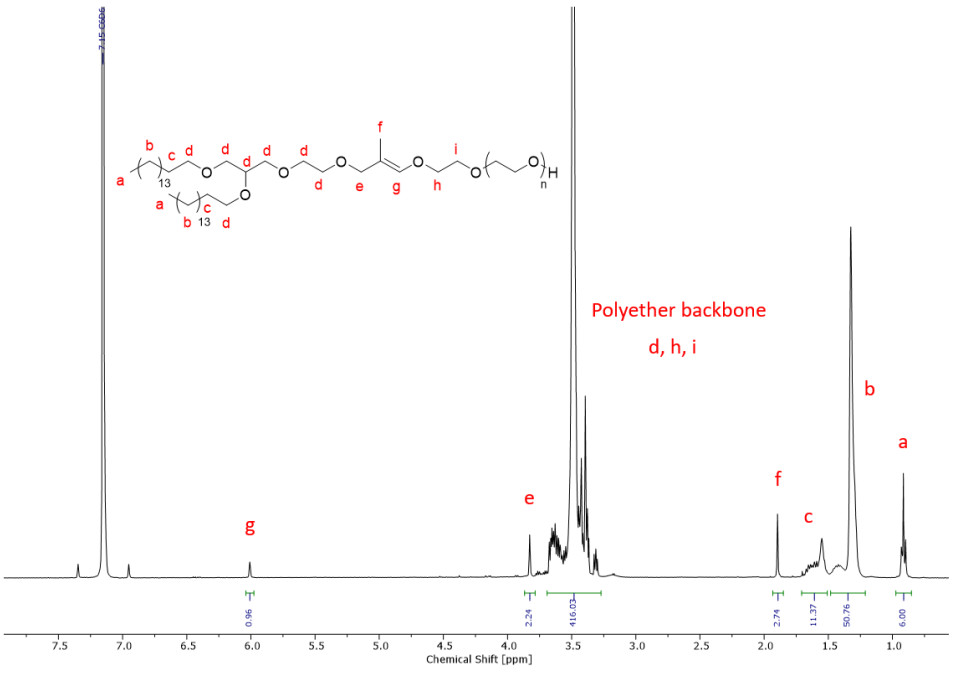

Figure 6: ^{1}H NMR spectrum (400 MHz, benzene-d_6) of the BisHD-*iso*MBE-PEG polymer

In order to exclude a cleavage of the polymer due to the isomerization, SEC measurements were performed in addition to the NMR spectra (**Figure 7**). The dashed curves correspond to the polymers before isomerization, the continuous curves after isomerization. The curves are congruent. Degradation or cleavage of the product could not be detected, neither by NMR spectroscopy nor in SEC measurements.

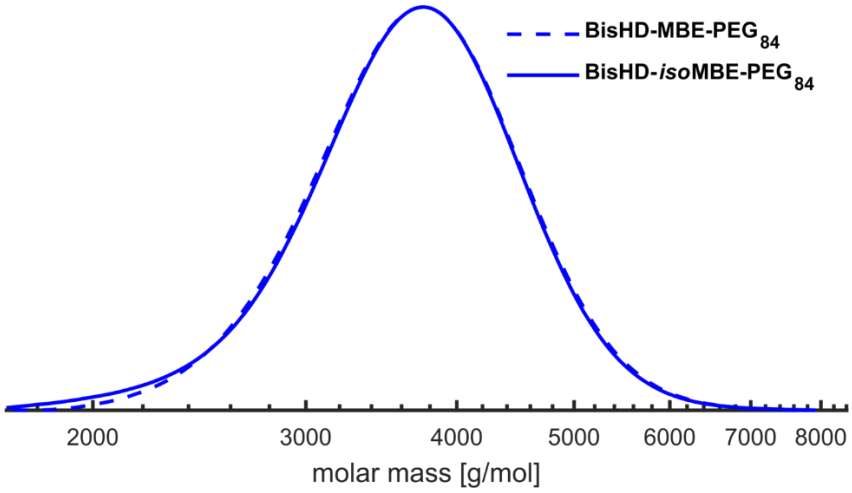

Figure 7: SEC traces (RI detector, DMF, PEG standards) of the BisHD-MBE-PEG (dashed) and BisHD-*iso*MBE-PEG polymers (continuous).

Post-polymerization modification

To enable subsequent modification of the liposomes, for example with a drug or a dye, the amphiphilic polyether lipids were post-functionalized. Established systems for this are click reactions, such as the azide-alkyne click.[43] In this work, the polymers were equipped with an alkyne group. This post-polymerization modification was carried out according to known synthesis procedures from our group.[38,44–46] For the attachment of the alkyne moieties, the amphiphilic polymer lipids were deprotonated with sodium hydride (NaH) and functionalized with propargyl bromide. Both polymers, the BisHD-PEG polymer and the BisHD-*iso*MBE-PEG polymer were modified. Successful functionalization was evidenced *via* NMR spectroscopy. The synthesis route for the post-polymerization modification for the polymers is shown in **Scheme 8**.

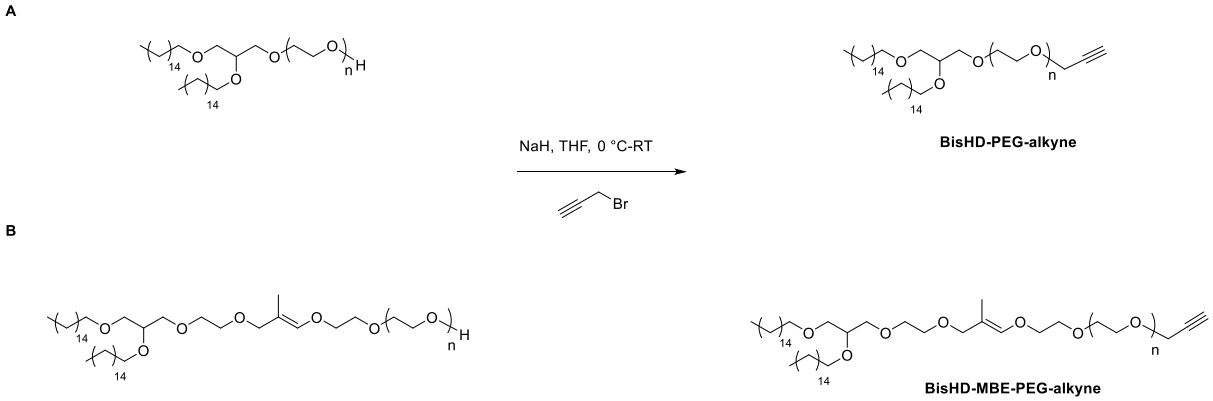

Scheme 8: Synthesis route of the post-polymerization modification of BisHD-PEG (**A**) and BisHD-*iso*MBE-PEG (**B**) with propargyl bromide.

In **Figure 8** the ^{1}H NMR spectra of BisHD-*iso*MBE-PEG before and after functionalization is shown. The characteristic signals for the protons of the alkyne moieties are highlighted in blue. Details regarding NMR spectra and the SEC measurements of the reference structure BisHD-PEG-alkyne can be found in the Supporting Information (**SI-Figure 18**, **SI-Figure 20**).

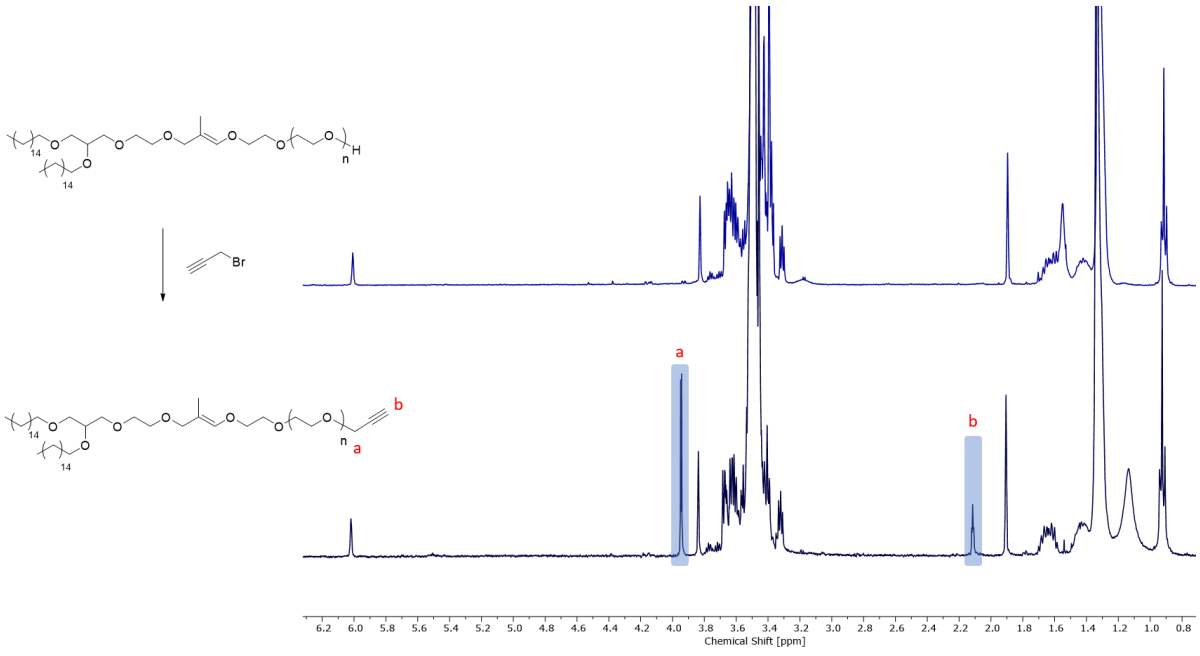

Figure 8: ^{1}H NMR spectra (400 MHz, benzene-d_6) of the BisHD-*iso*MBE-PEG polymer before (top) and after (bottom) post-polymerization modification with propargyl bromide.

SEC measurements showed no significant changes in the polymer distributions before and after functionalization. The SEC data of BisHD-*iso*MBE-PEG and BisHD-*iso*MBE-PEG-alkyne can be taken from the following **Figure 9**.

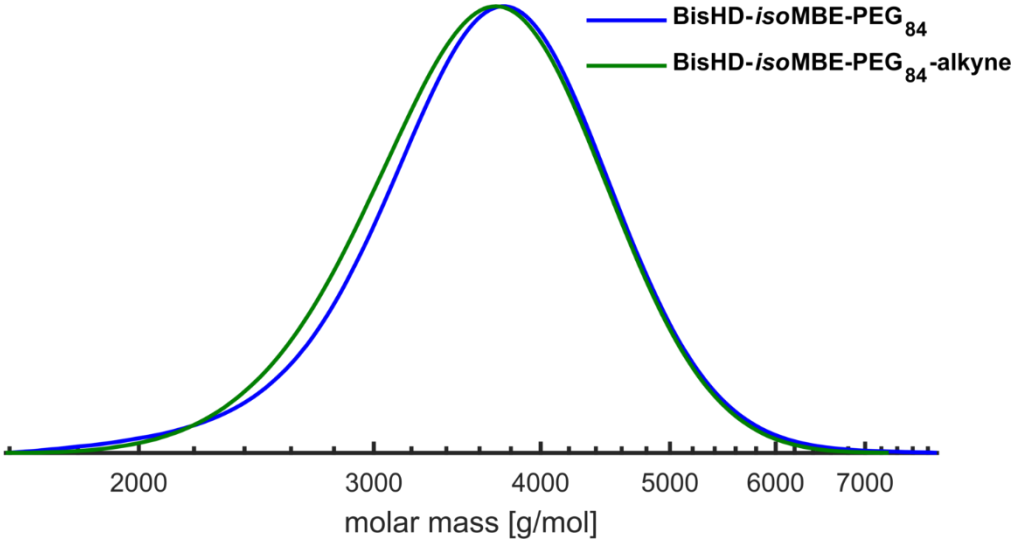

Figure 9: SEC traces (RI detector, DMF, PEG standards) of the BisHD-isoMBE-PEG polymer before (blue) and after (green) post-modification with propargyl bromide.

Degradation Studies of the Chol-isoMBE-PEG polymers

To obtain detailed information about the degradation products of the amphiphilic polymer lipids, they were incubated at acidic pH value. For this purpose, the BisHD-*iso*MBE-PEG polymer (5 mg) was dissolved in a dilute hydrochloric acid solution (1 mL) and treated for 24 hours with continuous shaking. The pH value was chosen low enough to ensure complete cleavage of all polymers. After 24 hours, the aqueous polymer solution was filtered over basic aluminum oxide to neutralize it and dried in high vacuum. Finally, the hydrolysis fragments were analyzed by SEC. **Figure 10** shows the SEC traces of the polymer before and after hydrolysis. The hydrolysis products of acidic cleavage are shown in **Scheme 9**.

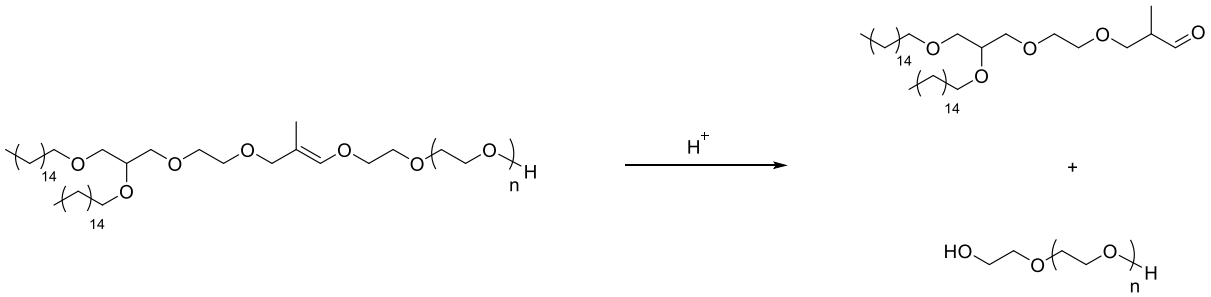

Scheme 9: Products of the acidic hydrolysis.

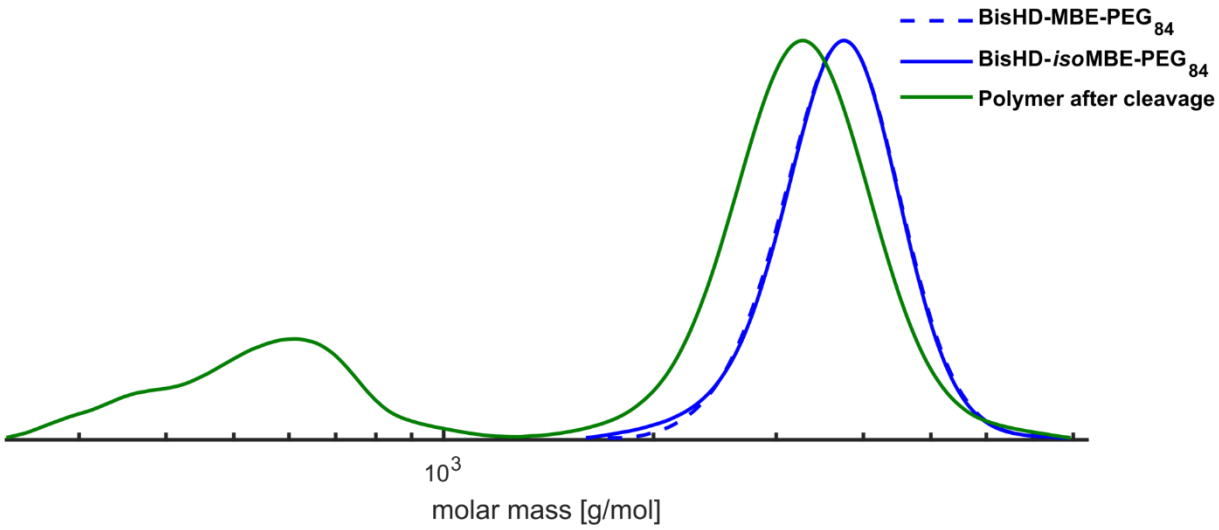

Figure 10: SEC traces (RI detector, DMF, PEG standards) of the BisHD-MBE-PEG polymer (dashed), the BisHD-*iso*MBE-PEG polymer (continuous) and the fragments after acidic hydrolysis (green).

For the analysis of the fragments by SEC measurement, the polymer solution was neutralized and the solvent removed. The hydrolysis products were then added to the SEC column as a mixture without purification. As expected, two compounds could be detected. One compound with a molecular weight of about 3200 g/mol, the other with a molecular weight of about 500 g/mol. These molecular weights correspond quite closely to the hydrolysis products. A shift to lower molecular weights in the higher molecular range additionally confirms the cleavage of the hydrophobic initiator from the PEG backbone.

2.2.3.3 Liposome preparation

The composition of the liposomes can be found in **Table 2**. The preparation was carried out by dual centrifugation. Purification was carried out by size exclusion chromatography.

Table 2: Lipid compositions of liposomal formulations in mol%.

	Lipid 1	Percentage	Lipid 2	Percentage	Lipid 3	Percentage
1	EPC3	55 mol%	Chol	45 mol%	-	-
2	EPC3	54 mol%	Chol	45 mol%	BisHD-PEG	1 mol%
3	EPC3	50 mol%	Chol	45 mol%	BisHD-PEG	5 mol%
4	EPC3	54 mol%	Chol	45 mol%	BisHD-PEG-alkyne	1 mol%
5	EPC3	50 mol%	Chol	45 mol%	BisHD-PEG-alkyne	5 mol%
6	EPC3	54 mol%	Chol	45 mol%	BisHD-*iso*MBE-PEG	1 mol%
7	EPC3	50 mol%	Chol	45 mol%	BisHD-*iso*MBE-PEG	5 mol%
8	EPC3	54 mol%	Chol	45 mol%	BisHD-*iso*MBE-PEG-alkyne	1 mol%
9	EPC3	50 mol%	Chol	45 mol%	BisHD-*iso*MBE-PEG-alkyne	5 mol%

EPC3: egg phosphatidyl choline 3; Chol: cholesterol.

2.2.3.4 Characterization of the liposomes

To determine the size of the liposomes, the vesicles were measured using dynamic light scattering (DLS). The results are shown in **Figure 11**. The composition of the liposomes is shown in **Table 2**, where L0 again corresponds to the standard liposome without modification. The size of liposomes was determined at the beginning and after incubation at 37 °C at a pH of 7.4 and 5.4 after 8 hours. The size of the liposomes was monodisperse at about 130-160 nm for all samples. Further details can be found in the **SI-Table 1**. No change in size was observed at any pH after 8 h of incubation. One reason for this is, according to literature significant cleavage of the vinyl ether sites only at a lower pH value (pH = 5-4.5) within the 8 hours.[30,32] In addition, it cannot be excluded that the PEG chains have only a minor influence on the size of the liposomes and that cleavage does not have a major effect on the size.

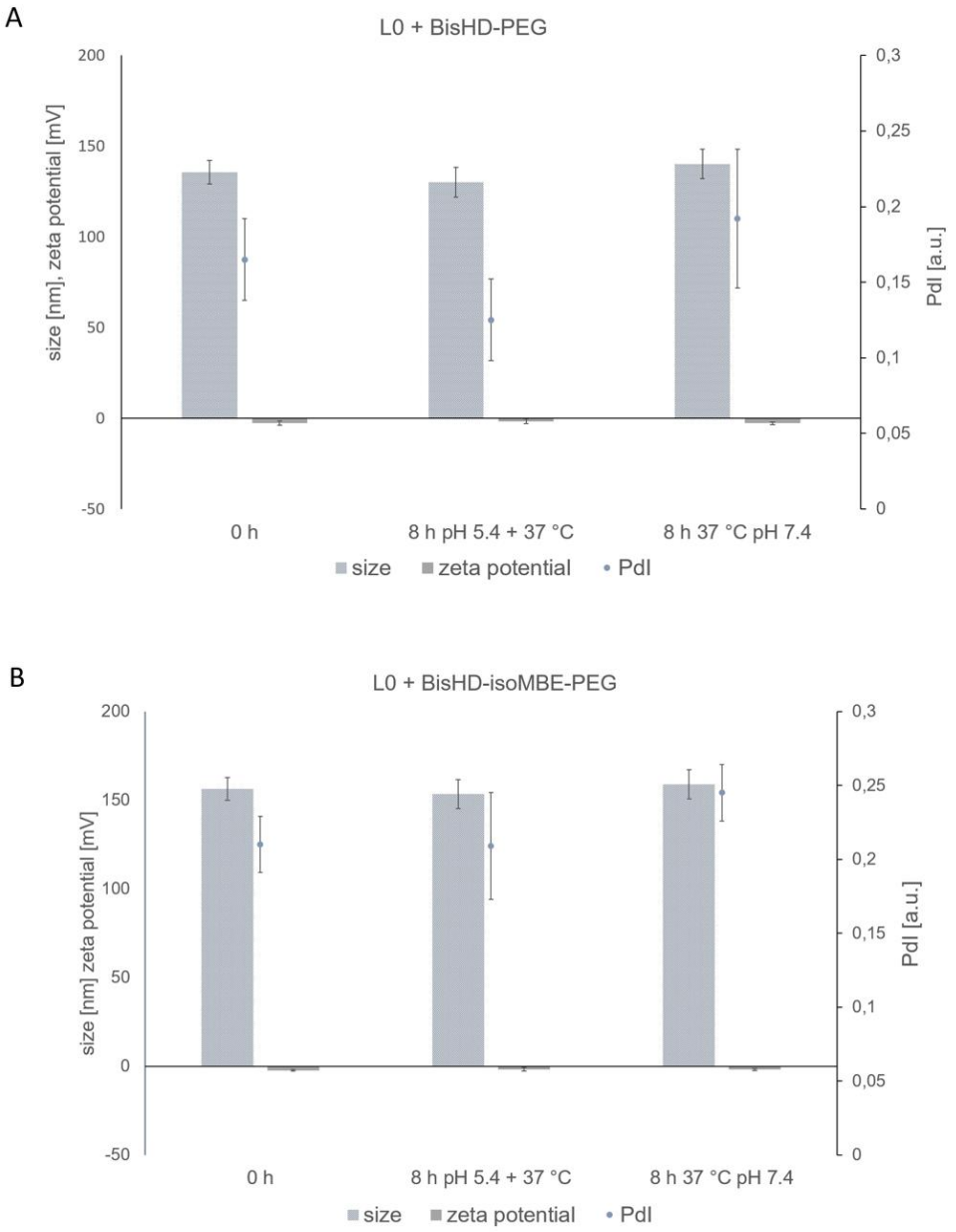

Figure 11: DLS measurements of the liposomes without a pH-responsive cleavage site (**A**) and with a pH-responsive cleavage site (**B**).

To check the stability of the liposomes, the model cargo Sulforhodamine B (SRB) was encapsulated in the liposomes. Sulforhodamine B is a highly water-soluble fluorescent dye. After encapsulation of the dye, the liposomes were purified by HPLC, so that fluorescence can only be measured due to the destabilization of the liposomal structure. Liposomes were then incubated at 37 °C at pH values of 7.4 and 5.9. At these pH values, no release of the model cargo from the liposomes could be detected (see **Figure 12**). It can therefore be

concluded that a possible cleavage of the PEG groups at these pH values has no influence on the stability of the liposomes. This plays a role especially in the storage of liposomes. Storage stability is the basic requirement for the use of these liposomes in biological applications.

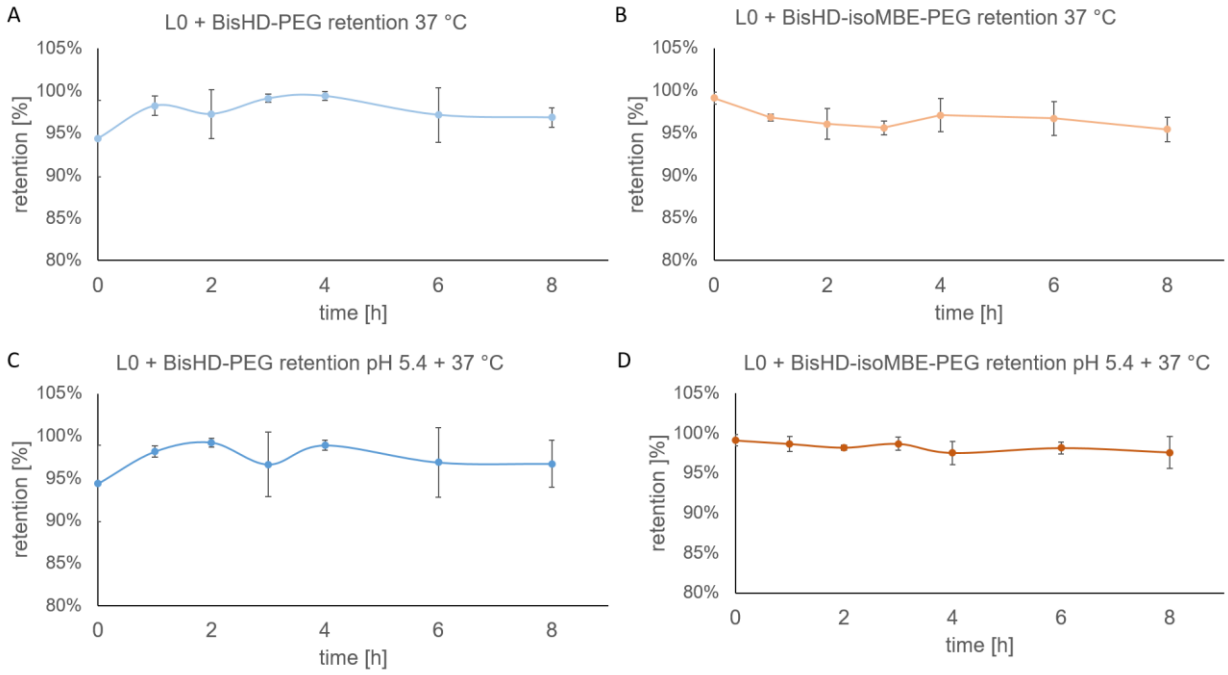

Figure 12: Stability measurements by encapsulation of Sulforhodamine B.

2.2.3.5 Cell viability studies

For the use of synthetically produced compounds in biomedical applications, it is essential to exclude toxicity. To verify this, the standard liposome L0 (**Table 2**, entry 1), liposomes modified with BisHD-PEG (**Table 2**, entry 3), BisHD-*iso*MBE-PEG (**Table 2**, entry 7), BisHD-PEG-alkyne (**Table 2**, entry 5) and BisHD-*iso*MBE-PEG-alkyne (**Table 2**, entry 9), were examined by cell assays. To remove chemical residues from the synthesis of the polymers, they were purified by dialysis. HeLa cells and HEK cells were used as cell lines. The liposomes were incubated for 24 h with the cells. Concentrations of 0.1 µg/mL up to 100 µg/mL were tested. The MTT assays are displayed in **Figure 13**.

At all concentrations and with all modifications, also in comparison with the standard liposome, no influence on the cells could be detected. The liposomes therefore show no toxicity and can be used unconditionally in biological systems.

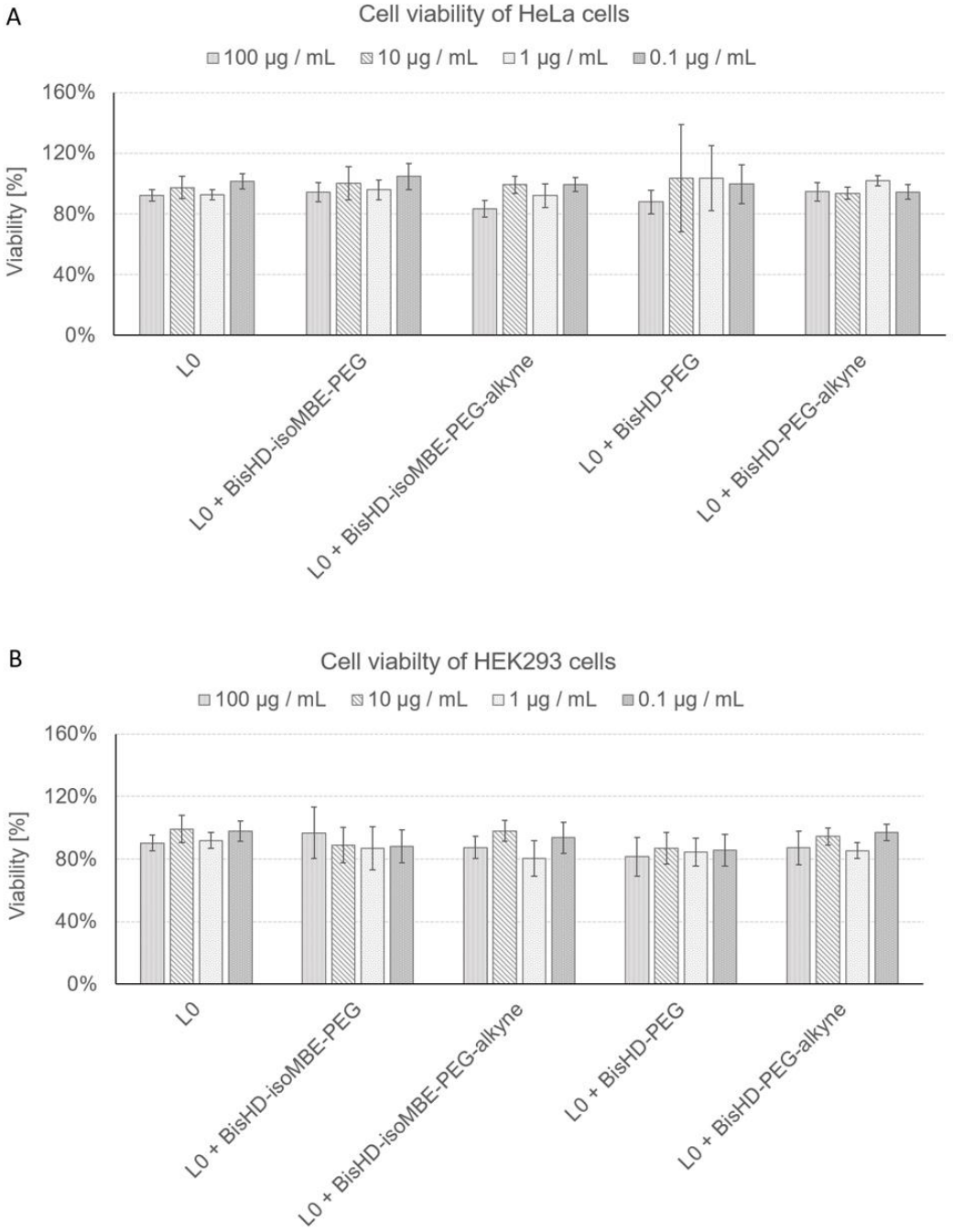

Figure 13: MTT assays of HeLa cells (**A**) and HEK cells (**B**) incubated with the standard liposome L0, liposomes modified with BisHD-PEG, BisHD-*iso*MBE-PEG, BisHD-PEG-alkyne and BisHD-*iso*MBE-PEG-alkyne.

2.2.4 Conclusion

This work introduces the synthesis of a pH-sensitive polyether lipid for the preparation of pH-responsive stealth liposomes by dual centrifugation. First, an initiator for the anionic ring-opening polymerization (AROP) was prepared based on a long-chain dialkyl anchor, which was endowed with an allyl function. Subsequently, the initiator was used in a polymerization with ethylene oxide (EO) to form the amphiphilic polyether lipids. Narrowly monodisperse polymers could be obtained ($Đ$ = 1.07-1.04). To convert the polyether lipid to its pH-responsive form, isomerization of the allyl function to the vinyl ether was carried out. Vinyl ethers exhibit excellent pH sensitivity in the range 5-4.5 and are therefore ideal for pH-responsive systems. In a post-modification with propargyl bromide, the polyether lipid was endowed with an alkyne end group. This allows for further functionalization *via* Cu(I)-catalyzed alkyne-azide cycloaddition (CuAAC), for example with a dye, a radioactive tracer, a small molecule or a ligand for targeted drug delivery. In addition, comparative structures without pH-sensitive cleavage sites were synthesized. The polyether lipids were then used to prepare liposomes by dual centrifugation. The size of the liposomes was determined by DLS. The liposomes were monodisperse with a size of about 150 nm. To investigate the stability of the liposomes, the model cargo Sulforhodamine B was encapsulated in the liposomes and they were incubated at pH values of 7.4 and 5.4 at 37 °C. No release of the dye was detected after 8 h and the size of the liposomes was unchanged in both cases. Therefore, it can be concluded that the liposomes are stable under slightly acidic conditions. In the last step, the liposomes were tested for possible toxicity by MTT assays. For this purpose, they were incubated with the cell lines HeLa and HEK293 for 24 h, and the cell activity was measured afterwards. No reduction in cell activity was detected, which rules out the toxicity of the systems. pH-sensitive polyether lipids are promising candidates for use in nanocarriers for targeted drug delivery. A combination of the pH-sensitive vinyl ether-based PEG lipids with targeted moieties, for example of folate or mannose receptors, is only one of many possible applications. The results of this work demonstrate the great potential of pH-sensitive polyether lipids for liposomal drug carrier systems.

2.2.5 Acknowledgment

E.B. thanks the DFG in the context of the SFB 1066 for financial support.

References

(1) Torchilin, V. Multifunctional and Stimuli-Sensitive Pharmaceutical Nanocarriers. *Eur. J. Pharm. Biopharm.* **2009**, *71* (3), 431–444. https://doi.org/10.1016/j.ejpb.2008.09.026.

(2) Chamundeeswari, M.; Jeslin, J.; Verma, M. L. Nanocarriers for Drug Delivery Applications. *Environ. Chem. Lett.* **2019**, *17* (2), 849–865. https://doi.org/10.1007/s10311-018-00841-1.

(3) Bangham, A. D.; Glover, J. C.; Hollingshead, S.; Pethica, B. A. The Surface Properties of Some Neoplastic Cells. *Biochem. J.* **1962**, *84* (3), 513–517. https://doi.org/10.1042/bj0840513.

(4) Malam, Y.; Loizidou, M.; Seifalian, A. M. Liposomes and Nanoparticles: Nanosized Vehicles for Drug Delivery in Cancer. *Trends Pharmacol. Sci.* **2009**, *30* (11), 592–599. https://doi.org/10.1016/j.tips.2009.08.004.

(5) Ahl, P. L.; Bhatia, S. K.; Meers, P.; Roberts, P.; Stevens, R.; Dause, R.; Perkins, W. R.; Janoff, A. S. Enhancement of the in Vivo Circulation Lifetime of L-α-Distearoylphosphatidylcholine Liposomes, Importance of Liposomal Aggregation versus Complement Opsonization. *Biochim. Biophys. Acta - Biomembr.* **1997**, *1329* (2), 370–382. https://doi.org/10.1016/S0005-2736(97)00129-6.

(6) Bradley, A. J.; Devine, D. V.; Ansell, S. M.; Janzen, J.; Brooks, D. E. Inhibition of Liposome-Induced Complement Activation by Incorporated Poly(Ethylene Glycol)-Lipids. *Arch. Biochem. Biophys.* **1998**, *357* (2), 185–194. https://doi.org/10.1006/abbi.1998.0798.

(7) Woodle, M. C.; Engbers, C. M.; Zalipsky, S.; Technology, L.; Court, H.; Park, M. New Amphipatic Polymer-Lipid Conjugates Forming Long-Circulating Reticuloendothelial System-Evading Liposomes. *BioconjugateChemistry* **1994**, *5* (6), 494–496. https://doi.org/10.1021/ac00087a707.

(8) Lasic, D. .; Needham, D. The "Stealth" Liposome: A Prototypical Biomaterial. *Chem. Rev.* **1995**, *95* (8), 2601–2628.

(9) Woodle, M. C. Surface-Modified Liposomes: Assessment and Characterization for Increased Stability and Prolonged Blood Circulation. *Chem. Phys. Lipids* **1993**, *64* (1–3), 249–262. https://doi.org/10.1016/0009-3084(93)90069-F.

(10) Veronese, F. M.; Pasut, G. PEGylation, Successful Approach to Drug Delivery. *Drug Discov. Today* **2005**, *10* (21), 1451–1458.

(11) Pasut, G.; Veronese, F. . . Polymer-Drug Conjugation, Recent Achievements and General Strategies. *Prog. Polym. Sci.* **2007**, *32*, 933–961. https://doi.org/10.1016/j.progpolymsci.2007.05.008.

(12) Pasut, G.; Paolino, D.; Celia, C.; Mero, A.; Joseph, A. S.; Wolfram, J.; Cosco, D.; Schiavon, O.; Shen, H.; Fresta, M. Polyethylene Glycol (PEG)-Dendron Phospholipids as Innovative Constructs for the Preparation of Super Stealth Liposomes for Anticancer Therapy. *J. Control. Release* **2015**, *199*, 106–113. https://doi.org/10.1016/j.jconrel.2014.12.008.

(13) Herzberger, J.; Niederer, K.; Pohlit, H.; Seiwert, J.; Worm, M.; Wurm, F. R.; Frey, H. Polymerization of Ethylene Oxide, Propylene Oxide, and Other Alkylene Oxides: Synthesis, Novel Polymer Architectures, and Bioconjugation. *Chem. Rev.* **2015**, acs.chemrev.5b00441. https://doi.org/10.1021/acs.chemrev.5b00441.

(14) De Vrieze, J.; Van Herck, S.; Nuhn, L.; De Geest, B. G. Design of PH-Degradable Polymer-Lipid Amphiphiles Using a Ketal-Functionalized RAFT Chain Transfer Agent. *Macromol. Rapid Commun.* **2020**, *41* (18), 1–6. https://doi.org/10.1002/marc.202000034.

(15) Gerweck, L. E.; Seetharaman, K. Cellular PH Gradient in Tumor versus Normal Tissue: Potential Exploitation for the Treatment of Cancer. *Cancer Res.* **1996**, *56* (6), 1194–1198.

(16) Abu Lila, A. S.; Kiwada, H.; Ishida, T. The Accelerated Blood Clearance (ABC) Phenomenon: Clinical Challenge and Approaches to Manage. *J. Control. Release* **2013**, *172* (1), 38–47. https://doi.org/10.1016/j.jconrel.2013.07.026.

(17) Chen, D.; Liu, W.; Shen, Y.; Mu, H.; Zhang, Y.; Liang, R.; Wang, A.; Sun, K.; Fu, F. Effects of a Novel PH-Sensitive Liposome with Cleavable Esterase-Catalyzed and PH-Responsive Double Smart MPEG Lipid Derivative on ABC Phenomenon. *Int. J. Nanomedicine* **2011**, *6*, 2053–2061. https://doi.org/10.2147/ijn.s24344.

(18) Dufort, S.; Sancey, L.; Coll, J. L. Physico-Chemical Parameters That Govern Nanoparticles Fate Also Dictate Rules for Their Molecular Evolution. *Adv. Drug Deliv. Rev.* **2012**, *64* (2), 179–189. https://doi.org/10.1016/j.addr.2011.09.009.

(19) Legendre, J. Y.; Szoka, F. C. Delivery of Plasmid DNA into Mammalian Cell Lines Using PH-Sensitive Liposomes: Comparison with Cationic Liposomes. *Pharmaceutical Research: An Official Journal of the American Association of Pharmaceutical Scientists*. 1992, pp 1235–1242.

https://doi.org/10.1023/A:1015836829670.

(20) Ishiwata, H.; Sato, S. B.; Vertut-Doï, A.; Hamashima, Y.; Miyajima, K. Cholesterol Derivative of Poly(Ethylene Glycol) Inhibits Clathrin-Independent, but Not Clathrin-Dependent Endocytosis. *Biochim. Biophys. Acta - Mol. Cell Res.* **1997**, *1359* (2), 123–135. https://doi.org/10.1016/S0167-4889(97)00061-X.

(21) Chen, D.; Jiang, X.; Huang, Y.; Zhang, C.; Ping, Q. Ph-Sensitive MPEG-Hz-Cholesterol Conjugates as a Liposome Delivery System. *J. Bioact. Compat. Polym.* **2010**, *25* (5), 527–542. https://doi.org/10.1177/0883911510379996.

(22) Wang, L.; Liu, G.; Wang, X.; Hu, J.; Zhang, G.; Liu, S. Acid-Disintegratable Polymersomes of PH-Responsive Amphiphilic Diblock Copolymers for Intracellular Drug Delivery. *Macromolecules* **2015**, *48* (19), 7262–7272. https://doi.org/10.1021/acs.macromol.5b01709.

(23) Guo, X.; Szoka, F. C. Steric Stabilization of Fusogenic Liposomes by a Low-PH Sensitive PEG - Diortho Ester - Lipid Conjugate. *Bioconjug. Chem.* **2001**, *12* (2), 291–300. https://doi.org/10.1021/bc000110v.

(24) Li, W.; Huang, Z.; MacKay, J. A.; Grube, S.; Szoka, F. C. Low-PH-Sensitive Poly(Ethylene Glycol) (PEG)-Stabilized Plasmid Nanolipoparticles: Effects of PEG Chain Length, Lipid Composition and Assembly Conditions on Gene Delivery. *J. Gene Med.* **2005**, *7* (1), 67–79. https://doi.org/10.1002/jgm.634.

(25) Masson, C.; Garinot, M.; Mignet, N.; Wetzer, B.; Mailhe, P.; Scherman, D.; Bessodes, M. PH-Sensitive PEG Lipids Containing Orthoester Linkers: New Potential Tools for Nonviral Gene Delivery. *J. Control. Release* **2004**, *99* (3), 423–434. https://doi.org/10.1016/j.jconrel.2004.07.016.

(26) Mustapa, M. F. M.; Grosse, S. M.; Kudsiova, L.; Elbs, M.; Raiber, E. A.; Wong, J. B.; Brain, A. P. R.; Armer, H. E. J.; Warley, A.; Keppler, M.; Ng, T.; Lawrence, M. J.; Hart, S. L.; Hailes, H. C.; Tabor, A. B. Stabilized Integrin-Targeting Ternary LPD (Lipopolyplex) Vectors for Gene Delivery Designed to Disassemble within the Target Cell. *Bioconjug. Chem.* **2009**, *20* (3), 518–532. https://doi.org/10.1021/bc800450r.

(27) Shin, J.; Shum, P.; Thompson, D. H. Acid-Triggered Release via DePEGylation of DOPE Liposomes Containing Acid-Labile Vinyl Ether PEG-Lipids. *J. Control. Release* **2003**, *91* (1–2), 187–200. https://doi.org/10.1016/S0168-3659(03)00232-3.

(28) Shin, J.; Shum, P.; Grey, J.; Fujiwara, S. I.; Malhotra, G. S.; González-Bonet, A.; Hyun, S. H.; Moase, E.; Allen, T. M.; Thompson, D. H. Acid-Labile MPEG-Vinyl Ether-1,2-Dioleylglycerol Lipids with Tunable Ph Sensitivity: Synthesis and Structural Effects on Hydrolysis Rates, DOPE Liposome Release Performance, and Pharmacokinetics.

Mol. Pharm. **2012**, *9* (11), 3266–3276. https://doi.org/10.1021/mp300326z.

(29) Luvino, D.; Khiati, S.; Oumzil, K.; Rocchi, P.; Camplo, M.; Barthélémy, P. Efficient Delivery of Therapeutic Small Nucleic Acids to Prostate Cancer Cells Using Ketal Nucleoside Lipid Nanoparticles. *J. Control. Release* **2013**, *172* (3), 954–961. https://doi.org/10.1016/j.jconrel.2013.09.006.

(30) Worm, M.; Leibig, D.; Dingels, C.; Frey, H. Cleavable Polyethylene Glycol: 3,4-Epoxy-1-Butene as a Comonomer to Establish Degradability at Physiologically Relevant PH. *ACS Macro Lett.* **2016**, *5* (12), 1357–1363. https://doi.org/10.1021/acsmacrolett.6b00735.

(31) Steiert, E.; Ewald, J.; Wagner, A.; Hellmich, U. A.; Frey, H.; Wich, P. R. PH-Responsive Protein Nanoparticles: Via Conjugation of Degradable PEG to the Surface of Cytochrome C. *Polym. Chem.* **2020**, *11* (2), 551–559. https://doi.org/10.1039/c9py01162e.

(32) Rui, Y.; Wang, S.; Low, P. S.; Thompson, D. H. Diplasmenylcholine-Folate Liposomes: An Efficient Vehicle for Intracellular Drug Delivery. *J. Am. Chem. Soc.* **1998**, *120* (44), 11213–11218. https://doi.org/10.1021/ja9742949.

(33) Gleue, L.; Schupp, J.; Zimmer, N.; Becker, E.; Frey, H.; Tuettenberg, A.; Helm, M. Stability of Alkyl Chain-Mediated Lipid Anchoring in Liposomal Membranes. *Cells* **2020**, *9* (10), 1–13. https://doi.org/10.3390/cells9102213.

(34) Massing, U.; Cicko, S.; Ziroli, V. Dual Asymmetric Centrifugation (DAC)-A New Technique for Liposome Preparation. *J. Control. Release* **2008**, *125* (1), 16–24. https://doi.org/10.1016/j.jconrel.2007.09.010.

(35) Stauch, O.; Uhlmann, T.; Fröhlich, M.; Thomann, R.; El-Badry, M.; Kim, Y. K.; Schubert, R. Mimicking a Cytoskeleton by Coupling Poly(N-Isopropylacrylamide) to the Inner Leaflet of Liposomal Membranes: Effects of Photopolymerization on Vesicle Shape and Polymer Architecture. *Biomacromolecules* **2002**, *3* (2), 324–332. https://doi.org/10.1021/bm015613y.

(36) An, H.; Bradshaw, J. S.; Krakowiak, K. E.; Zhu, C.; Dailey, N. K.; Izatt, R. M. Synthesis and Complexation Properties of Suitcase-Shaped Macrotricyclic and Butterfly-Shaped Macrobicyclic Polyether Ligands. *J.Org.Chem.* **1992**, No. 13, 4998–5005.

(37) de Vries, E. F. J.; Steenwinkel, P.; Brussee, J.; Kruse, C. G.; van der Gen, A. Synthesis of Chiral Diaza-18-Crown-6 Derivatives from Optically Active Diethanolamines. *J. Org. Chem.* **1993**, *58* (16), 4315–4325. https://doi.org/10.1021/jo00068a029.

(38) Hofmann, A. M.; Wurm, F.; Frey, H. Rapid Access to Polyfunctional Lipids with

Complex Architecture via Oxyanionic Ring-Opening Polymerization. *Macromolecules* **2011**, *44* (12), 4648–4657. https://doi.org/10.1021/ma200367c.

(39) Reibel, A. T.; Müller, S. S.; Pektor, S.; Bausbacher, N.; Miederer, M.; Frey, H.; Rösch, F. Fate of Linear and Branched Polyether-Lipids in Vivo in Comparison to Their Liposomal Formulations by 18F-Radiolabeling and Positron Emission Tomography. *Biomacromolecules* **2015**, *16* (3), 842–851. https://doi.org/10.1021/bm5017332.

(40) Worm, M.; Leibig, D.; Dingels, C.; Frey, H. Cleavable Polyethylene Glycol: 3,4-Epoxy-1-Butene as a Comonomer to Establish Degradability at Physiologically Relevant PH. *ACS Macro Lett.* **2016**, *5* (12), 1357–1363. https://doi.org/10.1021/acsmacrolett.6b00735.

(41) Ewald, J. Vinyl Ether Moieties as a Key Component for Cleavable Poly (Ethylene Glycol) Copolymers. **2020**.

(42) Bajaj, A.; Mishra, S. K.; Kondaiah, P.; Bhattacharya, S. Effect of the Headgroup Variation on the Gene Transfer Properties of Cholesterol Based Cationic Lipids Possessing Ether Linkage. *Biochim. Biophys. Acta - Biomembr.* **2008**, *1778* (5), 1222–1236. https://doi.org/10.1016/j.bbamem.2007.12.010.

(43) Van Dijk, M.; Rijkers, D. T. S.; Liskamp, R. M. J.; Van Nostrum, C. F.; Hennink, W. E. Synthesis and Applications of Biomedical and Pharmaceutical Polymers via Click Chemistry Methodologies. *Bioconjug. Chem.* **2009**, *20* (11), 2001–2016. https://doi.org/10.1021/bc900087a.

(44) Wagener, K.; Bros, M.; Krumb, M.; Langhanki, J.; Pektor, S.; Worm, M.; Schinnerer, M.; Montermann, E.; Miederer, M.; Frey, H.; Opatz, T.; Rösch, F. Targeting of Immune Cells with Trimannosylated Liposomes. *Adv. Ther.* **2020**, *3* (6), 1900185. https://doi.org/10.1002/adtp.201900185.

(45) Herzberger, J.; Fischer, K.; Leibig, D.; Bros, M.; Thiermann, R.; Frey, H. Oxidation-Responsive and "Clickable" Poly(Ethylene Glycol) via Copolymerization of 2-(Methylthio)Ethyl Glycidyl Ether. *J. Am. Chem. Soc.* **2016**, jacs.6b04548. https://doi.org/10.1021/jacs.6b04548.

(46) Fritz, T.; Hirsch, M.; Richter, F. C.; Müller, S. S.; Hofmann, A. M.; Rusitzka, K. A. K.; Markl, J.; Massing, U.; Frey, H.; Helm, M. Click Modification of Multifunctional Liposomes Bearing Hyperbranched Polyether Chains. *Biomacromolecules* **2014**, *15* (7), 2440–2448. https://doi.org/10.1021/bm5003027.

2.2.6 Supporting Information

2.2.6.1 Initiator synthesis

Synthesis of bifunctional MBE

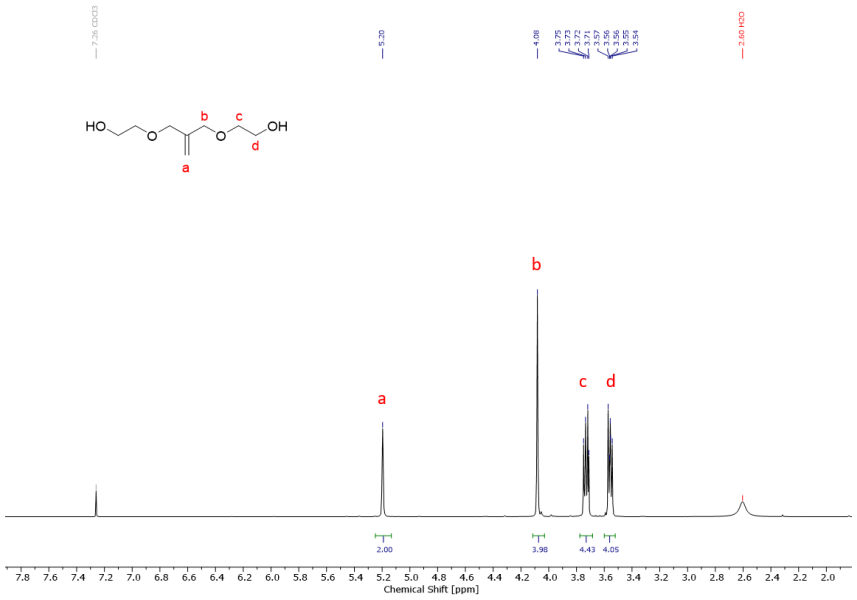

SI-Figure 1: ^{1}H NMR spectrum (300 MHz, chloroform-d_3) of MBE.

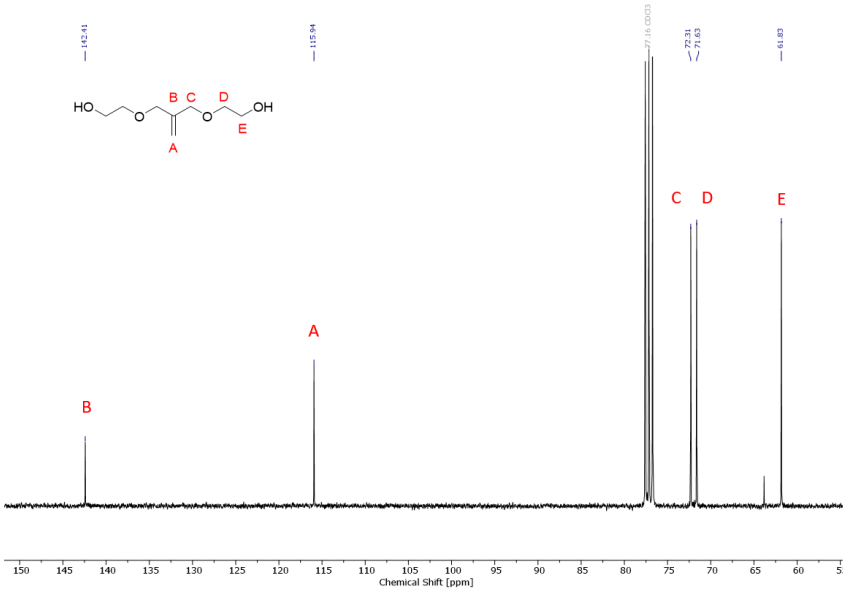

SI-Figure 2: ^{13}C NMR spectrum (75 MHz, chloroform-d_3) of MBE.

Synthesis of monofunctional THP-MBE-OH

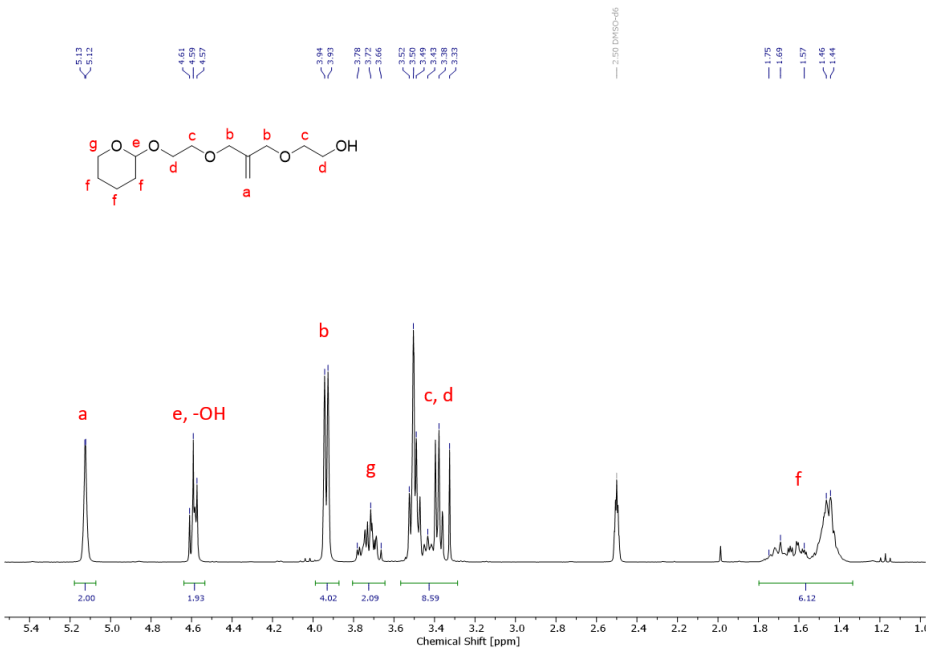

SI-Figure 3: ^{1}H NMR spectrum (300 MHz, DMSO-d_6) of THP-MBE-OH.

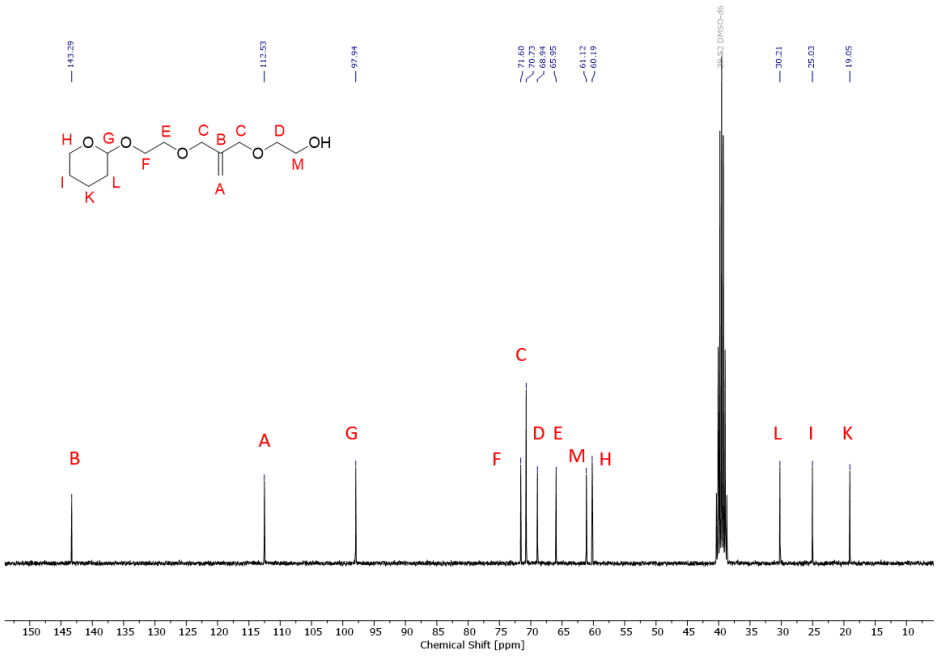

SI-Figure 4: ^{13}C NMR spectrum (75 MHz, DMSO-d_6) of THP-MBE-OH.

Synthesis of THP-MBE-Ts

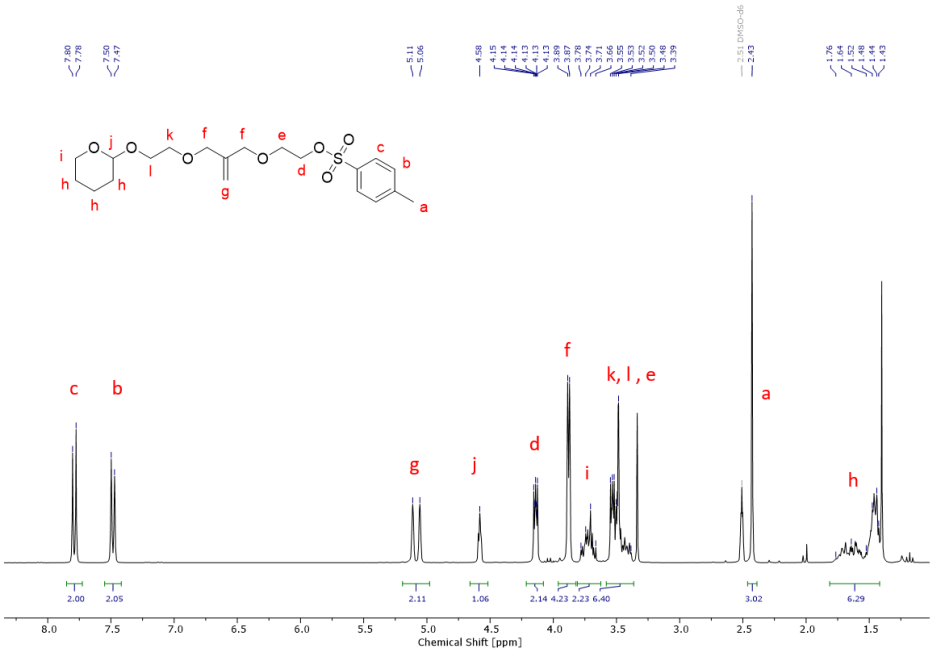

SI-Figure 5: ^{1}H NMR spectrum (300 MHz, DMSO-d_6) of THP-MBE-Ts.

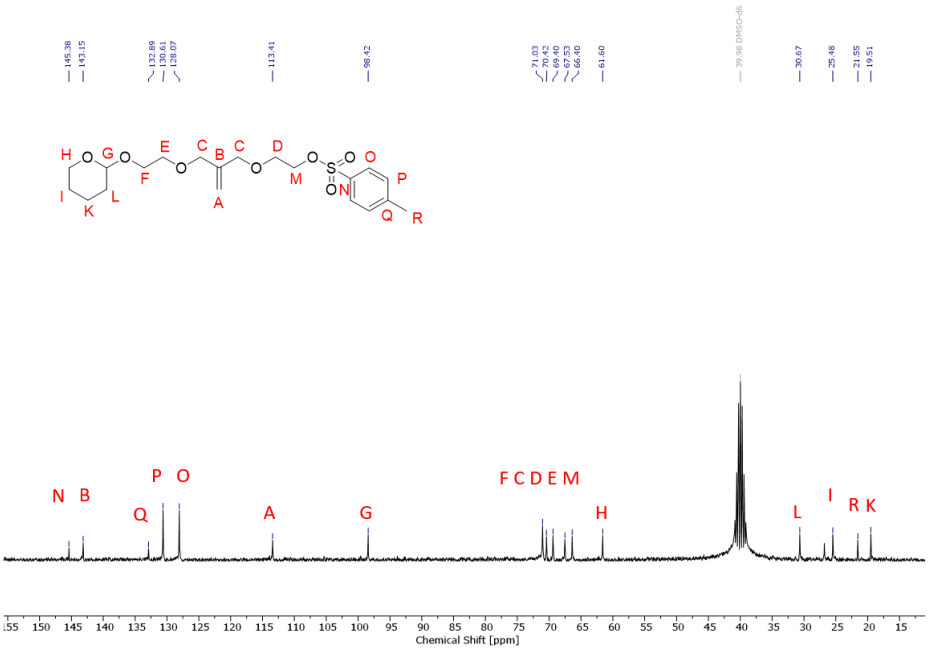

SI-Figure 6: ^{13}C NMR spectrum (75 MHz, DMSO-d_6) of THP-MBE-Ts.

Synthesis of BisHD-OH

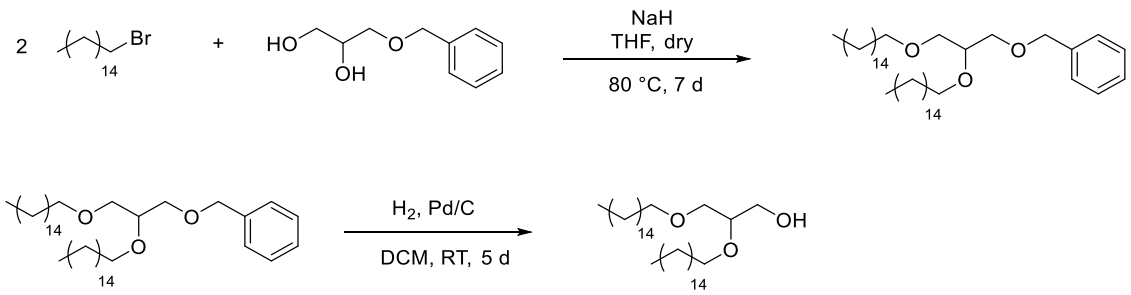

SI-Scheme 1: Synthesis route of the hydrophobic anchor structure.

^{1}H NMR (400 MHz, chloroform-*d*) δ [ppm] = 3.72 – 3.41 (m, 9H, C*H*$_2$-O and CH$_2$-C*H*-O), 1.61 – 1.49 (m, 4H, C*H*$_2$-CH$_2$-O), 1.25 (s, 52H, C*H*$_2$), 0.88 (t, *J* = 6.8 Hz, 6H, C*H*$_3$-CH$_2$).

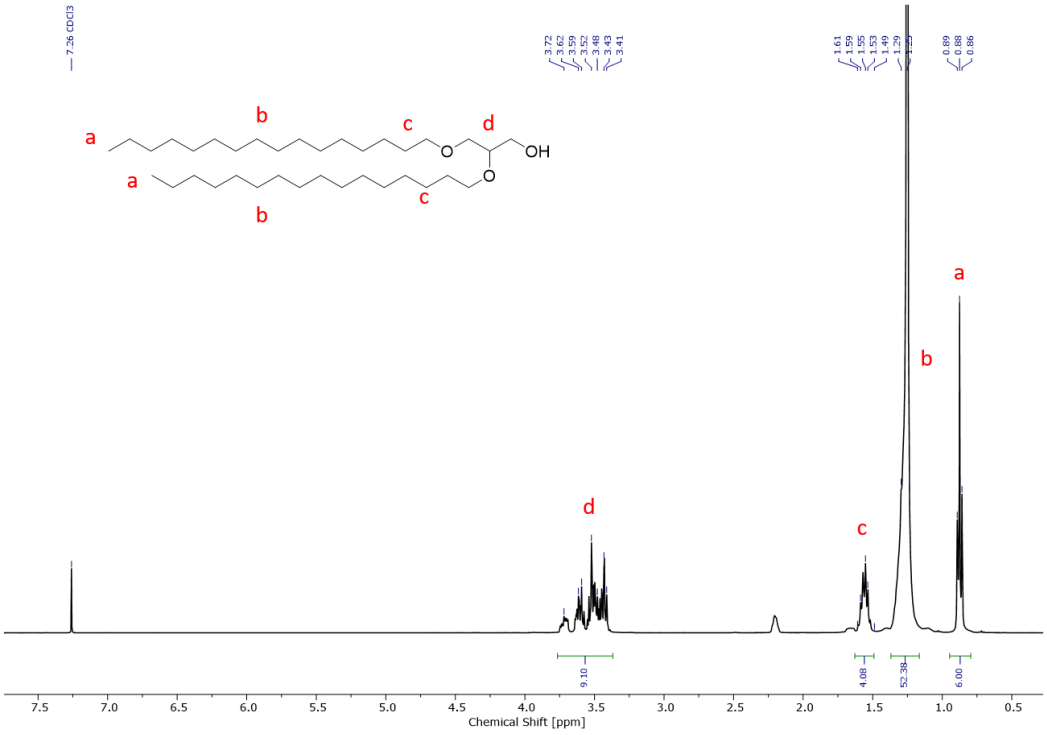

SI-Figure 7: ^{1}H NMR spectrum (400 MHz, chloroform-*d*$_3$) of BisHD-OH.

Synthesis of BisHD-MBE-OH

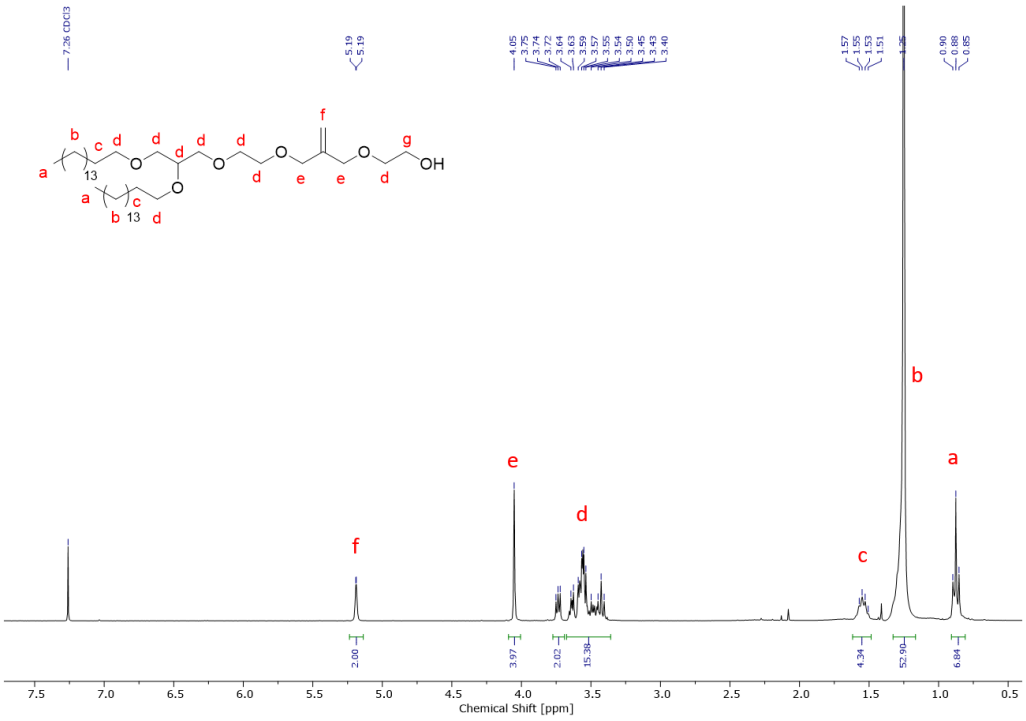

SI-Figure 8: ^{1}H NMR spectrum (300 MHz, chloroform-*d*) of BisHD-MBE-OH.

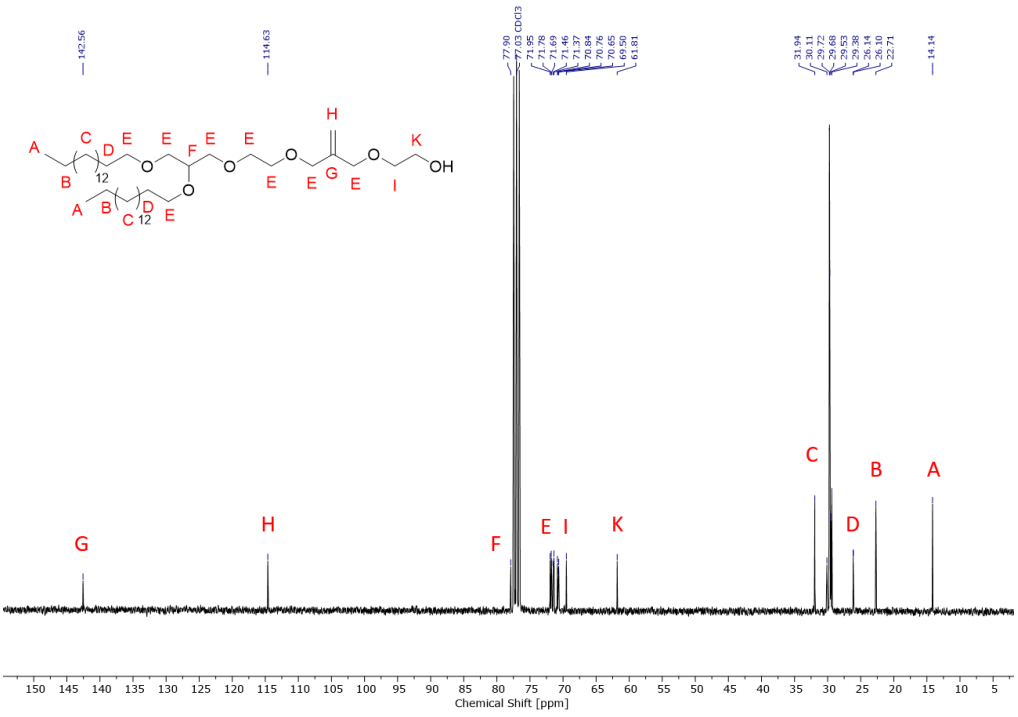

SI-Figure 9: ^{13}C NMR spectrum (75 MHz, chloroform-*d*) of BisHD-MBE-OH.

Synthesis of BisHD-PEG

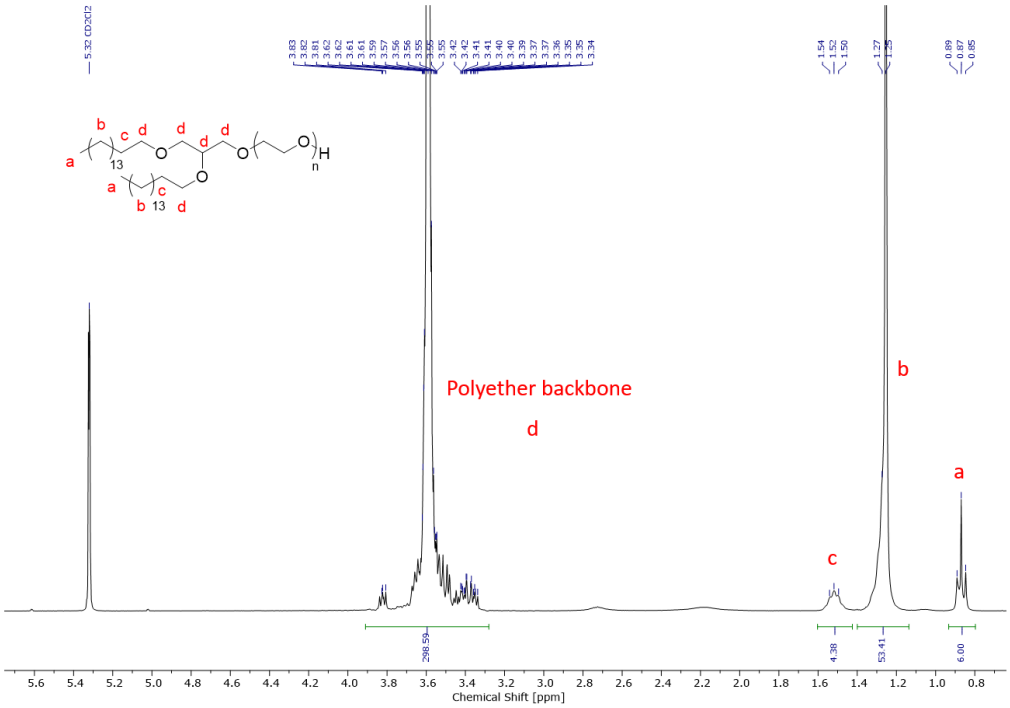

SI-Figure 10: ^{1}H NMR spectrum (300 MHz, methylene chloride-d_2) of BisHD-PEG.

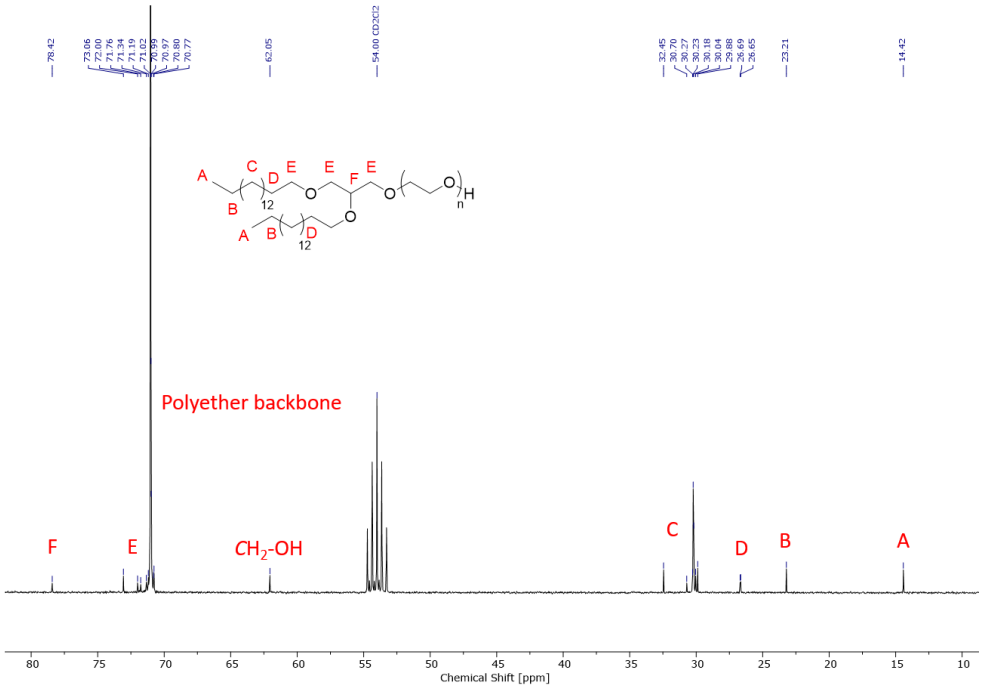

SI-Figure 11: ^{13}C NMR spectrum (75 MHz, methylene chloride-d_2) of BisHD-PEG.

Synthesis of BisHD-MBE-PEG

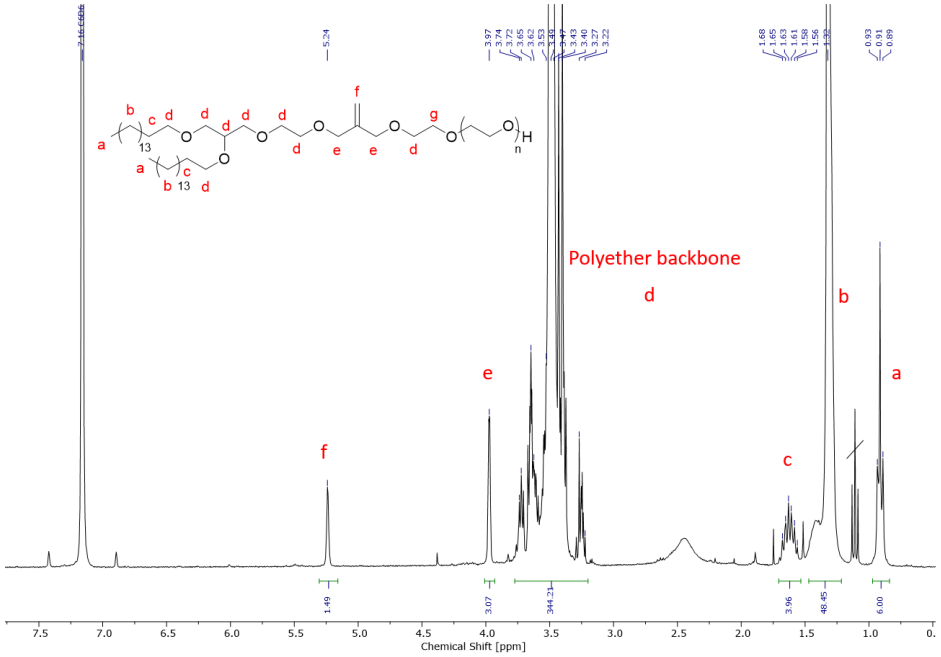

SI-Figure 12: ^{1}H NMR spectrum (300 MHz, benzene-d_6) of BisHD-MBE-PEG.

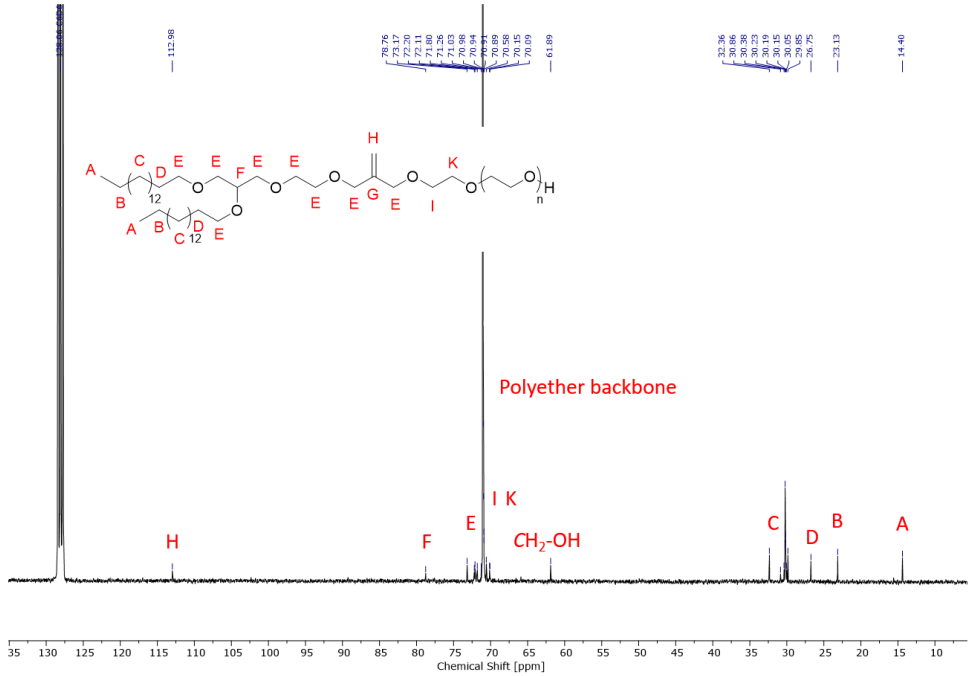

SI-Figure 13: ^{13}C NMR spectrum (75 MHz, benzene-d_6) of BisHD-MBE-PEG.

Synthesis of BisHD-isoMBE-PEG

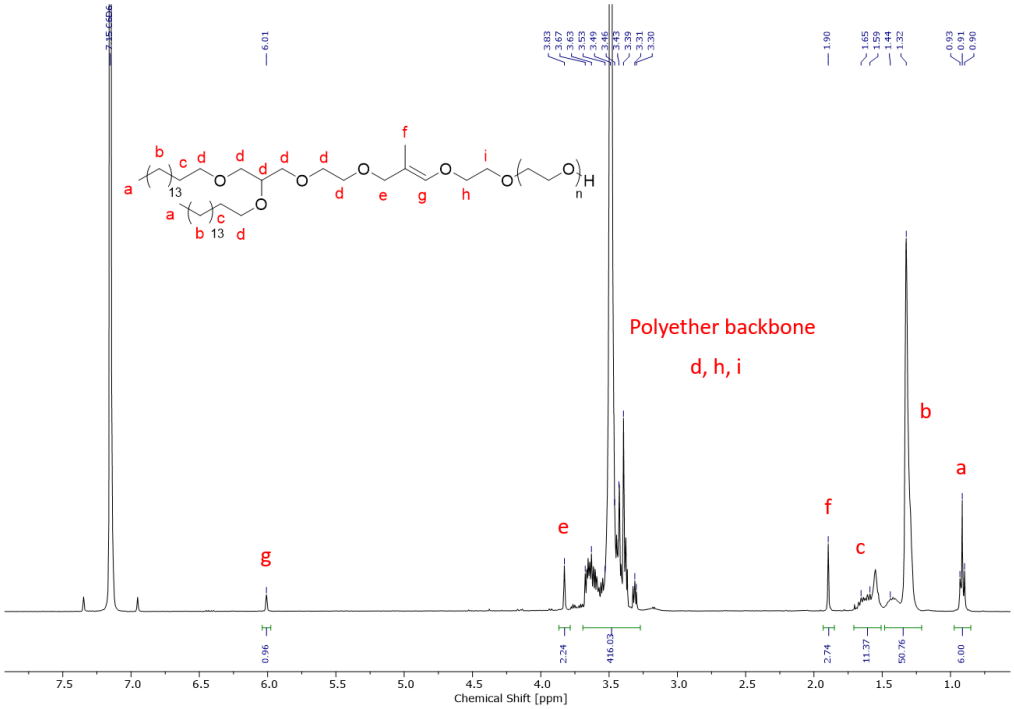

SI-Figure 14: ^{1}H NMR spectrum (400 MHz, benzene-d_6) of BisHD-*iso*MBE-PEG.

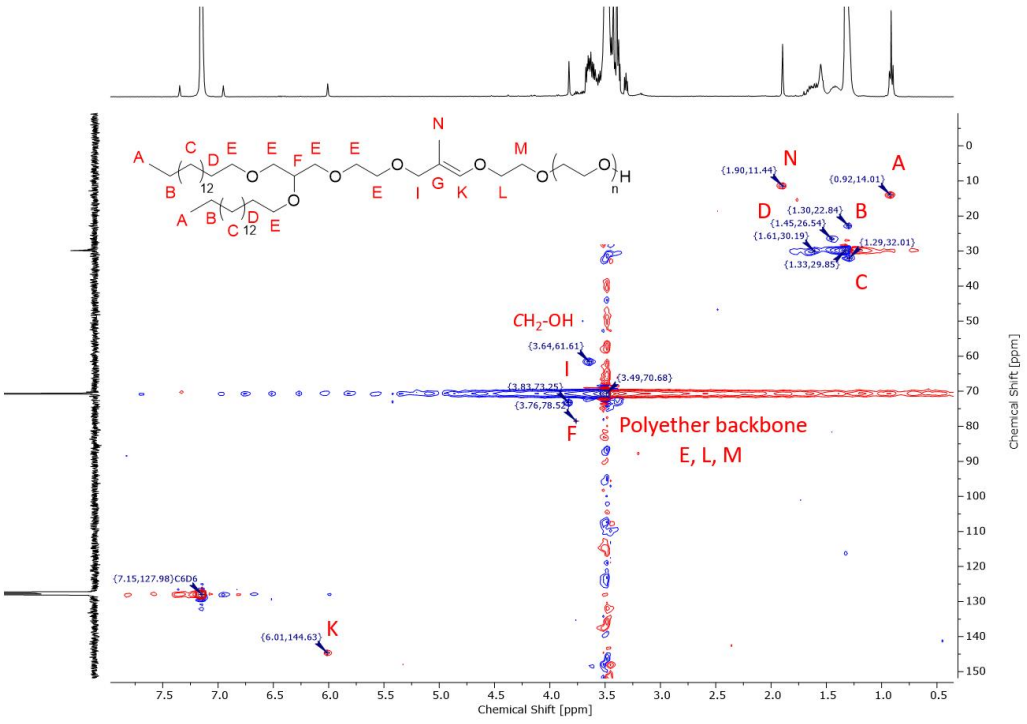

SI-Figure 15: ^{1}H, ^{13}C HSQC NMR spectrum (400 MHz, benzene-d_6) of BisHD-*iso*MBE-PEG.

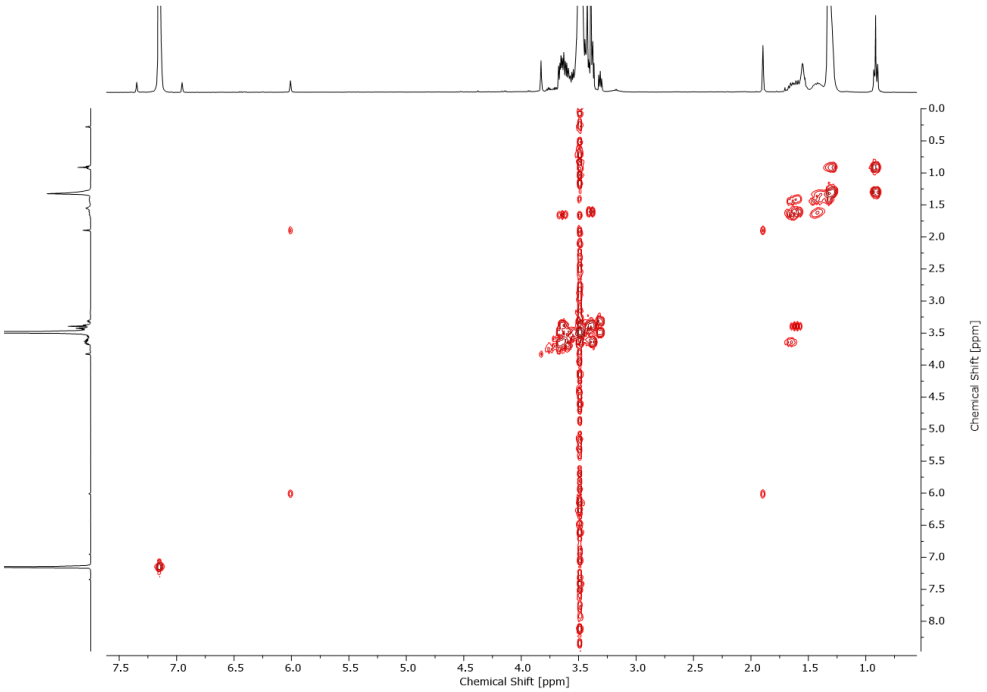

SI-Figure 16: ^{1}H, ^{1}H COSY NMR spectrum (400 MHz, benzene-d_6) of BisHD-*iso*MBE-PEG.

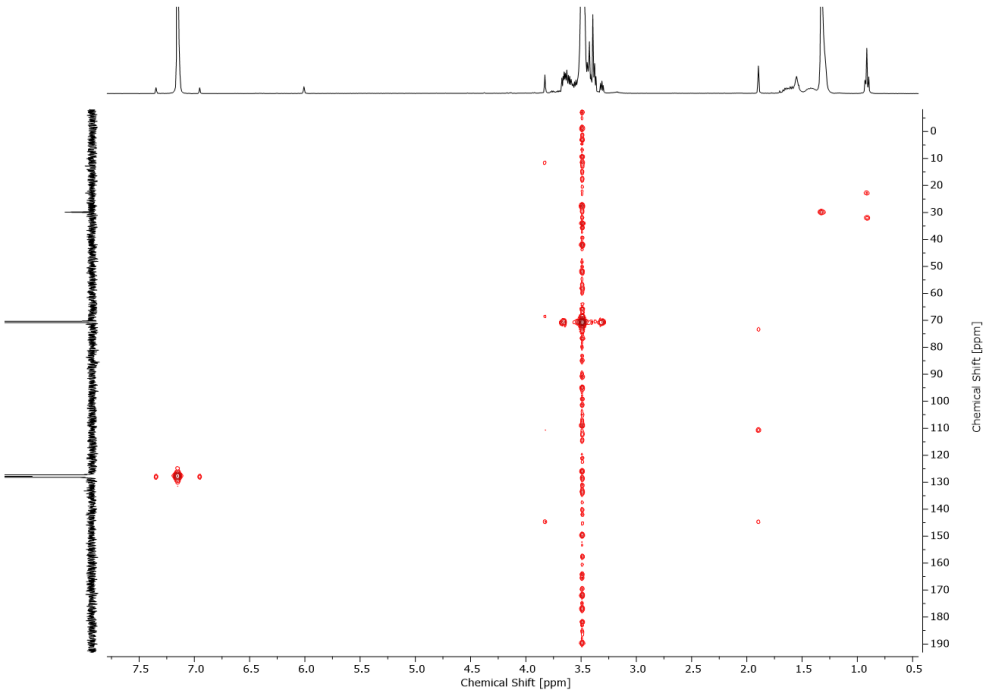

SI-Figure 17: ^{1}H, ^{13}C HMBC NMR spectrum (400 MHz, benzene-d_6) of BisHD-*iso*MBE-PEG.

Post-modification of BisHD-PEG

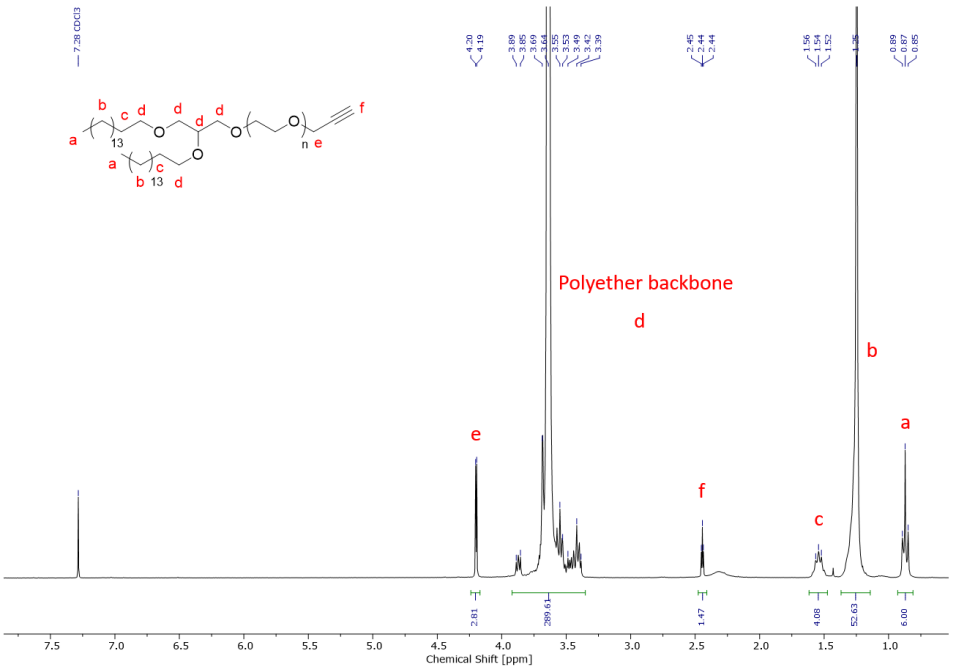

SI-Figure 18: ^{1}H NMR spectrum (300 MHz, chloroform-*d*) of BisHD-PEG-alkyne.

Post-modification of BisHD-isoMBE-PEG

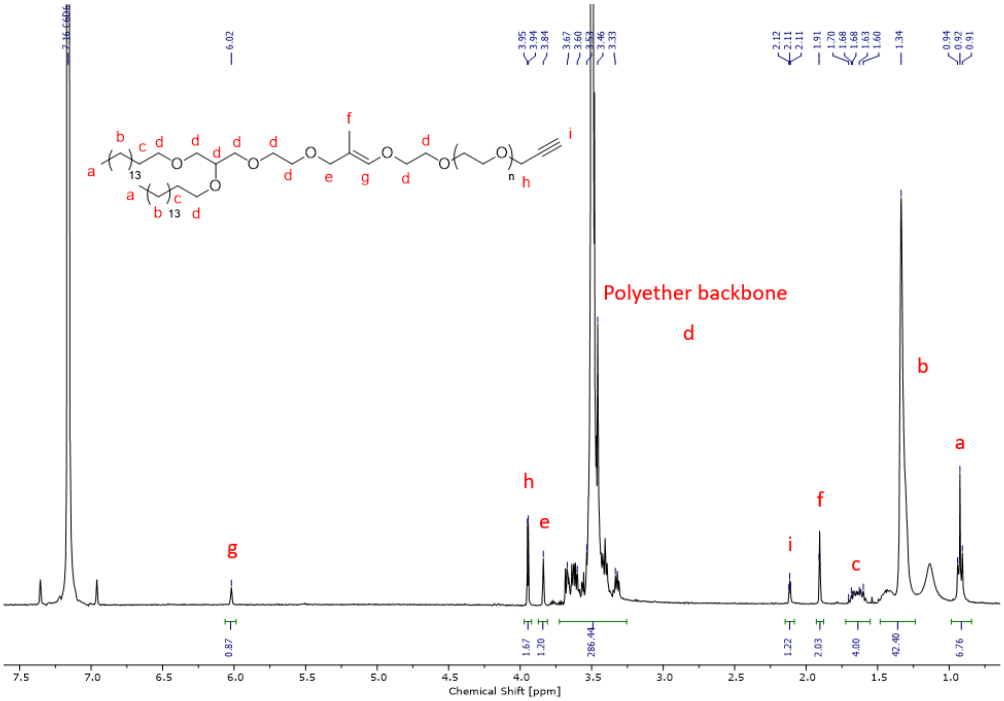

SI-Figure 19: ^{1}H NMR spectrum (400 MHz, benzene-d_6) of BisHD-*iso*MBE-PEG-alkyne.

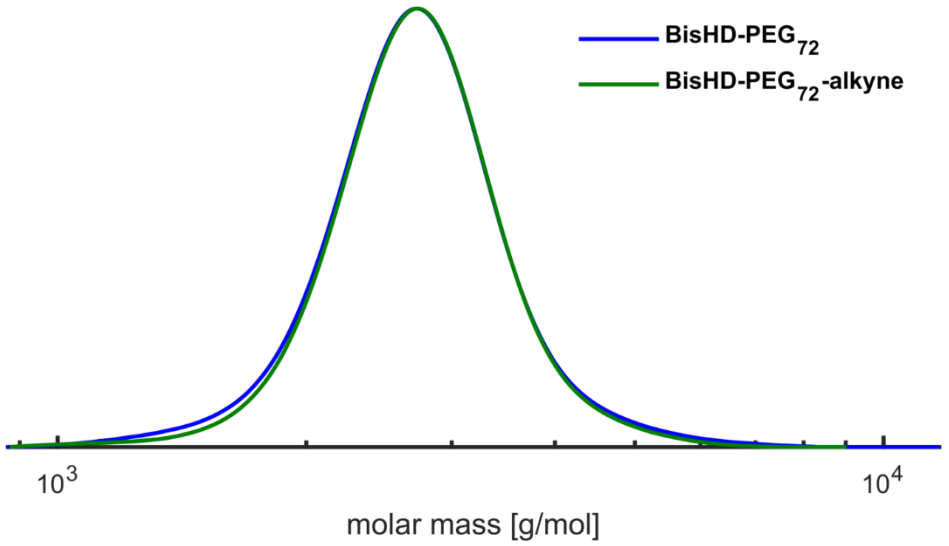

SI-Figure 20: SEC traces (RI detector, DMF, PEG standards) of the BisHD-PEG polymer before (blue) and after (green) post-modification with propargyl bromide.

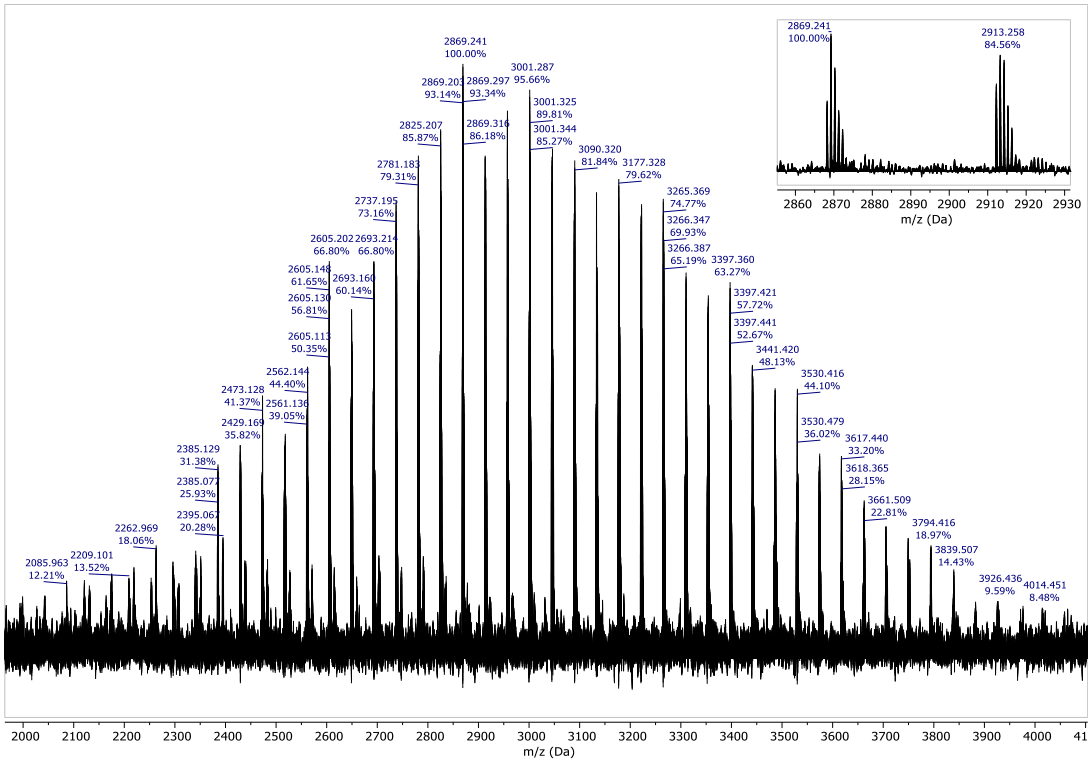

SI-Figure 21: MALDI-ToF MS spectrum of BisHD-PEG (left) and the zoom-in spectrum (right).

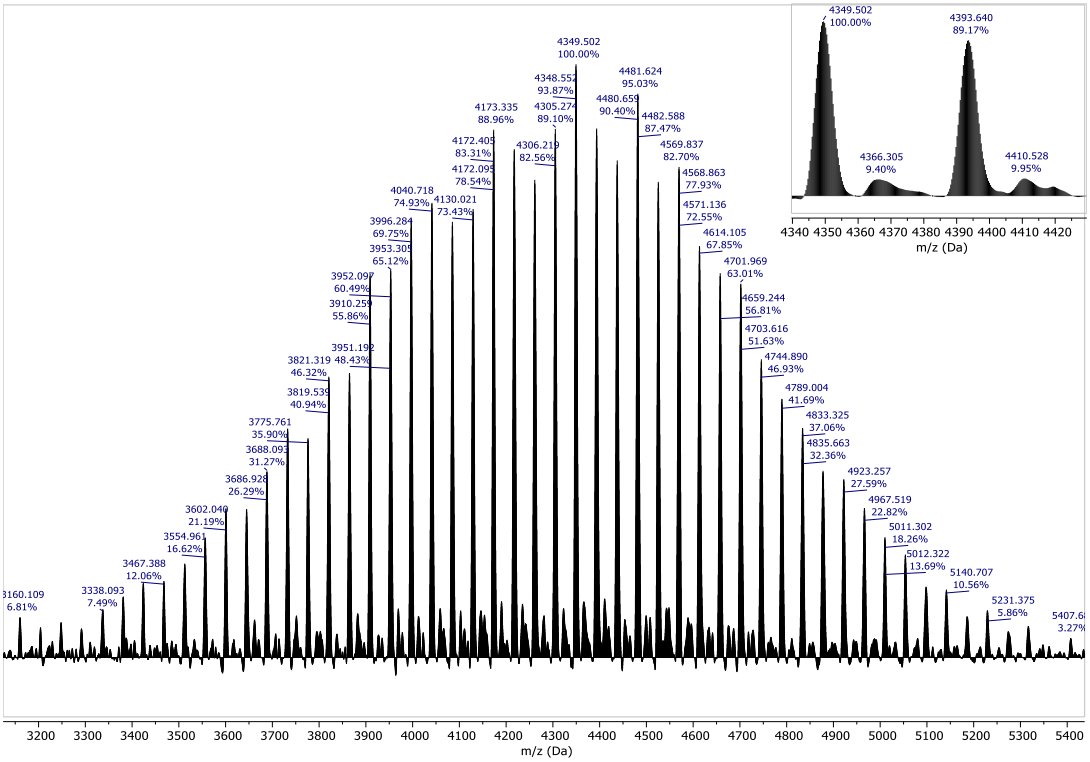

SI-Figure 22: MALDI-ToF MS spectrum of BisHD-MBE-PEG (left) and the zoom-in spectrum (right).

2.2.6.2 Dynamic light scattering

SI-Table 1: DLS measurement data.

Incubation	pH	Composition	Size	PDI
0 h		BisHD-PEG	135.6±9.31 nm	0.165±0.027
		BisHD-*iso*MBE-PEG	156.4±6.40 nm	0.210±0.019
8 h	5.4	BisHD-PEG	130.1±11.07 nm	0.125±0.027
		BisHD-*iso*MBE-PEG	153.3±8.19 nm	0.209±0.036
8 h	7.4	BisHD-PEG	140.2±8.43 nm	0.192±0.046
		BisHD-*iso*MBE-PEG	159.0±8.13 nm	0.245±0.019

3 Hyperbranched Polyether Lipids for Liposomal Application

3.1 ^{18}F-labeled, PSMA-specific liposomes: promising and PET-traceable tool for future targeted drug delivery in the treatment of prostate cancer

Eyleen Becker,[†] [redacted],[§] [redacted],[§] [redacted],[*,†] [redacted]*,[§]

[†]Department of Chemistry, Johannes Gutenberg University Mainz, Duesbergweg 10-14, 55128 Mainz, Germany

[§]Department of Chemistry - TRIGA site, Johannes Gutenberg University Mainz, Fritz-Strassmann-Weg 2, 55128 Mainz, Germany

*E-Mail: [redacted], [redacted]

to be submitted

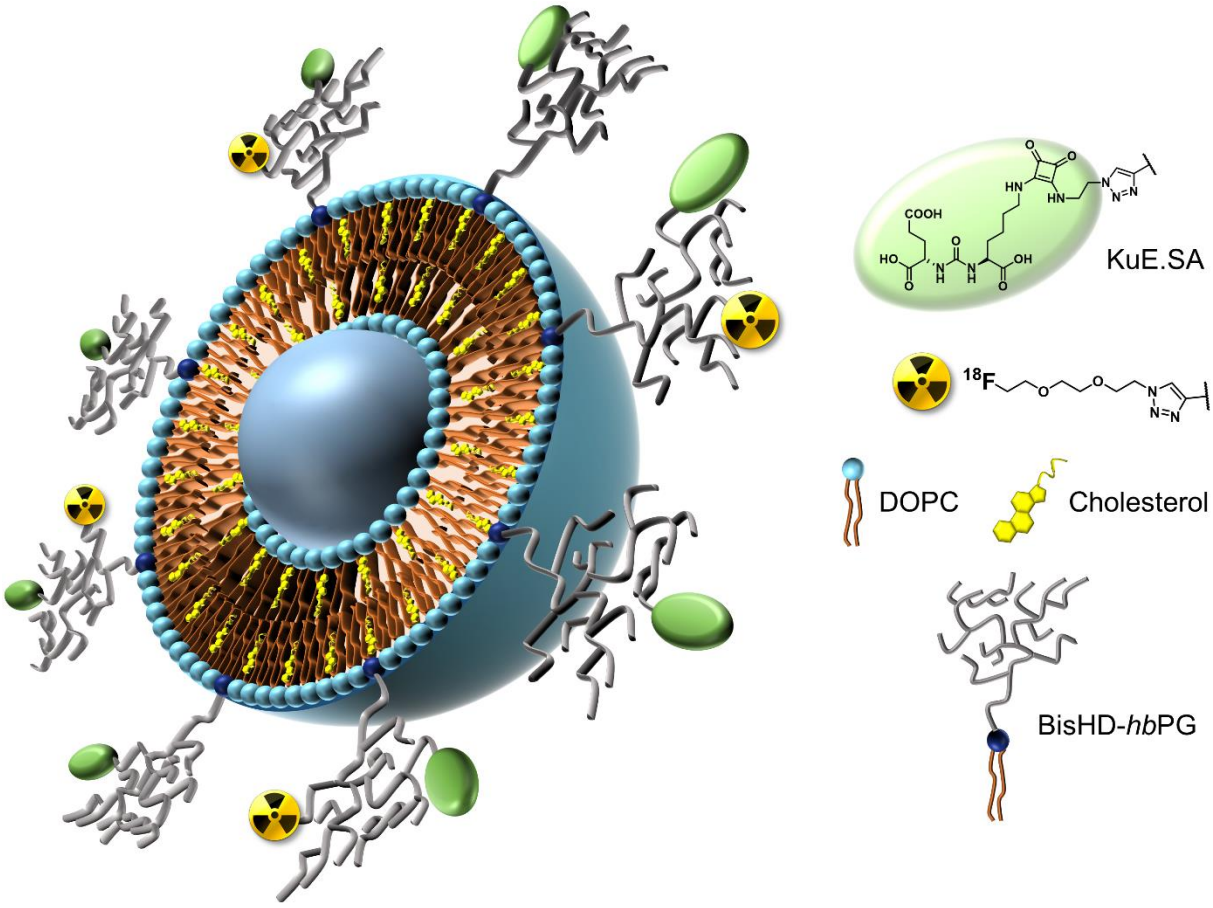

Abstract

Inhibitors of the prostate-specific membrane antigen (PSMA) belong to one of the most important substance classes in nuclear medicine. L-lysine-urea-L-glutamate (KuE) represents a key motif in recent diagnostics and therapeutic radiopharmaceuticals targeting the PSMA. Multifunctional polyether structures play a crucial role in shielding liposomes from degradation in the blood stream due to their stealth effect. In this work alkyne-functionalized hyperbranched polyglycerols (*hb*PG) with a long hydrophobic alkyl chain anchor (BisHD) were synthesized and consecutively modified with an azide-bearing, squaramide coupled PSMA inhibitor (KuE.SA.Azide) *via* Cu(I)-catalyzed alkyne-azide cycloaddition (CuAAC). Subsequent radiolabeling *via* similar reaction of [^{18}F]F-TEG-Azide with residual alkyne-groups followed by liposomal preparation led to a promising system for future targeted drug delivery in the treatment of prostate cancer that can be pre-evaluated *in vitro* and *in vivo via* positron emission tomography (PET).

3.1.1 Introduction

Among men, prostate cancer is the most common cancer in industrialized countries and the fifth leading cause of cancer death worldwide.[1,2] However, with early detection, there are good treatment options leading to a five-year survival rate of more than 90 %.[2,3] The prostate specific membrane antigen (PSMA) is associated with the diagnosis of prostate cancer. This membrane-bound glycoprotein belongs to the group of carboxypeptidases, which cleaves off C-terminal glutamate and for example catalyzes the hydrolysis of *N*-acetylaspartylglutamate to *N*-acetylaspartate. It is rarely found in healthy tissues but shows overexpression in prostate cancer cells.[4,5] For this reason, a variety of radiopharmaceutical drugs based on longer peptides, antibodies and small molecules targeting PSMA have been used for the diagnosis and treatment of prostate cancer.[6,7] These compounds have similar structures to *N*-acetylaspartyl glutamate with a C-terminal glutamate to address the glutamate recognition domain of PSMA.[8] Furthermore, the glutamate moiety must be attached to another non-cleavable group to prevent cleavage by PSMA *in vivo*. The presence of an aromatic moiety in the linker region significantly improves the affinity of the radiopharmaceutical by addressing an aromatic binding moiety in the binding pocket of the PSMA.[9] A variety of PSMA inhibitors are urea-based, such as the most important PSMA radiopharmaceuticals PSMA-11 and PSMA-617.[8,10,11] The lead structure of these molecules is a L-lysine-urea-L-glutamate (KuE) motif that resembles the structure of *N*-acetylaspartyl glutamate and is not cleavable by PSMA.

The use of squaric acid diethyl ester (3,4-Diethoxycyclobut-3-ene-1,2-dione; SADE) as coupling reagent provides a unique strategy for conjugation of target vectors, linker units and other molecules. It is already widely used in the coupling of biomolecules for preparation of e.g. carbohydrate- or protein-polymer-conjugates.[12]

The application of SADE simplifies the synthetic process. For example, no protective groups or further coupling reagents are required. There are also no by-products that need to be removed.

The two ester groups react selectively with amines under mild conditions.[13] The amidation can be carried out asymmetrically *via* pH control, since formation of the monoamide in the first step leads to reduced reactivity. By increasing the pH value, deprotonation occurs,

whereby the aromatic stabilization of the monoamide is lost and the second amidation can take place.[14–16] This prevents dimerization and enables asymmetric amidation with high selectivity and high yields.

Squaric acid shows a high acidity (pK_{a1} = 0.5-1.2; pK_{a2} = 2.2-3.5) and due to Hückel rule ([4n + 2] π-electrons, n = 0) for aromatic systems, it represents an aromatic unit.[17,18] In PSMA-specific radiopharamceuticals, squaric acid thus provides a moiety that interacts with the aromatic binding site in the binding pocket leading to increased affinity.[19,20]

The problem with small molecules, however, is their rapid excretion by the kidney and the associated short retention in the blood. In order to increase the circulation time, a variety of approaches have been pursued in recent decades.[21-22] One possible approach is to use drug delivery systems such as liposomes.[23,24] Liposomes are vesicular structures that mimic a biomembrane. They typically consist of amphiphilic phospholipids and are often additionally stabilized using cholesterol. The problem with these systems is that they are easily recognized by macrophages of the mononuclear phagocyte system (MPS) due to their size, which leads to increased uptake in the liver and spleen.[23,25-26] To increase the circulation time in the blood, the stealth effect of PEGylated systems is used. Polyethylene glycol chains are attached to the surface of the liposomes to shield them from macrophages.[27,28] PEG has been the "gold standard" for creating stealth liposomes for years.[29] In recent years, however, antibody-mediated immune responses have been increasingly observed.[30] In addition, functional groups for further functionalization are missing because methoxy PEG (mPEG) is commonly used. A promising alternative is the highly biocompatible and water-soluble hyperbranched polyglycerol (*hb*PG).[31] Hyperbranched polyglycerol has a large number of hydroxyl groups, which allows functionalization with targeting vectors, radiolabels or targeting ligands for direct drug delivery.[32] Wagener *et al.* investigated and compared liposome shielding *in vivo via* PET using ^{18}F-labeled, linear and hyperbranched polyether lipids. They observed comparably high stability and prolonged blood circulation of all investigated structures with differences in spleen accumulation mainly due to the different liposomal sizes.[33] Furthermore, very recently, they analogously prepared and investigated either fluorescence- or radiolabeled liposomes being functionalized with trimannose moieties for active targeting of dendritic

cells (DCs). Compared to non-functionalized liposomes, the trimannosylated analogues provided significantly increased uptake in the spleen and liver, presumably due to the presence of DCs.[34] Hofmann *et al.* introduced different strategies to synthesize a variety of linear-hyperbranched polyether lipids. For this purpose, cholesterol or dialkyl-based anchors with different chain length are directly used as initiators in an anionic ring opening polymerization (AROP) of various epoxide monomers. This procedure enables a variety of polyether architectures with an adjustable number of hydroxyl groups.[35] Furthermore, a study showed the stability of liposomes depending on the used anchor structure. Anchor structures with an alkyl chain between 18-20 methylene units showed an inherently higher stability of the liposomal membrane compared to cholesterol.[36]

The cyclotron-produced positron emitter fluorine-18 provides several advantageous properties for radiolabeling and *in vivo* evaluation of liposomal structures *via* PET. Although it belongs to the shorter-lived radionuclides, its half-life of 109.7 min is longer than that of many other commonly used PET-isotopes (such as ^{68}Ga, ^{11}C, ^{13}N, ^{15}O) allowing for more time-consuming synthesis and making it suitable not only for imaging of small molecules but also larger systems with prolonged circulation such as peptides, polymers and liposomes.[37,38] Furthermore, the almost exclusive β^+-decay (96.9 %) of fluorine-18 produces low energy positrons ($E_{\beta+,max}$ = 635 keV) ensuring a high spatial PET-resolution.[39] In contrast to radiometals, fluorine-18 is typically covalently bound to the respective molecule. Therefore, utilization of larger chelating structures that may impair liposome preparation or affect the shielding properties of the liposomal surface, is not required. Application of a structurally compliant, ^{18}F-labeled synthon such as the frequently used 1-Azido-2-(2-(2-[^{18}F]fluoroethoxy)ethoxy)ethane ([^{18}F]F-TEG-N_3) enables indirect radiolabeling of the hyperbranched polyether construct without significantly affecting its chemical and biological properties.[33,34,40,41]

In the present study the initial steps included synthesis of both an alkyne-functionalized hyperbranched polyglycerol with a long hydrophobic alkyl chain anchor and an azide-bearing squaramide coupled KuE-derivative. In the next step the corresponding KuE-functionalized polyether lipid was formed *via* CuAAC. Subsequently, the previously synthesized precursor 2-(2-(2-Azidoethoxy)ethoxy)ethyl-*p*-toluenesulfonate (Ts-TEG-N_3)

was ^{18}F-labeled using a custom-built semiautomatic modular system. A second copper(I)-catalyzed click-reaction between the resulting [^{18}F]F-TEG-N_3 and residual alkyne groups of the polyether led to the desired radiolabeled lipid. In the final step, the corresponding liposomes were prepared *via* thin film hydration method using DOPC and cholesterol as additives and liposomal size was adjusted by repeated extrusion. SEC purification finally resulted in ^{18}F-labeled, KuE-functionalized, *hb*PG-shielded liposomes representing a promising system for future drug delivery in the treatment of prostate cancer that can be traced and pre-evaluated *in vivo via* PET.

3.1.1.1 Experimental part

Terminology

The amphiphilic block copolymer based on the hydrophobic initiator 1,2-bis-*n*-hexadecyl glyceryl ether (BisHD-OH) and the monomer ethoxyethyl glycidyl ether (EEGE) to synthesize the protected macroinitiator is named BisHD-P(EEGE). After cleavage of the acetal protecting groups the resulting linear poly(glycerol) (*lin*PG) is named BisHD-*lin*PG. After the slow monomer addition (SMA) with the monomer glycidol the resulting hyperbranched polyglycerol (*hb*PG) polymer is named BisHD-*hb*PG. The precursor 2-(2-(2-Azidoethoxy)ethoxy)ethyl-*p*-toluenesulfonate is named Ts-TEG-N_3 and the ^{18}F-labeled click-synthon 1-Azido-2-(2-(2-[^{18}F]fluoroethoxy)ethoxy)ethane is named [^{18}F]F-TEG-N_3. The PSMA-inhibitor 2-(3-(5-Amino-1-carboxy-pentyl)ureido)pentanedioic acid (L-lysine-urea-L-glutamate) is named KuE.SA. The KuE.SA-functionalized BisHD-*hb*PG is named BisHD-*hb*PG-KuE.SA.

Instrumentation and Materials

^{1}H NMR (300 MHz), ^{13}C NMR (75 MHz) and 2D spectra were recorded on a Bruker Avance III HD 300 (5 mm BBFO-Probe with z-Gradient and ATM). ^{1}H NMR (400 MHz), ^{13}C NMR (100 MHz) and 2D spectra were measured on a Bruker Avance II 400 MHz (5 mm BBFO-Probe Z-gradient and ATM, SampleXPress 60 auto sampler). ^{1}H NMR (600 MHz), ^{13}C NMR (151 MHz) and 2D spectra were measured on a Bruker Avance III 600 MHz (5 mm TCI-CryoProbe Z-gradient and ATM, SampleXPress lite 16 sampler).The chemical shifts were

internally referred to residual proton signals of the deuterated solvent. The NMR spectra were analyzed *via* MestReNova v11.0 software.

Mass spectrometry was measured *via* Agilent Technologies 1220 Infinity LC system coupled to an Agilent Technologies 6130 Single Quadrupole LC/MS system. HPLC purification and analysis was performed using a Merck LaChrom system with Hitachi L7100 pump and L7400 UV-detector and the respectively mentioned column and conditions. Spin Filtration was carried out using Pall Microsep Advance centrifugal filters (MWCO = 1000 g/mol).

Size exclusion chromatography (SEC) for the synthesized polymers was performed at 50 °C in *N,N*-dimethylformamide (with 1 g/L lithium bromide added) as eluent on an Agilent 1,100 Series equipped with Polymer Standards Service (PSS) HEMA columns with 300/100/40 Å porosity and a RI detector. The determination of the molecular weights was determined by a calibration with poly(ethylene glycol) standards by PSS.

During radiosynthesis, activity of the samples was measured using a PC-based dose calibrator (ISOMED 2010, Nuklear Medizintechnik Dresden GmbH). Radio thin layer chromatography (radio-TLC) was performed using Merck Silica 60 F_{254} TLC plates; and ethylacetate:hexane (1:1) as mobile phase. Radio-TLC results were analyzed *via* image plate scanner (CR35-Bio, Elysia Raytest) and AIDA Image Analysis software (Elysia Raytest).

Dynamic light scattering (DLS) was measured using a Malvern Zetasizer Nano ZS. The cell holder was equipped with a Peltier-controlled thermostat. The samples were prepared with a concentration of 1 µL per 1 mL of PBS buffer solution from Sigma Aldrich (dilution 1:1000) and measured at a laser wavelength of 633 nm and a scattering angle of 173°. All samples were measured at a constant temperature of 25 °C. Measurements were performed in disposable polystyrene cuvettes from the company Brand. The analysis was carried out using Malvern Zetasizer Software 7.11 from Macromedia.

All solvents and reagents were purchased generally from the suppliers Acros Organics, Tokyo Chemical Industry (TCI), Sigma-Aldrich, Fluka, Fisher Scientific, Alfa Aesar, IRIS Biotech and VWR and were used as received unless otherwise stated. Deuterated solvents were purchased from Deutero GmbH. Dialysis membranes (regenerated cellulose, MWCO = 500 g/mol and MWCO = 1000 g/mol) were purchased from Orange Scientific.

EEGE was synthesized according to literature.[42] Glycidol was stirred over CaH_2 and freshly distilled before use. Dry *N*-methylpyrrolidone (NMP) was stored over molecular sieve before use.

Aqueous [^{18}F]fluoride was produced *via* proton-irradiation of enriched [^{18}O]H_2O using a PETtrace 700S cyclotron (GE Healthcare).

Synthesis procedure

Synthesis of the hydrophobic alkyl chain anchor (BisHD-OH)

BisHD-OH was synthesized as described in literature.[43] More details are in the Supporting Information (**SI-Scheme 1**, **SI-Figure 1**).

Synthesis of BisHD-linPG macroinitiator

The synthesis was carried out according to literature.[44]

The synthesis is described for BisHD-*lin*PG_{22} as a representative example.

1,2-bis-*n*-hexadecyl glyceryl ether (BisHD-OH) (2.00 g, 3.70 mmol, 1 eq.) and CsOH mono hydrate (0.56 mg, 3.33 mmol, 0.9 eq.) was placed in a dry Schlenk flask and dissolved in benzene (10 mL). The solution was stirred at 60 °C for at least 30 min and dried in vacuo overnight to remove moisture. Dry Dioxan (50 mL) was added and after 20 min EEGE (11.89 g, 81.34 mmol, 12.01 mL, 22 eq.) *via* syringe. The solution was stirred at 80 °C for 6 d. The solvent was removed in vacuo. The polymer was dissolved again in methanol (50 mL) and 4 g of an acidic ion exchange resin (Dowex 50WX8) was added to the polymer solution to cleave the acetal protecting groups of BisHD-P(EEGE). The solution was stirred and heated to 50 °C overnight. Afterwards, the resin was removed by filtration and the solvent was removed partly in vacuo. The crude polymer was precipitated twice in cold diethyl ether. The resulting block copolymer was dried in vacuo. The polymer was isolated as a brownish resin in a yield of 90 %.

^{1}H NMR (400 MHz, DMSO-d_6) δ [ppm] = 4.78 – 4.25 (m, 15H, OH), 3.67 – 3.13 (m, 123H, CH_2-O and CH_2-CH-O), 1.48 – 1.43 (m, 4H, CH_2-CH_2-O), 1.35 – 1.05 (m, 52H, CH_2), 0.85 (t, J = 6.8 Hz, 6H, CH_3-CH_2).

Synthesis of BisHD-hbPG

The synthesis was carried out according to literature.[44]

Hypergrafting of glycidol is described for the macroinitiator BisHD-*lin*PG_{22} as a representative example.

The macroinitiator BisHD-*lin*PG_{22} (0.20 g, 0.10 mmol, 1 eq.) was placed in a Schlenk flask, dissolved in benzene (3 mL) and dried in vacuo overnight. BisHD-*lin*PG_{22} was again dissolved in benzene (2 mL) and CsOH mono hydrate (33.58 mg, 0.20 mmol, 2 eq., equates to a degree of deprotonation of 10% of hydroxyl groups) was added. The solution was stirred at 60 °C for at least 1 hour and dried in vacuo overnight to remove moisture. The macroinitiator was dissolved in *N*-methylpyrrolidone (NMP) (1 mL) and a solution of glycidol (0.59 mg, 7.90 mmol, 0.51 mL, 40 eq.) (5 %) in NMP was added to the initiator solution over a time period of 16 h (0.5 mL/h) at 100 °C. The solution was stirred for additional 2 h to ensure complete conversion of glycidol. Subsequently, the solvent was removed under reduced pressure and the crude product was dialyzed for 16 h against methanol (MWCO = 1000 g/mol). The solvent was removed under reduced pressure and the product was dried in vacuo. The polymer was isolated in a yield of 60 %.

^{1}H NMR (400 MHz, pyridine-d_5) δ [ppm] = 6.58 – 5.80 (m, 74H, OH), 4.44 – 3.45 (m, 380H, CH_2-O and CH_2-CH-O), 1.73 – 1.60 (s, 4H, CH_2-CH_2-O), 1.44 – 1.20 (m, 52H, CH_2), 0.88 (t, J = 6.5 Hz, 6H, CH_3-CH_2).

Functionalization of BisHD-hbPG with propargyl bromide

The functionalization is described for BisHD-*hb*PG_{74} as representative example.

BisHD-*hb*PG_{74} (0.70 g, 0.12 mmol, 1 eq.) was placed in a Schlenk flask and dissolved in dimethylformamide (DMF) (15 mL). The solution was cooled to 0 °C and sodium hydride (19.6 mg, 0.82 mmol, 7 eq.) was added. The solution was stirred for 1 h at 0 °C to ensure complete deprotonation. Subsequently, propargyl bromide (0.52 mL, 0.46 mmol, 4 eq.) (80 wt% in toluene) was added and the mixture was allowed to slowly reach room temperature. The solution was stirred at room temperature for 2 days. Afterwards, water (2 mL) was added and the solvent was removed under reduced pressure. The crude product

was dialyzed against methanol (MWCO = 500 g/mol) for 24 h. The solvent was removed under reduced pressure and the product was dried in vacuo overnight. The alkyne-functionalized polymer was isolated in a yield of 75 %.

^{1}H NMR (400 MHz, pyridine-d_5) δ [ppm] = 6.61 – 5.86 (s, 67H, OH), 4.73 – 4.49 (s, 4H, OCH_2-CCH), 4.46 – 3.48 (m, 383H, CH_2-O and CH_2-CH-O), 1.74 – 1.60 (m, 4H, CH_2-CH_2-O), 1.49 – 1.17 (s, 52H, CH_2), 0.88 (t, J = 6.8 Hz, 6H, CH_3-CH_2).

Synthesis of KuE.SA.N$_3$

Synthesis of the squaramide functionalized PSMA inhibitor KuE.SA was carried out according to the already published procedure.[20]

Synthesis of 2-(3-(5-Amino-1-carboxy-pentyl)ureido)pentanedioic acid (L-lysine-urea-L-glutamate (KuE)

H-Glu(*t*Bu)-O*t*Bu (0.9 g, 3 mmol) and DIPEA (2 mL, 12 mmol) were dissolved in dry dichloromethane (150 mL). The solution was cooled to 0 °C and triphosgene (300 mg, 1 mmol) was added over a period of 4 h. The solution was then stirred for 1 h at room temperature. The H-Lys(Boc)-2CT-polystyrene solid phase (0.78 mmol/g, 390 mg, 0.3 mmol) was added to the reaction solution and stirred for additional 16 h at room temperature. The solid phase was filtered and washed with dichloromethane. The product was cleaved from the solid phase with TFA (3 x 7 mL, 10 min, RT) and purified by semi-preparative HPLC (column: Phenomenex Luna C18 (250 x 10 mm) 10 µ, flow rate: 5 mL/min, H_2O/MeCN + 0.1 % TFA, 0-5 % MeCN in 20 min, t_R = 9.0 min). KuE was obtained as a colorless oil (67.9 mg, 0.21 mmol, 71 %).

^{1}H-NMR (300 MHz, D_2O) δ [ppm] = 4.22 (ddd, *J* = 12.4, 9.0, 5.0 Hz, 2H, HOOC-CH-NH-CO), 2.98 (t, *J* = 7.5 Hz, 2H, NH_2-CH_2), 2.50 (t, *J* = 7.3 Hz, 2H, HOOC-CH_2-CH_2), 2.16 (dtd, *J* = 14.9, 7.5, 5.1 Hz, 1H, HOOC-CH_2-CH_2), 2.00 – 1.76 (m, 2H, HOOC-CH_2-CH_2, NH_2-$(CH_2)_3$-CH_2), 1.76 – 1.60 (m, 3H, NH_2-CH_2-CH_2, NH_2-$(CH_2)_3$-CH_2), 1.55 – 1.22 (m, 2H, NH_2-$(CH_2)_2$-CH_2)).

MS (ESI$^+$): 320.1 $[M+H]^+$, calculated for $C_{12}H_{21}N_3O_7$: 319.14 $[M]^+$.

Synthesis of 2-(3-(1-Carboxy-5-((2-ethoxy-3,4-dioxocyclobut-1-en-1-yl)amino)-pentyl)ureido)-pentanedioic acid (KuE.SA)

KuE (10 mg, 31.3 µmol) was dissolved in 0.5 M phosphate buffer (pH 7; 250 µL). To this solution 3,4-diethoxycyclobut-3-ene-1,2-dione (5.3 mg, 4.6 µL, 31.3 µmol) was added. The pH was adjusted to pH 7 using 1 M NaOH. The solution was shaken for 16 h. The product KuE.SA was purified by semi-preparative HPLC (column: Phenomenex Luna C18 (250 x 10 mm) 10 µ, flow rate: 5 mL/min, H_2O/MeCN + 0.1 % TFA, 12-30 % MeCN in 20 min, t_R = 10.0 min) and obtained as a colorless solid (27.8 mg, 62.7 µmol, 23 %).

^{1}H-NMR (300 MHz, D_2O) δ [ppm] = 4.75 – 4.65 (m, 2H, HOOC-C*H*-NH-CO), 4.30 – 4.12 (m, 2H, O-CH_2-CH_3), 3.59 (dt, *J* = 23.5 Hz, 6.6 Hz, 1H, NH-CH_2), 3.48 (t, *J* = 6.6 Hz, 1H, NH-CH_2) 2.49 (t, *J* = 7.3 Hz, 2H, HOOC-CH_2-CH_2), 2.16 (dtd, *J* = 15.3 Hz, 7.4 Hz, 5.2 Hz,1H, HOOC-CH_2-CH_2), 2.04 – 1.90 (m, 1H, HOOC-CH_2-CH_2) 1.86 – 1.75 (m, 2H, NH-$(CH_2)_3$-CH_2), 1.73 – 1.46 (m, 2H, NH-CH_2-CH_2), 1.41 (dt, *J* = 7.1 Hz, 3.6 Hz, 5H, NH-$(CH_2)_2$-CH_2, O-CH_2-CH_3).

^{13}C-NMR (300 MHz, D_2O) δ [ppm] = 188.86 (NH-C-*C*O), 182.94 (O-C-*C*O), 177.13 (HOO*C*-CH-$(CH_2)_2$-COOH), 176.95 (HOO*C*-CH_2-CH_2), 176.05 (NH-C=*C*-O), 173.15 (NH-*C*=C-O), 159.08 (NH-*C*O-NH), 70.41 (O-*C*H_3-CH_2), 52.91 (HOOC-*C*H-NH (Lys)), 52.48 (HOOC-*C*H-NH (Glu)), 44.03 ((NH-CH_2-*C*H_2)), 30.26 (NH-*C*H_2), 29.91 (HOOC-*C*H_2-CH_2), 28.86 (NH-$(CH_2)_3$-*C*H_2), 26.15 (HOOC-CH_2-*C*H_2), 21.59 (NH-$(CH_2)_2$-*C*H_2), 14.95 (O-CH_3-*C*H_2).

MS (ESI^+): 444.2 $[M+H]^+$, calculated for $C_{18}H_{25}N_3O_{10}$: 443.15 $[M]^+$.

Synthesis of 2-Azidoethylamine

2-Bromoethylamine hydrobromide (1 g, 4.9 mmol) and sodium azide (952 mg, 14.6 mmol) were dissolved in water (15 mL) and stirred overnight at 75 °C. The reaction mixture was cooled to 0 °C and potassium hydroxide (1.2 g, 21.4 mmol) was added. The product was extracted from the aqueous solution with diethyl ether (3 x 20 mL). The organic layer was evaporated under reduced pressure and 2-Azidoethylamine was obtained as colorless oil (372 mg, 4.3 mmol, 87 %).

^{1}H-NMR (300 MHz, chloroform-*d*$_3$) δ [ppm] = 3.37 (t, *J* = 5.7 Hz, 2H, C*H*$_2$-NH$_2$), 2.92 – 2.84 (m, 2H, N$_3$-C*H*$_2$), 1.42 (s, 2H, -N*H*$_2$).

^{13}C-NMR (300 MHz, chloroform-*d*$_3$) δ [ppm] = 54.50 (*C*H$_2$-N$_3$), 41.47 (*C*H$_2$-NH$_2$).

MS (ESI$^+$): 87.1 [M+H]$^+$ calculated for $C_2H_6N_4$: 86.06 [M]$^+$.

Synthesis of 2-(3-(5-((2-((2-azidoethyl)amino)-3,4-dioxocyclobut-1-en-1-yl)amino)-1-carboxypentyl)ureido)-pentanedioic acid (KuE.SA.N$_3$)

2-Azidoethylamine (40 mg, 0.46 µmol) and KuE.SA (6 mg, 13.5 µmol) were dissolved in 0.5 M phosphate buffer (pH 9, 300 µL) and the pH was readjusted to pH 9 with 1 M NaOH solution. The reaction mixture was shaken overnight and the product (6 mg, 12.4 µmol, 92 %) was obtained as a colorless oil after semi-preparative HPLC purification (column: Phenomenex Luna C18 (250 x 10 mm) 10 µ, flow rate: 5 mL/min, H$_2$O/MeCN + 0.1 % TFA, 10-40 % MeCN in 20 min, t_R = 8.2 min).

^{1}H-NMR (400 MHz, D$_2$O) δ [ppm] = 4.25 (dd, *J* = 9.1, 5.1 Hz, 1H, HOOC-C*H*-Glu), 4.19 (dd, *J* = 8.8, 4.9 Hz, 1H, HOOC-C*H*-Lys), 3.55 – 3.49 (m, 2H, NH-C*H*$_2$-CH$_2$-N$_3$), 3.17 (t, *J* = 5.5 Hz, 1H, C*H*$_2$-N$_3$), 2.50 (t, *J* = 7.3 Hz, 2H, HOOC-C*H*$_2$), 2.17 (dq, *J* = 12.5 Hz, 7.3 Hz, 1H, NH-CH$_2$-C*H*$_2$), 2.00 – 1.89 (m, 1H, NH-C*H*$_2$-CH$_2$), 1.85 (p, *J* = 7.9 Hz, 7.2 Hz, 1H, HOOC-CH$_2$-C*H*$_2$), 1.73 (dt, *J* = 13.7 Hz, 6.9 Hz, 1H, HOOC-CH$_2$-C*H*$_2$), 1.64 (p, *J* = 7.3 Hz, 6.4 Hz, 2H, NH-(CH$_2$)$_3$-C*H*$_2$), 1.45 (q, *J* = 8.4 Hz, 2H, NH-(CH$_2$)$_2$-C*H*$_2$).

^{13}C-NMR (400 MHz, D$_2$O) δ [ppm] = 177.26 (SA.*C*=O), 176.86 (HOO*C*-CH$_2$-CH$_2$), 176.10 (2C, HOO*C*-CH), 159.15 (NH-*C*O-NH), 117.66 (, NH-C-*C*-NH), 114,80 (NH-*C*-C-NH), 53.06 (HOOC-*C*H-Lys), 52.47 (HOOC-*C*H-Glu), 51.45 (*C*H$_2$-N$_3$), 43.50 (NH-*C*H$_2$-CH$_2$-N$_3$), 30.37 (NH-(CH$_2$)$_3$-*C*H$_2$), 29.87 (HOOC-*C*H$_2$), 29.36 (NH-CH$_2$-*C*H$_2$), 26.07 (HOOC-CH$_2$-*C*H$_2$), 21.62 (NH-(CH$_2$)$_2$-*C*H$_2$).

MS (ESI$^+$): 484.4 [M+H]$^+$, 506.2 [M+Na]$^+$, calculated for $C_{18}H_{25}N_7O_9$: 483.17 [M]$^+$.

Synthesis of the KuE.SA.triazolyl-BisHD-hbPG

KuE.SA-functionalization of BisHD-*hb*PG *via* CuAAC was performed according to a modified protocol by Yamamoto *et al.*[45] The synthesis is described for KuE.SA-triazolyl-BisHD-*hb*PG$_{74}$ as representative example.

Alkyne-BisHD-*hb*PG$_{74}$ (23 mg, 3.8 µmol, ca. 7 alkyne-groups per polymer) was dissolved in PBS (1 mL). KuE.SA.N$_3$ (4.6 mg, 9.5 µmol) in PBS (1 mL), DMSO (36 µL), *N,N,N′,N″,N‴*-pentamethyldiethylenetriamine and PMDETA (1 µL, 3.8 µmol) were added. The mixture was heated to 45 °C and CuBr (5.4 µL of a 1 mg/mL solution in DMSO; 5.4 µg, 0.038 µmol) was added and stirred at 45 °C and under argon atmosphere for 16 h. Purification was carried out by spin filtration. The solution was transferred into a centrifuge tube (Pall Microsep Advance 1K) and centrifuged for 30 min (4696 *g*). The concentrate was dissolved in water (1 mL) and centrifuged again for 15 min (4696 *g*). This washing step was repeated 7 times. In the last step the concentrate was centrifuged (4696 *g*) for 1 h. Lyophilisation gave the product as brownish solid (24.2 mg).

Synthesis of the precursor 2-(2-(2-Azidoethoxy)ethoxy)ethyl-p-toluenesulfonate (Ts-TEG-N$_3$)

Ts-TEG-N$_3$ was synthesized as described in literature.[40]

Radiosynthesis of 1-Azido-2-(2-(2-[^{18}F]fluoroethoxy)ethoxy)ethane ([^{18}F]F-TEG-N$_3$)

Radiolabeling of the precursor Ts-TEG-N$_3$ and subsequent purification to produce [^{18}F]F-TEG-N$_3$ was performed *via* semiautomatic custom modular system using cyclotron-produced [^{18}F]fluoride according to the procedure already reported in literature.[40]

[^{18}F]fluoride was first trapped on a preconditioned (10 mL 1 M K_2CO_3 solution, 10 mL Milli-Q water, 20 mL air) Sep-Pak QMA light cartridge (Waters) and subsequently eluted into a reaction vial using a mixture of 1 M K_2CO_3 solution (15 µL, 15 µmol), Kryptofix® 222 (15 mg, 40 µmol) and acetonitrile (1 mL). Azeotropic removal of residual water was achieved *via* evaporation of the solvent under reduced pressure and helium flow at 80 °C. After cooling to 40 °C, a solution of Ts-TEG-N$_3$ (10.0 mg, 30.4 µmol) in acetonitrile (1 mL) was added and the reaction vial was heated to 90 °C for 10 min. After completion of the radiolabeling reaction, the mixture was cooled down again to 40 °C and MeCN/H_2O (1:1) (1 mL) was added. The resulting solution of crude compound was subsequently purified *via* semipreparative HPLC (column: Phenomenex Luna C18 semipreparative (250 x 10 mm) 10 µ, flow rate: 3 mL/min, MeCN/H_2O 1:1, t_R = 8.0 min). The collected product fraction was diluted by Milli-Q water (35 mL) and passed through a preconditioned (10 mL acetonitrile,

10 mL Milli-Q water, 20 mL air) Lichrolut EN cartridge (Merck). Subsequently, the cartridge was dried with a stream of helium and eluted with anhydrous diethylether (1.5 mL) into a vial equipped with a stirring bar and a septum. Evaporation of the solvent under reduced pressure and helium flow (10 mL/min) at 40 °C led to the product ([^{18}F]F-TEG-N_3) with a decay corrected radiochemical yield of 53 %.

Synthesis of ([^{18}F]F-TEG-triazolyl)(KuE-SA-triazolyl)-BisHD-hbPG

^{18}F-labeling of the KuE-SA-triazolyl-BisHD-*hb*PG *via* copper(I)-catalyzed azide-alkyne cycloaddition (CuAAC) was performed similarly to the method already published.[33] The synthesis is described for ([^{18}F]F-TEG-triazolyl)-(KuE-SA-triazolyl)-BisHD-*hb*PG_{63} as representative example.

In detail, a solution of KuE-SA-triazolyl-BisHD-*hb*PG_{63} (3.1 mg, 0.56 µmol) in 1 mL PBS was added to a vial containing a layer of [^{18}F]F-TEG-N_3 and a stirring bar. Successively, 12.5 µL DMSO, 15 µL 1 M $CuSO_4$ solution (15 µmol) and 25 µL 2.4 M sodium ascorbate in PBS (60 µmol) were added and the resulting mixture was heated to 70 °C for 15 min while stirring. Completion of the reaction was confirmed *via* radio-TLC (radiolabeled product: R_f = 0, [^{18}F]F-TEG-N_3: R_f = 0.8-0.9). Subsequently, the solution was passed through preconditioned (0.8 mL 1 M HCl, 5 mL H_2O, 0.8 mL 1 M NaOH, 5 mL H_2O, 10 mL air) Chelex 100 chelating resin (600 mg, Bio-Rad) to remove catalytic copper. The cartridge was flushed with 1.5 mL abs. ethanol and the eluate was combined with the first aqueous flow-through yielding a solution of purified, ^{18}F-labeled polyether lipid with a decay corrected radiochemical yield of 73 %.

Synthesis of ([^{18}F]F-TEG-triazolyl)-BisHD-hbPG

^{18}F-labeling of the non-KuE-functionalized, alkyne-bearing BisHD-*hb*PG (3.5 mg, 0.65 µmol) was accomplished *via* CuAAC analogously to the synthesis of ([^{18}F]F-TEG-triazolyl)(KuE-SA-triazolyl)-BisHD-*hb*PG resulting in a decay-corrected radiochemical yield of 81 %.

Liposome formation

^{18}F-labeled, KuE-functionalized liposomes were prepared *via* thin film hydration and automatic extrusion similar to the method already published in literature.[33,34]

1,2-dioleoyl-*sn*-glycero-3-phosphocholine (DOPC, 241 µL, 20 mg/mL in ethanol, 6.13 µmol, 55 mol%) and cholesterol (246 µL, 7 mg/mL in ethanol, 4.46 µmol, 40 mol%) were added to the obtained aqueous-ethanolic solution of the ^{18}F-labeled polyether lipid ([^{18}F]F-TEG-triazolyl)(KuE-SA-triazolyl)-BisHD-hbPG (0.56 µmol, 5 mol%). The solvents were removed under reduced pressure *via* rotary evaporator providing a thin oily layer. Addition of 0.8 mL PBS and subsequent ultrasonication for 10 min at 50 °C led to a turbid yellow suspension. To obtain uniform liposomes of small size, the suspension was extruded automatically through polycarbonate membranes of different pore sizes (400 nm, 100 nm and 50 nm, 21 times each) *via* custom-built extrusion device equipped with a LiposoFast extruder unit (AVESTIN Europe GmbH). In order to separate smaller components and structures, the resulting liposomes were finally purified *via* fractionated size exclusion chromatography (SEC) using Sephacryl S-400 HR resin (Cytiva, 4 mL in a 6 mL SPE tube) and PBS as mobile phase (0.5 mL per fraction). The radiolabeled KuE-functionalized liposomes eluted in fractions 3-5 as a slightly turbid suspension with a decay-corrected radiochemical yield of 25 %.

3.1.2 Results and discussion

3.1.2.1 Polymer synthesis and characterization

The amphiphilic block copolymer BisHD-*hb*PG was synthesized in a multi-step procedure.

Synthesis of the hydrophobic BisHD-OH anchor

The hydrophobic anchor structure BisHD-OH was synthesized as initiator for the anionic ring opening polymerization (AROP) of epoxides. The initiator was prepared in a straightforward two-step synthesis based on a procedure of Stauch *et al.*, performing a Williamson etherification and using 1-*O*-benzyl glycerol and hexadecyl bromide, followed by hydrogenation to remove the benzyl protecting group.[43] In the past, two other hydrophobic anchors 1,2-bis-*n*-icosanyl glyceryl ether (BisID-OH) with longer and 1,2-bis-*n*-octadecyl glyceryl ether (BisOD-OH) with shorter alkyl chain lengths of the anchor

structures were also used for the AROP.[44] In a study of Gleue *et al.*, the influence of the length of the amphiphilic anchors on the stability of the liposome membrane and the exchange between liposome membrane and cell membrane was investigated.[36] Due to the good stability of BisHD-OH, this anchor was used as an initiator for our structures.

Synthesis of BisHD-linPG macroinitiator

In the first reaction step a BisHD-P(EEGE) precursor polymer was synthesized *via* AROP with ethoxy ethyl glycidyl ether (EEGE). For the polymerization of EEGE the BisHD-OH was first deprotonated with cesium hydroxide monohydrate and dried in vacuo overnight to remove any moisture. Cesium hydroxide monohydrate was used as base for the deprotonation to ensure a good reactivity for the polymerization due to the formation of a dissociated ion pair.[46,47] The resulting initiator salt was dissolved in dioxane and the AROP of EEGE was performed under slightly reduced pressure and at elevated temperatures (80 °C) for 6 days. High temperatures were necessary to enable a polymerization clearly above the melting point of the initiator and to increase the overall reactivity. The polymerization of EEGE leads to linear structures (PEEGE) with acetal-protected hydroxyl groups, which can be released upon acidic treatment according to literature.[48] The resulting linear polyglycerol (BisHD-*lin*PG) structure exhibits numerous hydroxyl groups and can therefore be used as a macroinitiator to prepare the hyperbranched polyglycerol (*hb*PG) block (**Scheme 1**).

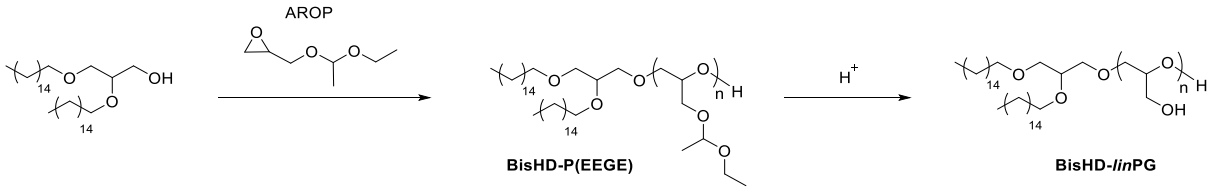

Scheme 1: Synthesis route for the macroinitiator BisHD-P(EEGE) and cleavage of the protecting acetal groups resulting in BisHD-*lin*PG.

Synthesis of BisHD-hbPG

BisHD-*lin*PG was used for "hypergrafting" of glycidol *via* slow monomer addition (SMA) technique to obtain the BisHD-*hb*PG polyether lipids. For the synthesis, the free hydroxyl groups of the BisHD-*lin*PG macroinitiator were deprotonated using cesium hydroxide monohydrate and dried overnight to remove any moisture. The initiator salt was dissolved

in *N*-methyl-2-pyrrolidone (NMP) to guarantee a good solubility of the macroinitiator and the resulting BisHD-*hb*PG. The monomer glycidol was added *via* SMA approach over a time period of 16 h to obtain well-defined BisHD-*hb*PG (**Scheme 2**).

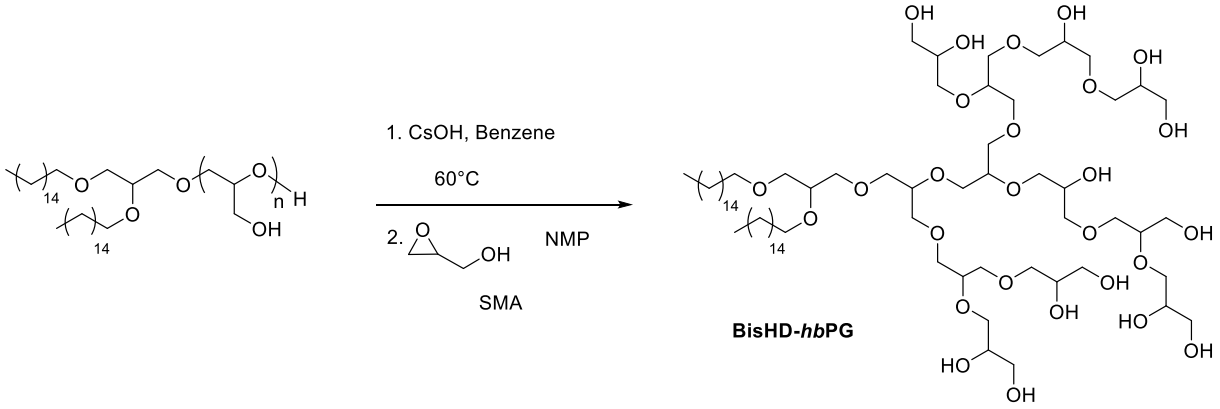

Scheme 2: Synthesis route for BisHD-*hb*PG *via* slow monomer addition (SMA) of glycidol.

The key characterization data of BisHD-P(EEGE), BisHD-*lin*PG and BisHD-*hb*PG are summarized in **Table 1**.

Table 1: Characterization data of the precursor BisHD-P(EEGE), the macroinitiator BisHD-*lin*PG and the block copolymer BisHD-*hb*PG.

Sample	M_n NMR a g·mol^{-1}	M_n SEC b g·mol^{-1}	$Đ$ b
BisHD-P(EEGE)$_{22}$	3750	2230	1.06
BisHD-*lin*PG$_{22}$	2170	1990	1.07
BisHD-*hb*PG$_{74}$	6010	3830	1.26

[a] Obtained from ^{1}H NMR spectroscopy. [b] Determined via SEC (RI, DMF, PEG standards).

AROP of BisHD and EEGE yielded the macroinitiator BisHD-P(EEGE), which was obtained with 22 EEGE units and a molecular weight (M_n) of 3750 g·mol^{-1} with a low dispersity ($Đ$=1.06). The BisHD-*lin*PG had a lower molecular weight of 2170 g·mol^{-1}, because of the acidic cleavage of the acetal groups. After the SMA with glycidol the BisHD-*hb*PG was obtained with 74 glycidol units and a molecular weight of 6010 g·mol^{-1}. The dispersity ($Đ$=1.26) is quiet good for this kind of "hypergrafting" reaction. The molecular weights determined *via* SEC are deviating from the results determined *via* ^{1}H NMR, due to the

applied PEG standards in the calibration and the varying hydrodynamic volume (V_h), especially for the BisHD-*hb*PG polymer compared to PEG.

An overlay of the monomodal SEC traces of the precursor BisHD-P(EEGE), the macroinitiator BisHD-*lin*PG and the amphiphilic block copolymer BisHD-*hb*PG is shown in **Figure 1**. An expected slight shift to a lower molecular weight is observed between the SEC trace before (blue) and after cleavage of the protecting groups (green). Furthermore, a shift to a higher molecular weight due to the changing V_h of the hyperbranched block copolymer can be observed (red).

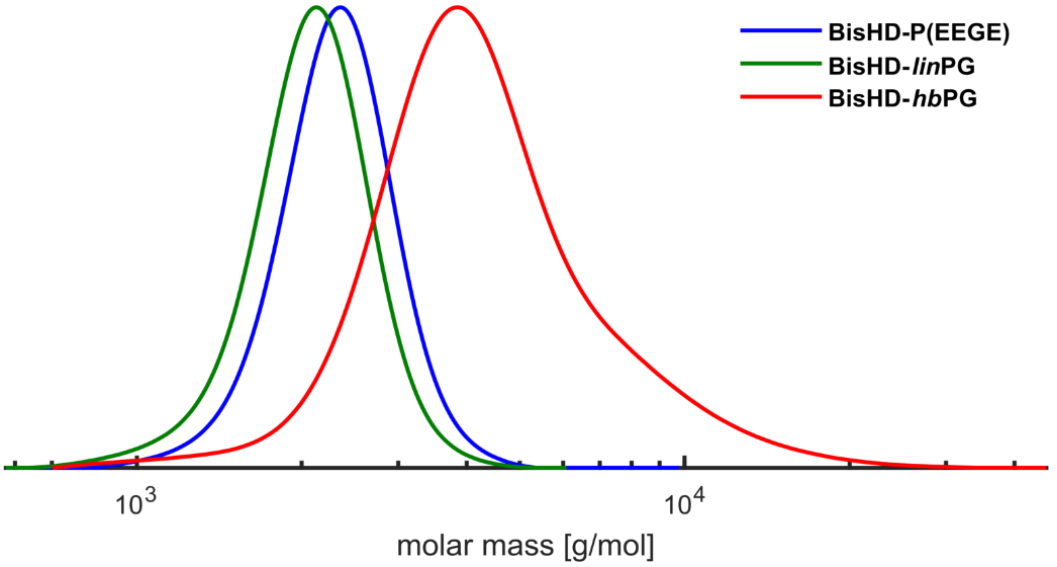

Figure 1: SEC traces (RI detector, DMF, PEG standards) of the precursor BisHD-P(EEGE), the macroinitiator BisHD-*lin*PG and the block copolymer BisHD-*hb*PG.

The ^{1}H NMR spectra of BisHD-P(EEGE) and the spectra of BisHD-*lin*PG after the deprotection are shown in **SI-Figure 2** and **SI-Figure 3**. The acetal protecting groups could be completely cleaved off. The ^{1}H NMR spectra of BisHD-*hb*PG$_{74}$ is shown in **Figure 2** with assigned signals.

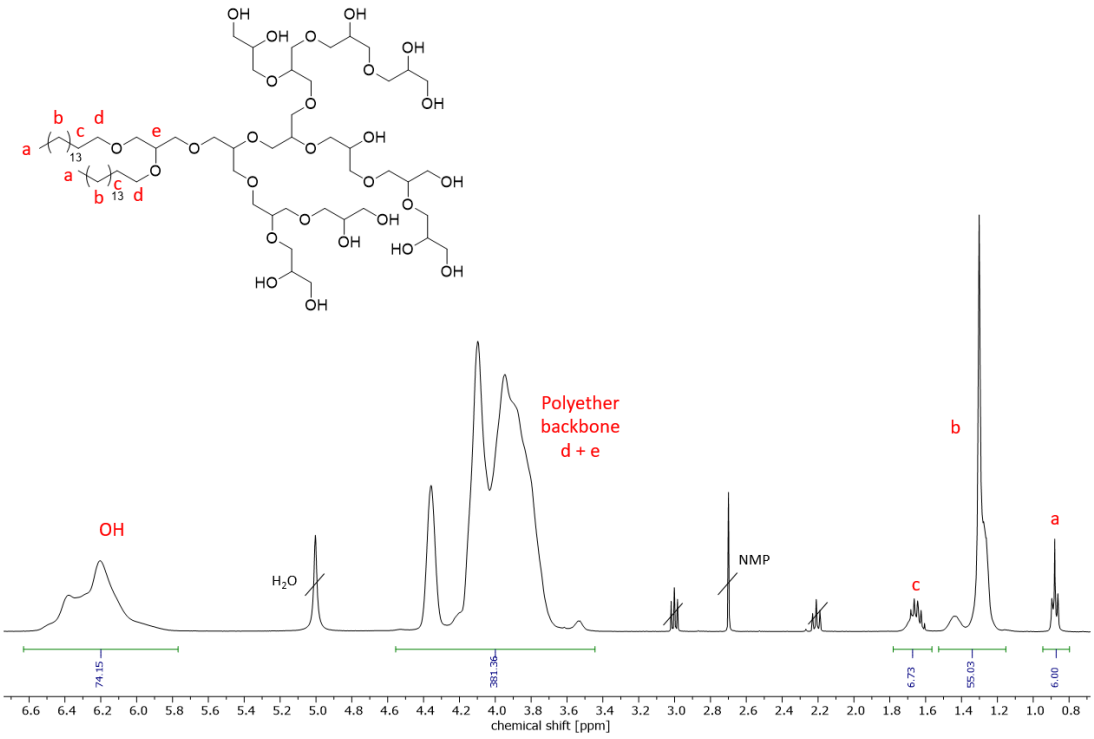

Figure 2: ^{1}H NMR spectrum (400 MHz, pyridine-d_5) of BisHD-*hb*PG$_{74}$ (entry 3, **Table 1**).

Post-polymerization modification

The amphiphilic BisHD-*hb*PG block copolymer was functionalized with propargyl bromide to attach alkyne-moieties. The alkyne-groups enables a copper(I)-catalyzed azide alkyne cycloaddition (CuAAC) with azide-bearing molecules. This reaction is known from literature and was adapted for the synthesized amphiphilic block copolymer.[40] For the functionalization, the hydroxyl groups of BisHD-*hb*PG were deprotonated using sodium hydride (NaH). The degree of functionalization was controlled *via* the amount of applied propargyl bromide. The successful functionalization was proven *via* NMR spectroscopy. The characteristic resonances for the propargyl group could be assigned *via* ^{1}H NMR spectrum (**Figure 3**) and ^{1}H, ^{13}C-HSQC NMR spectrum (**SI-Figure 6**). The number of alkyne groups cannot be accurately determined by integrating the signals in the ^{1}H NMR spectrum. The characteristic NMR signals of the alkyne group are strongly broadened in deuterated pyridine. However, from the decrease in the number of protons of the hydroxyl group from 74 to 67 protons, it can be concluded that an average of 7 alkyne groups per polymer are bound for further functionalization.

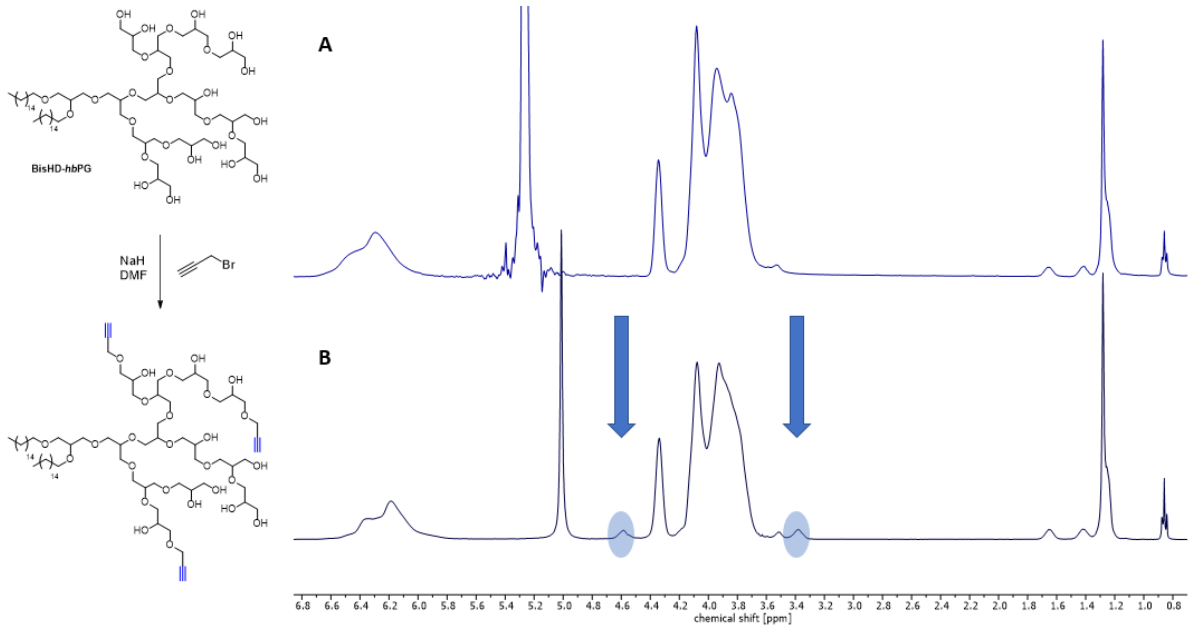

Figure 3: ^{1}H NMR spectra (400 MHz, pyridine-d_5) of BisHD-*hb*PG$_{74}$ (**A**, top) and BisHD-*hb*PG$_{74}$-alkyne (**B**, bottom). The appearing signals for the propargyl group are emphasized in blue.

In **Table 2** the characteristics of BisHD-*hb*PG before and after functionalization with propargyl bromide is summarized.

Table 2: Characterization data of the BisHD-*hb*PG and BisHD-*hb*PG-alkyne.

Sample	M_n NMR [a] g·mol^{-1}	M_n SEC [b] g·mol^{-1}	$Đ$ [b]	Alkyne moieties[b]
BisHD-*hb*PG$_{74}$	6010	3830	1.26	
BisHD-*hb*PG$_{74}$-alkyne	6500	4470	1.22	7

[a] Obtained from ^{1}H NMR spectroscopy. [b] Determined via SEC (RI, DMF, PEG standards).

SEC measurements reveal moderate size distribution for the functionalized BisHD-*hb*PG-alkyne polymer. Moreover, the successful attachment of alkyne-moieties to BisHD-*hb*PG is proven due to the shift of the SEC trace to lower elution volume translating to higher molecular weight (**Figure 4**). Polydispersity decreases minimally after functionalization due to purification by dialysis.

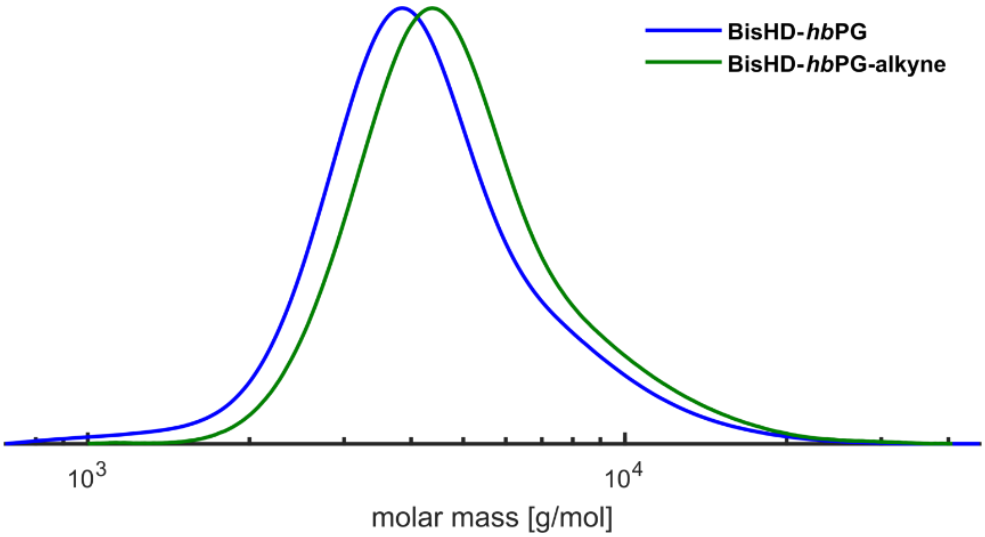

Figure 4: SEC traces (RI detector, DMF, PEG standards) of BisHD-*hb*PG before (blue) and after functionalization (green) with propargyl bromide.

3.1.2.2 Synthesis of the PSMA inhibitor and functionalization of the hyperbranched polyether lipid

Synthesis of the azide-functionalized PSMA inhibitor KuE.SA.N₃

Synthesis of the actual PSMA inhibitor L-lysine-urea-L-glutamate (KuE) was adopted from the procedure described by Greifenstein *et al.*[20] In the first step, slow addition of triphosgene to a cooled solution of twice *tert*-butyl protected L-glutamic acid and DIPEA led to the corresponding isocyanate, which was directly reacted with Nε-Boc-protected L-lysine bound to a chlorotrityl polystyrene resin (**Scheme 3**). Nucleophilic attack of the partially positively charged isocyanate-carbon by the α-nitrogen of lysine resulted in the solid phase-bound, urea coupled and protected amino acids. Simultaneous cleavage and deprotection using TFA followed by HPLC purification finally provided the desired product KuE with a yield of 71 %.

Subsequently, the squaric acid moiety was introduced using SADE at pH 7 *via* formation of the corresponding monoamide (**Scheme 3**). In this step, a severe pH control using a buffered medium is required to prevent further amidation and therefore KuE-dimerization, which occurs at more basic conditions. The HPLC-purified KuE.SA was obtained with a yield of 23 %. The rather moderate yield does not reflect low formation of the product (as confirmed *via* LC/MS), but is mainly attributed to a loss during HPLC purification.

The next step finally included azide-functionalization *via* second amidation of the squaric acid monoamide at pH 9 using 2-azidoethylamine (**Scheme 3**). The azide-bearing precursor was previously synthesized starting from 2-bromoethylamine hydrobromide by means of sodium azide and potassium hydroxide. After HPLC purification, the desired clickable PSMA inhibitor KuE.SA.N_3 was finally obtained with a yield of 86 %.

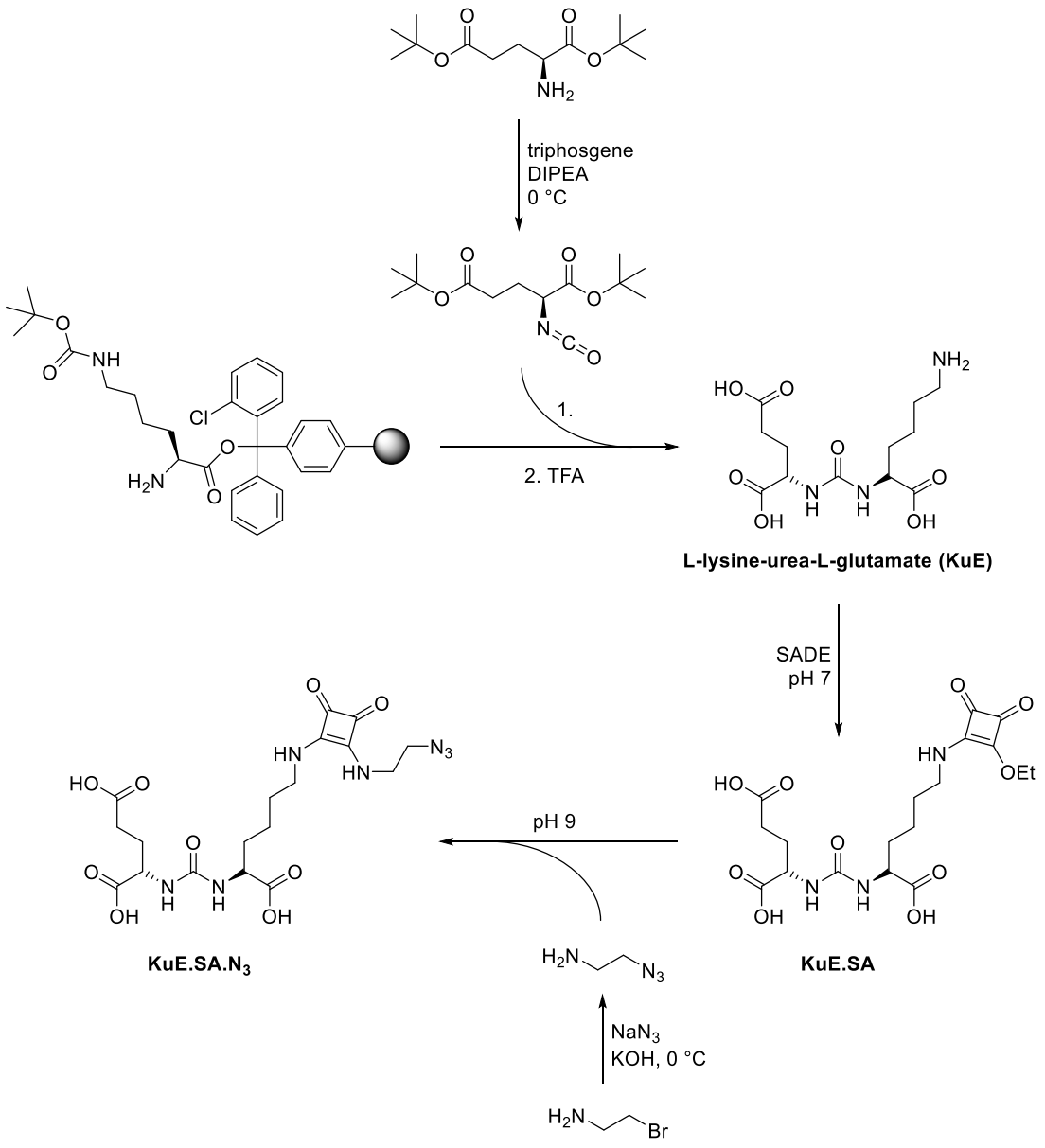

Scheme 3: Synthesis of the PSMA inhibitor L-lysine-urea-L-glutamate (KuE) and subsequent azide-functionalization *via* formation of the corresponding squaric acid diamide.

KuE.SA-functionalization of alkyne-bearing BisHD-hbPG

In order to ensure specific binding to PSMA expressing cancer of the later prepared liposomal system, the alkyne-bearing hyperbranched polyether lipid was functionalized with KuE.SA *via* CuAAC, also named click-reaction (**Scheme 4**). This modification was achieved similarly to the method Wagener *et al.* used for preparation of trimannosylated lipids.[34] Therefore, BisHD-*hb*PG-alkyne was reacted with the previously synthesized KuE.SA.N_3 using copper(I) bromide and PMDETA as base. According to the mechanism proposed by Worrel *et al.*, a catalytically active complex containing of a σ-bound copper acetylide being additionally supplemented by a second π-bound copper atom, is formed in situ.[34] The base PMDETA is added to promote the formation of the copper acetylide.[49] Subsequent coordination of the azide leads to the formation of a six-membered metallacycle, which in turn is then converted to the triazolyl-connected product through ring contraction and protonolytic cleavage of the catalyst. To ensure sufficient functionalization of the polyether lipid with the PSMA inhibitor on the one hand and to leave binding sites unoccupied for subsequent radiolabeling on the other hand, 2.5 equivalents KuE.SA.N_3 were used. Purification of the product for removal of small reaction components and unbound reactant was achieved *via* spin filtration (MWCO = 1000 g/mol).

To verify the successful binding of KuE.SA.N_3 to the polymer using CuAAC, NMR spectra were prepared. In the ^{1}H and ^{13}C spectra, only very weak characteristic signals could be detected. Reasons for this are on the one hand the large molecular weight of the polymer compared to the molecular weight of the attached group, many signals overlap with the signals of the polymer and the deuterated solvent pyridine has an additional strong shielding effect. However, by ^{1}H, ^{13}C HSQC analysis, the successful binding could be confirmed. The spectra can be taken from the Supporting Information (**SI-Figure 14**-**SI-Figure 18**). Furthermore, a decrease in the protons of the alkyne groups on the polymer was observed and the KuE.SA functionalized liposomes showed fluorescence in the DLS later on, further confirming the successful functionalization.

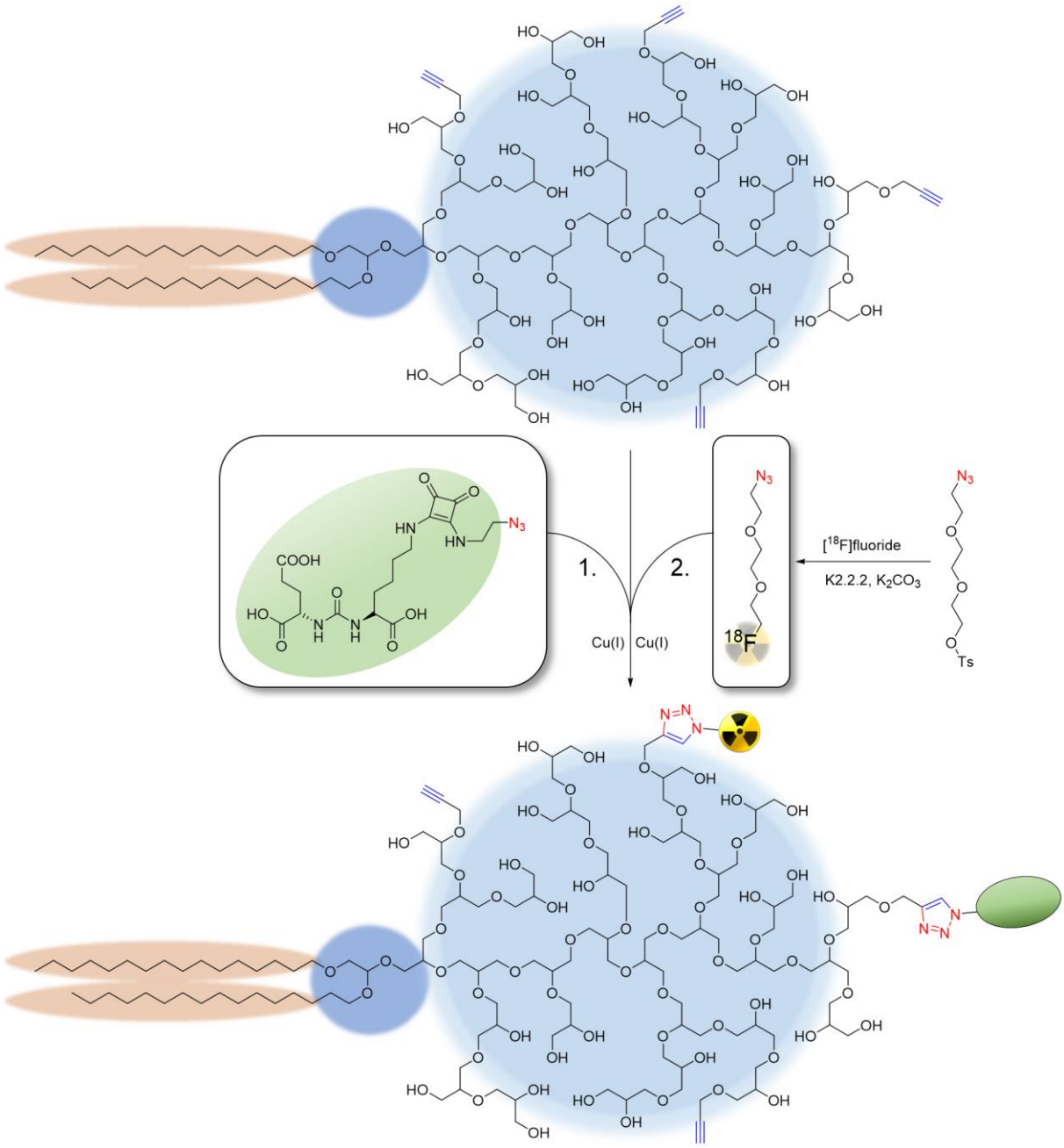

Scheme 4: Consecutive KuE.SA-functionalization and ^{18}F-labeling of the alkyne-bearing hyperbranched polyether lipid BisHD-*hb*PG using CuAAC.

3.1.2.3 Radiosynthesis

Radiosynthesis first included nucleophilic ^{18}F-labeling of the prior synthesized click-synthon Ts-TEG-N_3 according to the procedure of previous reports.[33,34,40] In this step a semiautomatic custom-built modular system was used significantly simplifying and accelerating the synthesis and minimizing radiation exposure to the experimentalist. Cyclotron produced [^{18}F]fluoride was first separated from target [^{18}O]water *via* trapping on

a quaternary methyl ammonium (QMA) anion exchange cartridge and subsequently eluted using a mixture of aqueous K_2CO_3, [2.2.2]cryptand (Kryptofix® 222) and acetonitrile. The aminopolyether Kryptofix® 222 serves as phase transfer catalysator enhancing fluoride-nucleophilicity and -solubility in organic solvents *via* complexation of the potassium counter ion.[50,51] Since hydrated [^{18}F]fluoride is strongly inactivated for nucleophilic reactions, complete removal of residual water plays a crucial role and was realized *via* azeotropic evaporation of the solvent. Nucleophilic substitution of the added precursor Ts-TEG-N_3 was achieved within 10 min at 90 °C. Further processing of the crude product consecutively included HPLC purification, dilution, polymer-based solid phase extraction using diethylether as eluent and evaporation of the solvent. The whole procedure lasted 100 min and therefore slightly less than one half-life of the radionuclide. The ^{18}F-labeled click synthon [^{18}F]F-TEG-N_3 was obtained with a decay corrected radiochemical yield of 53 %.

As shown in **Scheme 4**, residual unoccupied alkyne groups were used for radiolabeling of the KuE.SA-functionalized BisHD-*hb*PG *via* repeated CuAAC using previously synthesized [^{18}F]F-TEG-N_3. Therefore, the polyether lipid was combined with the radiolabeled synthon and the click reaction was initiated *via* addition of copper(II) sulfate and sodium ascorbate analogously to the KuE-functionalization described above. In this case, an elevated temperature of 70 °C was used to accelerate the conversion of reactants. As determined *via* radio-TLC (**Figure 5**), completion of the reaction could be confirmed already after 15 min as indicated by almost quantitative radiochemical yield (98.8 %). To separate cytotoxic copper, the reaction mixture was subsequently passed through a Chelex 100 chelating resin. A distinct blue layer at the very top of the cartridge indicated successful removal of the catalytic metal ion. Furthermore, Wagener *et al.* confirmed the efficiency of this method *via* the absence of precipitated copper sulfide after addition of sodium sulfide to the purified solution.[33] For maximum product recovery, the resin was additionally flushed with ethanol resulting in an aqueous-ethanolic solution of radiolabeled polyether lipid. In the case of BisHD-*hb*PG-KuE.SA, total duration of this synthesis step accounted for 32 min and the ^{18}F-labeled analogue could be obtained with a decay corrected radiochemical yield of 73 %.

For comparison, non-KuE-modified BisHD-*hb*PG was radiolabeled analogously (81 % RCY, 45 min).

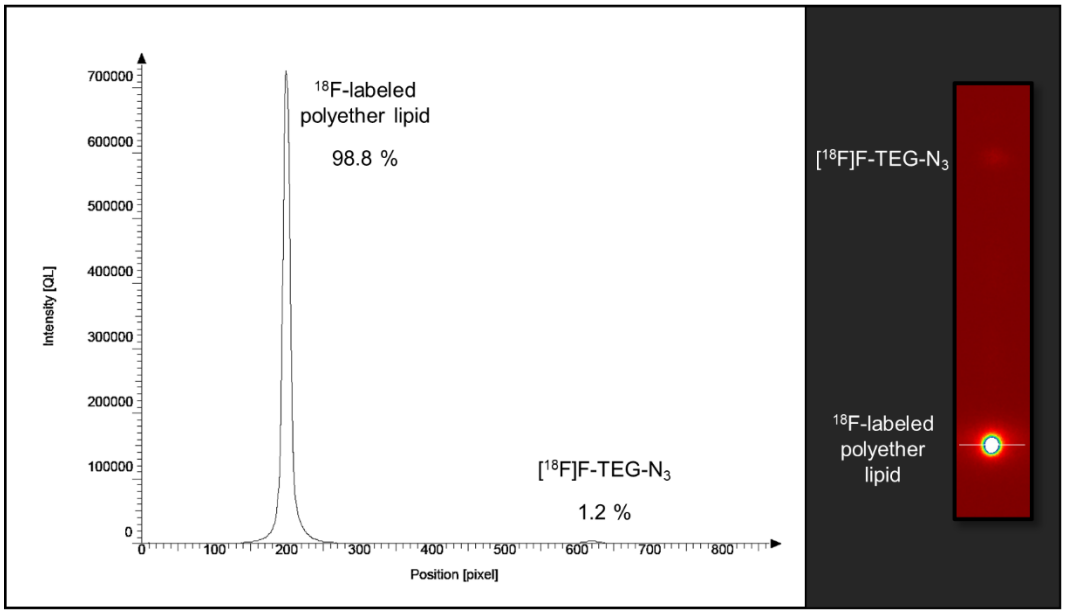

Figure 5: Radio-TLC image (right) and analyzed TLC chromatogram (left) showing the ^{18}F-labeling (CuAAC) results of ([^{18}F]F-TEG-triazolyl)-BisHD-*hb*PG-KuE.SA after 15 min at 70 °C (solid phase: silica gel, mobile phase: ethylacetate:hexane 1:1; ^{18}F-labeled polyether lipid: R_f = 0, [^{18}F]F-TEG-N_3: R_f = 0.8-0.9). The chromatogram position of 200 pixels indicates the TLC-baseline.

3.1.2.4 Liposome Formation and Characterization

As already mentioned, liposomes are typically prepared using amphiphilic phospholipids containing of a hydrophylic "head" and two hydrophobic "tails". Upon contact with polar solvents (e.g. water), these molecules spontaneously arrange themselves to form mono- and bilayers as well as spheric structures such as micelles or vesicular liposomes. In this study we used DOPC as structure-defining component. This zwitterionic phospholipid has a low gel-fluid phase transition temperature of approx. -22 °C and therefore enables preparation of fluid-state liposomes at room temperature.[52,53] For further stabilization, we additionally used cholesterol, which occupies free space of the bilayer and therefore decreases the flexibility and mobility of surrounding fluid-phase lipids leading to an increased mechanical rigidity, decreased water permeability and reduced aggregation-tendency of the liposomal system.[54–58] Ethanolic solutions of these two components (55 mol% DOPC, 40 mol%

cholesterol) were blended with the previously ^{18}F-labeled, KuE-functionalized BisHD-*hb*PG (5 mol%) and liposome preparation *via* thin film hydration was achieved according to the procedure described by Wagener *et al.*[33,34] Therefore, removal of the solvents under reduced pressure using a rotary evaporator led to a thin oily layer of the different constituents. Subsequently, large multilamellar vesicles of hetereogeneous size distribution were formed *via* hydration using PBS and ultrasonication. In order to obtain small uniform unilamellar liposomes, the suspension was extruded repeatedly through polycarbonate membranes of different pore sizes (400, 100 and 50 nm) using a custom-built automatic extrusion device. In contrast to manually driven extrusion, the applied device ensures constant speed and pressure leading to reproducible and narrow size distribution while minimizing the radiation exposure to the experimentalist.[33] Removal of smaller components like unassembled lipids and micelles was achieved *via* fractionated SEC (**SI-Figure 19**) resulting in a purified suspension of ^{18}F-labeled, KuE-functionalized and *hb*PG shielded liposomes with a decay corrected radiochemical yield of 25 %. Duration of the entire procedure accounted for 82 min. For comparison, ^{18}F-labeled but non-KuE-functionalized liposomes were prepared analogously (14 % RCY, 75 min). The following **Figure 6** shows the schematic structure of the ^{18}F-labeled, KuE-SA-functionalized and *hb*PG shielded liposomes.

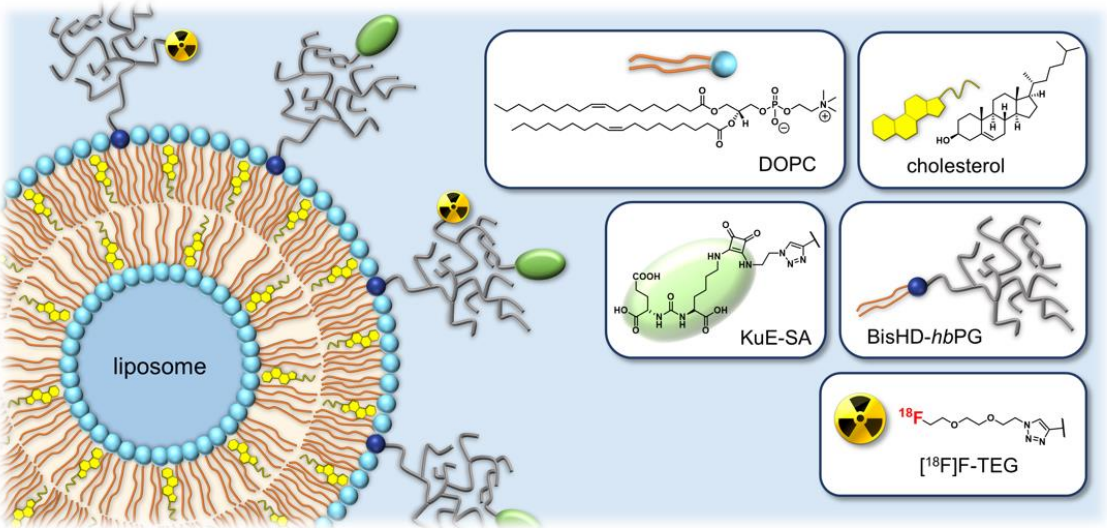

Figure 6: Schematic cross-section displaying the structure of the ^{18}F-labeled, KuE-SA-functionalized and *hb*PG-shielded liposomes.

After complete decay of the activity, the size of both KuE.SA-bearing and non-KuE-functionalized liposomes was measured *via* DLS (**SI-Table 1**, **SI-Figure 20**-**SI-Figure 22**). The BisHD-*hb*PG-alkyne liposomes indicated a diameter of 157.5 nm, for the analogous KuE.SA-bearing liposomes a higher value of 199.1 nm was measured. The significant difference in size may result from the measurement, as the sample of functionalized liposomes exhibits fluorescence, which may distort the measurement result. For this reason, the PDIs of the measured samples also differ (**SI-Table 1**). Since preparation, processing and extrusion was carried out analogously for both systems, the difference in size is presumably based on an increased steric demand due to KuE.SA-functionalization of the polyether lipid. Additionally, it may also be partly influenced by the measurement itself, as the sample of functionalized liposomes exhibits fluorescence, which may distort the DLS-results. The liposomal size plays a crucial role for the pharmacological behavior *in vivo*. Ideally, the hydrodynamic diameter should on the one hand be large enough to prevent interaction with hepatocytes and thus filtration through the liver, which occurs up to a particle size of 50-100 nm.[59] On the other hand, it should not exceed 300 nm to avoid an increased accumulation in the spleen.[60] Furthermore, (non-functionalized) liposomes with sizes ranging from 100 to 200 nm were reported to take advantage of tumor permeability most effectively resulting in optimal target uptake.[59,61] The dimensions of both liposomal systems described herein meet these requirements and were comparable to the values of similar vesicles reported in the literature.[34] The liposomes containing KuE.SA-functionalized BisHD-*hb*PG therefore represent promising tools for targeted drug delivery in the treatment of PSMA-expressing prostate cancer. Furthermore, utilization of the ^{18}F-labeled vesicles should ensure *in vivo* evaluation of the pharmacokinetics *via* PET in future follow-up studies.

3.1.3 Conclusion

In this study, the synthesis of an alkyne-functionalized hyperbranched polyglycerol with a long hydrophobic alkyl chain anchor (BisHD-*hb*PG) *via* AROP on the one hand and of a squaramide coupled PSMA inhibitor (KuE.SA) on the other hand is described. To combine these two structures, Cu(I)-catalyzed alkyne-azide cycloaddition (CuAAC) was used. For this purpose, BisHD-*hb*PG was functionalized with alkyne groups and the PSMA inhibitor

was modified with an azide group. In a second CuAAC the BisHD-*hb*PG-KuE.SA polymers were radiolabeled with a previously synthesized ^{18}F-labeled precursor. To obtain PSMA-specific drug delivery systems with a prolonged circulation behavior in the blood stream, liposomes were formed *via* thin film hydration method. The syntheses and radiolabeling were straightforward and achieved high yields. By combining the KuE.SA functionalized liposomes and the radiolabeling with fluorine-18, a promising system for future targeted drug delivery in the treatment of prostate cancer was introduced. This enables prostate cancer-targeted delivery of liposome-entrapped therapeutics and pre-evaluation of liposome behavior *in vitro* and *in vivo via* positron emission tomography (PET).

3.1.4 Acknowledgment

We thank [redacted] for technical assistance, [redacted] for SEC measurements, [redacted] and [redacted] for production and provision of fluorine-18. E.B. and B.K. thank the DFG in the context of the SFB 1066 for financial support. T.G. thanks the MPGC (Max Planck Graduate Center) for financial support.

Authors contribution: E.B., T.G. and B.K. planned and conceived the present study and wrote the manuscript. E.B. was in charge for synthesis and characterization of the alkyne-functionalized polyether lipids. T.G. performed KuE-functionalization of the polyether lipids. B.K. and T.G. were in charge for radiochemical and liposomal synthesis and evaluation. H.F. and F.R. supervised the whole part of the study. All authors read and approved the manuscript.

References

(1) Torre, L. A.; Bray, F.; Siegel, R. L.; Ferlay, J.; Lortet-Tieulent, J.; Jemal, A. Global Cancer Statistics, 2012. *CA. Cancer J. Clin.* **2015**, *65* (2), 87–108. https://doi.org/10.3322/caac.21262.

(2) Sung, H.; Ferlay, J.; Siegel, R. L.; Laversanne, M.; Soerjomataram, I.; Jemal, A.; Bray, F. Global Cancer Statistics 2020: GLOBOCAN Estimates of Incidence and Mortality Worldwide for 36 Cancers in 185 Countries. *CA. Cancer J. Clin.* **2021**, *0* (0), 1–41. https://doi.org/10.3322/caac.21660.

(3) Rawla, P. Epidemiology of Prostate Cancer. *World J. Oncol.* **2019**, *10* (2), 63–89. https://doi.org/10.1016/j.mednuc.2007.11.003.

(4) Perner, S.; Hofer, M. D.; Kim, R.; Shah, R. B.; Li, H.; Möller, P.; Hautmann, R. E.; Gschwend, J. E.; Kuefer, R.; Rubin, M. A. Prostate-Specific Membrane Antigen Expression as a Predictor of Prostate Cancer Progression. *Hum. Pathol.* **2007**, *38* (5), 696–701. https://doi.org/10.1016/j.humpath.2006.11.012.

(5) Silver, D. A.; Pellicer, I.; Fair, W. R.; W.D., H.; Cordon-Cardo, C. Prostate-Specific Membrane Antigen Expression in Normal and Malignant Human Tissues. *Clin. Cancer Res.* **1997**, *3* (January), 81–85.

(6) Okarvi, S. M. Recent Developments of Prostate-Specific Membrane Antigen (PSMA)-Specific Radiopharmaceuticals for Precise Imaging and Therapy of Prostate Cancer: An Overview. *Clin. Transl. Imaging* **2019**, *7* (3), 189–208. https://doi.org/10.1007/s40336-019-00326-3.

(7) Wester, H. J.; Schottelius, M. PSMA-Targeted Radiopharmaceuticals for Imaging and Therapy. *Semin. Nucl. Med.* **2019**, *49* (4), 302–312. https://doi.org/10.1053/j.semnuclmed.2019.02.008.

(8) Pillai, M. R. A.; Nanabala, R.; Joy, A.; Sasikumar, A.; Russ Knapp, F. F. Radiolabeled Enzyme Inhibitors and Binding Agents Targeting PSMA: Effective Theranostic Tools for Imaging and Therapy of Prostate Cancer. *Nucl. Med. Biol.* **2016**, *43* (11), 692–720. https://doi.org/10.1016/j.nucmedbio.2016.08.006.

(9) Kopka, K.; Benešová, M.; Bařinka, C.; Haberkorn, U.; Babich, J. Glu-Ureido-Based Inhibitors of Prostate-Specific Membrane Antigen: Lessons Learned during the Development of a Novel Class of Low-Molecular-Weight Theranostic Radiotracers. *J. Nucl. Med.* **2017**, *58*, 17S-26S. https://doi.org/10.2967/jnumed.116.186775.

(10) Benesová, M.; Schäfer, M.; Bauder-Wüst, U.; Afshar-Oromieh, A.; Kratochwil, C.; Mier, W.; Haberkorn, U.; Kopka, K.; Eder, M. Preclinical Evaluation of a Tailor-Made DOTA-Conjugated PSMA Inhibitor with Optimized Linker Moiety for Imaging and Endoradiotherapy of Prostate Cancer. *J. Nucl. Med.* **2015**, *56* (6), 914–920. https://doi.org/10.2967/jnumed.114.147413.

(11) Kozikowski, A. P.; Zhang, J.; Nan, F.; Petukhov, P. A.; Grajkowska, E.; Wroblewski, J. T.; Yamamoto, T.; Bzdega, T.; Wroblewska, B.; Neale, J. H. Synthesis of Urea-Based Inhibitors as Active Site Probes of Glutamate Carboxypeptidase II: Efficacy as Analgesic Agents. *J. Med. Chem.* **2004**, *47* (7), 1729–1738. https://doi.org/10.1021/jm0306226.

(12) Wurm, F. R.; Klok, H. A. Be Squared: Expanding the Horizon of Squaric Acid-Mediated Conjugations. *Chem. Soc. Rev.* **2013**, *42* (21), 8220–8236. https://doi.org/10.1039/c3cs60153f.

(13) Tietze, L. F.; Arlt, M.; Beller, M.; Glüsenkamp, K.-H.; Jähde, E.; Rajewsky, M. F. Anticancer Agents, 15. Squaric Acid Diethyl Ester: A New Coupling Reagent for the Formation of Drug Biopolymer Conjugates. Synthesis of Squaric Acid Ester Amides and Diamides. *Chem. Ber.* **1991**, *124* (5), 1215–1221. https://doi.org/10.1002/cber.19911240539.

(14) Dingels, C.; Wurm, F.; Wagner, M.; Klok, H. A.; Frey, H. Squaric Acid Mediated Chemoselective PEGylation of Proteins: Reactivity of Single-Step-Activated α-Amino Poly(Ethylene Glycol)S. *Chem. - A Eur. J.* **2012**, *18* (52), 16828–16835. https://doi.org/10.1002/chem.201200182.

(15) Quiñonero, D.; Frontera, A.; Ballester, P.; Deyà, P. M. A Theoretical Study of Aromaticity in Squaramide and Oxocarbons. *Tetrahedron Lett.* **2000**, *41* (12), 2001–2005.

(16) Prohens, R.; Portell, A.; Font-Bardia, M.; Bauzá, A.; Frontera, A. Experimental and Theoretical Study of Aromaticity Effects in the Solid State Architecture on Squaric Acid Derivatives. *Cryst. Growth Des.* **2014**, *14* (5), 2578–2587. https://doi.org/10.1021/cg500264k.

(17) Semmingsen, D. The Structure of Squaric Acid (3,4-Dihydroxy-3-Cyclobutene-1,2-Dione). *Tetrahedron Lett.* **1973**, *11*, 807–808.

(18) West, R.; Powell, D. L. New Aromatic Anions. III. Molecular Orbital Calculations on Oxygenated Anions. *J. Am. Chem. Soc.* **1963**, *85*, 2577–2579.

(19) Zhang, A. X.; Murelli, R. P.; Barinka, C.; Michel, J.; Cocleaza, A.; Jorgensen, W. L.; Lubkowski, J.; Spiegel, D. A. A Remote Arene-Binding Site on Prostate Specific Membrane Antigen Revealed by Antibody-Recruiting Small Molecules. *J. Am. Chem. Soc.* **2010**, *132* (36), 12711–12716. https://doi.org/10.1021/ja104591m.

(20) Greifenstein, L.; Engelbogen, N.; Lahnif, H.; Sinnes, J. P.; Bergmann, R.; Bachmann, M.; Rösch, F. Synthesis, Labeling and Preclinical Evaluation of a Squaric Acid Containing PSMA Inhibitor Labeled with 68Ga: A Comparison with PSMA-11 and PSMA-617. *ChemMedChem* **2020**, *15* (8), 695–704. https://doi.org/10.1002/cmdc.201900559.

(21) Wicki, A.; Witzigmann, D.; Balasubramanian, V.; Huwyler, J. Nanomedicine in Cancer Therapy: Challenges, Opportunities, and Clinical Applications. *J. Control. Release* **2015**, *200*, 138–157. https://doi.org/10.1016/j.jconrel.2014.12.030.

(22) Shi, J.; Kantoff, P. W.; Wooster, R.; Farokhzad, O. C. Cancer Nanomedicine: Progress, Challenges and Opportunities. *Nat. Rev. Cancer* **2017**, *17* (1), 20–37. https://doi.org/10.1038/nrc.2016.108.

(23) Allen, T. M.; Cullis, P. R. Liposomal Drug Delivery Systems: From Concept to Clinical Applications. *Adv. Drug Deliv. Rev.* **2013**, *65* (1), 36–48. https://doi.org/10.1016/j.addr.2012.09.037.

(24) Pattni, B. S.; Chupin, V. V.; Torchilin, V. P. New Developments in Liposomal Drug Delivery. *Chem. Rev.* **2015**, *115* (19), 10938–10966. https://doi.org/10.1021/acs.chemrev.5b00046.

(25) Akbarzadeh, A.; Rezaei-sadabady, R.; Davaran, S.; Joo, S. W.; Zarghami, N. Liposome : Classification , PrepNew Aspects of Liposomesaration , and Applications. *Nanoscale Res. Lett.* **2013**, *8* (102), 1–9.

(26) Ishida, T.; Harashima, H.; Kiwada, H. Liposome Clearance. *Biosci. Rep.* **2002**, *22* (2), 197–224. https://doi.org/10.1023/A:1020134521778.

(27) Herzberger, J.; Niederer, K.; Pohlit, H.; Seiwert, J.; Worm, M.; Wurm, F. R.; Frey, H. Polymerization of Ethylene Oxide, Propylene Oxide, and Other Alkylene Oxides: Synthesis, Novel Polymer Architectures, and Bioconjugation. *Chem. Rev.* **2015**, acs.chemrev.5b00441. https://doi.org/10.1021/acs.chemrev.5b00441.

(28) Veronese, F. M.; Pasut, G. PEGylation, Successful Approach to Drug Delivery. *Drug Discov. Today* **2005**, *10* (21), 1451–1458.

(29) Immordino, M. L.; Dosio, F.; Cattel, L. Stealth Liposomes: Review of the Basic Science, Rationale, and Clinical Applications, Existing and Potential. *Int. J. Nanomedicine* **2006**, *1* (13), 297–315.

(30) Huckaby, J. T.; Jacobs, T. M.; Li, Z.; Perna, R. J.; Wang, A.; Nicely, N. I.; Lai, S. K. Structure of an Anti-PEG Antibody Reveals an Open Ring That Captures Highly Flexible PEG Polymers. *Commun. Chem.* **2020**, *3* (1), 1–8. https://doi.org/10.1038/s42004-020-00369-y.

(31) Daniel, W.; Stiriba, S. E.; Holger, F. Hyperbranched Polyglycerols: From the Controlled Synthesis of Biocompatible Polyether Polyols to Multipurpose Applications. *Acc. Chem. Res.* **2010**, *43* (1), 129–141. https://doi.org/10.1021/ar900158p.

(32) Kasza, G.; Kali, G.; Domján, A.; Petho, L.; Szarka, G.; Iván, B. Synthesis of Well-Defined Phthalimide Monofunctional Hyperbranched Polyglycerols and Its Transformation to Various Conjugation Relevant Functionalities. *Macromolecules* **2017**, *50* (8), 3078–3088. https://doi.org/10.1021/acs.macromol.7b00413.

(33) Wagener, K.; Worm, M.; Pektor, S.; Schinnerer, M.; Thiermann, R.; Miederer, M.; Frey, H.; Rösch, F. Comparison of Linear and Hyperbranched Polyether Lipids for

Liposome Shielding by 18 F-Radiolabeling and Positron Emission Tomography. *Biomacromolecules* **2018**, *19* (7), 2506–2516. https://doi.org/10.1021/acs.biomac.8b00115.

(34) Wagener, K.; Bros, M.; Krumb, M.; Langhanki, J.; Pektor, S.; Worm, M.; Schinnerer, M.; Montermann, E.; Miederer, M.; Frey, H.; Opatz, T.; Rösch, F. Targeting of Immune Cells with Trimannosylated Liposomes. *Adv. Ther.* **2020**, *3* (6), 1900185. https://doi.org/10.1002/adtp.201900185.

(35) Hofmann, A. M.; Wurm, F.; Huhn, E.; Nawroth, T.; Langguth, P.; Frey, H. Hyperbranched Polyglycerol-Based Lipids via Oxyanionic Polymerization: Toward Multifunctional Stealth Liposomes. *Biomacromolecules* **2010**, *11* (3), 568–574. https://doi.org/10.1021/bm901123j.

(36) Gleue, L.; Schupp, J.; Zimmer, N.; Becker, E.; Frey, H.; Tuettenberg, A.; Helm, M. Stability of Alkyl Chain-Mediated Lipid Anchoring in Liposomal Membranes. *Cells* **2020**, *9* (10), 1–13. https://doi.org/10.3390/cells9102213.

(37) Jacobson, O.; Kiesewetter, D. O.; Chen, X. Fluorine-18 Radiochemistry, Labeling Strategies and Synthetic Routes. *Bioconjug. Chem.* **2015**, *26* (1), 1–18. https://doi.org/10.1021/bc500475e.

(38) Cole, E.; Stewart, M.; Littich, R.; Hoareau, R.; Scott, P. Radiosyntheses Using Fluorine-18: The Art and Science of Late Stage Fluorination. *Curr. Top. Med. Chem.* **2014**, *14* (7), 875–900. https://doi.org/10.2174/1568026614666140202205035.

(39) Bé, M.-M.; Chisté, V.; Dulieu, C.; Chechev, V.; Kuzmenko, N.; Helmer, R.; Nichols, A.; Schönfeld, E.; Dersch, R. *Table of Radionuclides*; 2004; Vol. 1.

(40) Reibel, A. T.; Müller, S. S.; Pektor, S.; Bausbacher, N.; Miederer, M.; Frey, H.; Rösch, F. Fate of Linear and Branched Polyether-Lipids in Vivo in Comparison to Their Liposomal Formulations by 18F-Radiolabeling and Positron Emission Tomography. *Biomacromolecules* **2015**, *16* (3), 842–851. https://doi.org/10.1021/bm5017332.

(41) Kettenbach, K.; Schieferstein, H.; Ross, T. L. 18 F-Labeling Using Click Cycloadditions. *Biomed Res. Int.* **2014**, *2014*, 1–16. https://doi.org/10.1155/2014/890540.

(42) Fitton, A. O.; Hill, J.; Jane, D. E.; Millar, R. Synthesis of Simple Oxetanes Carrying Reactive 2-Substituents. *Synthesis (Stuttg).* **1987**, 1140–1142.

(43) Stauch, O.; Uhlmann, T.; Fröhlich, M.; Thomann, R.; El-Badry, M.; Kim, Y. K.; Schubert, R. Mimicking a Cytoskeleton by Coupling Poly(N-Isopropylacrylamide) to the Inner Leaflet of Liposomal Membranes: Effects of Photopolymerization on

Vesicle Shape and Polymer Architecture. *Biomacromolecules* **2002**, *3* (2), 324–332. https://doi.org/10.1021/bm015613y.

(44) Hofmann, A. M.; Wurm, F.; Frey, H. Rapid Access to Polyfunctional Lipids with Complex Architecture via Oxyanionic Ring-Opening Polymerization. *Macromolecules* **2011**, *44* (12), 4648–4657. https://doi.org/10.1021/ma200367c.

(45) Yamamoto, S.; Nakahama, S.; Yamaguchi, K. A Heterobifunctional Linker Bearing Azide-Reactive Alkyne and Thiol-Reactive Maleimide Connected with N-(2-Nitrobenzyl)Imide to Synthesize Photocleavable Diblock Copolymers. *Chem. Lett.* **2013**, *4* (8), 791–793.

(46) Brocas, A. L.; Mantzaridis, C.; Tunc, D.; Carlotti, S. Polyether Synthesis: From Activated or Metal-Free Anionic Ring-Opening Polymerization of Epoxides to Functionalization. *Prog. Polym. Sci.* **2013**, *38* (6), 845–873. https://doi.org/10.1016/j.progpolymsci.2012.09.007.

(47) Penczek, S.; Cypryk, M.; Duda, A.; Kubisa, P.; Słomkowski, S. Living Ring-Opening Polymerizations of Heterocyclic Monomers. *Prog. Polym. Sci.* **2007**, *32* (2), 247–282. https://doi.org/10.1016/j.progpolymsci.2007.01.002.

(48) Schömer, M.; Frey, H. Water-Soluble "Poly(Propylene Oxide)" by Random Copolymerization of Propylene Oxide with a Protected Glycidol Monomer. *Macromolecules* **2012**, *45* (7), 3039–3046. https://doi.org/10.1021/ma300249c.

(49) Binder, W. H.; Sachsenhofer, R. "Click" Chemistry in Polymer and Materials Science. *Macromol. Rapid Commun.* **2007**, *28* (1), 15–54. https://doi.org/10.1002/marc.200600625.

(50) Lu, S.; Lepore, S. D.; Song, Y. L.; Mondal, D.; Cohn, P. C.; Bhunia, A. K.; Pike, V. W. Nucleophile Assisting Leaving Groups: A Strategy for Aliphatic 18F-Fluorination. *J. Org. Chem.* **2009**, *74* (15), 5290–5296. https://doi.org/10.1021/jo900700j.

(51) Stewart, M. N.; Hockley, B. G.; Scott, P. J. H. Green Approaches to Late-Stage Fluorination: Radiosyntheses of 18F-Labelled Radiopharmaceuticals in Ethanol and Water. *Chem. Commun.* **2015**, *51* (79), 14805–14808. https://doi.org/10.1039/C5CC05919D.

(52) Ladbrooke, B. D.; Chapman, D. Thermal Analysis of Lipids, Proteins and Biological Membranes a Review and Summary of Some Recent Studies. *Chem. Phys. Lipids* **1969**, *3* (4), 304–356. https://doi.org/https://doi.org/10.1016/0009-3084(69)90040-1.

(53) Siwak, D. R.; Tari, A. M.; Lopez-Berestein, G. Liposomal Antisense Oligonucleotides for Cancer Therapy. *Methods Enzymol.* **2004**, *387*, 241–253.

https://doi.org/10.1016/S0076-6879(04)87015-0.

(54) Corvera, E.; Mouritsen, O. G.; Singer, M. A.; Zuckermann, M. J. The Permeability and the Effect of Acyl-Chain Length for Phospholipid Bilayers Containing Cholesterol: Theory and Experiment. *Biochim. Biophys. Acta - Biomembr.* **1992**, *1107* (2), 261–270. https://doi.org/https://doi.org/10.1016/0005-2736(92)90413-G.

(55) Needham, D.; Nunn, R. S. Elastic Deformation and Failure of Lipid Bilayer Membranes Containing Cholesterol. *Biophys. J.* **1990**, *58* (4), 997–1009. https://doi.org/10.1016/S0006-3495(90)82444-9.

(56) Demel, R. A.; De Kruyff, B. The Function of Sterols in Membranes. *Biochim. Biophys. Acta - Rev. Biomembr.* **1976**, *457* (2), 109–132. https://doi.org/https://doi.org/10.1016/0304-4157(76)90008-3.

(57) Virden, J. W.; Berg, J. C. NaCl-Induced Aggregation of Dipalmitoylphosphatidylglycerol Small Unilamellar Vesicles with Varying Amounts of Incorporated Cholesterol. *Langmuir* **1992**, *8* (6), 1532–1537. https://doi.org/10.1021/la00042a007.

(58) Bhattacharya, S.; Haldar, S. Interactions between Cholesterol and Lipids in Bilayer Membranes. Role of Lipid Headgroup and Hydrocarbon Chain-Backbone Linkage. *Biochim. Biophys. Acta - Biomembr.* **2000**, *1467* (1), 39–53. https://doi.org/10.1016/S0005-2736(00)00196-6.

(59) Ernsting, M. J.; Murakami, M.; Roy, A.; Li, S. D. Factors Controlling the Pharmacokinetics, Biodistribution and Intratumoral Penetration of Nanoparticles. *J. Control. Release* **2013**, *172* (3), 782–794. https://doi.org/10.1016/j.jconrel.2013.09.013.

(60) Moghimi, S. M.; Hunter, A. C.; Murray, J. C. Long-Circulating and Target-Specific Nanoparticles: Theory to Practice. *Pharmacol. Rev.* **2001**, *53* (2), 283–318.

(61) Liu, D.; Mori, A.; Huang, L. Role of Liposome Size and RES Blockade in Controlling Biodistribution and Tumor Uptake of GM1-Containing Liposomes. *Biochim. Biophys. Acta - Biomembr.* **1992**, *1104* (1), 95–101. https://doi.org/https://doi.org/10.1016/0005-2736(92)90136-A.

3.1.5 Supporting Information

3.1.5.1 Synthesis of the hydrophobic anchor structure

Synthesis of BisHD-OH

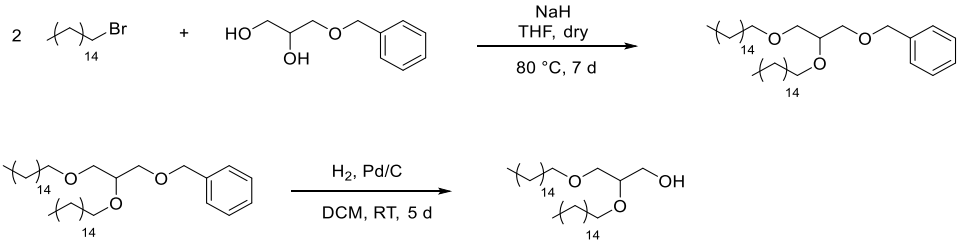

SI-Scheme 1: Synthesis route of the hydrophobic anchor structure.

^{1}H NMR (400 MHz, Chloroform-*d*) δ (ppm) = 3.72 – 3.41 (m, 9H, C*H*$_2$-O and CH$_2$-C*H*-O), 1.61 – 1.49 (m, 4H, C*H*$_2$-CH$_2$-O), 1.25 (s, 52H, C*H*$_2$), 0.88 (t, *J* = 6.8 Hz, 6H, C*H*$_3$-CH$_2$).

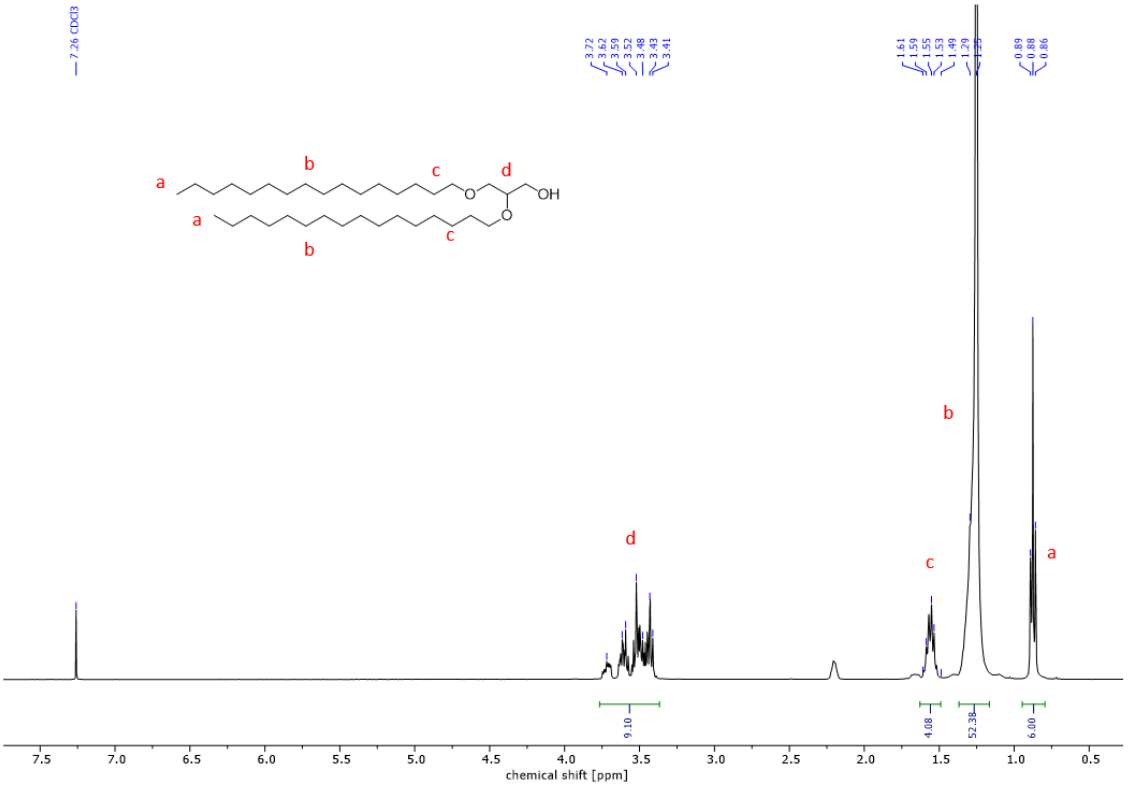

SI-Figure 1: ^{1}H NMR spectrum (400 MHz, chloroform-*d*$_3$) of BisHD-OH.

3.1.5.2 Polymer synthesis and characterization

Synthesis of BisHD-linPG macroinitiator

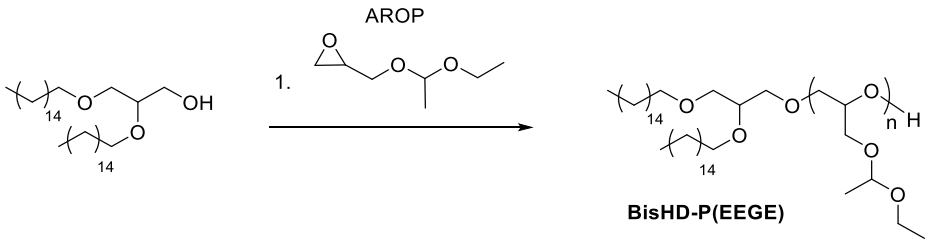

SI-Scheme 2: Synthesis route of BisHD-P(EEGE).

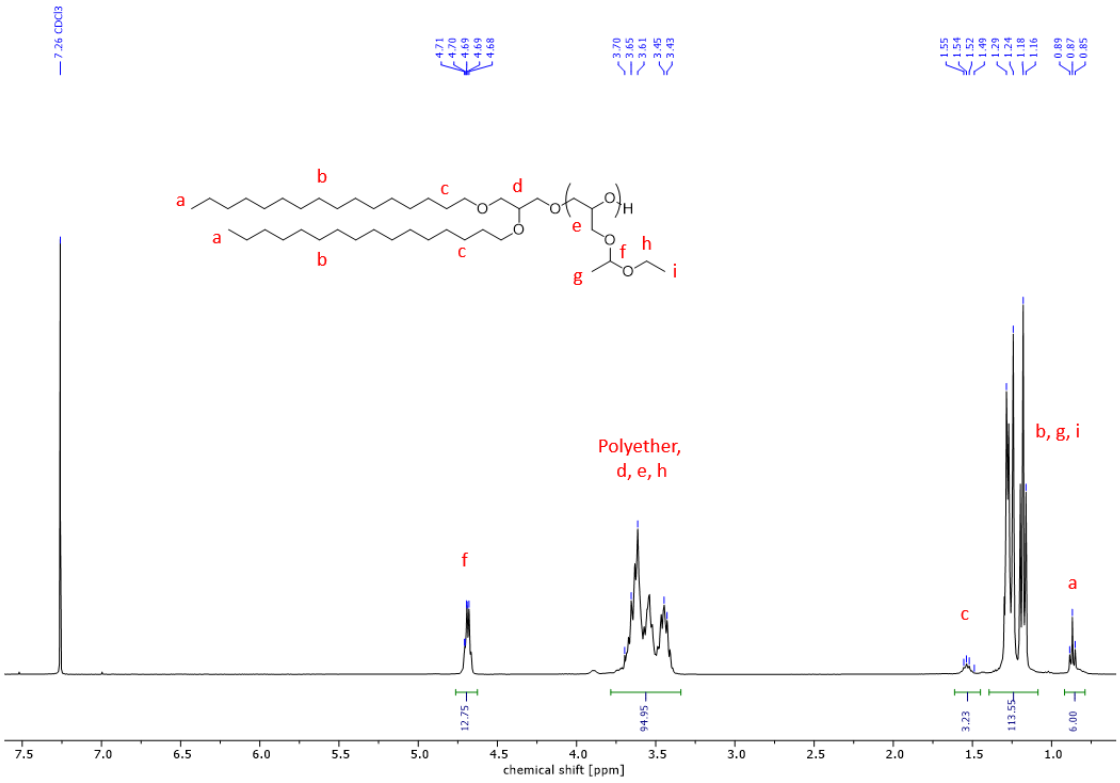

SI-Figure 2: ^{1}H NMR spectrum (400 MHz, chloroform-*d*$_3$) of BisHD-P(EEGE).

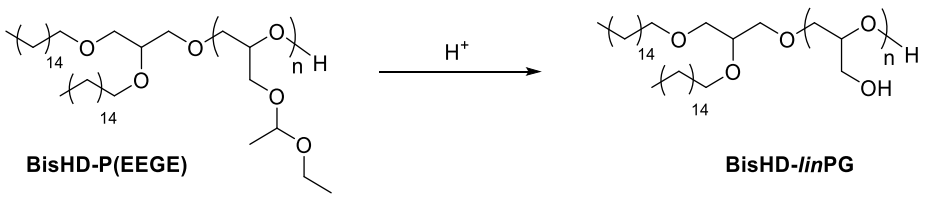

SI-Scheme 3: Synthesis route of the macroinitiator BisHD-*lin*PG.

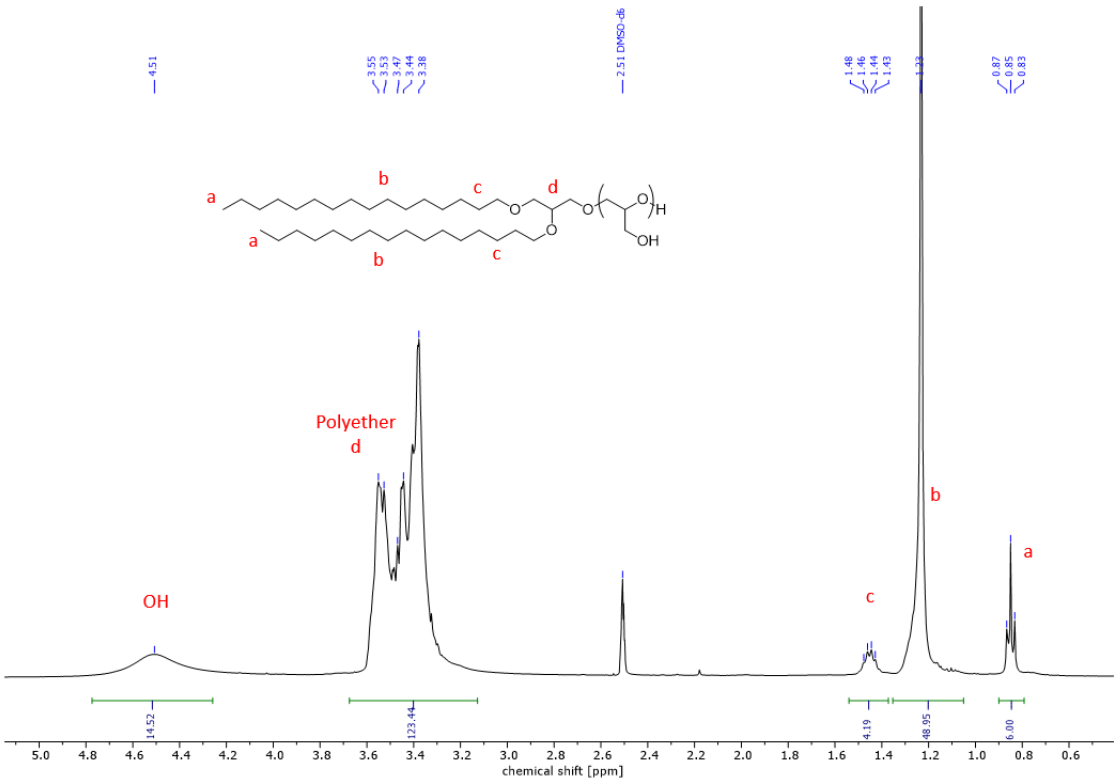

SI-Figure 3: ^{1}H NMR spectrum (400 MHz, DMSO-d_6) of BisHD-*lin*PG.

Synthesis of BisHD-hbPG

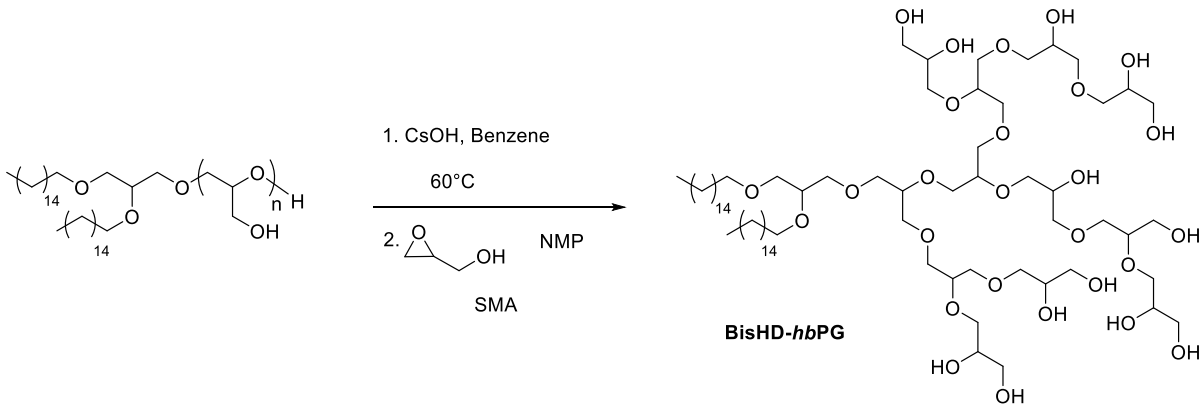

SI-Scheme 4: Synthesis route of BisHD-*hb*PG.

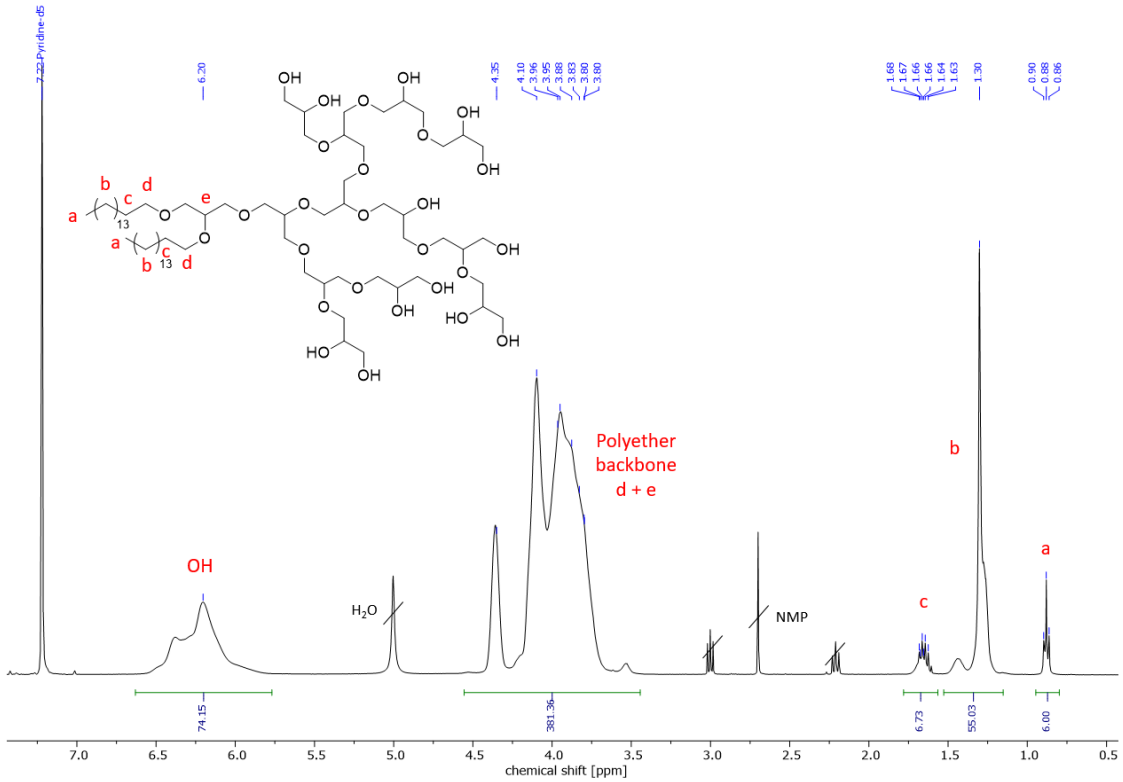

SI-Figure 4: ^{1}H NMR spectrum (400 MHz, pyridine-d_5) of BisHD-*hb*PG.

Synthesis of BisHD-hbPG-alkyne

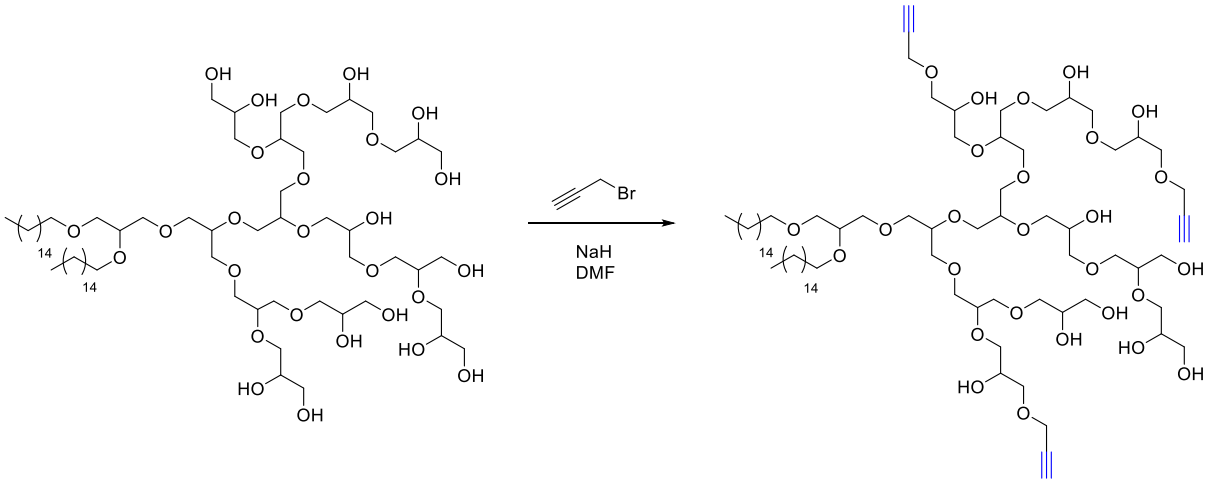

SI-Scheme 5: Synthesis route of BisHD-*hb*PG-alkyne.

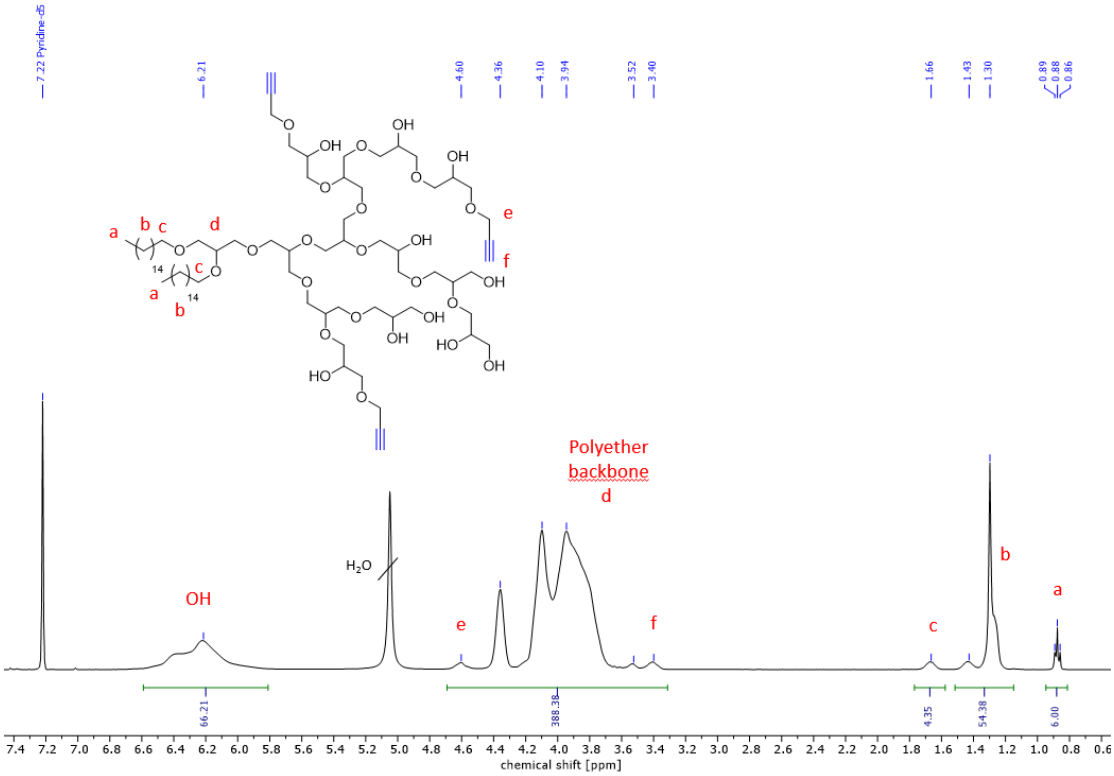

SI-Figure 5: ^{1}H NMR spectrum (400 MHz, pyridine-d_5) of BisHD-*hb*PG-alkyne.

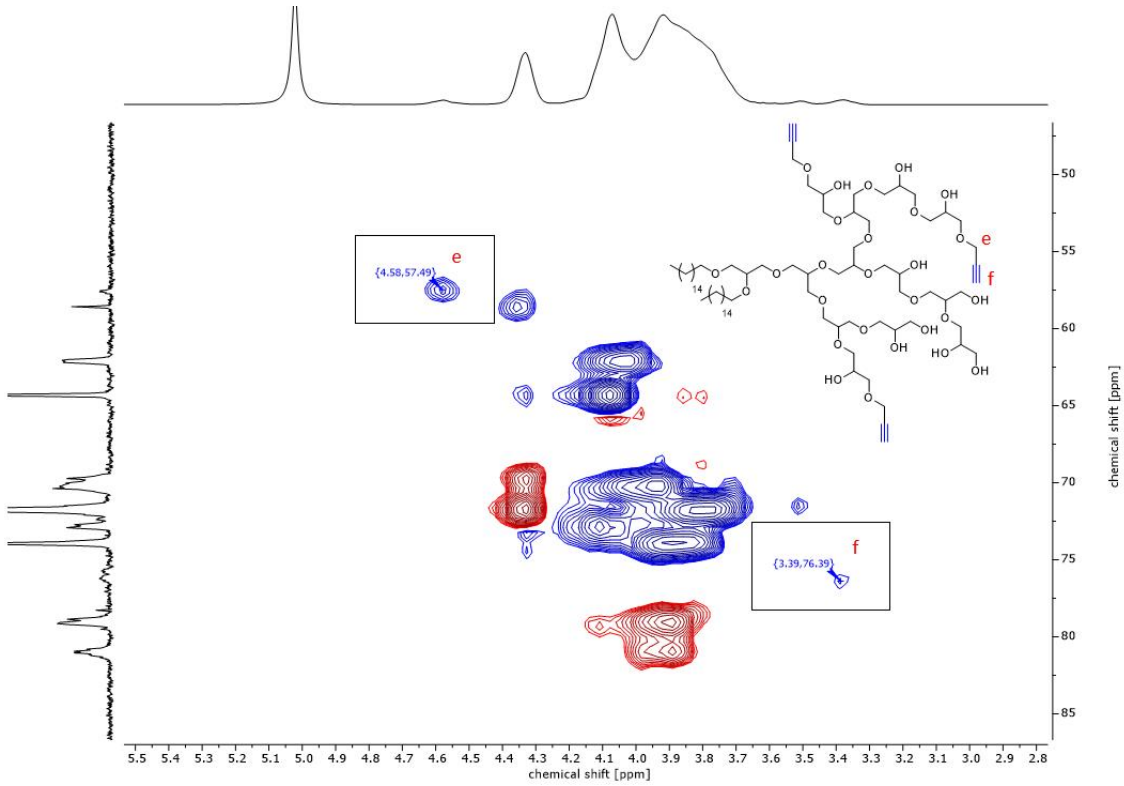

SI-Figure 6: ^{1}H, ^{13}C HSQC NMR spectrum (400 MHz, pyridine-d_5) of BisHD-*hb*PG-alkyne.

3.1.5.3 Synthesis of KuE.SA.N_3

Synthesis of 2-(3-(5-Amino-1-carboxy-pentyl)ureido)pentanedioic acid (L-lysine-urea-L-glutamate (KuE)

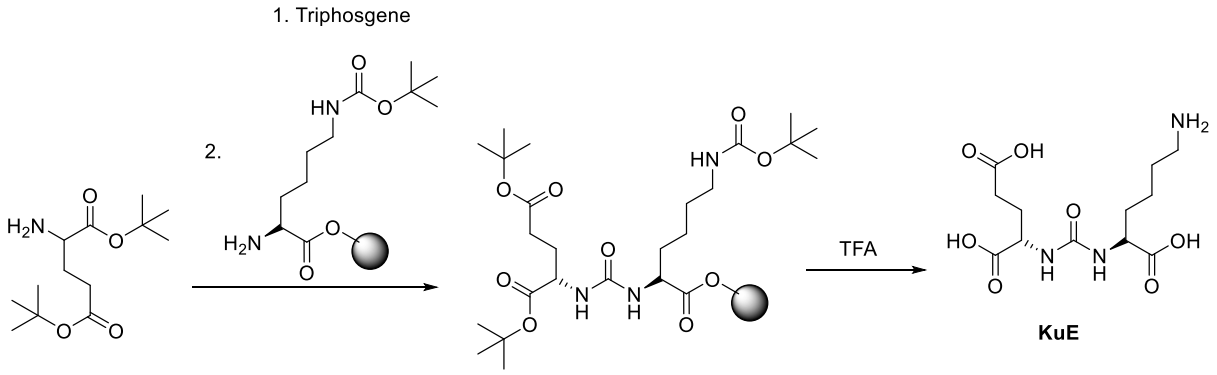

SI-Scheme 6: Synthesis route of KuE.

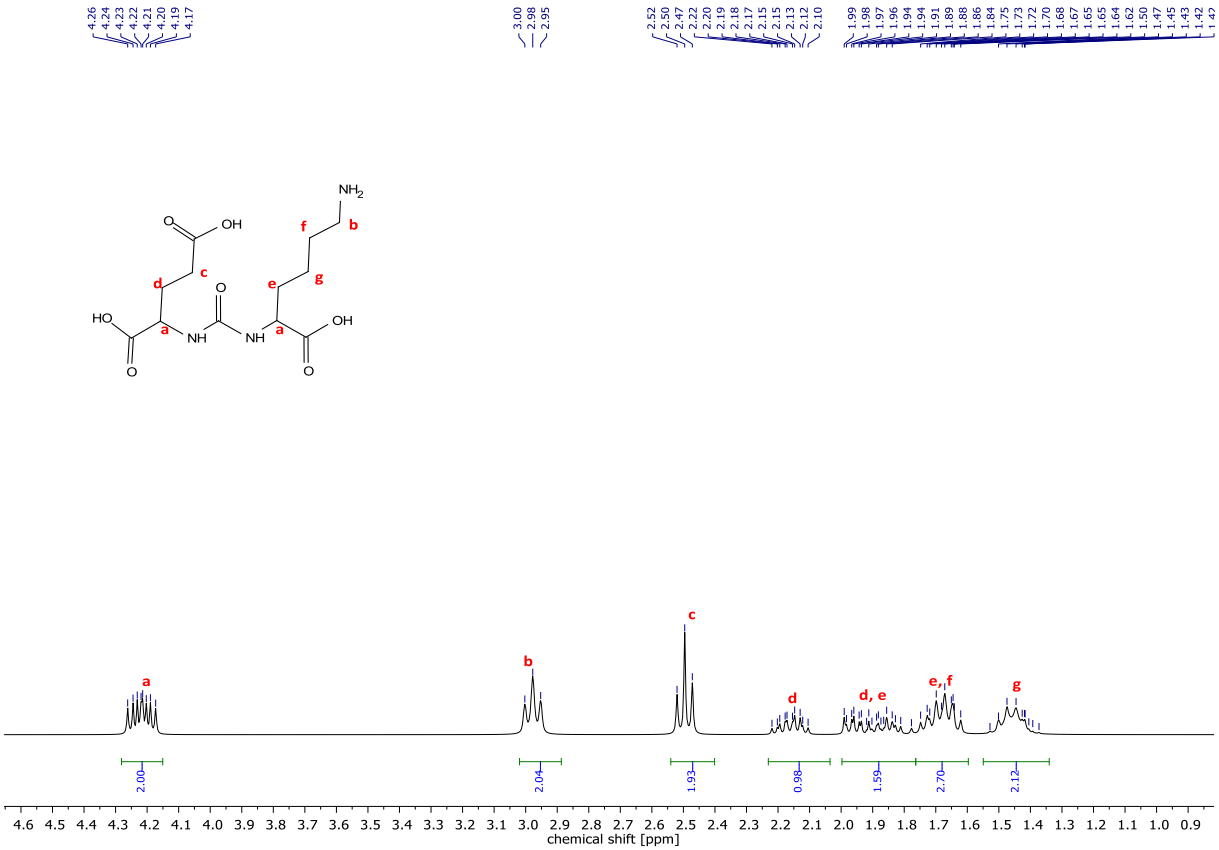

SI-Figure 7: ^{1}H NMR spectra (300 MHz, D_2O) of KuE.

Synthesis of 2-(3-(1-Carboxy-5-((2-ethoxy-3,4-dioxocyclobut-1-en-1-yl)amino)pentyl)-ureido)-pentanedioic acid (KuE.SA)

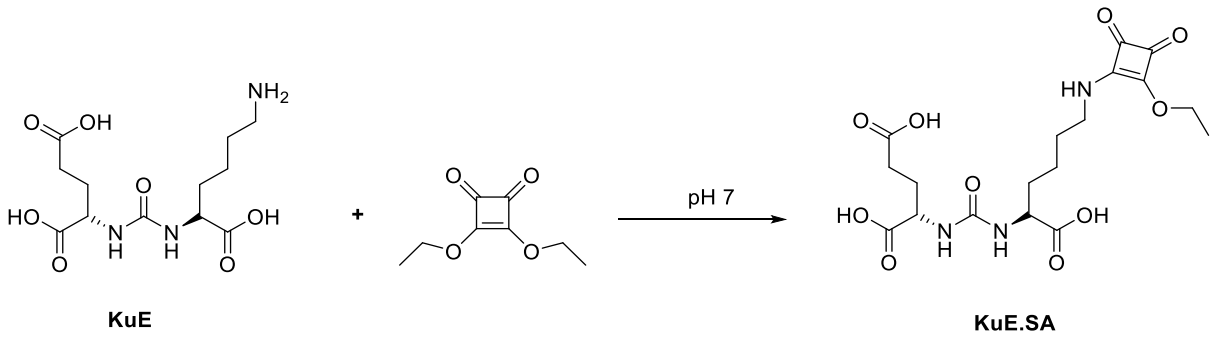

SI-Scheme 7: Synthesis route of KuE.SA.

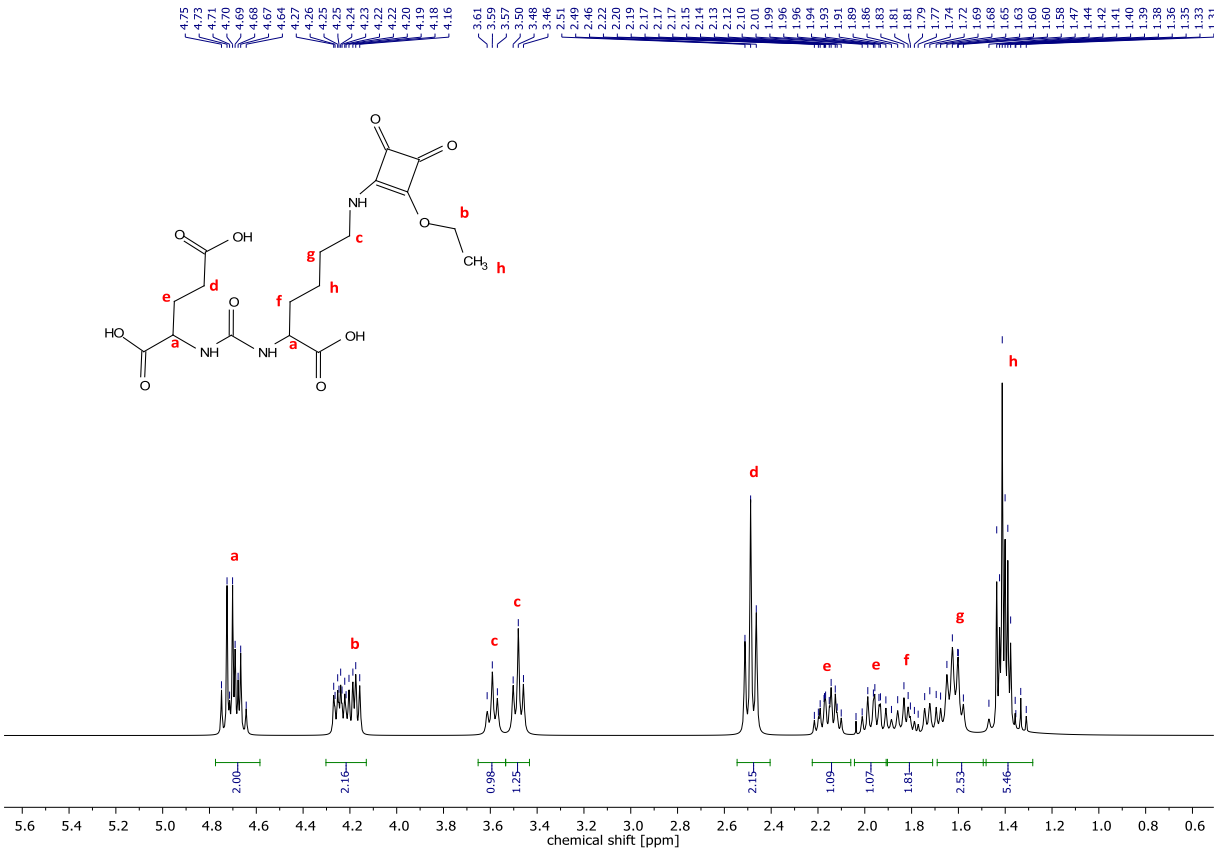

SI-Figure 8: ^{1}H NMR spectrum (300 MHz, D_2O) of KuE.SA.

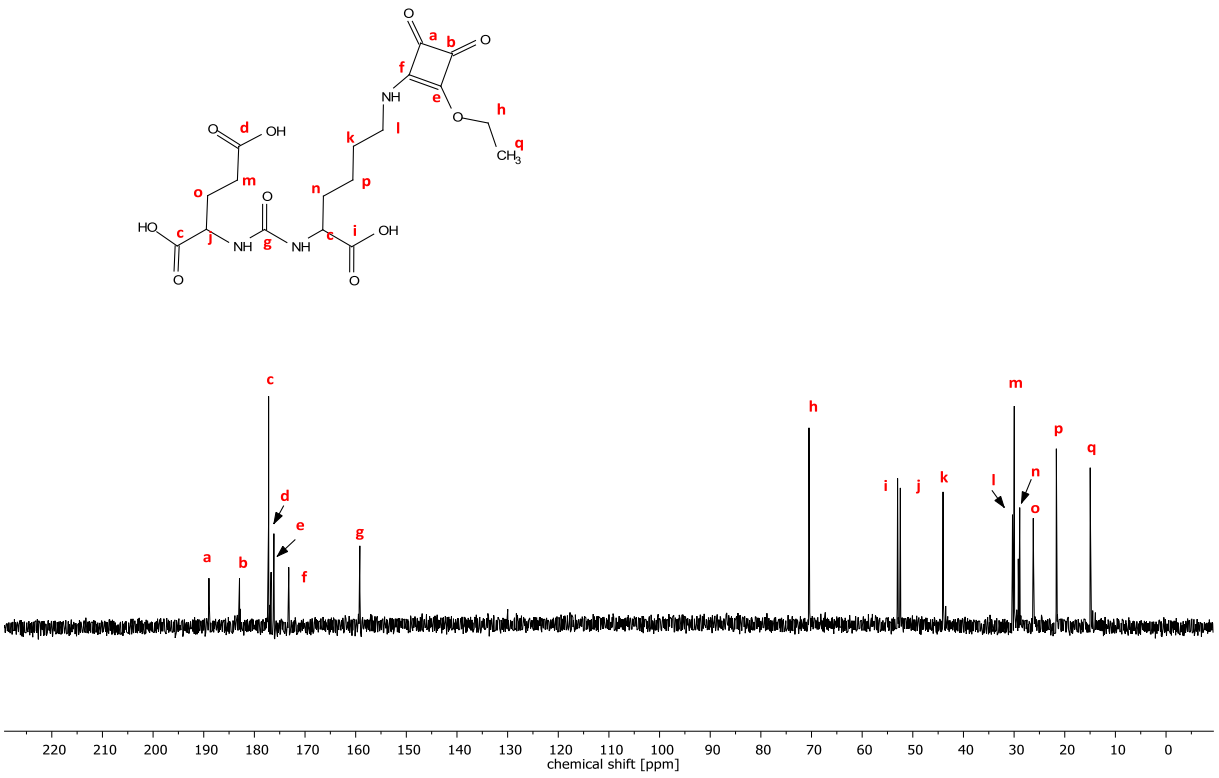

SI-Figure 9: ^{13}C NMR spectrum (300 MHz, D_2O) of KuE.SA.

Synthesis of 2-Azidoethylamine

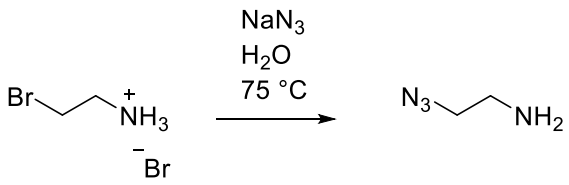

SI-Scheme 8: Synthesis route of 2-Azidoethylamine.

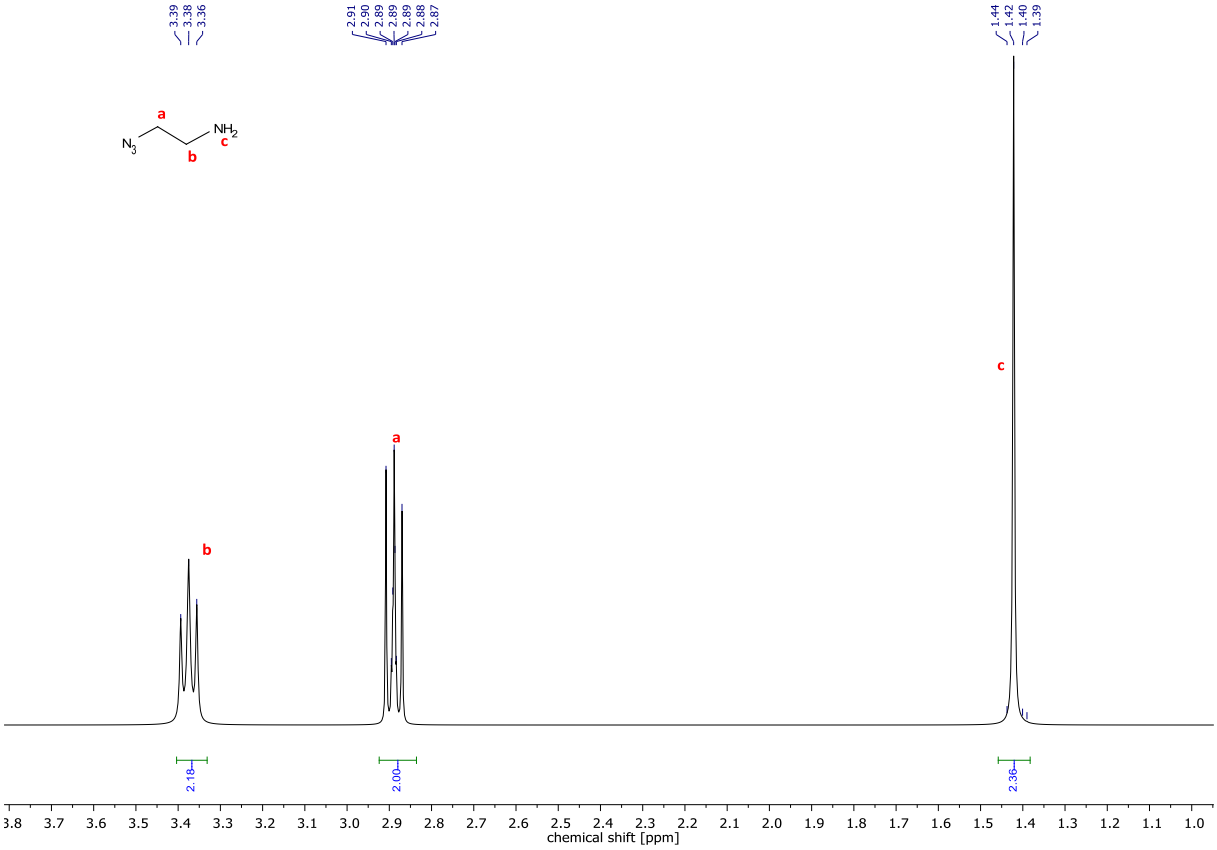

SI-Figure 10: ^{1}H NMR spectrum (300 MHz, $CDCl_3$) of 2-Azidoethylamine.

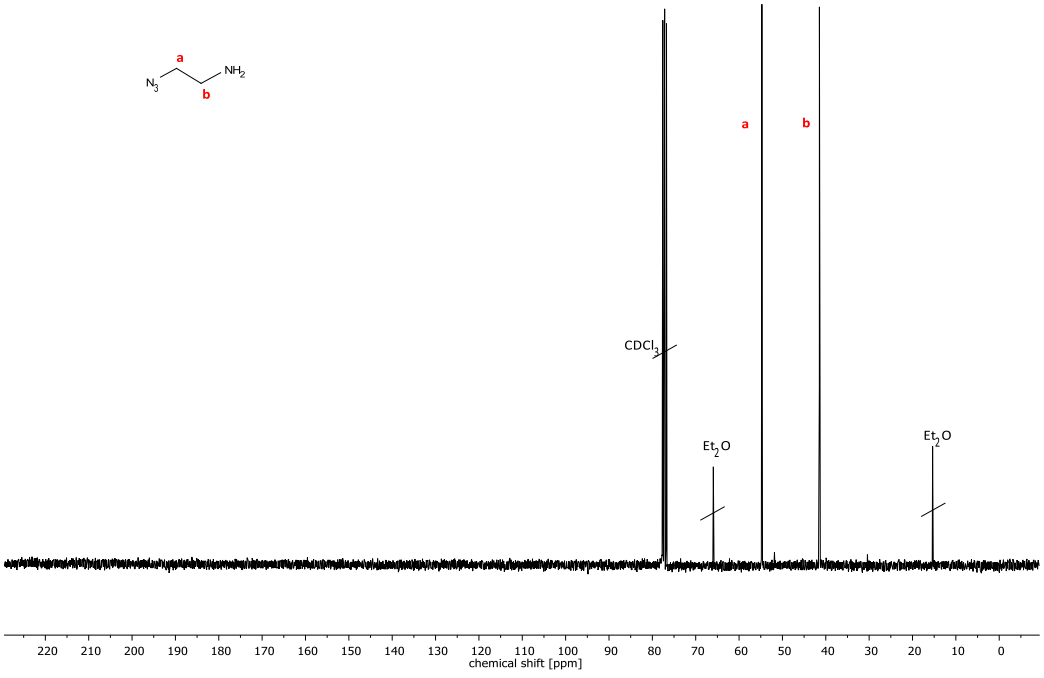

SI-Figure 11: ^{13}C NMR spectrum (300 MHz, $CDCl_3$) of 2-Azidoethylamine.

Synthesis of 2-(3-(5-((2-((2-azidoethyl)amino)-3,4-dioxocyclobut-1-en-1-yl)amino)-1-carboxypentyl)ureido)pentanedioic acid (KuE.SA.N₃)

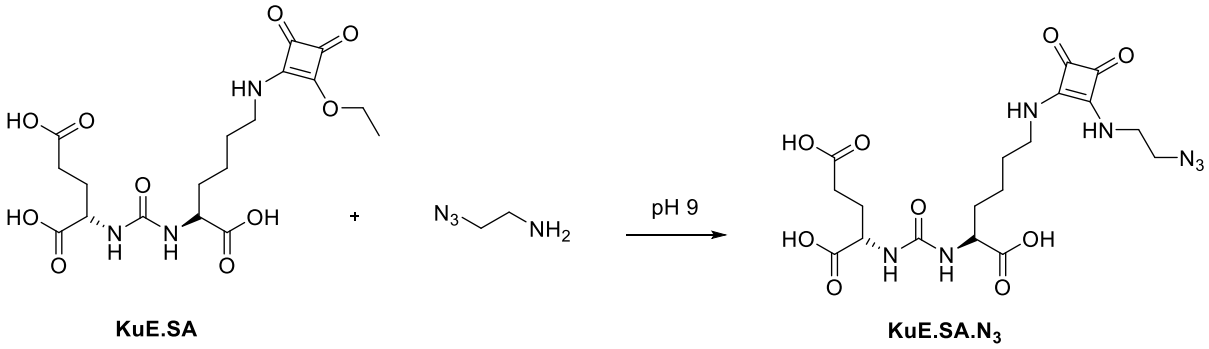

SI-Scheme 9: Synthesis route of KuE.SA.N₃.

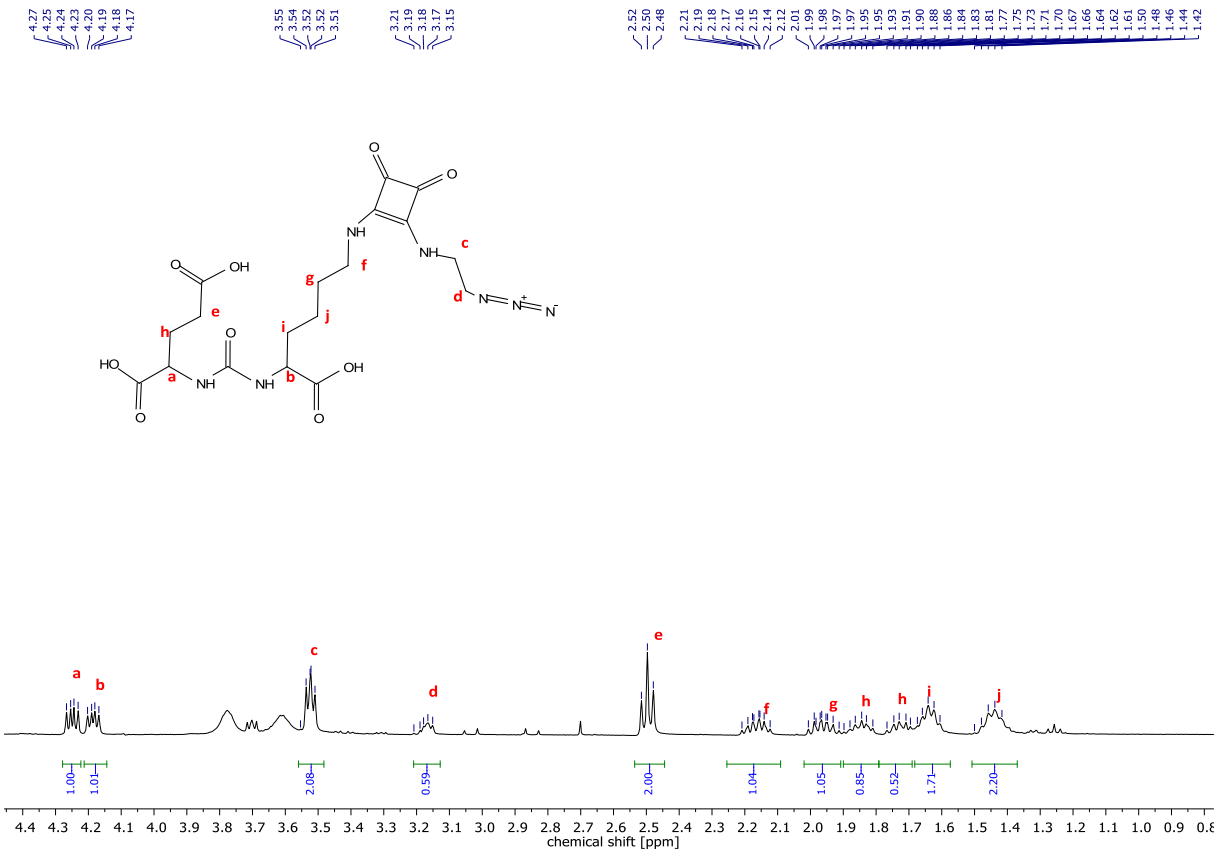

SI-Figure 12: ^{1}H NMR spectrum (400 MHz, D_2O) of KuE.SA.N₃.

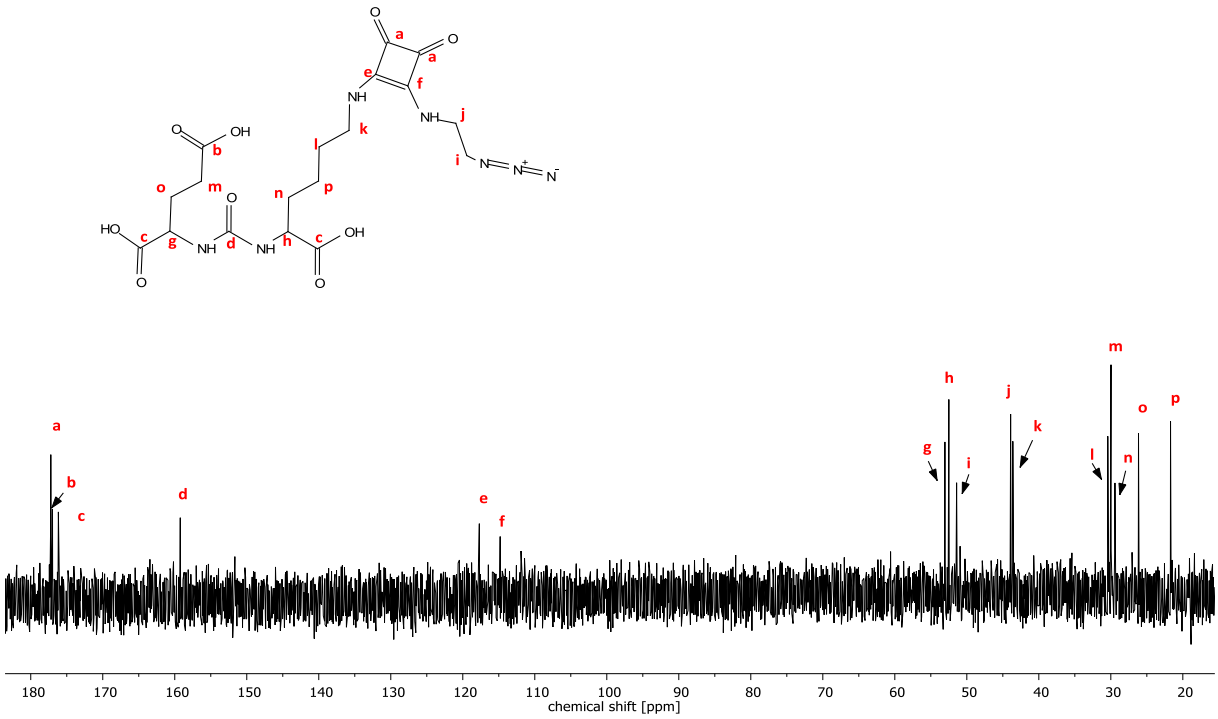

SI-Figure 13: ^{13}C NMR spectrum (400 MHz, D_2O) of KuE.SA.N_3.

Synthesis of the KuE.SA.triazolyl-BisHD-hbPG

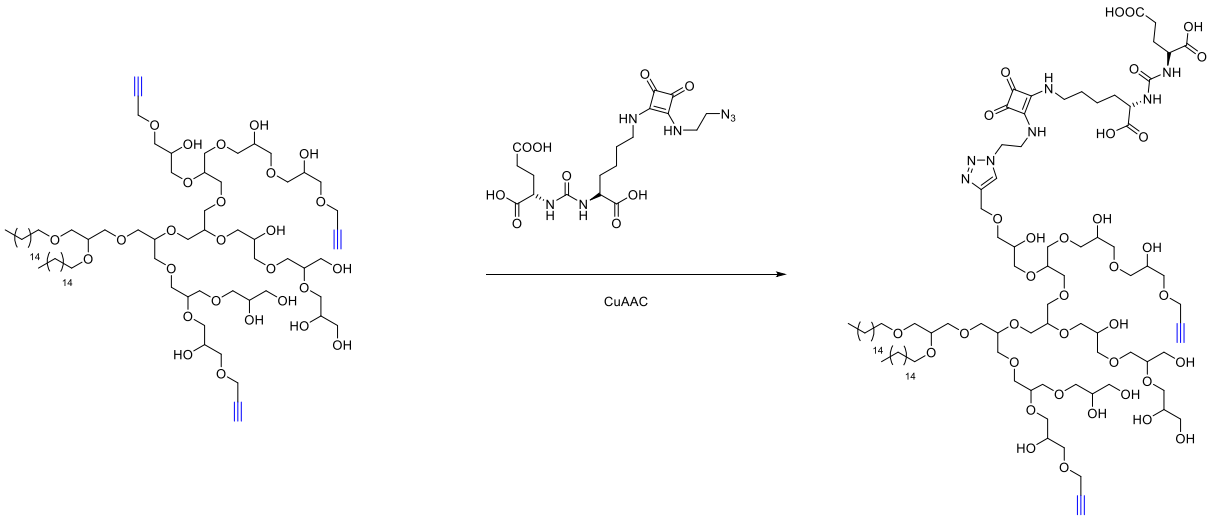

SI-Scheme 10: Synthesis of the KuE.SA.triazolyl-BisHD-*hb*PG.

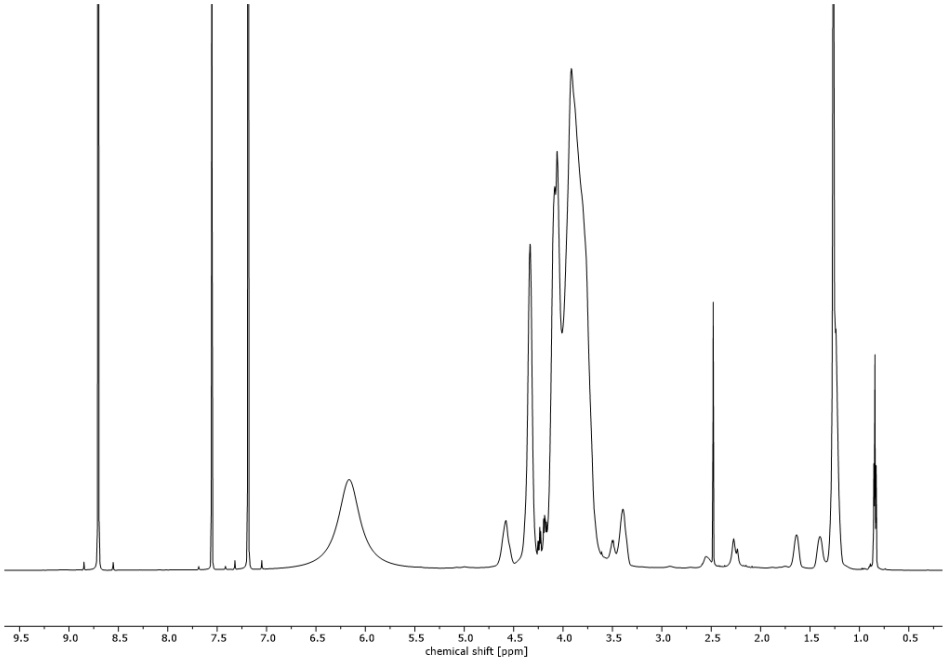

SI-Figure 14: ^{1}H NMR spectrum (600 MHz, pyridine-d_5) of the KuE.SA.triazolyl-BisHD-*hb*PG.

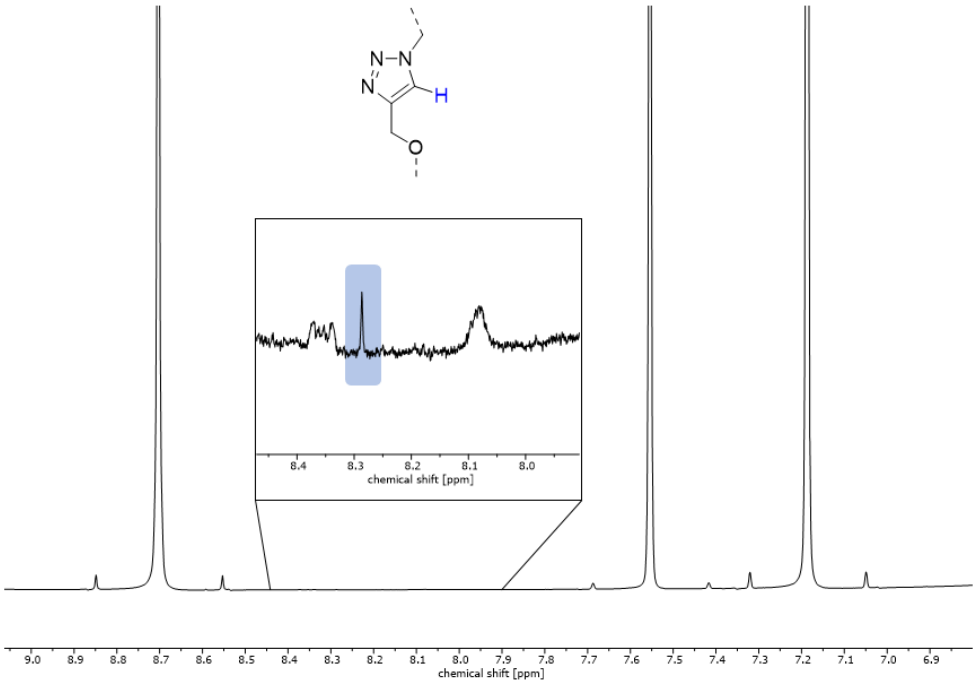

SI-Figure 15: Zoom-in ^{1}H NMR spectrum (600 MHz, pyridine-d_5) of the KuE.SA.triazolyl-BisHD-*hb*PG.

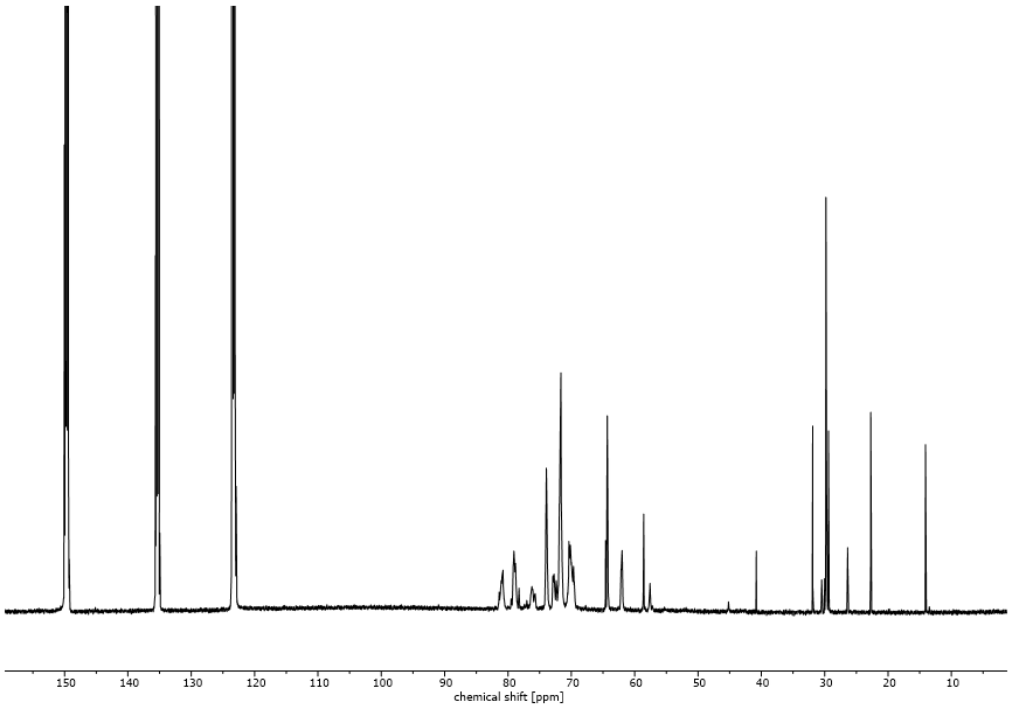

SI-Figure 16: ^{13}C NMR spectrum (151 MHz, pyridine-d_5) of the KuE.SA.triazolyl-BisHD-*hb*PG.

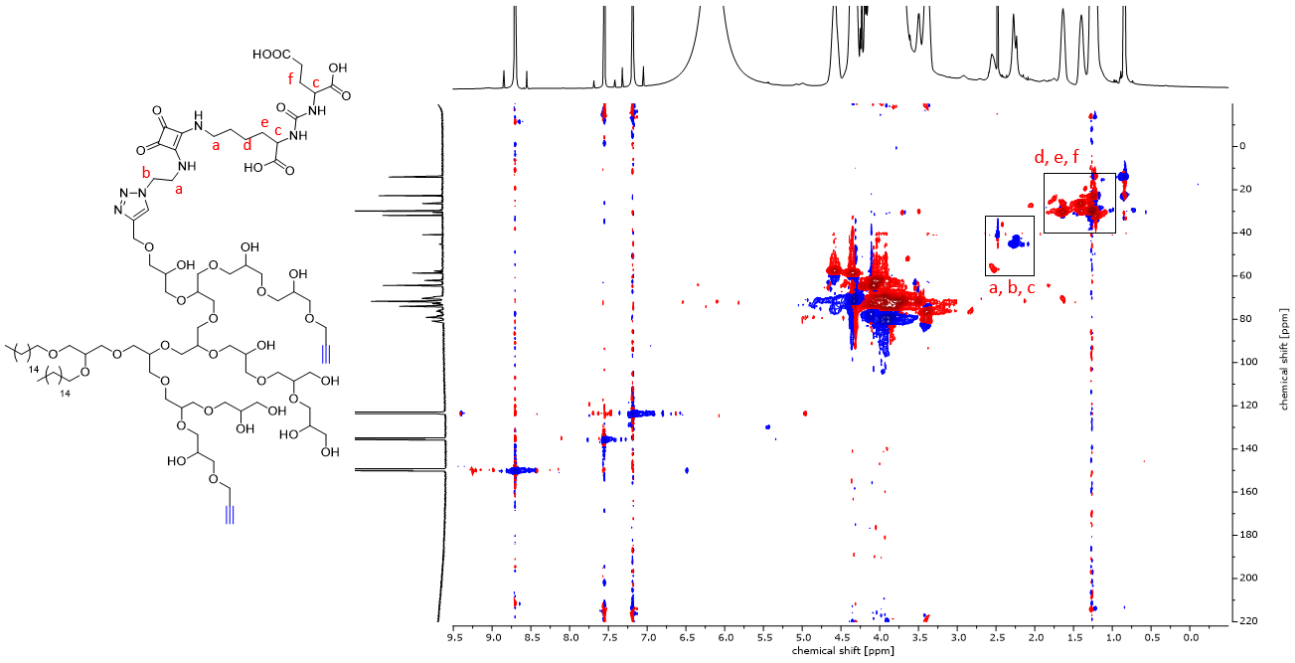

SI-Figure 17: ^{1}H, ^{13}C HSQC NMR spectrum (600 MHz, pyridine-d_5) of the KuE.SA.triazolyl-BisHD-*hb*PG.

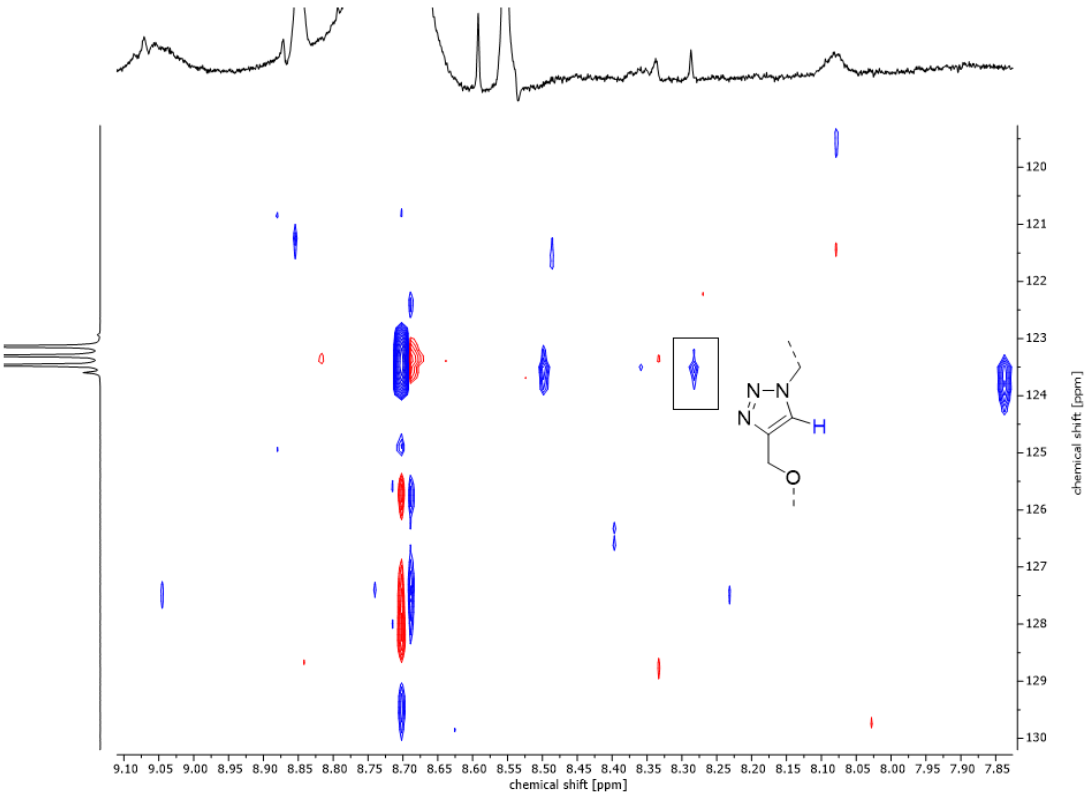

SI-Figure 18: Zoom-in ^{1}H, ^{13}C HSQC NMR spectrum (600 MHz, pyridine-d_5) of the KuE.SA.triazolyl-BisHD-*hb*PG.

3.1.5.4 SEC elugram of the ^{18}F-labeled BisHD-hbPG-KuE.SA liposomes

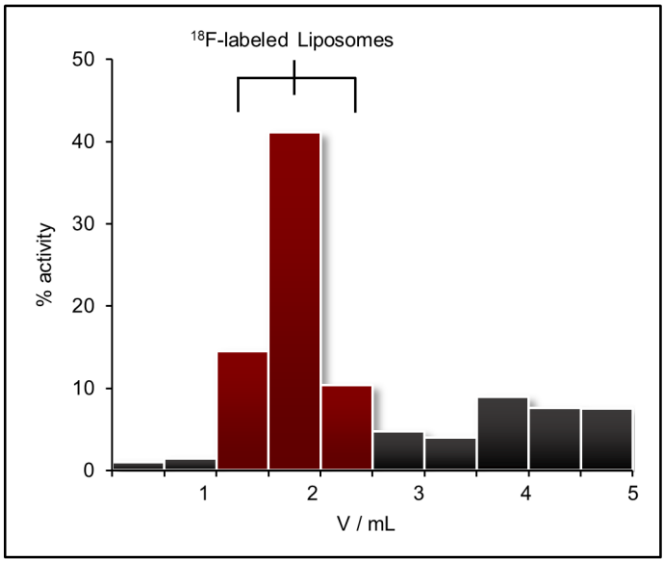

SI-Figure 19: SEC elugram displaying the distribution of radioactivity in consecutive fractions of 0.5 mL PBS during purification of ^{18}F-labeled BisHD-*hb*PG-KuE.SA liposomes.

3.1.5.5 DLS measurement

SI-Table 1: DLS measurement data of the liposomes BisHD-*hb*PG-alkyne and BisHD-*hb*PG-KuE.SA.

Sample	*Z-Average*[a] d.nm	*Size*[a] d.nm	*Intensity*[a] %	*PDI*[a]
BisHD-*hb*PG-alkyne liposomes	144.9	157.5	100	0.071
BisHD-*hb*PG-KuE.SA liposomes	167.4	199.1	100	0.206

[a] Determined by DLS via Zetasizer.

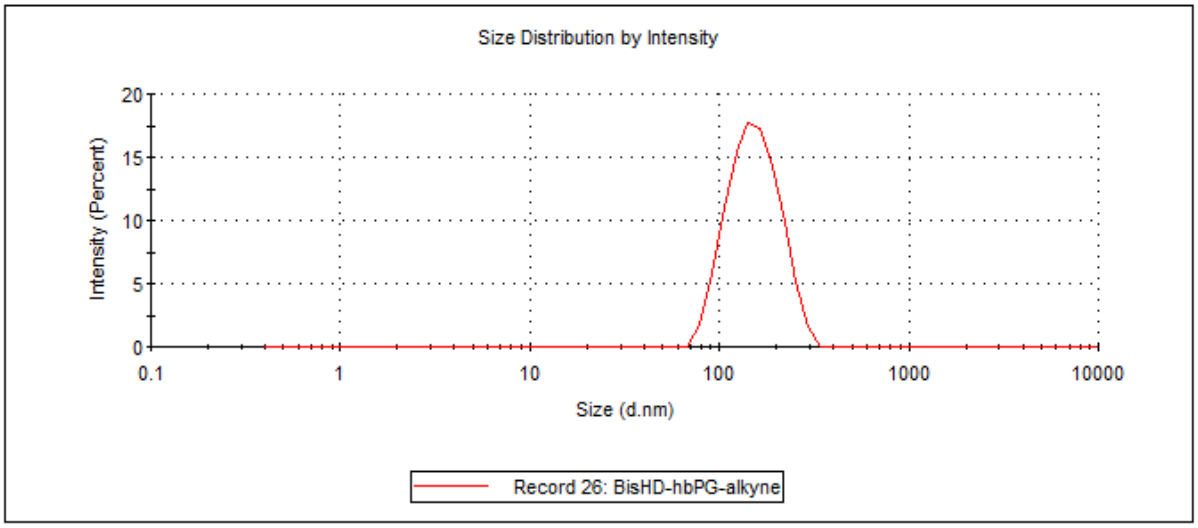

SI-Figure 20: DLS measurement of the liposomes BisHD-*hb*PG-alkyne.

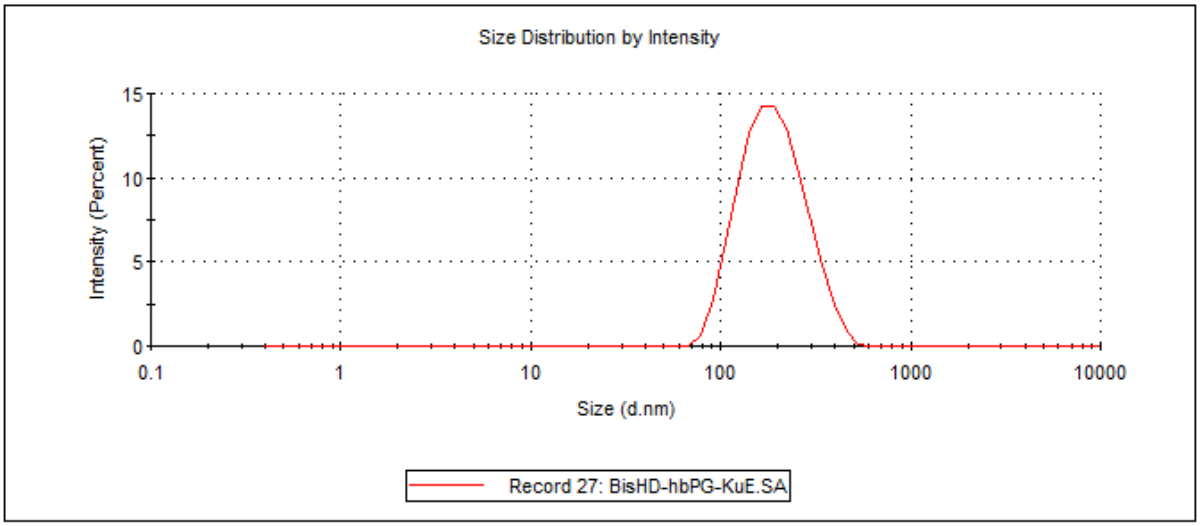

SI-Figure 21: DLS measurement of the liposomes BisHD-*hb*PG-KuE.SA.

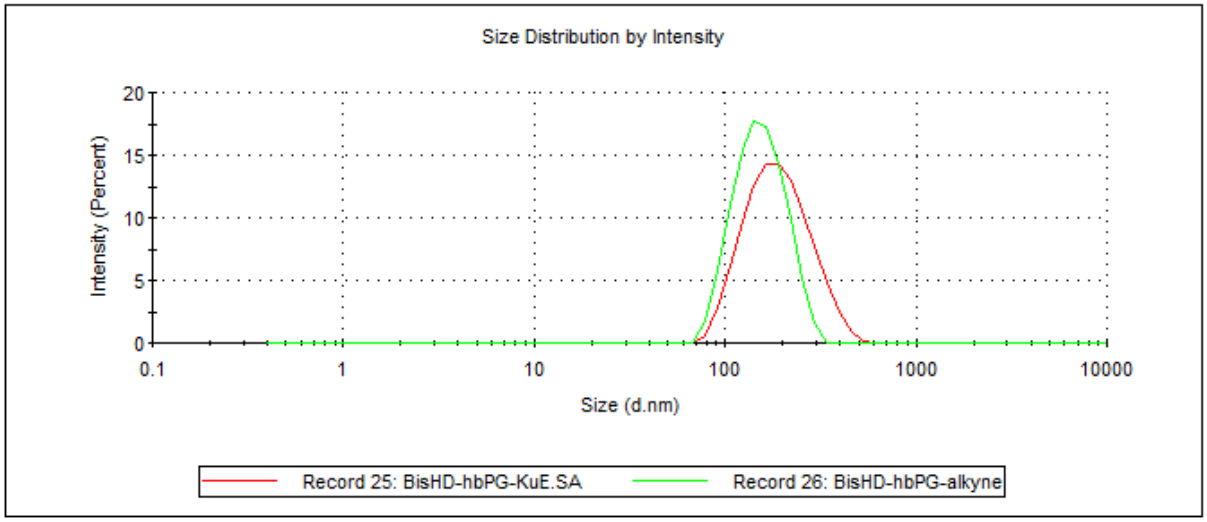

SI-Figure 22: Overlay of the DLS measurements of the liposomes BisHD-*hb*PG-alkyne (green) and BisHD-*hb*PG-KuE.SA (red).

4 Thiazolidine Functional Polyethers

4.1 Thiazolidine-based Glycidyl Ethers for the Anionic Ring-Opening Polymerization

Eyleen Becker,[1] [redacted],[1] [redacted],[1] [redacted],[2] [redacted],[2,*] [redacted][1,*]

[1]Department of Chemistry, Johannes Gutenberg University Mainz, Duesbergweg 10-14, 55128 Mainz, Germany

[2]Institute of Pharmacy and Biochemistry, Johannes Gutenberg University Mainz, Staudingerweg 5, 55128 Mainz, Germany

*E-Mail: [redacted], [redacted]

to be submitted

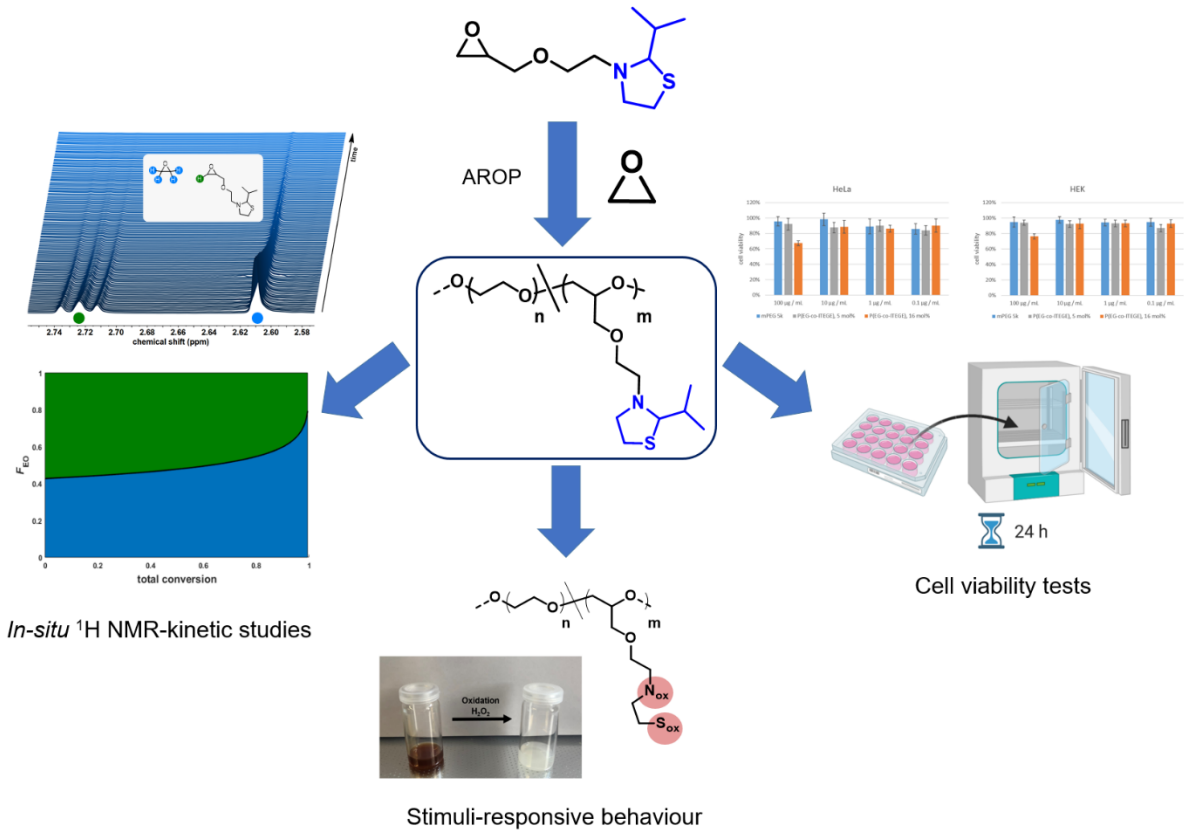

Abstract

Poly(ethylene glycol) (PEG) is a commonly used polymer for a wide variety of applications. In this work, the synthesis route for a new glycidyl ether monomer based on the structure of thiazolidine derivatives is described to prepare well-defined, multifunctional PEGs with stimuli-responsive moieties in the side chains. The thiazolidine ethanol derivatives used as precursors for the preparation of glycidyl ethers were used as initiators for the polymerization of ethylene oxide (EO) to study the stability of the compounds under the conditions of the anionic ring-opening polymerization (AROP).

Both homopolymers and statistical copolymers with different amounts of thiazolidine moieties and EO were obtained *via* anionic ring-opening polymerization with comparable molecular weights of approx. 5000 g/mol. The microstructure of the copolymers was studied by *in situ* ^{1}H NMR kinetics and showed a random monomer distribution (reactivity ratios: r_{EO} = 0.74 ± 0.00 and r_{TEGE} = 1.34 ± 0.00). The responsive properties of the copolymers were investigated using the example of oxidation by hydrogen peroxide solution *via* NMR spectroscopy and SEC measurements. To verify the application in biological or medical systems, toxicity tests were performed by MTT assays.

4.1.1 Introduction

Polyethylene glycol (PEG) is a versatile material that is used in numerous pharmaceutical and medical applications, due to its good water solubility, low toxicity, immunogenicity. Its shielding properties are exploited in nanomedicine, generally known as the "stealth" effect of PEGylated therapeutics.[1,2] In addition to the advantageous properties, however, there is one significant disadvantage: the low functionality.[3,4] Only the polymer terminus can be used for further functionalization. However, this problem can be counteracted by using other epoxide monomers with functional groups that can be designed as required. By copolymerizing these epoxide monomers with ethylene oxide (EO) *via* anionic ring-opening polymerization (AROP), tailored, narrowly distributed, multifunctional polymers can be prepared. Of particular interest for the selection of epoxide monomers are systems that can vary their properties by a stimulus. From a biological point of view possible stimuli can be divided into two classes: physiological stimuli, such as pH values, redox processes, enzymatic activities, electrolyte and monosaccharide concentrations, and external physical stimuli, such as light, electromagnetic fields, mechanical forces and ultrasound.[5,6]

In particular, pH-responsive polymers are of significant interest, because pH values can vary widely within the body. These range extends from the acidic environment in the stomach (pH = 2) to basic pH values in the intestine (pH = 5-8), which must be taken into account especially for the oral administration of active ingredients.[7] In contrast, the pH differences of different tissue structures and cellular compartments are much smaller. For example, the extracellular pH of tumor tissue and inflammatory tissue (pH = 6.5-7.2) is minimally lower than in healthy tissue and blood (pH ~ 7.4).[7–9] In the endosome (pH = 5.0-6.5) and lysosome (pH = 4.5-5.0), pH is even lower.[10,11] Physiological pH gradients render pH-responsive polymers promising candidates for the use in biomedical applications.[12]

pH-responsive and ionizable polymers possess acidic functional groups, such as carboxylic or sulfonic acid groups and/or basic groups such as primary, secondary or tertiary amines.[5,13,14] The change in pH leads to ionization (protonation or deprotonation) of the pH-sensitive group, commonly resulting in drastic changes in the solubility of the respective polymers.

The use of tertiary amines as pH-responsive moieties is well established in (meth)acrylate based polymers and is widely used in pharmaceutical technology, for instance in case of Eudragit® used to control the release of drugs.[15,16] Although there is a variety of different structures in this field, tertiary amines are underrepresented in the field of functional polyethers.[17–19] Only a few groups have already addressed the use of polyethers with tertiary amines for the synthesis of pH-responsive copolymers with ethylene oxide (EO).[20–23] For example, Lynd *et al.* introduced statistical copolymers with *N,N*-diisopropylamine units as a promising possibility for pH-responsive systems.[24] Furthermore, glycidyl amines are known for the AROP with EO, but they differ from glycidyl ether amines not only structurally, but mainly with regard to the reactivity ratios. For this reason, glycidyl amines form in most cases a tapered microstructure in copolymerizations with EO, whereas glycidyl ether amines show a random monomer distribution in copolymerizations with EO.[22]

As already mentioned, redox processes can also act as a stimulus on polymers and have led to an important class of polymers besides pH-responsive systems. Similar to the different pH ranges in the body, there are naturally occurring redox processes, which can also be used as a stimulus. Both oxidative and reductive processes are possible. Oxidative processes occur in the extracellular fluid, inflamed tissue and tumor tissue, whereas reductive processes occur in the cell.[25] An example of an oxidation-responsive system is the triblock copolymer PEG-PPS-PEG, consisting of PEG-polypropylene sulfide (PPS). Oxidizing substances such as hydrogen peroxide (H_2O_2), e.g. from a glucose-oxidase/glucose-oxygen system, oxidize the hydrophobic PPS core and convert it into hydrophilic polysulfoxides and polysulfones. Due to the oxidation, a change in the properties of the polymer takes place.[26]

An epoxide monomer with a thioether group was introduced by our group in previous work.[27] This monomer was copolymerized with EO to prepare thioether functional PEGs. These could subsequently be used as oxidation-responsive systems.

In this work, we present the development of an epoxide monomer, that combines the beneficial properties of tertiary amines and thioethers in one molecule. To incorporate both functionalities into a glycidyl ether, the synthesis was based on thiazolidine derivatives. Various thiazolidine derivatives were synthesized and these were converted to thiazolidine alcohols. To test the stability of the thiazolidine ring of the different derivatives under the

conditions of AROP, the thiazolidine alcohols were used as initiators for the polymerization of EO. In the process, a suitable candidate for the synthesis of a glycidyl ether was found. After successful synthesis of the thiazolidine-based glycidyl ether 2-isopropylthiazolidine ethyl glycidyl ether (ITEGE), it was copolymerized with EO to produce thiazolidine-functional PEGs and also the homopolymer. The monomer sequence statistics of the copolymers was investigated by *in situ* ^{1}H NMR kinetics. Furthermore, the toxicity was investigated by cell viability studies.

4.1.2 Experimental part

Terminology

The thiazolidine derivatives employed are 2,2-dimethylthiazolidine (DMT), 2-isopropyl–thiazolidine (IT) and 2-(*tert*-butyl)thiazolidine (TBT). They were used for the synthesis of the 2-alkylthiazolidine ethanol derivatives 2-(2,2-dimethylthiazolidin-3-yl)ethan-1-ol (DMTOH), 2-(2-isopropylthiazolidin-3-yl)ethan-1-ol (ITOH), 2-(2-(*tert*-butyl)thiazolidin-3-yl)ethan-1-ol and thiazolidine for the synthesis of 2-(thiazolidin-3-yl)ethan-1-ol (TOH). TOH and ITOH were used for the synthesis of the 2-alkylthiazolidine ethyl glycidyl ethers: thiazolidine ethyl glycidyl ether (TEGE) and 2-isopropylthiazolidine ethyl glycidyl ether (ITEGE). Copolymers with ethylene oxide (EO) and ITEGE prepared *via* anionic ring-opening polymerization (AROP) are named P(EG-*co*-ITEGE), the homopolymer is named P(ITEGE).

Instrumentation

^{1}H NMR (300 MHz), ^{13}C NMR (75 MHz) and 2D spectra were recorded on a Bruker Avance III HD 300 (5 mm BBFO-Probe with z-Gradient and ATM). ^{1}H NMR (400 MHz), ^{13}C NMR (100 MHz), ^{31}P NMR (121.5 MHz) and 2D spectra were measured on a Bruker Avance II 400 MHz (5 mm BBFO-Probe Z-gradient and ATM, SampleXPress 60 auto sampler). The chemical shifts were internally referred to residual proton signals of the deuterated solvent.

Size exclusion chromatography (SEC) was performed at 50 °C in *N,N*-dimethylformamide (with 1 g/L lithium bromide added) as eluent on an Agilent 1,100 Series equipped with Polymer Standards Service (PSS) HEMA columns with 300/100/40 Å porosity and a RI

detector. The determination of the molecular weights was determined by a calibration with poly(ethylene glycol) standards by PSS.

Differential scanning calorimetry (DSC) measurements were carried out under a nitrogen atmosphere using a Perkin Elmer DSC 8,500 in the temperature range of -95 °C to 100 °C, with heating rates of 20 °C/min for the first and 10 °C/min for the second heating run.

Cell viability studies (MTT assays) were measured using a Spark 10M plate reader from the Tecan group.

Materials

All solvents and reagents were purchased generally from the suppliers Acros Organics, Tokyo Chemical Industry (TCI), Sigma-Aldrich, Fluka, Fisher Scientific, Alfa Aesar and were used as received unless otherwise stated. Deuterated solvents were purchased from Deutero GmbH. Dialysis membranes (regenerated cellulose, MWCO = 1000 g/mol) were purchased from Orange Scientific. HeLa and HEK293 cell lines were purchased from DSMZ.

Synthesis procedure

Synthesis of 2-Alkylthiazolidines

All thiazolidine derivatives were prepared analogously according to a synthesis procedure by Shibamoto *et al.*[28]

The synthesis procedure is described as a representative example for the preparation of 2-isopropylthiazolidine (IT) with isobutyraldehyde as carbonyl component.

In a round bottom flask, cysteamine hydrochloride (30.0 g, 0.26 mol, 1 eq.) was dissolved in water (300 mL). Isobutyraldehyde (19.0 g, 0.26 mol, 24.1 mL, 1 eq.) was then added and the solution was stirred for 24 hours at room temperature. After 24 hours, a cold K_2CO_3-solution (0.28 g/mL, 200 mL) was added to the reaction solution. The organic phase was extracted with dichloromethane (3x100 mL), dried with $MgSO_4$ and the organic solvent was evaporated. The colorless oil was used without further workup (yield: 28.87 g, 0.22 mol, 85 %).

^{1}H NMR (400 MHz, chloroform-*d*) δ[ppm] = 4.30 (d, *J* = 7.5 Hz, 1H, NH-C*H*-S), 3.63 – 3.49 (m, 1H, NH-C*H*$_2$-CH$_2$-S), 3.03 – 2.91 (m, 2H, NH-C*H*$_2$-CH$_2$-S, NH-CH$_2$-C*H*$_2$-S), 2.83 – 2.74 (m, 1H, NH-CH$_2$-C*H*$_2$-S), 1.98 – 1.84 (m, 1H, CH$_3$-C*H*-CH$_3$), 1.60 (s, 1H, -N*H*), 1.08 (dd, *J* = 18.1, 6.7 Hz, 6H, C*H*$_3$).

^{13}C NMR (101 MHz, Chloroform-*d*) δ= 79.16 (1C, NH-*C*H-S), 52.61 (1C, NH-*C*H$_2$-CH$_2$-S), 34.82 (1C, NH-CH$_2$-*C*H$_2$-S), 34.07 (1C, CH$_3$-*C*H-CH$_3$), 20.80 (1C, *C*H$_3$), 20.46 (1C, *C*H$_3$).

Synthesis of 2-Alkylthiazolidine ethanol

All thiazolidine ethanol derivatives were prepared according to literature.[29]

The synthesis procedure is described as a representative example for the preparation of 2-(2-isopropylthiazolidin-3-yl)ethan-1-ol (ITOH).

In a three-necked flask equipped with a Dimroth condenser, dropping funnel and stirrer, *N,N*-Diisopropylethylamine (59.09 g, 0.46 mol, 60.30 mL, 1.5 eq.) was placed in dry chloroform (300 mL) under argon atmosphere. 2-Isopropylthiazolidine (40.00 g, 0.30 mol, 1 eq.) was added to the solution *via* dropping funnel with stirring. The solution was stirred for 30 min at room temperature. Bromoethanol (49.51 g, 0.40 mol, 28.13 mL, 1.3 eq.) was added and the solution was heated at 50 °C for 5 days. The organic solvent was removed in vacuo, the residue was taken up in ethyl acetate, the resulting salt was filtered off and the residue was extracted with saturated NaHCO$_3$-solution. The solvent was evaporated from the crude product and the final purification was carried out by fractional distillation (b.p.=86 °C, 0.001 mbar). The product was obtained as a colorless liquid (yield: 25.50 g, 0.15 mol, 50 %).

^{1}H NMR (400 MHz, chloroform-*d*) δ [ppm] = 3.86 (d, *J* = 9.7 Hz, 1H, N-C*H*-S), 3.65 (dt, *J* = 9.6, 4.2 Hz, 2H, OH-C*H*$_2$-CH$_2$), 3.24 (dddd, *J* = 12.3, 5.8, 2.1, 0.9 Hz, 1H, N-C*H*$_2$-CH$_2$-S), 3.08 – 2.98 (m, 1H, N-C*H*$_2$-CH$_2$-S), 2.97 – 2.84 (m, 2H, N-CH$_2$-C*H*$_2$-S), 2.64 – 2.57 (m, 1H, OH-CH$_2$-C*H*$_2$), 2.56 – 2.48 (m, 1H, OH-CH$_2$-C*H*$_2$), 1.71 – 1.60 (m, 1H, CH$_3$-C*H*-CH$_3$), 1.01 (dd, *J* = 21.3, 6.6 Hz, 6H, C*H*$_3$).

^{13}C NMR (101 MHz, chloroform-*d*) δ [ppm] = 83.91 (1C, N-*C*H-S), 60.22 (1C, OH-*C*H$_2$-CH$_2$), 56.73 (1C, OH-CH$_2$-*C*H$_2$), 55.99 (1C, N-*C*H$_2$-CH$_2$-S), 35.59 (1C, CH$_3$-*C*H-CH$_3$), 30.79 (1C, N-CH$_2$-*C*H$_2$-S), 20.75 (1C, *C*H$_3$), 20.15 (1C, *C*H$_3$).

Synthesis of 2-Alkylthiazolidine ethyl glycidyl ether

All thiazolidine ethyl glycidyl ether derivatives were prepared in slightly modified form *via* phase transfer catalysis.[30]

The synthesis procedure is described as a representative example for the preparation of 2-isopropylthiazolidine ethyl glycidyl ether (ITEGE).

Isopropylthiazoldine ethanol (10.00 g, 57.00 mmol, 1 eq.) was added to a mixture of 50 % aqueous NaOH solution (150 mL) and benzene (150 mL) in a three-necked flask with dropping funnel and electric stirrer. The phase transfer catalyst Tetrabutylammonium hydrogen sulfate (TBAHS) (1.94 g, 5.70 mmol, 0.1 eq.) was added to this solution with rapid stirring. The reaction mixture was cooled to 0 °C and epichlorohydrin (15.83 g, 171.10 mmol, 13.40 mL, 3 eq.) was slowly added *via* dropping funnel. The reaction was stirred at room temperature until no alcohol was detectable *via* TLC (approximately 5 hours reaction time). After the reaction time, benzene (150 mL) was added to the solution, the solid was filtered off, and the organic phase was extracted with brine. The combined organic phases were dried over NaSO$_4$ and the solvent was removed in vacuo. The final purification was performed by fractional distillation in high vacuum (b.p.=98 °C, 0.001 mbar). The product was obtained as a colorless, viscous liquid (yield: 7.25 g, 31.34 mmol, 55 %).

^{1}H NMR (300 MHz, chloroform-*d*) δ [ppm] = 3.95 (d, *J* = 9.8 Hz, 1H, N-C*H*-S), 3.80 (dd, *J* = 11.6, 2.9 Hz, 1H, O-CH-C*H$_2$*-O), 3.74 – 3.54 (m, 2H, O-C*H$_2$*-CH$_2$), 3.47 – 3.36 (m, 1H, O-CH-C*H$_2$*-O), 3.32 – 3.21 (m, 1H, N-C*H$_2$*-CH$_2$-S), 3.21 – 3.12 (m, 1H, O-C*H*-CH$_2$), 3.10 – 2.97 (m, 1H, N-C*H$_2$*-CH$_2$-S), 2.88 (dd, *J* = 10.1, 3.1 Hz, 2H, N-CH$_2$-C*H$_2$*-S), 2.81 (t, *J* = 4.6 Hz, 1H, O-C*H$_2$*-CH), 2.66 – 2.51 (m, 3H, O-C*H$_2$*-CH, O-CH$_2$-C*H$_2$*), 1.70 – 1.53 (m, 1H, CH$_3$-C*H*-CH$_3$), 1.07 – 0.93 (m, 6H, C*H$_3$*).

^{13}C NMR (75 MHz, chloroform-*d*) δ [ppm] = 84.87 (1C, N-*C*H-S), 71.87 (1C, O-CH-*C*H$_2$-O), 71.78 (1C, O-CH-*C*H$_2$-O), 70.99 (1C, O-*C*H$_2$-CH$_2$), 56.89 (1C, N-*C*H$_2$-CH$_2$-S), 53.95 (1C, O-CH$_2$-*C*H$_2$), 53.93(1C, O-CH$_2$-*C*H$_2$), 50.86 (1C, O-*C*H-CH$_2$), 50.84 (1C, O-*C*H-CH$_2$), 44.23 (1C,

O-*C*H$_2$-CH), 44.18 (1C, O-*C*H$_2$-CH), 35.36 (1C, CH$_3$-*C*H-CH$_3$), 30.91 (1C, N-CH$_2$-*C*H$_2$-S), 20.96 (1C, *C*H$_3$), 20.19 (1C, *C*H$_3$).

Synthesis of 2-alkylthiazolidine ethanol initiated PEG polymers

The polymerization of ethylene oxide (EO) using the 2-alkylthiazolidine ethanol derivatives as initiators was performed based on literature for other glycidyl ethers with adjusted reaction procedure.[30]

The synthesis is described for IT-PEG$_{117}$ with 2-(2-isopropylthiazolidin-3-yl)ethan-1-ol (ITOH) as initiator as a representative example. All other samples were synthesized in the same fashion.

In a dry flask the initiator ITOH (68.00 mg, 0.39 mmol, 1 eq.) and CsOH mono hydrate (59.00 mg, 0.35 mmol, 0.9 eq.) were dissolved in benzene (5 mL) and dry THF (5 mL), stirred under slightly reduced pressure at 50 °C for 30 minutes and subsequently dried in high vacuum for 16 hours. The resulting initiator salt was dissolved in dry DMSO (6 mL), and the flask was cooled to -80 °C with an ethanol/nitrogen cooling bath. Ethylene oxide (1.94 g, 44.10 mmol, 2.00 mL, 113 eq.) was condensed *via* a graduated ampule into the flask. The reaction mixture was stirred in vacuo at room temperature for 48 hours. Subsequently, methanol (1 mL) was added, and the flask was flushed with argon. The resulting polymer IT-PEG$_{117}$ was precipitated three times in a mixture of diethyl ether/acetone (70:30 vol%) and separated *via* centrifuge. The polymer was dried under reduced pressure at room temperature for 24 hours (yield: 90 %).

^{1}H NMR (300 MHz, DMSO-d_6) δ [ppm] = 3.82 (d, *J* = 5.0 Hz, 1H, N-C*H*-S), 3.51 (s, 469H, backbone, N-CH$_2$-C*H$_2$*-O), 3.16 – 3.02 (m, 1H, N-C*H$_2$*-CH$_2$-S), 2.74 – 2.57 (m, 5H, N-C*H$_2$*-CH$_2$-S, N-CH$_2$-C*H$_2$*-S, N-C*H$_2$*-CH$_2$-O), 1.70 – 1.54 (m, 1H, CH$_3$-C*H*-CH$_3$), 0.85 (dd, *J* = 12.1, 6.8 Hz, 6H, C*H$_3$*).

^{13}C NMR (75 MHz, DMSO-d_6) δ [ppm] = 100.73 (1C, N-*C*H-S), 72.81, 70.95 – 70.01 (234C, backbone), 64.33 (1C, N-CH$_2$-*C*H$_2$-O), 60.66 (1C, *C*H$_2$-OH), 54.68 (1C, N-*C*H$_2$-CH$_2$-O), 52.09 (1C, N-*C*H$_2$-CH$_2$-S), 31.62, 31.39 (2C, CH$_3$-*C*H-CH$_3$, N-CH$_2$-*C*H$_2$-S) 19.17 (1C, *C*H$_3$), 16.96 (1C, *C*H$_3$).

Synthesis of P(ITEGE) homopolymer

In a dry Schlenk flask the initiator 2-(benzyloxy)ethanol (9.00 mg, 0.06 mmol, 1 eq.) and CsOH mono hydrate (8.00 mg, 0.05 mmol, 0.8 eq.) were dissolved in benzene (5 mL) and stirred under slightly reduced pressure at 50 °C for 30 minutes and subsequently dried in high vacuum for 16 hours. The monomer was dried over CaH_2. The initiator salt was dissolved in dry DMSO (3 mL) and the monomer ITEGE (1.73 mmol, 400.24 mg, 28 eq.) was added to the solution. The solution was stirred and heated to 40 °C for 3 days. Subsequently, methanol (1 mL) was added, and the flask was flushed with argon. The resulting polymer $P(ITEGE)_{29}$ was precipitated three times in a mixture of diethyl ether/acetone (70:30 vol%) and separated *via* centrifuge. The polymer was dried under reduced pressure at room temperature for 24 hours (yield: 90 %).

^{1}H NMR (400 MHz, methylene chloride-d_2) δ [ppm] = 7.36 – 7.22 (m, 5H, H_{arom}), 4.52 (s, 2H, C_{arom}-CH_2-O), 3.89 (d, J = 9.7 Hz, 29H, N-CH-S), 3.78 – 3.35 (m, 203H, backbone, O-CH_2-CH_2-O, O-CH_2-CH_2-N), 3.30 – 3.16 (m, 29H, N-CH_2-CH_2-S), 3.01 – 2.90 (m, 29H, N-CH_2-CH_2-S), 2.87 – 2.74 (m, 58H, N-CH_2-CH_2-S), 2.62 – 2.43 (m, 58H, O-CH_2-CH_2-N), 1.64 – 1.45 (m, 29H, CH_3-CH-CH_3), 1.02 – 0.85 (m, 169H, CH_3).

^{13}C NMR (101 MHz, methylene chloride-d_2) δ [ppm] = 128.27, 127.58 (6C, C_{arom}), 84.88 (1C, N-CH-S), 78.88 (29C, O-CH_2-$C$$H_2$-N), 73.03 (1C, C_{arom}-$C$$H_2$), 72.69 – 69.57 (89C, backbone, O-$C$$H_2$-$C$$H_2$-O), 64.52 (1C, $C$$H_2$-OH), 56.67 (29C, N-$C$$H_2$-$CH_2$-S), 35.45 (29C, CH_3-CH-CH_3), 30.76 (29C, N-CH_2-$C$$H_2$-S), 20.81 (29C, $C$$H_3$), 19.89 (29C, $C$$H_3$).

Synthesis of P(EG-co-ITEGE) copolymers

The polymerization was performed according to a standard procedure for the anionic ring-opening polymerization of glycidyl ethers.[27,31]

The following synthesis refers to $P(EG_{98}$-*co*-$ITEGE_2)$. All other samples were synthesized in the same fashion with varied comonomer equivalents.

In a dry flask the initiator 2-(benzyloxy)ethanol (9.00 mg, 0.06 mmol, 1 eq.) and potassium *tert*-butoxide (10.00 mg, 0.09 mmol, 0.8 eq.) were dissolved in benzene (5 mL) and stirred under slightly reduced pressure at 50 °C for 30 minutes and subsequently dried in high

vacuum for 16 hours. The monomer ITEGE was dried over CaH_2. The initiator salt was dissolved in dry DMSO (5 mL) and the monomer ITEGE (52.00 mg, 0.23 mmol, 2 eq.) were added *via* syringe, and the flask was cooled to -80 °C in an ethanol/nitrogen cooling bath. Ethylene oxide (0.49 g, 11.00 mmol, 0.50 mL, 98 eq.) was condensed *via* a graduated ampule into the flask. The reaction mixture was stirred in vacuo at 50 °C for 48 hours. Subsequently, methanol (1 mL) was added, and the flask was flushed with argon. The resulting polymer P(EG_{98}-$ITEGE_2$) was precipitated three times in a mixture of diethyl ether/acetone (70:30 vol%) and separated *via* centrifuge. Polymers with higher ITEGE contents were purified *via* dialysis against MeOH (MWCO = 1000 g/mol). The polymers were dried under reduced pressure at room temperature for 24 hours (yields: 75-90 %).

^{1}H NMR (400 MHz, methylene chloride-d_2) δ [ppm] = 7.45 – 7.25 (m, 5H, H_{arom}), 4.56 (s, 2H, C_{arom}-CH_2-O), 3.93 (d, J = 9.7 Hz, 2H, N-CH-S), 3.86 – 3.39 (m, 472H, backbone, O-CH_2-CH_2-O, O-CH_2-CH_2-N), 3.31 – 3.20 (m, 2H, N-CH_2-CH_2-S), 3.05 – 2.80 (m, 6H, N-CH_2-CH_2-S), 2.67 – 2.46 (m, 6H, N-CH_2-CH_2-S, O-CH_2-CH_2-N), 1.67 – 1.50 (m, 2H, CH_3-CH-CH_3), 0.98 (dd, J = 29.4, 6.6 Hz, 12H, CH_3).

^{13}C NMR (101 MHz, methylene chloride-d_2) δ [ppm] = 128.24, 127.66 (6C, C_{arom}), 84.87 (2C, N-CH-S), 78.33 (2C, O-CH_2-$C$$H_2$-N), 73.05 (1C, C_{arom}-$C$$H_2$), 72.52 – 69.66 (236C, backbone, O-$C$$H_2$-$C$$H_2$-O), 61.57 (1C, $C$$H_2$-OH), 56.64 (2C, N-$C$$H_2$-$CH_2$-S), 35.44 (2C, CH_3-CH-CH_3), 30.70 (2C, N-CH_2-$C$$H_2$-S), 20.67 (2C, $C$$H_3$), 19.82 (2C, $C$$H_3$).

Sample preparation for in situ ^{1}H NMR kinetic studies

Note that very small amounts of EO were necessary for kinetics measurements. It is rather difficult to measure such small amounts, which means that the targeted and calculated comonomer compositions of the NMR kinetics studies may differ. The sample preparation for in situ ^{1}H NMR kinetics was performed in adaption to Herzberger and co-workers.[32] The following procedure refers to a P(EG-*co*-ITEGE) kinetics experiment.

A stock solution of the initiator was prepared in a dry Schlenk flask. For this purpose, five times the required equivalents of the initiator 2-(benzyloxy)ethanol (47.50 mg, 0.31 mmol, 1 eq.) and five times of the required potassium *tert*-butoxide (31.50 mg, 0.28 mmol, 0.9 eq.) were dissolved in benzene (5 mL) and heated to 50 °C for 30 min and freeze dried overnight.

Subsequently, the flask was flushed with argon and dry DMSO-d_6 (0.5 mL) was added. A dry Norell S-5-400-VT-7 NMR tube with Teflon seal was evacuated and cooled to -80 °C in a nitrogen/acetone cooling bath. Approximately EO (96.00 mg, 2.20 mmol, 0.1 mL, 35 eq.) were condensed in a NMR tube. The NMR tube was flushed with argon and the initiator stock solution (0.1 mL) was introduced into the NMR tube *via* syringe with constant argon counterflow and cooling. Subsequently, ITEGE (216.00 mg, 0.90 mmol, 0.24 mL, 15 eq.) and dry DMSO-d_6 (0.4 mL) were added *via* syringe. The NMR tube was evacuated for several minutes under cooling and sealed afterwards. Before the kinetics measurement was started, the NMR tube was shaken vigorously to ensure a homogeneous reaction solution. The NMR tube was transferred in a pre-warmed (50 °C) NMR spectrometer and the measurement was started after stabilization of the temperature (~5 min, ΔT = 0.1 °C). Sample spinning was turned off during the measurement and two spectra were recorded per minute with one scan each. After 6 h data collection was stopped. Full monomer conversion was determined *via* NMR spectroscopy (**Figure 7**).

Cell viability studies

Prior to the cytotoxicity tests the corresponding polymers were purified by dialysis (regenerated cellulose, MWCO = 1000 g/mol) in PBS buffer solution and dried *via* freeze-pump technique.

The influence of polymers on HeLa and HEK293 cell lines was determined through a 3-(4,5-Dimethylthiazol-2-yl)-2,5-diphenyltetrazoliumbromid (MTT) based cell viability assay.

HeLa or HEK293 cells were cultured in growth medium without phenol red containing 0.1 vol-% Penicilin and Streptomycin, 10 vol-% Fetal Bovine Serum, 0.1 vol-% Glutamax™ supplement, 0.2 vol-% glucose solution and 0.1 vol-% sodium pyruvate solution and seeded 24 h before treatment in 200 µl medium (37,5k cells/ml) in 96-well plates. After the exchange of growth medium, cells were treated with lipid concentrations of 100, 10, 1 and 0.1 mg/mL for 24 h. Afterwards 30 µL of a 5 mg/mL MTT solution in DPBS were added per well and incubated for 1 h. Medium was replaced with 200 µL of a (1:8 v/v) glycine buffer pH 10 and DMSO mixture and afterwards the 96-well plate was shaken for 15 min until the formazan crystals were dissolved. For analysis of cell viability, the absorbance at 595 nm

with background correction at 670 nm was measured using a plate reader. All measurements were performed in technical triplicates.

4.1.3 Results and discussion

4.1.3.1 Monomer synthesis

The thiazolidine-based glycidyl ethers were synthesized in a three-step reaction procedure.

Synthesis of the thiazolidine derivatives

In the first step of the glycidyl ether monomer synthesis, different thiazolidine derivatives were synthesized. All thiazolidine derivatives were prepared according to a synthesis procedure reported by Shibamoto *et al.*[28]

Thiazolidines are saturated five-membered heterocycles containing a thioether and a secondary amine.[33] Their derivatives can be easily synthesized by the condensation of cysteamine hydrochloride and an aldehyde or ketone (**Scheme 1**).[34] However, the thiazolidine formation is reversible. The ring can be reopened by addition of water and thus the reaction can be reversed. Different thiazolidine derivatives were prepared to prevent possible ring opening during polymerization. Ring opening could cause uncontrolled side reactions and should thus be prevented by using a suitable derivative. Since no suitable literature is available in this field with reaction parameters comparable to those of AROP, the influence on the stability of the ring is investigated in a subsequent section.

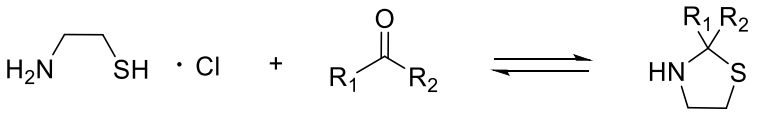

Scheme 1: General procedure for the synthesis of thiazolidine derivatives by the condensation of cysteamine hydrochloride and an aldehyde or ketone.

For the thiazolidine synthesis cysteamine hydrochloride was dissolved in water, one equivalent of the aldehyde/ketone was added, and the solution was stirred for 24 hours. After purification, the products could be obtained in high yields (over 75 %). The NMR spectra of the products can be taken from the SI (**SI-Figure 1**-**SI-Figure 4**). In **Table 1** the aldehydes/ketones and the following thiazolidine derivatives are listed.

Table 1: Aldehyde/Ketone compound and the resulting thiazolidine derivative.

Aldehyde/Ketone	Product
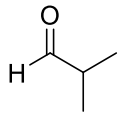 isobutyraldehyde	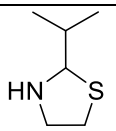 2-isopropylthiazolidine (IT)
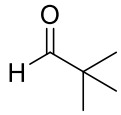 pivalaldehyde	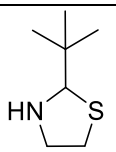 2-(*tert*-butyl)thiazolidine (TBT)
 acetone	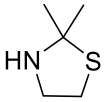 2,2-dimethylthiazolidine (DMT)

Synthesis of 2-alkylthiazolidine ethanol

In the next step, the thiazolidine derivatives were reacted to give the 2-alkylthiazolidine ethanol. The synthesis was carried out according to a prescription of Fernandéz-Zertuche *et al.*[29]

In a nucleophilic substitution, the thiazolidine derivatives and bromoethanol were reacted with DIPEA as an auxiliary base at 40 °C. In addition to the synthesized thiazolidine derivatives, thiazolidine was purchased and reacted in the same manner. The general synthesis route is shown in **Scheme 2**. An overview of the products after the reaction of the thiazolidine derivatives with bromoethanol is shown in **Figure 1**. Characterization data obtained by ^{1}H NMR spectroscopy can be found in the SI (**SI-Figure 5**-**SI-Figure 9**).

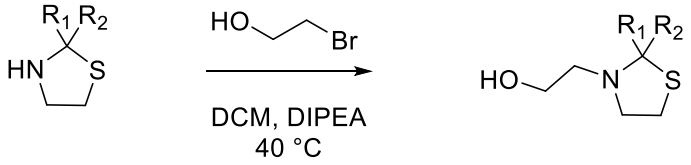

Scheme 2: General synthesis route for 2-alkylthiazolidine ethanol.

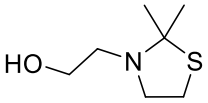

2-(2,2-dimethylthiazolidin-3-yl)ethan-1-ol

DMTOH

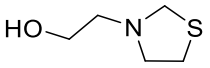

2-(thiazolidin-3-yl)ethan-1-ol

TOH

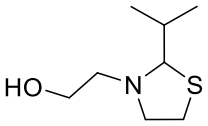

2-(2-isopropylthiazolidin-3-yl)ethan-1-ol

ITOH

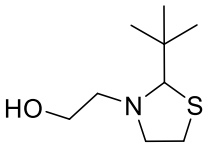

2-(2-*tert*-butyl)thiazolidine-3-yl)ethan-1-ol

TBTOH

Figure 1: Overview of the products after the reaction of the thiazolidine derivatives with bromoethanol.

Synthesis of thiazolidine-based glycidyl ethers

The alcohols 2-(thiazolidin-3-yl)ethan-1-ol (TOH) and 2-(2-isopropylthiazolidin-3-yl)ethan-1-ol (ITOH) were used to prepare the thiazolidine-based glycidyl ethers. The synthesis was first carried out following the monomer synthesis of MTEGE by solid phase reaction according to a description of Herzberger *et al.*[27] The alcohol was mixed with sodium hydroxide, and epichlorohydrin was added in excess. Final purification was carried out by fractional distillation. However, the yields obtained with this synthesis route were very low (between 15-25 %), and for this reason the process was switched to phase-transfer catalysis. The synthesis was carried out according to a procedure by Mangold *et al.*[30] The synthesis routes of both methods are exemplified by the reaction of ITOH with epichlorohydrin in **Scheme 3**.

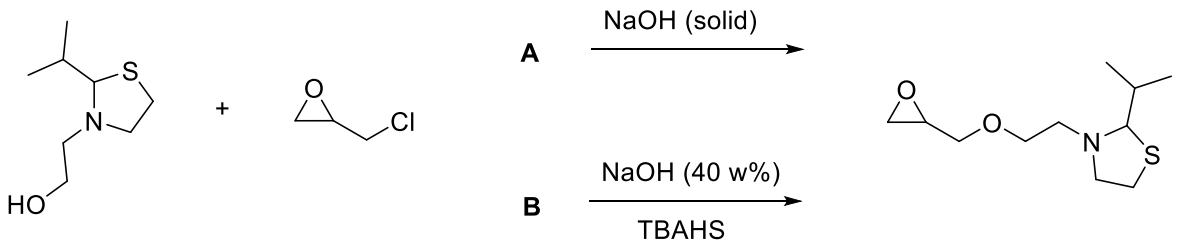

Scheme 3: Synthesis routes for the synthesis of 2-isopropylthiazolidine ethyl glycidyl ether (ITEGE) *via* solid phase reaction (**A**) and phase-transfer catalysis (**B**).

Using phase-transfer catalysis, yields between 55-70 % were obtained after purification by distillation. In this method in particular, by-products may take place due to the basic elimination on epichlorohydrin followed by nucleophilic substitution, so the adjustment of reaction parameters to increase the yield is mandatory. The yield obtained here is in a good agreement with the yields of other glycidyl ethers prepared by phase-transfer catalysis.[30] The following **Figure 2** shows the ^{1}H NMR spectrum of ITEGE. All signals could be clearly assigned. Especially the diastereotopic protons of the epoxide ring (**h**, **i**, **k**) are clearly visible. More details of the ^{1}H NMR spectrum of TEGE can be found in the SI (**SI-Figure 10**).

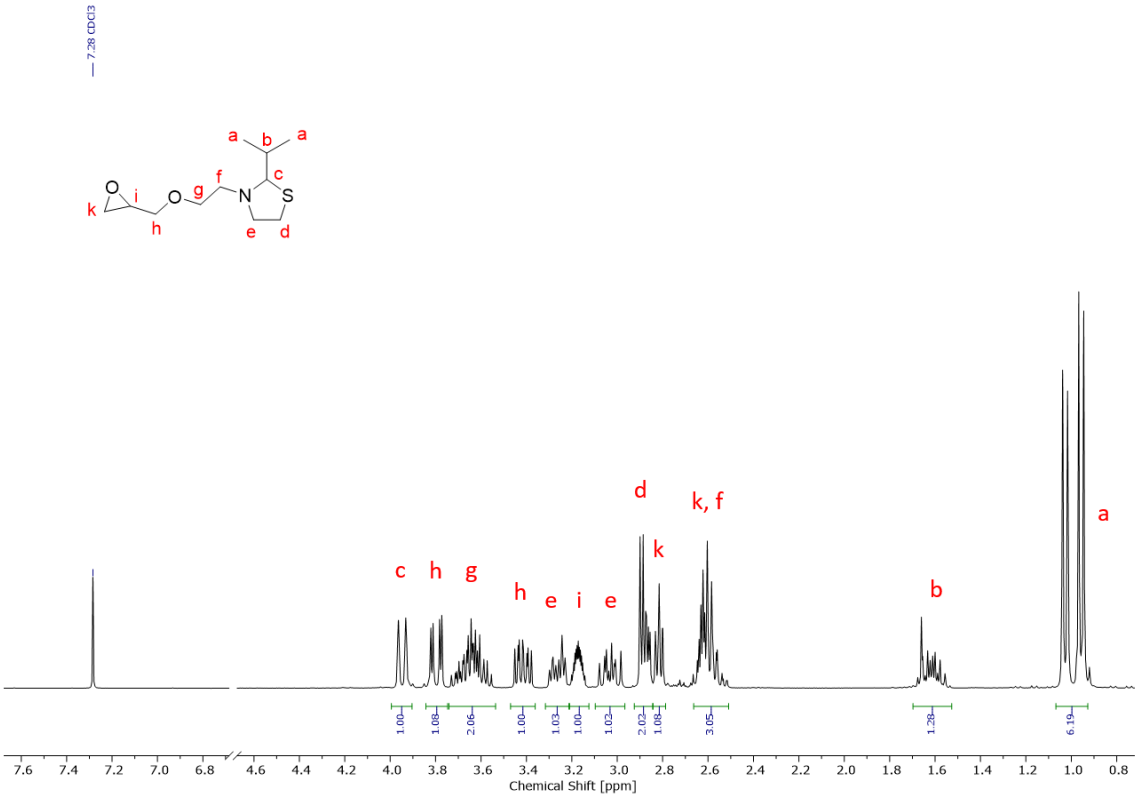

Figure 2: ^{1}H NMR spectrum (300 MHz, chloroform-*d*) of ITEGE.

4.1.3.2 Polymer synthesis and characterization.

DMTOH, TOH and ITOH initiated PEG polymers

Ring opening of thiazolidine derivatives in AROP may lead to undesirable side reactions. For this reason, prior to the synthesis of the glycidyl ether amines, the stability of the ring was tested under the conditions of AROP using the thiazolidine ethanol derivatives as initiators to determine the best possible precursor for the synthesis of the glycidyl ether

amines. In a first series of experiments the alcohols DMTOH, TOH and ITOH were used as initiators for the polymerization of EO. The general synthesis procedure is shown in **Scheme 4**. A degree of deprotonation of 90 % was chosen and the polymerizations were performed in DMSO at room temperature. Full monomer conversion was found *via* ^{1}H NMR spectroscopy.

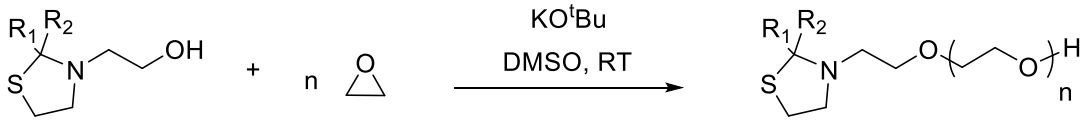

DMTOH: R_1 R_2 = CH_3 TOH: R_1 R_2 = H ITOH: R_1 = H , R_2 = isopropyl

Scheme 4: General synthesis procedure for the initiation of PEG with DMTOH, TOH and ITOH.

Upon initiation with DMTOH and TOH, cleavage of the thiazolidine ring was detected by ^{1}H NMR spectroscopy. Furthermore, bimodal SEC elugrams could be observed for the polymers. This can be attributed to the fact that cleavage of the ring can lead to the formation of another initiation-capable by-product. In addition, the targeted molecular weights of 5000 g/mol could not be obtained, the molecular weights were always below 3000 g/mol and lower (determined by NMR). More details can be found in the SI (**SI-Figure 24**).

In pronounced contrast, initiation by ITOH gave good results. Key characterization data of the resulting polymers is summarized in **Table 2**. The targeted degree of polymerization is in good agreement with the determined values for the obtained PEG. The molecular weight (M_n) was obtained from SEC in DMF using PEG standards and a monomodal molecular weight distribution with narrow dispersity was obtained ($Đ$ = 1.15). The corresponding SEC trace of IT-PEG is shown in **Figure 3**.

Table 2: Characterization data of the ITOH initiated PEG polymer.

Sample [a]	EO^{theo}	$M_n^{NMR\ a}$ g·mol^{-1}	$M_n^{SEC\ b}$ g·mol^{-1}	$Đ^{b}$
IT-PEG$_{117}$	110	5320	3790	1.15

[a] Obtained from ^{1}H NMR spectroscopy. [b] Determined *via* SEC (RI, DMF, PEG standards).

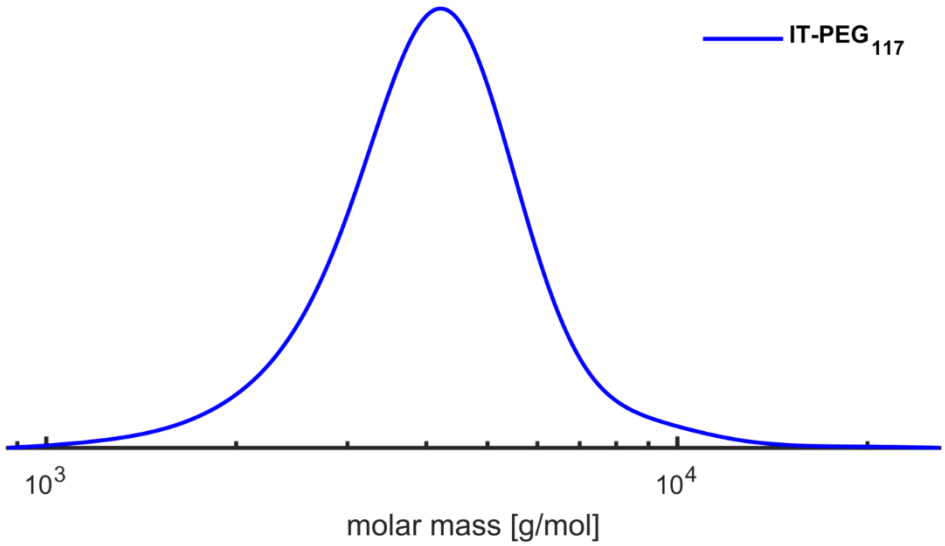

Figure 3: SEC trace (RI detector, DMF, PEG standards) of the ITOH initiated PEG polymer.

The ^{1}H NMR spectrum of the ITOH initiated PEG polymer is shown in **Figure 4** with assigned signals. The molecular weight from ^{1}H NMR spectroscopy was determined *via* integration of the proton (signal **c**) of the initiator.

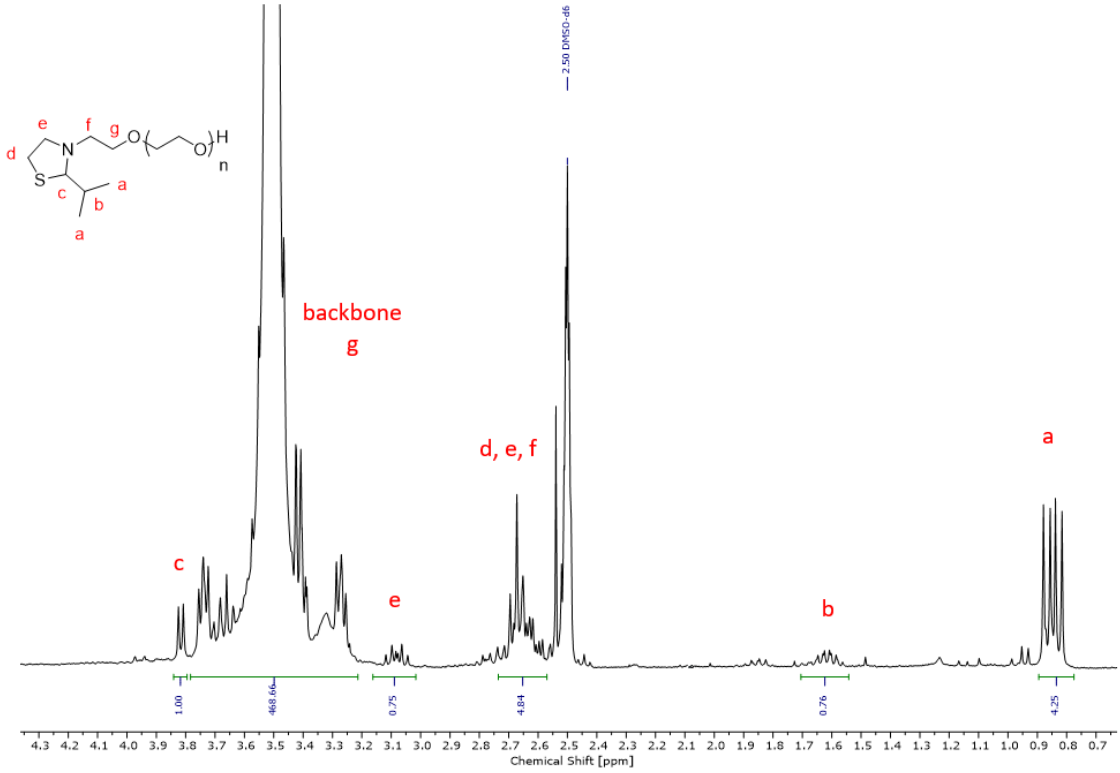

Figure 4: ^{1}H NMR spectrum (300 MHz, DMSO-d_6) of IT-PEG.

Based on the initiation tests with the thiazolidine ethanol derivatives, the monomer ITEGE proved to be promising due to the stability of the ring under AROP conditions. With the other derivatives, good results could not be obtained, so the following sections focused on the application of ITEGE. However, the other compounds could be polymerized *via* monomer activated ring-opening polymerization (MAROP) in future work, because this polymerization technique is characterized by its high tolerance for functional groups and mild reaction conditions (e.g. low temperature).[35]

Copolymerization of EO and ITEGE (PEG-co-ITEGE) and homopolymerization of ITEGE (PITEGE)

To synthesize copolymers by AROP of EO and ITEGE, the molar fractions of the two epoxide monomers were varied. As initiator 2-(benzyloxy)ethanol was used, because this allows the determination of the molecular weight *via* ^{1}H NMR spectroscopy by integration of the isolated methylene group of the initiator. Furthermore, potassium *tert*-butoxide was used as a base, and DMSO as a solvent, which allowed full monomer conversion at all molar

fractions, as determined *via* ^{1}H NMR spectroscopy. Quantitative removal of the solvent was achieved *via* precipitation of the copolymers in diethyl ether/acetone. The synthesis route is shown in **Scheme 5**.

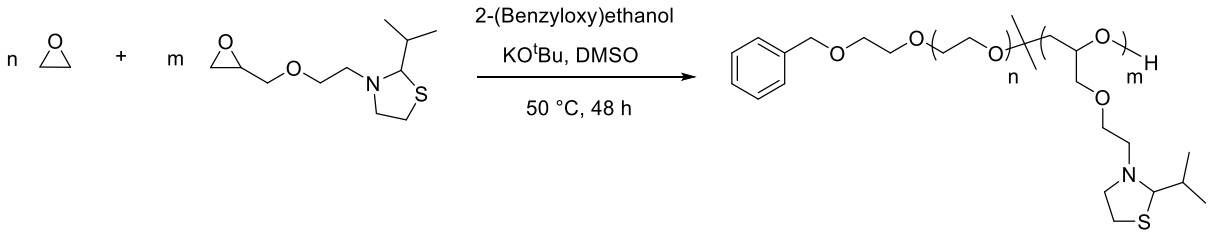

Scheme 5: Synthesis route for the copolymerization of EO and ITEGE to P(EO-*co*-ITEGE) *via* AROP.

Homopolymerization was also carried out with the initiator 2-(benzyloxy)ethanol and potassium *tert*-butoxide, albeit solvent-free in bulk. However, this resulted in a broader molecular weight distribution ($Đ$ = 1.17). Therefore, the approach was repeated, this time with the addition of crown ether ([18]crown-6). A better result was obtained in terms of dispersity ($Đ$ = 1.12), but a shoulder in the higher molecular range was detected by SEC measurement. In the last approach, the homopolymer was prepared using cesium hydroxide mono hydrate in DMSO at 40 °C (**Scheme 6**). This synthesis route gave the best results with monomodal molecular weight distribution with a narrow dispersity ($Đ$ = 1.06). The ^{1}H NMR spectrum and ^{13}C NMR spectrum as well as the results of the SEC measurements can be found in the SI (**SI-Figure 15**, **SI-Figure 16**, **SI-Figure 25**)

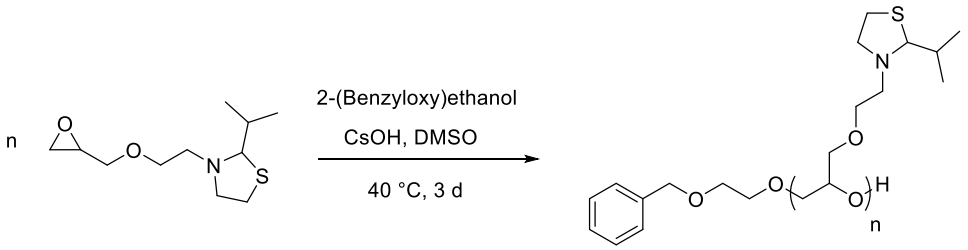

Scheme 6: Synthesis route for the homopolymerization of ITEGE to P(ITEGE).

The key characterization results for the P(EG-*co*-ITEGE) copolymers and the P(ITEGE) homopolymer are summarized in **Table 3**.

Table 3: Key characterization results for the P(EG-*co*-ITEGE) copolymers and the P(ITEGE) homopolymer.

Sample [a]	ITEGE [theo] mol%	ITEGE [a] mol%	M_n [NMR a] g·mol^{-1}	M_n [SEC b] g·mol^{-1}	$Đ$ [b]	T_g °C	T_m °C
P(EG$_{98}$-*co*-ITEGE$_2$)	1	1	4920	3970	1.07	-55	30
P(EG$_{79}$-*co*-ITEGE$_3$)	5	5	4320	2880	1.06	-53	18
P(EG$_{84}$-*co*-ITEGE$_9$)	10	10	5920	2830	1.05	-52	19
P(EG$_{53}$-*co*-ITEGE$_{10}$)	15	16	4780	2210	1.06	-49	16
P(EG$_{44}$-*co*-ITEGE$_{10}$)	20	19	4390	1620	1.09	-49	15
P(EG$_{15}$-*co*-ITEGE$_7$) [c]	30	32	2420	1130	1.10	-	-
P(ITEGE$_{28}$)	100	100	6590	1430	1.06	-25	-

[a] Obtained from ^{1}H NMR spectroscopy. [b] Determined *via* SEC (RI, DMF, PEG standards). [c] ^{1}H NMR kinetics performed in a NMR tube.

Copolymers with a molecular weight in the range of 4320 g·mol^{-1} to 5920 g·mol^{-1} (NMR) were synthesized with molar contents of ITEGE between 1 mol% and 32 mol%, which were in good agreement with the targeted values. The corresponding SEC traces of the series of copolymers are depicted in **Figure 5**, showing monomodal distributions with $Đ \leq 1.10$. Molecular weights were determined *via* SEC and show a systematic deviation from the molecular weights determined *via* ^{1}H NMR spectroscopy with increasing amount of incorporated ITEGE. This effect can be attributed to the hydrodynamic radii of the copolymers, which differ from the applied PEG standard with increasing amount of ITEGE.

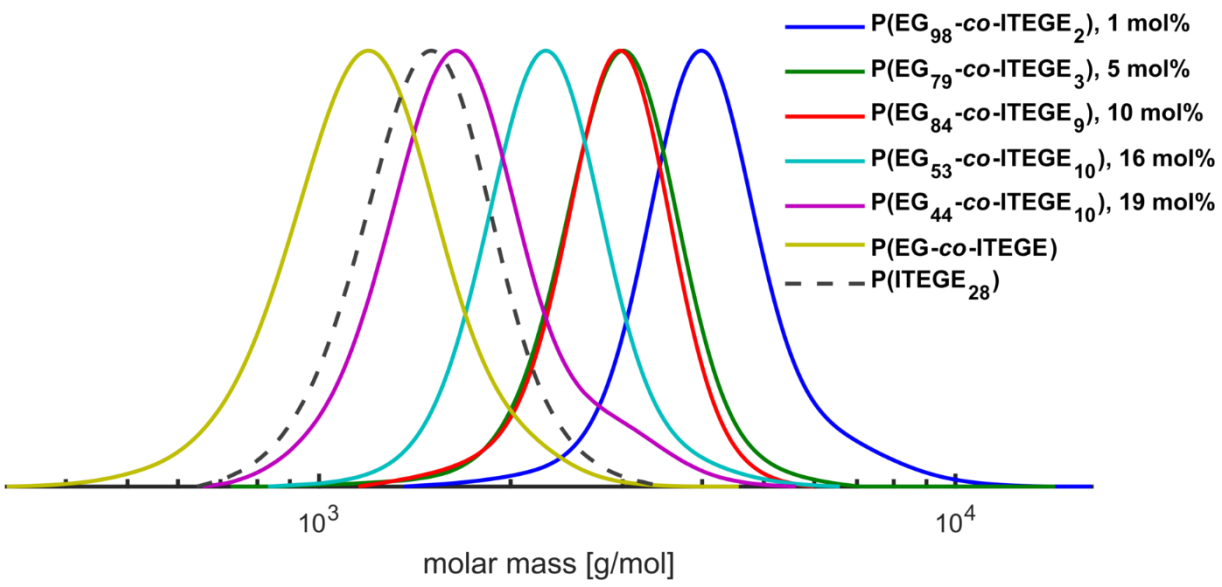

Figure 5: SEC traces (RI detector, DMF, PEG standards) of P(EG-*co*-ITEGE) copolymers.

A representative ^{1}H NMR spectrum of a P(EG-*co*-ITEGE) copolymer is depicted in **Figure 6** with assignment of all characteristic proton signals. Further NMR spectra of P(EG-*co*-ITEGE) are shown in **SI-Figure 17**-**SI-Figure 21**.

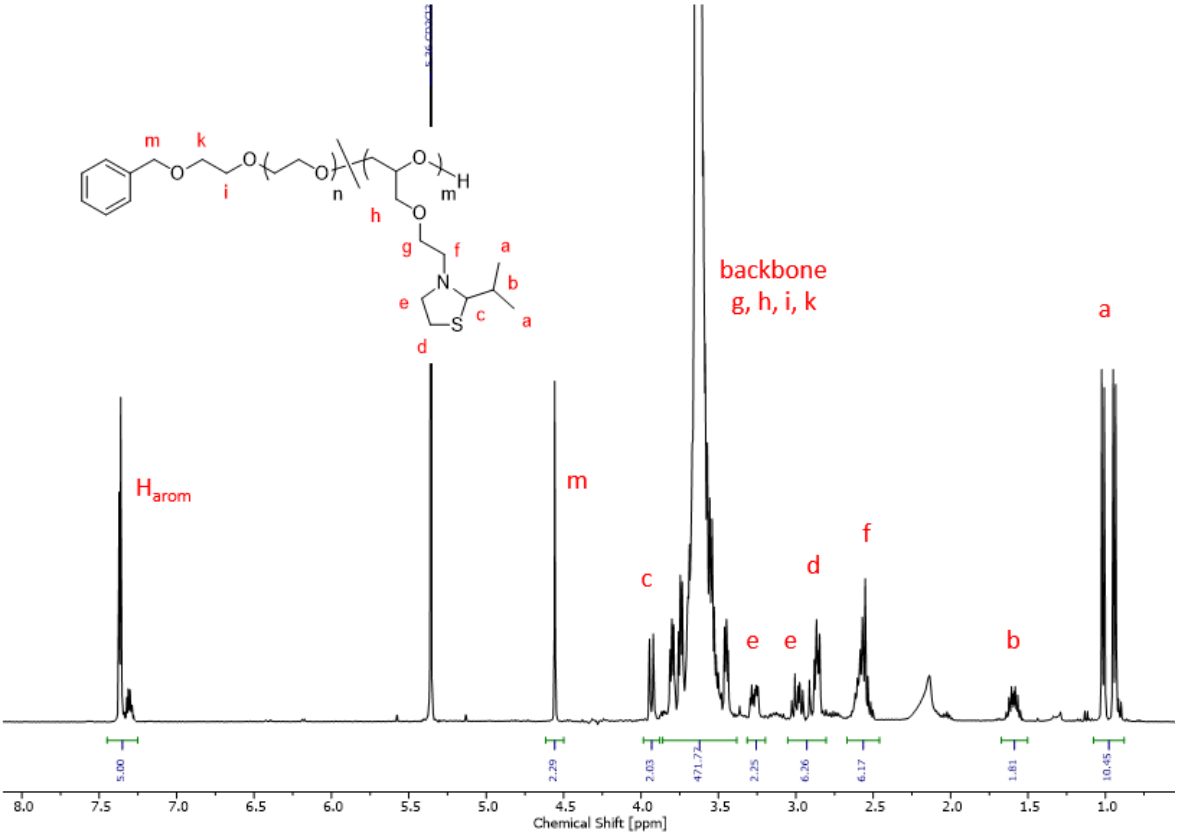

Figure 6: ^{1}H NMR spectrum (400 MHz, methylene chloride-d_2) of P(EG$_{98}$-*co*-ITEGE$_2$).

The thermal behavior of the copolymers and the homopolymer was investigated via DSC measurements. For all copolymers, a T_g between -55 to -49 °C was determined. With increasing amounts of ITEGE units, a slight increase in T_g was observed. The lower T_g compared to PEG (T_g= -53 °C, T_m= 66 °C)[1] can be explained by the flexibility of the side chains of the ITEGE units. Furthermore, for all copolymers melting temperatures (T_m) in the range of 50-15 °C were determined for all measured copolymers. The larger the ITEGE content of the polymers, the lower the melting temperature, since crystallization of the PEG chains is disturbed by the hydrophobic ITEGE moieties. The homopolymer had a T_g of -25 °C, and a T_m could not be determined. This behavior is explained by the atactic nature of the polyethers formed, which renders crystallization impossible, as has been observed for a variety of other poly(glycidyl ethers) before.

4.1.3.3 *In situ* ^{1}H NMR kinetic studies.

In the past, kinetic investigations by *in situ* ^{1}H NMR spectroscopy on anionic copolymerization of EO with various glycidyl ethers (GE) revealed an almost random distribution of GE units in the polyether chains, which translates to similar reactivity ratios.[32] In 2016, our group investigated the copolymerization of EO and 2-(methylthio)ethyl glycidyl ether (MTEGE) in *in situ* ^{1}H NMR experiments in DMSO-d_6. The application of a nonterminal modal of chain copolymerization introduced by Jaacks *et al.*[36] revealed a random copolymerization with reactivity ratios of r_{EO} = 0.92 ± 0.02. and r_{MTEGE} = 1.06 ± 0.02. Note that reactivity ratios are defined as $r_1 = k_{11}/k_{12}$ and $r_2 = k_{22}/k_{21}$ with 1 representing EO and 2 representing ITEGE as well as the rate constant k. Thus, we performed an *in situ* ^{1}H NMR kinetic experiment of the copolymerization P(EO-*co*-ITEGE) to elucidate the distribution of ITEGE units along the polyether backbone (**Figure 7**).

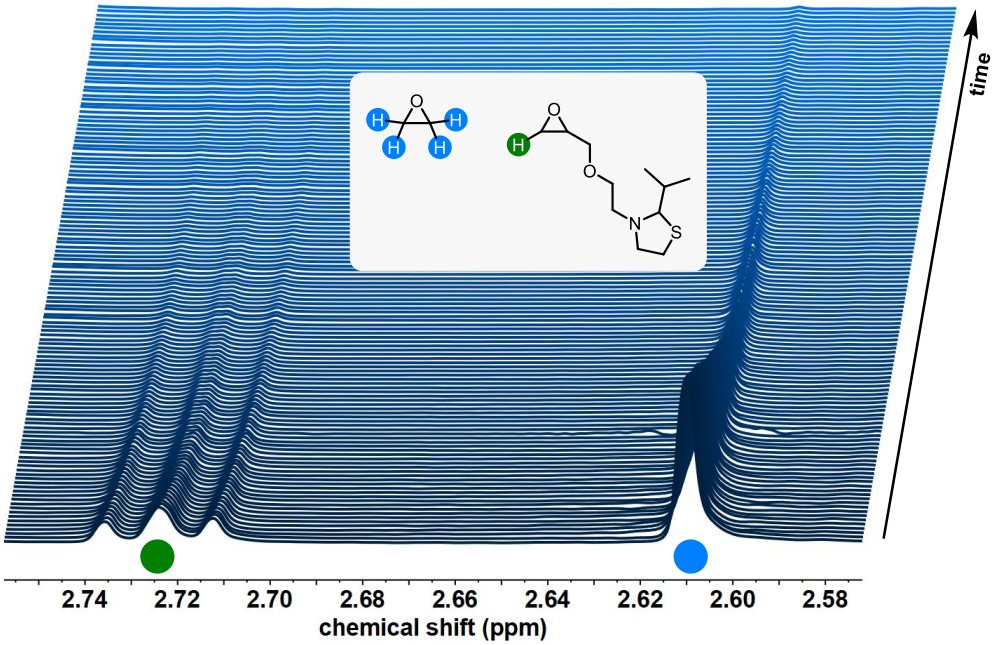

Figure 7: *In situ* ^{1}H NMR experiment of the anionic copolymerization of P(EO-*co*-ITEGE) in DMSO-d_6 at 50 °C.

The anionic copolymerization was initiated by potassium 2-(benzyloxy)ethan-1-olate in DMSO-d_6 at 50 °C. The monomer consumption $M_{x,t}/M_{x,t=0}$ over time was monitored for both monomers, enabling the determination of the consumption versus total conversion (**Figure 8**). One spectrum every 30 s was recorded with one scan.

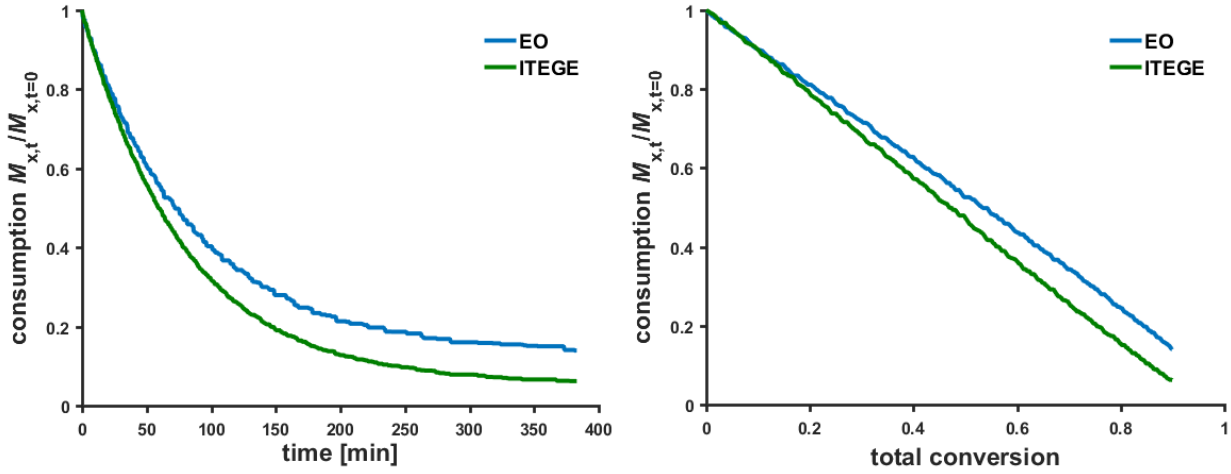

Figure 8: Monomer consumption versus time (left) and total conversion (right) evaluated by *in situ* ^{1}H NMR experiments of the anionic copolymerization of P(EO-*co*-ITEGE) in DMSO-d_6 at 50 °C.

By utilization of the Jaacks formalism, reactivity ratios were determined as r_{EO} = 0.74 ± 0.00 and r_{ITEGE} = 1.34 ± 0.00 with a coefficient of determination (R^2) of 0.99 (**SI-Figure 27**).[36] As expected, slightly preferred incorporation of ITEGE was observed in the early stages, resulting in a slight gradient shown in the molar composition diagram (**SI-Figure 28**). The presented results are in good agreement with the explanation given for P(EO-*co*-MTEGE). The authors ascribe the slightly increased reactivity of the glycidyl ether compared to EO to an enhanced coordination of the side chain to the potassium counterion, which is an equally suitable explanation for ITEGE. Hence, the Lewis basicity of the epoxide ring of the comonomer is increased, resulting in a higher reactivity.

4.1.3.4 Stimuli-responsive behavior

The responsive behavior of the copolymers was investigated using oxidation with hydrogen peroxide as an example. The oxidation of the polymers is of particular interest because both, the tertiary amine and the thioether of the thiazolidine ring can be oxidized.[20,27,37] For the oxidation, 100 mg of the copolymer P(EG-*co*-ITEGE) containing 16 mol% ITEGE was mixed with 1 mL of H_2O_2 solution (30 %) and stirred for overnight at room temperature. At first glance, an optical change could be observed after about 30 min: the viscous, brownish-colored polymer solution turned to a colorless, slightly turbid solution (see **Figure 9**).

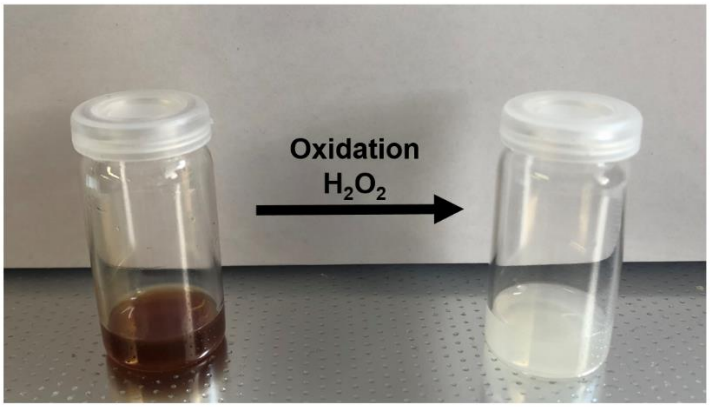

Figure 9: Polymer before and after oxidation with H_2O_2 solution.

The polymer was precipitated in ice-cold diethyl ether after the reaction time. This was not possible before oxidation; after oxidation, the polymer precipitated as a colorless solid in diethyl ether. After drying, the polymer could be obtained as a colorless transparent film. For further characterization, NMR measurements were performed and the polymer was analyzed by SEC.

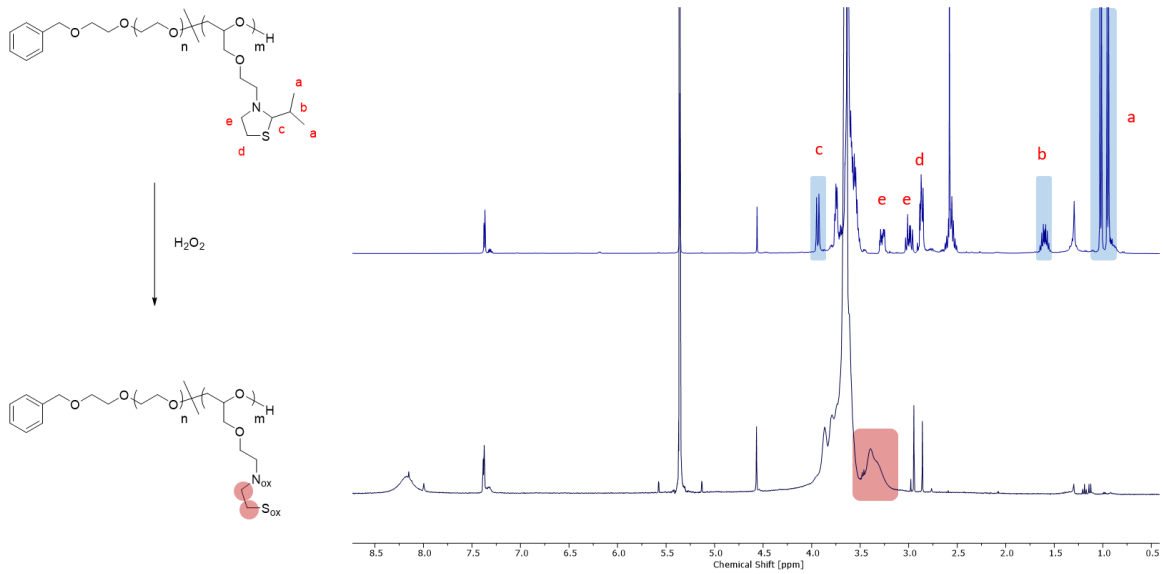

Figure 10: ^{1}H NMR spectra (400 MHz, methylene chloride-*d*) of the P(EG-co-ITEGE) copolymer before and after oxidation with H_2O_2 solution.

After oxidation, the NMR spectrum showed that the signals from the isopropyl groups of the thiazolidine ring has completely disappeared (**Figure 10**). This suggests that the groups are not stable under oxidative conditions. The characteristic signals a-c of the groups are

marked in blue in the spectrum (**Figure 10**). Furthermore, a shift of the signals of the methyl groups (**e** and **d**, marked in red) between the nitrogen and sulfur atom could be detected. The exact structure of the polymer cannot be determined precisely from the NMR spectrum, but a possible structure can be determined from the shifts in the ^{1}H and ^{1}H, ^{13}C HSQC spectra (see **SI-Figure 22**, **SI-Figure 23**). **Scheme 7** and **Scheme 8** below lists the oxidation states of various nitrogen and sulfur compounds to identify a possible structure.[38,39]

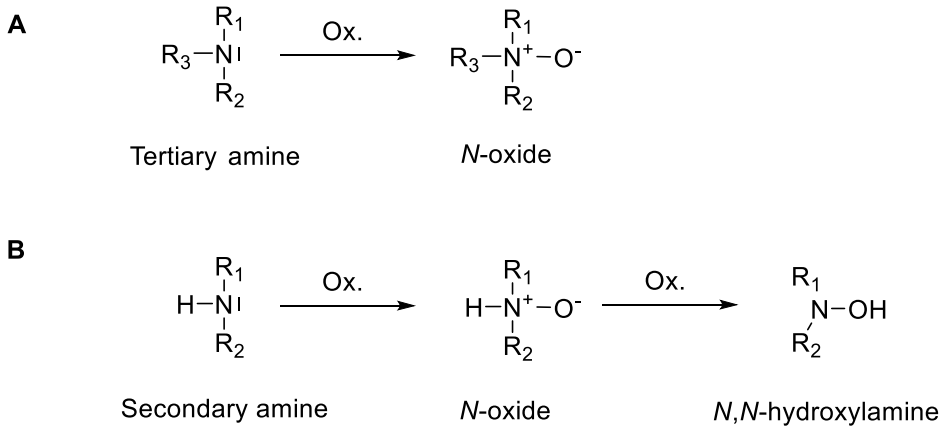

Scheme 7: Oxidation states of nitrogen compounds.

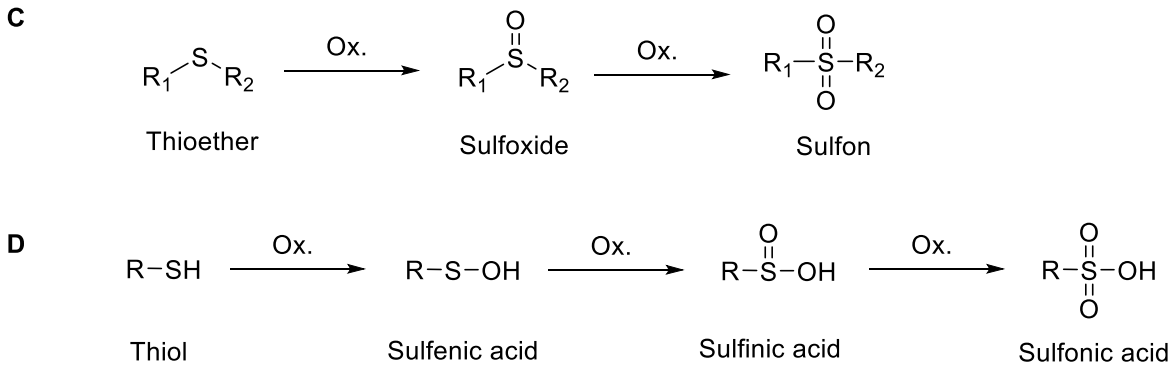

Scheme 8: Oxidation states of sulfur compounds.

If we consider the case where the isopropyl groups on the ring remain stable during oxidation, an *N*-oxide would form on the nitrogen and a sulfoxide or sulfone on the sulfur (paths **A** and **C**). More likely, because of the very strong oxidant, a sulfone would form along with the *N* oxide. In our case, however, we know that the isopropyl groups cannot withstand oxidation. Therefore, paths **B** and **D** must be considered: an *N,N*-hydroxylamine and a

sulfonic acid are formed with high probability. This assumption can be confirmed on the basis of the NMR spectra (**SI-Figure 22**, **SI-Figure 23**).

When the polymer was measured after oxidation *via* SEC, a slight decrease in molecular weight from previously 2210 g/mol to 1960 g/mol was observed. However, the molecular weight distribution of 1.06 remained constant (see **SI-Figure 26**).

The influence of different pH values on the copolymers was not investigated in this work, but will be studied by further experiments in the future.

4.1.3.5 Cell viability studies

PEG is used for many biomedical applications due to its low toxicity, antigenicity and immunogenicity.[1] Copolymers of PEG used for potential application in biomedical and pharmaceutical fields, it is therefore imperative to determine the cytotoxicity. The polymerization takes place in DMSO, which is strongly cytotoxic to any cells. For this reason, it is crucialto purify the polymers by dialysis. In the next step, cell tests of the P(EG-*co*-ITEGE) copolymers containing 5 mol% (17 wt%) and 16 mol% (50 wt%) ITEGE were carried out, using HeLa cells and HEK cells as cell lines. The polymers were incubated for 24 h with the cells. Copolymer concentrations of 0.1 µg/mL up to 100 µg/mL were tested to investigate the influence of the copolymer. As a reference, a commercially available mPEG with a similar molecular weight to that of the copolymers was also analyzed. The results of the MTT assays are displayed in **Figure 11**.

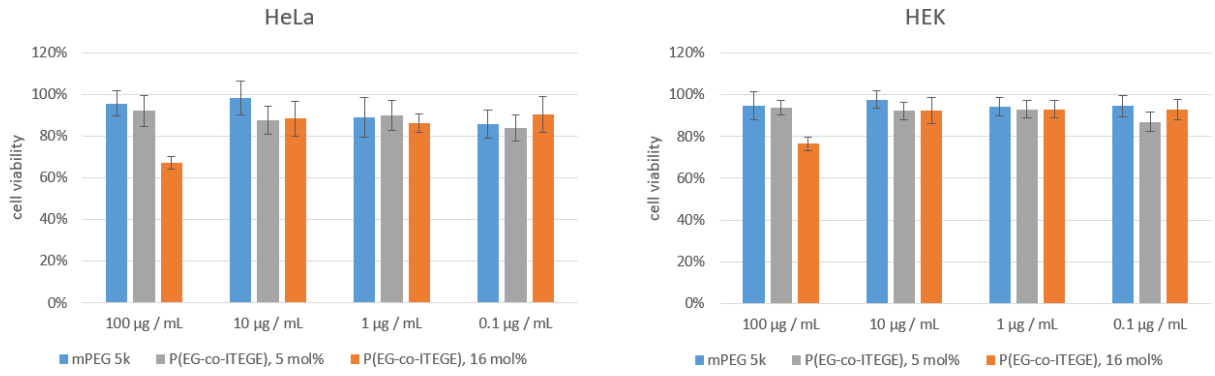

Figure 11: MTT assays of HeLa and HEK cells incubated with $mPEG_{5k}$ (blue) as reference and P(EG-*co*-ITEGE) copolymers with 5 mol% ITEGE (grey) and 16 mol% ITEGE (orange).

Concentrations of the polymers between 0.1 μg/mL-10 μg/mL showed no effect on cell viability. The copolymer with 16 mol% ITEGE at a concentration of 100 μg/mL showed a reduction of cell viability in HeLa cells to 67 ± 3 %, and in HEK cells to 76±3 %. Since 16 mol% corresponds to approximately 50 wt% of the polymer, a concentration of 100 μg/mL is rather high. For this reason, a decrease in cell viability is not surprising. Nevertheless, a toxic effect of the copolymers on the cells at lower ITEGE content and concentrations below 100 μg/mL was not observed.

4.1.4 Conclusion

In this work, the synthesis of several thiazolidine derivatives was demonstrated for the preparation of thiazolidine-based glycidyl ethers. in the first step, the thiazolidine derivatives were prepared by condensation of cysteamine hydrochloride and an aldehyde or ketone. In this process, 2-isopropylthiazolidines (IT), 2-(tert-butyl)thiazolidines (TBT) and 2,2-dimethylthiazolidines (DMT) were synthesized. In the next step, the compounds were used to prepare the corresponding 2-alkylthiazolidine ethanol derivatives 2-(2,2-dimethylthiazolidin-3-yl)ethan-1-ol (DMTOH), 2-(thiazolidin-3-yl)ethan-1-ol (TOH), 2-(2-isopropylthiazolidin-3-yl)ethan-1-ol (ITOH) and 2-(2-(tert-butyl)thiazolidin-3-yl)ethan-1-ol (TBTOH). To test the stability of the alkylthiazolidinethanol compounds under the conditions of AROP, the alcohols were used as initiators for the polymerization with EO. ITOH turned out to be a suitable candidate to function for the further synthesis of the glycidyl ether and the subsequent copolymerization. By reacting ITOH and epichlorohydrin, the glycidyl ether 2-isopropylthiazolidine ethyl glycidyl ether (ITEGE) could be prepared.

AROP was used to synthesize the homopolymer P(ITEGE) and various copolymers P(EG-*co*-ITEGE) with EO. The amount of ITEGE in the copolymers was varied from 1 mol% to 32 mol%, and the molecular weight was kept constant at approx. 5000 g/mol. Narrow molecular weight distributions with dispersities below 1.10 were obtained. The polymers were characterized by NMR spectroscopy and SEC measurements. In addition, the thermal behavior was analyzed *via* DSC.

To obtain information on the distribution of ITEGE units in the polyether backbone, *in situ* ^{1}H NMR kinetic studies were performed. Reactivity ratios were determined as

r_{EO} = 0.74 ± 0.00 and r_{ITEGE} = 1.34 ± 0.00 with a coefficient of determination (R^2) of 0.99. Slightly preferred incorporation of ITEGE was observed in the early stages of the copolymerization, resulting in a slight gradient displayed by the molar based composition diagram.

The responsive behavior of the copolymers was investigated by oxidation. A change in the solubility behavior of the polymers after oxidation was observed. Furthermore, the structure of the polymer was analyzed by NMR spectroscopy and SEC. The pH-responsive behavior was not investigated in this work, but will be investigated in the future.

Finally, the toxicity of the polymers was investigated by MTT assay. Only at a higher concentration of ITEGE units a reduction of cell activity could be detected.

4.1.5 Acknowledgment

We thank [redacted] for the DSC measurements, [redacted] for SEC measurements and [redacted] for assistance in the NMR kinetic measurements. E.B. thanks the DFG in the context of the SFB 1066 for financial support.

References

(1) Herzberger, J.; Niederer, K.; Pohlit, H.; Seiwert, J.; Worm, M.; Wurm, F. R.; Frey, H. Polymerization of Ethylene Oxide, Propylene Oxide, and Other Alkylene Oxides: Synthesis, Novel Polymer Architectures, and Bioconjugation. *Chem. Rev.* **2015**, acs.chemrev.5b00441. https://doi.org/10.1021/acs.chemrev.5b00441.

(2) Shen, H.; Wang, G. *Ethylene Oxide Polymers: Synthesis, Modification, Topology, and Applications*; 2018. https://doi.org/10.1002/0471440264.pst528.pub2.

(3) Harris, J. M.; Chess, R. B. Effect of Pegylation on Pharmaceuticals. *Nat. Rev. Drug Discov.* **2003**, *2* (3), 214–221. https://doi.org/10.1038/nrd1033.

(4) Pressly, E. D.; Rossin, R.; Hagooly, A.; Fukukawa, K. I.; Messmore, B. W.; Welch, M. J.; Wooley, K. L.; Lamm, M. S.; Hule, R. A.; Pochan, D. J.; Hawker, C. J. Structural Effects on the Biodistribution and Positron Emission Tomograpgy (PET) Imaging of Well-Defined 64Cu-Labeled Nanoparticles Comprised of Amphiphilic Block Graft Copolymers. *Biomacromolecules* **2007**, *8* (10), 3126–3134. https://doi.org/10.1021/bm700541e.

(5) Meng, F.; Zhong, Z.; Feijen, J. Stimuli-Responsive Polymersomes for Programmed Drug Delivery. *Biomacromolecules* **2009**, *10* (2), 197–209. https://doi.org/10.1021/bm801127d.

(6) Lu, Y.; Aimetti, A. A.; Langer, R.; Gu, Z. Bioresponsive Materials. *Nat. Rev. Mater. 2* **2016**, *2*, 16075.

(7) Schmaljohann, D. Thermo- and PH-Responsive Polymers in Drug Delivery. *Adv. Drug Deliv. Rev.* **2006**, *58* (15), 1655–1670. https://doi.org/10.1016/j.addr.2006.09.020.

(8) Vaupel, P.; Kallinowski, F.; Okunieff, P. Blood Flow, Oxygen and Nutrient Supply, and Metabolic Microenvironment of Human Tumors: A Review. *Cancer Res.* **1989**, *49*, 6449–6465.

(9) Rofstad, E. K.; Mathiesen, B.; Kindem, K.; Galappathi, K. Acidic Extracellular PH Promotes Experimental Metastasis of Human Melanoma Cells in Athymic Nude Mice. *Cancer Res.* **2006**, *66* (13), 6699–6707. https://doi.org/10.1158/0008-5472.CAN-06-0983.

(10) Grabe, M.; Oster, G. Regulation of Organelle Acidity. *J. Gen. Physiol.* **2001**, *117* (4), 329–344. https://doi.org/10.1085/jgp.117.4.329.

(11) Watson, P.; Jones, A. T.; Stephens, D. J. Intracellular Trafficking Pathways and Drug Delivery: Fluorescence Imaging of Living and Fixed Cells. *Adv. Drug Deliv. Rev.* **2005**, *57* (1 SPEC. ISS), 43–61. https://doi.org/10.1016/j.addr.2004.05.003.

(12) Mura, S.; Nicolas, J.; Couvreur, P. Stimuli-Responsive Nanocarriers for Drug Delivery. *Nat. Mater.* **2013**, *12*, 991–1103.

(13) Wang, L.; Liu, G.; Wang, X.; Hu, J.; Zhang, G.; Liu, S. Acid-Disintegratable Polymersomes of PH-Responsive Amphiphilic Diblock Copolymers for Intracellular Drug Delivery. *Macromolecules* **2015**, *48* (19), 7262–7272. https://doi.org/10.1021/acs.macromol.5b01709.

(14) Li, M.-H.; Keller, P. Stimuli-Responsive Polymer Vesicles. *Soft Matter* **2009**, *5* (5), 927. https://doi.org/10.1039/b815725a.

(15) Madsen, J.; Armes, S. P. (Meth)Acrylic Stimulus-Responsive Block Copolymer Hydrogels. *Soft Matter* **2012**, *8* (3), 592–605. https://doi.org/10.1039/c1sm06035j.

(16) Thakral, S.; Thakral, N. K.; Majumdar, D. K. Eudragit®: A Technology Evaluation.

Expert Opin. Drug Deliv. **2013**, *10* (1), 131–149. https://doi.org/10.1517/17425247.2013.736962.

(17) Verkoyen, P.; Frey, H. Amino-Functional Polyethers: Versatile{,} Stimuli-Responsive Polymers. *Polym. Chem.* **2020**, *11* (24), 3940–3950. https://doi.org/10.1039/D0PY00466A.

(18) Zhang, Q.; Kelland, M. A.; Frey, H.; Blankenburg, J.; Limmer, L. Amine N-Oxide Kinetic Hydrate Inhibitor Polymers for High-Salinity Applications. *Energy and Fuels* **2020**, *34* (5), 6298–6305. https://doi.org/10.1021/acs.energyfuels.0c00838.

(19) Zhang, Q.; Limmer, L.; Frey, H.; Kelland, M. A. N-Oxide Polyethers as Kinetic Hydrate Inhibitors: Side Chain Ring Size Makes the Difference. *Energy and Fuels* **2021**, *35* (5), 4067–4074. https://doi.org/10.1021/acs.energyfuels.0c04333.

(20) Herzberger, J.; Kurzbach, D.; Werre, M.; Fischer, K.; Hinderberger, D.; Frey, H. Stimuli-Responsive Tertiary Amine-Functional PEGs Based on N , N -Dialkyl Glycidyl Amines. *Macromolecules* **2014**, *47* (22), 7679–7690.

(21) Kurzbach, D.; Wilms, V. S.; Frey, H.; Hinderberger, D. Impact of Amino-Functionalization on the Response of Poly(Ethylene Glycol) (PEG) to External Stimuli. *ACS Macro Lett.* **2013**, *2* (2), 128–131. https://doi.org/10.1021/mz300596r.

(22) Reuss, V. S.; Werre, M.; Frey, H. Thermoresponsive Copolymers of Ethylene Oxide and N,N-Diethyl Glycidyl Amine: Polyether Polyelectrolytes and PEGylated Gold Nanoparticle Formation. *Macromol. Rapid Commun.* **2012**, *33* (18), 1556–1561. https://doi.org/10.1002/marc.201200307.

(23) Lundberg, P.; Lynd, N. A.; Zhang, Y.; Zeng, X.; Krogstad, D. V.; Paffen, T.; Malkoch, M.; Nyström, A. M.; Hawker, C. J. PH-Triggered Self-Assembly of Biocompatible Histamine-Functionalized Triblock Copolymers. *Soft Matter* **2013**, *9* (1), 82–89. https://doi.org/10.1039/c2sm26996a.

(24) Lee, A.; Lundberg, P.; Klinger, D.; Lee, B. F.; Hawker, C. J.; Lynd, N. A. Physiologically Relevant, PH-Responsive PEG-Based Block and Statistical Copolymers with N,N-Diisopropylamine Units. *Polym. Chem.* **2013**, *4* (24), 5735. https://doi.org/10.1039/c3py00747b.

(25) Meng, F. H.; Zhong, Z. Y.; Feijen, J. Stimuli-Responsive Polymersomes for

Programmed Drug Delivery. *Biomacromolecules* **2009**, *10* (2), 197–209. https://doi.org/10.1021/bm801127d.

(26) Napoli, A.; Boerakker, M. J.; Tirelli, N.; Nolte, R. J. M.; Nico A. J. M. Sommerdijk; Hubbell, J. A. Glucose-Oxidase Based Self-Destructing Polymeric Vesicles. **2004**, *20* (9). https://doi.org/10.1021/LA0357054.

(27) Herzberger, J.; Fischer, K.; Leibig, D.; Bros, M.; Thiermann, R.; Frey, H. Oxidation-Responsive and "Clickable" Poly(Ethylene Glycol) via Copolymerization of 2-(Methylthio)Ethyl Glycidyl Ether. *J. Am. Chem. Soc.* **2016**, jacs.6b04548. https://doi.org/10.1021/jacs.6b04548.

(28) Yasuhara, A.; Shibamoto, T. Determination of Physical and Spectral Data on Thiazolidines for Trace Aldehyde Analysis. *Agric. Biol. Chem.* **1989**, *53* (8), 2273–2274. https://doi.org/10.1271/bbb1961.53.2273.

(29) Rodríguez-Lozada, J.; Tovar-Gudiño, E.; Guevara-Salazar, J. A.; Razo-Hernández, R. S.; Santiago, Á.; Pastor, N.; Fernández-Zertuche, M. QSAR and Molecular Docking Studies of the Inhibitory Activity of Novel Heterocyclic GABA Analogues over GABA-AT. *Molecules* **2018**, *23* (11). https://doi.org/10.3390/molecules23112984.

(30) Mangold, C.; Dingels, C.; Obermeier, B.; Frey, H.; Wurm, F. PEG-Based Multifunctional Polyethers with Highly Reactive Vinyl-Ether Side Chains for Click-Type Functionalization. *Macromolecules* **2011**, *44* (16), 6326–6334. https://doi.org/10.1021/ma200898n.

(31) Obermeier, B.; Frey, H. Poly (Ethylene Glycol- Co -Allyl Glycidyl Ether) S : A PEG-Based Modular Synthetic Platform for Multiple Bioconjugation. **2011**, 436–444.

(32) Herzberger, J.; Leibig, D.; Liermann, J. C.; Frey, H. Conventional Oxyanionic versus Monomer-Activated Anionic Copolymerization of Ethylene Oxide with Glycidyl Ethers: Striking Differences in Reactivity Ratios. *ACS Macro Lett.* **2016**, *5* (11), 1206–1211. https://doi.org/10.1021/acsmacrolett.6b00701.

(33) Rather, S.; Clarke, H. T. The Action of Formaldehyde upon Cysteine. *J. Am. Chem. Soc.* **1937**, *59* (1), 200–206. https://doi.org/10.1021/ja01280a050.

(34) Esterbauer, H.; Ertl, A.; Scholz, N. The Reaction of Cysteine with α,β-Unsaturated Aldehydes. *Tetrahedron* **1976**, *32* (2), 285–289. https://doi.org/10.1016/0040-

4020(76)87015-9.

(35) Labbé, A.; Carlotti, S.; Deffieux, A.; Hirao, A. Controlled Polymerization of Glycidyl Methyl Ether Initiated by Onium Salt/Triisobutylaluminum and Investigation of the Polymer LCST. *Macromol. Symp.* **2007**, *249–250*, 392–397. https://doi.org/10.1002/masy.200750409.

(36) Jaacks, V. A Novel Method of Determination of Reactivity Ratios in Binary and Ternary Copolymerizations. *Die Makromol. Chemie* **1972**, *161* (1), 161–172. https://doi.org/10.1002/macp.1972.021610110.

(37) Blankenburg, J.; Stark, M.; Frey, H. Oxidation-Responsive Polyether Block Copolymers Lead to Non-Ionic Polymer Surfactants with Multiple Amine: N -Oxides. *Polym. Chem.* **2019**, *10* (13), 1569–1574. https://doi.org/10.1039/c9py00093c.

(38) Latscha, H. P.; Kazmaier, U. Stickstoffverbindungen. In *Chemie für Biologen*; Springer Berlin Heidelberg: Berlin, Heidelberg, 2016; pp 497–512. https://doi.org/10.1007/978-3-662-47784-7_30.

(39) Latscha, H. P.; Kazmaier, U. Schwefelverbindungen. In *Chemie für Biologen*; Springer Berlin Heidelberg: Berlin, Heidelberg, 2016; pp 489–495. https://doi.org/10.1007/978-3-662-47784-7_29.

4.1.6 Supporting Information

4.1.6.1 Monomer synthesis and characterization.

Synthesis of 2-alkylthiazolidines

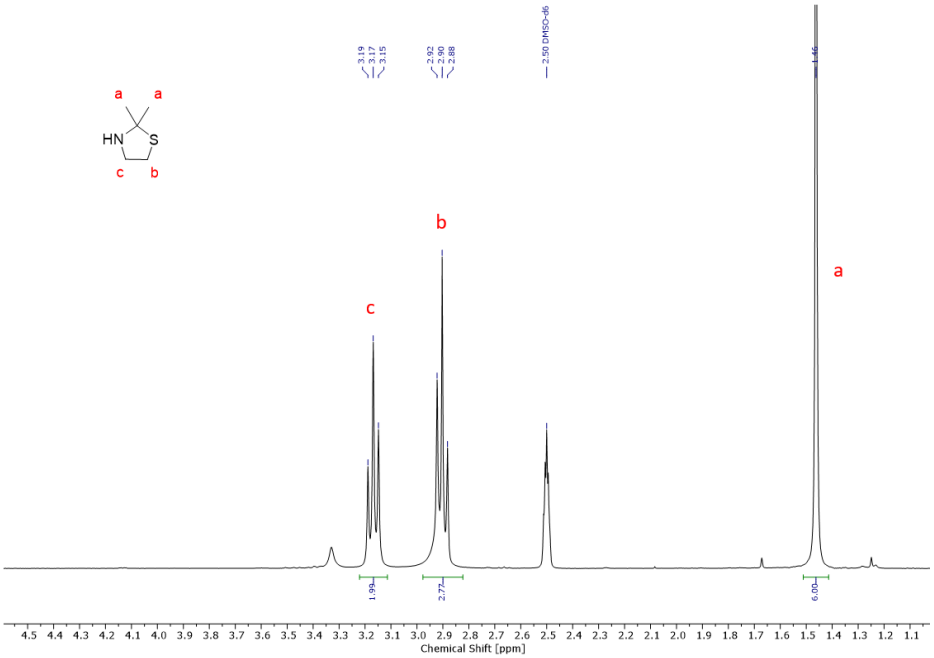

SI-Figure 1: ^{1}H NMR spectrum (300 MHz, DMSO-d_6) of DMT.

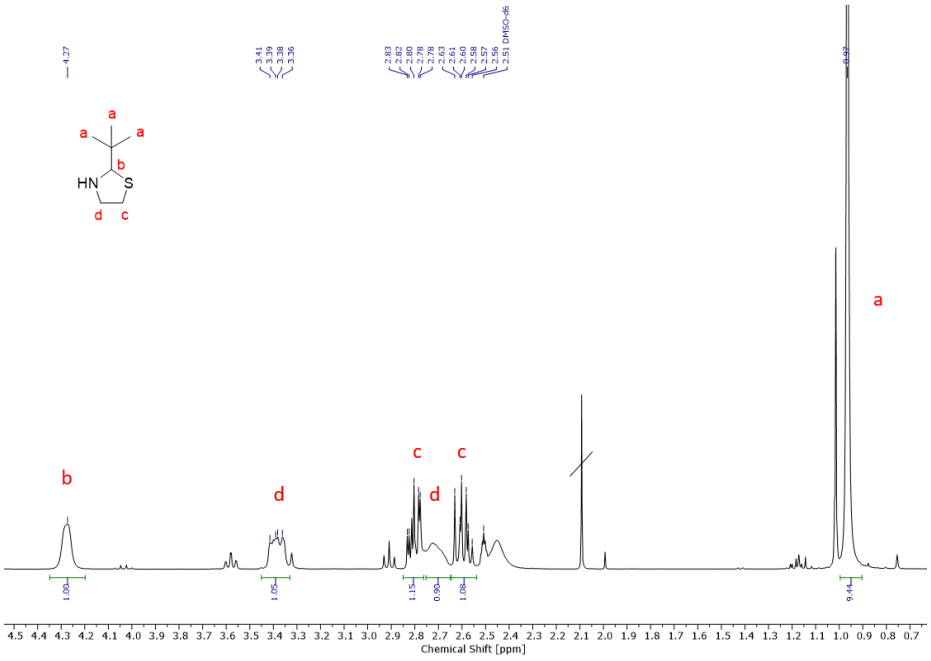

SI-Figure 2: ^{1}H NMR spectrum (300 MHz, DMSO-d_6) of TBT.

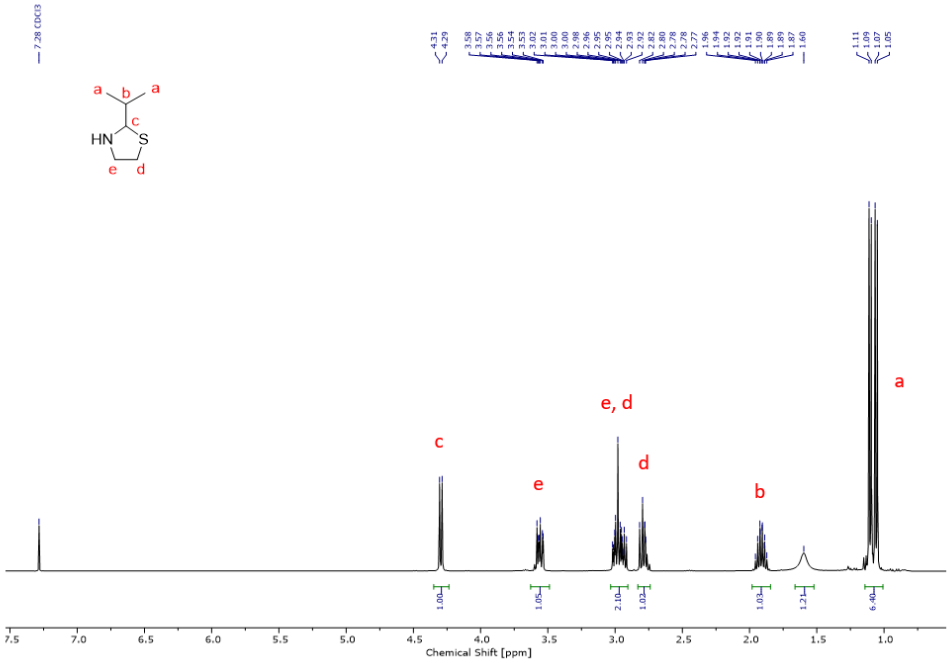

SI-Figure 3: ^{1}H NMR spectrum (300 MHz, chloroform-*d*) of IT.

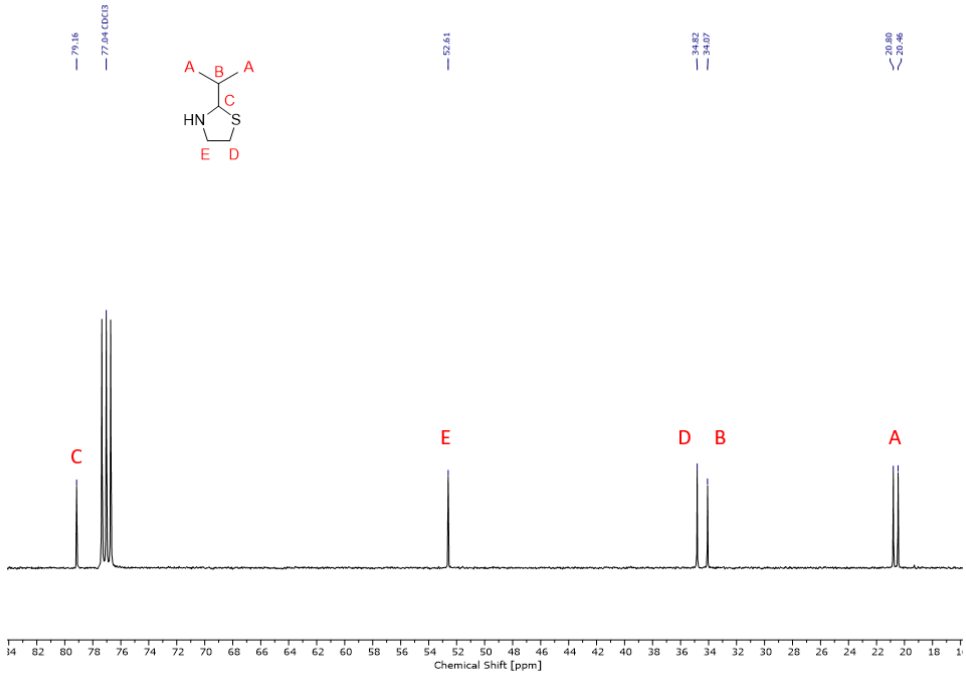

SI-Figure 4: ^{13}C NMR spectrum (75 MHz, chloroform-*d*) of IT.

Synthesis of 2-alkylthiazolidine ethanol

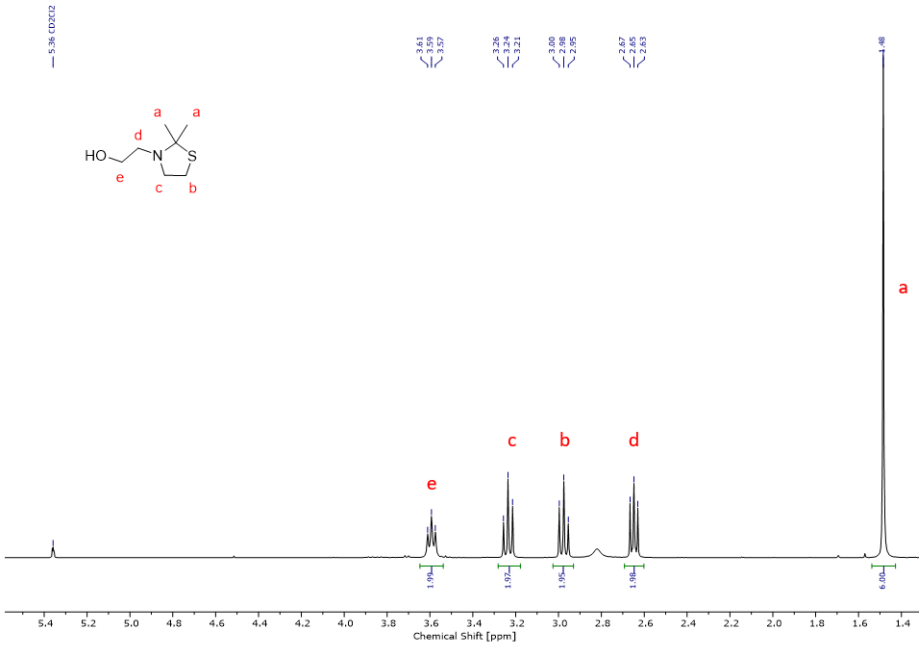

SI-Figure 5: ^{1}H NMR spectrum (300 MHz, methylene chloride-d_2) of DMTOH.

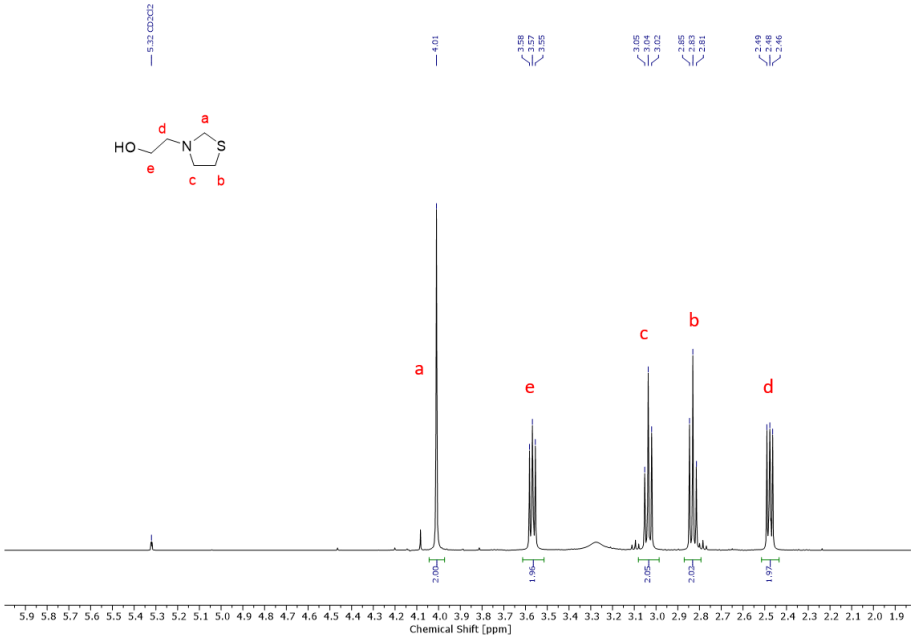

SI-Figure 6: ^{1}H NMR spectrum (300 MHz, methylene chloride-d_2) of TOH.

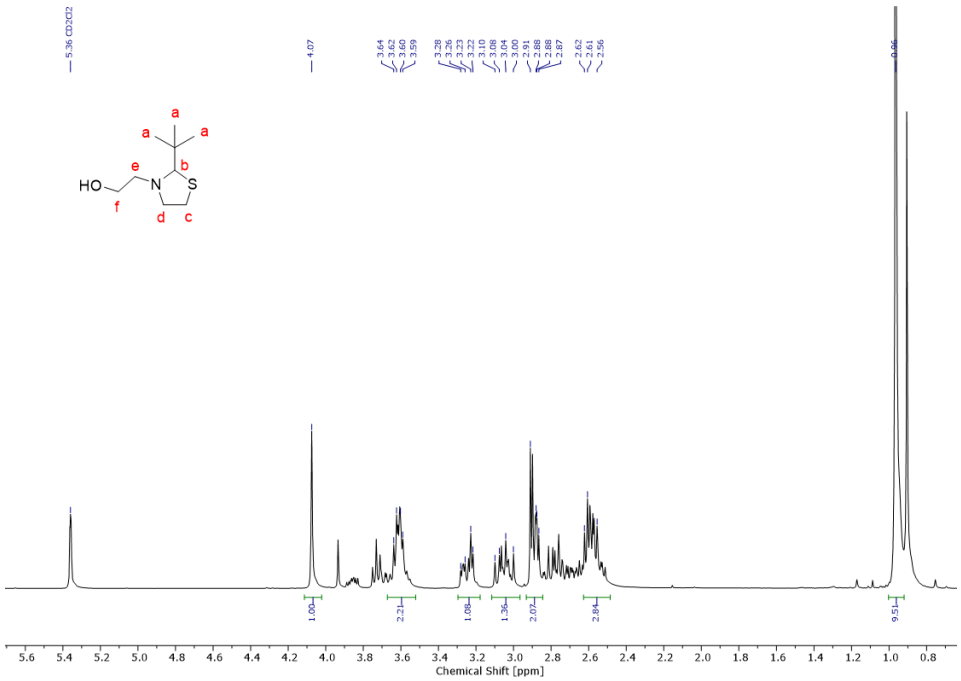

SI-Figure 7: ^{1}H NMR spectrum (300 MHz, methylene chloride-d_2) of TBTOH.

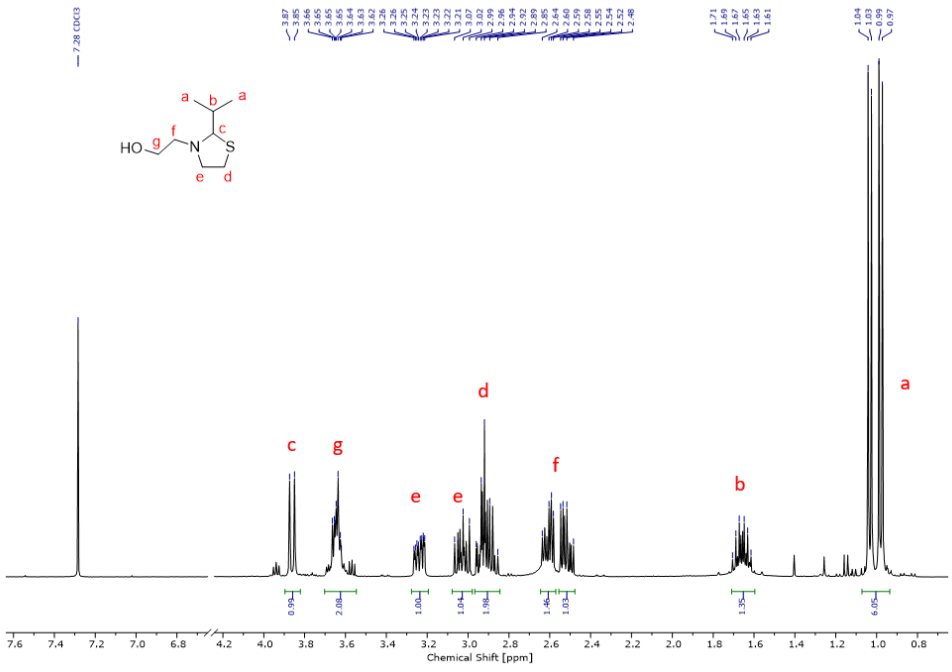

SI-Figure 8: ^{1}H NMR spectrum (300 MHz, chloroform-d) of ITOH.

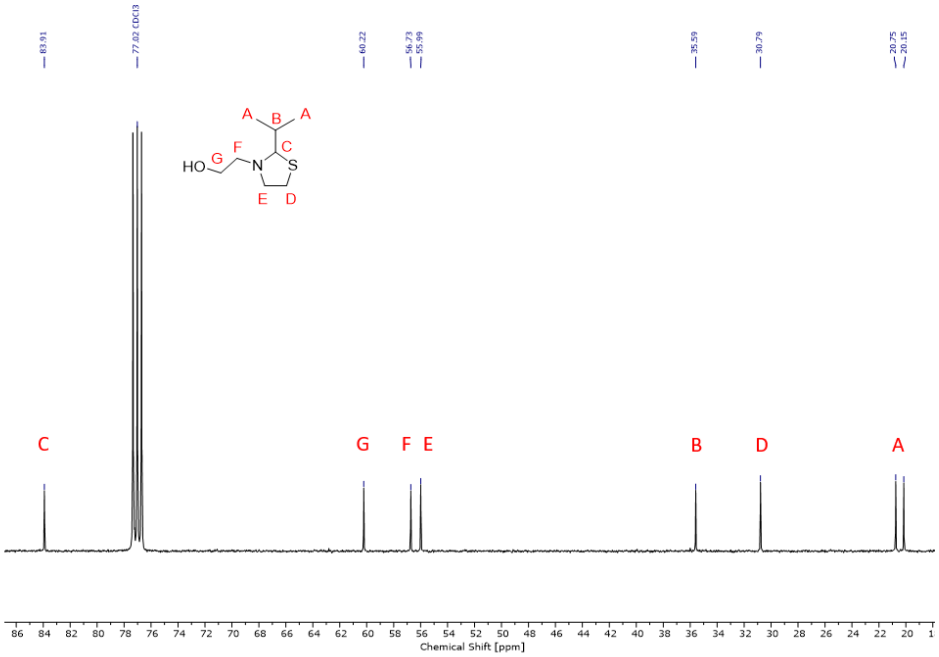

SI-Figure 9: ^{13}C NMR spectrum (75 MHz, chloroform-*d*) of ITOH.

Synthesis of 2-alkylthiazolidine ethyl glycidyl ether

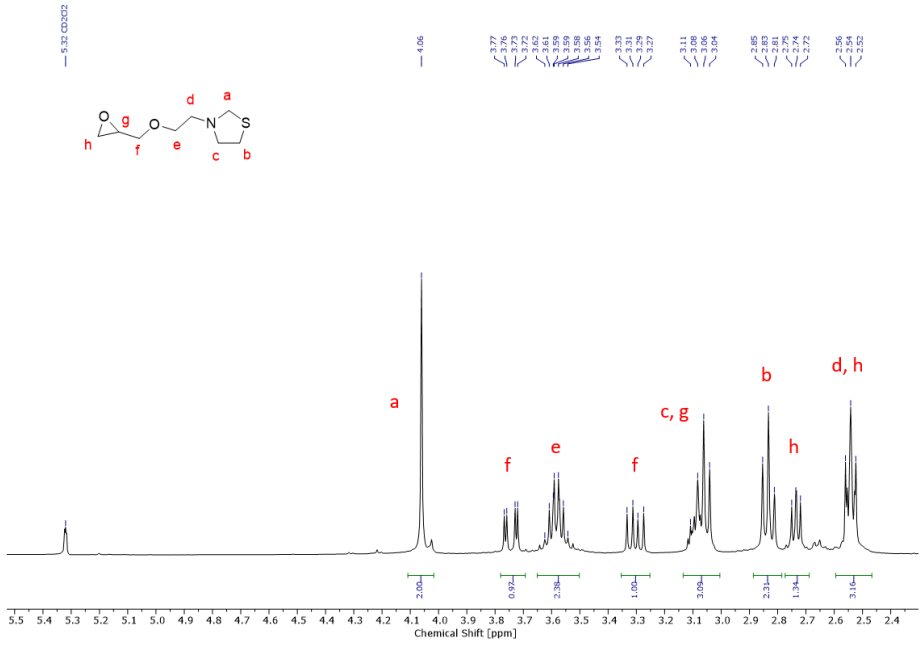

SI-Figure 10: ^{1}H NMR spectrum (300 MHz, methylene chloride-d_2) of TEGE.

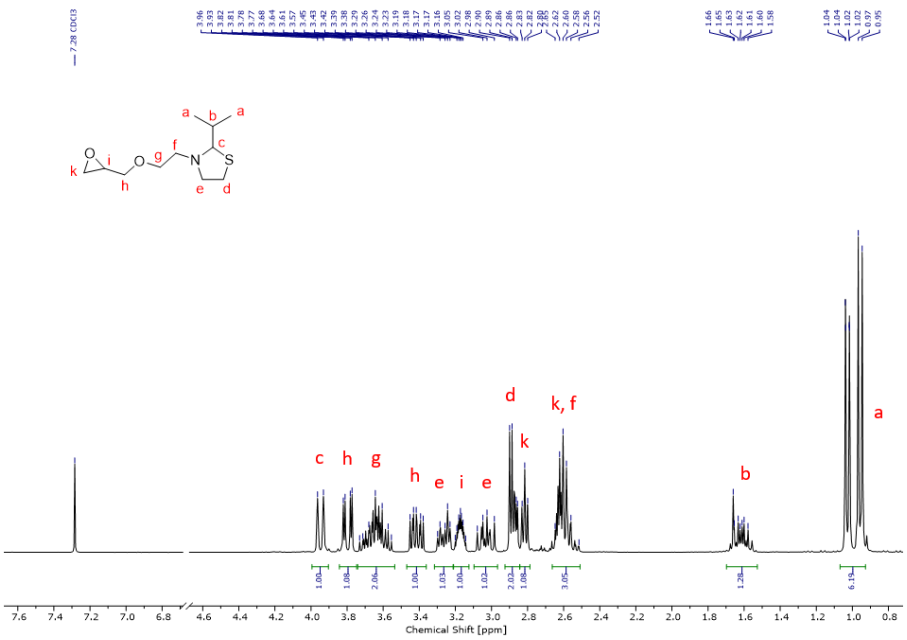

SI-Figure 11: ^{1}H NMR spectrum (300 MHz, chloroform-*d*) of ITEGE.

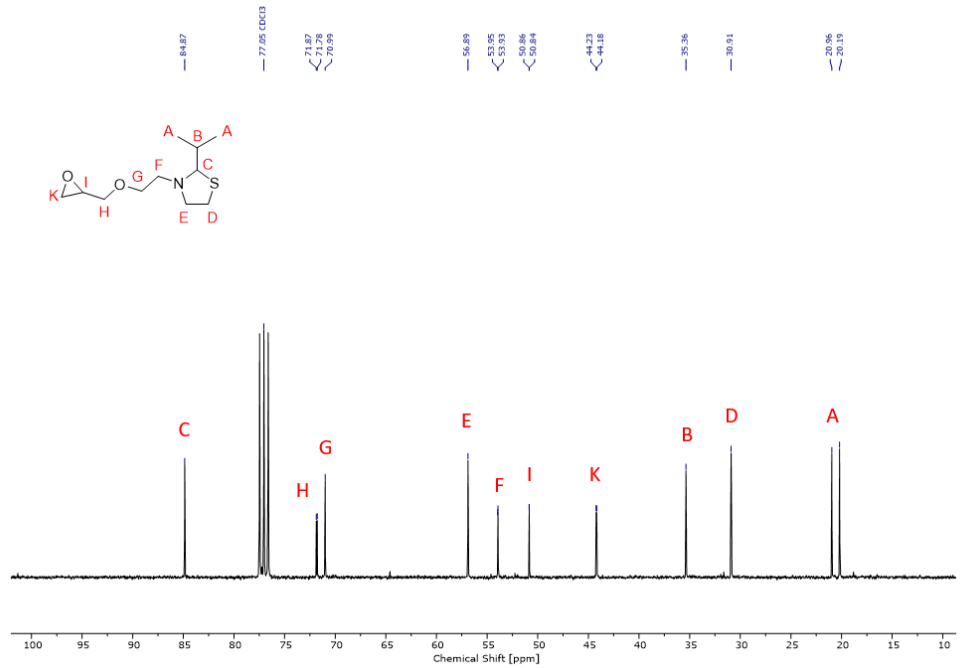

SI-Figure 12: ^{13}C NMR spectrum (75 MHz, chloroform-*d*) of ITEGE.

4.1.7 Polymer synthesis and characterization.

Synthesis of 2-alkylthiazolidine ethanol initiated PEG polymers

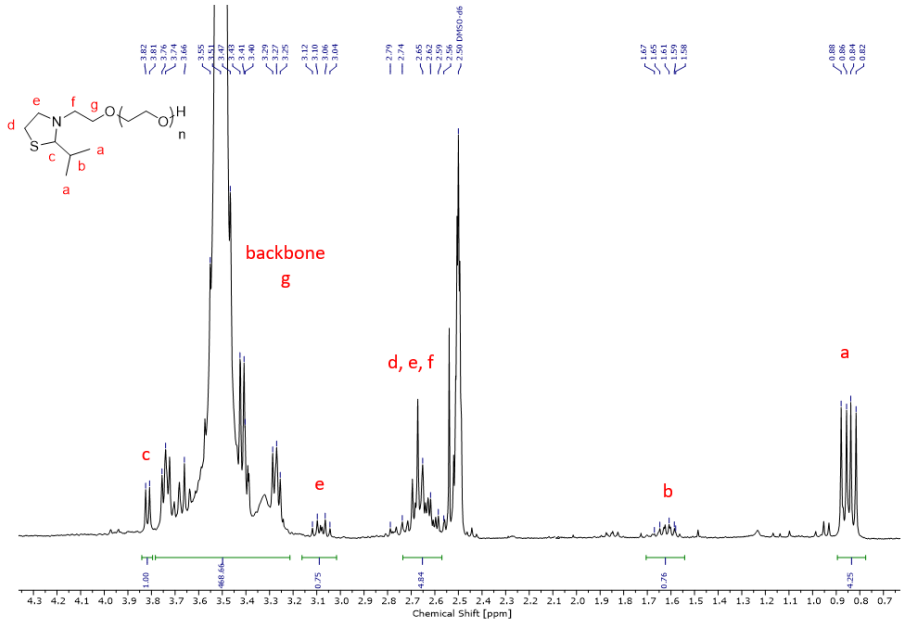

SI-Figure 13: ^{1}H NMR spectrum (300 MHz, DMSO-d_6) of IT-PEG.

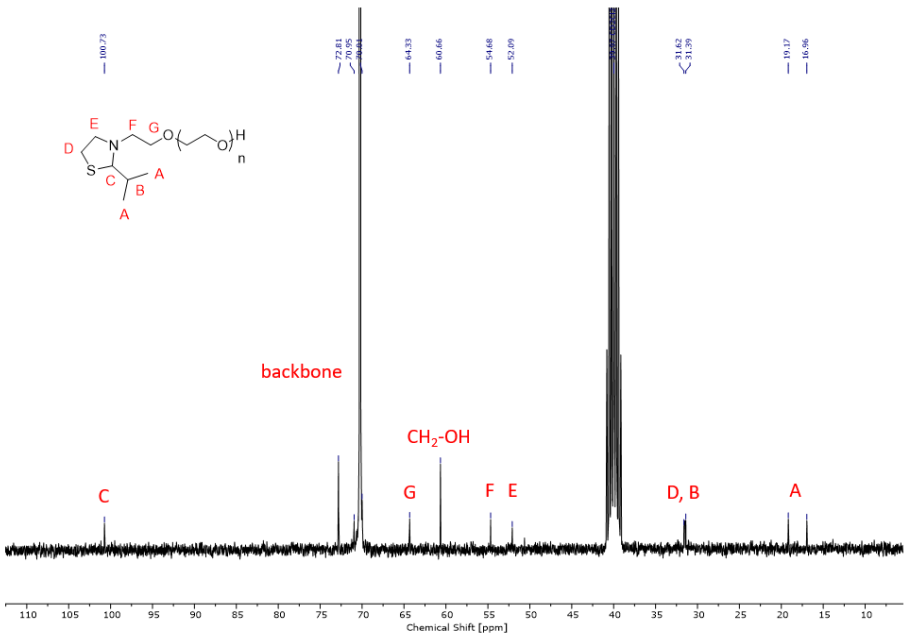

SI-Figure 14: ^{13}C NMR spectrum (75 MHz, DMSO-d_6) of IT-PEG.

Synthesis of P(ITEGE) homopolymer

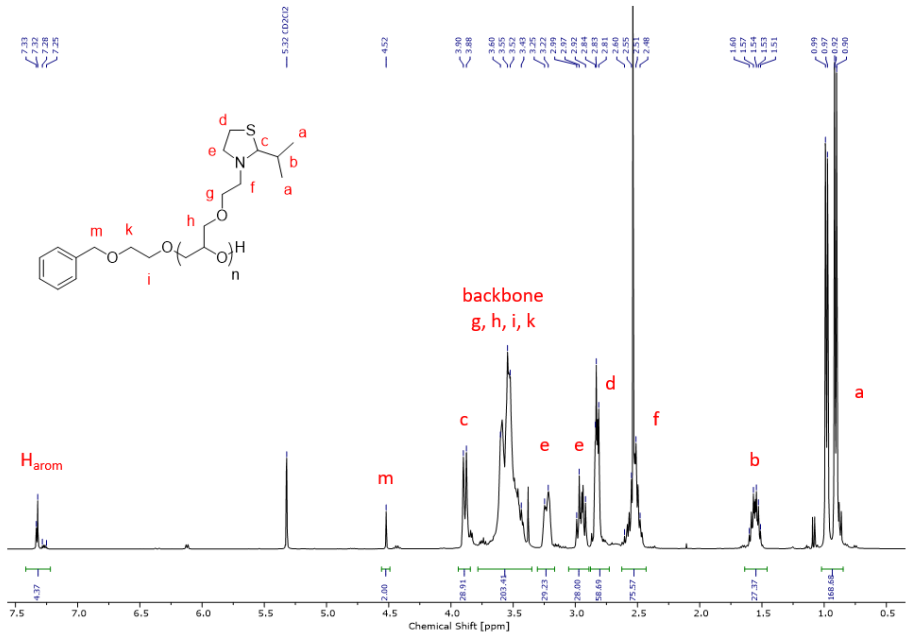

SI-Figure 15: ^{1}H NMR spectrum (400 MHz, methylene chloride-d_2) of the P(ITEGE) homopolymer.

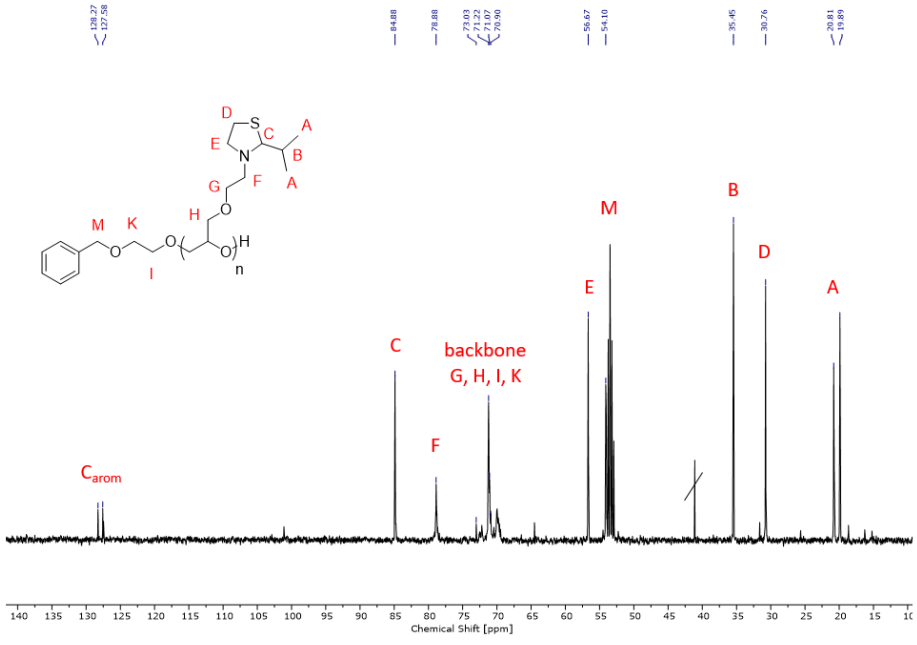

SI-Figure 16: ^{13}C NMR spectrum (101 MHz, methylene chloride-d_2) of the P(ITEGE) homopolymer.

Synthesis of P(EG-co-ITEGE) copolymer

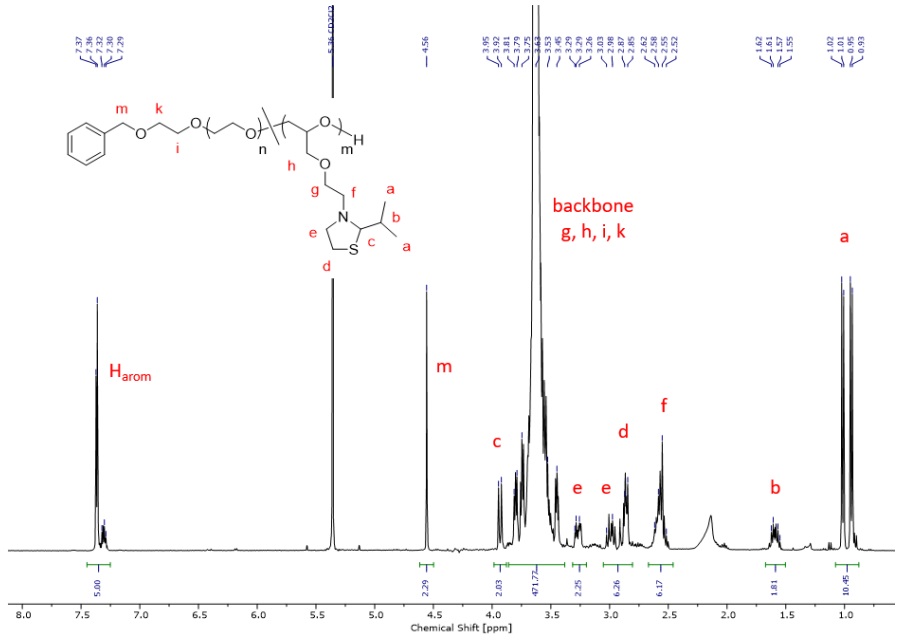

SI-Figure 17: ^{1}H NMR spectrum (400 MHz, methylene chloride-d_2) of P(EG$_{98}$-*co*-ITEGE$_2$).

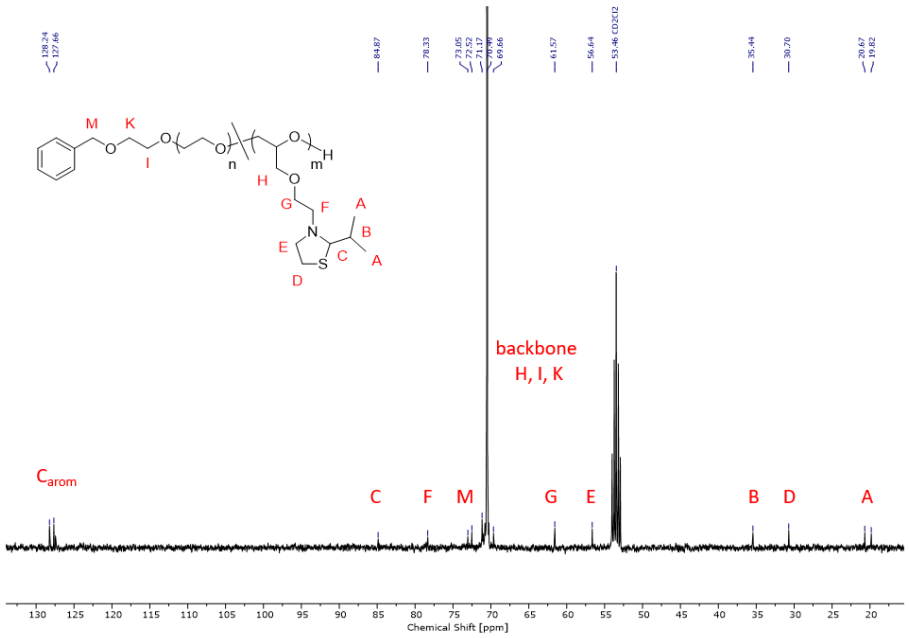

SI-Figure 18: ^{13}C NMR spectrum (101 MHz, methylene chloride-d_2) of P(EG$_{98}$-*co*-ITEGE$_2$).

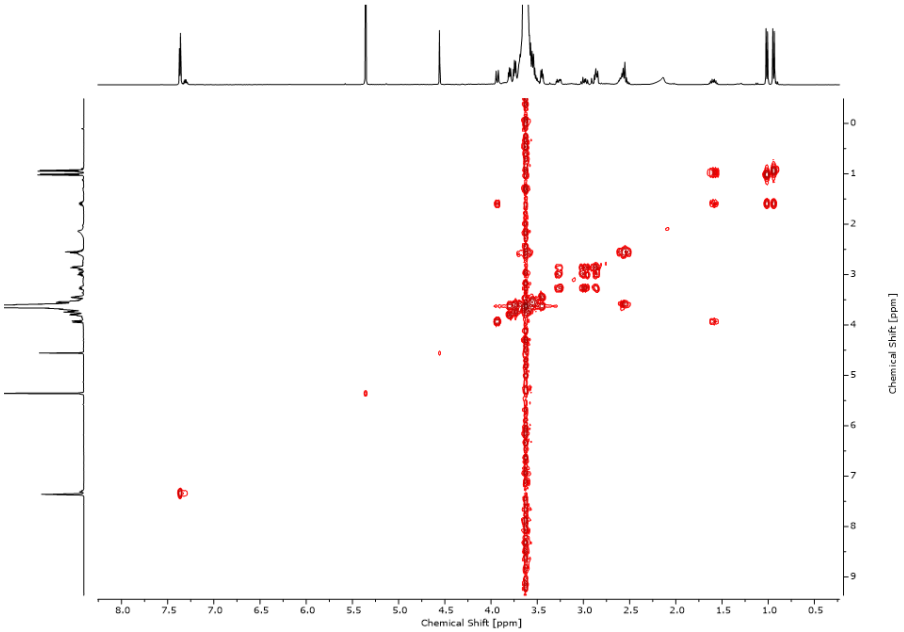

SI-Figure 19: ^{1}H, ^{1}H COSY NMR spectrum (400 MHz, methylene chloride-d_2) of P(EG$_{98}$-*co*-ITEGE$_2$).

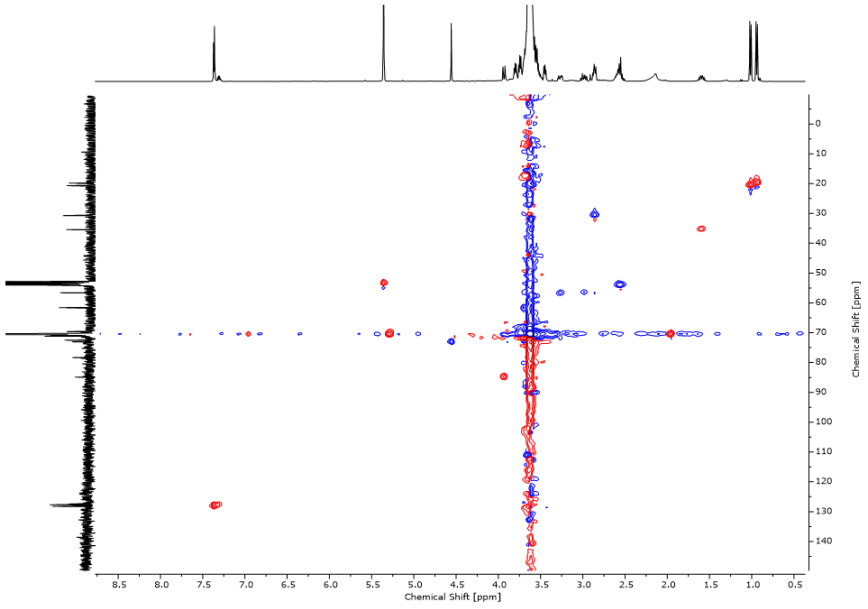

SI-Figure 20: ^{1}H, ^{13}C HSQC NMR spectrum (400 MHz, methylene chloride-d_2) of P(EG$_{98}$-*co*-ITEGE$_2$).

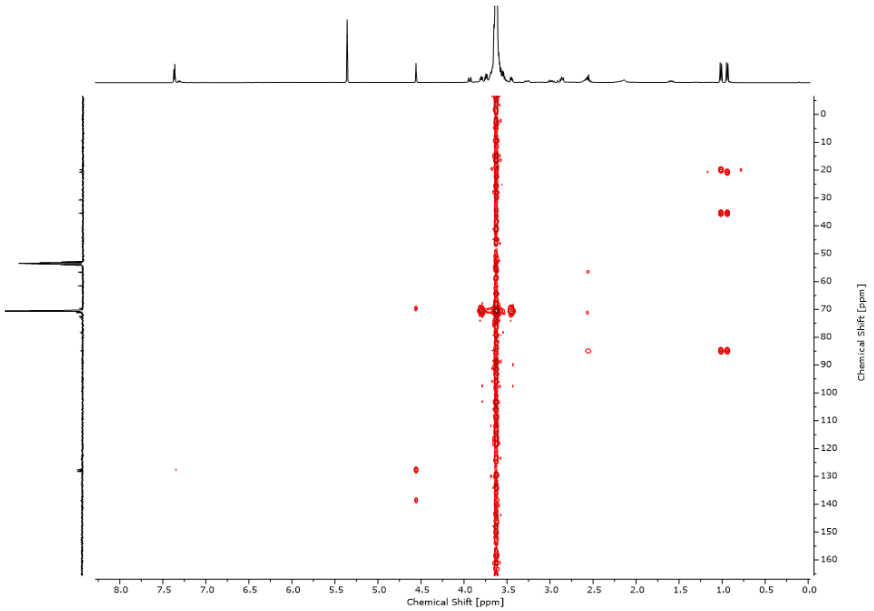

SI-Figure 21: ^{1}H, ^{13}C HMBC NMR spectrum (400 MHz, methylene chloride-d_2) of P(EG_{98}-*co*-$ITEGE_2$).

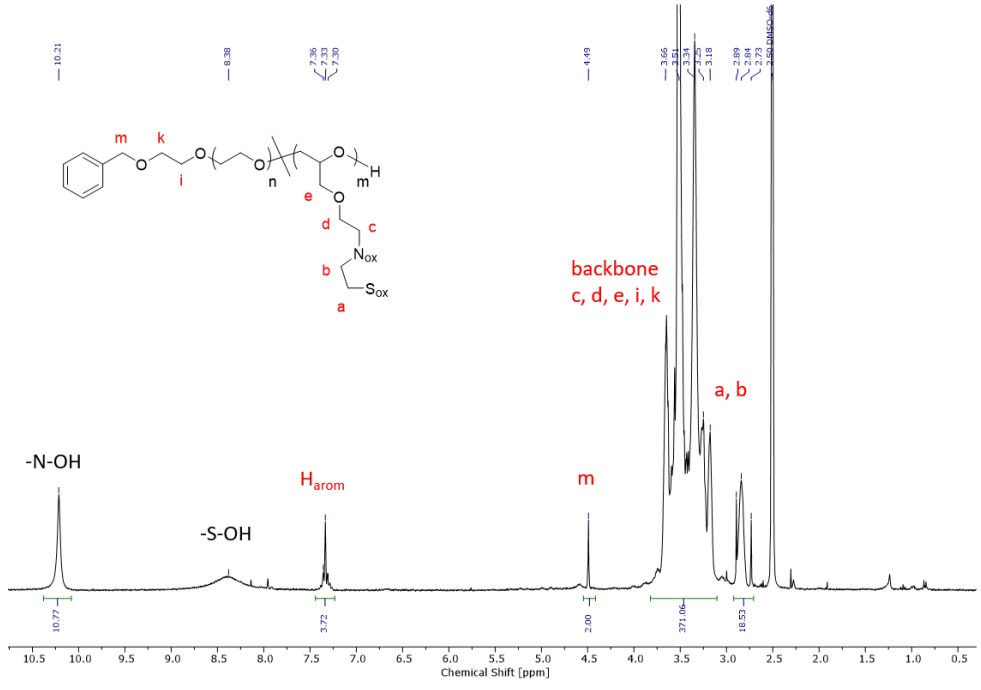

SI-Figure 22: ^{1}H NMR spectrum (400 MHz, DMSO-d_6) of P(EG-*co*-ITEGE) after oxidation with H_2O_2 solution.

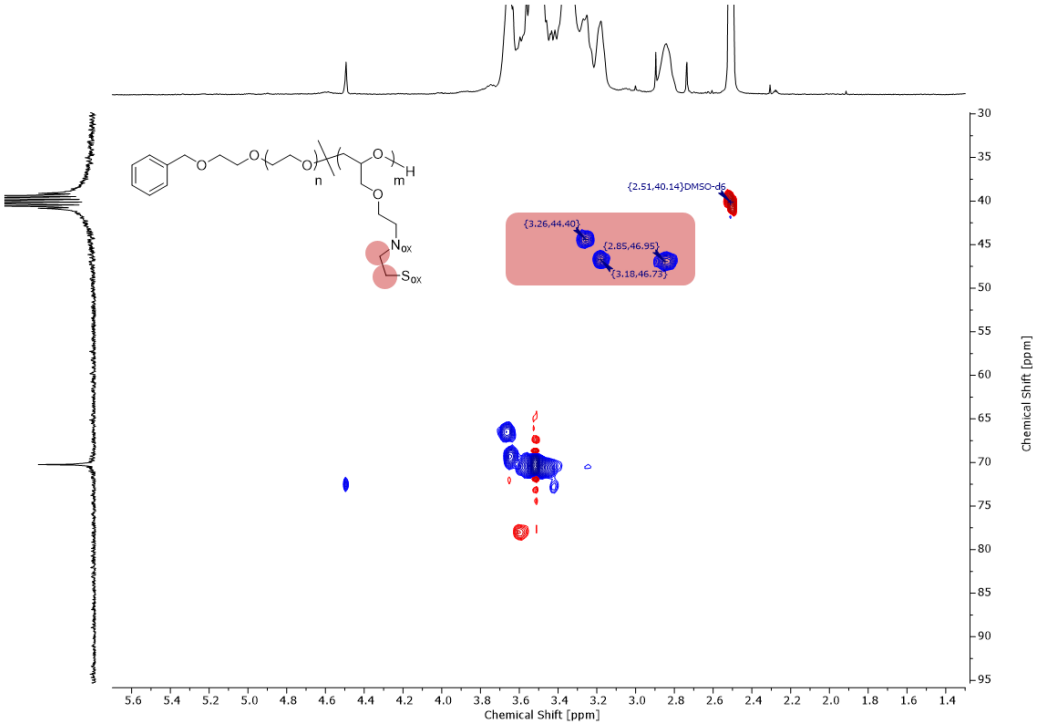

SI-Figure 23: ^{1}H, ^{13}C HSQC NMR spectrum (400 MHz, DMSO-d_6) of P(EG-*co*-ITEGE) after oxidation with H_2O_2 solution.

SEC measurements

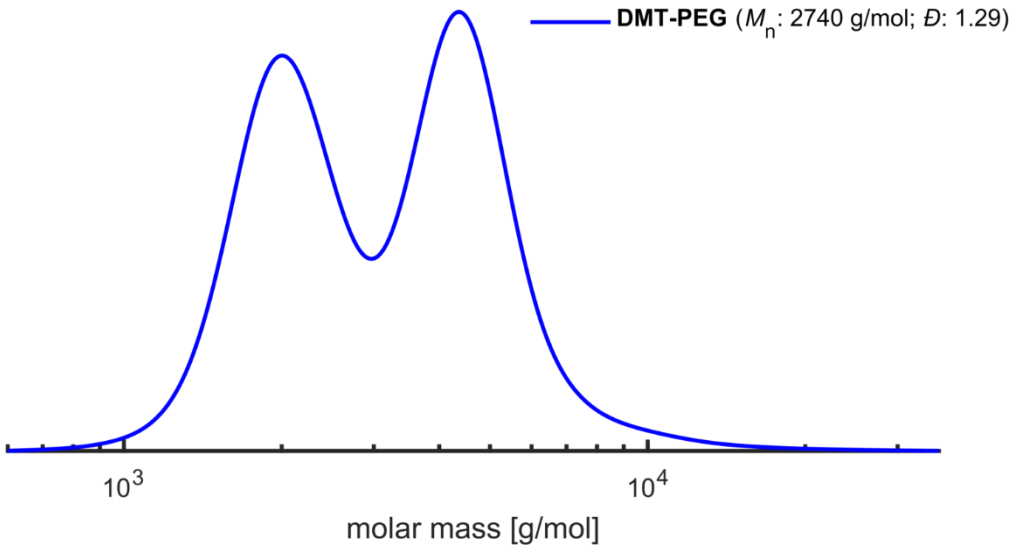

SI-Figure 24: SEC trace (RI detector, DMF, PEG standards) of DMT-PEG.

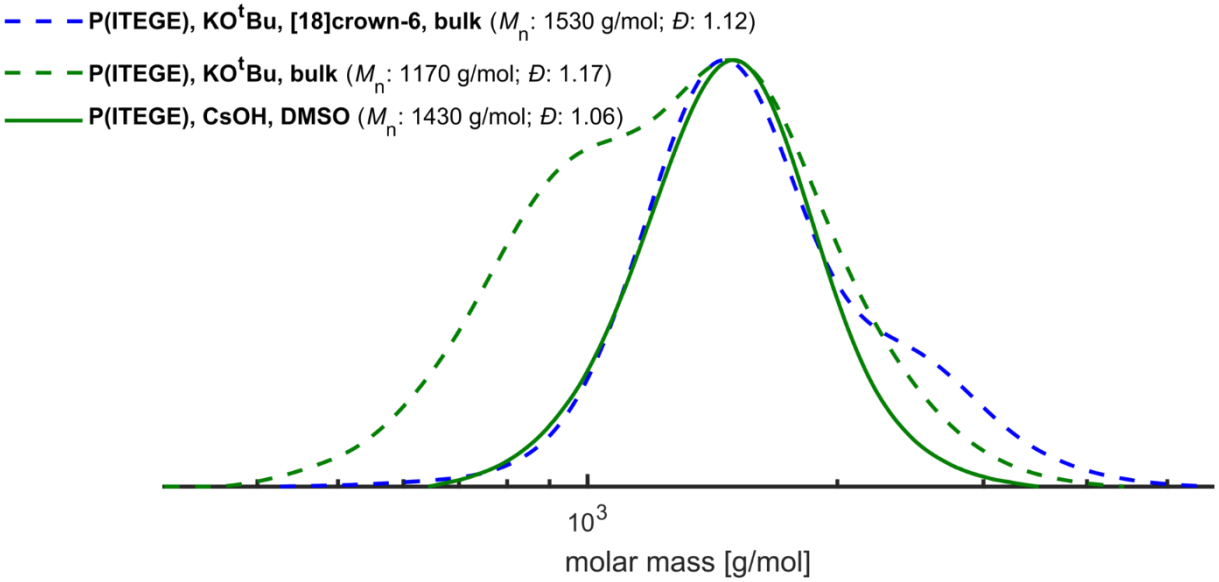

SI-Figure 25: SEC traces (RI detector, DMF, PEG standards) of P(ITEGE) synthesized *via* different synthesis routes.

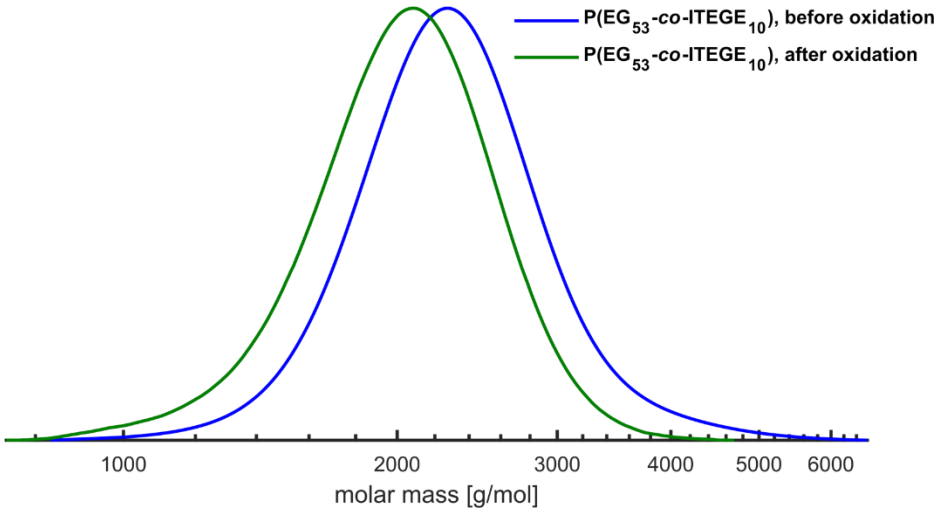

SI-Figure 26: SEC traces (RI detector, DMF, PEG standards) of P(EG-co-ITEGE) before (blue) and after oxidation (green).

4.1.7.1 *In situ* ^{1}H NMR kinetic studies.

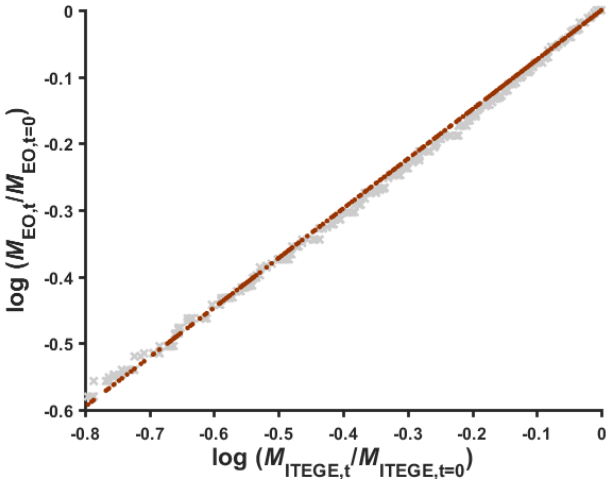

SI-Figure 27: Jaacks plot of the anionic copolymerization of P(EO-*co*-ITEGE) in DMSO-d_6 at 50 °C evaluated by *in situ* ^{1}H NMR experiments (R^2 = 0.99).

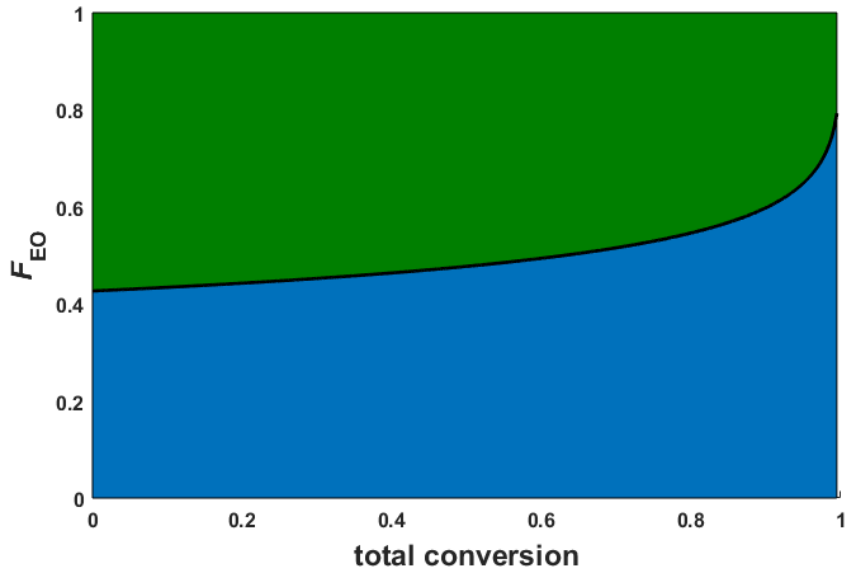

SI-Figure 28: Molar based composition diagram of P(EO-*co*-ITEGE) in DMSO-d_6 at 50 °C with an initial molar ratio of 0.5:0.5. F_{EO} = EO incorporation.

5 Appendix

5.1 Ketal- and Acetal-Functional Dialkyl-PEG Lipids for pH-Sheddable Stealth Liposomes

[redacted], † [redacted], § Eyleen Becker, † [redacted], § [redacted], †,c [redacted],*,§ and [redacted]*,†

†Department of Chemistry, Johannes Gutenberg University Mainz, Duesbergweg 10-14, 55128 Mainz, Germany

§Institute of Pharmacy and Biochemistry, Johannes Gutenberg University Mainz, Staudingerweg 5, 55128 Mainz, Germany

c Graduate School, Materials Science in Mainz, Staudinger Weg 9, 55128 Mainz, Germany

*E-Mail: [redacted], [redacted]

to be submitted

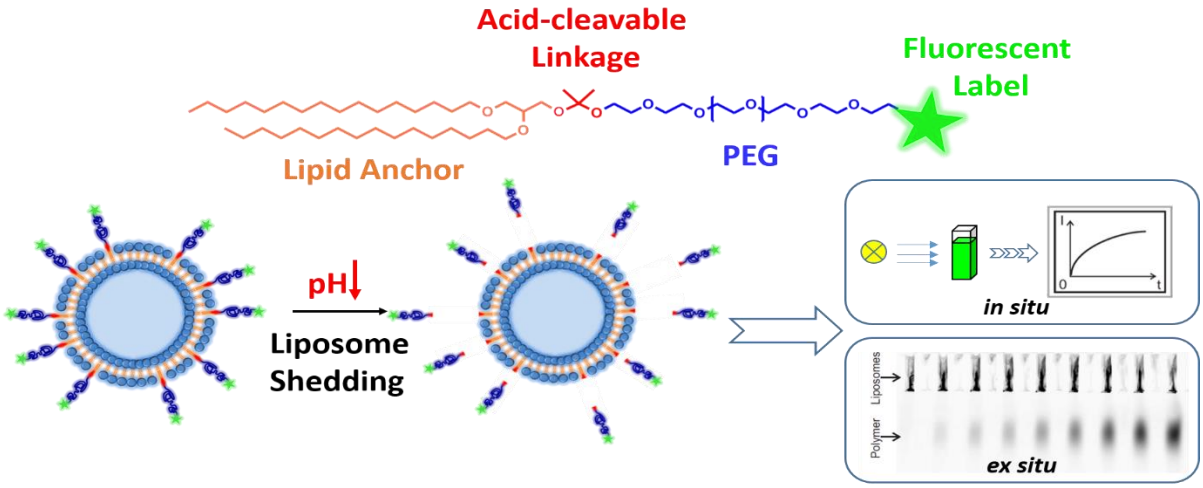

Abstract

In nanomedicine, stealth liposomes with PEG-lipids entrenched in their membranes represent potent drug delivery systems for the treatment of tumors. However, in the presence of a PEG stealth layer, cellular uptake and drug release can be hampered. Here we introduce a novel class of pH-sensitive PEG-lipids containing ketals and acetals as cleavable linkages to facilitate shedding of the PEG shell inside the tumor tissue or in a cellular compartment. A prototype one-step synthesis towards ketals is introduced to conveniently incorporate asymmetric ketals into PEG-based block structures. Modified bishexadecyl glycerols were used as initiators for the anionic ring-opening polymerization of ethylene oxide to access well-defined PEG-lipids ($Đ$ = 1.04 - 1.08) with tunable molecular weights (M_n = 2000 - 3500 g mol^{-1}). Online ^{1}H NMR spectroscopy served to evaluate kinetics of acidic hydrolysis. Fluorescence spectroscopy and agarose gel electrophoresis were employed to monitor pH-triggered shedding of liposomes, revealing highly promising cleavage profiles for the ketal-functional lipids ($t_{1/2}$ ~ 4h, pH 6.4). The findings demonstrate the potential of these functionalizable, pH-sensitive lipids for pH-triggered drug release strategies from liposomes.

Keywords

liposomes, poly(ethylene glycol), PEG, lipids, pH-cleavable, ketals

5.1.1 Introduction

In recent years, stimuli-responsive polymers have gained increasing attention in various fields of research due to their unique properties.[1,2] Stimuli-responsive materials are sensitive to an external trigger, such as pH, oxidation/reduction, light or temperature, upon which a structural change is induced. Structural changes may encompass solubility switches due to temperature/light-induced conformational changes, protonation,[3–5] or cleavage of pH-labile, redox-responsive, or light-sensitive moieties.[6,7] Especially in nanomedicine, pH-responsive polymers have proven advantageous for the design of drug carrier systems, since acidic compartments are present in various parts of human tissue. Lowered pH values have been reported for endosomal and lysosomal cellular compartments,[8] as well as for the microenvironment of various tumor cell lines and for inflammatory tissue.[9,10]

Poly(ethylene glycol) (PEG) is generally regarded as the gold standard polymer for medical applications due to its excellent biocompatibility and very low immunogenicity,[11,12] and increasing effort is devoted to incorporating pH-cleavable building blocks into PEG and its conjugates.[13,14] In liposomal research, pH-sensitive PEG-lipids have recently become attractive, as they enable shedding of stealth liposomes inside the targeted tissue to enhance efficacy of the drug carriers. The presence of a PEG stealth layer can hamper cellular uptake of liposomes and drug release.[15–17] Moreover, PEGylated nanoparticles can be subjected to accelerated blood clearance upon repetitive drug administration leading to an increased uptake by the liver.[18,19] PEG-lipids bearing pH-cleavable linkages can be employed to avoid these drawbacks of PEG in liposomes.[20,21] Examples of acid-cleavable moieties incorporated into pH-sensitive liposomes (PSL) include hydrazones,[21–24] orthoesters,[24–26] acetals,[27] vinyl ethers,[28,29] and cyclic ketals.[30] The corresponding strategies are generally based on chemical modification of commercially available monomethoxy PEG (mPEG) and therefore lack the possibility to attach further functionalities such as dye labels or radioactive tracers, for instance to unravel the fate of the cleaved PEG chains. Also linking of targeting ligands to enable directed drug delivery is not possible. Furthermore, molecular compositions are restricted to the commercially available molecular weights of PEG, limiting precise tuning of lipid properties.

Within the class of acid-hydrolyzable moieties, acetals and ketals constitute highly potent representatives, as the substitution patterns provides a means of fine-tuning their susceptibility towards hydrolysis.[31] Generally, acetals are hydrolyzed several orders of magnitude slower than respective ketals.[32] These circumstances allow for the design of hydrolysis profiles to match the specific requirements for controlled release strategies. Increasing effort has been expended on incorporating acetals and ketals into polymeric structures.[33–38] However, to date, no synthetic routes are available to conveniently access ketals composed of two different alcohol components without tedious purification or multi-step reactions. A straightforward approach to these asymmetric ketals may grant access to novel, pH-cleavable block-type structures and polymer conjugates, thereby extending the scope of pH-sensitive materials for triggered drug release purposes. The design of lipids that combine suitable pH-dependent hydrolysis with tailored molecular compositions and, in addition, facilitate the attachment of further functional groups remains a challenge.

Recent findings in liposomal research have elucidated higher membrane integrity of polyether-based lipids containing dialkyl-derived anchor groups compared to cholesterol-functional lipids.[39] These results motivate a stronger focus on dialkyl-containing polyether-based lipids, since stable anchorage in the membrane can further enhance stability profiles of stealth liposomes and therefore prevent extracellular leakage of the cargo, while ligand-mediated targeting efficiencies are increased as well. In this work, we introduce a novel class of acid-cleavable dialkyl glycerol PEG-lipids containing ketals and acetals as scissile linkages and demonstrate their potential for pH-sensitive stealth liposomes. A prototype one-step strategy based on vinyl ether chemistry is presented, offering straightforward access to asymmetric ketals in polymers. Acetal- and ketal-containing dialkyl glycerol derivatives have been synthesized and used as initiators for the anionic ring-opening polymerization of ethylene oxide to obtain pH-cleavable lipids with precisely tunable molecular weights of PEG and narrow molecular weight distributions. The susceptibility of the PEG-lipids towards acidic hydrolysis has been evaluated *via* real-time ^{1}H NMR kinetic studies. Furthermore, functionalization of the lipids *via* copper(I)-catalyzed azide-alkyne click chemistry with fluorescent dyes has been demonstrated *via* a post-preparational approach at the liposomal surface. pH-triggered shedding of the liposomes endowed with

the fluorescent-labelled PEG-lipids have been monitored by fluorescence spectroscopy and gel electrophoresis, revealing promising cleavage profiles for the ketal-functional lipid species.

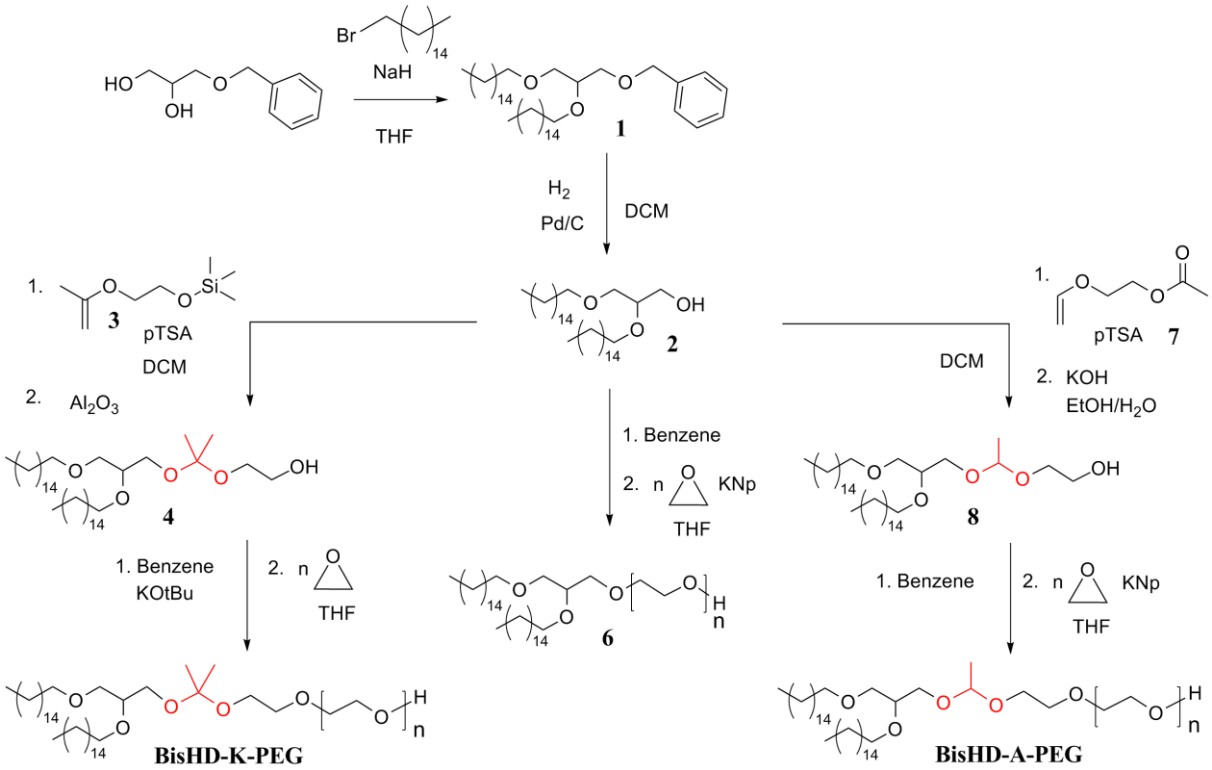

Scheme 1: Synthesis of bishexadecyl glycerol-based lipids.

5.1.2 Experimental part

Instrumentation

^{1}H NMR spectra were measured on a Bruker Avance II 400 MHz (5 mm BBO probe, 256 Scans, and B-ACS 60 auto sampler) at 294 K. 2D NMR and ^{13}C NMR spectra were recorded on a Bruker Avance II 400 (100.5 MHz, 5 mm BBO probe, and B-ACS 60 auto sampler) at 294 K, if not stated otherwise. ^{13}C inverse gated NMR spectra were recorded with 2048 scans and a relaxation delay of 10 s. Relaxation times T_1 for the ketal species were determined *via* saturation recovery methods. All spectra were processed with MestReNova v9.0 software.

GPC (SEC) data were obtained using Agilent 1100 Series endowed with a PSS HEMA-column ($10^6/10^4/10^2$ Å porosity), LiBr/DMF (1 g/L) as eluent using RI detection. Molecular weights and dispersity ($Đ = M_w/M_n$) were determined with monodisperse PEG standards from *Polymer Standard Service GmbH (PSS)*.

MALDI-ToF mass spectrometry was conducted on an Axima CFR MALDI-ToF mass spectrometer using pencil lead or α-cyano-4-hydroxy-cinnamonic acid (CHCH) as matrix and potassium trifluoroacetate (KTFA) as a source for cations.

Materials

All chemicals were obtained from *Sigma Aldrich, TCI Europe*, or *Acros Organics* unless stated otherwise. Deuterated solvents (C_6D_6, CD_2Cl_2, $CDCl_3$, DMSO-d_6, D_2O) were purchased from *Deutero GmbH*. Egg phosphatidylcholine (EPC, fully hydrogenated EPC3) was kindly provided by *Lipoid GmbH* (Ludwigshafen, Germany). Cholesterol was purchased from *Carl Roth* (Karlsruhe, Germany). Atto 488 azide was obtained from *Atto-Tec* (Siegen, Germany). 2-[2-[(Trimethylsilyl)oxy]ethoxy]propene (**3**),[40] and 2-Acetoxyethoxy vinyl ether (**7**)[41] were synthesized according to reported procedures. THF used for the anionic ring-opening polymerization was dried and stored over sodium/benzophenone. Care must be taken when handle the flammable, toxic, and gaseous ethylene oxide.

Methods

Liposome preparation was conducted *via* dual centrifugation (DC) according to a method previously described.[42] Briefly, ethanolic solutions of hydrated egg phosphatidyl choline (EPC, Lipoid, Ludwigshafen, Germany), cholesterol (Carl Roth, Karlsruhe, Germany) and the respective polymeric amphiphile were combined to yield 85 µmol (~5 mg) in a molar ratio of 50:45:5, respectively, and dried *in vacuo*. Lipid samples were stored at -80 °C until use to prevent degradation of the ketal structures. 9.3 µL of Dulbecco's phosphate buffered saline (DPBS, Thermo-Fisher Scientific, Waltham, MA, USA) and 70 mg of ceramic beads (SiLyBeads ZY 0.3 – 0.4 mm) were added and the sample subjected to a 20 min dual centrifugation run at 2500 RPM, utilizing a customized Hettich Rotanta 400 centrifuge (Hettich, Tuttlingen, Germany) with a custom made inset. 28 µL DPBS were added and the obtained vesicular phospholipid gel subjected to two more 2 min DC runs, in between of which the sample orientation was reversed. Stock liposome suspensions were stored at 4 °C until usage, highly sensitive ketal compounds were used immediately.

Liposome functionalization was carried out according to a previously established protocol.[43] For copper-catalyzed azide alkyne cycloaddition, the following reactants were added in the

listed order: MilliQ water (to a total volume of 40 µL), phosphate buffer (5.3 mM NaH_2PO_4, 94.7 mM Na_2HPO_4, pH 8), THPTA (0.5 mM), $CuSO_4$ (0.1 mM), and sodium ascorbate (2.5 mM), Atto 488 azide (Atto-Tec, Siegen, Germany, 50 µM), liposome suspension (10 µL). After incubation for 2 h at 25 °C, the reaction was stopped by addition of 1 µL of 50 mM EDTA (Carl Roth) solution. Liposome suspensions were purified *via* gel filtration over custom-made Sepharose 2B-CL (Sigma-Aldrich, St. Louis, MO, USA) columns, fluorimetric determination assured a complete removal of residual free fluorophore azide.

Liposome cleavage was quantified either *via* a fluorescence spectrometric *in situ* approach or *via* an *ex situ* approach, utilizing separation of cleavage products *via* polyacrylamide gel electrophoresis (PAGE). For the fluorimetric assay, quartz glass cuvettes (Hellma, Müllheim, Germany) with a 1 cm path length and tight PTFE plugs were used in a Jasco FP-6500 Fluorimeter (Jasco, Tokyo, Japan) equipped with an ETC-273T temperature controller, a Peltier element stage with a magnetic stirrer and a HAAKE WKL26 cooling unit (Thermo-Fisher Scientific). 2.5 µL of conventional liposomes, consisting only of EPC and cholesterol were combined with 3.8 mL DPBS for 24 h to saturate the glass surface in order to prevent adsorption of labeled amphiphiles. After removal, a liposome sample was added to the cuvette in PBS in a total volume of 2.53 mL, while the amount of liposomes was adjusted to yield Atto 488 in a concentration of 50 nM. After equilibration for 1 h, 1.26 mL of citric acid solutions were added to yield 3.8 mL total volume and no gas phase in the cuvette. Citric acid concentrations were previously determined to yield final pH values of 2.4, 3.4, 4.4, 5.4 and 6.4. For pH 7.4, DPBS was used. For pH 8.4, a sodium tetraborate buffer (12 mM $Na_2B_4O_7$, 126 mM NaCl) was used instead. Fluorescence emission (exc. 490 nm, em. 520 nm) was measured with data rates between 5 sec^{-1} and 7.5 h^{-1} under constant stirring and at 25 °C. Other measurement parameters: em./exc. Bandwith 5 nm, PMT voltage "high". For the *ex situ* approach, samples of liposome suspensions were combined with solutions of citric acid as described above, to obtained the previously determined pH values. Samples were taken at the intended timepoints and neutralized with Na_2HPO_4 solutions of specific and previously tested concentrations. As a gel loading buffer, 4 µL of a 60% (v/v) glycerol solution in DPBS was added and samples were stored at -80 °C until further analysis. PAGE was conducted with 10 cm x 20 cm x 2 mm 15% denaturing polyacrylamide gels (PAGE

system, Carl Roth) for 2 h and 15 min at a constant power of 15 W, employing a CBS LSG-400-20 adjustable vertical electrophoresis stand (CBS Scientific, San Diego, USA) and a Consort EV232 power supply (Consort, Turnhout, Belgium). Gels were imaged with a Typhoon 9600 multimode imager with a blue laser unit (GE Healthcare), illuminated at 488 nm and analyzed with a 520 nm bandpass 40 nm filter. ImageJ was used for analysis and measurement of background-corrected band intensities.[44] The data was fit with Origin (Origin-Lab, Northampton, MA; USA) to the first order exponential decay function $y = A_1 * e^{(-x/t1)} + y_0$, while fluorescence intensities were normalized to target values y_0 obtained from a first order fit. The half-life time was calculated from $t_{1/2} = \ln(2) * t_1$.

Cytotoxicity: MTT Assay

Cytotoxicity of liposomal suspensions was assessed by a 3-(4,5-Dimethylthiazol-2-yl)-2,5-diphenyltetrazoliumbromid (MTT) assay. HeLa cells were seeded in a density of 10,000 per well in 96-well optical bottom plates (Greiner, Frickenhausen, Germany) 12 h before incubation. To test liposome toxicity, medium was replaced with fresh medium containing liposomes in total lipid concentrations of 100, 10, 1 and 0.1 mg/mL. After 24 h, 40 µL of a 5 mg/mL solution of MTT in D-PBS (Thermo-Fisher Scientific, Waltham, MA, USA) were added to the cells and incubated for 1 hour. After careful removal of the medium, 225 µL of a 1:8 v/v mixture of glycine buffer pH 10 and DMSO were added and the cells shaken for 15 min to dissolve the precipitated crystals. 25 µL from each well diluted with 150 µL of glycine buffer pH 10-DMSO mixture (1:8 v/v) in a fresh 96-well plate. Absorbance of MTT was measured at 595 nm with background correction at 670 nm on a Tecan M200 plate reader, values were normalized to untreated cells. All measurements were performed in technical triplicates.

^{1}H NMR Kinetics

Deuterated phosphate/citrate phosphate buffer solutions were produced by mixing of two stock solutions and adjustment of the pH with a pH electrode. Stock solutions of K_2HPO_4 (100 mmol L^{-1}) and KH_2PO_4 (100 mmol L^{-1}) in deuterated water were used for phosphate buffer at pD 6.4. Accordingly, stock solutions of citric acid (100 mmol L^{-1}) and K_2HPO_4 (100

mmol L^{-1}) in deuterated water were used for the citrate phosphate buffer at pD 3.4 and pD 5.4. The respective pD values were obtained *via* the equation pD = pH + 0.4.[45]

For *in-situ* ^{1}H NMR degradation kinetics, 50 mg of the respective polymer were dissolved in 0.7 mL of deuterated buffer and transferred into a NMR tube immediately after dissolving. The NMR tube was placed in a preheated NMR spectrometer (37 °C) and the sample was locked to the solvent signal and shimmed after the sample temperature was constant (ΔT = 0.1 K) for 2 min. Spectra were recorded with 16 scans at 2-minute intervals during the first hour, then at 5-minute intervals for 2 hours, at 10-minute intervals within the next 5 hours due to a decrease in the reaction rate. The kinetic analysis was stopped manually after complete cleavage was achieved.

Synthesis procedure

3-Benzyl-1,2-bishexadecyl-rac-glycerol **1**. In a 1000mL three-necked round-bottom flask equipped with a reflux condenser and a mechanical stirrer 1-benzyl-*rac*-glycerol (5.0 g, 27.4 mmol) and sodium hydride (2.6 g, 109.7 mmol) were dissolved in dry THF (400 mL) under argon atmosphere. 1-Bromohexadecane (33.5 g, 109.7 mmol) was added via syringe and the reaction mixture was stirred at reflux for 6 d. The solvent was evaporated under reduced pressure and the resulting residue was dissolved in a 1/1-mixture of diethyl ether/water (500 mL). After stirring for 16 h, the aqueous phase was neutralized via addition of diluted sulfuric acid (1 mol L^{-1}) and the organic phase was separated. The aqueous solution was extracted three times with diethyl ether and the combined organic layers were dried over sodium sulfate and filtrated. The solvent was evaporated under reduced pressure and excess 1-bromohexadecane was removed under high vacuum. The pure product (10.1 g, 16.0 mmol, 58 %) was obtained after column chromatography (eluent: petrol ether/ diethyl ether 30:1) over silica.

^{1}H NMR (400 MHz, $CDCl_3$): δ [ppm] 7.40–7.23 (m, 5H, CH_{Ar}), 4.56 (s, 2H, ArCH_2), 3.65–3.37 (m, 9H, CH_2-CH_2-O, CH-CH_2-O and CH_2-CH-O), 1.66–1.48 (m, 4H, CH_2-CH_2-O), 1.43–1.15 (m, 52H, CH_2), 0.88 (t, 6H, J_{AB} = 6.3 Hz, CH_3-CH_2).

1,2-Bishexadecyl-rac-glycerol **2**. **1** (10.1 g, 16.0 mmol) was dissolved in DCM (200 mL) and stirred with 10wt%-palladium on activated charcoal (505 mg) under hydrogen atmosphere

for 3 d. The residue was subsequently filtrated through Celite and the filter cake was washed with DCM. After evaporation of the solvent, the pure product was afforded as colorless crystals in quantitative yield.

^{1}H NMR (400 MHz, $CDCl_3$): δ [ppm] 3.78–3.36 (m, 9H, CH_2-C*H*$_2$-O, CH-C*H*$_2$-O and CH_2-C*H*-*O*), 1.63–1.49 (m, 4H, C*H*$_2$-CH_2-O), 1.40–1.17 (m, 52H, CH_2), 0.88 (t, 6H, J_{AB} = 6.6 Hz, C*H*$_3$-CH_2).

2-[2-[(Trimethylsilyl)oxy]ethoxy]propene **3**. This compound was synthesized according to literature.[40] Storage under argon atmosphere at 8 °C was essential to prevent decomposition.

2-((2-[2,3-bis(hexadecyloxy)propoxy]propan-2-yl)oxy)ethanol **4**. *p*-Toluenesulfonic acid monohydrate (9.6 mg, 0.056 mmol) and **2** (300 mg, 0.557 mmol) were dissolved in benzene (15 mL) in a dry Schlenk flask and stirred at 40 °C under slightly reduced pressure for 15 min keeping the stopcock closed. Moisture was removed via azeotropic distillation with benzene, and subsequent drying in high vacuum at 40 °C for 16 h. After cooling to RT, the residue was dissolved in dry DCM (15 mL) and **3** (969 mg, 5.57 mmol) was added. The reaction was stirred for 90 min and quenched with triethylamine. After removing all volatiles in high vacuum, the pure product (147 mg, 41 %) was afforded via column chromatography over alox (neutral, 6wt% H_2O) applying a stepwise alteration of the eluent from petrol ether to petrol ether/ethyl acetate (20:1) to petrol ether/ethyl acetate (10:1).

^{1}H NMR (400 MHz, C_6D_6): δ [ppm] 3.77–3.43 (m, 11H, CH_2-O and CH_2-C*H*-*O*), 3.37 (t, 2H, J_{AB} = 6.5 Hz, CH_2-C*H*$_2$-O-CH_2), 1.71–1.54 (m, 4H, CH_2-C*H*$_2$-CH_2-O), 1.34–1.10 (m, 58H, CH_2 and CO_2-$(CH_3)_2$), 0.91 (t, 6H, J_{AB} = 6.7 Hz, C*H*$_3$-CH_2).

^{13}C NMR (100.6 MHz, C_6D_6): δ [ppm] = 99.95 (1C, *CO*$_2$$(CH_3)_2$), 78.97 (1C, *CH*-$CH_2O$), 71.89 (1C, CH_2-*CH*$_2$*O*-CH_2), 71.46 (1C, CH-*CH*$_2$*O*-CH_2), 70.97 (1C, CH_2-*CH*$_2$*O*-CH), 62.82 (1C, CH-*CH*$_2$*O*-$CO(CH_3)_2$), 62.47 (1C, CH_2OH), 61.85 (1C, *CH*$_2$-CH_2OH), 32.38 (2C, CH_3-CH_2-*CH*$_2$), 30.79-29.88 (24C, CH_2), 26.74 (2C, CH_2), 25.11 (2C, CO_2(CH_3)$_2$), 23.16 (2C, *CH*$_2$-CH_3), 14.41 (2C, CH_2-*CH*$_3$).

α-(2-[2,3-bis(hexadecyloxy)propoxy]propan-2-yl) ω-hydro PEG ***BisHD-K-PEG***. Compound **4** (100 mg, 0.155 mmol) and dry potassium *tert*-butoxide (15.6 mg, 0.139 mmol) were dissolved in benzene (10 mL) and stirred in a dry Schlenk flask under slightly reduced

pressure at 50 °C for 15 min keeping the stopcock closed. Moisture and generated *tert*-butanol were removed by azeotropic distillation of benzene and subsequent drying at 50 °C in high vacuum for 16 h. After cooling to RT, dry THF (15 mL) was cryo-transferred into the Schlenk flask and ethylene oxide (1.11 mL, 22.3 mmol) was cryo-transferred via a graduated ampule into the initiator solution. The reaction was proceeded at 40 °C for 2 d and the polymerization was quenched with methanol (2 mL). After precipitation in cold diethyl ether, all volatiles were removed in vacuum and the pure polymer was obtained. (Yield: 81 %)

^{1}H NMR (400 MHz, C_6D_6): δ [ppm] 3.77–3.25 (m, 158H, CH_2O and CH_2-C*HO*), 1.71–1.53 (m, 4H, C*H*$_2$-CH_2-O), 1.51–1.10 (m, 58H, CH_2 and CO_2-$(CH_3)_2$), 0.90 (t, 6H, J_{AB} = 6.7 Hz, C*H*$_3$-CH_2).

^{13}C NMR (100.6 MHz, C_6D_6): δ [ppm] = 100.00 (1C, *CO*$_2$$(CH_3)_2$), 78.97 (1C, *CH*-$CH_2O$), 73.17-60.74 (79C, CH_2O), 32.35 (2C, CH_3-CH_2-*CH*$_2$), 30.87-29.84 (24C, CH_2), 26.76 (2C, *CH*$_2$-CH_2-CH_2O), 25.12 (2C, CO_2(*CH*$_3$)$_2$), 23.12 (2C, *CH*$_2$-CH_3), 14.40 (2C, CH_2-*CH*$_3$).

1,2-Bishexadecylglycerol PEG **6**. Compound **2** (200 mg, 0.371 mmol) was dissolved in benzene (10 mL) and stirred in a dry Schlenk flask under slightly reduced pressure at 60 °C for 15 min keeping the stopcock closed. Moisture was removed by azeotropic distillation of benzene and subsequent drying at 70 °C in high vacuum for 16 h. After cooling to RT, dry THF (15 mL) was cryo-transferred into the Schlenk flask and potassium naphthalenide in THF (0.37 mL, 0.18 mmol, c = 0.5 mol L^{-1}, prepared from potassium (235 mg, 6.0 mmol) and naphthalene (770 mg, 6.0 mmol) in dry THF (12 mL) in a glovebox under argon) was added via syringe. Generated hydrogen was removed in vacuum and ethylene oxide (1.11 mL, 22.3 mmol) was cryo-transferred via a graduated ampule into the initiator solution. The reaction was carried out at 40 °C for 3 h and subsequently continued at 60 °C for 3 d. The polymerization was quenched with methanol (2 mL) and the polymer was precipitated in cold diethyl ether. After removing all volatiles under vacuum, the pure polymer was obtained. (Yield: 82 %) ^{1}H NMR (400 MHz, DMSO-*d*$_6$): δ [ppm] 3.70–3.20 (m, 250H, C*H*$_2$-O and CH_2-C*H*-*O*), 1.50–1.38 (m, 4H, C*H*$_2$-CH_2-O), 1.34–1.10 (m, 52H, CH_2), 0.84 (t, 6H, J_{AB} = 6.4 Hz, C*H*$_3$-CH_2).

2-Acetoxyethoxy vinyl ether **7**. This compound was synthesized according to prescriptions described in the literature.[41]

2-(2-[2,3-bis(hexadecyloxy)propoxy]ethoxy)ethyl acetate ***BisHD-Acetal-Acetate***. Compound **2** (600 mg, 1.11 mmol) and *p*-toluenesulfonic acid monohydrate (19 mg, 0.11 mmol) were dissolved in a dry Schlenk flask in benzene (15 mL) and stirred under slightly reduced pressure at 40 °C for 15 min keeping the stopcock closed. Moisture was removed by azeotropic distillation of benzene and subsequent drying at 40 °C in high vacuum for 2 h. After cooling to RT, the mixture was dissolved in dry DCM (15 mL) and a solution of 2-acetoxy ethoxy vinyl ether **7** (724 mg, 5.57 mmol) in dry DCM (15 mL) was added via syringe. The reaction was stirred for 15 min and subsequently quenched via addition of triethylamine (5 mL). After washing of the solution with 1N sodium hydroxide (100 mL), the aqueous phase was extracted with DCM (50 mL) and the combined organic layers were dried over sodium sulfate. The solvent was evaporated under reduced pressure and excess vinyl ether was removed in high vacuum for 16 h. The pure product (712 mg, 1.06 mmol, 96 %) was obtained by column chromatography (eluent: petrol ether/ethyl acetate, 10:1) over silica.

^{1}H NMR (400 MHz, C_6D_6): δ [ppm] 4.68 (q, 1H, J_{AB} = 5.4 Hz, O_2CHCH_3), 4.25–4.09 (m, 2H, CH_2-$COOCH_3$), 3.85–3.44 (m, 9H, CH_2-O and CH_2-CH-O), 3.40 (t, 2H, J_{AB} = 6.3 Hz, CH_2-CH_2-O-CH_2), 1.72 (s, 3H, CH_3OOCH_2), 1.70–1.54 (m, 4H, CH_2-CH_2-CH_2-O), 1.52–1.27 (m, 52H, CH_2), 1.25 (d, 3H, J_{AB} = 5.4 Hz, O_2CH-CH_3), 0.92 (t, 6H, J_{AB} = 6.7 Hz, CH_3-CH_2).

^{13}C NMR (100.6 MHz, C_6D_6): δ [ppm] 170.11 (1C, $COOCH_3$), 100.19 (1C, O_2CH-CH_3), 78.73 (1C, CH-CH_2O), 71.88 (1C, CH_2-CH_2O-CH_2), 71.62 (1C, CH-CH_2O-CH_2), 70.97 (1C, CH_2-CH_2O-CH), 65.76 (1C, CH-CH_2O-$CHOCH_3$), 63.82 (1C, CH_2O-$COCH_3$), 63.03 (1C, CH_2-CH_2O-$COCH_3$), 32.38 (2C, CH_3-CH_2-CH_2), 30.79-29.88 (24C, CH_2), 26.77 (2C, CH_2-CH_2-CH_2-O), 23.16 (2C, CH_2-CH_3), 20.52 (2C, CH_2O-$COCH_3$), 19.73 (2C, O_2CH-CH_3), 14.40 (2C, CH_2-CH_3).

2-(2-[2,3-bis(hexadecyloxy)propoxy]ethoxy)ethanol **8**. Potassium hydroxide (1.78 g, 31.8 mmol) and ***BisHD-Acetal-Acetate*** (712 mg, 1.06 mmol) were dissolved in a mixture of ethanol (320 mL)/water (19 mL, 1.06 mmol). The solution was stirred at reflux for 2 h and

ethanol was removed under reduced pressure. The residue was dispersed in diethyl ether (300 mL) and washed with diluted sodium hydroxide (300 mL, 0.1 mol L^{-1}). Subsequently, the organic phase was dried over sodium sulfate and the solvent was evaporated in vacuum. The crude product was purified by column chromatography over silica (petrol ether/ethyl acetate, 6:1) yielding a ceraceous, yellowish solid (605 mg, 0.96 mmol, 91 %) as the pure product.

^{1}H NMR (400 MHz, CD_2Cl_2): δ [ppm] 4.73 (q, 1H, J_{AB} = 5.3 Hz, O_2CHCH_3), 3.70–3.37 (m, 13H, CH_2O and CH_2-C*H-O*), 2.31 (s, 1H, OH), 1.58–1.47 (m, 4H, CH_2-CH_2-CH_2-O), 1.37–1.16 (m, 52H, CH_2), 1.29 (d, 3H, J_{AB} = 5.3 Hz, O_2CH-CH_3), 0.92 (t, 6H, J_{AB} = 6.7 Hz, CH_3-CH_2).

α-(2-[2,3-bis(hexadecyloxy)propoxy]ethoxy) ω-hydro PEG ***BisHD-A-PEG*** . Compound **8** (200 mg, 0.371 mmol) was dissolved in benzene (10 mL) and stirred in a dry Schlenk flask under slightly reduced pressure at 60 °C for 15 min keeping the stopcock closed. Moisture was removed by azeotropic distillation of benzene and subsequent drying at 70 °C in high vacuum for 16 h. After cooling to RT, dry THF (15 mL) was cryo-transferred into the Schlenk flask and potassium naphthalenide in THF (0.37 mL, 0.18 mmol, c = 0.5 mol L^{-1}, prepared from potassium (235 mg, 6.0 mmol) and naphthalene (770 mg, 6.0 mmol) in dry THF (12 mL) in a glovebox under argon) was added via syringe. Generated hydrogen was removed in vacuum and ethylene oxide (1.11 mL, 22.3 mmol) was cryo-transferred via a graduated ampule into the initiator solution. The reaction proceeded at 40 °C for 3 h and subsequently continued at 60 °C for 3 d. The polymerization was quenched with methanol (2 mL) and the polymer was precipitation in cold diethyl ether. After removing all volatiles under vacuum, the pure polymer was obtained. (Yield: 82 %)

^{1}H NMR (400 MHz, C_6D_6): δ [ppm] 4.74 (q, 1H, J_{AB} = 5.3 Hz, O_2CHCH_3), 3.88–3.26 (m, 190H, CH_2O and CH_2-C*H-O*), 1.69–1.55 (m, 4H, CH_2-CH_2-O), 1.49–1.21 (m, 52H, CH_2), 1.29 (d, 3H, J_{AB} = 5.3 Hz, O_2CH-CH_3), 0.91 (t, 6H, J_{AB} = 6.4 Hz, CH_3-CH_2).

^{13}C NMR (100.6 MHz, C_6D_6): δ [ppm] = 100.46 (1C, *O_2CH*-CH_3), 78.86 (1C, *CH*-CH_2O), 73.24–61.89 (87C, CH_2O), 32.36 (2C, CH_3-CH_2-*CH_2*), 30.86-29.85 (24C, CH_2), 26.76 (2C, *CH_2*-CH_2-CH_2O), 23.14 (2C, *CH_2*-CH_3), 19.96 (1C, O_2CH-*CH_3*), 14.40 (2C, CH_2-*CH_3*).

General procedure applied to access alkyne-functional lipids. Example: BisHD-A-PEG Alkyne. In a dry Schlenk flask, compound **9** (300 mg, 0.115 mmol) was dissolved in dry THF (15 mL) under argon atmosphere. The solution was cooled to 0 °C, sodium hydride (8.3 mg, 0.34 mmol) was added and the mixture was stirred for 10 min. Propargyl bromide (51.1 mg, 0.34 mmol, 80 wt% in toluene) was injected via syringe and the reaction was carried out at RT for 20 h. After filtration, the solution was reduced to a small volume and the polymer was precipitated in cold diethyl ether. (280 mg, 92 %)

^{1}H NMR (400 MHz, C_6D_6): δ [ppm] 4.74 (q, 1H, J_{AB} = 5.3 Hz, O_2CHCH_3), 3.94 (d, 2H, $^{4}J_{AB}$ = 2.4 Hz, OCH_2-CCH), 3.86–3.25 (m, 190H, CH_2O and CH_2-CH-O), 2.14 (m, 1H, OCH_2-CCH), 1.71–1.54 (m, 4H, CH_2-CH_2-O), 1.52–1.19 (m, 52H, CH_2), 1.29 (d, 3H, J_{AB} = 5.3 Hz, O_2CH-CH_3), 0.90 (t, 6H, J_{AB} = 6.4 Hz, CH_3-CH_2).

^{13}C NMR (100.6 MHz, C_6D_6): δ [ppm] 100.46 (1C, O_2CH-CH_3), 80.47 (1C, OCH_2-CCH), 78.86 (1C, CH-CH_2O), 74.70 (1C, OCH_2-CCH), 73.24–64.97 (87C, CH_2O), 58.38 (1C, OCH$_2$-CCH), 32.36 (2C, CH_3-CH_2-CH_2), 30.86-29.85 (24C, CH_2), 26.76 (2C, CH_2-CH_2-CH_2O), 23.14 (2C, CH_2-CH_3), 19.96 (1C, O_2CH-CH_3), 14.40 (2C, CH_2-CH_3).

5.1.3 Results and discussion

5.1.3.1 Synthesis of Acid-Labile 1,2-Bis-*n*-hexadecyl Glycerol Macroinitiators.

Recent findings confirmed superior membrane stability of 1,2-dialkyl-glycerol-based lipids compared in comparison to cholesterol-functional polyether-based lipids.[39] Stable anchorage of lipids in the membrane of liposomes constitutes one crucial parameter contributing to the overall stability and serum half-life of stealth liposomes.[46] Therefore, in this work we focused on designing PEG-lipids with dialkyl anchor units endowed with acetals and ketals as pH-sensitive linkages. An overview of the synthesis of lipids discussed in this study is depicted in **Scheme 1**. At first, 1,2-bis-*n*-hexadecyl glycerol **2** was synthesized in a two-step procedure by alkylation of 1-*O*-benzyl glycerol **1** and subsequent hydrogenation of the protecting group. This protocol has been reported in the literature before,[47] however reaction conditions were slightly altered. 1,2-bis-*n*-hexadecyl glycerol **2** represents the key synthon in this reaction scheme and served as the precursor for further modification.

The first approach shown in **Scheme 1** (left path) aims at incorporating acid-cleavable ketal moieties into dialkyl-based PEG-lipid. To this end, a novel synthetic route was introduced to access the ketal-functional alcohol **4** in a one-step protocol utilizing a TMS-protected vinyl ether **3** under acid catalysis. Cleavage of the TMS-protecting group was conveniently accomplished on a pre-hydrated alox-based chromatography column in the purification step. Compound **3** was synthesized according to reported protocols.[40] Quenching of the reaction after 90 min prevented formation of a symmetric ketal compound (spectrum not shown). The structure of the macroinitiator **4** was verified by means of ^{1}H NMR and ^{13}C NMR spectroscopy. (See **SI-Figure 1** and **SI-Figure 2**) In ^{1}H NMR spectra methyl proton signals of the ketal moiety overlapped with the resonances of the alkyl chains between 1.5 and 1.2 ppm as confirmed *via* 2D NMR (HSQC, HMBC) analysis (See **SI-Figure 3**, **SI-Figure 4**).

Complete functionalization of the precursor **2** was concluded from the integration ratio of the terminal alkyl methyl proton signals (6H) compared to the superimposed resonances of the alkyl methylene protons and the ketal methyl protons (58H). The presence of the ketal moiety is evident from the ^{13}C NMR spectrum by the characteristic chemical shifts of 99.95 ppm for the quaternary carbon and 25.11 ppm for the methyl carbon atoms. In summary, this is, to the best of our knowledge, the first report on a one-step protocol to asymmetric, acyclic ketals in polymers.

The second approach provided access to acid-labile acetal-containing lipids (right path, **Scheme 1**). For this purpose, the acetate-protected vinyl ether **7** was used to derivatize 1,2-bis-*n*-hexadecyl glycerol **2** in an acid-catalyzed transformation, introducing an acetal moiety. Compared to the ketal synthesis described above, acetal formation proceeded at a faster rate, and the reaction was complete after 15 min. Reactivity of vinyl ethers towards acid-catalyzed electrophilic addition has been reported to occur at a faster rate in case of higher degrees of alkylation due to accelerated, rate-determining protonation of the olefin.[29] The difference in reaction kinetics of the two vinyl ethers in this study towards addition of **2** might be a consequence of the bulkiness of the alcohol component and the more sterically hindered 2-propenyl ether moiety of **3**. Saponification of the acetate group liberated a terminal hydroxyl functionality forming the macroinitiator **8**. **SI-Figure 7** contains the ^{1}H

NMR spectrum of **8** revealing the acetal resonances at 4.73 ppm and 1.30 ppm, respectively. The loss of the acetate proton signals at 1.7 ppm confirmed successful hydrolysis of the ester protecting group (Compare **SI-Figure 6** and **SI-Figure 7**). This second approach builds upon a synthetic route previously reported by our group for other acetal-containing polymers.[48–50] Herein, we extended the scope of the concept to dialkyl-based lipids.

5.1.3.2 Synthesis of Acid-Labile PEG-Lipid.

Subsequently, the pH-sensitive, dialkyl-based alcohols were used as macroinitiators for the anionic ring-opening polymerization (AROP) of ethylene oxide to attach the lipids' hydrophilic PEG blocks. In case of the ketal-functional macroinitiator **4**, potassium *tert*-butoxide proved suitable to deprotonate the macroinitiator prior drying. Unexpectedly, drying of **4** in the non-deprotonated state led to partial decomposition of the ketal moieties. Furthermore, it is important to note that all AROPs were performed at ambient temperature to retain integrity of the ketal linkage. In this study, three ketal-functional polymers are presented in a range of molecular weights M_n from 2000 to 3600 g mol^{-1} exhibiting narrow molecular weight distributions (~~*Đ*~~) below 1.1. **Table 1** summarizes the molecular characteristics of the pH-sensitive PEG-lipids discussed in this work. Molecular weights M_n were calculated from ^{1}H NMR spectroscopy considering the integration ratio of the polyether backbone signals and the terminal methyl proton resonances of the alkyl chains. Apparently, molecular weights obtained from SEC analysis were generally underestimated compared to the molecular weights determined from NMR which could be ascribed to differences in hydrodynamic radii of the lipids and the PEG standards used for calibration. **Figure 1** shows the SEC traces of the polymers synthesized in this study, revealing monomodal molecular weight distributions for all samples and shifts to lower elution volume with increasing molecular weights. As an example, the ^{1}H NMR spectrum of **BisHD-K-PEG$_{37}$** is included in the SI (**SI-Figure 5**). As stated above for the macroinitiator, an overlap of the ketal and the alkyl proton signals was observed for the ketal-functional lipids as well (See 2D NMR analysis, **SI-Figure 3**, **SI-Figure 4**).

Table 1: Molecular Characteristics of **BisHD-K-PEG** and **BisHD-A-PEG** Lipids prepared.

Composition [a]	M_n NMR [a] g·mol^{-1}	M_n SEC [b] g·mol^{-1}	$Đ$ [b]
BisHD-K-PEG$_{37}$	2230	2000	1.06
BisHD-K-PEG$_{40}$	2350	2100	1.07
BisHD-K-PEG$_{68}$	3590	3400	1.08
BisHD-A-PEG$_{46}$	2650	2400	1.05
BisHD-A-PEG$_{60}$	3140	3100	1.04
BisHD-A-PEG$_{68}$	3560	3400	1.07
BisHD-PEG$_{62}$	2870	2200	1.05

[a] Obtained from ^{1}H NMR spectroscopy. [b] Determined *via* SEC (RI, DMF, PEG standards).

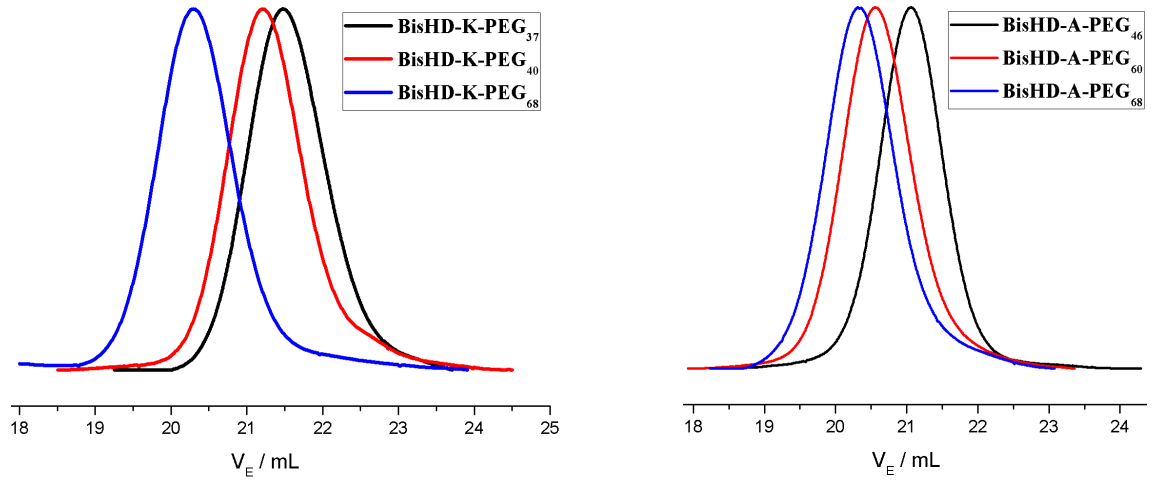

Figure 1: SEC traces (RI detector signal/eluent: DMF) of **BisHD-K-PEGs** and **BisHD-A-PEGs** with varying degrees of polymerization.

In order to confirm incorporation of the ketal moiety in the lipid structure, inverse gated ^{13}C NMR spectroscopy (IG ^{13}C NMR) and MALDI ToF mass spectrometry were conducted. The IG ^{13}C NMR spectrum of **BisHD-K-PEG** is given in **Figure 2** including the integration ratios for a set of characteristic carbon atoms normalized to alkyl methyl carbon signals. Herein, a comparison of the integrals for the alkyl methyl carbon at 14.40 ppm, the methyl ketal carbon at 25.12 ppm and the quaternary ketal carbon at 100.00 ppm, respectively provided evidence for the complete integrity of the ketal linkages. It is noteworthy that IG

^{13}C NMR analysis was performed under customized parameters of the measurements, including a relaxation delay d_1 of 10 s and 2048 scans in order to record accurate signal intensities. These prerequisites proved necessary due to the long relaxation time T_1 of the quaternary ketal carbon of 7.10 s in C_6D_6 determined via saturation recovery. **Figure 3** depicts a MALDI ToF mass spectrum of the ketal-functional PEG-lipid detected as an ionized potassium complex, using a pencil lead matrix. The use of a non-acidic matrix prevented decomposition of the ketal during sample preparation. Apparently, no PEG diol was observed in the spectra, which could be formed in the presence of water during the polymerization or cleavage of the lipid in the work-up process. The two methods retrospectively demonstrate stability of the ketal-functional macroinitiator **4** under the strongly basic conditions of AROP and further on, prove the absence of non-cleavable PEG-lipids.

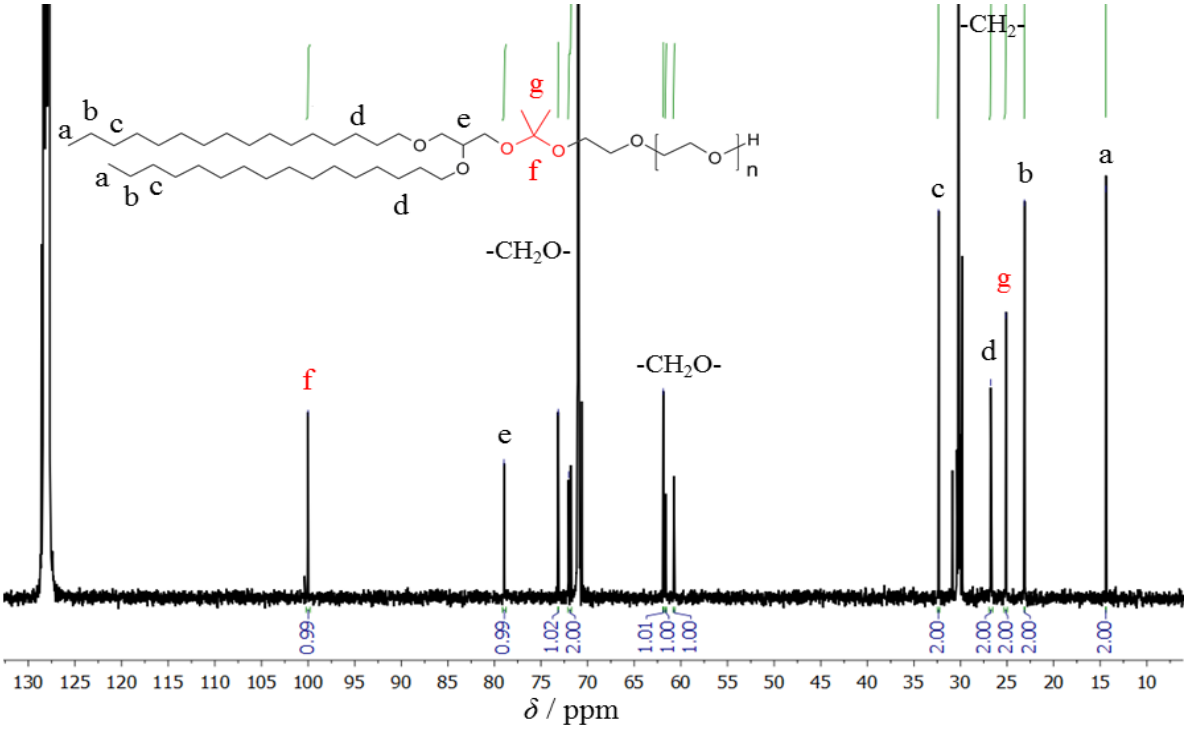

Figure 2: Inverse gated ^{13}C NMR spectrum of **BisHD-K-PEG$_{37}$** measured in C_6D_6 at 100 MHz.

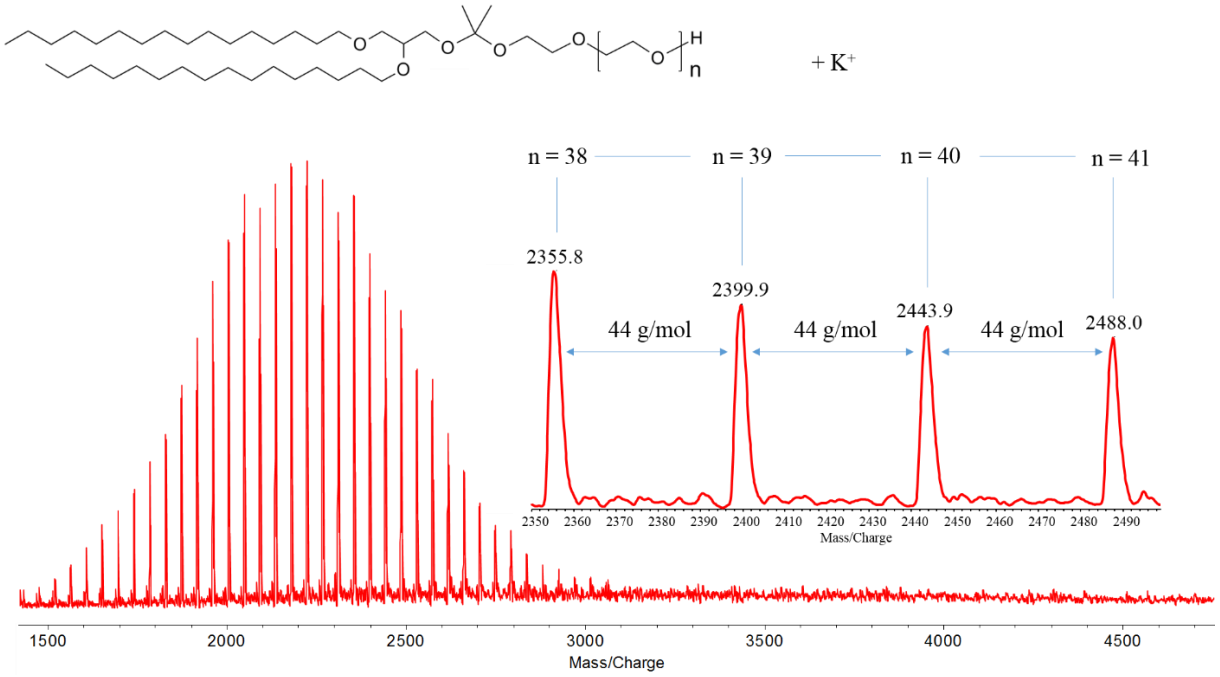

Figure 3: MALDI-ToF mass spectrum of **BisHD-K-PEG$_{37}$** using pencil lead as a matrix recorded in reflectron mode.

In an analogous manner, the acetal-functional alcohol **8** was utilized as a macroinitiator for the AROP of ethylene oxide. In contrast, however, the integrity of the acetals remained unaffected by drying of the macroinitiator without prior deprotonation. Three acetal-containing PEG-lipids are presented in this study covering a molecular weight range of 2400 to 3600 g mol^{-1} comparable to the ketal-functional lipids discussed above. SEC analysis revealed narrow, monomodal molecular weight distributions with dispersities $Đ$ below 1.1 (see **Table 1**). As an example, **Figure 4** shows the ^{1}H NMR spectrum of **BisHD-A-PEG$_{46}$** measured in C_6D_6. The characteristic multiplet between 4.77 and 4.69 ppm corresponds to the acetal proton and verifies complete incorporation of the pH-cleavable moiety into the lipid structure. The complex splitting pattern of the signal derives from two diastereoisomers of the lipid and was observed for all polymer samples. As stated above for the ketal-functional lipids, molecular weights obtained from SEC were consistently underestimated compared to the values determined by NMR spectroscopy, however, results of both methods were in good agreement. Molecular weights were calculated from ^{1}H NMR spectra considering the integral of the polyether backbone in relation to the alkyl methyl resonances.

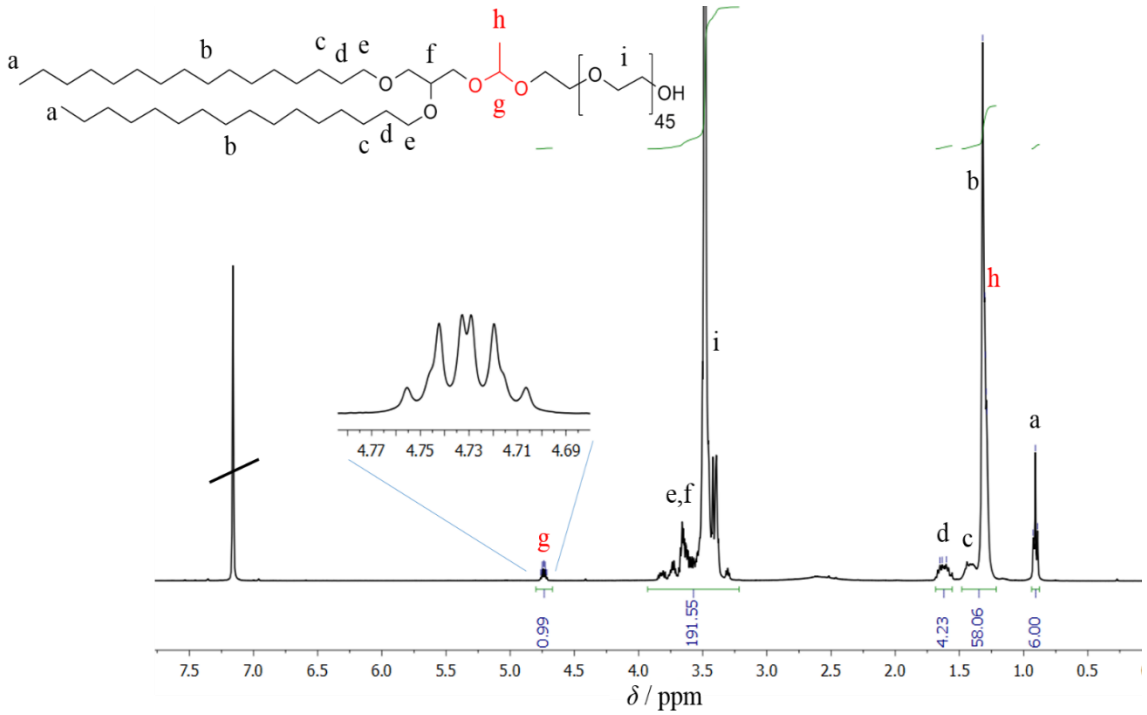

Figure 4: ^{1}H NMR spectrum of **BisHD-A-PEG$_{46}$** measured in C_6D_6 at 400 MHz. The region between 4.77 and 4.69 ppm was magnified to clarify the splitting pattern of the acetal signal.

Furthermore, MALDI ToF mass spectroscopy served to prove the proposed lipid structure, revealing two sub-distributions in the spectrum of **BisHD-A-PEG$_{60}$** corresponding to sodium and potassium counterions of the polymer (See **SI-Figure 10**). Although α-cyano-4-hydroxycinnamic acid (CHCA) and potassium trifluoroacetate (KTFA) were used as matrix/salt with slight acidity, no sign of acetal hydrolysis was apparent from the spectra. For comparative purposes, we additionally synthesized a non-cleavable PEG-lipid **6** with a molecular weight M_n of 2870 g mol^{-1} by implementing 1,2-bis-*n*-hexadecyl glycerol **2** as a macroinitiator (middle path, **Scheme 1**). The molecular characteristics of this polymer are given in **Table 1**. The straightforward access to a portfolio of structurally varied lipids discussed in the section above allows for a systematic investigation of the effect of different acid-labile moieties on the overall lipid properties. In the following section, we focus on kinetic studies with respect to pH-dependent hydrolysis of the novel acetal- and ketal-containing, dialkyl-derived PEG-lipids.

5.1.3.3 Online ^{1}H NMR Kinetics.

In order to evaluate susceptibility of the pH-sensitive lipids towards acidic hydrolysis, time-resolved ^{1}H NMR spectroscopy in deuterated buffer was employed. This technique enables online monitoring of reaction kinetics in an NMR tube by examining time-dependent intensity changes of characteristic NMR signals and has been utilized recently to screen cleavage profiles of acetals and ketals.[50] Since slightly acidic conditions (pH 5.5 to 6.5) have been reported for the tumor microenvironment of various cancer cells lines and inflammatory tissue,[9] we studied the behavior of the lipids in a physiologically relevant pH range. To this end, cleavage profiles of **BisHD-K-PEG$_{68}$** and **BisHD-A-PEG$_{68}$** were investigated in buffered solutions of deuterium oxide with pD 5.4 (citrate-phosphate buffer) and 6.4 (phosphate buffer) at 37°C recording a set of 105 spectra in a time period of 8 h and 24 h, respectively. An excerpt of the spectra obtained for the cleavage of **BisHD-K-PEG$_{68}$** at pD 6.4 is illustrated in Figure 5, revealing a consistent increase of the signal intensity at 2.3 ppm corresponding to acetone formed by hydrolysis of the ketal. (See expected reaction equation in **Figure 5**) To assess the respective half-life $t_{1/2\text{-}D2O}$ of the lipid according to first order kinetics, the integral of the acetone signal was plotted against time t and analyzed by means of an exponential fit function (See **Figure 5**). **Table 2** summarizes the results for the ketal-functional lipid exhibiting half-lives of ~ 40 min at pD 5.4, and ~ 4.5 h at pD 6.4, respectively.

Table 2: Results of ^{1}H NMR hydrolysis studies for **BisHD-K-PEG$_{68}$**.

BisHD-K-PEG$_{68}$	$t_{1/2\text{-}D2O}$ / h [a]
pD 5.4	0.67 ± 0.01
pD 6.4	4.68 ± 0.08
BisHD-A-PEG$_{68}$	$t_{1/2\text{-}D2O}$ / h
pD 3.4	10.98 ± 0.34

[a] half-life of the lipid in buffered D_2O at a given pD value.

Closer examination of the cleavage profile reveals that the signal intensity of the PEG backbone remains constant, whereas alkyl resonances roughly prevail unaltered first, but

gradually decrease after a certain degree of decomposition. This observation might be explained by the presence of micelles in the NMR tube, causing solubilization of the cleaved alkyl chains in the micellar cores, thereby keeping their magnetic environment unchanged. As hydrolysis of the lipids progressed, stability of the micelles decreased, effecting an assembly of the hydrophobic fragments at the air-D_2O interface that led to a drop in the signal intensity. Kim *et al.* performed NMR kinetic studies in buffered D_2O by manual analysis of aliquots to determine the half-life of an acetone ketal-containing PEG dimethacrylate and found values ~ 14 min at pH 5.0. Given the structural difference and the slightly lower pH, these reports are consistent with our findings.[51]

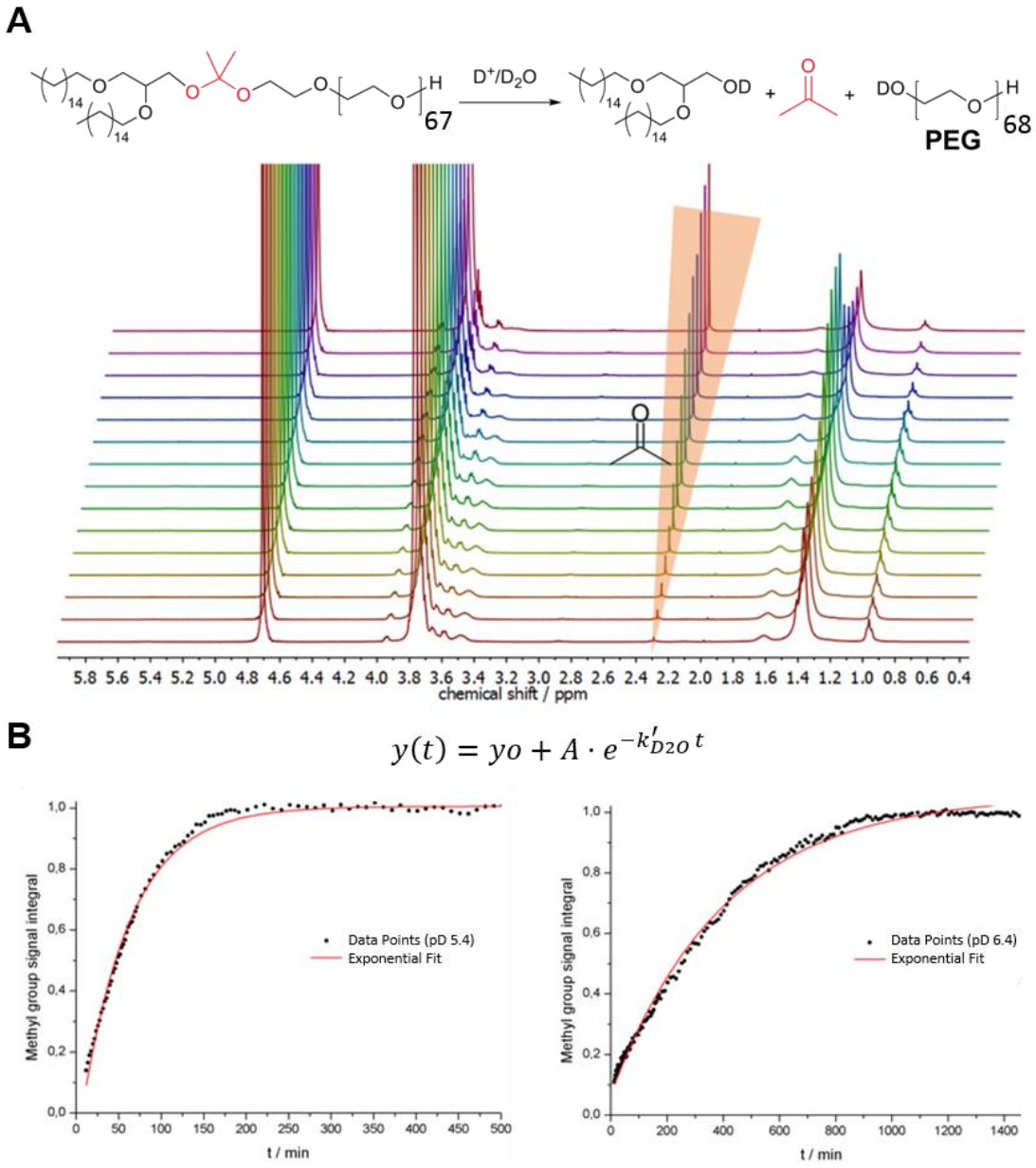

Figure 5: A: Reaction equation for the hydrolysis of ketals (top). Online ^{1}H NMR kinetic study monitoring ketal cleavage of the lipid in phosphate buffered D_2O at 37°C. For illustrative purposes, an excerpt of 16 spectra is shown for the measurement of **BisHD-K-PEG$_{68}$** at pD 6.4. However, a series of 105 spectra was recorded and analyzed for the study (bottom). **B:** Experimental results from ^{1}H NMR kinetic studies for the hydrolysis of **BisHD-K-PEG$_{68}$** at pD 5.4 and 6.4. The integrals of the acetone signal at 2.3 ppm are plotted against time t using an exponential fit of the general form given above to determine $t_{1/2\text{-}D2O}$.

In case of the acetal-functional lipid **BisHD-A-PEG$_{68}$**, no sign of acetal hydrolysis was observed within a time period of 24 h at pD 5.4. Thereupon, the experiment was repeated

at pD 3.4. A selection of the spectra is presented in **Figure 6**, indicating the formation of acetaldehyde and acetaldehyde hydrate as hydrolysis products. Due to an overlap of the acetal proton signals with the NMR solvent peak, direct monitoring of acetal cleavage was not possible. Instead, combined signal intensities of the two hydrolysis products were considered to determine the half-life $t_{1/2\text{-}D2O}$ of ~ 11h.

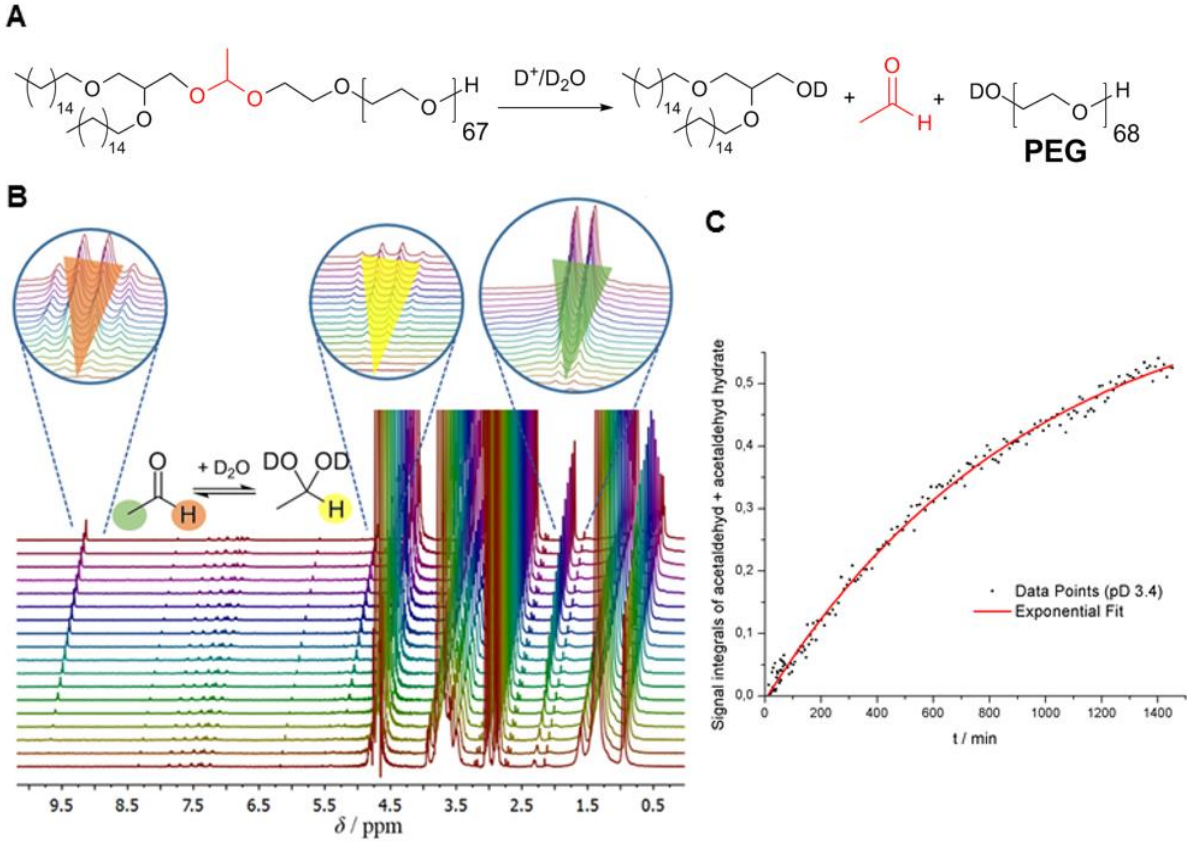

Figure 6: A: Expected reaction for the hydrolysis of acetals. **B:** Online ^{1}H NMR kinetic study monitoring acetal cleavage of the lipid in citrate-phosphate buffered D_2O at 37°C. For illustrative purposes, an excerpt of 18 spectra is shown for the measurement of **BisHD-A-PEG$_{68}$** at pD 3.4, though a series of 105 spectra was recorded and analyzed for the study. **C:** Experimental results of ^{1}H NMR kinetic studies for the hydrolysis of **BisHD-A-PEG$_{68}$** at pD 3.4. The combined integrals of the acetaldehyde signal (9.8 ppm) and acetaldehyde hydrate (5.4 ppm) are plotted vs. time t, using an exponential fit to determine $t_{1/2\text{-}D2O}$.

The results of the NMR kinetics indicate that cleavage of ketals occurs at a rate several orders of magnitude higher than the hydrolysis rate of acetal. These findings have motivated

us to take a closer look at the behavior of the pH-sensitive lipids in liposomal formulations via alternative techniques.

5.1.3.4 pH-triggered Liposome Shedding

In this section we aim at elucidating the behavior of liposomes modified with the pH-sensitive lipids introduced in the sections above to evaluate their potential for pH-responsive drug carriers. For this purpose, two parallel experiments were designed to investigate shedding of the PEG stealth layer from the liposomal surface. To monitor the cleavage profiles, fluorescent dyes (Atto 488 azide) were covalently attached to the pH-sensitive PEG-lipids using copper(I)-catalyzed azide-alkyne click chemistry (CuAAC), and PEG shedding from liposomes was analyzed by fluorescence spectroscopy (FS) and polyacrylamide gel electrophoresis (PAGE). The in situ fluorescence spectroscopy assay has been introduced in a previous study,[52] however, has so far not been used to quantify rates of hydrolysis. Liposomes were prepared by means of dual centrifugation (DC) replacing 5 mol% of the total amount of lipids (egg phosphatidylcholine EPC, and cholesterol) with the novel pH-sensitive PEG-lipids. Cell viability of liposomes containing alkyne-functional lipids was evaluated *via* MTT assays (**Figure 7**), revealing high cellular compatibility comparable to conventional liposomes (CL) and sterically stabilized liposomes (SSL, DSPE-mPEG$_{2000}$).

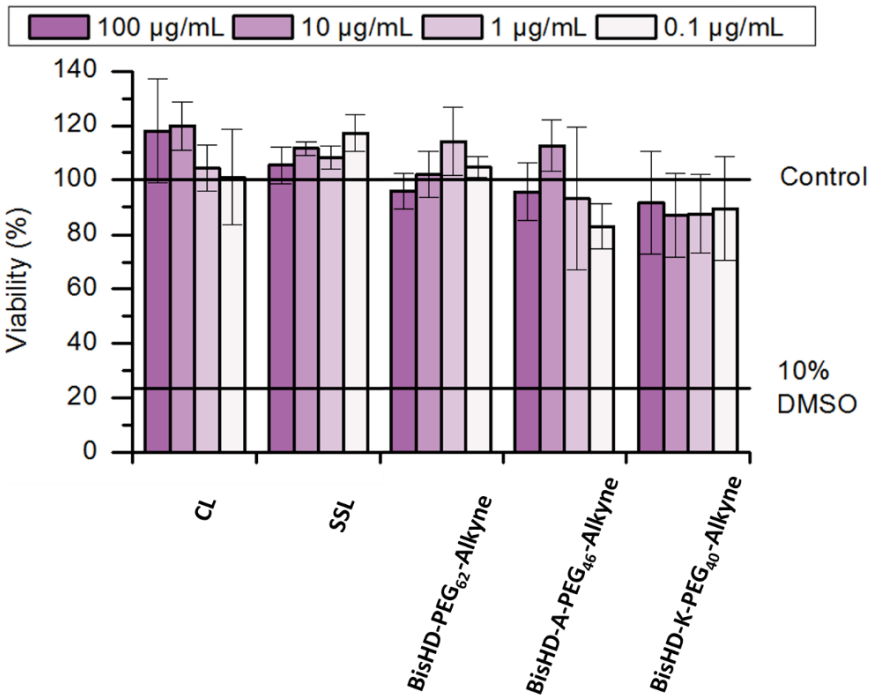

Figure 7: Cell viability test (MTT assay) for liposomes containing alkyne-functional PEG-lipids (**BisHD-PEG$_{62}$**, **BisHD-A-PEG$_{46}$**, **BisHD-K-PEG$_{40}$**) in comparison to conventional liposomes (CL) and sterically stabilized liposomes (SSL, DSPE-mPEG$_{2000}$).

The post-preparational dye-labelling of stealth liposomes via CuAAC has been demonstrated in previous works.[43] In case of FS analysis, fluorescently labelled liposomes were studied in buffered solutions in a pH range of 2.4 to 5.4. Prior to use, cuvette surfaces were incubated with plain EPC/cholesterol liposomes to prevent amphiphile adsorption. At first, susceptibility of acetal-containing PEG-lipids in liposomes towards acidic hydrolysis was pursued, as slower rates of hydrolysis could be expected. **Figure 8 B** illustrates the results of time-dependent FS analysis for dye-labelled liposomes prepared from **BisHD-A-PEG$_{46}$-Alkyne**. The fluorescence intensities are plotted vs. time *t* for spectra recorded within a period of 24 h at 37 °C.

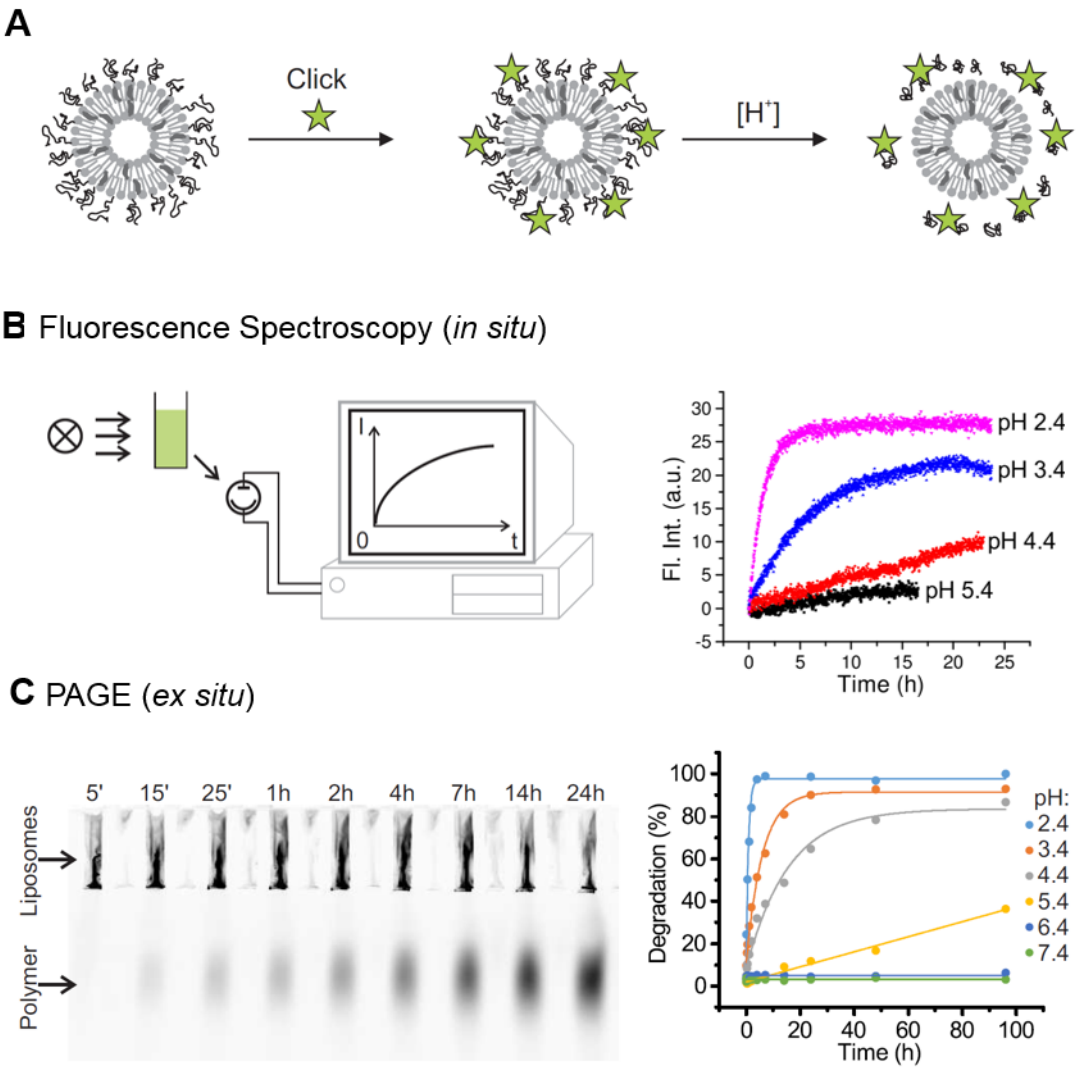

Figure 8: A: Schematic post-preparational dye-labelling of liposomes and subsequent pH-triggered shedding. **B:** Fluorescence spectroscopy analysis of pH-dependent shedding for dye-labelled **BisHD-A-PEG$_{46}$** liposomes at 37 °C. **C:** Example of a PAGE fluorescence scan for the cleavage analysis of **BisHD-A-PEG$_{46}$** in liposomes at pH 3.4.(left) pH-dependent cleavage profiles for **BisHD-A-PEG$_{46}$** liposomes analyzed *via* PAGE analysis (right) at 37 °C.

A systematic increase of the fluorescence signal was detected for pH values of 2.4 to 4.4, whereas at higher pH, intensities remained approximately constant throughout the time of measurement (see **Figure 8 B**). Control measurements assured that the fluorescence increase was not due to reaction of the fluorophore itself and that compounds without a cleavable group (**BisHD-PEG$_{62}$-Alkyne**) did not show this fluorescence increase (compare **SI-Figure 13**). The incline of fluorescence intensities can be associated with the cleavage of acetal moieties and consequently the detachment of dye-labelled PEGs from the liposomes.

Presumably, in case of unscathed acetal linkages, dyes were located in proximity to the liposomal surface, promoting thermal relaxation of excited fluorophores that lead to quenching of the fluorescence intensity. After acidic cleavage of acetals, the weakened interactions of fluorophores with the vesicles' surfaces effected an increased fluorescence emission. In addition, inner filter effects were expected to lower fluorescence emission while fluorophores were bound to the surfaces. Half-lifes $t_{1/2}$ were determined *via* an exponential fit revealing values of ~ 1 h (pH 2.4) and ~ 4 h (pH 3.4). (See **Table 3**) At pH 4.4, a slow gradual increase was observed, albeit unsuitable for quantitative analysis.

Table 3: Half-lives of **BisHD-A-PEG$_{46}$** and **BisHD-K-PEG$_{40}$** liposomes at different pH values.

Half-life	$t_{1/2}$ / h					
pH	**2.4**	**3.4**	**4.4**	**5.4**	**6.4**	**7.4**
BisHD-A-PEG$_{46}$						
FS	1.04 ± 0.01	4.48 ± 0.32	n.d.	n.d.	s.h.	s.h.
PAGE	0.59 ± 0.08	4.16 ± 0.45	10.72 ± 1.47	21.09 ± 2.83	s.h.	s.h.
BisHD-K-PEG$_{40}$						
FS	r.h.	r.h.	0.01	0.17 ± 0.02	4.01 ± 0.70	19.50 ± 0.28
PAGE	r.h.	r.h.	0.01	0.15 ± 0.01	3.11 ± 0.28	13.10 ± 0.80

r.h.(rapid hydrolysis): $t_{1/2}$ < 10s; n.d.: not determinable; s.h.(slow hydrolysis): half-life exceeds 24 h.

As a reference experiment, polyacrylamide gel electrophoresis (PAGE) was conducted to evaluate the results from FS and furthermore to investigate the cleavage profiles on a longer time scale. To this end, dye-labelled liposomes of **BisHD-A-PEG$_{46}$-Alkyne** were prepared as discussed above and incubated at 37 °C in buffered solutions (pH 2.4 to 7.4). Samples were taken within a period of 96 h, neutralized in PBS buffer (pH 7.4) to prevent further acetal hydrolysis and subsequently analyzed on an agarose gel by measuring the fluorescence intensity of the cleaved PEG-dye fractions (See **Figure 8 C**). The data suggest that intact liposomes showed no migration, whereas cleaved polymers migrated through the gel effecting increased emission intensities with longer times of incubation. **Figure 8 C** (right) shows the time-dependent fluorescence signal for different pH values revealing a continuous increase of the signal intensities at pH values below 6.4. As expected, faster cleavage rates were observed at lower pH values. Half-lifes $t_{1/2}$ were determined from an

exponential fit ranging from 1 h (pH 2.4) to 21 h (pH 5.4). (See **Table 3**) A comparison of the half-lives at pH 2.4 and 3.4 obtained from FS and PAGE reveals that results of both methods are in good agreement. At pH values exceeding 5.4, the rates of acetal hydrolysis were too slow to be detected by the two techniques.

In an analogous manner, liposomes were prepared from the ketal-functional PEG-lipid **BisHD-K-PEG$_{40}$-Alkyne** and subsequently, their susceptibility towards acidic hydrolysis was analyzed via FS and PAGE, as described above in a pH range from 3.4 to 7.4 at 37 °C. (See **Figure 9**) Due to significant differences in the rates of hydrolysis at different pH values, separate plots were chosen for each set of data points. Half-lifes $t_{1/2}$ were calculated from exponential fits and values are summarized in **Table 3**. Both techniques consistently demonstrated rapid cleavage of ketals at pH 4.4 ($t_{1/2}$ ~ 40 s) and 5.4 ($t_{1/2}$ ~ 10 min), whereas at pH 6.4 slower rates of hydrolysis with values of $t_{1/2}$ in the order of ~ 3.5 h were determined. As observed above, results obtained via FS fit well with the results from PAGE analysis. **Figure 9** visualizes the concordant curve profiles for the two measurements. At pH 7.4, small discrepancies between the two techniques are visible, however values are in the same order of magnitude. Below pH 4.4, complete scission of the PEG-lipids occurred in less than 10 s and was beyond the time resolution of the techniques employed in this study. Slow hydrolysis of ketals at pH 7.4 might require storage of the liposomal formulations at higher pH values after preparation. Therefore, we investigated the stability of ketal residues at pH 8.4 and found half-lifes (PAGE analysis) exceeding 130 h (data not shown) that account for the high stability of the liposomes under slightly basic storage conditions.

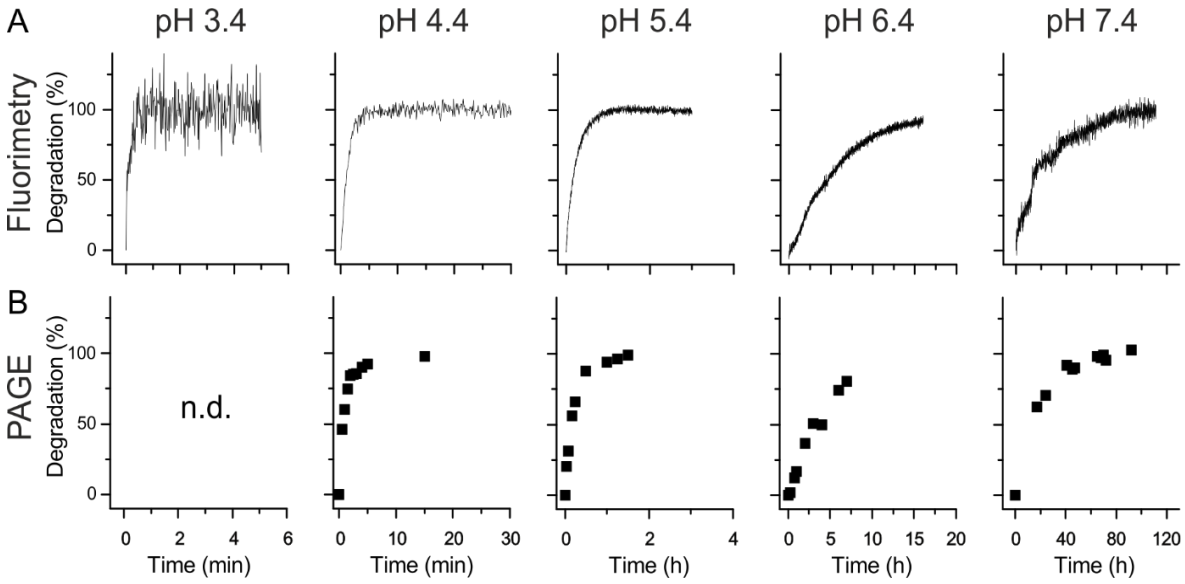

Figure 9: A: Fluorimetric analysis of liposome disintegration at 37 °C for dye-labelled **BisHD-K-PEG$_{40}$** liposomes at different pH. Data points are visualized in separate plots as time scales differ significantly. **B:** PAGE analysis of the dye-labelled **BisHD-K-PEG$_{40}$** liposomes in a pH range of 4.4 to 7.4 at 37 °C.

Clearly, values obtained for the half-life $t_{1/2}$ of acetal- and ketal-containing lipids in liposomes via FS/PAGE were generally lower than values calculated from online ^{1}H NMR kinetics for the pure lipids (Compare **Table 2** and **Table 3**). Several factors might contribute to these differences. For instance, the liposomal surface contains multiple, negatively charged moieties, creating a more polar environment in closer proximity to the cleavable linkages that might lead to accelerated rates of hydrolysis. Similar findings have been observed for lipids containing vinyl ethers as pH-cleavable units in the presence of negatively charged phosphates.[29] Another influence might derive from the different hydrolysis kinetics of acetals and ketals in D_2O and H_2O, respectively due to the kinetic deuterium isotope effect.[53] It is noteworthy that discrepancies were more pronounced for acetal-based lipids, whereas, in case of ketals, values were of the same order of magnitude. This might be due to the transition of volatile acetaldehyde into the gas phase, rendering it undetectable by NMR, and hence, causing a drop in signal intensities. These findings suggest great potential for these functionalizable, pH-sensitive lipids in liposomal research, as they allow for pH-triggered release strategies combined with active cell targeting and/or

simultaneous polymer/carrier trafficking. The *in vivo* behavior of the PSLs discussed in this study is under current investigation.

5.1.4 Conclusion

In this work, we introduce a novel class of pH-sensitive PEG-lipids based on bishexadecyl glycerol anchor groups containing acetal and ketal moieties as cleavable linkages. The use of polyether-based lipids with dialkyl chains in liposomes has recently been proven particularly advantageous, as dialkyl anchors are stably entrenched in liposomal membranes.[39] A prototype synthesis route has been developed that provides straightforward access to asymmetric ketals in PEG-lipids. Acetal- and ketal-functional dialkyl glycerol derivatives were utilized as macroinitiators for the anionic ring-opening polymerization (AROP) of ethylene oxide to obtain amphiphilic PEG-block structures in a molecular weight range of 2000 to 3500 g mol^{-1} with narrow molecular weight distributions ($Đ$ = 1.04 - 1.08). Integrity of the acid-cleavable moieties was proven by ^{1}H, IG ^{13}C NMR spectroscopy and MALDI ToF mass spectrometry.

In order to evaluate susceptibility of the lipids towards acidic hydrolysis, real-time ^{1}H NMR kinetic studies were performed in D_2O revealing rapid cleavage of the ketals $t_{1/2\text{-}D2O}$ ~ 1h (pD 5.4), ~ 5 h (pD 6.4) and significantly slower hydrolysis for the acetals. Furthermore, pH-responsiveness of the scissile PEG-lipids in liposomes at physiologically relevant pH was investigated by means of fluorescence spectroscopy and agarose gel electrophoresis. In accordance with the results from NMR kinetic studies, acetal hydrolysis occurs at a distinctly slower rate with half-lives of ~ 21 h (pH 5.4) compared to the fast cleavage of ketals with half-lives $t_{1/2}$ of ~ 10 min (pH 5.4), ~ 3.5 h (pH 6.4). These cleavage profiles, in particular, render the ketal-functional PEG-lipids promising candidates for pH-triggered drug release strategies from liposomes. Due to lowered pH values in the microenvironment of various tumor cell lines,[9] pH-sensitive stealth liposomes represent a promising class of drug carrier systems for anticancer treatment. A combination of the slowly hydrolyzing acetal PEG-lipid species endowed with target moieties such as folate or mannose to achieve active cell targeting, and the rapidly hydrolyzing ketal PEG-lipid ensuring pH-triggered shedding of the liposome inside the tumor tissue, might further improve cellular uptake and may reduce accelerated blood clearance (ABC phenomenon). These results demonstrate the

great potential of the pH-sensitive lipids enabling further post-functionalization strategies and render them an innovation for pH-triggered release strategies from liposomal drug carriers. Future experiments will focus on the *in vivo* performance of these acid-sensitive PEG dialkyl-lipids in liposomal formulations.

5.1.5 Acknowledgment

The authors thank [redacted]n for customized NMR measurements, [redacted] for MALDI-ToF mass spectrometry, and [redacted] for technical support. Furthermore, we thank [redacted] for scientific input and [redacted] for technical assistance. M.W. and T.F. are grateful for a fellowship by the Max Planck Graduate Center (MPGC). D.L. acknowledges a fellowship through the Excellence Initiative (DFG/GSC 266) in the context of MAINZ "Materials Science in Mainz". The Rotanta 400 DC prototype was kindly provided by Andreas Hettich GmbH, Tuttlingen, Germany. This work was supported by funding of the DFG research center SFB 1066, project grant A7.

References

(1) Gil, E. S.; Hudson, S. M. Stimuli-Reponsive Polymers and Their Bioconjugates. *Prog. Polym. Sci.* **2004**, *29* (12), 1173–1222. https://doi.org/10.1016/j.progpolymsci.2004.08.003.

(2) Guragain, S.; Bastakoti, B. P.; Malgras, V.; Nakashima, K.; Yamauchi, Y. Multi-Stimuli-Responsive Polymeric Materials. *Chem. - A Eur. J.* **2015**, *21* (38), 13164–13174. https://doi.org/10.1002/chem.201501101.

(3) Vancoillie, G.; Frank, D.; Hoogenboom, R. Thermoresponsive Poly(Oligo Ethylene Glycol Acrylates). *Prog. Polym. Sci.* **2014**, *39* (6), 1074–1095. https://doi.org/10.1016/j.progpolymsci.2014.02.005.

(4) Moon, H. J.; Ko, D. Y.; Park, M. H.; Joo, M. K.; Jeong, B. Temperature-Responsive Compounds as in Situ Gelling Biomedical Materials. *Chem. Soc. Rev.* **2012**, *41* (14), 4860–4883. https://doi.org/10.1039/c2cs35078e.

(5) Schattling, P.; Jochum, F. D.; Theato, P. Multi-Stimuli Responsive Polymers-the All-in-One Talents. *Polym. Chem.* **2014**, *5* (1), 25–36. https://doi.org/10.1039/c3py00880k.

(6) Gohy, J. F.; Zhao, Y. Photo-Responsive Block Copolymer Micelles: Design and Behavior. *Chem. Soc. Rev.* **2013**, *42* (17), 7117–7129. https://doi.org/10.1039/c3cs35469e.

(7) Wei, H.; Zhuo, R. X.; Zhang, X. Z. Design and Development of Polymeric Micelles with Cleavable Links for Intracellular Drug Delivery. *Prog. Polym. Sci.* **2013**, *38* (3–4), 503–535. https://doi.org/10.1016/j.progpolymsci.2012.07.002.

(8) Asokan, A.; Cho, M. J. Exploitation of Intracellular PH Gradients in the Cellular Delivery of Macromolecules. *J. Pharm. Sci.* **2002**, *91* (4), 903–913. https://doi.org/10.1002/jps.10095.

(9) Gerweck, L. E.; Vijayappa, S.; Kozin, S. Tumor PH Controls the in Vivo Efficacy of Weak Acid and Base Chemotherapeutics. *Mol. Cancer Ther.* **2006**, *5* (5), 1275–1279. https://doi.org/10.1158/1535-7163.MCT-06-0024.

(10) Patel, N. R.; Pattni, B. S.; Abouzeid, A. H.; Torchilin, V. P. Nanopreparations to Overcome Multidrug Resistance in Cancer. *Adv. Drug Deliv. Rev.* **2013**, *65* (13–14), 1748–1762. https://doi.org/10.1016/j.addr.2013.08.004.

(11) Pasut, G.; Veronese, F. . . Polymer-Drug Conjugation, Recent Achievements and General Strategies. *Prog. Polym. Sci.* **2007**, *32*, 933–961. https://doi.org/10.1016/j.progpolymsci.2007.05.008.

(12) Herzberger, J.; Niederer, K.; Pohlit, H.; Seiwert, J.; Worm, M.; Wurm, F. R.; Frey, H. Polymerization of Ethylene Oxide, Propylene Oxide, and Other Alkylene Oxides: Synthesis, Novel Polymer Architectures, and Bioconjugation. *Chem. Rev.* **2015**, acs.chemrev.5b00441. https://doi.org/10.1021/acs.chemrev.5b00441.

(13) Hatakeyama, H.; Akita, H.; Harashima, H. A Multifunctional Envelope Type Nano Device (MEND) for Gene Delivery to Tumours Based on the EPR Effect: A Strategy for Overcoming the PEG Dilemma. *Adv. Drug Deliv. Rev.* **2011**, *63* (3), 152–160. https://doi.org/10.1016/j.addr.2010.09.001.

(14) Dingels, C.; Frey, H. From Biocompatible to Biodegradable: Poly(Ethylene Glycol)s with Predetermined Breaking Points. In *Hierarchical Macromolecular Structures: 60 Years after the Staudinger Nobel Prize II*; Percec, V., Ed.; Springer International Publishing: Cham, 2013; pp 167–190. https://doi.org/10.1007/12_2013_235.

(15) Dufort, S.; Sancey, L.; Coll, J. L. Physico-Chemical Parameters That Govern Nanoparticles Fate Also Dictate Rules for Their Molecular Evolution. *Adv. Drug Deliv. Rev.* **2012**, *64* (2), 179–189. https://doi.org/10.1016/j.addr.2011.09.009.

(16) Legendre, J. Y.; Szoka, F. C. Delivery of Plasmid DNA into Mammalian Cell Lines Using PH-Sensitive Liposomes: Comparison with Cationic Liposomes. *Pharmaceutical Research: An Official Journal of the American Association of Pharmaceutical Scientists*. 1992, pp 1235–1242. https://doi.org/10.1023/A:1015836829670.

(17) Ishiwata, H.; Sato, S. B.; Vertut-Doï, A.; Hamashima, Y.; Miyajima, K. Cholesterol Derivative of Poly(Ethylene Glycol) Inhibits Clathrin-Independent, but Not Clathrin-Dependent Endocytosis. *Biochim. Biophys. Acta - Mol. Cell Res.* **1997**, *1359* (2), 123–135. https://doi.org/10.1016/S0167-4889(97)00061-X.

(18) Dams, E. T. M.; Laverman, P.; Oyen, W. J. G.; Storm, G.; Scherphof, G. L.; van der Meer, J. W. M.; Corstens, F. H. M.; Boerman, O. C. Accelerated Blood Clearance and Altered Biodistribution of Repeated Injections of Sterically Stabilized Liposomes. *J. Pharmacol. Exp. Ther.* **2000**, *292* (3), 1071–1079.

(19) Laverman, P.; Carstens, M. G.; Boerman, O. C.; Th. M. Dams, E.; Oyen, W. J. G.; van Rooijen, N.; Corstens, F. H. M.; Storm, G. Factors Affecting the Accelerated Blood Clearance of Polyethylene Glycol-Liposomes upon Repeated Injection. *J. Pharmacol. Exp. Ther.* **2001**, *298* (2), 607–612.

(20) Abu Lila, A. S.; Kiwada, H.; Ishida, T. The Accelerated Blood Clearance (ABC) Phenomenon: Clinical Challenge and Approaches to Manage. *J. Control. Release* **2013**, *172* (1), 38–47. https://doi.org/10.1016/j.jconrel.2013.07.026.

(21) Chen, D.; Liu, W.; Shen, Y.; Mu, H.; Zhang, Y.; Liang, R.; Wang, A.; Sun, K.; Fu, F. Effects of a Novel PH-Sensitive Liposome with Cleavable Esterase-Catalyzed and PH-Responsive Double Smart MPEG Lipid Derivative on ABC Phenomenon. *Int. J. Nanomedicine* **2011**, *6*, 2053–2061. https://doi.org/10.2147/ijn.s24344.

(22) Chen, D.; Jiang, X.; Huang, Y.; Zhang, C.; Ping, Q. Ph-Sensitive MPEG-Hz-Cholesterol Conjugates as a Liposome Delivery System. *J. Bioact. Compat. Polym.* **2010**, *25* (5), 527–542. https://doi.org/10.1177/0883911510379996.

(23) Zhang, L.; Wang, Y.; Yang, Y.; Liu, Y.; Ruan, S.; Zhang, Q.; Tai, X.; Chen, J.; Xia, T.; Qiu, Y.; Gao, H.; He, Q. High Tumor Penetration of Paclitaxel Loaded PH Sensitive Cleavable Liposomes by Depletion of Tumor Collagen i in Breast Cancer. *ACS Appl. Mater. Interfaces* **2015**, *7* (18), 9691–9701. https://doi.org/10.1021/acsami.5b01473.

(24) Guo, X.; Szoka, F. C. Steric Stabilization of Fusogenic Liposomes by a Low-PH Sensitive PEG - Diortho Ester - Lipid Conjugate. *Bioconjug. Chem.* **2001**, *12* (2), 291–300. https://doi.org/10.1021/bc000110v.

(25) Li, W.; Huang, Z.; MacKay, J. A.; Grube, S.; Szoka, F. C. Low-PH-Sensitive Poly(Ethylene Glycol) (PEG)-Stabilized Plasmid Nanolipoparticles: Effects of PEG Chain Length, Lipid Composition and Assembly Conditions on Gene Delivery. *J. Gene Med.* **2005**, *7* (1), 67–79. https://doi.org/10.1002/jgm.634.

(26) Masson, C.; Garinot, M.; Mignet, N.; Wetzer, B.; Mailhe, P.; Scherman, D.; Bessodes, M. PH-Sensitive PEG Lipids Containing Orthoester Linkers: New Potential Tools for

Nonviral Gene Delivery. *J. Control. Release* **2004**, *99* (3), 423–434. https://doi.org/10.1016/j.jconrel.2004.07.016.

(27) Mustapa, M. F. M.; Grosse, S. M.; Kudsiova, L.; Elbs, M.; Raiber, E. A.; Wong, J. B.; Brain, A. P. R.; Armer, H. E. J.; Warley, A.; Keppler, M.; Ng, T.; Lawrence, M. J.; Hart, S. L.; Hailes, H. C.; Tabor, A. B. Stabilized Integrin-Targeting Ternary LPD (Lipopolyplex) Vectors for Gene Delivery Designed to Disassemble within the Target Cell. *Bioconjug. Chem.* **2009**, *20* (3), 518–532. https://doi.org/10.1021/bc800450r.

(28) Shin, J.; Shum, P.; Thompson, D. H. Acid-Triggered Release via DePEGylation of DOPE Liposomes Containing Acid-Labile Vinyl Ether PEG-Lipids. *J. Control. Release* **2003**, *91* (1–2), 187–200. https://doi.org/10.1016/S0168-3659(03)00232-3.

(29) Shin, J.; Shum, P.; Grey, J.; Fujiwara, S. I.; Malhotra, G. S.; González-Bonet, A.; Hyun, S. H.; Moase, E.; Allen, T. M.; Thompson, D. H. Acid-Labile MPEG-Vinyl Ether-1,2-Dioleylglycerol Lipids with Tunable Ph Sensitivity: Synthesis and Structural Effects on Hydrolysis Rates, DOPE Liposome Release Performance, and Pharmacokinetics. *Mol. Pharm.* **2012**, *9* (11), 3266–3276. https://doi.org/10.1021/mp300326z.

(30) Luvino, D.; Khiati, S.; Oumzil, K.; Rocchi, P.; Camplo, M.; Barthélémy, P. Efficient Delivery of Therapeutic Small Nucleic Acids to Prostate Cancer Cells Using Ketal Nucleoside Lipid Nanoparticles. *J. Control. Release* **2013**, *172* (3), 954–961. https://doi.org/10.1016/j.jconrel.2013.09.006.

(31) Nakamura, N.; Suzuki, K. Study on Ketalization Reaction of Poly (Vinyl Alcohol) by Ketones. IX. Kinetic Study on Acetalization and Ketalization Reaction of 1,3-Butanediol as a Model Compound for Poly (Vinyl Alcohol). *J. Polym. Sci. Part A Polym. Chem.* **1997**, *35* (9), 1719–1731. https://doi.org/10.1002/(SICI)1099-0518(19970715)35:9<1719::AID-POLA13>3.0.CO;2-8.

(32) Pierre, T. S.; Chiellini, E. Biodegradability of Synthetic Polymers for Medical and Pharmaceutical Applications: Part 2—Backbone Hydrolysis. *J. Bioact. Compat. Polym.* **1987**, *2* (1), 4–30. https://doi.org/10.1177/088391158700200101.

(33) Gillies, E. R.; Goodwin, A. P.; Fréchet, J. M. J. Acetals as PH-Sensitive Linkages for Drug Delivery. *Bioconjug. Chem.* **2004**, *15* (6), 1254–1263. https://doi.org/10.1021/bc049853x.

(34) Gillies, E. R.; Fréchet, J. M. J. PH-Responsive Copolymer Assemblies for Controlled Release of Doxorubicin. *Bioconjug. Chem.* **2005**, *16* (2), 361–368. https://doi.org/10.1021/bc049851c.

(35) Shenoi, R. A.; Lai, B. F. L.; Imran Ul-Haq, M.; Brooks, D. E.; Kizhakkedathu, J. N. Biodegradable Polyglycerols with Randomly Distributed Ketal Groups as Multi-

Functional Drug Delivery Systems. *Biomaterials* **2013**, *34* (25), 6068–6081. https://doi.org/10.1016/j.biomaterials.2013.04.043.

(36) Binauld, S.; Stenzel, M. H. Acid-Degradable Polymers for Drug Delivery: A Decade of Innovation. *Chem. Commun.* **2013**, *49* (21), 2082–2102. https://doi.org/10.1039/c2cc36589h.

(37) Chen, D.; Wang, H. Novel PH-Sensitive Biodegradable Polymeric Drug Delivery Systems Based on Ketal Polymers. *J. Nanosci. Nanotechnol.* **2014**, *14* (1), 983–989. https://doi.org/10.1166/jnn.2014.9190.

(38) Zhang, S.; Zhao, Y. Controlled Release from Cleavable Polymerized Liposomes upon Redox and PH Stimulation. *Bioconjug. Chem.* **2011**, *22* (4), 523–528. https://doi.org/10.1021/bc1003197.

(39) Fritz, T.; Voigt, M.; Worm, M.; Negwer, I.; M??ller, S. S.; Kettenbach, K.; Ross, T. L.; Roesch, F.; Koynov, K.; Frey, H.; Helm, M. Orthogonal Click Conjugation to the Liposomal Surface Reveals the Stability of the Lipid Anchorage as Crucial for Targeting. *Chem. - A Eur. J.* **2016**, *22* (33), 11578–11582. https://doi.org/10.1002/chem.201602758.

(40) Gassman, P. G.; Burns, S. J.; Pfister, K. B. Synthesis of Cyclic and Acyclic Enol Ethers (Vinyl Ethers). *J. Org. Chem.* **1993**, *58*, 1449–1457.

(41) Greenland, B. W.; Liu, S.; Cavalli, G.; Alpay, E.; Steinke, J. H. G. Synthesis of Beaded Poly(Vinyl Ether) Solid Supports with Unique Solvent Compatibility. *Polymer (Guildf).* **2010**, *51* (14), 2984–2992. https://doi.org/10.1016/j.polymer.2010.04.026.

(42) Massing, U.; Cicko, S.; Ziroli, V. Dual Asymmetric Centrifugation (DAC)-A New Technique for Liposome Preparation. *J. Control. Release* **2008**, *125* (1), 16–24. https://doi.org/10.1016/j.jconrel.2007.09.010.

(43) Fritz, T.; Hirsch, M.; Richter, F. C.; Müller, S. S.; Hofmann, A. M.; Rusitzka, K. A. K.; Markl, J.; Massing, U.; Frey, H.; Helm, M. Click Modification of Multifunctional Liposomes Bearing Hyperbranched Polyether Chains. *Biomacromolecules* **2014**, *15* (7), 2440–2448. https://doi.org/10.1021/bm5003027.

(44) Abràmoff, M. D.; Magalhães, P. J.; Ram, S. J. Image Processing with ImageJ. *Biophotonics Int.* **2004**, *11* (7), 36–41. https://doi.org/10.1201/9781420005615.ax4.

(45) Glasoe, P. K.; Long, F. A. Use of Glass Electrodes to Measure Acidities in Deuterium Oxide. *J. Phys. Chem.* **1960**, *64* (1), 188–190. https://doi.org/10.1021/j100830a521.

(46) Pattni, B. S.; Chupin, V. V.; Torchilin, V. P. New Developments in Liposomal Drug Delivery. *Chem. Rev.* **2015**, *115* (19), 10938–10966.

https://doi.org/10.1021/acs.chemrev.5b00046.

(47) Stauch, O.; Uhlmann, T.; Fröhlich, M.; Thomann, R.; El-Badry, M.; Kim, Y. K.; Schubert, R. Mimicking a Cytoskeleton by Coupling Poly(N-Isopropylacrylamide) to the Inner Leaflet of Liposomal Membranes: Effects of Photopolymerization on Vesicle Shape and Polymer Architecture. *Biomacromolecules* **2002**, *3* (2), 324–332. https://doi.org/10.1021/bm015613y.

(48) Dingels, C.; Müller, S. S.; Steinbach, T.; Tonhauser, C.; Frey, H. Universal Concept for the Implementation of a Single Cleavable Unit at Tunable Position in Functional Poly(Ethylene Glycol)S. *Biomacromolecules* **2013**, *14* (2), 448–459. https://doi.org/10.1021/bm3016797.

(49) Worm, M.; Kang, B.; Dingels, C.; Wurm, F. R.; Frey, H. Acid-Labile Amphiphilic PEO-b-PPO-b-PEO Copolymers: Degradable Poloxamer Analogs. *Macromol. Rapid Commun.* **2016**, 1–6. https://doi.org/10.1002/marc.201600080.

(50) Pohlit, H.; Bellinghausen, I.; Schömer, M.; Heydenreich, B.; Saloga, J.; Frey, H. Biodegradable PH-Sensitive Poly(Ethylene Glycol) Nanocarriers for Allergen Encapsulation and Controlled Release. *Biomacromolecules* **2015**, *16* (10), 3103–3111. https://doi.org/10.1021/acs.biomac.5b00458.

(51) Kim, S.; Linker, O.; Garth, K.; Carter, K. R. Degradation Kinetics of Acid-Sensitive Hydrogels. *Polym. Degrad. Stab.* **2015**, *121*, 303–310. https://doi.org/10.1016/j.polymdegradstab.2015.09.014.

(52) Müller, S. S.; Fritz, T.; Gimnich, M.; Worm, M.; Helm, M.; Frey, H. Biodegradable Hyperbranched Polyether-Lipids with in-Chain PH-Sensitive Linkages. *Polym. Chem.* **2016**, *7* (40), 6257–6268. https://doi.org/10.1039/C6PY01308B.

(53) Cordes, E. H. Mechanism and Catalysis for the Hydrolysis of Acetals, Ketals, and Ortho Esters. *Prog. Phys. Org. Chem.* **2007**, *4*, 1–44.

5.1.6 Supporting Information

5.1.7 Polymer synthesis and characterization.

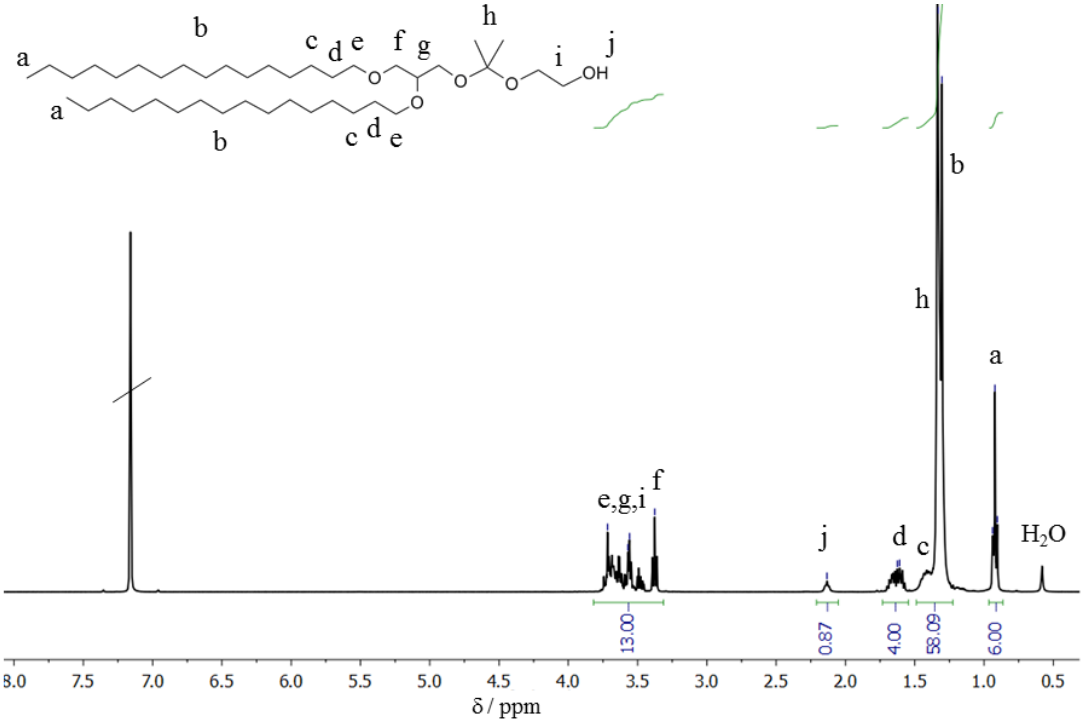

SI-Figure 1: ^{1}H NMR spectrum of the macroinitiator 4 measured in C_6D_6 at 400 MHz.

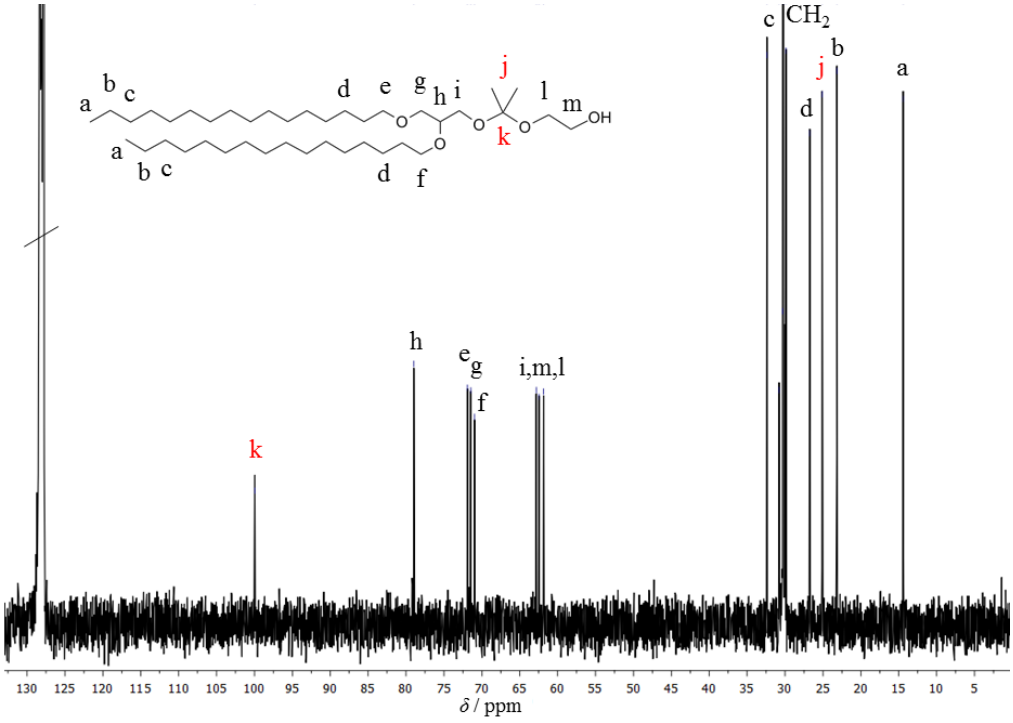

SI-Figure 2: ^{13}C NMR spectrum of the macroinitiator 4 measured in C_6D_6 at 100 MHz.

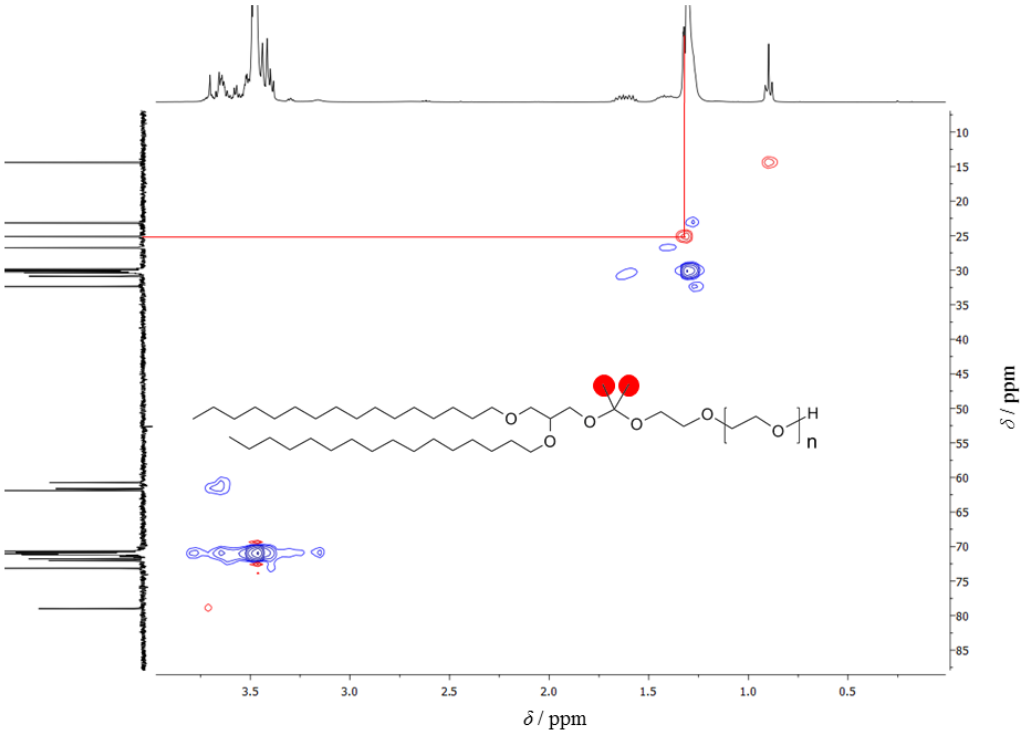

SI-Figure 3: HSQC 2D NMR spectrum of BisHD-K-PEG measured in C_6D_6.

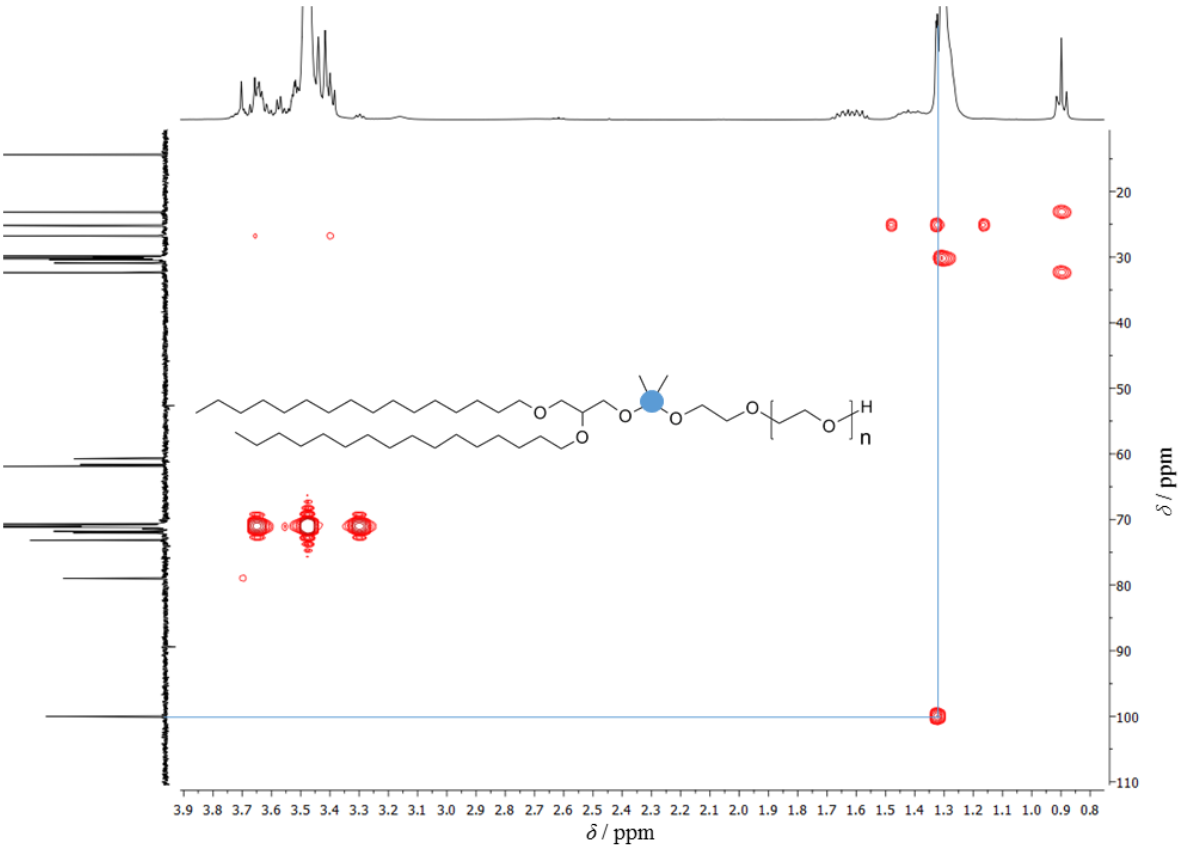

SI-Figure 4: HMBC 2D NMR spectrum of BisHD-K-PEG measured in C_6D_6.

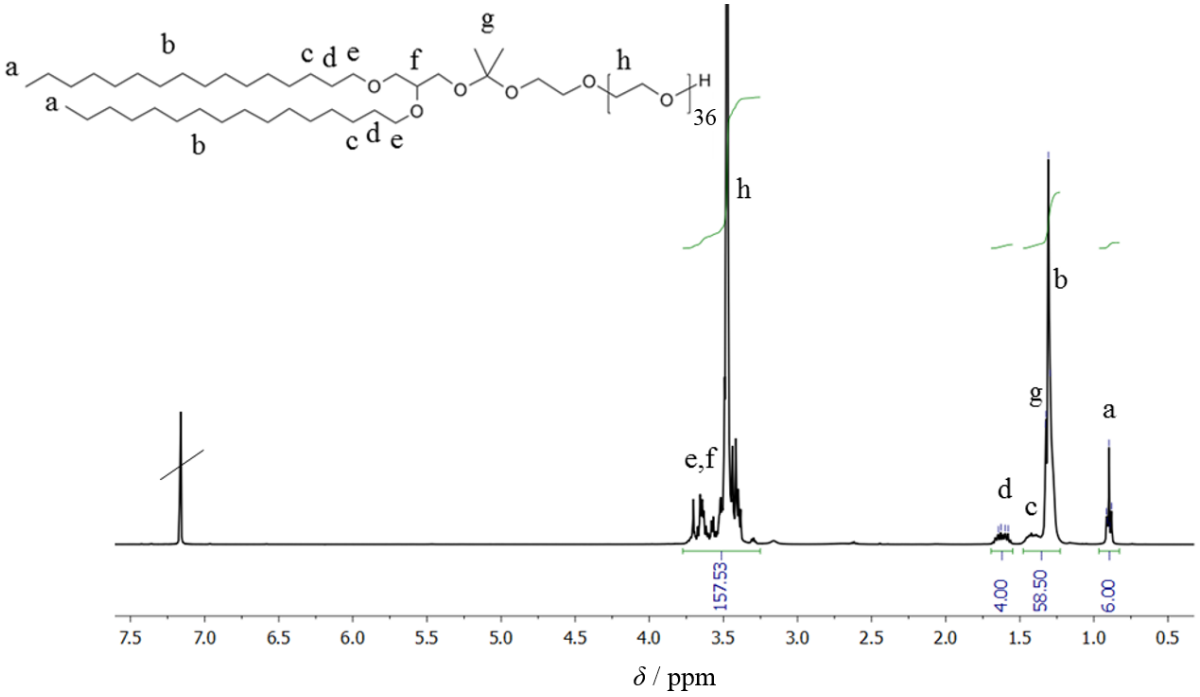

SI-Figure 5: ^{1}H NMR Spectrum of BisHD-K-PEG$_{37}$ measured in C_6D_6 at 400 MHz.

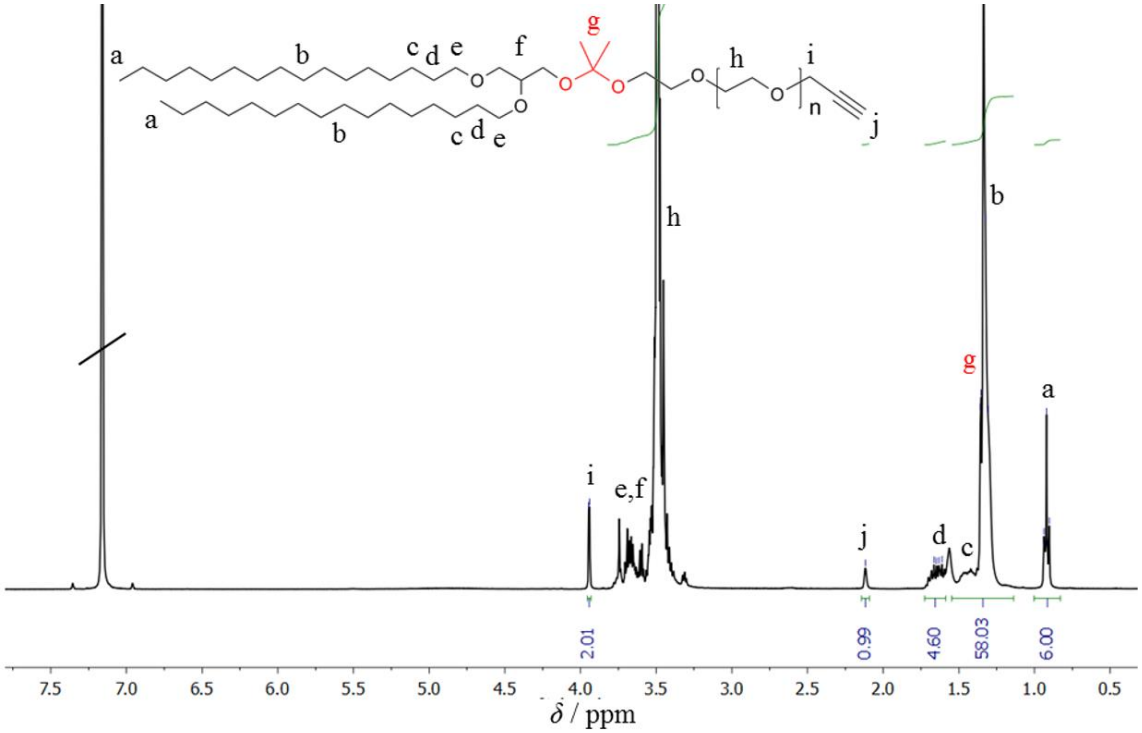

SI-Figure 6: ^{1}H NMR Spectrum of BisHD-K-PEG$_{40}$-Alkyne in C_6D_6 measured at 400 MHz.

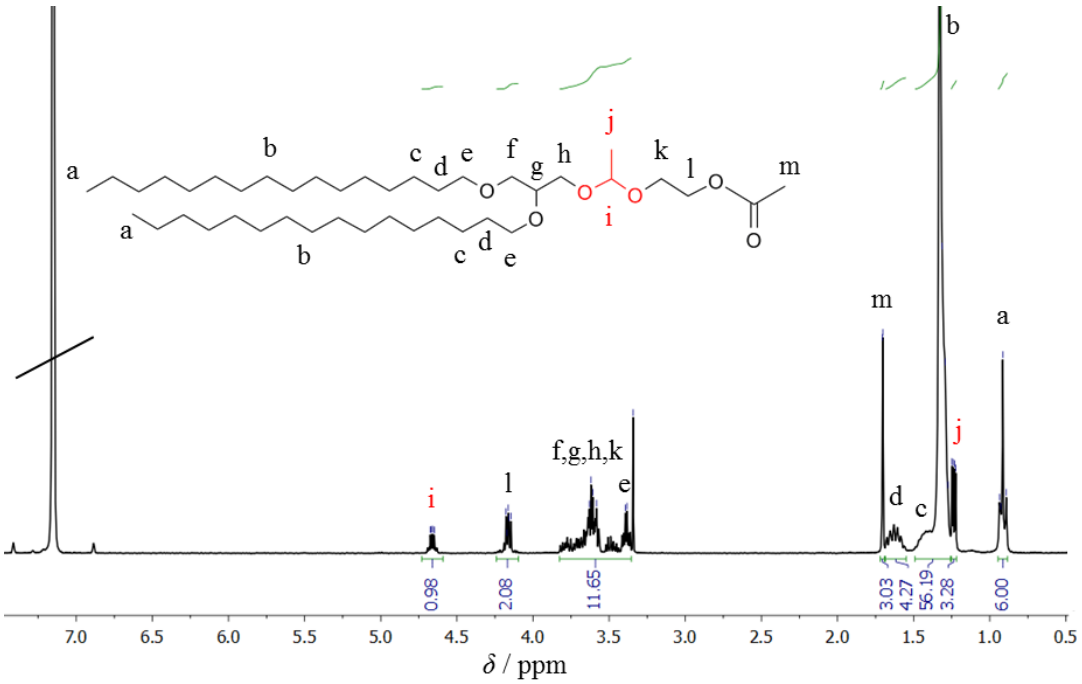

SI-Figure 7: ^{1}H NMR spectrum of BisHD-Acetal-Acetate measured in C_6D_6 at 400 MHz.

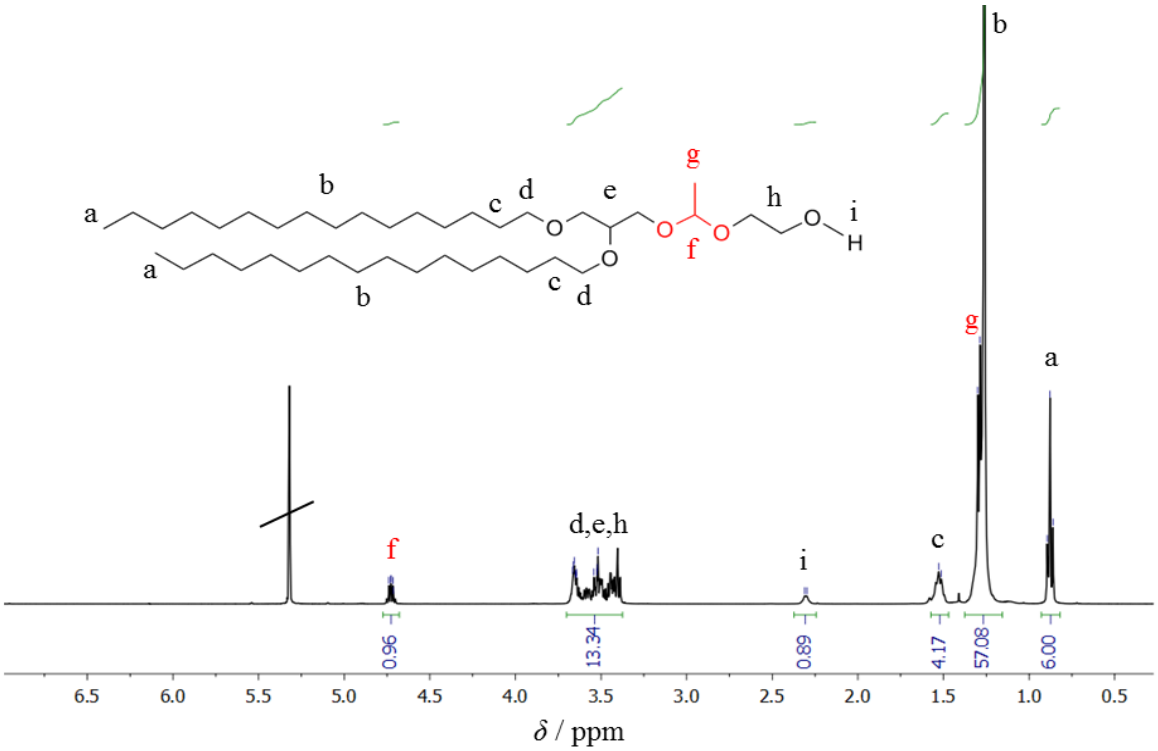

SI-Figure 8: ^{1}H NMR spectrum of the macroinitiator 8 measured in CD_2Cl_2 at 400 MHz.

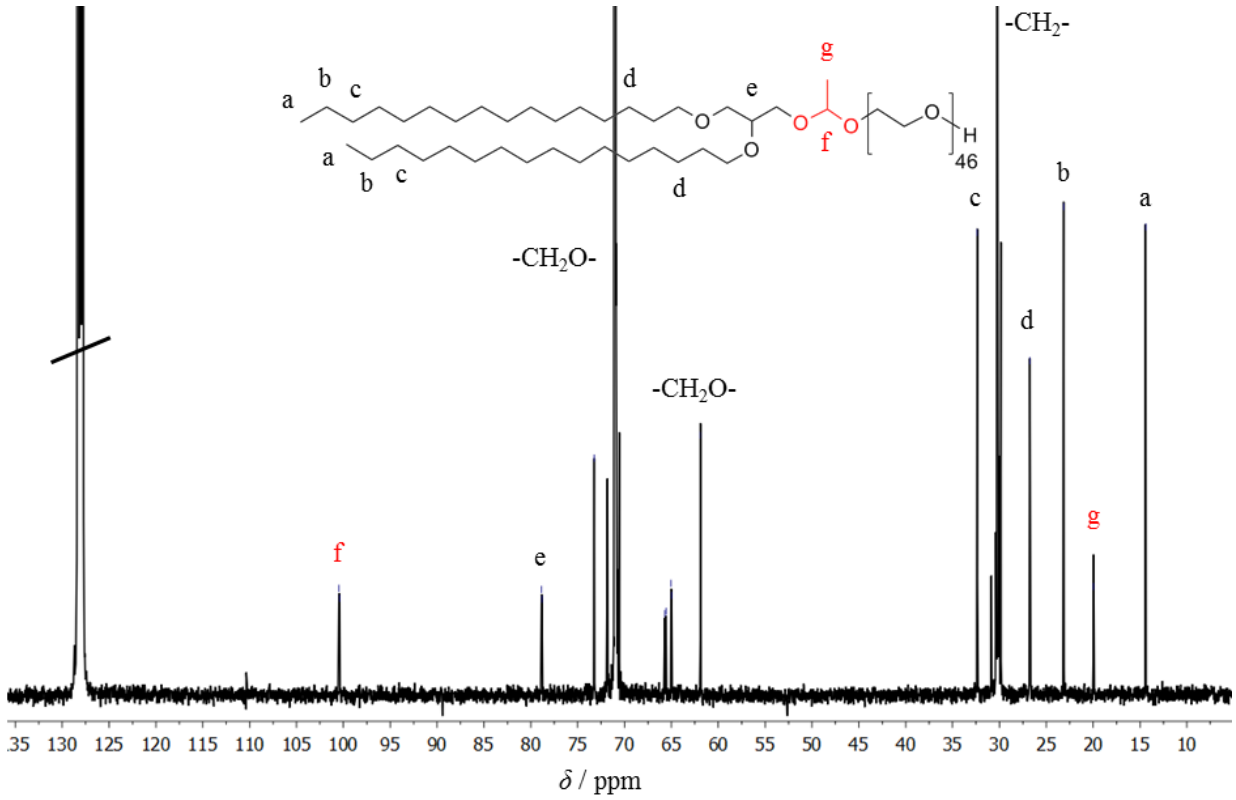

SI-Figure 9: ^{13}C NMR spectrum of BisHD-A-PEG_{46} measured in C_6D_6 at 100 MHz.

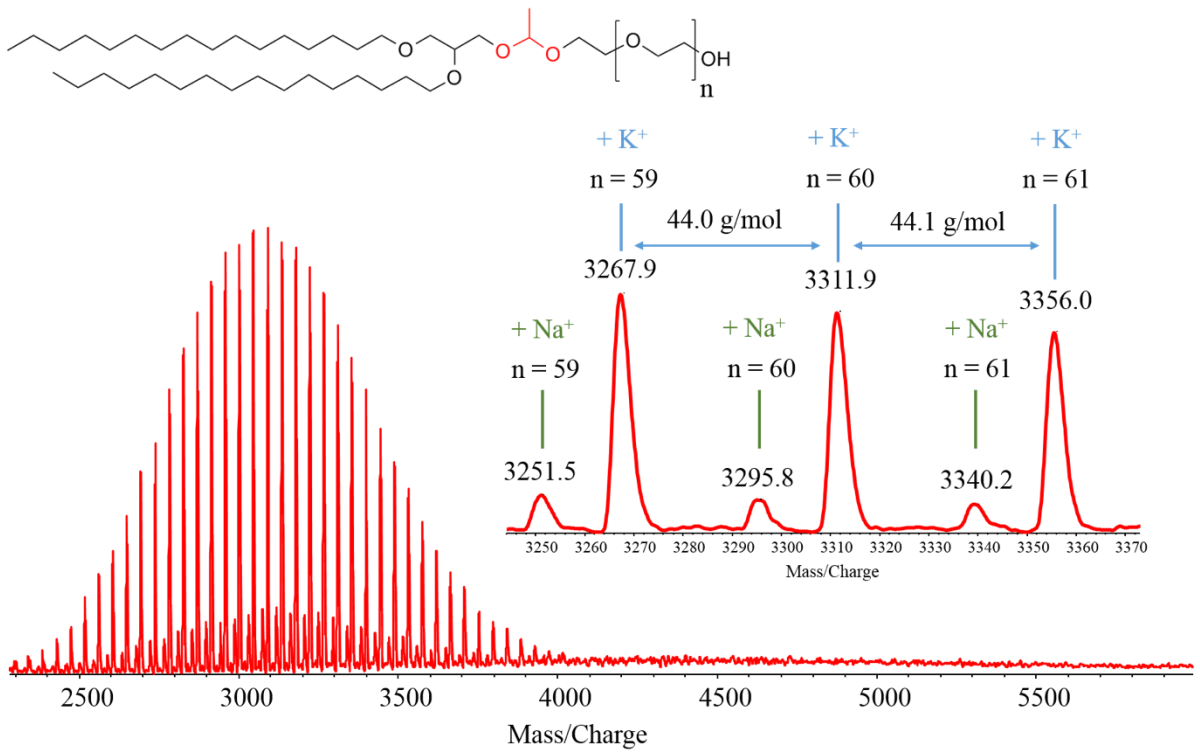

SI-Figure 10: MALDI-ToF mass spectrum of BisHD-A-PEG using a KTFA/CHCA matrix recorded in reflectron mode.

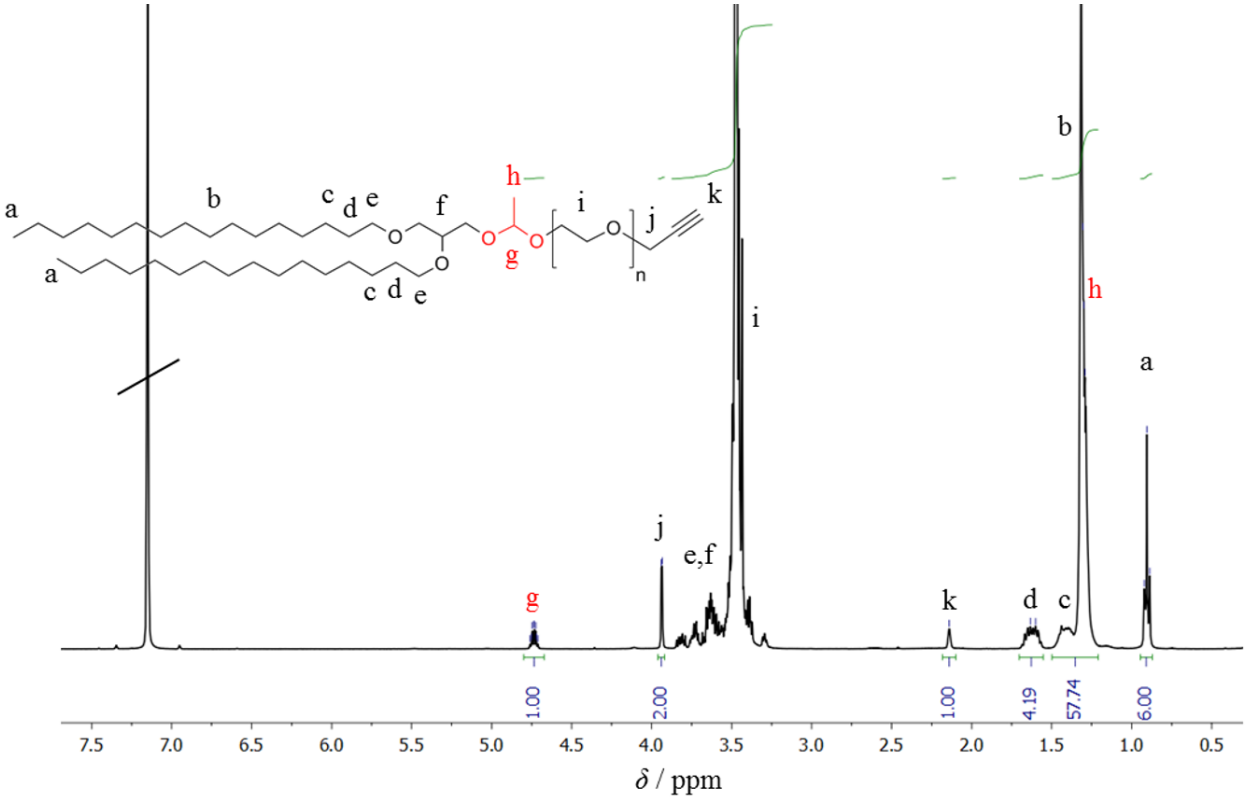

SI-Figure 11: ^{1}H NMR spectrum of BisHD-A-PEG$_{46}$-Alkyne measured in C_6D_6 at 400 MHz.

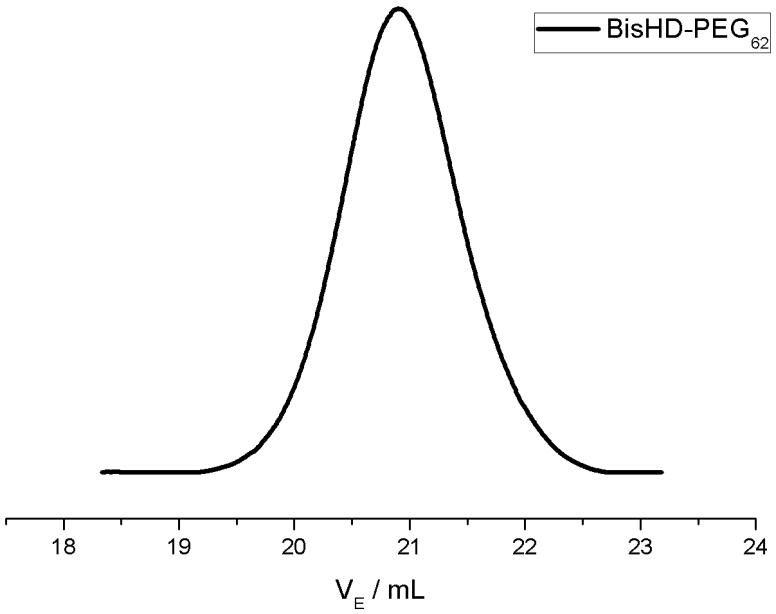

SI-Figure 12: SEC trace of BisHD-PEG$_{62}$ measured in DMF using RI detection.

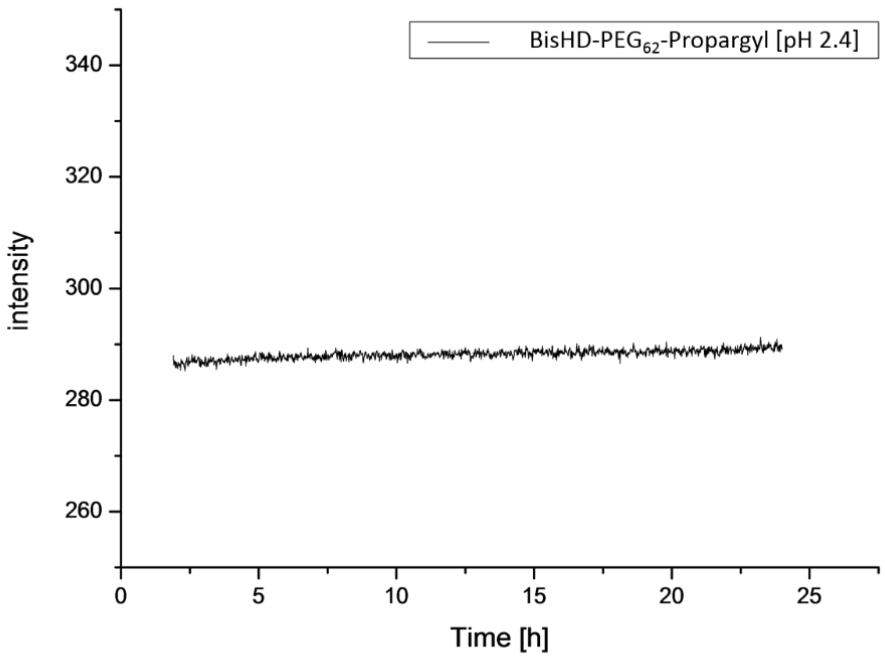

SI-Figure 13: Fluorescence trace of amphiphile without a cleavable group at pH 2.4. No increase in fluorescence was measurable.

5.2 Stability of Alkyl Chain-Mediated Lipid Anchoring in Liposomal Membranes

Lukas Gleue,[1] Jonathan Schupp,[2] Niklas Zimmer,[2] Eyleen Becker,[3] Holger Frey,[3] Andrea Tuettenberg,[2,*] Mark Helm[1,*]

[1] Institute of Pharmaceutical and Biomedical Science, Johannes Gutenberg-University Mainz, 55128 Mainz, Germany; lugleue@uni-mainz.de

[2] Department of Dermatology, University Medical Center, Johannes Gutenberg-University Mainz, 55131 Mainz, Germany; jonschup@uni-mainz.de (J.S.); Niklas.Zimmer@unimedizin-mainz.de (N.Z.)

[3] Department of Chemistry, Johannes Gutenberg-University Mainz, 55128 Mainz, Germany; ebecker@uni-mainz.de (E.B.); hfrey@uni-mainz.de (H.F.)

* Correspondence: antuette@uni-mainz.de (A.T.); mhelm@uni-mainz.de (M.H.)

Published in Cells, **2020**, *9* (10), 1-13, DOI: https://doi.org/10.3390/cells9102213.

cells

MDPI

Article

Stability of Alkyl Chain-Mediated Lipid Anchoring in Liposomal Membranes

Lukas Gleue [1], Jonathan Schupp [2], Niklas Zimmer [2], Eyleen Becker [3], Holger Frey [3], Andrea Tuettenberg [2,*] and Mark Helm [1,*]

[1] Institute of Pharmaceutical and Biomedical Science, Johannes Gutenberg-University Mainz, 55128 Mainz, Germany; lugleue@uni-mainz.de

[2] Department of Dermatology, University Medical Center, Johannes Gutenberg-University Mainz, 55131 Mainz, Germany; jonschup@uni-mainz.de (J.S.); Niklas.Zimmer@unimedizin-mainz.de (N.Z.)

[3] Department of Chemistry, Johannes Gutenberg-University Mainz, 55128 Mainz, Germany; ebecker@uni-mainz.de (E.B.); hfrey@uni-mainz.de (H.F.)

* Correspondence: antuette@uni-mainz.de (A.T.); mhelm@uni-mainz.de (M.H.)

Received: 30 July 2020; Accepted: 24 September 2020; Published: 29 September 2020

Abstract: Lipid exchange among biological membranes, lipoprotein particles, micelles, and liposomes is an important yet underrated phenomenon with repercussions throughout the life sciences. The premature loss of lipid molecules from liposomal formulations severely impacts therapeutic applications of the latter and thus limits the type of lipids and lipid conjugates available for fine-tuning liposomal properties. While cholesterol derivatives, with their irregular lipophilic surface shape, are known to readily undergo lipid exchange and interconvert, e.g., with serum, the situation is unclear for lipids with regular, linear-shaped alkyl chains. This study compares the propensity of fluorescence-labeled lipid conjugates of systematically varied lengths to migrate from liposomal particles consisting mainly of egg phosphatidyl choline 3 (EPC3) and cholesterol into biomembranes. We show that dialkyl glyceryl lipids with chains of 18–20 methylene units are inherently stable in liposomal membranes. In contrast, C16 lipids show some lipid exchange, albeit significantly less than comparable cholesterol conjugates. Remarkably, the C18 chain length, which confers noticeable anchor stability, corresponds to the typical chain length in biological membranes.

Keywords: liposomes; click chemistry; polyglycerol; bioconjugates; drug delivery

1. Introduction

Liposomes are spherical nanovesicles consisting of lipids, which were first produced in the 1960s by Alex Bangham et al. [1]. Due to the amphiphilic properties of phosphatidyl choline lipids in combination with cholesterol-based lipids, liposomes possess an aqueous core and one or more hydrophobic phospholipid bilayers. This enables the incorporation of hydrophobic molecules into the membranes as well as the transport of water-soluble molecules in the core compartment. Because of these properties, liposomes have found application in cancer treatment, gene therapy, cell biology and as a powerful drug delivery system [2–10].

Phospholipids, glycerophospholipids and derivatives of cholesterol can be used for the production of liposomes, and this variety of lipids allows the formulation of liposomes with different properties, especially adapted to the respective application.

For example, by adding cholesterol up to 50 mol-% to a liposome formulation, membrane stability and tightness can be increased or particle uptake by macrophages can be reduced by using lipids with linked polyethylene glycol (PEG) chains [11]. These commonly called "PEGylated" liposomes show peculiar behavior, known as the "stealth effect", i.e., significantly increased blood

circulation half-life [12,13]. This effect results from shielding by the long polyethylene glycol chains, which reduces the binding of blood plasma components and interaction with macrophages, leading to increase half-life in blood circulation [14,15]. In addition to the classic example of PEGylation, the conjugation of liposomes to antibodies, folic acid, biotin or peptides can be used for specific tumor targeting [16–20].

We have previously established hyperbranched polyglycerol (*hbPG*)-derived stealth-like polyether lipid structures, possessing either a dialkyl or cholesterol anchor [21]. In human blood serum, liposomes containing hyperbranched polyglycerols showed lower aggregation than comparable PEGylated liposomes by comparable biodistribution [22,23]. Furthermore, hbPG-functionalization leads to increased interaction with macrophages, probably triggered by the lower amount of adsorbed proteins on the surface compared to classical PEGylated particles. This effect might possibly result from the larger number of free hydroxy groups in hbPG-functionalized liposomes, although experimental verification of this hypothesis is not yet available [5].

Cholesterol and many of its metabolic derivatives (such as steroid hormones) are distributed in the bloodstream by lipid–protein particles of variegated density. In addition to receptor-mediated uptake, steroid structures are thought to insert into, or pass through, cell membranes in the frame of a dynamic equilibrium [24,25]. Hence, lipid extraction from liposomes in a similar equilibrium is quite relevant for the sustained properties of liposomal formulations. Previous research of our group established the monitoring of lipid escape from the liposomal membrane and insertion into other membranes. This behavior was particularly evident for cholesterol lipids, which, presumably due to their irregular scaffold structure, are less stably anchored in membranes than typical biomembrane lipids whose two long hydrocarbon chains are known to form a dense network of van-der-Waals interactions in a symmetric lipophilic environment such as a cell membrane [26]. In order to demonstrate this effect, we prepared liposomes based on functionalizable cholesterol and dialkyl lipid derivatives, to which fluorescent dyes were covalently attached by click chemistry. After 4 h incubation of cells with the fluorescently labelled liposomes, confocal laser scanning microscopy images showed a significant fluorescence of labeled cholesterol derivatives in the cell membrane, in contrast to labeled dialkyl lipids which rarely inserted into the cell membrane [25].

The choice of appropriate lipid anchors can therefore influence a number of important parameters of liposomal formulations, e.g., the sustained transport (or release) of a model cargo during extended circulation, or the durability of molecular structures conjugated to the liposomal surface, which are important for stealth shielding or for targeting to specific receptors involving molecular recognition of bioconjugates [27,28].

In the present study, we identify a lower limit for dialkyl chain length in lipids, which leads to the exchange between the liposomal membrane and the cell membrane.

2. Materials and Methods

2.1. Synthesis of Dialkyl-Based Anchors

Three different hydrophobic anchor structures were synthesized for use as initiators for the anionic ring-opening polymerization (AROP) of epoxides. The initiators were prepared in a straightforward two-step procedure based on a procedure of Stauch et al., performing a Williamson etherification and using 1-*O*-benzyl glycerol and hexadecyl bromide, octadecyl bromide as well as icosane bromide, followed by hydrogenation to remove the benzyl protecting group [29]. In order to investigate the influence of the chain lengths, the anchors 1,2-bis-*n*-icosanyl glyceryl ether (BisID), 1,2-bis-*n*-hexadecyl glyceryl ether (BisHD) and 1,2-bis-*n*-octadecyl glyceryl ether (BisOD) were synthesized. The alkyl chain lengths of the anchor structures were 20 (BisID), 18 (BisHD) and 16 (BisOD) carbon atoms.

2.2. Synthesis of Amphiphilic Polyethers

The anionic ring-opening polymerization (AROP) of ethylene oxide was applied to synthesize well-defined PEG chains with tailored molecular weights [30]. The 1,2 bis-*n*-alkyl glyceryl ethers were

used as initiators for the polymerization to obtain amphiphilic polyether-based lipids (see supplement scheme S1). The combination of a hydrophobic initiator and a hydrophilic polyether results in polymers with amphiphilic behavior, which are suitable for the integration into liposomes to obtain sterically stabilized liposomal nanocarriers.

The AROP for the polymerization of ethylene oxide (EO) was carried out in dry tetrahydrofuran (THF), and potassium naphthalenide was used as a base to deprotonate the initiator. The deprotonation process was followed by color change of the initiator solution. The polymerization was carried out at 60 °C for 24 h to obtain full conversion. Molecular weights are controlled via the ratio of employed initiator and epoxide monomer.

2.3. *Functionalization of Amphiphilic Polyethers with Propargyl Bromide*

To attach alkyne-moieties, the polyether-based lipids were functionalized with propargyl bromide at the polyether end group. An alkyne-group enables the copper(I)-catalyzed azide-alkyne cycloaddition (CuAAC) with functional groups, e.g., dyes like atto 488 azide or other azide-bearing molecules [25]. This reaction is known from literature and was adapted for the synthesized amphiphilic polyethers [31,32]. For this purpose, the terminal hydroxyl group of PEG was deprotonated using sodium hydride (NaH) (see supplement scheme S1). The terminal propargyl group was then introduced by a substitution reaction with propargyl bromide (structures: Figure 1B).

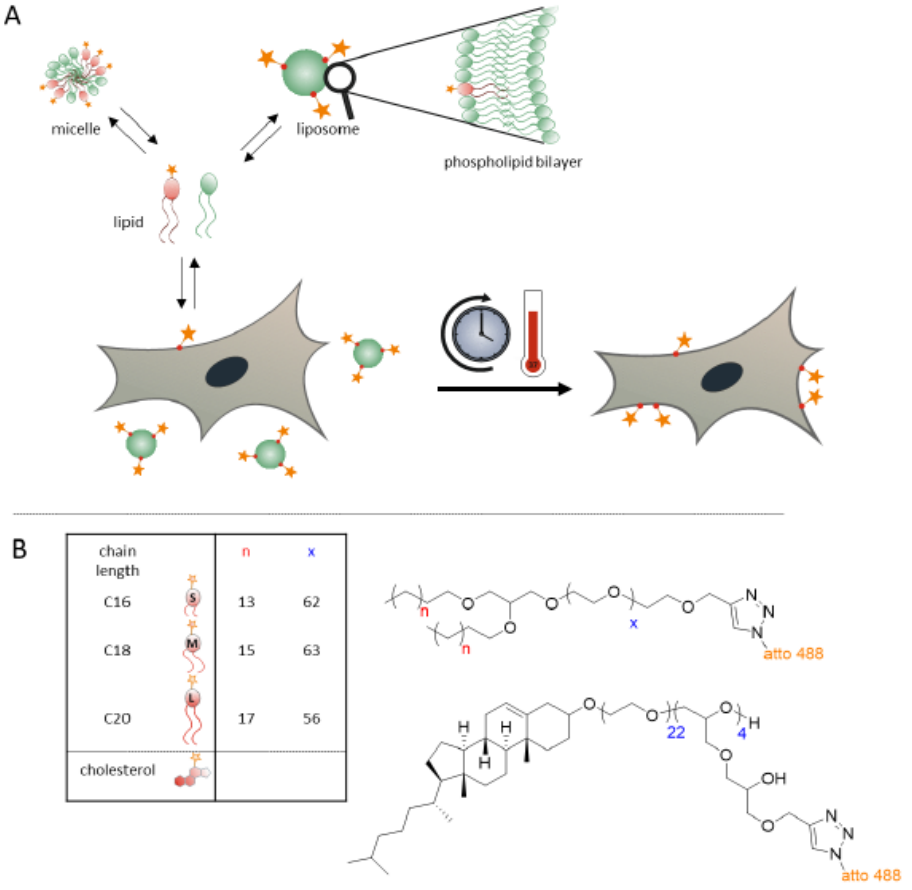

Figure 1. (**A**) Conceptual sketch of the approach. Lipid compounds are distributed among a variety of lipid-containing bodies in a complex equilibrium with ill-defined dynamics. The star symbolizes the attached fluorescence dye atto 488. (**B**) Synthetic experimental polyether lipids employed in the investigations: n describes the number of carbon atoms in alkyl chains, x the number of polyethylene glycol (PEG)-units.

2.4. Synthesis of Cholesterol-Based Linear-Hyperbranched Polyethers

As a drawback, despite its combination of favorable properties, such as excellent aqueous solubility, low toxicity and biocompatibility, PEG exhibits the disadvantage of low functionality, i.e., only the terminal hydroxyl groups [30,33]. Hyper-branched structures based on polyglycerol (*hb*PG) are therefore a promising alternative, due to the multitude of hydroxyl groups available for post-polymerization modification. Furthermore, *hb*PG is highly water-soluble and also exhibits excellent biocompatibility [34]. Hofmann et al. introduced amphiphilic *hb*PGs using different hydrophobic initiators (cholesterol, 1,2-bis-*n*-tetradecyl glyceryl ether (BisTD), 1,2-bis-*n*-hexadecyl glyceryl ether (BisHD) and 1,2-bis-*n*-octadecyl glyceryl ether (BisOD)) [21,35].

In the first reaction step a cholesterol-PEG-PEEGE precursor polymer was synthesized via AROP with EO and ethoxyethyl glycidyl ether (EEGE) (see supplement scheme S2). The polymerization of EEGE leads to linear structures (PEEGE) with acetal-protected hydroxyl groups, which can be released upon acidic treatment. The resulting linear polyglycerol (*lin*PG) structure exhibits numerous hydroxyl groups and can therefore be used as a macroinitiator to prepare a hyperbranched polyglycerol (*hb*PG) block. Consequently, after the deprotection under acidic conditions, the cholesterol-PEG-*lin*PG macroinitiator was used for "hypergrafting" of glycidol via the slow monomer addition (SMA) technique to obtain the cholesterol-PEG-*hb*PG polyether lipids (Figure 1B).

2.5. Functionalization of Cholesterol-PEG-hbPG with Propargyl Bromide

Polymer derivatization for subsequent functionalization by click chemistry was carried out using propargyl bromide. The hydroxyl groups of *hb*PG were deprotonated using sodium hydride (NaH). In the case of the functionalization of *hb*PG, the degree of functionalization was controlled via the amount of propargyl bromide employed. The average degree of functionalization was determined via ^{1}H NMR spectroscopy [29].

2.5.1. Liposome Preparation

In the first step, for the preparation of 5 mM liposomes, lipids dissolved in chloroform (see Table 1) were added to a PCR tube (#G001 F, Kisker Biotech, Steinfurt, Germany) depending on their percentage of total lipid amount and the solvent was removed by vacuum centrifugation (#5305, Eppendorf, Hamburg, Germany).

For complete removal of solvents, lipids were then freeze-dried at -80 °C (Alpha 2–4 LD, Martin Christ Gefriertrocknungsanlagen, Osterode/Harz, Germany) overnight and stored in a freezer until use at −20 °C.

To prepare liposomes, dried lipids were incubated together with 325 mg SiLibeads (#96035, Typ ZY-S 0.3–0.4 mm, Sigmund Lindner, Warmensteinach, Germany) and 9.3 µL DPBS (Dulbecco's phosphate-buffered saline (#14190-094, Thermo Fisher Scientific, Waltham, MA, USA)) for 10 min at room temperature and then mixed for 20 min at 4 °C by dual centrifugation (#3200 + #3205, Andreas Hettich, Tüttlingen, Germany) to form a phospholipid gel. To finally form liposomes, the gel was homogenized again together with 77.2 µL DPBS twice for 2 min at 4 °C.

Table 1. Lipid compositions of liposomal formulations in mol-%.

Lipid 1	Percentage	Lipid 2	Percentage	Lipid 3	Percentage
EPC3	50 mol-%	Cholesterol	45 mol-%	C16 or C18 or C20 or Cholesterol alkyne lipid	5 mol-%
EPC3	60 mol-%	Cholesterol	35 mol-%		
EPC3	70 mol-%	Cholesterol	35 mol-%		
DPPC	50 mol-%	Cholesterol	45 mol-%	C16 or C18 alkyne lipid	5 mol-%
DSPC	50 mol-%	Cholesterol	45 mol-%		
20:0 PC	50 mol-%	Cholesterol	45 mol-%		

EPC3: egg phosphatidyl choline 3 (#527600, lipoid, Ludwigsharfen, Germany); DPPC: 1,2-dipalmitoyl-sn-glycero-3-phosphocholine (#850355C-200MG, Sigma-Aldrich, St. Louis, MO, USA); DSPC: 1,2-distearoyl-sn-glycero-3-phosphocholine (#850365C-200MG, Sigma-Aldrich); 20:0 PC: 1,2-diarachidoyl-sn-glycero-3-phosphocholine (#850368C-25MG, Sigma-Aldrich).

2.5.2. Liposome Modification and Purification

To label alkyne liposomes with fluorescent dye atto 488-azide, 30 µL liposome stock was dissolved in 100 mM phosphate buffer pH 8 (PB) (94.7 mM disodium hydrogen phosphate (#P030.1, Carl Roth, Karlsruhe, Germany), 5.3 mM sodium dihydrogen phosphate dihydrate (#T879.1, Carl Roth)), 0.5 mM Tris (hydroxypropyltriazolylmethyl) amine (THPTA, Helm Group, Johannes Gutenberg University Mainz, Germany), 0.1 mM copper sulfate pentahydrate (#8175.1, Carl Roth,), 2.5 mM soduim ascorbate (#3149.1, Carl Roth), 0.1 mM atto 488-azide (#AD 488-101, Atto-Tec, Siegen, Germany) in a PCR tube (#G001 F, Kisker Biotech) and filled up with MiliQ-Water (#ZRQSVR5WW, Merk Millipore, Darmstadt, Germany) to a finale volume of 120 µL.

The reaction mixture was agitated at room temperature for two hours and after completion of the transformation, 20 mM EDTA (ethylenediaminetetraacetic acid (#8040.1, Carl Roth, solved in water)) was added to stop the reaction.

2.5.3. Cell Culture and Cell Lines Employed

The human melanoma cell line UKRV-Mel-15a was cultured in RPMI 1640 medium (#31870, Thermo Fisher Scientific, Waltham, MA, USA) supplemented with 10% FBS (fetal bovine serum (#10500064, Thermo Fisher Scientific)), 1% GlutaMAX™ (#35050038, Thermo Fisher Scientific) and 0.1% primocin (#ant-pm-2, InvivoGen, San Diego, CA, USA). Cells were detached via incubation Trypsin-EDTA (#T3924, Merck, Darmstadt, Germany) for 5 min at 37 °C every 3 to 4 days.

2.5.4. Flow Cytometry

For analysis of lipid exchange via flow cytometry UKRV-Mel-15a cells were seeded in 24 well tissue culture plates (#3524, Corning, Corning, NY, USA) at a density of 100,000 in 1 mL medium and incubated for 4 or 24 h with liposomes at a concentration of 1% or 5% (v/v). For Section 3.5, adherent cells were treated additionally with 10 µM cytochalasin D (#C2618, Merck) 30 min prior to liposome addition [36–38]. Cells were detached via incubation with Trypsin-EDTA (#T3924, Merck)) for 5 min at 37 °C. Singe cell suspension was stained with 200fold diluted Fixable Viability Dye eFluor™ 780 (#65-0865-18, Thermo Fisher Scientific) in DPBS (#14190-094, Thermo Fisher Scientific) for 20 min at 4 °C for dead cell exclusion, fixed with 4% PFA (paraformaldehyde (#0335.1, Carl Roth)) in DPBS for 20 min at 4 °C and measured in FACS buffer containing 0.5% HSA (#10530a/96, CSL Behring, Marburg, Germany), 1 mM EDTA (#A3553, AppliChem, Darmstadt, Germany), 10 µg/mL human IgG (#EU/1/08/446/001, CSL Behring GmbH, Marburg, Germany) in DPBS.

Flow cytometry was performed on an LSRII flow cytometer (BD Biosciences, Franklin Lakes, NJ, USA) and samples were measured by 488 nm (FITC-channel 505LP, 530/30) and by 633 nm (APC-channel 660/20; FVD780 735LP, 780/60). Data were analyzed by using Cytobank [39].

2.5.5. Microscopy

For the confocal imaging, the Leica SP8 with HyD Detector (Wetzlar, Germany) was used with lasers for 405 nm, 488 nm and 638 nm. Melanoma cell line UKRV-Mel-15awas cultured for 24 h in ibidi µ-slides 8 well (#80826, Ibidi, Gräfelfing, Germany), 30,000 cells/well each, in supplemented RPMI 1640 medium (see cell culture cell line). After treatment for 4 and 24 h with the same endpoint, cells were checked for adherence and then fixed with 4% PFA (#0335.1, Carl Roth, Karlsruhe, Germany) in DPBS for 20 min at 4 °C. Additionally DNA was stained by Hoechst 33342 (#PK-CA707-40046, PromoCell, Heidelberg, Germany)) and the membrane by DiD (1,1-Dioctadecyl-3,3,3,3-tetramethylindodicarbocyanine (#PK-CA707-30021, PromoCell, Heidelberg, Germany)) for 30 min at RT each. For image analysis, Fiji was used [40].

2.5.6. Dynamic Light Scattering

For liposome characterization, 20 µL purified liposome suspension was diluted in 1 mL MiliQ-water and polydispersity (PDI), size and zeta-potential (ζ-potential) were measured in a disposable folded capillary cell (#dts1070, Malvern, Worcestershire, United Kingdom) at 25 °C by using a Malvern Zetasizer Nano series (Malvern). The refractive index was set to 1.33 (1.59 for liposomes) with a water viscosity of 0.8872 and the scattering angle was configured to 173.

3. Results

3.1. Concept and Approach

The strategy for monitoring of the fate of different dye-conjugated lipids is shown in Figure 1A. The upper part depicts in a general manner the behavior of single lipid molecules in equilibrium between micelles, free lipids and liposomal structures. In in vitro cell culture, the latter also includes the cell membranes, which participate in an exchange equilibrium with liposomes.

To monitor the exchange equilibrium, we labelled the polyether model lipids with a fluorescent dye and traced their location both by microscopy and by flow cytometry. Suspension of liposomes containing fluorescence-labelled lipids were added to cell cultures, and after a certain incubation period, the localization and intensity of fluorescence in the cell membranes were analyzed. Of note, we are aware that we cannot directly distinguish between lipid exchange taking place at the cell membrane with liposomes in suspension or phagocytosis of liposomes and their subsequent degradation and incorporation into the cell membrane system. However, time-lapse imaging with this approach has previously enabled us to efficiently monitor the fast exchange of cholesterol derivatives between liposomes and cell membranes [26]. We observed a rapid exchange rate in the single-minutes digit for cholesterol derivates, with fluorescent lipids first appearing in the cell membrane and only later being incorporated into intracellular vesicles [26]. In this work, we observed a significantly slower exchange for alkyl chains up to a time of 4 h, leading us to conduct the current observation at 4 h and 24 h. The latter time point was chosen to obtain a measure of the duration of the lipid exchange. To guard against the potential adverse effects of endocytosis, we also performed experiments in the presence of cytochalasin D, an endocytosis inhibitor.

3.2. Experimental Lipids and Liposome Preparation

Figure 1B depicts the different compounds employed in this setting, which were synthesized based on our prior discovery that revealed high dynamics of a cholesterol derivative in transitions from liposomal preparations to cell membranes [26]. The model compounds employed are conceptually similar to biological membrane lipids containing two long alkyl chains as well as a hydrophilic headgroup, which in the current work is a polyethylene glycol chain (or alternatively a *hb*PG structure) that additionally equips the liposomes with a stealth effect. The synthesis of these compounds was conducted along the lines described previously by Frey et al. [21,23,35]. Briefly, the synthesis of PEGylated lipids was performed by anionic ring-opening polymerization (ROP) starting from dialkyl-substituted glycerol. Subsequent to the polymerization of EO, the resulting PEGylated

ether lipids were reacted with propargyl bromides to functionalize the chain ends with a propargyl-ether.

The terminal alkyne moieties allowed for subsequent derivatization by click chemistry either before (pre) or after (post) liposomal formulation. Our current investigation relies on post-formulation CuAAc of liposomes with fluorescent dyes, which were then purified by gel filtration chromatography. The advantages of this formulation–derivatization sequence include mild reaction conditions and fast product isolation by routine semi-automated methods [41].

The production of liposomes was conducted by dual centrifugation, a technique based on the simultaneous rotation of two sample plates around two axes. This results in the mixing of the samples instead of sedimentation as in classical centrifugation. The advantages of using dual centrifugation to produce liposomal formulations are the choice of flexible preparation sizes with simultaneous sterile and endotoxin-free conditions. In addition, this cost-effective method allows for the simultaneous preparation of several samples [26,42].

The liposome suspensions prepared by dual centrifugation were then fully automatically purified by using semi-automated gel filtration on an HPLC (high-performance liquid chromatography) setup to remove free lipids. Routine characterization included size determination by dual light scattering and measurement of surface potential. For this work, we used liposomes with 162.60 ± 29.51 nm diameter, 0.26 ± 0.07 a.u. polydispersity and −13.87 ± 0.07 mV zeta-potential.

3.3. Analysis of Lipid Exchange Via Flow Cytometry

To compare the transfer of fluorescently labelled experimental lipids from liposomes to cells in tissue culture, cells were cultivated for 4 h and 24 h with liposomal formulations containing the fluorescence-labeled lipids in two different concentrations. In comparison to previously investigated RBE4 cells [26], we found the human melanoma cell line UKRV-Mel-15a more amenable to rapid and reproducible analyses, presumably because of their relatively large size. After incubation with liposomal preparations, the medium was removed, cells were fixed and then analyzed by flow cytometry.

The results after gating signals for the atto 488 are presented in Figure 2A,B. Figure 2A, reflecting the fluorescence intensity obtained after an incubation of 4h, clearly reproduces the behavior of cholesterol-anchor derived lipids as previously published, showing strong signals corresponding to a transfer of cholesterol derived lipids to the cell membranes [26]. For the dialkyl lipids, most signals remained near a baseline of 5.0×10^3 with the visually apparent, but not significant, exception of the liposomal preparation containing 5 mol-% C16 compounds, i.e., the shortest alkyl chain used in this study. Additionally, cells incubated with C18 and C20 liposomes for 4 h showed moderately, but not significantly, increased fluorescence.

Data obtained after 24 h (Figure 2B) demonstrate the progression of lipid exchange for all preparations containing 5 mol-% polyether lipids, albeit only to a very limited extent for the C18 and C20 anchor chains. Meanwhile, in further confirmation of our previous observations, the signal resulting from the cholesterol derivative outdistanced all others by far, more subtle differences were observable among the polyether lipids.

Thus, the C16 preparations both at 1 mol-% and 5 mol-% now gave rise to significantly higher signals than those of the corresponding longer C18 and C20 alkyl chains. These observations suggest that for the anchoring of stealth structures with alkyl chains, a minimum alkyl chain length of C18 is very efficient, whereas a length of 16 carbon atoms delineates a border, below which anchoring might be insufficient. Future studies including, e.g., C14 and C12 polyether lipids, must be undertaken to understand if chain length is the only determinant of membrane anchorage.

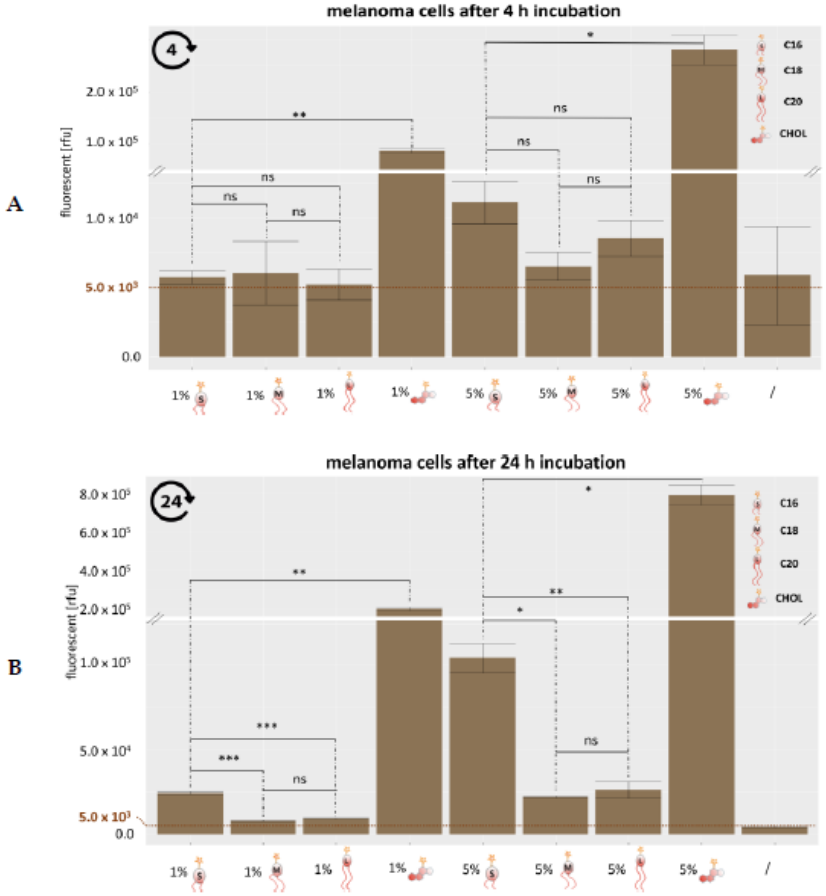

Figure 2. Quantification of lipid exchange after 4 h (**A**) and 24 h (**B**) by flow cytometry. 1.0×10^5 UKRV-Mel-15a cells were incubated with 1 or 5 vol-% atto 488 linked liposomes at 37 °C and fixed with a 4% formaldehyde solution before flow cytometric analysis. The significance between two values is illustrated by * p = 0.05–0.01, ** $p < 0.001$, *** $p < 0.0001$ and ns = no significance. The statistically significant was calculated using the Welch and Brown–Forsythe version of the one-way ANOVA test.

3.4. Tracking Labeled Lipids by Fluorescence Microscopy

For a more spatially resolved, detailed investigation, cells exposed to liposomes as described above for the flow cytometry analyses were imaged by confocal fluorescence microscopy. The results for 4 h and 24 h incubation at 37 °C are shown side-by-side in Figure 3.

As a positive control for lipid exchange, the liposomes contained a DiD label, which is observed to stain the cells' biomembranes in the red fluorescence channel clearly. In comparison to this efficient exchange from liposomes to cell membranes, C18 and C20 lipids hardly show signals of relocation, which is coherent with the observations in flow cytometry stated above. In contrast, relocation was easily visible for cholesterol-conjugated dye, which rapidly stained cell membranes, indicated by green fluorescence from the atto 488 dye, or by an overlay of red and green fluorescence visualized in orange in Figure 3, this observation, too, is well in line with the flow cytometry data. To a lesser extent, but clearly visible, the relocalization of green fluorescence was observed for the labeled C16 lipid after 24 h (upper right panel in Figure 3), signaling a certain extent of lipid exchange from liposomes to the cell membrane. In summary, these images thus confirm the tendency of C16 alkyl lipid to enter into a dynamic equilibrium as depicted in Figure 1A in a time frame comprising a few hours to one day.

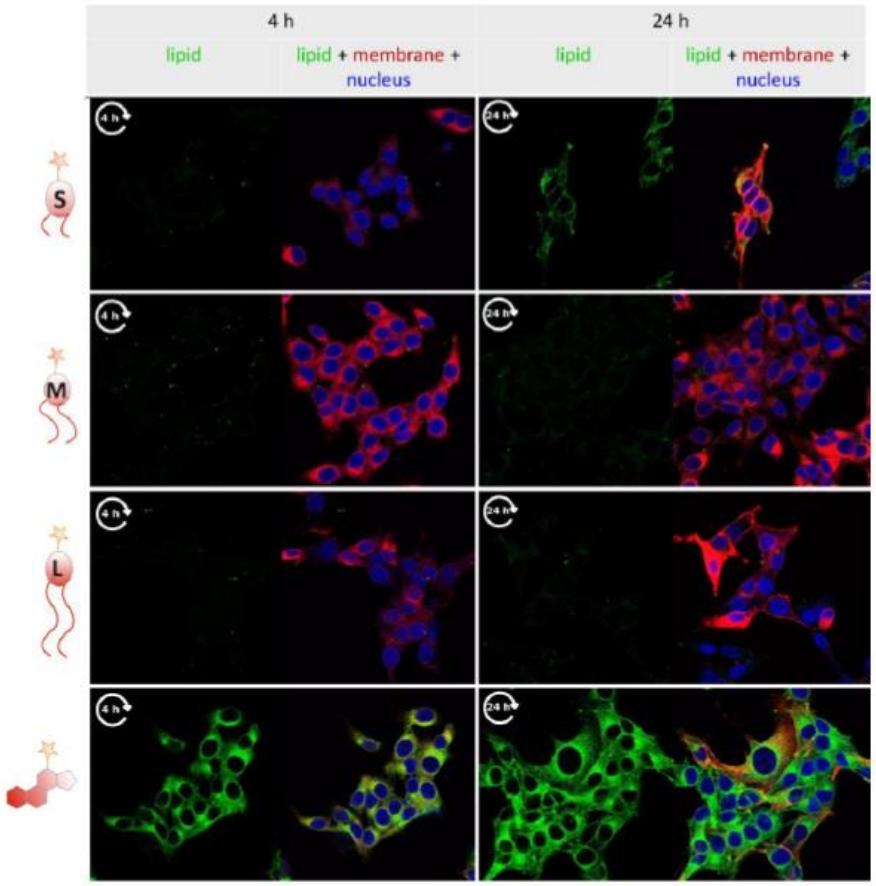

Figure 3. Confocal fluorescence imaging of UKRV-Mel-15a cells, observed at 4 h and 24 h after incubation with liposomes containing membrane label (DiD, red) and click-labeled experimental lipids with varied chain length (atto 488, green). Cell nuclei were stained with Hoechst (blue). Together with the cell membrane shown in red, the insertion of lipids becomes visible as an orange signal in the merge view.

3.5. Analysis of Lipid Exchange Depending on Liposome Composition

To further characterize the differential behavior of C1b versus longer alkyl lipids in some more depth, we investigated the influence of liposome composition on the lipid exchange. Liposomes containing 5 mol-% C16 versus C18 alkyne lipids were prepared with different EPC3: Chol ratios, namely 50/45, 60/35 and 70/25. Lipid exchange after 24 h incubation was analyzed by flow cytometry as described above. To suppress the potential influence of endocytotic uptake, cell culture experiments were carried out in the presence of 10 µM endocytosis inhibitor cytochalasin D.

The results shown in Figure 4A show slightly decreased exchange and thus more stable anchoring for C18 lipids at higher EPC3 content, while the exchange of the C16 lipid peaks at medium EPC3 content. The principle insight obtained here, though, is that the difference between C16 and C18 is highly significant at all ratios, and that C16 maintains similarly high lipid exchange rates even at increased EPC3 content.

In a similar experiment, we investigated the effect of phosphocholines with different dialkyl chain lengths. Correspondingly liposomes were prepared, which contained phosphocholine with chain lengths of C16, C18, or C20 instead of EPC3. Each formulation contained 5 mol-% C16 or C18 alkyne lipid. The results after 24 h incubation shown in Figure 4B suggest a slightly increased anchoring of our C18-hbPG-lipid in membranes containing long-chain phosphocholine, but this

visual impression is not statistically significant. Similarly, our C16-hbPG-lipid displays reduced lipid exchange in longer EPC chains, and this effect is highly significant. Throughout, the mobility of the C16 compound is clearly higher than that of the C18 compound.

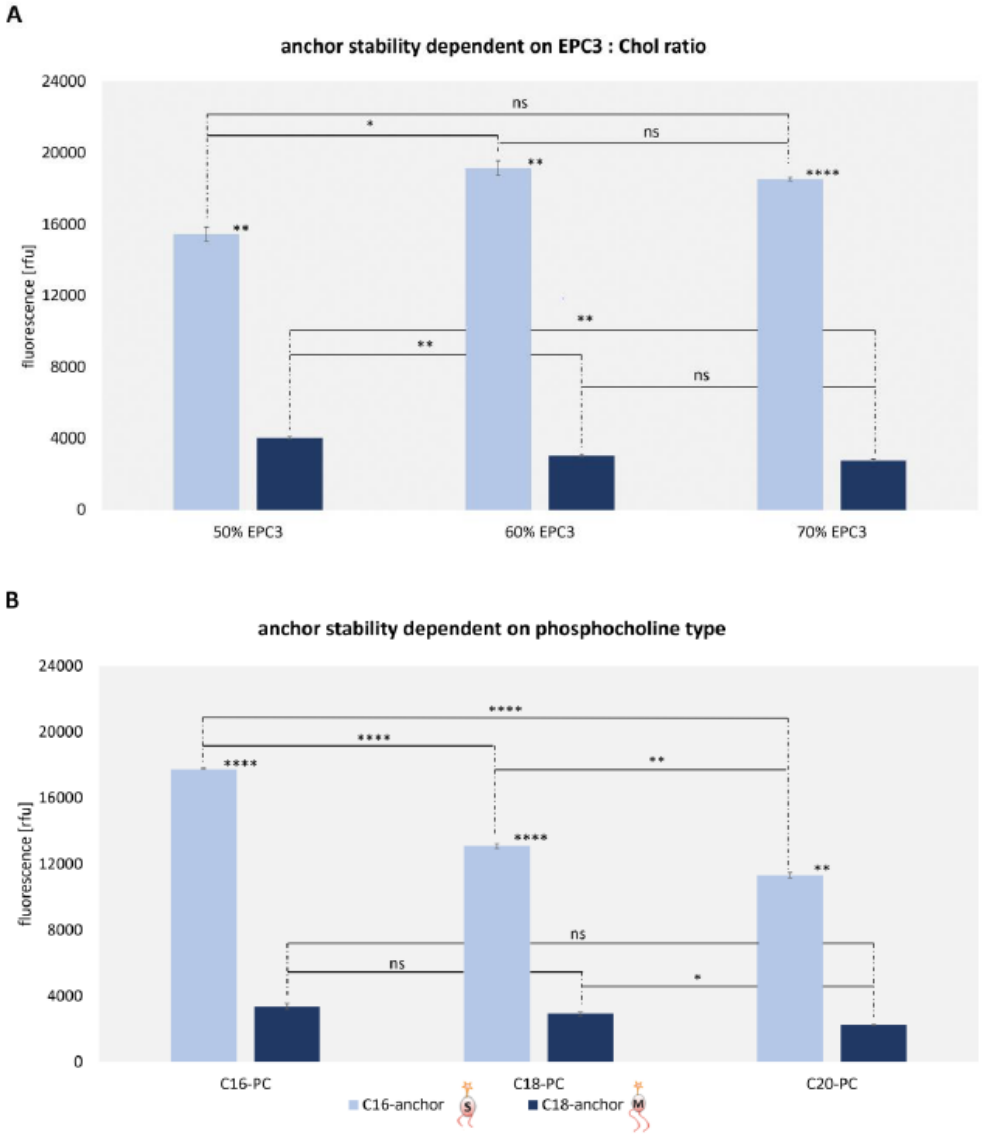

Figure 4. Quantification of lipid exchange depending on (**A**) the EPC3: Chol (cholesterol) ratio (**B**) and on the carbon atom number of phosphocholines used for liposome preparation. 1.0 × 10^5 UKRV Mel-15a cells were incubated with 5 vol-% atto 488 linked liposomes and cytochalasin D at 37 °C and fixed with a 4% formaldehyde solution before flow cytometric analysis. The significance between two values is illustrated by * p = 0.05–0.01, ** p < 0.001, **** p > 0.0001 and ns = no significance. The statistically significant was calculated using the Welch and Brown–Forsythe version of the one-way ANOVA test.

4. Discussion

In the present study, we showed results on the mobility of amphiphilic polyether lipids in liposomal membranes with respect to their propensity to insert into cell membranes in a time frame

of up to one day, which is a relevant time span for testing liposomal formulations in either in vitro or in vivo.

We used fast exchanging cholesterol derivatives as a positive control in the comparative analysis of a mini-series of homologous lipids containing dialkyl chains of increasing length [26]. The data firmly established that dialkyl anchors of any tested length are much more stably anchored in the liposomal membrane than cholesterol derivatives, extending previous observations to lipids as short as C16 [26]. This is plausible, given the irregular shape of cholesterol, yet interesting with respect to the behavior of biological lipids with chain lengths shorter than the classical C18. Of interest, the lipids forming the liposomal double-membrane consisted of nearly equal parts cholesterol, and phosphatidylcholine, the latter being structurally more similar to the dialkyl lipids. Although the lipid-dye conjugate used here to trace the lipid exchange contained a rather hydrophilic polyglycerol chain, which is likely to enhance its extraction from a membrane, our results support a view of "aging" liposomes, which may dramatically change their composition when exposed to a "lipid extraction equilibrium" as depicted in Figure 1B. This may give rise to disadvantages on multiple levels [43,44]. One such level is the structural integrity of the liposome, required to retain or release its therapeutic cargo in a reproducible fashion. Clearly, this important property may be subject to dramatic alterations, depending on the lipid extraction conditions in vivo, but also depending on the propensity of a given liposomal constituent compound for lipid exchange. While previous work identified cholesterol conjugates as problematic, our current data offer an approximation for the choice of non-steroid lipids capable of reducing the risk of undesired lipid exchange [26].

On another level, the molecular surface of liposomes, especially when decorated with targeting or stealth structures, is likely to suffer from lipid exchange. Here, too, our studies provide important results. In particular, we show that dialkyl lipids with 16C chains are more likely to escape from liposomal membranes than longer-chain lipids. This behavior may be important for the choice of dialkyl lipids as anchors for modifications, such as PEGylation or antibody conjugation, because the number of carbon atoms in dialkyl chains may have an influence on stability and half-life time of a modification in the application of liposomes as drug delivery systems. Particularly after intravenous application, liposomes encounter various moieties capable of lipid exchange, including cellular components of blood such as erythrocytes and thrombocytes, but also various protein–lipid particles involved in lipid transport such as HDLP, LDLP, and the like.

As a final comment, we would like to point out the striking fact that we detect increasing propensity for lipid exchange for lipids with alkyl chains just below the typical length encountered in many biomembranes, namely C18 (e.g., oleic acid, vaccenic acid or stearic acid) [45,46]. While ours is but a single data point of one lipid with C16 chains, it might be worth looking into this border in a more systematic fashion.

Supplementary Materials: The following are available online at www.mdpi.com/2073-4409/9/10/2213/s1, Scheme S1: Synthesis Route of the Dialkyl PEG-Lipids and Functionalization with propargyl bromide., Scheme S2: Synthesis Route of the Cholesterol-PEG-hbPEG Lipids and Functionalization with propargyl bromide.

Author Contributions: Conceptualization, M.H., H.F. and A.T.; methodology, J.S., M.H. and A.T.; validation, L.G., N.Z. and J.S.; synthesis E.B.; formal analysis, J.S., N.Z. and L.G. writing—original draft preparation, M.H.; writing—review and editing, J.S., L.G., H.F., M.H. and A.T.; visualization, J.S. and L.G.; supervision, M.H. and A.T.; project administration, J.S.; funding acquisition, M.H., H.F. and A.T. All authors have read and agreed to the published version of the manuscript.

Funding: This research was founded by German Research Foundation (CRC1066), Project A7 to MH and H.F. and Project B3 to AT, and by the Wilhelm-Sander Stiftung to A.T.

Acknowledgments: We thank the imaging core facility of Gregory Harms in the University Medical Center Mainz for providing the Leica TCS SP8 microscope and excellent technical advice. We also thank Anna-Maria Hofmann, Matthias Worm and Ann-Kathrin Danner, former members of the Frey Group, Johannes Gutenberg-University of Mainz, for the synthesis of lipids used in this study. Matthias Voigt, former member of the Helm group, is acknowledged for technical assistance in initial phases of this study.

Conflicts of Interest: The authors declare no conflict of interest.

References

1. Bangham, A.D.; Horne, R.W. Negative Staining of Phospholipids and Their Structural Modification by Surface-Active Agents as Observed in the Electron Microscope. *J. Mol. Biol.* **1964**, *8*, 660–668, doi:10.1016/S0022-2836(64)80115-7.
2. Allen, T.M.; Cullis, P.R. Liposomal Drug Delivery Systems: From Concept to Clinical Applications. *Adv. Drug Deliv. Rev.* **2013**, *65*, 36–48, doi:10.1016/j.addr.2012.09.037.
3. Florence, A. Targeted and Controlled Drug Delivery: Novel Carrier Systems. *Int. J. Pharm.* **2003**, *267*, 157, doi:10.1016/S0378-5173(03)00356-9.
4. Shashi, K.; Satinder, K.; Bharat, P. A Complete Review on: Liposomes. *Int. Res. J. Pharm.* **2012**, *3*, 10–16.
5. Weber, C.; Voigt, M.; Simon, J.; Danner, A.-K.; Frey, H.; Mailänder, V.; Helm, M.; Morsbach, S.; Landfester, K. Functionalization of Liposomes with Hydrophilic Polymers Results in Macrophage Uptake Independent of the Protein Corona. *Biomacromolecules* **2019**, *20*, 2989–2999, doi:10.1021/acs.biomac.9b00539.
6. Geusens, B.; Lambert, J.; De Smedt, S.C.; Buyens, K.; Sanders, N.N.; Van Gele, M. Ultradeformable Cationic Liposomes for Delivery of Small Interfering RNA (SiRNA) into Human Primary Melanocytes. *J. Control. Release* **2009**, *133*, 214–220, doi:10.1016/j.jconrel.2008.10.003.
7. Weissig, V.; Boddapati, S.V.; Cheng, S.-M.; D'souza, G.G.M. Liposomes and Liposome-like Vesicles for Drug and DNA Delivery to Mitochondria. *J. Liposome Res.* **2006**, *16*, 249–264, doi:10.1080/08982100600851169.
8. Lindner, L.H.; Eichhorn, M.E.; Eibl, H.; Teichert, N.; Schmitt-Sody, M.; Issels, R.D.; Dellian, M. Novel Temperature-Sensitive Liposomes with Prolonged Circulation Time. *Clin. Cancer Res.* **2004**, *10*, 2168–2178, doi:10.1158/1078-0432.CCR-03-0035.
9. Zimmermann, K.; Hossann, M.; Hirschberger, J.; Troedson, K.; Peller, M.; Schneider, M.; Brühschwein, A.; Meyer-Lindenberg, A.; Wess, G.; Wergin, M.; et al. A Pilot Trial of Doxorubicin Containing Phosphatidyldiglycerol Based Thermosensitive Liposomes in Spontaneous Feline Soft Tissue Sarcoma. *Int. J. Hyperth.* **2017**, *33*, 178–190, doi:10.1080/02656736.2016.1230233.
10. Parmentier, J.; Hofhaus, G.; Thomas, S.; Cuesta, L.C.; Gropp, F.; Schröder, R.; Hartmann, K.; Fricker, G. Improved Oral Bioavailability of Human Growth Hormone by a Combination of Liposomes Containing Bio-Enhancers and Tetraether Lipids and Omeprazole. *J. Pharm. Sci.* **2014**, *103*, 3985–3993, doi:10.1002/jps.24215.
11. Briuglia, M.-L.; Rotella, C.; McFarlane, A.; Lamprou, D.A. Influence of Cholesterol on Liposome Stability and on in Vitro Drug Release. *Drug Deliv. Transl. Res.* **2015**, *5*, 231–242, doi:10.1007/s13346-015-0220-8.
12. Vemuri, S.; Rhodes, C.T. Preparation and Characterization of Liposomes as Therapeutic Delivery Systems: A Review. *Pharm. Acta Helv.* **1995**, *70*, 95–111, doi:10.1016/0031-6865(95)00010-7.
13. Kirby, C.; Clarke, J.; Gregoriadis, G. Effect of the cholesterol content of small unilamellar liposomes on their stability in vivo and in vitro. *Biochem. J.* **1980**, *186*, 591–598, doi:10.1042/bj1860591.
14. Awad, N.; Paul, V.; Mahmoud, M.; Sawaftah, N.; Kawak, P.; Al-Sayah, M.; Husseini, G. The Effect of Pegylation and Targeting Moieties on the Ultrasound-Mediated Drug Release from Liposomes. *ACS Biomater. Sci. Eng.* **2019**, doi:10.1021/acsbiomaterials.8b01301.
15. Drummond, D.C.; Meyer, O.; Hong, K.; Kirpotin, D.B.; Papahadjopoulos, D. Optimizing Liposomes for Delivery of Chemotherapeutic Agents to Solid Tumors. *Pharmacol. Rev.* **1999**, *51*, 691–743.
16. Moghimipour, E.; Rezaei, M.; Ramezani, Z.; Kouchak, M.; Amini, M.; Angali, K.A.; Dorkoosh, F.A.; Handali, S. Folic Acid-Modified Liposomal Drug Delivery Strategy for Tumor Targeting of 5-Fluorouracil. *Eur. J. Pharm. Sci.* **2018**, *114*, 166–174, doi:10.1016/j.ejps.2017.12.011.
17. Lu, R.; Zhou, L.; Yue, Q.; Liu, Q.; Cai, X.; Xiao, W.; Hai, L.; Guo, L.; Wu, Y. Liposomes Modified with Double-Branched Biotin: A Novel and Effective Way to Promote Breast Cancer Targeting. *Bioorg. Med. Chem.* **2019**, *27*, 3115–3127, doi:10.1016/j.bmc.2019.05.039.
18. Wu, H.-C.; Chang, D.-K. Peptide-Mediated Liposomal Drug Delivery System Targeting Tumor Blood Vessels in Anticancer Therapy. *J. Oncol.* **2010**, *2010*, 723798, doi:10.1155/2010/723798.
19. Heath, T.D.; Fraley, R.T.; Papahdjopoulos, D. Antibody targeting of liposomes: Cell specificity obtained by conjugation of F (ab') 2 to vesicle surface. *Science* **1980**, *210*, 539–541, doi:10.1126/science.7423203.
20. Bendas, G.; Krause, A.; Bakowsky, U.; Vogel, J.; Rothe, U. Targetability of Novel Immunoliposomes Prepared by a New Antibody Conjugation Technique. *Int. J. Pharm.* **1999**, *181*, 79–93, doi:10.1016/s0378-5173(99)00002-2.

21. Hofmann, A.M.; Wurm, F.; Hühn, E.; Nawroth, T.; Langguth, P.; Frey, H. Hyperbranched Polyglycerol-Based Lipids via Oxyanionic Polymerization: Toward Multifunctional Stealth Liposomes. *Biomacromolecules* **2010**, *11*, 568–574, doi:10.1021/bm901123j.
22. Mohr, K.; Müller, S.S.; Müller, L.K.; Rusitzka, K.; Gietzen, S.; Frey, H.; Schmidt, M. Evaluation of Multifunctional Liposomes in Human Blood Serum by Light Scattering. *Langmuir* **2014**, *30*, 14954–14962, doi:10.1021/la502926e.
23. Wagener, K.; Worm, M.; Pektor, S.; Schinnerer, M.; Thiermann, R.; Miederer, M.; Frey, H.; Rösch, F. Comparison of Linear and Hyperbranched Polyether Lipids for Liposome Shielding by (18)F-Radiolabeling and Positron Emission Tomography. *Biomacromolecules* **2018**, *19*, 2506–2516, doi:10.1021/acs.biomac.8b00115.
24. Cooper, R.A. Influence of Increased Membrane Cholesterol on Membrane Fluidity and Cell Function in Human Red Blood Cells. *J. Supramol. Struct.* **1978**, *8*, 413–430, doi:10.1002/jss.400080404.
25. Feingold, K.R.; Grunfeld, C. *Introduction to Lipids and Lipoproteins*; Feingold, K.R., Anawalt, B., Boyce, A., Chrousos, G., Dungan, K., Grossman, A., Hershman, J.M., Kaltsas, G., Koch, C., Kopp, P., et al., Eds.; South Dartmouth: Dartmouth, MA, USA, 2000.
26. Fritz, T.; Voigt, M.; Worm, M.; Negwer, I.; Müller, S.S.; Kettenbach, K.; Ross, T.L.; Roesch, F.; Koynov, K.; Frey, H.; et al. Orthogonal Click Conjugation to the Liposomal Surface Reveals the Stability of the Lipid Anchorage as Crucial for Targeting. *Chem. A Eur. J.* **2016**, *22*, 11578–11582, doi:10.1002/chem.201602758.
27. Mohammed, A.R.; Weston, N.; Coombes, A.G.A.; Fitzgerald, M.; Perrie, Y. Liposome Formulation of Poorly Water Soluble Drugs: Optimisation of Drug Loading and ESEM Analysis of Stability. *Int. J. Pharm.* **2004**, *285*, 23–34, doi:10.1016/j.ijpharm.2004.07.010.
28. Nogueira, E.; Gomes, A.C.; Preto, A.; Cavaco-Paulo, A. Design of Liposomal Formulations for Cell Targeting. *Coll. Surf. B Biointerfaces* **2015**, *136*, 514–526, doi:10.1016/j.colsurfb.2015.09.034.
29. Stauch, O.; Uhlmann, T.; Fröhlich, M.; Thomann, R.; El-Badry, M.; Kim, Y.-K.; Schubert, R. Mimicking a Cytoskeleton by Coupling Poly(N-Isopropylacrylamide) to the Inner Leaflet of Liposomal Membranes: Effects of Photopolymerization on Vesicle Shape and Polymer Architecture. *Biomacromolecules* **2002**, *3*, 324–332, doi:10.1021/bm015613y.
30. Herzberger, J.; Niederer, K.; Pohlit, H.; Seiwert, J.; Worm, M.; Wurm, F.R.; Frey, H. Polymerization of Ethylene Oxide, Propylene Oxide, and Other Alkylene Oxides: Synthesis, Novel Polymer Architectures, and Bioconjugation. *Chem. Rev.* **2016**, *116*, 2170–2243, doi:10.1021/acs.chemrev.5b00441.
31. Reibel, A.T.; Müller, S.S.; Pektor, S.; Bausbacher, N.; Miederer, M.; Frey, H.; Rösch, F. Fate of Linear and Branched Polyether-Lipids In Vivo in Comparison to Their Liposomal Formulations by 18F-Radiolabeling and Positron Emission Tomography. *Biomacromolecules* **2015**, *16*, 842–851, doi:10.1021/bm5017332.
32. Wagener, K.; Bros, M.; Krumb, M.; Langhanki, J.; Pektor, S.; Worm, M.; Schinnerer, M.; Montermann, E.; Miederer, M.; Frey, H.; et al. Targeting of Immune Cells with Trimannosylated Liposomes. *Adv. Ther.* **2020**, *3*, 1900185, doi:10.1002/adtp.201900185.
33. Sawant, R.; Torchilin, V. Challenges in Development of Targeted Liposomal Therapeutics. *AAPS J.* **2012**, *14*, 303–315, doi:10.1208/s12248-012-9330-0.
34. Kainthan, R.K.; Janzen, J.; Levin, E.; Devine, D.V.; Brooks, D.E. Biocompatibility Testing of Branched and Linear Polyglycidol. *Biomacromolecules* **2006**, *7*, 703–709, doi:10.1021/bm0504882.
35. Hofmann, A.M.; Wurm, F.; Frey, H. Rapid Access to Polyfunctional Lipids with Complex Architecture via Oxyanionic Ring-Opening Polymerization. *Macromolecules* **2011**, *44*, 4648–4657, doi:10.1021/ma200367c.
36. Fujimoto, L.M.; Roth, R.; Heuser, J.E.; Schmid, S.L. Actin Assembly Plays a Variable, but Not Obligatory Role in Receptor-Mediated Endocytosis. *Traffic* **2000**, *1*, 161–171, doi:10.1034/j.1600-0854.2000.010208.x.
37. Ribes, S.; Ebert, S.; Regen, T.; Agarwal, A.; Tauber, S.C.; Czesnik, D.; Spreer, A.; Bunkowski, S.; Eiffert, H.; Hanisch, U.-K.; et al. Toll-like receptor stimulation enhances phagocytosis and intracellular killing of nonencapsulated and encapsulated Streptococcus pneumoniae by murine microglia. *Infect. Immun.* **2010**, *78*, 865–871, doi:10.1128/IAI.01110-09.
38. Dutta, D.; Donaldson, J.G. Search for Inhibitors of Endocytosis. *Cell. Logist.* **2012**, *2*, 203–208, doi:10.4161/cl.23967.
39. Kotecha, N.; Krutzik, P.O.; Irish, J.M. Web-Based Analysis and Publication of Flow Cytometry Experiments. *Curr. Protoc. Cytom.* **2010**, *53*, 10.17.1–10.17.24, doi:10.1002/0471142956.cy1017s53.

40. Schindelin, J.; Arganda-Carreras, I.; Frise, E.; Kaynig, V.; Longair, M.; Pietzsch, T.; Preibisch, S.; Rueden, C.; Saalfeld, S.; Schmid, B.; et al. Fiji: An Open-Source Platform for Biological-Image Analysis. *Nat. Methods* **2012**, *9*, 676–682, doi:10.1038/nmeth.2019.
41. Kolb, H.C.; Finn, M.G.; Sharpless, K.B. Click Chemistry: Diverse Chemical Function from a Few Good Reactions. *Angew. Chemie Int. Ed.* **2001**, *40*, 2004–2021, doi:10.1002/1521-3773(20010601)40:11<2004::AID-ANIE2004>3.0.CO;2-5.
42. Massing, U.; Ingebrigtsen, S.G.; Škalko-Basnet, N.; Holsæter, A.M. Dual Centrifugation—A Novel "in-Vial" Liposome Processing Technique. *Liposomes* **2017**, doi:10.5772/intechopen.68523.
43. Huang, Z.; Jaafari, M.R.; Szoka, F.C., Jr. Disterolphospholipids: Nonexchangeable Lipids and Their Application to Liposomal Drug Delivery. *Angew. Chemie Int. Ed.* **2009**, *48*, 4146–4149, doi:doi:10.1002/anie.200900111.
44. Phillips, M.C.; Johnson, W.J.; Rothblat, G.H. Mechanisms and Consequences of Cellular Cholesterol Exchange and Transfer. *Biochim. Biophys. Acta Rev. Biomembr.* **1987**, *906*, 223–276, doi:10.1016/0304-4157(87)90013-X.
45. Schumann, J.; Leichtle, A.; Thiery, J.; Fuhrmann, H. Fatty Acid and Peptide Profiles in Plasma Membrane and Membrane Rafts of PUFA Supplemented RAW264.7 Macrophages. *PLoS ONE* **2011**, *6*, e24066, doi:10.1371/journal.pone.0024066.
46. Abbott, S.K.; Else, P.L.; Atkins, T.A.; Hulbert, A.J. Fatty Acid Composition of Membrane Bilayers: Importance of Diet Polyunsaturated Fat Balance. *Biochim. Biophys. Acta Biomembr.* **2012**, *1818*, 1309–1317, doi:10.1016/j.bbamem.2012.01.011.

cells

MDPI

Supplementary Material

S1. Materials and Methods

S1.1. Reagents

Unless mentioned otherwise, all chemicals were obtained from *Sigma Aldrich*, *Acros Organics*, *Fisher Scientific* or *TCI Europe*. Deuterated solvents (pyridine-*d5*, benzene-*d6* or chloroform-*d*) were purchased from *Deutero GmbH*. Ethylene oxide (EO) was received from *Sigma Aldrich* and must be handled with high precaution. Ethoxyethyl glycidyl ether (EEGE) was synthesized according to literature[1] and was dried over CaH_2 for at least 30 min. Subsequently it was freshly cryo-transferred prior to use. For the anionic ring-opening polymerization (AROP) dry THF was stored over benzophenone/sodium.

S1.2. Instrumentation

^1H, ^{13}C NMR and 2D spectra were measured on a Bruker Avance III HD 300 (300 MHz, 5 mm, BBFO probe, and B-ACS 60 auto sampler) or rather a Bruker Avance II spectrometer operated at 400 MHz (5 mm BBFO smart probe and SampleXPress 60 auto sampler) at 296 K. Pyridine-*d5*, benzene-*d6* , chloroform-*d* or DMSO-*d6* was used as a solvent. The NMR spectra were referenced internally to the respective signals of the deuterated solvent. Analysis of all spectra was carried out using the software MestReNova version 9.0.

S1.3. Handling of Ethylene Oxide (EO)

The gaseous, flammable and highly toxic ethylene oxide (EO) must be handled carefully and has to be stored in pressure-proof gas bottles. It must be used only in an adequate fume hood under appropriate safety precautions. Polymerizations in which EO is involved are performed in flame-dried glassware to enable the conversion of EO inside the sealed and evacuated glass apparatus and to guarantee secure handling via cryo-transfer techniques. To avoid abrupt detachment of the septum and hence release of EO the maximum batch-sizes of 8 g EO in a 500 mL flask must not be exceeded.

S2. Synthesis

S2.1. Synthesis of Ethoxyethyl Glycidyl Ether (EEGE)

EEGE was synthesized as described in literature.[1]

^1H NMR, COSY (300 MHz, chloroform-*d*, δ): 4.75–4.68 (qd, *J* = 5.3 Hz; 3.4 Hz, 1H, acetal H), 3.86–3.29 (m, 4H, -CHC*H*$_2$OCOCH$_2$-, -CHCH$_2$OCOC*H*$_2$-) 3.13–3.07 (m, 1H, CH$_2$OC*H*CH$_2$-), 2.77–2.74 (ddd, *J* = 5.1 Hz; 4.1 Hz; 1.0 Hz, 1H, C*H*$_2$OCHCH$_2$-), 2.61–2.55 (ddd, *J* = 10.7 Hz; 5.1 Hz; 2.7 Hz, 1H, C*H*$_2$OCHCH$_2$-), 1.29–1.26 (dd, *J* = 5.4 Hz; 4.7 Hz, 3H, -OCHC*H*$_3$), 1.18–1.13 (td, *J* = 7.1 Hz; 0.9 Hz, 3H, -OCH$_2$C*H*$_3$).

S2.2. Synthesis of 1,2-Bis-N-Octadecyl Glyceryl Ether (BisOD)

The synthesis was carried out according to literature.[2]

^1H NMR, COSY (400 MHz, chloroform-*d*, δ): 3.74–3.41 (m, 9H, glycerol H), 1.59–1.53 (m, 4H, -OCH$_2$C*H*$_2$-), 1.31–1.25 (m, 60H, -OCH$_2$CH$_2$(C*H*$_2$)$_{15}$CH$_3$), 0.88 (t, *J* = 13.1 Hz; 7.2 Hz, 6H; -O(CH$_2$)$_{17}$C*H*$_3$).

^{13}C NMR, HSQC, HMBC (101 MHz, chloroform-*d*, δ): 78.4 (glycerol C), 72.0 (-OCH$_2$CH$_2$-), 71.1 (glycerol C), 70.6 (-OCH$_2$CH$_2$-), 63.3 (glycerol C), 32.1 (-OCH$_2$CH$_2$(CH$_2$)$_{17}$CH$_3$), 30.3 (-OCH$_2$*C*H$_2$-), 29.9–29.5 (-OCH$_2$CH$_2$(*C*H$_2$)$_{17}$CH$_3$), 26.3 (-OCH$_2$CH$_2$(*C*H$_2$)$_{17}$CH$_3$), 22.9

(-$OCH_2CH_2(CH_2)_{17}CH_3$), 14.3 (-$O(CH_2)_{19}CH_3$).

S2.3. Polymer Synthesis of BisOD-PEG

The synthesis is described for BisOD-PEG81 as a representative example.

1,2-Bis-*n*-octadecyl glyceryl ether (BisOD) (0.2 g, 0.36 mmol, 1 eq.) was placed in a dry Schlenk flask and dissolved in benzene (10 mL). The solution was stirred at 60 °C for 30 min and dried in vacuo for 16 h to remove moisture. Dry tetrahydrofuran (approx. 10 mL) was cryo-transferred to the Schlenk flask to dissolve the initiator. Afterwards, the initiator was deprotonated with a 0.5 M solution of potassium naphthalenide in THF (0.36 mL, 0.18 mmol, 0.5 eq.) while stirring. The solution was cooled down to –80 °C and ethylene oxide (EO) (1.70 mL, 37.57 mmol, 105 eq.) was cryo-transferred using a graduated ampule. The polymerization was carried out at 60 °C for 24 h. In order to quench the polymerization, an excess of ethanol was added. The solvent was removed under reduced pressure, the crude product was dissolved in methanol and precipitated twice in cold diethyl ether to obtain the pure product. Yield: 99%.

^{1}H NMR, **COSY** (400 MHz, benzene-*d6*, δ): 3.67–3.30 (m, 359H, polyether backbone and glycerol H), 1.66–1.56 (m, 4H, -OCH_2CH_2-), 1.44–1.28 (m, 58H, -$OCH_2CH_2(CH_2)_{15}CH_3$), 0.92–0.89 (m, 6H, -$O(CH_2)_{17}CH_3$).

^{13}C NMR, **HSQC**, **HMBC** (101 MHz, benzene-*d6*, δ): 79.0 (glycerol C), 73.4 (polyether backbone and glycerol C), 72.4-70.9 (polyether backbone and glycerol C), 62.2 (polyether backbone and glycerol C), 32.6 (-$OCH_2CH_2(CH_2)_{14}CH_2CH_3$), 31.1–30.1 (-$OCH_2CH_2$- and -$OCH_2CH_2$ $(CH_2)_{14}CH_2CH_3$), 27.0 (-$OCH_2CH_2(CH_2)_{14}CH_2CH_3$), 23.4 (-$OCH_2CH_2(CH_2)_{14}CH_2CH_3$), 14.64 (-$O(CH_2)_{17}CH_3$).

S2.4. Functionalization of BisOD-PEG with Propargyl Bromide

The functionalization is described for BisOD-PEG81-alkyne as a representative example.

BisOD-PEG81 (0.3 g, 0.074 mmol, 1 eq.) was placed in a dry Schlenk flask and dissolved in dry THF. The solution was cooled to 0 °C and sodium hydride (0.005 g, 0.223 mmol, 3 eq.) was added while stirring. Subsequently, propargyl bromide (0.020 mL, 0.223 mmol, 3 eq.) was added and the solution was stirred for 24 h at room temperature. The reaction mixture was filtered and the solvent was slightly reduced under reduced pressure. The remaining solution was precipitated twice in cold diethyl ether and the pure product was dried in vacuo. Yield: 66%.

^{1}H NMR, **COSY** (300 MHz, benzene-*d6*, δ): 3.95–3.94 (d, *J* = 2.4 Hz, 2H, -OCH_2CCH), 3.77–3.24 (m, 374H, polyether backbone and glycerol H), 2.13–2.12 (t, *J* = 2.4 Hz, 1H, -OCH_2CCH), 1.69–1.57 (m, 12H, -OCH_2CH_2-), 1.47–1.30 (m, 60H, -$OCH_2CH_2(CH_2)_{15}CH_3$), 0.94–0.90 (m, 6H, -$O(CH_2)_{17}CH_3$).

S2.5. Synthesis of 1,2-Bis-N-Octadecyl Glyceryl Ether (BisHD)

The synthesis was carried out according to literature.[2]

^{1}H NMR, **COSY** (400 MHz, chloroform-*d*, δ): 3.78–3.36 (m, 9H, glycerol H), 1.63–1.49 (m, 4H, -OCH_2CH_2-), 1.40–1.17 (m, 52H, -$OCH_2CH_2(CH_2)_{13}CH_3$), 0.88 (t, *J* = 13.1 Hz; 7.2 Hz, 6H; -$O(CH_2)_{17}CH_3$).

S2.6. Synthesis of 1,2-Bis-N-Icosanyl Glyceryl Ether (BisID)

The synthesis was carried out according to literature.[3]

Dry tetrahydrofuran (THF) was placed in three-necked round bottom flask equipped with Dimroth condenser and sealed precision glass (KPG) stirrer. Under argon atmosphere and stirring 3-benzyloxy-1,2-propanediol (2.7 mL, 0.017 mol, 1 eq.), sodium hydride (1.62 g, 0.068 mol, 4 eq.) and 1-bromoicosane (24.42 g, 0.068 mol, 4 eq.) was added. The reaction mixture was stirred at 80 °C for 9 days. Additional NaH was added (1.00 g, 0.042 mol, 2.5 eq) and the solution was stirred for another 23 days. The solvent was removed under reduced pressure to obtain a total volume of 250 mL. Water

(250 mL) and diethyl ether (250 mL) was added and the mixture was stirred overnight at room temperature. To neutralize the reaction mixture, sulfuric acid (1 mol·L^{-1}, 15 mL, 0.015 mol) was added and again stirred overnight. The organic phase was extracted three times with diethyl ether (150 mL each) and dried over sodium sulfate. The solvent was removed under reduced pressure and the crude product was purified using flash column chromatography (petroleum ether/diethyl ether 40:1). The intermediate 1,2-bis-*n*-icosanyl-3-benzyl glyceryl ether (4.97 g, 0.007 mol) was obtained as colorless solid. Yield: 41%.

1,2-Bis-*n*-icosanyl-3-benzyl glyceryl ether (4.97 g, 0.007 mol, 1 eq.) was dissolved in dichloromethane. Palladium on activated charcoal was added (5 weight percent). Hydrogen was introduced and the mixture was stirred at room temperature for 20 days. The catalyst was removed via filtration over celite®. Afterwards the solvent was removed under reduced pressure to obtain 1,2-bis-*n*-icosanyl glyceryl ether (1.84 g, 0.003 mol) as colorless solid. Yield: 42%.

^{1}H NMR, COSY (400 MHz, chloroform-*d*, δ): 3.74–3.41 (m, 9H, glycerol H), 1.60–1.52 (m, 4H, -OCH_2CH_2-), 1.34–1.21 (m, 68H, -$OCH_2CH_2(CH_2)_{17}CH_3$), 0.89–0.86 (m, 6H, -$O(CH_2)_{19}CH_3$).

^{13}C NMR, HSQC, HMBC (101 MHz, chloroform-*d*, δ): 78.4 (glycerol C), 72.0 (-OCH_2CH_2-), 71.1 (glycerol C), 70.6 (-OCH_2CH_2-), 63.25 (glycerol C), 32.1 (-$OCH_2CH_2(CH_2)_{17}CH_3$), 30.2 (-OCH_2CH_2-), 29.9–29.5 (-$OCH_2CH_2(CH_2)_{17}CH_3$), 26.3 (-$OCH_2CH_2(CH_2)_{17}CH_3$), 22.9 (-$OCH_2CH_2(CH_2)_{17}CH_3$), 14.3 (-$O(CH_2)_{19}CH_3$).

S2.7. Polymer Synthesis of BisID-PEG

The synthesis is described for BisID-PEG_{62} as a representative example.

1,2-Bis-*n*-icosanyl glyceryl ether (BisID) (0.2 g, 0.307 mmol, 1 eq.) was placed in a dry Schlenk flask and dissolved in benzene (10 mL). The solution was stirred at 60 °C for at least 30 min and dried in vacuo for 16 h to remove moisture. Dry tetrahydrofuran (approx. 10 mL) was cryo-transferred to the Schlenk flask to dissolve the initiator. Afterwards, the solution was stirred and the initiator was deprotonated with a 0.5 M solution of potassium naphthalenide in THF (0.31 mL, 0.153 mmol, 0.5 eq.). The solution was cooled down to –90 °C and ethylene oxide (EO) (0.95 mL, 20.919 mmol, 68 eq.) was cryo-transferred using a graduated ampule. The polymerization was carried out at 60 °C for 24 h. Subsequently, the reaction mixture was heated to 80 °C for 16 h. To quench the polymerization, an excess of ethanol was added and the solvent was removed under reduced pressure. The crude product was dissolved in methanol and precipitated three times in cold diethyl ether to obtain the pure product. Yield: 95%.

^{1}H NMR, COSY (400 MHz, benzene-*d6*, δ): 3.73–3.31 (m, 256H, polyether backbone and glycerol H), 1.67–1.58 (m, 4H, -OCH_2CH_2-), 1.45–1.27 (m, 70H, -$OCH_2CH_2(CH_2)_{15}CH_3$), 0.93–0.89 (m, 6H, -$O(CH_2)_{19}CH_3$).

^{13}C NMR, HSQC, HMBC (101 MHz, benzene-*d6*, δ): 79.0 (glycerol C), 73.4 (polyether backbone and glycerol C), 72.4–70.8 (polyether backbone and glycerol C), 62.1 (polyether backbone and glycerol C), 32.6 (-$OCH_2CH_2(CH_2)_{16}CH_2CH_3$), 31.1–30.1 (-$OCH_2CH_2$- and -$OCH_2CH_2(CH_2)_{16}CH_2CH_3$ (BisID)), 27.0 (-$OCH_2CH_2(CH_2)_{16}CH_2CH_3$ (BisID)), 23.4 (-$OCH_2CH_2(CH_2)_{16}CH_2CH_3$ (BisID)), 14.6 (-$O(CH_2)_{19}CH_3$ (BisID)).

S2.8. Functionalization of BisID-PEG with Propargyl Bromide

The functionalization is described for BisID-PEG_{62}-alkyne as a representative example.

BisID-PEG_{62} (0.2 g, 0.059 mmol, 1 eq.) was placed in a Schlenk flask and dissolved in dry THF (10 mL). The solution was cooled to 0 °C and sodium hydride (0.004 g, 0.178 mmol, 3 eq.) was added. Afterwards, propargyl bromide (0.016 mL, 0.178 mmol, 3 eq.) was added, and the solution was stirred for 24 h at room temperature. The reaction mixture was filtered, and the solvent was reduced under reduced pressure. The remaining solution was precipitated twice in cold diethyl ether and the pure product was dried in vacuo. Yield: 61%.

^{1}H NMR, COSY (300 MHz, benzene-*d6*, δ): 3.95–3.94 (d, *J* = 2.4 Hz, 2H, -OC*H*$_2$CCH), 3.77–3.24 (m, 245H, polyether backbone and glycerol H), 2.12–2.11 (t, *J* = 2.4 Hz, 1H, -OCH$_2$CC*H*), 1.69–1.57 (m, 4H, -OCH$_2$C*H*$_2$-), 1.49–1.28 (m, 67H, -OCH$_2$CH$_2$(C*H*$_2$)$_{15}$CH$_3$), 0.94–0.90 (m, 6H, -O(CH$_2$)$_{17}$C*H*$_3$).

Scheme S1: Synthesis Route of the Dialkyl PEG-Lipids and Functionalization with propargyl bromide.

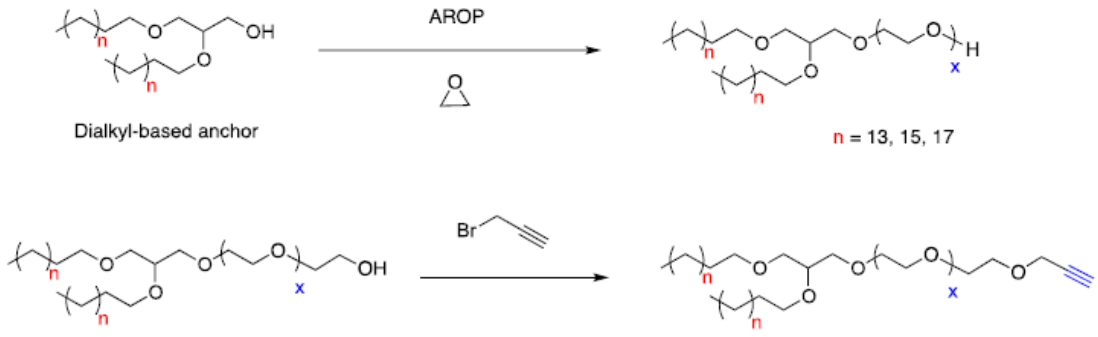

S2.9. Polymer Synthesis of Cholesterol-PEG-PEEGE

The synthesis protocol was described in previous reports.[3]

^{1}H NMR, COSY (300 MHz, DMSO-*d6*, δ): = 5.30 (C=CH cholesterol), 4.63 (br, CHO acetal), 3.72–3.21 (polyether backbone; CHO cholesterol), 2.28–0.82 (br, CH_2, CH cholesterol), 1.18–1.06 (br, CH_3 acetal), 0.64 (br, CH_3 cholesterol).

S2.10. Polymer Synthesis of Cholesterol-PEG-linPG

The synthesis protocol was described in previous reports.[3]

^{1}H NMR, COSY (300 MHz, DMSO-*d6*, δ): = 5.30 (C=CH cholesterol), 4.24 (br, OH), 3.72–3.21 (polyether backbone; CHO cholesterol), 2.28–0.82 (br, CH_2, CH cholesterol), 0.64 (br, CH_3 cholesterol).

S2.11. Polymer Synthesis of Cholesterol-PEG-hbPG

The synthesis protocol was described in previous reports.[3]

^{1}H NMR, COSY (300 MHz, DMSO-*d6*, δ): = 5.30 (C=CH cholesterol), 4.77–4.43 (br, OH, different signals due to hyperbranched PG), 3.76–3.22 (polyether backbone; CHO cholesterol), 2.28–0.82 (br, CH_2, CH cholesterol), 0.64 (br, CH_3 cholesterol).

S2.12. Functionalization of Cholesterol-PEG-hbPG with Propargyl Bromide

The synthesis protocol was described in previous reports.[3]

^{1}H NMR, COSY (300 MHz, DMSO-*d6*, δ): = 5.30 (C=CH cholesterol), 4.77–4.43 (br, OH, different signals due to hyperbranched PG), 4.31–4.17 (OCH$_2$C≡CH), 3.76–3.22 (polyether backbone; CHO cholesterol), 2.45 (C≡CH), 2.28–0.82 (br, CH_2, CH cholesterol), 0.63 (br, CH_3 cholesterol).

Scheme S2: Synthesis Route of the Cholesterol-PEG-hbPEG Lipids and Functionalization with propargyl bromide.

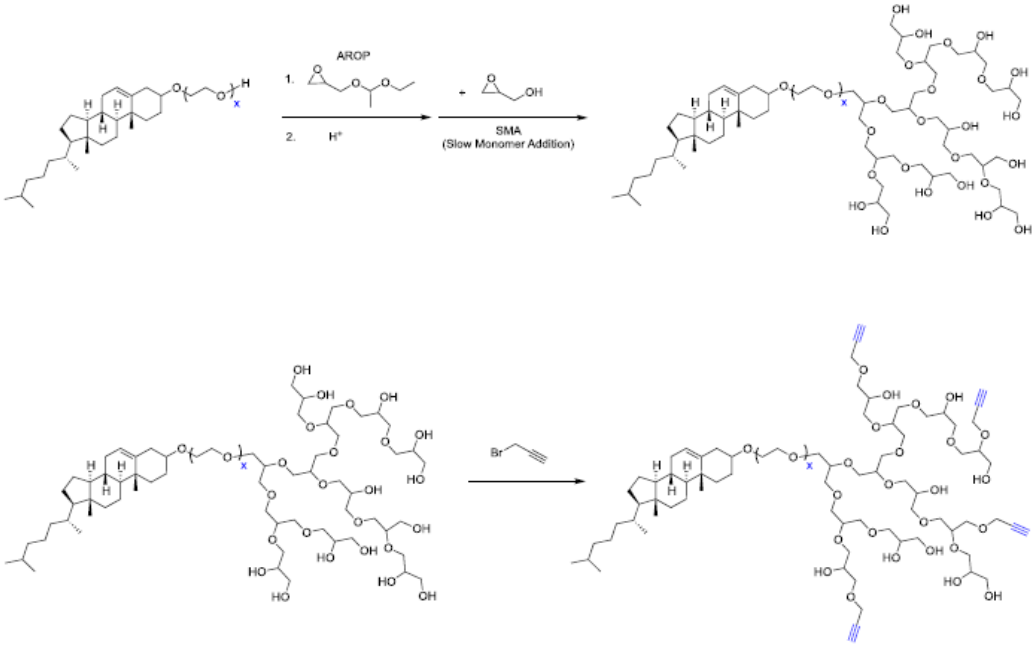

References

1. Fitton, A. O.; Hill, J.; Jane, D. E.; Millar, R. Synthesis of Simple Oxetanes Carrying Reactive 2-Substituents. *Synthesis* **1987**, 1140–1142, doi:10.1055/s-1987-28203.
2. Stauch, O.; Uhlmann, T.; Fröhlich, M.; Thomann, R.; El-Badry, M.; Kim, Y.-K.; Schubert, R. Mimicking a Cytoskeleton by Coupling Poly(*N*-isopropylacrylamide) to the Inner Leaflet of Liposomal Membranes: Effects of Photopolymerization on Vesicle Shape and Polymer Architecture. *Biomacromolecules* **2002**, *3*, 324–332, doi:10.1021/bm015613y.
3. Hofmann, A. M.; Wurm, F.; Frey, H. Rapid Acess to Polyfunctional Lipids with Complex Architecture via Oxyanionic Ring-Opening Polymerization. *Macromolecules* **2011**, *44*, 4648–4657, doi:10.1021/ma200367c.

6 Curriculum Vitea

Curriculum Vitae

Eyleen Becker

Kaiser-Karl-Ring 2, 55118 Mainz

Eyleen@gmx.net

Geburtsdatum:	09. April 1991
Geburtsort:	Landau/Pfalz
Nationalität:	Deutsch

Ausbildung

Seit 08/2017 **Promotion, Johannes Gutenberg-Universität Mainz**

Department Chemie, Betreuung von Prof. Dr. Holger Frey

Thema: „Linear and Hyperbranched Polyether-based Polymers as Nanocarriers for Drug Delivery“

09/2016 – 06/2017 **Diplomarbeit, Johannes Gutenberg-Universität Mainz**

Department Chemie, Betreuung von Prof. Dr. Holger Frey

Thema: „Synthese und Charakterisierung von pH- und redox-responsiven, amphiphilen Polyethern“

04/2010 – 06/2017 **Studium der Chemie, Johannes Gutenberg-Universität Mainz**

Abschluss: Diplom-Chemikerin

08/2001 – 03/2010 **Schulausbildung, Eduard-Spranger-Gymnasium Landau/Pfalz**

Abschluss: Abitur

Fortbildungen

06/2019	Sommerschule der Sonderforschungsbereiche 1066 und 1278 „Nanomedicine: Formulation, Characterization, Translation“, Fulda
12/2018	APV Academia Seminar „How to orientate for starting an industrial career“ Evonik Nutrition & Health Care GmbH, Darmstadt Kursleitung: Prof. Dr. Jörg Breitkreutz
07/2018	Sommerschule des Sonderforschungsbereichs 1066 „Nanodimensional Polymer Therapeutics for Tumor Therapy“, Bad Kreuznach
05/2018	Geprüfter Projektmanager Wirtschaftschemie GDCh, Münster Kursleitung: Prof. Dr. Jens Leker
03/2018	Grundlagen der guten Herstellungspraxis (GMP), Mainz Kursleitung: Prof. Dr. Michael Hildebrand

Praxiserfahrungen

04/2018 – 01/2020	Wissenschaftlicher Assistent für Organische Chemie und Polymerchemie Johannes Gutenberg-Universität Mainz Betreuung von Bachelorstudenten und Studenten im organisch-chemischen Grundpraktikum
03/2018 – 05/2018	Wissenschaftlicher Assistent für das Praktikum „Biopolymere und medizinisch relevante Polymere“ Johannes Gutenberg-Universität Mainz

10/2016 – 02/2017	Übungsleiter der Vorlesung „Biopolymere“ Johannes Gutenberg-Universität Mainz Kursleitung: Prof. Dr. Holger Frey, Prof. Dr. Volker Mailänder
06/2015 – 11/2015	Hilfswissenschaftler für das Praktikum „Chemie für Biologen“ Johannes Gutenberg-Universität Mainz Kursleitung: Dr. Manfred Müller

Qualifikationen

Sprachen	Deutsch:	Muttersprache
	Englisch:	Sehr gut in Wort und Schrift
	Französisch:	Grundkenntnisse
EDV	MS Office, LaTeX, MestReNova, ChemDraw, Scifinder, Reaxys, Mendeley, Biorender	

Nationale und internationale Konferenzen

02/2019	Macromolecular Colloquium, Freiburg „Polymers and the Digital Age“
09/2018	Symposium der Sonderforschungsbereiche 1066 und 1278 „Nanomedicine: Is there more than Tumor Targeting?“, Mainz
09/2018	CLINAM Konferenz, Basel, Schweiz „11th European and Global Summit for Clinical Nanomedicine, Targeted Delivery and Precision Medicine – The Building Blocks to Personalized Medicine“
05/2018	Bordeaux Polymer Conference 2018, Bordeaux, Frankreich

02/2018	Macromolecular Colloquium, Freiburg „Far from Equilibrium Macromolecular Systems“
09/2017	JGU & KIT Symposium on Polymer Science, Mainz

Publikationen und Beiträge

(1) Becker, E., Grus, T.; Klasen, B.; Frey, H.; Rösch, F. ^{18}F-labeled, PSMA-specific liposomes: promising and PET-traceable tool for future targeted drug delivery in the treatment of prostate cancer. *To be submitted.*

(2) Becker, E.; Fuß, F.; Frey, H. Design of pH-Degradable Cholesterol-based Polyether Lipids for the Conjugation of Small Molecules. *To be submitted.*

(3) Becker, E.; Gleue, L.; Frey, H., Helm, M. Vinylether-functional Dialkyl-PEG Lipids for pH-Responsive Liposomes. *To be submitted.*

(4) Becker, E.; Matthes, R.; Gleue, L.; Frey, H., Helm, M. Thiazolidine-based Glycidyl Ethers for the Anionic Ring-Opening Polymerization. *To be submitted.*

(5) Worm, M; Fritz, T.; Becker, E.; Jung, F.; Leibig, D.; Helm, M.; Frey, H. Ketal- and Acetal-Functional Dialkyl-PEG Lipids for pH-Sheddable Stealth Liposomes. *To be submitted.*

(6) Gleue, L.; Schupp, J.; Zimmer, N.; Becker, E.; Frey, H.; Tuettenberg, A.; Helm, M. Stability of Alkyl Chain-Mediated Lipid Anchoring in Liposomal Membranes. *Cells* **2020**, *9* (10), 1–13. https://doi.org/10.3390/cells9102213.

Referenzen

Prof. Dr. Holger Frey
Betreuer der Diplom- und Doktorarbeit
Department Chemie
Johannes Gutenberg-Universität Mainz
Duesbergweg 10-14
55128 Mainz, Deutschland

Tel.: +49 (0)6131 39 24078
Email: frey@uni-mainz.de